VOL. 461 JANUARY 6, 1989
COMPLETE IN ONE ISSUE

12th International Symposium on Column Liquid Chromatography Washington, DC, June 19–24, 1988 Part III

RNAL OF

HROMATOGRAPHY

RNATIONAL JOURNAL ON CHROMATOGRAPHY, ELECTROPHORESIS AND RELATED METHODS

SYMPOSIUM VOLUMES

ELSEVIER

JOURNAL OF CHROMATOGRAPHY

Scope. The *Journal of Chromatography* publishes papers on all aspects of chromatography, electrophoresis and related methods. Contributions consist mainly of research papers dealing with chromatographic theory, instrumental development and their applications. The section *Biomedical Applications*, which is under separate editorship, deals with the following aspects: developments in and applications of chromatographic and electrophoretic techniques related to clinical diagnosis or alterations during medical treatment; screening and profiling of body fluids or tissues with special reference to metabolic disorders; results from basic medical research with direct consequences in clinical practice; drug level monitoring and pharmacokinetic studies; clinical toxicology; analytical studies in occupational medicine.

Submission of Papers. Papers in English, French and German may be submitted, in three copies. Manuscripts should be submitted to: The Editor of *Journal of Chromatography*, P.O. Box 681, 1000 AR Amsterdam, The Netherlands, or to: The Editor of *Journal of Chromatography, Biomedical Applications*, P.O. Box 681, 1000 AR Amsterdam, The Netherlands. Review articles are invited or proposed by letter to the Editors. An outline of the proposed review should first be forwarded to the Editors for preliminary discussion prior to preparation. Submission of an article is understood to imply that the article is original and unpublished and is not being considered for publication elsewhere. For copyright regulations, see below.

Subscription Orders. Subscription orders should be sent to: Elsevier Science Publishers B.V., P.O. Box 211, 1000 AE Amsterdam, The Netherlands, Tel. 5803 911, Telex 18582 ESPA NL. The *Journal of Chromatography* and the *Biomedical Applications* section can be subscribed to separately.

Publication. The *Journal of Chromatography* (incl. *Biomedical Applications*) has 37 volumes in 1989. The subscription prices for 1989 are:

J. Chromatogr. + *Biomed. Appl.* (Vols. 461–497):
Dfl. 6475.00 plus Dfl. 999.00 (p.p.h.) (total *ca.* US$ 3933.75)

J. Chromatogr. only (Vols. 461–486):
Dfl. 5200.00 plus Dfl. 702.00 (p.p.h.) (total *ca.* US$ 3106.25)

Biomed. Appl. only (Vols. 487–497):
Dfl. 2200.00 plus Dfl. 297.00 (p.p.h.) (total *ca.* US$ 1314.25).

Our p.p.h. (postage, package and handling) charge includes surface delivery of all issues, except to subscribers in Argentina, Australia, Brasil, Canada, China, Hong Kong, India, Israel, Malaysia, Mexico, New Zealand, Pakistan, Singapore, South Africa, South Korea, Taiwan, Thailand and the U.S.A. who receive all issues by air delivery (S.A.L. — Surface Air Lifted) at no extra cost. For Japan, air delivery requires 50% additional charge; for all other countries airmail and S.A.L. charges are available upon request. Back volumes of the *Journal of Chromatography* (Vols. 1–460)are available at Dfl. 230.00 (plus postage). Claims for missing issues will be honoured, free of charge, within three months after publication of the issue. Customers in the U.S.A. and Canada wishing information on this and other Elsevier journals, please contact Journal Information Center, Elsevier Science Publishing Co. Inc., 655 Avenue of the Americas, New York, NY 10010. Tel. (212) 989-5800.

Abstracts/Contents Lists published in Analytical Abstracts, ASCA, Biochemical Abstracts, Biological Abstracts, Chemical Abstracts, Chemical Titles, Chromatography Abstracts, Current Contents/Physical, Chemical & Earth Sciences, Current Contents/Life Sciences, Deep-Sea Research/Part B: Oceanographic Literature Review, Excerpta Medica, Index Medicus, Mass Spectrometry Bulletin, PASCAL-CNRS, Referativnyi Zhurnal and Science Citation Index.

See inside back cover for Publication Schedule, Information for Authors and information on Advertisements.

0021-9673/89/$03.50

Printed in The Netherlands

For contents see p. VII.

Add supercritical capability to your GC

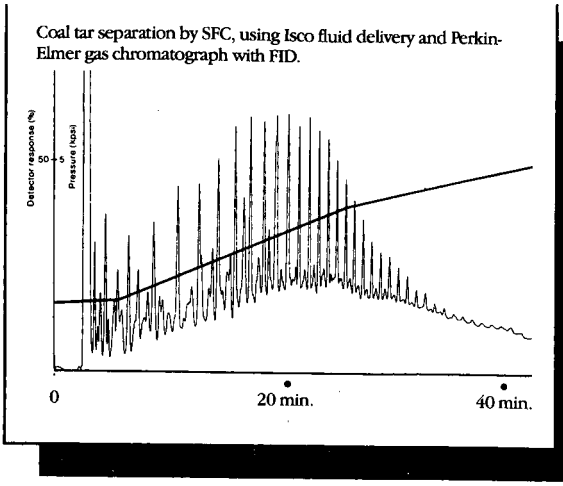

An Isco SFC-500 syringe pump with computer-based gradient control will push a whole new range of samples through your present GC. For relatively low cost, you can easily install an SFC fluid delivery system that gives you pulseless flow, programmability for virtually any pressure or density gradient, and unlimited method storage on computer disks.

If you're ready to try SFC, get the facts on Isco fluid delivery systems and complete chromatographs using 1 mm packed columns with absorbance detection. Contact your Isco representative now.

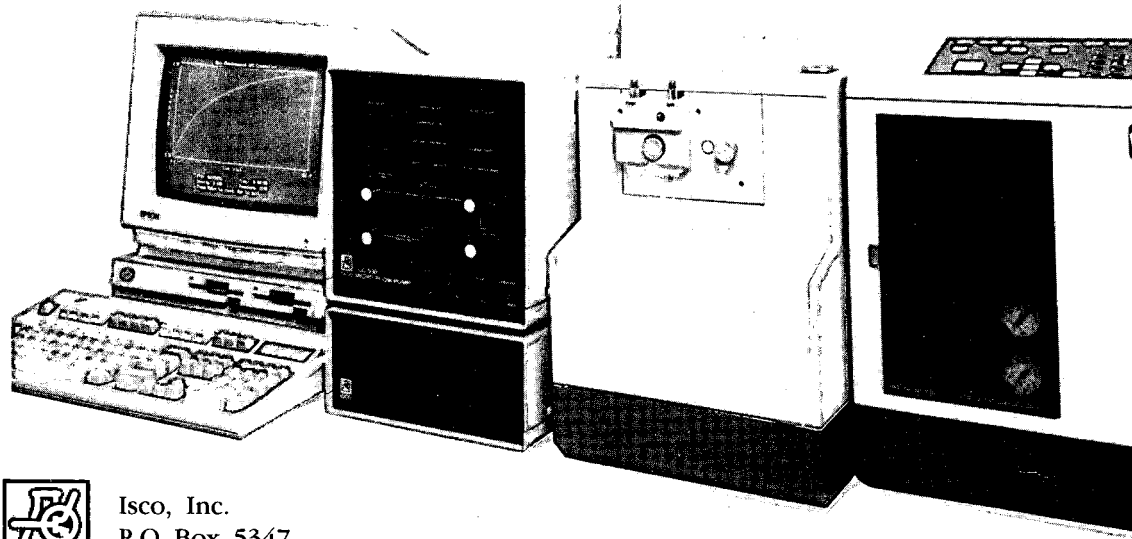

Isco, Inc.
P.O. Box 5347,
Lincoln, NE 68505. U.S.A

ISCO

Distributors • **The Netherlands:** Beun-de Ronde B.V Abcoude 02946-3119 • **Hungary:** Lasis Handelsges. mbH Wien 82 01 83 • **Spain:** Iberlabo, s.a. Madrid 01 251 1491 • **W. Germany:** Colora Messtechnik GmbH Lorch, Württ. 07172 1830 • **France:** Ets. Roucaire, S.A. Velizy (1) 39 46 96 33 • **Italy:** Gio. de Vita e C. s.r.l. Roma 4950611 • **U.K.:** Life Science Laboratories, Ltd, Luton (0582) 59767 **Norway:** Dipl. Ing. Houm A.S. Oslo 02 15 92 50 • **Switzerland:** IG Instrumenten-Gesellschaft AG Zurich 01 4613311 • **Belgium:** SA HVL NV Bruxelles (02) 720 48 30 • **Denmark:** Mikrolab Aarhus A/S Højbjerg 06-29 61 11 • **Austria:** Neuber Gesellschaft mbH Wien 42 62

Totally automated HPLC .....Hands off chromatography

Robust chromatography for analytes in "real world" samples, and no operator intervention! ASTED®, a new robotic system developed by Gilson, uses dialysis and trace enrichment. ASTED automates sample pretreatment, permitting chromatographic analysis of virtually any sample type.

ASTED mixes raw sample with standards and reagents, separates low molecular weight analytes from biological or industrial matrices, then injects into the analytical column. The system is on-line, requires no guard column and ensures a long lifetime for the column. Cycle time is typically 5 minutes, with one sample being prepared while the previous one elutes.

Compatibility? ASTED is compatible with most HPLC systems, with practically any existing HPLC method, with most data processors. No need to change your protocol or modify your system.

Flexibility? ASTED offers prechromatographic chemistry, dialysis, trace enrichment, and injection, as combined or separate functions for method development.

Savings? With low running costs and high sample throughput, ASTED is highly competitive for quantitative or fingerprint routines.

Validation? ASTED has been fully validated for various applications: amino acids and metabolites in biological fluids; total theophylline and xanthines, anticonvulsant drugs, cortisol and glucocorticoids in plasma or serum; free catecholamines in urine. Other applications are being developed in food quality control, pharmaceuticals, environmental analysis.

For more information about ASTED, please contact your nearest Gilson representative.

Selected references:
D.C. Turnell and J.D.H. Cooper, J. Chromatogr., 395 (1987) 613-621.
J.D.H. Cooper, D.C. Turnell, B. Green and F. Vérillon, J. Chromatogr., 456 (1988) 53-69.

ASTED® (Automated Sequential Trace Enrichment of Dialysates)
Original Patent : U.K. 2 124 370 and Registered Trademark of Coventry Health Authority, U.K.

JOURNAL OF CHROMATOGRAPHY

VOL. 461 (1989)

JOURNAL *of* CHROMATOGRAPHY

INTERNATIONAL JOURNAL ON CHROMATOGRAPHY,
ELECTROPHORESIS AND RELATED METHODS

SYMPOSIUM VOLUMES

ELSEVIER
AMSTERDAM — OXFORD — NEW YORK — TOKYO

Old Corcoran (Renwick) Gallery of Art, wood engraving, 1884

0021-9673/89/$03.50

Printed in The Netherlands

SYMPOSIUM VOLUME

SYMPOSIUM VOLUME

TWELFTH INTERNATIONAL SYMPOSIUM ON COLUMN LIQUID CHROMATOGRAPHY

PART III

Washington, DC (U.S.A.), June 19–24, 1988

Guest Editor

G. GUIOCHON

(Knoxville and Oak Ridge, TN)

The proceedings of the *Twelfth International Symposium on Column Liquid Chromatography, Washington, DC, June 19–24, 1988*, are published in three volumes of the *Journal of Chromatography*: Vols. 458 and 459 (1988) and 461 (1989). The Foreword to the proceedings, and information on the Sponsoring Scientific Organizations and the Scientific and Organization Committees only appear in Vol. 458. Vol. 459 is dedicated to the memory of **Dr. István Halász**, and opens with an obituary.

CONTENTS

12TH INTERNATIONAL SYMPOSIUM ON COLUMN LIQUID CHROMATOGRAPHY, WASHINGTON, DC, JUNE 19–24, 1988, PART III

In articles with more than one author, the name of the author to whom correspondence should be addressed is indicated in the article heading by a 6-pointed asterisk (*)

Journal of Chromatography, 461 (1989) 1–18
Elsevier Publishers B.V., Amsterdam — Printed in The Netherlands

CHROMSYMP. 1444

THEORETICAL STUDY OF SYSTEM PEAKS AND ELUTION PROFILES FOR LARGE CONCENTRATION BANDS IN THE CASE OF A BINARY ELUENT CONTAINING A STRONGLY SORBED ADDITIVE

SADRODDIN GOLSHAN-SHIRAZI and GEORGES GUIOCHON*

**Department of Chemistry, University of Tennessee, Knoxville, TN 37996-1600 (U.S.A.) and Division of Analytical Chemistry, Oak Ridge National Laboratory, Oak Ridge, TN (U.S.A.)*

SUMMARY

The profile of system peaks when using high concentrations and a binary mobile phase was studied using the semi-ideal model of chromatography. The profile of the sample band depends on the concentration of the strong solvent and on the sample size. It is very strongly influenced by the relative adsorption strength of the strong solvent and the sample. This relative strength is measured by the ratio of (a) the origin slope of the equilibrium isotherm of the strong solvent between the stationary phase and the pure weak solvent to (b) the origin slope of the isotherm of the sample (*i.e.*, the ratio between their respective column capacity factors in the pure weak solvent). When this ratio is smaller than 0.2, the sample band profile depends only on the equilibrium isotherm of the sample in the binary mixture. If the ratio becomes larger, the competition between the strong solvent and the sample molecules for interaction with the stationary phase becomes more intense. For Langmuir-competitive isotherms of the strong solvent and the sample, if the concentration of the strong solvent and/or its strength are progressively increased at constant sample size, the retention time of the band decreases (as expected), whereas its typical Langmuirian asymmetry decreases and, past a narrow transition range, reverses. Bands traditionally associated with an anti-Langmuir isotherm are then obtained.

Extremely unusual, broad, characteristic profiles, with a sharp front and a sharp rear, which sometimes exhibit two maxima, are obtained in the transition region. When the origin slope ratio is large, the profile of a high-concentration-sample band in the transition region has two shock layers. The occurrence of such band profiles, under experimental conditions similar to those predicted here, have been reported previously, but their origin has remained unexplained until now.

INTRODUCTION

Since the work of Wilson[1], DeVault[2], Glueckauf[3] and Thomas[4], it has been recognized that the elution profile of high-concentration chromatographic bands is the result of non-linear phenomena. These phenomena can be considered from either a kinetic or a thermodynamic point of view, as we know that thermodynamic equilibria

0021-9673/89/$03.50

are not static but kinetic in nature. The equilibrium constant, for example, is the ratio between the sorption and the desorption rates.

As explained in the following paragraphs, the rigorous solution of a chromatographic problem requires the use of a kinetic approach and, hence, a knowledge of the concentration dependence of the sorption and desorption rates. Equilibrium isotherms are easier to model and measure than mass-transfer rates, which explains the attraction and popularity of equilibrium and semi-equilibrium models that make simplifying assumptions regarding the kinetics of mass transfers. Most retention mechanisms used in chromatography have very fast kinetics. Hence the phase compositions are always, and everywhere in the column, close to equilibrium. Equilibrium isotherms are not linear. At high solute concentrations, they always exhibit some degree of non-linearity, the concentration in the stationary phase at equilibrium increasing either faster or more slowly than the concentration in the mobile phase. Accordingly, solutes at different concentrations tend to move along the column at different speeds, and either the front or rear of the band will tend to become steeper and steeper. However, the finite character of the kinetics of mass transfers between phases tends to relax all concentration gradients, especially those which the non-linear behavior of the chromatographic process at high concentrations tends to build up.

The elution profile of a chromatographic band is obtained as the solution of a classical mass balance equation, relating the time differential in the concentrations of the corresponding compound in the mobile and stationary phases[1,2]. A relationship between these two differentials is required in order to solve the problem, and it can be found by either a thermodynamic or a kinetic approach. The former assumes constant equilibrium between phases. The required relationship between the time differentials of the solute concentrations in both phases is obtained by differentiation of the equilibrium isotherm. The latter attempts to derive a relationship between (a) the rate of sorption/desorption and (b) the composition of the stationary and mobile phases, and is a much more difficult approach.

The first approach assumes, according to Haarhoff and Van der Linde[5], that the mass transfer is fast enough for the two phases to be always very near equilibrium, the effects of axial diffusion and finite rate of radial mass transfer merely combining and resulting in an apparent diffusion, larger than the true axial diffusion but having the same consequence. This is the basis of the semi-ideal model of chromatography, which is valid for columns having more than 1000 theoretical plates. This model is attracting much interest at present, because of the recently increased importance of preparative liquid chromatography in the pharmaceutical and biochemical industries, and because nearly all retention mechanisms used in the various implementations of high-performance liquid chromatography (HPLC) (normal- and reversed-phase chromatography, ion-exchange chromatography, hydrophobic interaction chromatography, ligand-exchange chromatography, size-exclusion chromatography) involve very fast mass transfers between phases. The related ideal model assumes further that the column efficiency is infinite[1–3,6]. An analytical solution of the ideal model can be derived in the case of a Langmuir isotherm[7]. The solutions of the ideal mode are very close to the profiles obtained with real columns of finite efficiency used in the semi-ideal model. It is important to note that the discontinuities or shocks predicted by the ideal model are replaced in the semi-ideal model with shock layers that have the steep fronts or rears recorded with overloaded elution bands, and that propagate at the same velocity as the shocks of the ideal model[8].

The second approach consists in writing the kinetic equation describing the processes of adsorption of the studied compounds by the stationary phase and their desorption as a function of their concentrations in the two phases of the system. In Langmuir kinetics, the corresponding equation has also been solved[4,9]. It gives profiles that are identical with those supplied by the previous approach, in the case of fast kinetics[10]. However, it permits the study of slow equilibria, such as those used in affinity chromatography, in some instances where the sorption/desorption rates are abnormally slow or in various processes of adsorption and absorption.

The choice between the two approaches will depend in many instances on the relative ease with which the thermodynamics or the kinetics of a certain retention mechanism can be studied and described. At present, it seems that thermodynamics leads to an easier route.

In previous papers we described the algorithmic approach to a numerical solution of the single- and two-component problems within the framework of the semi-ideal model[11,12]. We used the programs derived from these analyses to calculate elution profiles of single and two-component pulses and the influence of most experimental parametes on these profiles[11] and on the separation of a binary mixture[13]. However, in all instances, we neglected the adsorption of the mobile phase. This is acceptable provided that the mobile phase is a single solvent, as it can be shown that this is tantamount to making a choice of the reference state in adsorption thermodynamics[14]. However, this assumption falters when the mobile phase is a mixture of solvents[15].

In adsorption chromatography, it is common to use a mobile phase containing a strong solvent, which is adsorbed on the stationary phase, modifies its surface and competes with the eluites for access to the adsorption sites on this surface. Hence the prediction of the band profile of a single-component sample eluted with a binary eluent is really a two-component problem, whereas the prediction of the elution profiles and separation of a two-component sample is a three-component problem. The boundary and initial conditions of the problem are just slightly different from those for the elution of a two- and a three-component sample plug: one of the components (the sample) is injected as a plug, whereas the other one (the strong solvent) is injected continuously, at constant concentration as a component of the mobile phase.

In this paper, we discuss from a theoretical standpoint the phenomena associated with the elution of a single component with a binary eluent. In the accompanying paper[16], we present experimental evidence for the soundness of these theoretical results.

THEORY

As both the strong solvent and the solute can interact with the stationary phase (through whatever retention mechanism is involved), we must consider a mass balance equation for each of them. For the solute we have

$$\frac{\partial C_a}{\partial t} + \frac{V_s}{V_m} \cdot \frac{\partial q_a}{\partial t} + u \cdot \frac{\partial C_a}{\partial z} = D_L \cdot \frac{\partial^2 C_a}{\partial z^2} \qquad (1)$$

and for the strong solvent we have similarly

$$\frac{\partial C_s}{\partial t} + \frac{V_s}{V_m} \cdot \frac{\partial q_s}{\partial t} + u \cdot \frac{\partial C_s}{\partial z} = D_L \cdot \frac{\partial^2 C_s}{\partial z^2} \tag{2}$$

where t is the time and z the abscissa along the column, C is the concentration in the mobile phase [the subscripts a and s represent the analyte (sample, eluite or solute) and the strong solvent, respectively], q is the concentration in the stationary phase, V_s and V_m are the fractions of the column volume available for the stationary and the mobile phase, respectively, and D_L is the axial diffusion coefficient, assumed to be the same for both the strong solvent and the sample. In order to solve this system we need a proper set of relationships between the time differentials of the concentrations of the solute and the strong solvent in the stationary phase and their concentrations in the mobile phase (see Introduction).

It is impossible to derive exact solutions of the system of partial differential equations obtained, except when linearity applies (*e.g.*, first-order kinetics)[17]. Such a solution is valid only under analytical conditions. Numerical solutions of this system may be obtained using a finite-difference method[11,12], but only after some simplification to eliminate the right-hand side (RHS) of the equations.

Within the framework of the classical semi-ideal model[18], we make the following three assumptions. First, the axial diffusion term is negligible. Second, the relationship between (a) the concentrations of the solute and the strong solvent in the stationary phase at equilibrium and (b) the mobile-phase concentrations of these two components, at the same time and the same place in the column, are given by the mixed, competitive, ternary isotherms (see below). The combination of these two assumptions results in an infinite column efficiency. Thus, we account for the finite efficiency of the column by setting the length increment in the numerical integration of the system of partial differential equations equal to the column HETP. The time increment is related to the length increment[19]. It can be shown that, with this method, the errors introduced by the calculation in the derivation of the profiles solution of eqns. 1 and 2 with a zero RHS are made exactly equal to the neglected RHS. Accordingly, the procedure gives exact numerical solutions of the system of eqns. 1 and 2.

In the following, we have assumed the simplest possible form for the ternary isotherm, the competitive Langmuir isotherms

$$\frac{q_a}{q_o} = \frac{b_a C_a}{1 + b_a C_a + b_s C_s} \tag{3}$$

and

$$\frac{q_s}{q'_o} = \frac{b_s C_s}{1 + b_a C_a + b_s C_s} \tag{4}$$

where q_o and q'_o are the saturation concentrations of the sample and the strong solvent respectively, in the stationary phase. The column saturation limit is the product of q_o (or q'_o) and the column volume, and b_a and b_s are numerical coefficients.

This sytem of eqns. 1–4 is identical with that used in the study of the separation of the two components of a binary mixture when a sample pulse is injected in elution chromatography[12]. The difference from this previous problem is the set of boundary conditions. A constant stream of mobile phase with a constant concentration of strong solvent is flowing during the whole experiment, and a pulse of solute is injected over a very short period of time. Accordingly, the boundary conditions of the problem are as follows:

$$C_a(x,0) = 0 \tag{5a}$$

$$\begin{aligned} C_a(0,t) &= 0 \text{ if either } t < 0 \text{ or } t > t_p \\ &= C_o \text{ if } 0 < t \leqslant t_p \end{aligned} \tag{5b}$$

where t_p is the width of the sample pulse.

$$C_s(0,t) = C_{s,o} \tag{5c}$$

The calculations are carried out by means of a program similar to that described previously[15]. In all the simulations, the column dimensions are assumed to be 25 cm × 4.5 mm I.D., the flow-rate 1 ml/min (flow-velocity 0.122 cm/s) and the column efficiency 5000 theoretical plates. The isotherm parameters used and the sample size are given in the figure captions.

RESULTS AND DISCUSSION

Chromatography of a sample containing a single compound with a binary mobile phase gives a peak for that compound at a retention time resulting from the combined interaction of both the sample and the strong solvent with the stationary phase and gives two peaks for the strong solvent. The latter are usually called system peaks. They have been investigated extensively by previous workers[20–24] who were essentially preoccupied with the interference of these peaks with those of the sample in analytical chromatography.

In true linear chromatography, these system peaks should not occur. Analytical chromatography with a mixed mobile phase may be linear as far as the sample is concerned, but not as far as the mobile phase is concerned. In fact, the whole purpose of using mixtures as mobile phases is to manipulate the equilibrium constants so as to adjust the selectivity and retention volumes for successful analysis. The concentration of the strong solvent is usually high enough to modify the retention of the sample components, and therefore the column behavior cannot be linear towards this solvent modifier.

The solvent peaks are the result of the modification of the strong solvent–stationary phase equilibrium due to the injection of the sample. Hence they are the result of transitory changes in the composition of the mobile phase. They are detected by a non-selective detector, such as a refractive index detector, and are not detected by a selective detector, such as a UV detector. This is why the chromatograms obtained, even in analytical chromatography, can be very different, depending on the nature of the mobile phase used and whether a selective or a non-selective detector is chosen.

With a non-selective detector, the chromatogram may be nearly impossible to account for if there are numerous resolved components in the sample being analyzed.

If the sample injected is large, the non-linear effects are considerably amplified and a variety of situations may be encountered, depending on the relative strengths of the adsorption of the solute and the strong solvent on the stationary phase. Figs. 1–4 show the results of the simulation of the elution of a high-concentration band of a single-solute sample under different sets of experimental conditions. In all instances we observe three peaks, one for the solute and two for the strong solvent. The first of the latter two peaks is positive (excess of strong solvent, representing the amount replaced by the sample when it is injected). If the strong solvent is less strongly adsorbed than the sample, the first peak is eluted as a non-retained compound. If the strong solvent is equally or more strongly retained than the sample, the first peak is retained and eluted at a time that depends on the nature of the strong solvent (*i.e.*, the characteristics of its adsorption), on its concentration and on the nature and concentration of te sample.

The second solvent peak is negative. Usually, it is eluted at the same time as the solute. Sometimes, the negative peak is more strongly retained than the sample, and

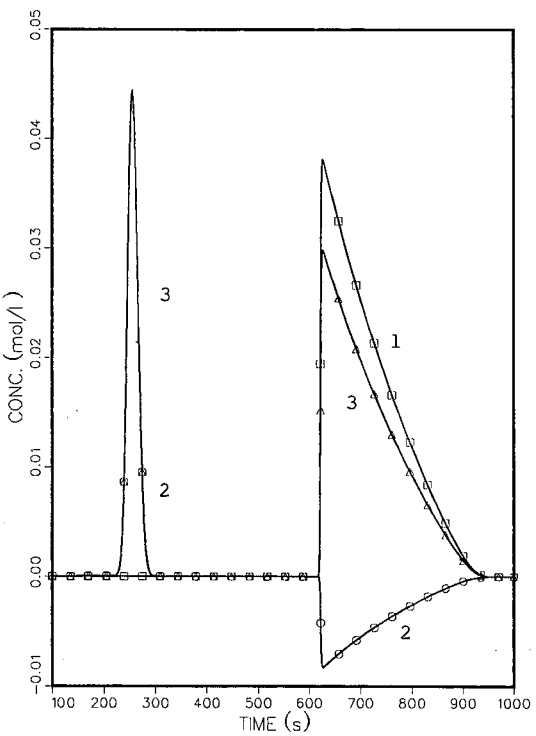

Fig. 1. Chromatogram obtained for a one-component sample on a chromatographic column with a binary mobile phase. Column length, 25 cm; column efficiency, 5000 theoretical plates; flow velocity, 0.122 cm/s ($t_0 = 205$ s); strong solvent concentration, 0.25 M; Langmuir isotherm coefficients, $a_s = 2.0$, $a_a = 20$, $b_s = 1.0$, $b_a = 10$; sample size, 83.3 μmole. 1, Elution profile of the sample (signal from a detector selective for the sample); 2, elution profile of the strong solvent (signal from a detector selective for the solvent); 3, sum of profiles 1 and 2 (signal from a non-selective detector with equal response factors for strong solvent and solute).

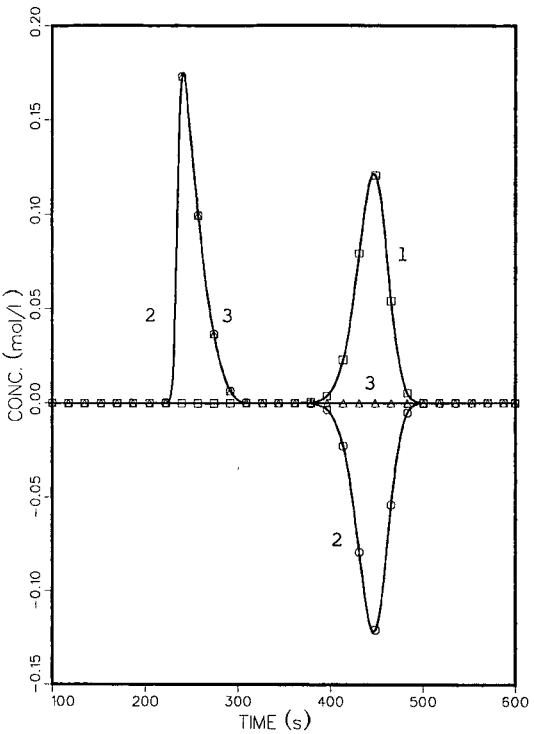

Fig. 2. Chromatogram obtained for a one-component sample on a chromatographic column with a binary mobile phase. Experimental conditions as in Fig. 1, except $a_s = 20$ and $b_s = 10$. 1, Elution profile of the sample; 2, elution profile of the strong solvent; 3, sum of profiles 1 and 2.

then the positive peak is eluted at the same time as this sample. The signal of a truly non-selective detector is a combination of these two concentration profiles. In the figures we have assumed that the total chromatogram was obtained this way.

In practice, however, there is no truly non-selective detector. The response factor of the differential refractive index detector may change by more than one order of magnitude from one compound to another. It may even change in sign[16]. In such an event, the combination of the asymmetric shapes of the two interfering peaks [the solvent (system) peak and the solute peak] and of unusual response factors may lead to unexpected chromatograms, which may be difficult to account for without an excellent understanding of the chromatographic processes involved. The shape of the sample band profile itself may become totally unexpected, very different from what is usually observed for an overloaded column, whether the isotherm is Langmuirian or anti-Langmuirian. Some unusual profiles of that kind have already been reported[25].

Fig. 1 shows the simulation chromatogram obtained for a large sample of a solute that is much more strongly retained than the strong solvent. However, as the concentration of the strong solvent is high its presence changes the retention behavior of the sample and, in particular, reduces its retention time (the column capacity factor is inversely proportional to $1 + b_s c_s$, where b_s and c_s are the second coefficient of the Langmuir isotherm of the strong solvent and its concentration in the mobile phase,

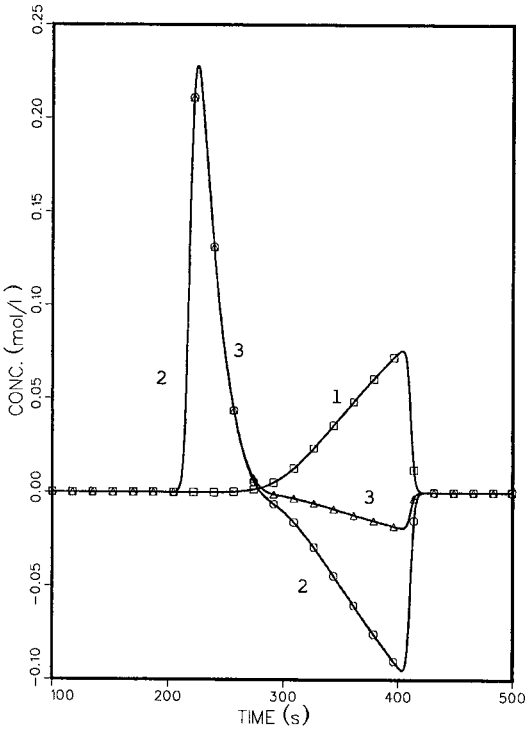

Fig 3. Chromatogram obtained for a one-component sample on a chromatographic column with a binary mobile phase. Experimental conditions as in Fig. 1, except $a_s=40$ and $b_s=20$. 1, Elution profile of the sample; 2, Elution profile of the strong solvent; 3, sum of profiles 1 and 2.

respectively[15]). We observe a sample peak with a very sharp front and a tail ending close to the retention time of a very small plug of sample, under the same experimental conditions. This profile is very close to that observed when the solute equilibrium isotherm is Langmuirian. It has been shown that when the ratio of the slopes at the origin of the adsorption isotherms of the sample and the strong solvent in the weak solvent is greater than about 5, the three following profiles are almost identical[15]: (i) the experimental profile, (ii) the profile calculated from the (correct) two-component model and the competitive isotherm and (iii) the profile calculated from the approximate one-component model (using the single-component isotherm, derived from the competitive isotherm by assuming that the strong solvent concentration is constant). Differences appear progressively as the isotherm slope ratio decreases.

As expected, there are two solvent peaks in Fig. 1. One, observed at the dead volume, is Gaussian. The other, appearing at the same time as the sample band, is negative; the concentration of the strong solvent decreases in the eluent during the elution of the sample band. Accordingly, the total concentration of solutes in the weak solvent varies less than would be indicated by the profile of the sample band. The signal of a non-selective detector is smaller than that of a detector selective for the sample only, which would have the same response factor. The strong solvent peak is proportional to the solute peak. This means that a detector that would respond to both

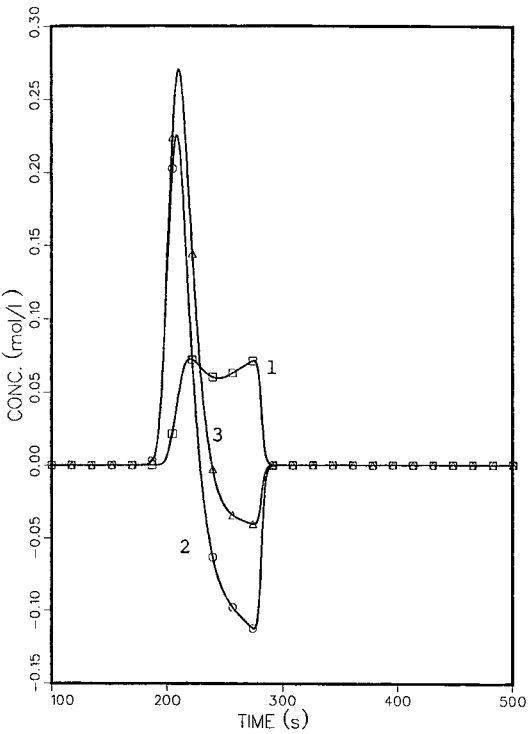

Fig. 4. Chromatogram obtained for a one-component sample on a chromatographic column with a binary mobile phase. Experimental conditions as in Fig. 1, except $a_s = 200$ and $b_s = 100$. 1, Elution profile of the sample; 2, elution profile of the strong solvent; 3, sum of profiles 1 and 2.

the sample and the strong solvent could exhibit a total lack of response during the elution of the composite band, should the two response factors be in the proper ratio. This proportionality is due to the fact that each molecule of sample that leaves the stationary phase is replaced with a certain number of molecules of strong solvent that were displaced at the time of injection of the sample. Obviously, the areas of the two bands of strong solvent are equal, as they correspond to the same amount of material, first displaced from the column, then replenished.

Fig. 2 shows the simulated chromatogram obtained under conditions very similar to those for Fig. 1, except that the slope at the origin of the adsorption isotherm (origin slope), of the strong solvent is steeper. The origin slopes of the sample and the strong solvent are now equal. The sample band has become less retained at infinite dilution and, altough the sample was of the same size for Figs. 1 and 2, the band shown in Fig. 2 is much more symmetrical, even nearly Gaussian. The first solvent peak, on the other hand, is now tailing slightly. Its retention time increases with increasing strength of the organic modifier. The profile of the second, negative, solvent band is equal to that of the sample band, but it is negative. Accordingly, the concentration of the weak solvent in the eluent remains constant during the entire elution of these bands and the only signal recorded by a non-selective detector would be the asymmetric first

solvent band. This is a paradoxical, unexpected result, which could be highly misleading.

Figs. 3 and 4 show simulated chromatograms obtained with samples that are less strongly adsorbed than the strong solvent. The ratios of the origin slopes of the adsorption isotherms for the strong solvent and the sample in the weak solvent are 2 and 10 for Figs. 3 and 4, respectively. Now, the profiles of the three bands, that for the sample and the two for the strong solvent, are all asymmetric. However, the elution profile of the sample has changed direction. Its front is diffuse, whereas its rear is very sharp, as if the adsorption isotherm were anti-Langmuirian. As explained under Theory, the isotherms used here are competitive Langmuir isotherms, wich cannot, in any way, be combined to result in an anti-Langmuir isotherm. The phenomenon is entirely due to the competition between the molecules of sample and strong solvent for access to the adsorbent surface. The increasing strength of the strong solvent is reflected by the decrease in the retention of the sample, at constant composition of the eluent. The mere competition between solute and strong solvent (or one of the mobile phase additives) explains why, in many instances, the profiles of overloaded bands obtained in reversed-phase or hydrophobic interaction chromatography correspond to an anti-Langmuir type of isotherm, not to a Langmuir type. This phenomenon

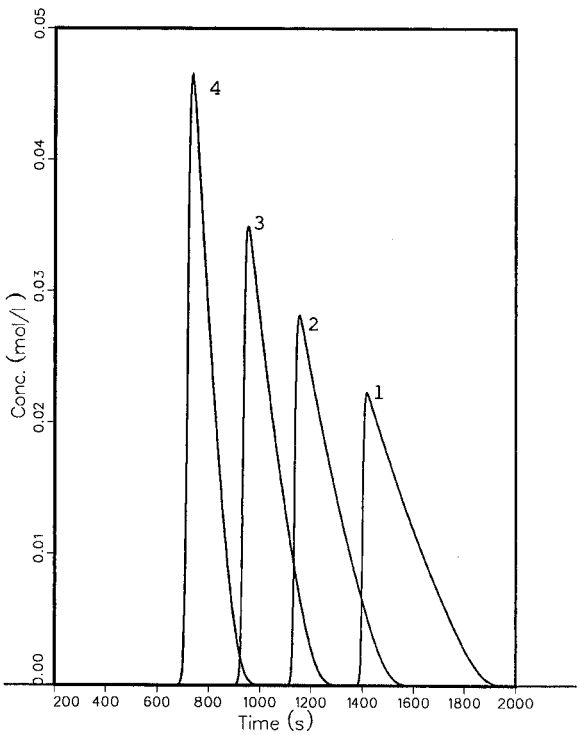

Fig. 5. Influence of the concentration of the strong solvent in the mobile phase on the elution profile of a single compound. Weakly adsorbed strong solvent. Experimental conditions as in Fig. 1, except $a_s = 4$, $a_a = 40$, $b_s = 0.80$; $b_a = 8$, and different strong solvent concentrations. Strong solvent concentration: 1, 0.1; 2, 0.5; 3, 1; 4, 2 *M*.

could explain why a change in the composition of the solvent can reverse the asymmetry direction of the band and replace an apparently anti-Langmuir band profile by a Langmuirian profile.

We also observe in Figs. 3 and 4 that the two solvent bands are now partially merged and that the negative second band is more concentrated than the sample band. As a consequence, the injection of the sample results in a negative signal with a non-selective detector, while a much simpler, positive signal is observed with a selective detector.

These phenomena are similar to those observed in analytical chromatography and reported by previous workers[20–24]. In the case of high-concentration sample bands, there is an additional complexity resulting from the fact that the perturbation due to the injection of the sample cannot be considered to be small and cannot be treated by assuming that the system behaves linearly near the steady equilibrium point.

The retention time of the sample band and the shape of its profile depend not only on the relative strengths of the adsorption of the strong solvent and the sample from their solution in the weak solvent, but also on the column efficiency, the concentration of the strong solvent in the mobile phase, the column saturation capacity and the size of the sample pulse.

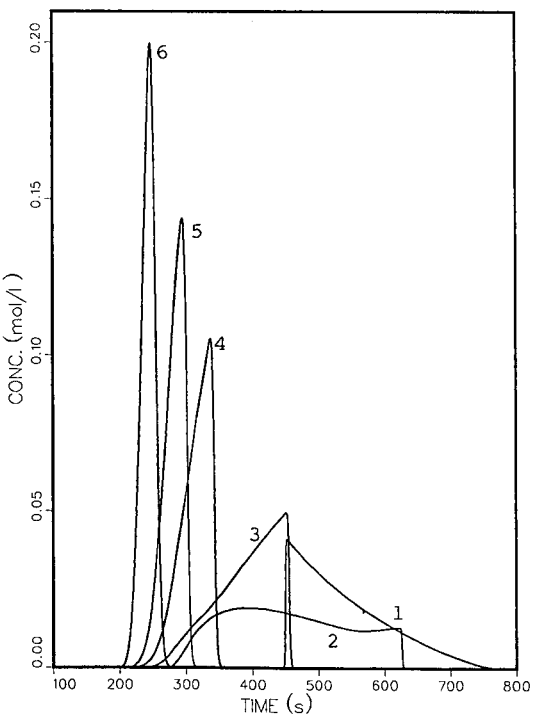

Fig. 6. Influence of the concentration of the strong solvent in the mobile phase on the elution profile of a pure compound. Strongly adsorbed strong solvent. Experimental conditions as in Fig. 5, except $a_s = 28.8$, $a_a = 14.4$, $b_s = 16$ and $b_a = 8$ and different strong solvent concentrations. Strong solvent concentration: 1, 0.017; 2, 0.085; 3, 0.17; 4, 0.34; 5, 0.5; 6, 1 *M*.

Fig. 5 shows a series of simulated chromatograms obtained with the same sample size of a compound that is much more strongly adsorbed than the strong solvent from a dilute solution in the weak solvent. The ratio of the origin slopes of the sample and the strong solvent is 10. The concentration of the strong solvent is increased from 0.1 to 0.5, 1 and 2 *M*. In all instances, the band profile corresponds to that observed in overloading a chromatographic system with a Langmuir isotherm. However, the degree of symmetry of the sample peak increases with increasing concentration of the strong solvent. Its retention time decreases, as does the limiting retention time at zero sample size of the sample. This is expected, as it is the reason why the concentration of strong solvent in the eluent is usually adjusted.

Fig. 6 shows the simulated chromatograms obtained by the same procedure, increasing the concentration of the strong solvent in the mobile phase at constant sample size, but this time the sample is less strongly adsorbed on the stationary phase than the strong solvent. The ratio of the origin slopes of the sample and the strong solvent is now 0.5. At high concentrations of the strong solvent, we observe the same effect as that seen in Fig. 3. The band profile is similar to the profiles associated with an anti-Langmuir isotherm, although the isotherms involved here are not anti-Langmuirian. When the concentration of the strong solvent decreases, the band profile

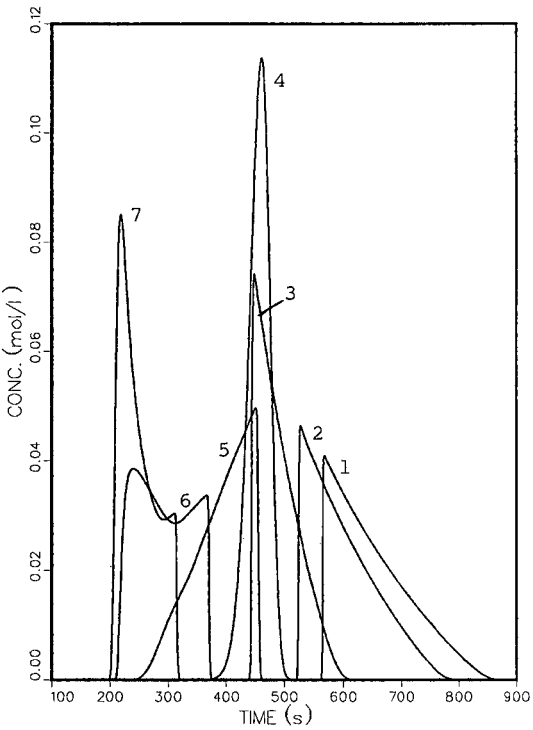

Fig. 7. Influence of the strength of adsorption of the strong solvent in the mobile phase on the elution profile of a single compound. Experimental conditions as in Fig. 6, except strong solvent concentration 0.17 *M* and different Langmuir coefficients a_s and b_s. a_s/a_a: 1, 0; 2, 0.1; 3, 0.5; 4, 1; 5, 2; 6, 5; 7, 10. b_s/b_a: 1, 0; 2, 0.1; 3, 0.5; 4, 1; 5, 2; 6, 5; 7, 10.

changes, a hump appears on its front, then its rear moves backwards rapidly and the profile becomes typical of the band of a compound having a Langmuir isotherm (see Fig. 6). Such a behavior is unexpected. The profiles obtained in the transition region are very unusual. Elution band profiles similar to those described in Fig. 6 have been reported previously by Kirkland[25] and have remained unexplained until now.

These phenomena can be explained by the fact that, even if the strong solvent is strongly adsorbed on the stationary phase, the fraction of the adsorbent surface that is covered by the strong solvent molecules at equilibrium is still small at low concentrations of this solvent (otherwise, with a more weakly adsorbed solute, there would be almost no retention). Hence the competition with the sample molecules has mainly the effect of reducing the retention time, but the band profile is not changed. The modification of the band profile occurs when the competition for adsorption between strong solvent and sample molecules becomes acute, *i.e.*, at strong solvent concentrations, in a range which depends on its strength of adsorption.

Fig. 7 shows a series of simulated chromatograms for the injection of a constant amount of a single-solute sample in a mobile phase of constant composition (*i.e.*, constant concentration of the strong solvent). From one band to the next, the relative adsorption strength of the sample and the strong solvent is changed. The ratio of the origin slopes of the isotherms between the strong solvent and the sample for adsorption

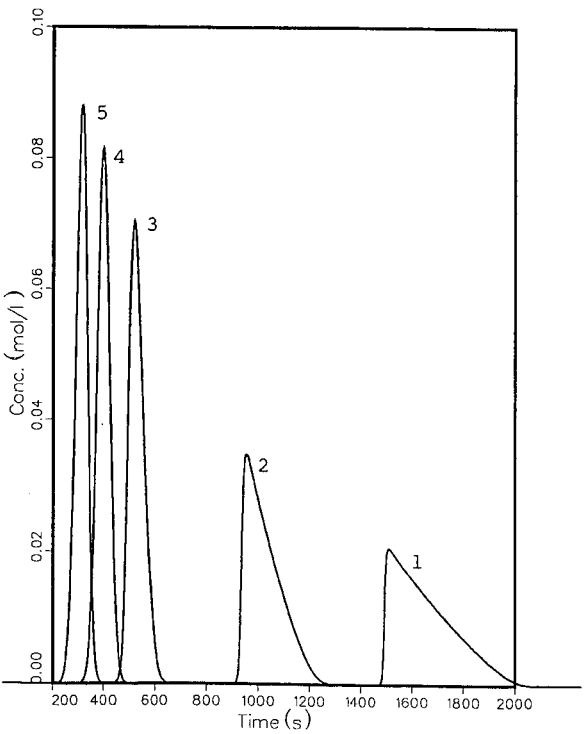

Fig. 8. Influence of the strength of adsorption of the strong solvent in the mobile phase on the elution profile of a single compound. Experimental conditions as in Fig. 7, except strong solvent concentration 1.0 *M* and different Langmuir coefficients a_s and b_s. a_s/a_a: 1, 0; 2, 0.1; 3, 0.5; 4, 1; 5, 2. b_s/b_a: 1, 0; 2, 0.1; 3, 0.5; 4, 1; 5, 2.

from their solutions in the weak solvent is increased from 0 to 0.1, 0.5, 1, 2, 5 and 10. As expected on the basis of our explanations, the sample band profile changes, and a reversal in the direction of the asymmetry is observed. The first three profiles have the shape normally associated with a Langmuir isotherm. The fourth is Gaussian. The fifth is similar to those associated with an anti-Langmuir isotherm. The last two bands have two steep fronts, *i.e.*, two shock layers. They show a progressive transformation of the sample band into a non-retained band (t_0 = 205 s).

Fig. 8 shows a series of simulated chromatograms, similar to those in Fig. 7, the only difference being in the higher concentration of the strong solvent in the mobile phase. The retention time of the sample band decreases rapidly with increasing ratios of the origin slopes of the isotherms between the strong solvent and the sample. The band profile remains similar to the profiles associated with a Langmuir isotherm. By the time the ratio has become large enough to promote a reversal in the direction of band asymmetry, the retention time is too small and the sample band just becomes unretained and symmetrical.

Whereas all Figs. 1–8 showed changes in the band profile associated with variations in the composition of the mobile phase and with the relative strength of adsorption of the sample and the strong solvent, while the sample size was kept constant, Figs. 9–11 show simulated chromatograms obtained with increasing sample

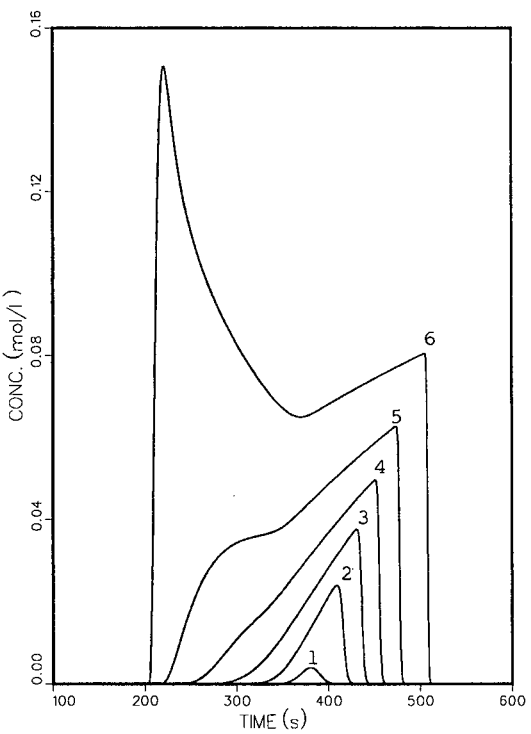

Fig. 9. Influence of the sample size on the elution profile of a single compound by a binary mobile phase. Strongly adsorbed solvent. Experimental conditions as in Fig. 6, except strong solvent concentration 0.17 *M* and different sample sizes. Sample size: 1, 1.66; 2, 16.6; 3, 41.6; 4, 83.3; 5, 166.6; 6, 416.5 μmole.

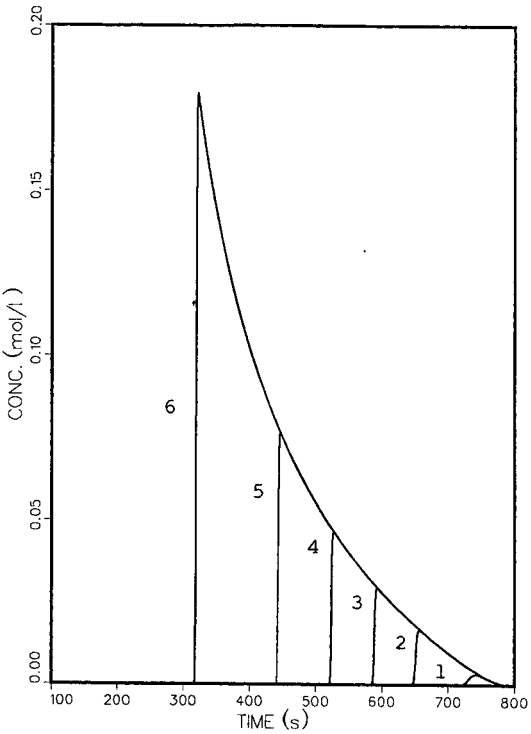

Fig. 10. Influence of the sample size on the eluting profile of a single compound by a binary mobile phase. Weakly adsorbed solvent. Experimental conditions as in Fig. 9, except Langmuir coefficients are $a_s = 1.44$ and $b_s = 0.8$. Same sample sizes.

sizes. Fig. 9 shows a series of such chromatograms corresponding to a strong solvent that is more strongly adsorbed on the stationary phase than the sample (ratio of the origin slopes equal to 2). At small sample sizes, the sample band profile evolves in a way that is typically associated with an anti-Langmuir isotherm, with a shock layer at the rear border of the band. We note, however, that the front does not remain stable, but that the front of the band moves backwards with increasing sample size. This does not occur with a true anti-Langmuir isotherm[11]. However, when the sample size becomes large a hump appears on the slanted front of the band. It grows and progressively gives rise to a second maximum, while a second shock layer[8] appears on the front. Such bands with two maxima for a pure compound are exceptional, but the phenomenon has been reported previously[25].

Fig. 10 shows a series of simulated band profiles obtained for increasing sample sizes of a single compound that is eluted by a binary mobile phase containing a strong solvent that is much less retained than the sample (ratio of the origin slopes of the strong solvent and the sample equal to 0.1). The progressive change in the profile, with a front becoming steeper and steeper and being eluted earlier and earlier, is classical of what is observed when a chromatographic column is overloaded with a compound exhibiting a Langmuir equilibrium isotherm between the stationary and mobile phases[11].

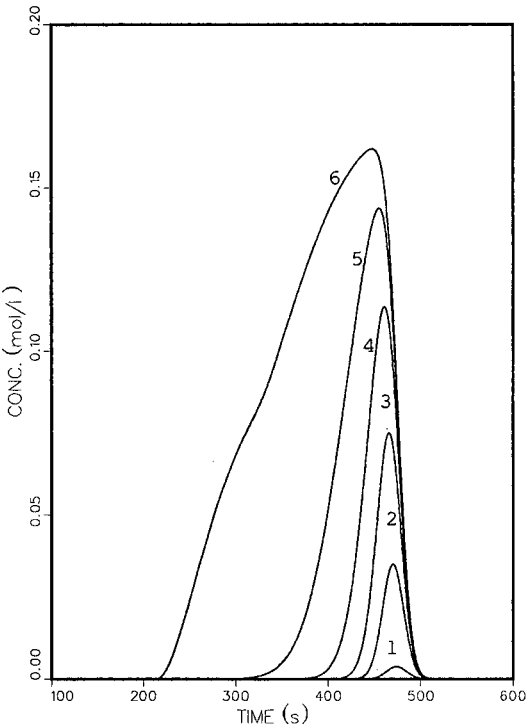

Fig. 11. Influence of sample size on the elution profile of a single compound by a binary mobile phase. Strong solvent and sample equally adsorbed. Experimental conditions as in Fig. 9, except Langmuir coefficients are $a_s = 14.4$ and $b_s = 8$. Same sample sizes.

Fig. 11 shows a series of simulated band profiles obtained for increasing sample sizes of a single compound that is as strongly retained by the stationary phase as the strong solvent (ratio of the origin slopes of the equilibrium isotherms equal to 1). Although the band profile changes progressively, becoming less and less symmetrical, it is remarkable that in this instance the retention time of the band maximum remains nearly constant until very large sample sizes are reached.

Fig. 12 shows a series of simulated band profiles obtained at constant sample size and constant composition of the mobile phase containing a strong solvent such that the ratio of the origin slopes of the strong solvent and the sample isotherms is constant. The values of the coefficients b_a and b_s of the isotherms (see eqns. 3 and 4) change from one band to the next. Accordingly, the column saturation capacity changes and the loading factor changes proportionally at constant sample size. At high values of the column saturation capacity the band profile is of the Langmuir type, but the loading factor is small, and hence the band profile is nearly symmetrical and the profile is close to Gaussian. As the column saturation capacity decreases, the column becomes more and more overloaded, the band asymmetry increases and its retention time decreases. At a certain intermediate value, the band profile shifts, the direction of asymmetry reverses and the profile acquires a rear shock layer, usually characterizing the anti-Langmuir isotherms.

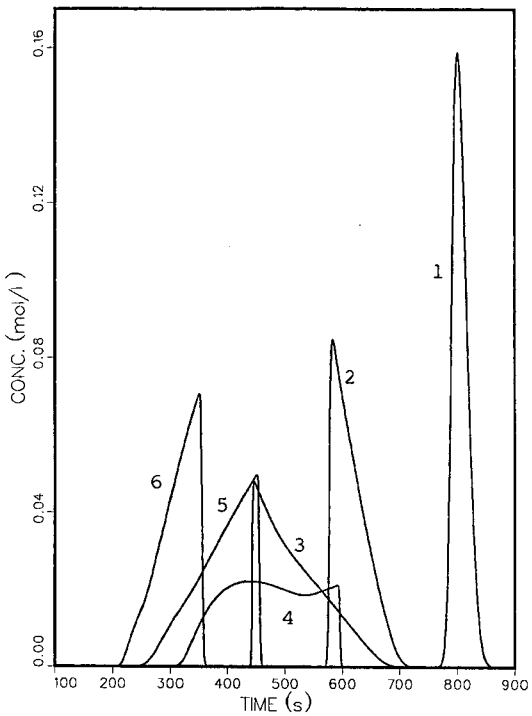

Fig. 12. Influence of the column saturation capacity on the elution profile of a single compound by a binary mobile phase. Experimental conditions as in Fig. 7 (including sample size), except stationary phase saturation capacity, Q. $a_s = 28.8$ and $b_s = 28.8/Q$; $a_a = 14.4$ and $b_a = 14.4/Q$. Stationary phase saturation capacity, Q: 1, 144; 2, 14; 3, 7.2; 4, 3.6; 5, 1.8; 6, 0.9 mol/l.

CONCLUSION

The use of mixed mobile phases containing a strong solvent that is not much less strongly adsorbed than the components of the samples studied generates system peaks that become very complex and may become extremely difficult to account for, especially if these compounds are not very well separated from each other and if a non-selective detector is used to record the chromatograms. The combination of several detectors, including a component-selective and a non-selective detector, may help considerably in accounting for the experimental results.

In the accompanying paper[16], we present a comparison between experimental results obtained in normal-phase adsorption chromatography with mixtures of a weak solvent and alkanols at low concentrations and the present theoretical results[16]. In further work, we shall extend the present observations on a single-component sample to the separation of multi-component mixtures[26].

ACKNOWLEDGEMENTS

This work was supported in part by grant CHE-8715211 from the National

Science Foundation and by the cooperative agreement between the University of Tennessee and the Oak Ridge National Laboratory.

REFERENCES

1 J. N. Wilson, *J. Am. Chem. Soc.*, 62 (1940) 1583.
2 D. DeVault, *J. Am. Chem. Soc.*, 65 (1943) 532.
3 E. Glueckauf, *Proc. R. Soc., London, Ser. A*, 186 (1946) 35.
4 H. C. Thomas, *J. Am. Chem. Soc.*, 66 (1944) 1664.
5 P. C. Haarhoff and H. J. van der Linde, *Anal. Chem.*, 38 (1966) 573.
6 G. Guiochon and L. Jacob, *Chromatogr. Rev.*, 14 (1971) 77.
7 S. Golshan-Shirazi and G. Guiochon, *Anal. Chem.*, 60 (1988) 2364.
8 B. C. Lin, S. Golshan-Shirazi, Z. Ma and G. Guiochon, *Anal. Chem.*, in press.
9 J. L. Wade, A. F. Bergold and P. W. Carr, *Anal. Chem.*, 59 (1987) 1286.
10 B. C. Lin, S. Golshan-Shirazi and G. Guiochon, *J. Phys. Chem.*, in press.
11 G. Guiochon, S. Golshan-Shirazi and A. Jaulmes, *Anal. Chem.*, 60 (1988) 1856.
12 G. Guiochon and S. Ghodbane, *J. Phys. Chem.*, 92 (1988) 3682.
13 S. Ghodbane and G. Guiochon, *J. Chromatogr.*, 440 (1988) 9.
14 E. sz. Kováts, in F. Bruner (Editor), *The Science of Chromatography*, Elsevier, Amsterdam, 1985, p. 205.
15 S. Golshan-Shirazi and G. Guiochon, *J. Phys. Chem.*, in press.
16 S. Golshan-Shirazi and G. Guiochon, *J. Chromatogr.*, 461 (1989) 19.
17 J. C. Giddings, *Dynamics of Chromatography*, Marcel Dekker, New York, 1966.
18 P. Rouchon, M. Schonauer, P. Valentin and G. Guiochon, in F. Bruner (Editor), *The Science of Chromatography*, Elsevier, Amsterdam, 1985, p. 131.
19 B. C. Lin and G. Guiochon, *Sep. Sci.*, in press.
20 D. J. Solms, T. W. Smuts and V. Pretorius, *J. Chromatogr. Sci.*, 9 (1971) 600.
21 M. Denkert, L. Hackzell, G. Schill and E. Sjögren, *J. Chromatogr.*, 218 (1981) 31.
22 S. Levin and E. Grushka, *Anal. Chem.*, 58 (1986) 1602.
23 S. Levin and E. Grushka, *Anal. Chem.*, 59 (1987) 1157.
24 R. M. McCormick and B. L. Karger, *J. Chromatogr.*, 199 (1980) 259.
25 J. J. Kirkland, *J. Chromatogr.*, 83 (1973) 149.
26 S. Golshan-Shirazi and G. Guiochon, in preparation.

Journal of Chromatography, 461 (1988) 19–34
Elsevier Publishers B.V., Amsterdam — Printed in The Netherlands

CHROMSYMP. 1445

EXPERIMENTAL STUDY OF SYSTEM PEAKS AND ELUTION PROFILES FOR LARGE CONCENTRATION BANDS IN THE CASE OF A BINARY ELUENT CONTAINING A STRONGLY SORBED ADDITIVE

SADRODDIN GOLSHAN-SHIRAZI and GEORGES GUIOCHON*

**Department of Chemistry, University of Tennessee, Knoxville, TN 37996-1600 (U.S.A.) and Division of Analytical Chemistry, Oak Ridge National Laboratory, Oak Ridge, TN (U.S.A.)*

SUMMARY

Band profiles of high-concentration samples of single compounds eluted from a silica column by a binary mobile phase were recorded under various sets of experimental conditions. The mobile phase was a dilute solution (0.02–2%, v/v) of light alkanols in dichloromethane or *n*-hexane. When the concentration of the strong solvent increases at a constant sample size, or the sample size increases at a constant strong solvent concentration, the elution profile, which is first of the type associated with a Langmuir adsorption isotherm with a sharp front and a slanted tail, changes the direction of its asymmetry and becomes similar in shape to the profiles associated with an anti-Langmuir isotherm, with a slanted front and a sharp tail. The shape of the profiles in the transition range is unusual and appears similar to the composite of two or three different bands. Finally, at large sample sizes and high strong solvent concentrations, the profile develops a hump on its front, which eventually may turn into a second peak.

These experimental profiles are in excellent qualitative agreement with those predicted by theory and described in the accompanying paper. Their variations with the experimental parameters follow the trends predicted in that study. The competition between the molecules of the strong solvent (or modifier) and those of the samples is entirely responsible for these profiles.

INTRODUCTION

In a previous paper[1], we discussed from a theoretical standpoint the profiles of high and very high concentration bands eluted by a binary solvent mixture. The aim of this work was to compare these theoretical results with experimental results and to show how a number of phenomena that have remained unexplained so far can be accounted for and possibly used.

When a sample is injected into a chromatographic column swept by a mobile phase that is not a single solvent but a mixture, several peaks are observed, some of which are negative. These peaks, which are usually called system peaks, have been known for a long time[2]. They have been used for isotherm determinations[3], as a method for the UV detection of compounds without a chromophore[4,5] and for the

0021-9673/89/$03.50

direct determination of equilibrium constants[6]. An excellent review of the origin, formation and importance of system peaks has been published by Levin and Grushka[7].

System peaks are due to the perturbation of the equilibrium between the mobile phase and the stationary phase as the sample penetrates the column and its molecules compete with those in the mobile phase which interact with the stationary phase. The net result of this competition, if the sample is retained at all, is in the expulsion from the stationary phase of a small amount of the adsorbed components of the mobile phase. This amount corresponds to the amount of sample adsorbed on the stationary phase at equilibrium, under the experimental conditions selected. The expelled amounts of these components travel along the column at their own speed, as a function of the extent of their adsorption. When the sample is eluted, the adsorbed solvent components of the mobile phase must replenish the stationary phase and thus equilibrium between the two phases is reached again. Accordingly, the elution of the sample band is accompanied by a negative solvent band. Depending on (i) the sample size, (ii) the adsorption strength ratio of the strong solvent and the sample and (iii) the ratio of the response factors of the detector for the sample and the strong solvent, the corresponding peak may be positive, negative or almost negligible in size.

Previous work on system peaks[2–8] dealt essentially with the quasi-linear aspect. Chromatography is certainly not linear in the present instance, as it involves two characteristic properties of non-linear chromatography: (i) the amount of strong solvent adsorbed at equilibrium is not proportional to its concentration in the mobile phase; the strong solvent adsorption isotherm is usually not linear in the concentration range used in the mobile phase; and (ii) the retention time of a small sample pulse depends on the concentration of the strong solvent, which is why the strong solvent (or additive) is used in the first place. However, it is possible to consider the problem of the elution of a small sample plug as a problem in linear chromatography, because a function can be replaced by its two-term expansion around any of its values, in order to calculate the effect of a very small change in the variable. The linear treatment of system peaks under analytical conditions is therefore justified, as they constitute small perturbations. However, it should not be forgotten that the isotherms involved are the mixed, competitive isotherms, expressing quantitatively how the amount of compound A_s (strong solvent, mobile phase additive or sample) which is sorbed by the stationary phase at equilibrium depends on the concentration of all the components present in the mobile phase.

The purpose of this work was different. We are interested in studying the problems involved in preparative liquid chromatography and the answers can only be obtained by considering the entire problem, which involves the solution of the system of non-linear mass balance equations describing the behavior of the components of the mobile phase and the sample. This requires a knowledge of the mixed, competitive equilibrium isotherms of all the species involved or, alternately, of the kinetics of mass transfers between phases of all these species. For most implementations of chromatography, the kinetics of mass transfer are fast enough to justify assuming the two phases to be near equilibrium at all times[9]. We can therefore use the semi-ideal model[10]. The prediction of the profiles of high-concentration bands eluted by a binary mobile phase is therefore a two-compound problem, requiring a system of two mass balance equations (one for the sample and one for the additive or strong solvent). If the

mobile phase is a ternary solvent or contains two additives, the prediction of the profile of a high-concentration band of a single compound becomes a three-component problem, and the prediction of the profiles for a two-component sample with a ternary mobile phase becomes a four-component problem.

In the accompanying theoretical paper[1] we considered the elution profile of a high-concentration band eluted by a binary mobile phase and the influence of various experimental parameters. Here we compare the theoretical results with those obtained experimentally.

EXPERIMENTAL

A Hewlett-Packard (Palo Alto, CA, U.S.A.) Model 1090 liquid chromatograph, equipped with a diode-array detector and a data station, was used for most of the experiments. Also employed for experiments involving the study of the solvent peaks was a Waters Assoc. (Milford, MA, U.S.A.) Model 410 differential refractive index detector, connected to the HP datastation through an HP dual-channel interface. A 25 cm × 1/4 in. O.D. × 4.6 mm I.D. stainless-steel column packed with 15–25-μm silica particles was used.

The mobile phases were derived either from dichloromethane, modified with various amounts of one of the strong organic solvents methanol, ethanol, 2-propanol and *tert.*-butanol, or from *n*-hexane, modified by mixing with different concentrations of 2-propanol. The compositions are reported in the figure captions.

The solutes investigated were 2-phenylethanol, 3-phenyl-1-propanol and 2-phenyl-1-propanol from Fluka (Ronkonkoma, NY, U.S.A.) and acetophenone from Fisher Scientific (Pittsburgh, PA, U.S.A.). The sample size was varied between 0.02 and 25 μl.

RESULTS AND DISCUSSION

Twenty years ago it was suggested that strongly polar organic solvents, such as alcohols, could be used as organic modifiers in weakly polar or non-polar mobile phases, such as *n*-hexane or dichloromethane, in order to control the activity of the silica[11]. Kirkland[12] published a detailed study on the influence of water and various alcohols as organic solvent modifiers in normal-phase liquid chromatography. Very small concentrations of these additives were required; typically, concentrations between 0.05 and 0.3% of methanol, ethanol or 2-propanol were recommended[12].

Kirkland[12] reported very unusual band shapes in some instances. He noted a change in the elution profile with increasing alcohol content, the direction of asymmetry of the peak changing from tailing to fronting, with an intermediate stage where the band "appears as the superimposition of two different chromatographic bands". Punčochářova *et al.*[13] noted similar phenomena in the elution profiles of bands of cyclohexanol and cyclohexanone on silica with various binary mobile phases.

As these experiments showed the importance of the effect of alkanols as organic modifiers, we decided to investigate the behavior of system peaks generated by the injection in this kind of mobile phase of large or very large sample sizes, and also the profiles of the sample peaks.

Experimental study of the solvent peak

Our theoretical results[1] showed that the elution of a high-concentration pulse of sample is accompanied by a solvent peak, which occurs as a result of the coupling between the adsorption of the solvent and the sample on the stationary phase. The use of a refractive index detector is necessary to record the solvent band, as the UV absorption of alkanols is negligibly small at accessible wavelengths.

We used dichloromethane containing 1% of 2-propanol as the mobile phase. Fig. 1 shows a chromatogram obtained with 2-phenylethanol as the sample. The refractive indices of dichloromethane, 2-propanol and 2-phenylethanol are 1.4244, 1.3772 and 1.532, respectively. Although the response factors are not directly proportional to the differences between the refractive indices of the solutes and that of the weak solvent, we may expect to see a negative peak when the concentration of the strong solvent increases in the weak solvent and a positive peak when the concentration of the sample increases[14]. This inversion of the response sign must be kept in mind when looking at the chromatograms and trying to understand what is happening in the column.

Fig. 1 shows the chromatograms for four pulses of 2-phenylethanol (1, 2, 5 and 10 μl). The inset is a simulated chromatogram corresponding to a strongly sorbed organic modifier (ratio of the origin slopes of the adsorption isotherms of the strong solvent and the sample from their dilute solution in the pure weak solvent equal to 2). It permits an easy understanding of what is happening here.

The simulated elution profile (Fig. 1, inset) exhibits one sample band and two bands for the strong solvent, a positive peak eluted before the sample band and a negative peak eluted at the same time as the sample band[1]. The area of these system peaks increases with increasing sample size. At large sample sizes, the positions of the first solvent band and of the sample peak depend not only on the adsorption strength

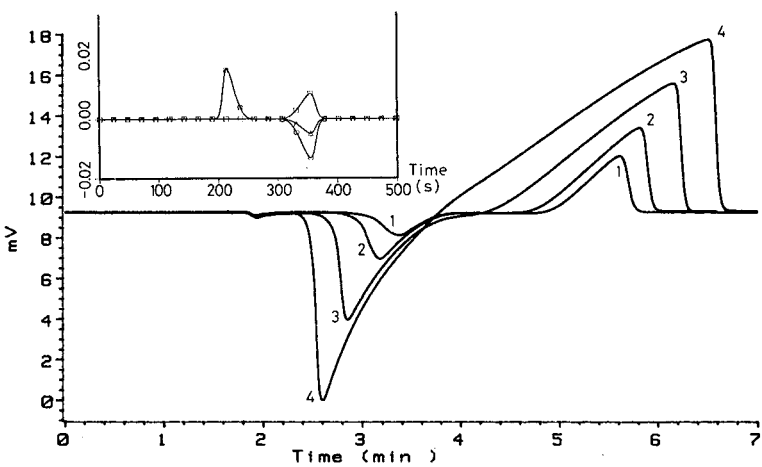

Fig. 1. Elution chromatograms of pulses of 2-phenylethanol of increasing sample size. Refractive index detector. Comparison with theoretical predictions. Column, 25 cm × 4.6 mm I.D.; mobile phase, dichloromethane containing 1% 2-propanol (*i.e.*, 0.17 *M*); stationary phase, silica, 15–25-μm particles; flow-rate 2 ml/min. Sample size: 1, 1 μl; 2, 2 μl; 3, 5 μl; 4, 10 μl. Inset. Simulated chromatogram with competitive Langmuir isotherms for the strong solvent and the sample. Langmuir coefficients: $a_a = 40$; $a_s = 80$; $b_a = 8$; $b_s = 16$ (see ref. 1). Concentration of strong solvent, 0.17 *M*; sample size, 1 μl.

of the strong solvent (*i.e.*, the slope at the origin of its adsorption isotherm between the pure weak solvent and the stationary phase), but also on the sample size (see Figs. 1 and 2). The position of the sample peak (at least at zero sample size) also depends on the strength of adsorption of this compound. With increasing sample size, the two bands of the pure solvent and the sample approach closer to each other and eventually interfere with each other[1].

The experimental results (see Fig. 1, curves 1–4) confirm these predictions. As the response factor is negative for the strong solvent and positive for the sample, the first peak (strong solvent) is recorded as a negative signal, while the effects of the strong solvent band add to those of the sample band in the recording of the second, mixed band (the second solvent band is negative in concentration, *i.e.*, positive in signal with the refractive index detector). The area of the first system peak increases with increasing sample size. The first system peak and the sample band approach closer to each other, and the resolution between these two bands becomes lower than unity for a sample size larger than 5 μl (see Fig. 1, curves 3 and 4).

The same phenomenon is observed in Fig. 2, which shows the chromatograms recorded for the elution of samples of increasing size (1, 5 and 10 μl) of 3-phenyl-1-propanol. The resolution between the system peak and the sample band is larger at small sample sizes, because 3-phenyl-1-propanol is more strongly adsorbed than 2-phenylethanol, and thus these bands begin to interfere with each other markedly only for the largest sample (see Fig. 2).

The strength of adsorption of the three phenylalkanols used in this work decreases in the order 3-phenyl-1-propanol, 2-phenylethanol and 2-phenyl-1-propanol. Fig. 3 shows the chromatograms obtained for the same amounts of these three compounds (5 μl) when injected separately. The retention time of the maximum of the system peak (first solvent peak) increases with increasing sample adsorption, whereas the retention of the sample band increases in order of increasing strength of adsorption (order of increasing retention times: 2-phenyl-1-propanol < 2-phenylethanol < 3-

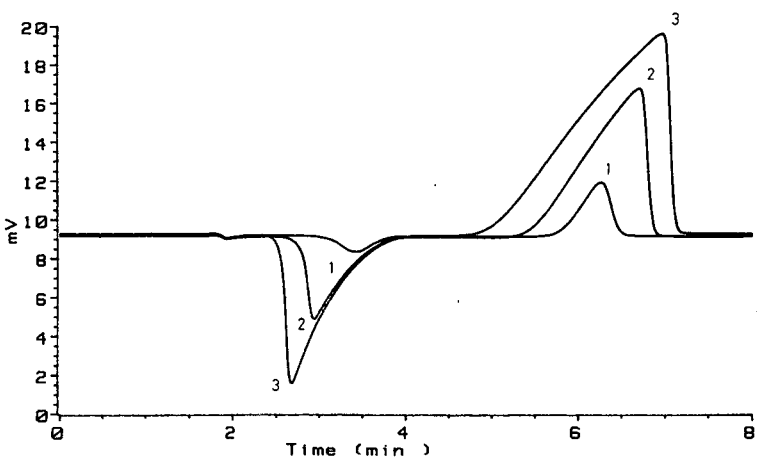

Fig. 2. Elution chromatograms of pulses of 3-phenyl-1-propanol of increasing sample size. Refractive index detector. Experimental conditions as in Fig. 1. Sample size: 1, 1 μl; 2, 5 μl; 3, 10 μl.

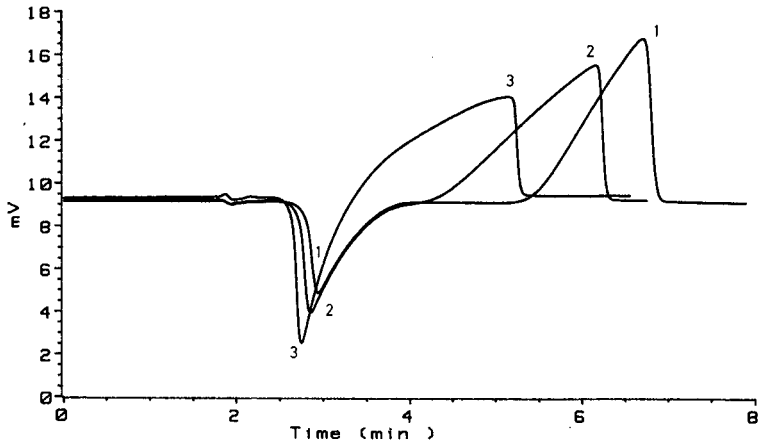

Fig 3. Elution chromatograms of pulses of different single compounds of same sample size (5 μl). Refractive index detector. Experimental conditions as in Fig. 1. 1, 3-Phenyl-1-propanol; 2, 2-phenylethanol; 3, 2-phenyl-1-propanol.

phenyl-1-propanol). The degree of resolution between the strong solvent and solute bands improves in the same order.

These experimental results confirm the predictions of our theoretical model[1].

Experimental study of the sample peak. Influence of the nature of the modifier

The remainder of this study was performed with a diode-array UV detector, and therefore there is no contribution of the changes in the strong solvent concentration and of the system peaks in the recorded chromatograms. The only effect of the strong solvent results from its competition with the sample for the adsorption sites at the surface of the silica.

Figs. 4–7 show the elution chromatograms of pulses of various amounts of 3-phenyl-1-propanol on silica when other alcohols are used as modifiers: 1% *tert.*-butanol (Fig. 4), 1% 2-propanol (Fig. 5), 1% ethanol (Fig. 6) and 0.5% methanol (Fig. 7). Comparison between Figs. 1 and 5 shows that there is little difference between the shapes of the true sample profiles (Fig. 5) and those of the profiles of the second band eluted from the column (Fig. 1).

In all instances, the elution profiles show leading peaks, with a sharp shock layer on their rear, and a retention time of the band maximum that increases with increasing sample size. This behavior is usually associated with an anti-Langmuir isotherm. This conclusion would be correct with a pure mobile phase but it is obviously not true here. The equilibrium isotherms may not be properly represented by true competitive Langmuir isotherms; this theoretical model is too crude to account quantitatively for the behavior of most real systems. Nevertheless, the curvature of the isotherms is negative. The behavior of the system when the sample size, the organic modifier concentration or its nature is changed is not consistent with an anti-Langmuir type of isotherm. For example, when the sample size is increased for a system with a true anti-Langmuir isotherm, all the bands start at the same time[15]. This is not the case in Figs. 4–7. Further, within some range of strong solvent concentrations (see Figs. 11

and 14), we observe band profiles that are typical of those traditionally associated with a Langmuir isotherm (or at least typical of an isotherm with a negative curvature).

The polarity of the alcohol and hence the strength of its adsorption on silica increase with decreasing length of its alkyl chain. The retention times of the bands, especially the limiting retention time (retention time of the smallest sample size that gives an almost symmetrical peak), decrease in the order *tert.*-butanol, 2-propanol, ethanol (see Figs. 4–7). The band shapes observed with methanol (see Fig. 7) are very unusual, but very similar to those predicted by the theoretical study (see ref. 1, Figs. 4 and 9).

Figs. 8 and 9 show chromtograms obtained with a weaker solvent (*n*-hexane instead of dichloromethane), modified with 1% of 2-propanol. Two compounds were used as pure samples, 3-phenyl-1-propanol and the much less polar acetophenone.

Because *n*-hexane is a weaker, less polar solvent than dichloromethane, the saturation capacity of the column is larger. Accordingly, the effect of the adsorption of the strong solvent on the band profile of the sample is smaller, as shown in Fig. 8 (*cf.*, Fig. 6). The elution profile of 3-phenyl-1-propanol is now similar to that observed with a pure mobile phase for a compound with a weakly curved Langmuir isotherm.

On the other hand, acetophenone is much less polar than 3-phenyl-1-propanol, less strongly adsorbed and less retained (*cf.*, Figs. 8 and 9). The strength of adsorption of the strong solvent is much higher than that of the sample and the elution profiles become very unusual, as shown in Fig. 9. At first, when the sample size increases from zero, the band profile evolves as in the case of an anti-Langmuir isotherm, but then (see curve 4 in Fig. 9) the front part of the band also becomes very steep, the profile becomes a smooth rectangle and eventually a sharp peak arises at low retention times. This corresponds precisely to the situation predicted by the theoretical study when the strong solvent is much more strongly retained than the sample (see ref. 1, Fig. 9).

Experimental study of the sample peak. Influence of the concentration of the modifier

Fig. 10 shows the elution bands obtained for the chromatography of increasing amounts of acetophenone with a binary mobile phase consisting of 2-propanol–*n*-hexane (2:98). Compared with Fig. 9 the change in elution profile is less pronounced, but it is as striking. The bands remain narrower and there is no trend towards a change in the direction of asymmetry, but now the large bands have two maxima. Common sense would lead one to think that either the sample is impure or there is something wrong with the entrance packing section of the column (it is not unusual that the packing at the column inlet becomes inhomogeneous or even that a hole forms, resulting in band profiles similar to those of chromatograms 5 and 6 in Fig. 10). The phenomenon is also reminiscent of that observed by Kirkland[12].

A systematic investigation of the influence of the concentration of the strong solvent on the elution band profile was carried out, using dichloromethane as the weak solvent and 2-propanol as the strong solvent. The concentration of 2-propanol was increased from 0.1 to 0.2 and 1%. Samples of various sizes of 2-phenylethanol and 3-phenyl-1-propanol were injected. The chromatograms are shown in Figs. 11–17. The theoretical study[1] showed that at low concentrations of strong solvent the behavior of the band profile is "normal", *i.e.*, it is similar to what would be expected when overloading a column in the case of a Langmuir isotherm. The band becomes increasingly asymmetric, with a very sharp front (shock layer) and a smooth tail

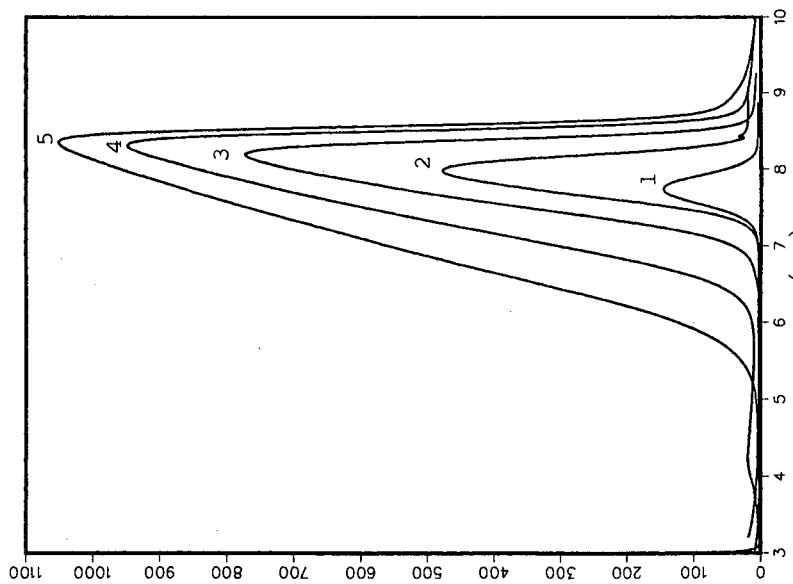

Fig. 4. Elution chromatograms of pulses of 3-phenyl-1-propanol of increasing sample size. UV detector at 270 nm (no response for the solvent). Column, 25 cm × 4.6 mm I.D.; mobile phase, dichloromethane containing 1% *tert.*-butanol; stationary phase, silica, 15–25-μm particles; flow-rate, 2 ml/min. 1, 0.4 μl; 2, 2 μl; 3, 6 μl; 4, 15 μl; 5, 25 μl.

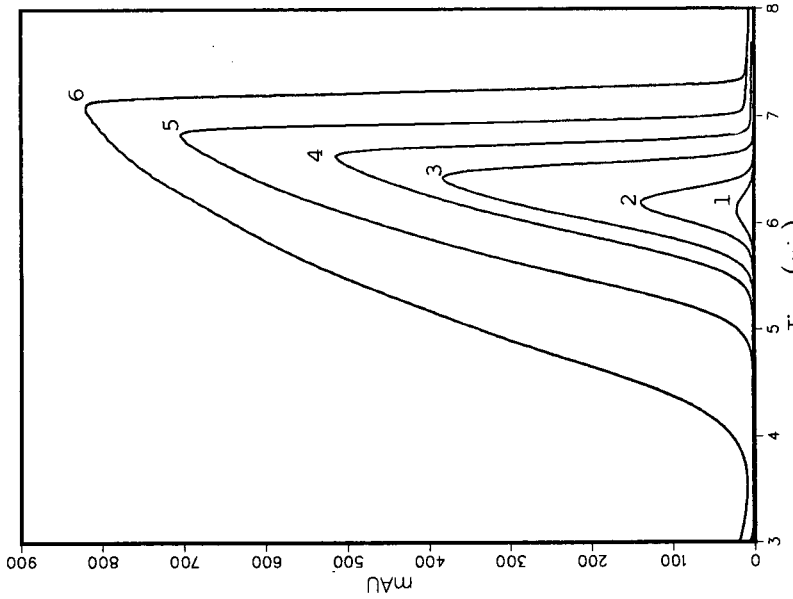

Fig. 5. Elution chromatograms of pulses of 3-phenyl-1-propanol of increasing sample size. UV detector (no response for the solvent). Experimental conditions as in Fig. 4, except 1% 2-propanol as strong solvent. 1, 0.08 μl; 2, 0.4 μl; 3, 2 μl; 4, 4 μl; 5, 8 μl; 6, 20 μl.

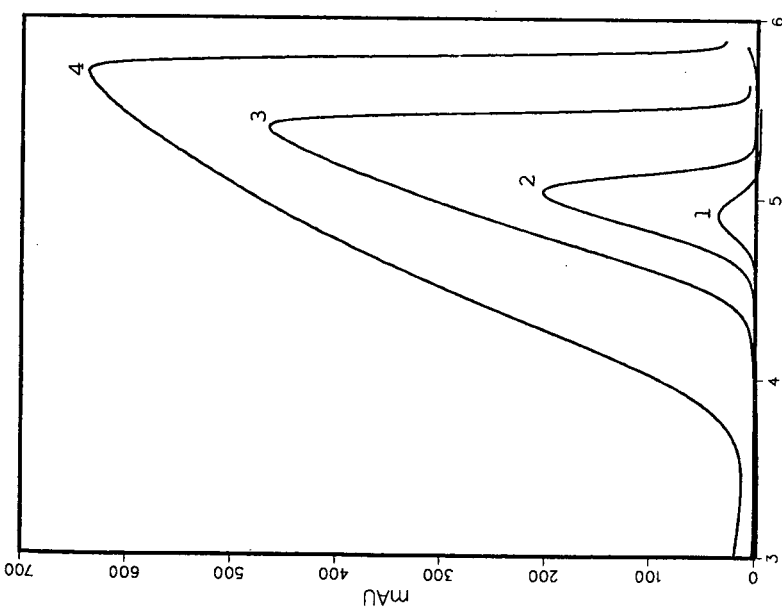

Fig. 6. Elution chromatograms of pulses of 3-phenyl-1-propanol of increasing sample size. UV detector (no response for the solvent). Experimental conditions as in Fig. 4, except 1% ethanol as strong solvent. 1, 0.08 μl; 2, 0.4 μl; 3, 2 μl; 4, 6 μl.

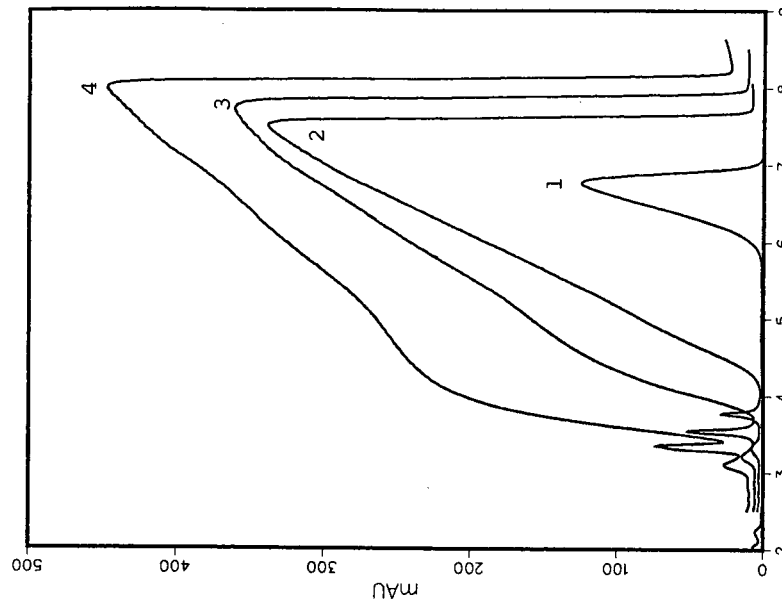

Fig. 7. Elution chromatograms of pulses of 3-phenyl-1-propanol of increasing sample size. UV detector (no response for the solvent). Experimental conditions as in Fig. 4, except 0.5% methanol as strong solvent. 1, 0.4 μl; 2, 4 μl; 3, 6 μl; 4, 10 μl.

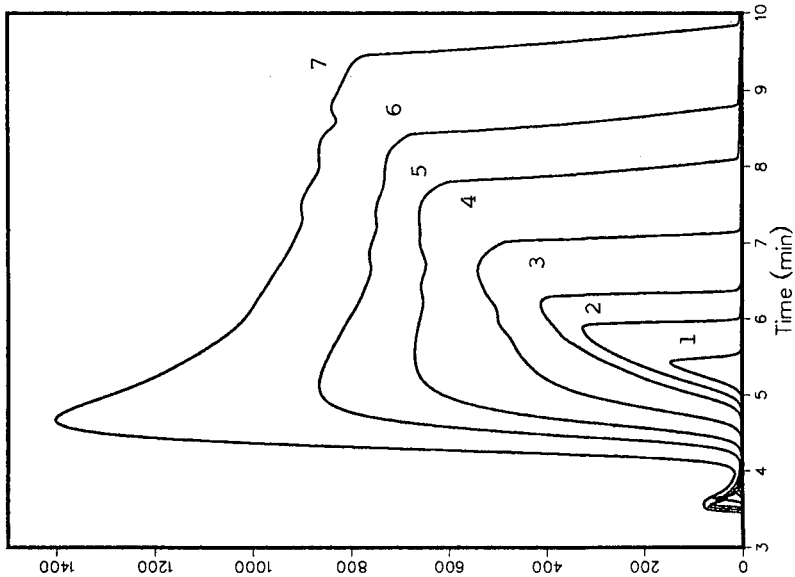

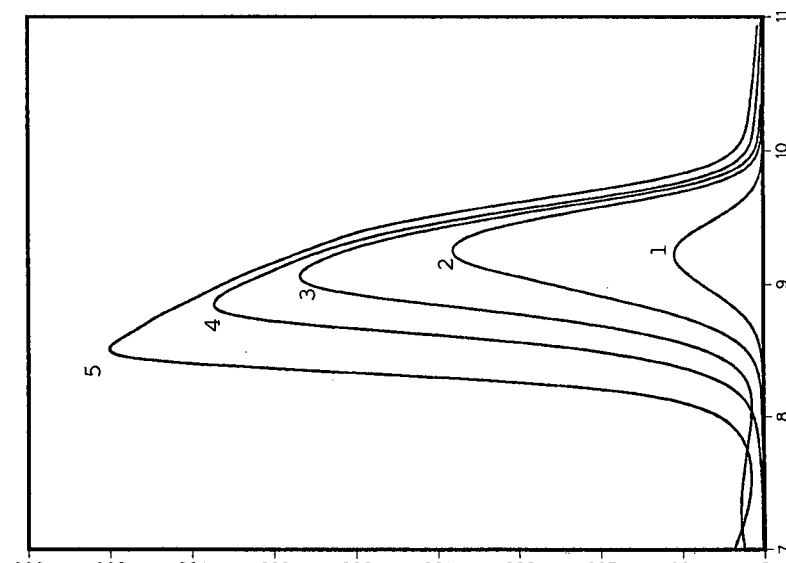

Fig. 8. Elution chromatograms of pulses of 3-phenyl-1-propanol of increasing sample size. UV detector (no response for the solvent). Experimental conditions as in Fig. 4, except 1% 2-propanol as strong solvent and *n*-hexane as weak solvent. Flow-rate, 3 ml/min. 1, 1 μl; 2, 5 μl; 3, 10 μl; 4, 15 μl; 5, 25 μl.

Fig. 9. Elution chromatograms of pulses acetophenone of increasing sample size. UV detector at 320 nm (no response for the solvent). Experimental conditions as in Fig. 4, except 1% 2-propanol as strong solvent and *n*-hexane as weak solvent. Flow-rate, 1 ml/min. 1, 0.02 μl; 2, 1 μl; 3, 2 μl; 4, 5 μl; 5, 10 μl; 6, 15 μl; 7, 25 μl.

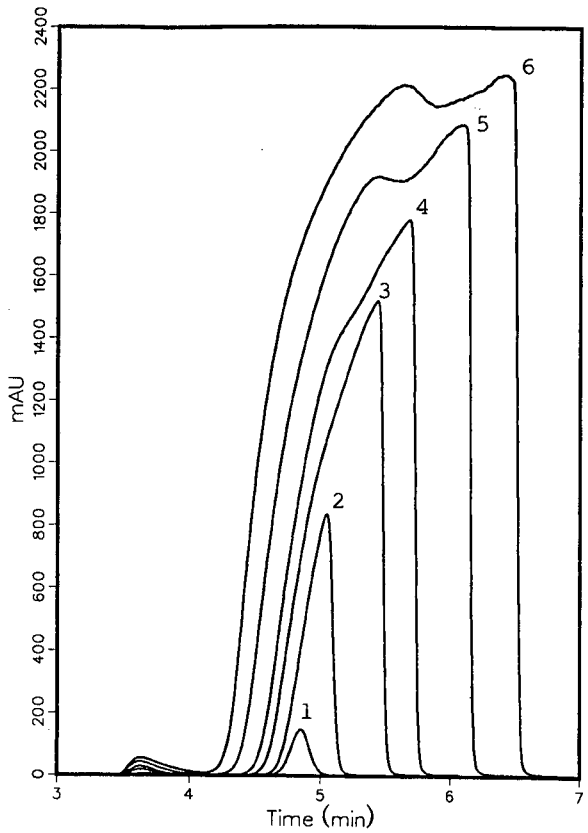

Fig. 10. Elution chromatograms of pulses of acetophenone of increasing sample size. UV detector (no response for the solvent). Experimental conditions as in Fig. 9, except 2% 2-propanol as strong solvent. 1, 0.02 μl; 2, 1 μl; 3, 3 μl; 4, 5 μl; 5, 10μl; 6, 15 μl.

extending until the retention time of the sample at infinite dilution. When the concentration of the strong solvent is high, the reverse behavior is predicted by the theory of chromatography. The bands are leading, with a smooth (diffuse) front and a sharp rear part. There is a narrow range of strong solvent concentrations in which the band profile reverses itself and the bands assume extremely odd shapes[1].

The experimental results confirm these predictions. Fig. 11 shows the profiles obtained with a concentration of 0.1% 2-propanol, with samples of 0.2, 1 and 10 μl of 2-phenylethanol. The profiles are typical of those obtained for a Langmuir isotherm. Fig. 12 shows the chromatograms obtained for sample sizes of 0.2, 1 and 5 μl of the same compound when the mobile phase contains 0.2% 2-propanol. The band profile has completely changed and is extremely unusual. However, it is very similar to the profiles calculated by our simulation program (see ref. 1, Figs. 6 and 12). Fig. 13 shows the chromatograms recorded with a mobile phase containing 1% 2-propanol with samples of the same compound of 0.2, 1, 5, 10 and 15 μl. The profile asymmetry has changed direction compared with the peaks in Fig. 11, and the bands are similar to (but

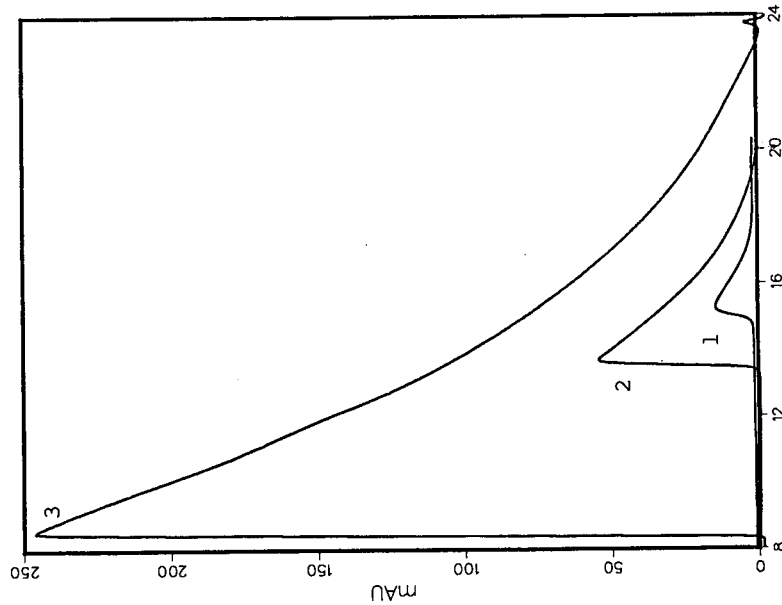

Fig. 11. Elution chromatograms of pulses of 2-phenylethanol of increasing sample size. UV detector (no response for the solvent). Experimental conditions as in Fig. 4, except 0.1% 2-propanol as strong solvent. 1, 0.2 μl; 2, 1 μl; 3, 10 μl.

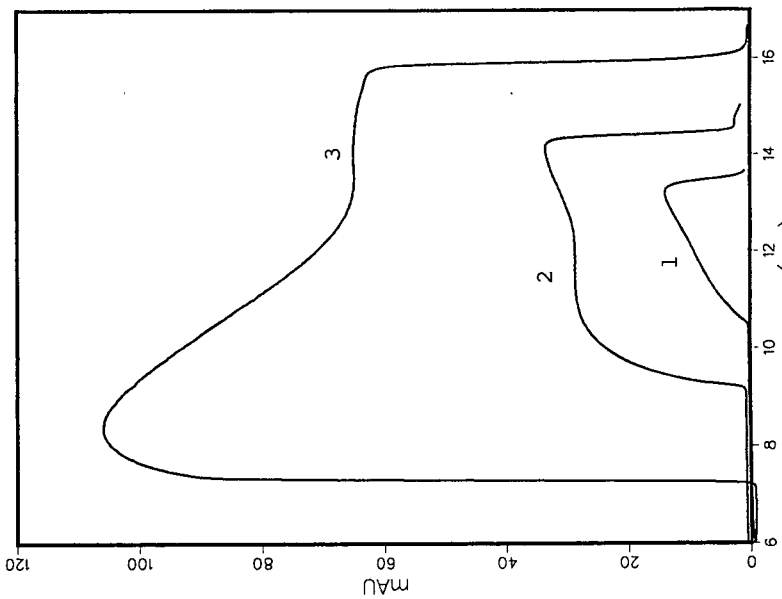

Fig. 12. Elution chromatograms of pulses of 2-phenylethanol of increasing sample size. UV detector (no response for the solvent). Experimental conditions as in Fig. 11, except 0.2% 2-propanol as strong solvent. 1, 0.2 μl; 2, 1 μl; 3, 5 μl.

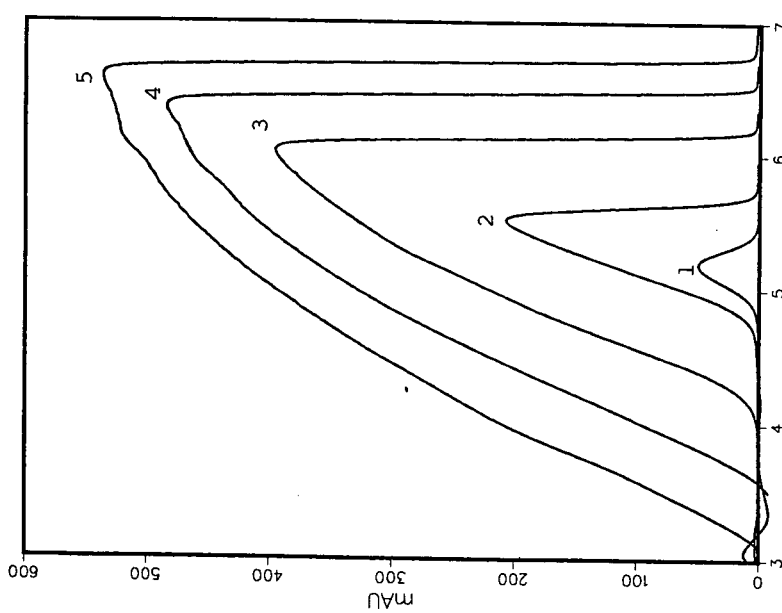

Fig. 13. Elution chromatograms of pulses of 2-phenylethanol of increasing sample size. UV detector (no response for the solvent). Experimental conditions as in Fig. 11, except 1% 2-propanol as strong solvent. 1, 0.2 μl; 2, 1 μl; 3, 5μl; 4, 10μl; 5, 15μl.

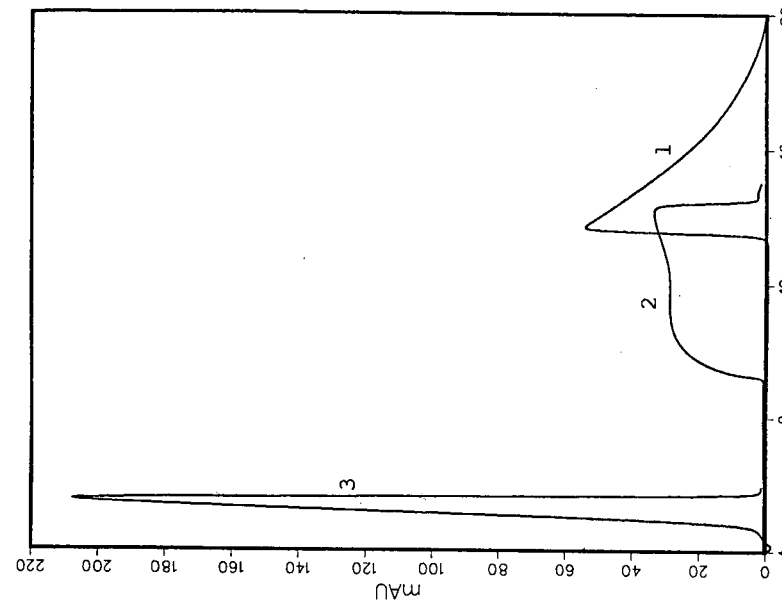

Fig. 14. Elution chromatograms of pulses of 2-phenylethanol of equal sample sizes (1 μl). UV detector (no response for the solvent). Experimental conditions as in Fig. 11, except variable concentration of the mobile phase in 2-propanol. 1, 0.1%; 2, 0.2%; 3, 1%.

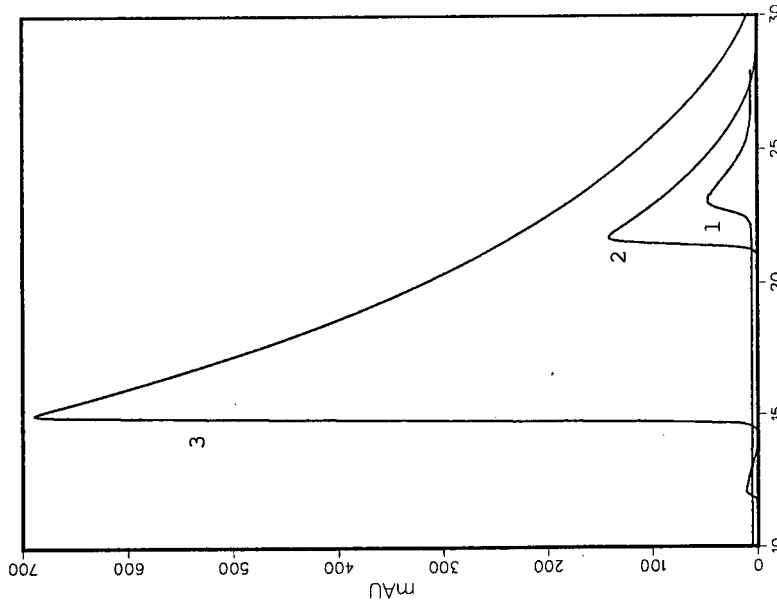

Fig. 15. Elution chromatograms of pulses of 3-phenyl-1-propanol of increasing sample size. UV detector (no response for the solvent). Experimental conditions as in Fig. 4, except 0.02% 2-propanol as strong solvent and detection wavelength 254 nm. 1, 0.2 μl; 2, 1 μl; 3, 10 μl.

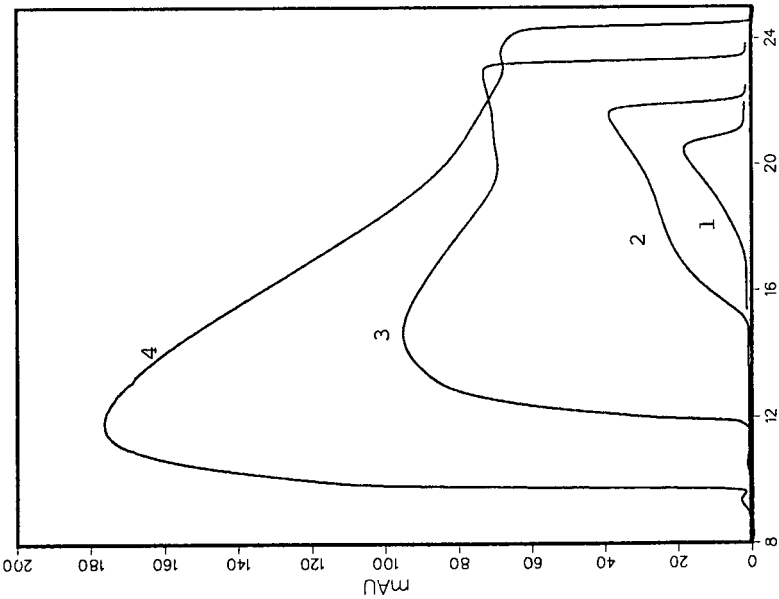

Fig. 16. Elution chromatograms of pulses of 3-phenyl-1-propanol of increasing sample size. UV detector (no response for the solvent). Experimental conditions as in Fig. 15, except 0.1% 2-propanol as strong solvent. 1, 0.2 μl; 2, 1 μl; 3, 5 μl; 4, 10 μl.

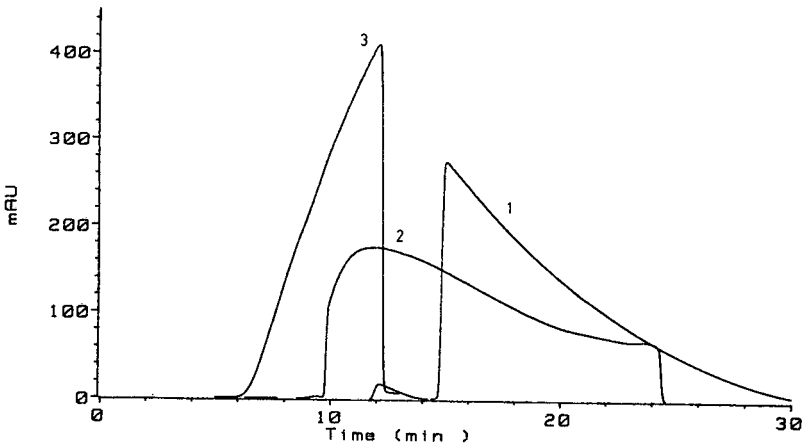

Fig. 17. Elution chromatograms of pulses of 3-phenyl-1-propanol of equal sample size (10 μl). UV detector (no response for the solvent). Experimental conditions as in Fig. 15, except variable concentration of the mobile phase in 2-propanol. 1, 0.02%; 2, 0.1%; 3, 0.4%.

not identical with) those observed with an anti-Langmuir isotherm. The bands are now leading, with a sharp rear boundary.

The dramatic character of the change in band profile with increasing concentration of the strong solvent in the mobile phase is illustrated by Fig. 14, which shows the band profiles obtained for the same amount of sample (1 μl of 2-phenylethanol) with three different mobile phases, containing 0.1, 0.2 and 1% 2-propanol. The marked decrease in retention time is obvious. The change in the profile is remarkable, as is the close agreement with the results of our theoretical study (see in ref. 1, Fig. 6).

Similar results were obtained with 3-phenyl-1-propanol under similar experimental conditions, although the numerical values are slightly different (see Figs. 15–17).

CONCLUSION

The results of this experimental investigation validate entirely the conclusion of the theoretical study[1]. The competition between the molecules of the strong solvent or other additives in the mobile phase and the components of the sample influence considerably the shape of the elution bands and probably the degree of resolution in addition to the production per unit time of a chromatographic column in preparative applications. It is indeed possible that a combination of additives could enhance the symmetry of the bands. It has been shown in the theoretical study that under some well defined set of experimental conditions the sample band could be both retained and eluted as a nearly symmetrical band. In this work we have not striven to duplicate these conditions, because we are interested in the profile of a single-component band only as an intermediate test of a complex theory.

Our work will be pursued by an investigation of the influence of the nature and strength of adsorption of the eluents compared with those of the solutes, of their

concentration and of the sample size, on the separation, yield and production rate for a binary mixture. This is the simplest problem of practical importance that the theoretician must tackle to the satisfaction of the chemical engineer.

ACKNOWLEDGEMENTS

This work was supported in part by grant CHE-8715211 from the National Science Foundation and by the cooperative agreement between the University of Tennessee and the Oak Ridge National Laboratory. We are grateful to Hewlett-Packard for the gift of the Model 1090A liquid chromatograph and datastation.

REFERENCES

1 S. Golshan-Shirazi and G. Guiochon, *J. Chromatogr.*, 461 (1989) 1.
2 D. J. Solms, T. W. Smuts and V. Pretorius, *J. Chromatogr. Sci.*, 9 (1971) 600.
3 P. Valentin and G. Guiochon, *J. Chromatogr. Sci.*, 14 (1976) 56 and 132.
4 B. A. Bidlingmeyer, S. N. Deming, W. P. Price, Jr., B. Sachok and M. Petrusek, *J. Chromatogr.*, 186 (1979) 419.
5 M. Denkert, L. Hackzell, G. Schill and E. Sjögren, *J. Chromatogr.*, 218 (1981) 31.
6 S. Levin and E. Grushka, *Anal. Chem.*, 59 (1987) 1157.
7 S. Levin and E. Grushka, *Anal. Chem.*, 58 (1986) 1602.
8 R. M. McCormick and B. L. Karger, *J. Chromatogr.*, 199 (1980) 259.
9 P. C. Haarhoff and H. J. van der Linde, *Anal. Chem.*, 38 (1966) 573.
10 G. Guiochon and S. Ghodbane, *J. Phys. Chem.*, 92 (1988) 3682.
11 R. J. Maggs, *J. Cromatogr. Sci*, 7 (1969) 145.
12 J. J. Kirkland, *J. Chromatogr.*, 83 (1973) 149.
13 J. Punčochářova, J. Kříž, L. Vodička and D. Průšová, *J. Chromatogr.*, 191 (1980) 81.
14 E. S. Yeung and R. Synovec, *Anal. Chem.*, 55 (1983) 1599.
15 G. Guiochon, S. Golshan-Shirazi and A. Jaulmes, *Anal. Chem.*, 60 (1988) 1856.

Journal of Chromatography, 461 (1989) 35–44
Elsevier Science Publishers B.V., Amsterdam — Printed in The Netherlands

CHROMSYMP. 1511

DIOXANYL HYDROPEROXIDE IN PREPARATIVE LIQUID CHROMATOGRAPHY

ELLEN M. DERRICO*, HELGA BUSH, PATRICIA M. FINNEGAN
G. D. Searle & Co., 4901 Searle Parkway, Skokie, IL 60077 (U.S.A.)

SUMMARY

A contaminant was discovered in the eluate from a preparative liquid chromatographic purification of a research drug. The contaminant was isolated by column chromatography and identified by spectral data as 1,4-dioxan-2-yl hydroperoxide (*p*-dioxanyl hydroperoxide). The hydroperoxide was characterized by NMR and IR spectroscopy and thin-layer and high-performance liquid chromatography. The conditions for safe removal and reduction were also investigated.

INTRODUCTION

Peroxides formed as a result of the autoxidation of ether solvents are known to be unstable and heat-, friction- and shock-sensitive compounds[1–5]. In the past, research has been carried out to characterize 1,4-dioxan-2-yl hydroperoxide (*p*-dioxanyl hydroperoxide), a peroxide found in dioxane. The single-crystal X-ray structure was determined by Nord and Lindberg[6], and IR and NMR characterization were carried out by Griere and Petterson (see ref. 6).

Safety issues regarding peroxide have been addressed in several publications[1–5,7–9], and the removal of peroxides from solvents by either scavenging with neutral alumina or reduction with metals, such as iron or silver, has been reported[10,11]. Peroxide formation in ether solvents when used in large volumes or in industrial applications has been acknowledged in several publications[10–12]. Verzele and DeWaele[12] suggested that the amount of peroxide generated is potentially hazardous.

Despite the problems, dioxane is a useful solvent in both normal and reversed-phase preparative chromatography for its unique selectivity and solubility properties. A peroxide of 1,4-dioxane, *p*-dioxanyl hydroperoxide, was isolated in our laboratory during normal-phase preparative liquid chromatography. This paper discusses the formation, isolation, identification, removal and hazards of *p*-dioxanyl hydroperoxide.

EXPERIMENTAL AND RESULTS

Materials and instrumentation

High-purity solvents (acetonitrile, dioxane, ethyl acetate, hexane, 2-propanol,

0021-9673/89/$03.50

dichloromethane, methyl *tert.*-butyl ether, tetrahydrofuran and trimethylpentane) were obtained from Baxter, Burdick and Jackson (Muskegon, MI, U.S.A.). High-performance liquid chromatography (HPLC) grade water, concentrated sulfuric acid and potato starch were from J. T. Baker (Phillipsburg, NJ, U.S.A.). Acetic acid, granular iron(II) sulfate, phosphomolybdic acid (PMA) crystals, potassium iodide, resublimed iodine crystals and sodium hydroxide pellets were obtained from Mallinckrodt (Paris, KY, U.S.A.). Acculute standard volumetric hydrochloric acid was from Anachemia Chemicals (Champlain, NY, U.S.A.). Analytical reagent grade potassium permanganate and EM Quant peroxide test strips were obtained from EM Science (Cincinnati, OH, U.S.A.). N,N-Dimethyl-*p*-phenylenediamine (DMPD), 1% spray reagent, was from Sigma (St. Louis, MO, U.S.A.).

For preparative HPLC experiments, Bio-Sil A (200–400 mesh) silica gel was obtained from Bio-Rad Labs. (Richmond, CA, U.S.A.). Woelm Super I neutral alumina was from Universal Scientific (Atlanta, GA, U.S.A.). ICN Adsorbents (formerly Woelm) 32–63-μm, 60-Å irregular silica gel was obtained from ICN Biomedicals (Cleveland, OH, U.S.A.). Partisil Prep 40 silica gel came from Whatman (Clifton, NJ, U.S.A.). For thin-layer chromatographic (TLC) analyses, Uniplate Woelm silica gel GF TLC plates were obtained from Analtech (Newark, DE, U.S.A.), and Merck silica gel $60F_{254}$ TLC plates were from EM Science. For the reduction experiments, analytical grade AG 50W-X4 H^+ (−400 mesh) cation-exchange resin was obtained from Bio-Rad Labs. The resin was prepared by washing with 1 *M* hydrochloric acid (Anachemia Chemicals), deionized water, 0.5 *M* iron(II) sulfate solution (Mallinckrodt), deionized water, 2-propanol and hexane.

The analytical system for the HPLC analyses of *p*-dioxanyl hydroperoxide consisted of an LC9533 ternary gradient liquid chromatograph from IBM Instruments (Danbury, CT, U.S.A.), a Schoeffel 770 variable-wavelength UV detector, obtained from Waters Chromatography Division, Millipore (Milford, MA, U.S.A.). an Erma ERC7510 refractive index detector, obtained from Anspec (Warrenville, IL, U.S.A.) and a Linear Instruments (Irvine, CA, U.S.A.) Model 585 recorder. The column used for the analyses was a μPorasil silica column (300 × 3.9 mm I.D.) from Waters Assoc.

The formation of *p*-dioxanyl hydroperoxide occurred initially during a preparative HPLC purification in which a SepTech ST/800C system from Separations Technology (Wakefield, RI, U.S.A.) with a stainless-steel column (1 m × 4 in. I.D.) obtained from HT Chemicals (St. Louis, MO, U.S.A.) was used. To isolate *p*-dioxanyl hydroperoxide, a Whatman (Clifton, NJ, U.S.A.) Magnum 40 stainless-steel column was utilized.

NMR data were obtained with a Varian (Palo Alto, CA, U.S.A.) VXR200 spectrometer. For IR data, a Perkin-Elmer (Norwalk, CT, U.S.A.) 283B spectrometer was utilized. The UV absorbance spectrum of *p*-dioxanyl hydroperoxide was obtained using a Beckman (Irvine, CA, U.S.A.) DU-7HS UV–VIS spectrophotometer.

Peroxide formation in dioxane

A contaminant was discovered during the analysis of purified drug products from a preparative HPLC purification which utilized dioxane, trimethylpentane and acetonitrile in the mobile phase. The contaminant was identified as *p*-dioxanyl hydroperoxide. Several experiments were then performed to investigate the formation of *p*-dioxanyl hydroperoxide in the solvent and during preparative HPLC.

Dioxane is stored in 1- or 4-l brown glass bottles, under nitrogen. Once they are opened, air enters the bottles and autoxidation of dioxane begins, according to the following reaction[1,3,5,10,11,13–18]:

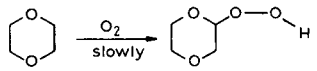

Dioxane *p*-dioxanyl hydroperoxide
(1,4-dioxan-2-yl hydroperoxide)

When a fresh 4-l bottle of dioxane was opened and immediately evaporated under vacuum at 40°C, 200 mg of fairly pure *p*-dioxanyl hydroperoxide were obtained. It was also demonstrated that amounts up to 200 mg/l could be generated when the dioxane was aerated with a stream of oxygen and irradiated with UV light in an open beaker for 100 h.

In experiments with preparative silica gel columns packed in the laboratory, a higher concentration of peroxide was found in the column eluate than in the initial solvent. Several brands of silica gel were investigated, and all produced an increase in peroxides (see Table I). In these experiments, the actual amount of peroxide produced during the chromatography and fraction work-up was determined by evaporating the solvent, weighing the peroxide residue and subtracting the amount contributed by the fresh dioxane from the bottle. The concentration of the peroxide present in the fresh solvent prior to chromatography was determined by evaporating the solvent and weighing the residual peroxide.

From these experiments with silica gel columns, one can expect the formation of peroxides during preparative HPLC. The amount produced can be minimized by using fresh dioxane, stored under nitrogen, and by limiting the exposure of the dioxane to oxygen during the preparation of mobile phases and the storage and work-up of fractions.

Isolation and detection of p-dioxanyl hydroperoxide

The original *p*-dioxanyl hydroperoxide contaminant was formed during a preparative HPLC purification in which a mobile phase consisting of dioxane–trimethylpentane–acetonitrile (25:75:0.5, v/v) was used. A total of 90 l of mobile phase was passed through a column containing 3.9 kg of silica gel. The peroxide was first observed when the column fractions were analysed by TLC on Analtech Woelm silica gel plates developed with 100% ethyl acetate (R_F = 0.55). The peroxide was rendered

TABLE I

COLUMN CHROMATOGRAPHY EXPERIMENTS

Experiment No.	*Silica gel brand*	*Volume of mobile phase (l)*	*Peroxide produced during chromatography (mg)*
1	Bio-Rad Bio-Sil A	2.7	8.7
2	ICN Adsorbents	2.7	27.0
3	Whatman Partisil Prep 40	2.5	43.7
4	Whatman Partisil Prep 40	2.6	38.2

visible by two techniques: (1) the plates were sprayed with 50% sulfuric acid and heated at 300°C for 3–5 min and then viewed under long-wavelength UV light (366 nm); (2) the same plates were then sprayed with 10% phosphomolybdic acid (PMA) solution and heated at 300°C for 1–3 min to produce blue spots against a yellow background. The peroxide contaminant was visible by both techniques and was present in every chromatographic fraction.

The contaminated drug product was purified and 400 mg of the peroxide were isolated by the following method. A Whatman Magnum 40 preparative column packed with silica gel was eluted with 2 l of ethyl acetate–hexane (3:2) followed by 4 l of ethyl acetate. The *p*-dioxanyl hydroperoxide was eluted in the first 2400 ml, completely resolved from the main drug product (Fig. 1).

HPLC analysis

HPLC was utilized to analyze samples and solvent for *p*-dioxanyl hydroperoxide. The initial system was similar to the method for the preparative HPLC isolation of the *p*-dioxanyl hydroperoxide. A μPorasil column was eluted with ethyl acetate–hexane (1:1) at a flow-rate of 2 ml/min. Both UV (265 nm, 0.2 a.u.f.s.) and refractive index (RI) (temperature 35°C, range = 1) detection were utilized. The retention time of *p*-dioxanyl hydroperoxide was *ca.* 3.9 min. The system was useful for separating *p*-dioxanyl hydroperoxide from impurities with RI detection. Owing to the high UV cut-off of ethyl acetate, UV detection was hindered.

The following system was developed to accommodate both UV and RI detection. A μPorasil column was eluted with 2-propanol–hexane (1:9) at a flow-rate of 2 ml/min. UV detection was effected at 210 nm, 0.4 a.u.f.s. and RI detection at a temperature of 40°C and range = 1. The retention time of the peroxide was *ca.* 4.6 min. The RI response is greater than the UV response, as there are no strong UV chromophores in dioxane or *p*-dioxanyl hydroperoxide. Typical chromatograms are shown in Fig. 2. All of the lots of *p*-dioxanyl hydroperoxide, dioxane and the original peroxide contaminant isolated by preparative HPLC were analyzed by HPLC.

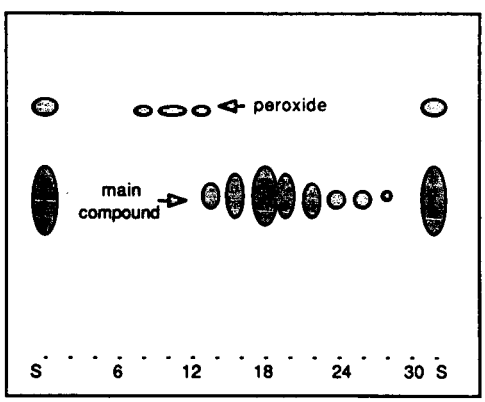

Fig. 1. TLC analysis of fractions for the preparative isolation of *p*-dioxanyl hydroperoxide. Mobile phase, ethyl acetate; detection, 10% PMA after 50% sulfuric acid. S is the sample prior to chromatography. Only the even-numbered fractions from the isolation were spotted on the TLC plate.

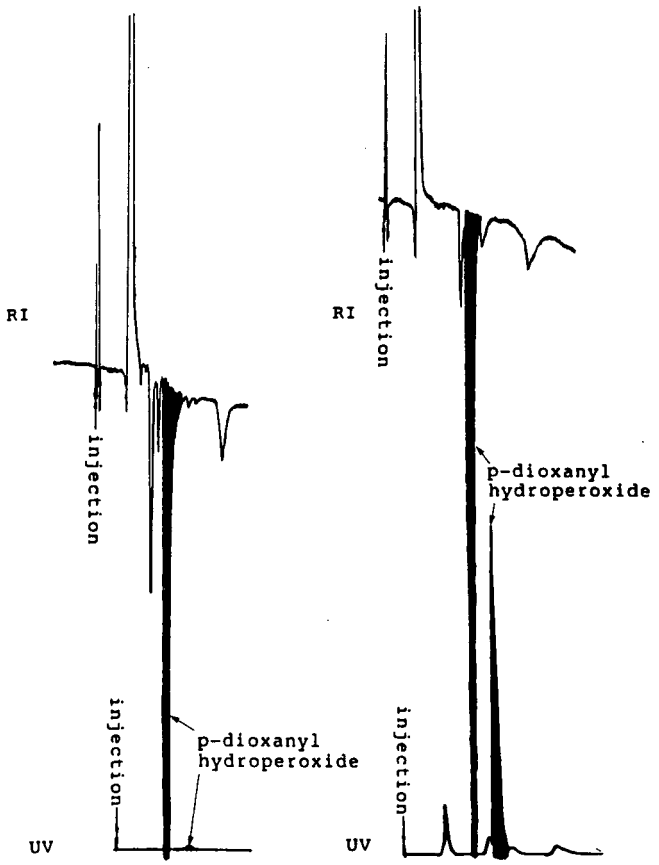

Fig. 2. HPLC methods for *p*-dioxanyl hydroperoxide. System (A): mobile phase, ethyl acetate–hexane (1:1); UV detection, 265 nm, 0.2 a.u.f.s.; RI detection at 35°C, range 1. System (B): mobile phase, 2-propanol–hexane (1:9); UV detection, 210 nm, 0.04 a.u.f.s.; RI detection at 40°C, range 1. Sample, 100 μl of 2 mg/ml *p*-dioxanyl hydroperoxide dissolved in the mobile phase.

This system is also suitable for determining the peroxide content in old bottles of dioxane and other ethers, such as tetrahydrofuran and methyl *tert.*-butyl ether. Both UV and RI detection are sufficiently sensitive to detect the ether peroxides at low levels when a 5-μl aliquot of the solvent is injected.

TLC analysis

A TLC method for analyzing samples containing *p*-dioxanyl hydroperoxide was developed to provide a quick and cost-effective method of analysis. The optimal system, with respect to convenience and R_F value, was 100% ethyl acetate on silica gel TLC plates, with the following detection techniques. (1) N,N-dimethyl-*p*-phenylenediamine (DMPD): the plates are sprayed with a 1% solution of DMPD in acidified methanol and heated very briefly at 300°C. A positive response is a purplish pink spot against a white background. The plates can be viewed in reflected or transmitted white light. This test is specific for organic peroxides and can be used to detect 1 μg. (2)

TABLE II

COMPARISON OF TLC DETECTION METHODS

Scale: 1 = best; 5 = worst.

No.	*Test*	*Detection limit (μg)*	*Contrast*	*Response*	*Ease of mechanics*	*Stability*
1	DMPD	1.0	3	1	1	2
2	DMPD–heat	5.0	1	1	2	2
3	DMPD–heat–LWUV* (366 nm)	1.0	1	1	2	2
4	Potassium permanganate–sodium hydroxide	0.5	2	1	2	2
5	50% sulfuric acid–LWUV*	5.0	2	4	2	1
6	50% sulfuric acid–10% PMA	5.0	4	5	2	2

* Long-wavelength UV detection.

DMPD with heating: the plates from technique 1 are heated for 5–10 min at 300°C and produce better contrast of the spots against the background. The sensitivity is decreased to 5 μg. The plates can be viewed under reflected white light. (3) DMPD with heating and long-wavelength UV detection: the plates from technique 2 are viewed under long-wavelength UV light (366 nm). The spots appear dark with a bright corona against a dark background. The sensitivity is 1 μg. (4) Potassium permanganate–sodium hydroxide: the TLC plates are sprayed with a solution of 0.5 g of potassium permangenate dissolved in 1 *M* sodium hydroxide solution and heated for *ca.* 20 s at 300°C. A positive response is a yellow spot against a magenta background. The plates can be viewed under reflected or transmitted white light. This test is not specific for peroxides, but can be used to detect 0.5 μg. (5) Sulfuric acid with long-wavelength UV detection: the plates are sprayed with 50% sulfuric acid and heated at 300°C for 3–5 min, then viewed under long-wavelength UV light (366 nm). The spots appear as light spots against a dark background. The sensitivity is 5 μg. (6) Sulfuric acid–PMA: After technique 5, the plates are sprayed with a 10% solution of PMA and heated at 300°C for 1–3 min. The peroxide gives blue spots against a yellow background when viewed under white light. The sensitivity is 5 μg.

In Table II, these detection methods are compared on the basis of limit of detection, contrast, response, ease of mechanics and stability of the spray reagent solution.

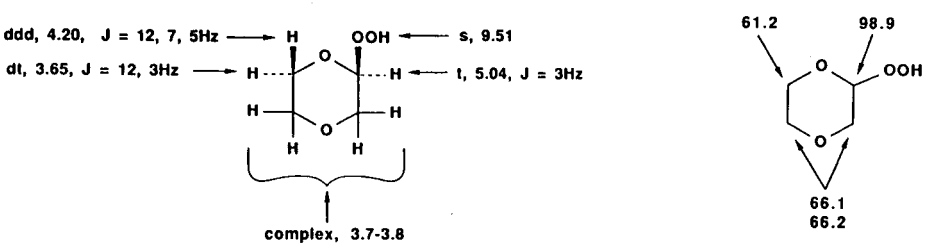

Fig. 3. (Left) Proton and (right) carbon-13 NMR assignments for *p*-dioxanyl hydroperoxide.

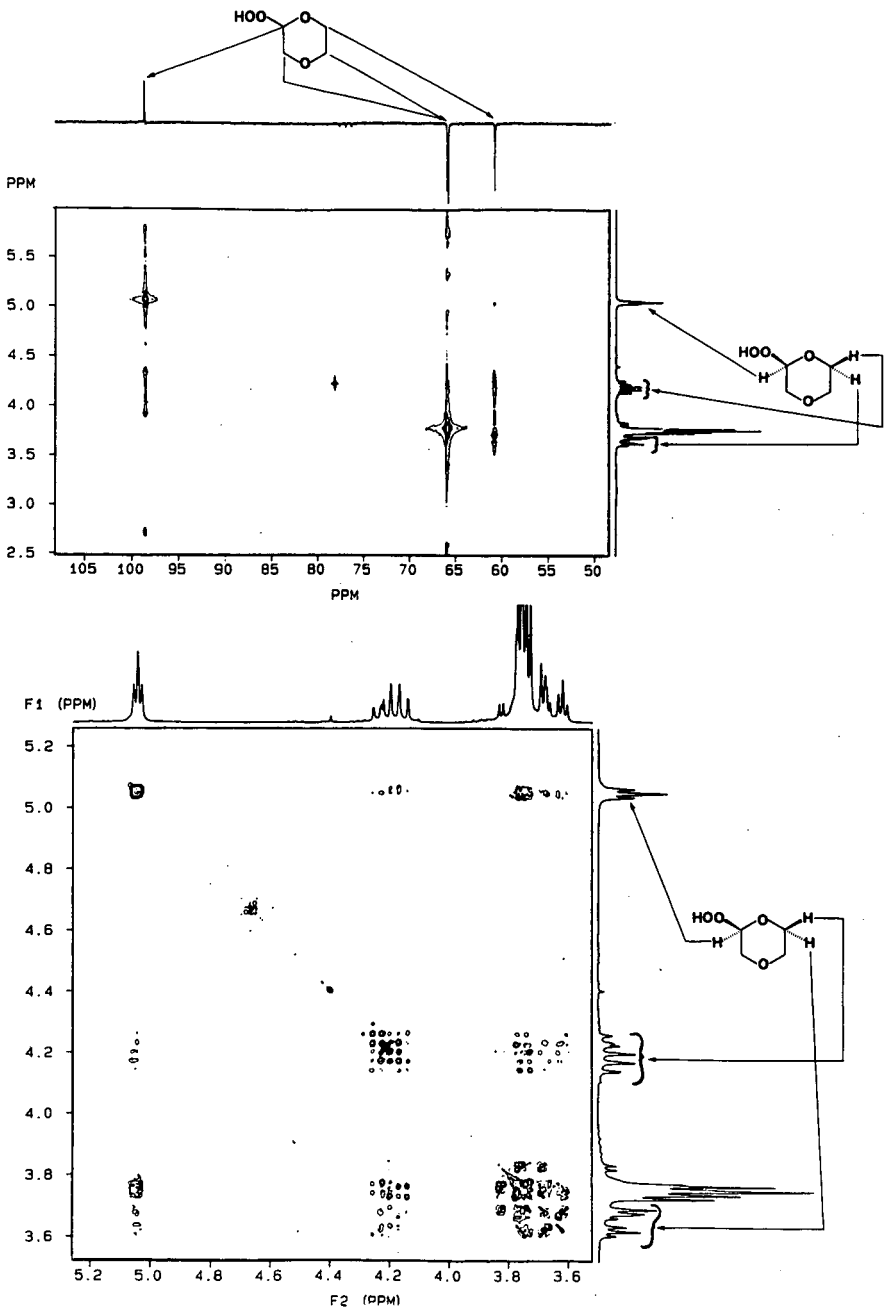

Fig. 4. (Top) 200 MHz proton–carbon heterocorrelation and (bottom) proton–proton homocorrelation spectra of *p*-dioxanyl hydroperoxide in deuterochloroform solution.

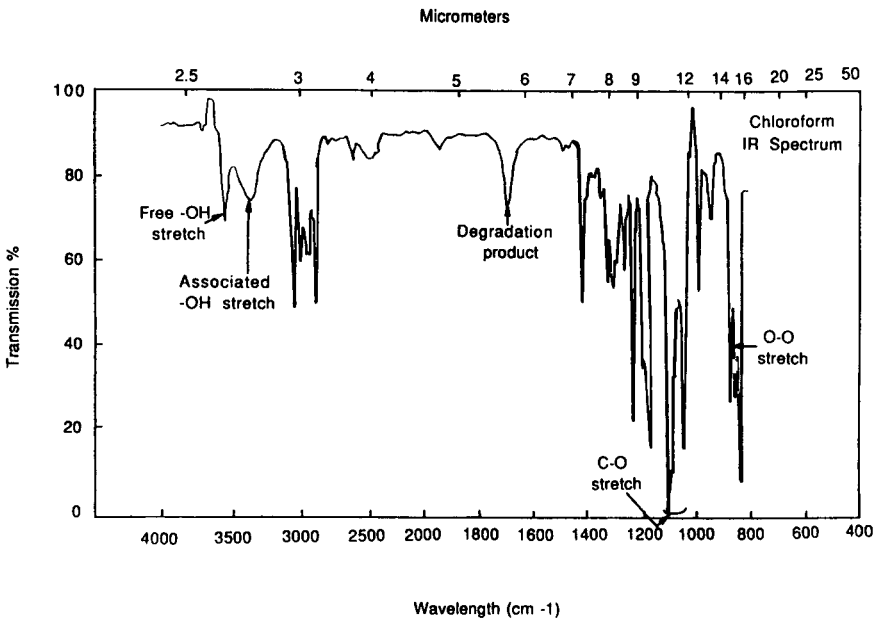

Fig. 5. Chloroform IR spectrum of isolated *p*-dioxanyl hydroperoxide.

Identification

The contaminant isolated by preparative HPLC was determined to be *p*-dioxanyl hydroperoxide based on elemental analysis (found, C 40.2, H 6.8; required for $C_4H_8O_4$, C 40.0, H 6.7%), spectral data and a positive response to EM Quant peroxide test strips.

The proton and carbon-13 NMR spectra obtained by using deuterated chloroform and a tetramethylsilane reference are fully consistent with the structure of *p*-dioxanyl hydroperoxide. Assignments shown in Fig. 3 were confirmed by double resonance, HOMCOR and HETCOR experiments. HOMCOR and HETCOR spectra are given in Fig. 4.

The IR spectrum shown in Fig. 5 contains bands due to free and associated –OH stretching and a band due to O–O stretch. The band at about 1725 cm^{-1} is probably due to a degradation product of the hydroperoxide, as no evidence of major impurities was present in the chromatographic data or other spectral data.

The UV spectrum of a concentrated solution of *p*-dioxanyl hydroperoxide, shown in Fig. 6, contains end absorption beyond 210 nm. Therefore, UV detection in HPLC can be utilized.

Removal of peroxide from dioxane

Several methods of removing *p*-dioxanyl hydroperoxide from dioxane were investigated. When *p*-dioxanyl hydroperoxide is present at concentrations greater than 5 mg/ml, preparative HPLC can be utilized to remove the hydroperoxide from the solvent. In this procedure, the peroxide is concentrated and is not chemically reduced and there exists a potential explosion hazard. Woelm states[10] that alumina scavenges peroxides while letting other compounds pass through unaltered. With *p*-dioxanyl

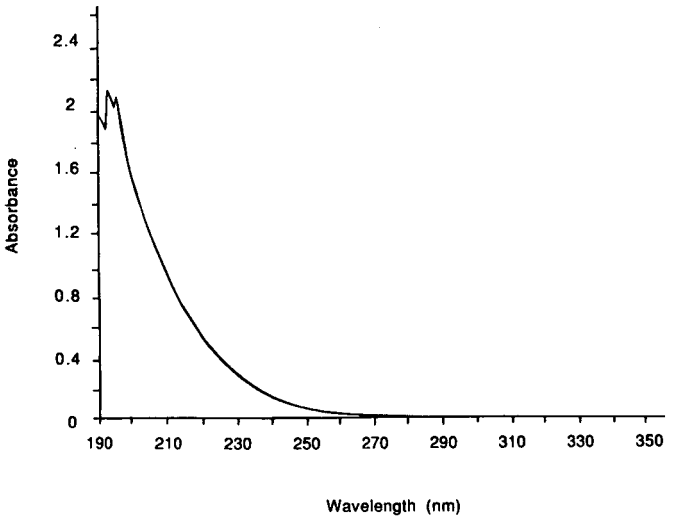

Fig. 6. UV absorbance spectrum of *p*-dioxanyl hydroperoxide, dissolved in acetonitrile (UV cut-off = 190 nm) at a concentration of 11.9 mg in 2.3 ml, 504.2 mg-%, 0.1-cm cell.

hydroperoxide, it has been reported[2,10,14,17] that alumina has been found to cause decomposition of this peroxide.

To investigate the chemical reduction of peroxides by alumina, two experiments were performed with columns containing Super I neutral alumina. In the first experiment, 0.2 g of *p*-dioxanyl hydroperoxide was injected into a column containing 4 g of alumina. The first mobile phase was dichloromethane. To elute the peroxide, a stepwise gradient with increasing amounts of 2-propanol in the mobile phase was applied. The peroxide was not eluted by 100% 2-propanol. Water is recommended for eluting the peroxide from alumina[10], and therefore an additional stepwise gradient from 100% 2-propanol to 100% water was used. No peroxide was eluted. In a second experiment, the maximum amount of peroxide effectively decomposed was calculated. The same experiment was repeated using *ca.* 0.6 g of *p*-dioxanyl hydroperoxide. A total of *ca.* 0.27 g was successfully decomposed. From this experiment, the maximum loading ratio for peroxide decomposition was calculated to be 1 part of peroxide on 17 parts of alumina.

An alternative method for the decomposition of *p*-dioxanyl hydroperoxide by chemical reduction was also investigated. In this method, a strong cation-exchange resin with iron in the 2+ oxidation state was slurried with the sample solution[11,14,19]. It was found that 10 mg of peroxide in 1 ml of solvent were decomposed in 1.5 h when in the presence of 120 mg of iron resin. For small amounts of hydroperoxides, at concentrations less than 5 mg/ml of peroxide in solvent, the solution can be disposed of as for general waste solvents.

CONCLUSION

Peroxides are known to be potentially unstable, explosive and friction-sensitive compounds[1–5,12,20]. Our work has demonstrated that *p*-dioxanyl hydroperoxide is

formed during preparative HPLC and chromatographers using dioxane need to be aware of the potentially hazardous situations when this peroxide is passed through packed columns or concentrated during fraction work-up. The detection and analysis procedure we have described can be useful in monitoring the peroxide content of solvents, samples and solutions during preparative HPLC. Precautions to minimize the exposure of dioxane or dioxane-containing mobile phases to air and UV radiation need to be implemented throughout the preparative chromatographic process.

ACKNOWLEDGEMENTS

The following assisted in the investigations by performing additional analyses and participating in helpful discussions: Clifford J. Seul, Paul W. Schoen, Arthur L. Campbell, Kevin A. Babiak, Elisabeth Hajdu and Lilian Garcia.

REFERENCES

1 *"CHAS" Notes*, American Chemical Society, Division of Chemical Health and Safety, Washington, DC, No. 1(4), 1982, p. 3.
2 H. L. Jackson, W. B. McCormack, C. S. Rondestvedt, K. C. Smeltz and I. E. Viele, *J. Chem. Educ.*, 47 (1970) A175.
3 M. C. Nagel, *J. Chem. Educ.*, 61 (1984) 250.
4 D. A. Pipetone and D. D. Hedberg, *J. Chem. Educ.*, 59 (1982) A159.
5 J. Varjavandi and O. L. Mageli, *J. Chem. Educ.*, 48 (1971) A451.
6 A. G. Nord and B. Lindberg, *Acta Chem. Scand.*, 27 (1973) 1175.
7 *Data Sheet*, No. 655, National Safety Council, Chicago, IL, 1976.
8 *B & J Solvent Applications Update*, Baxter, Burdick and Jackson, Muskegon, MI, 1986, p. 3.
9 *Fisher Methyl tert.-Butyl Ether (MTBE)*, Fisher Scientific, Pittsburgh, PA, Bulletin No. 625/0-1020-07, 1981.
10 *Purification of Solvents by Adsorbents Woelm, 1 and 1a*, Woelm Pharma., Eschwege, 1973.
11 H. G. Shertzer and W. M. Tabor, *J. Environ. Sci. Health*, A20 (1985) 845.
12 M. Verzele and C. DeWaele, *Preparative High Performance Liquid Chromatography*, Deinze, Gent, 1986, pp. 90–91.
13 B. C. Gilbert and A. J. Dobbs, *Organic Peroxides*, Vol. III, Interscience, New York, 1972, pp. 271–339.
14 D. Swern (Editor), *Organic Peroxides*, Vol. II, Wiley-Interscience, New York, 1971, pp. 17–19, 23–25, 31–59, 68–69, 94–127, 178–183 and 223–224.
15 S. Patai (Editor), *The Chemistry of Peroxides*, Wiley, Chichester, 1983, pp. 142–143, 501, 503–506, 652, 721–722, 755 and 760–761.
16 P. Bilski and J. Szychlinski, *J. Photochem.*, 38 (1987) 117.
17 F. Feigl, *Spot Tests in Organic Analysis*, Elsevier, Amsterdam, 1966, p. 14.
18 L. G. Wade, Jr., *Organic Chemistry*, Prentice-Hall, Englewood Cliffs, NJ, 1987, pp. 509–10.
19 A. M. Trzeciak and J. J. Ziolkowski, *J. Mol. Catal.*, 39 (1987) 85.
20 V. K. Mohan, K. R. Becker and J. E. Hay, *J. Hazardous Mater.*, 5 (1982) 197.

Journal of Chromatography, 461 (1989) 45–61
Elsevier Science Publishers B.V., Amsterdam — Printed in The Netherlands

CHROMSYMP. 1429

PRODUCTION SCALE PURIFICATION OF BIOSYNTHETIC HUMAN INSULIN BY REVERSED-PHASE HIGH-PERFORMANCE LIQUID CHROMATOGRAPHY

EUGENE P. KROEFF*, REBECCA A. OWENS, EDDIE L. CAMPBELL, RONALD D. JOHNSON* and HARLENE I. MARKS**

Department of Biosynthetic Isolation and Purification Development, Lilly Research Laboratories, A Division of Eli Lilly and Company, Lilly Corporate Center, Indianapolis, IN 46285 (U.S.A.)

SUMMARY

A process based on reversed-phase high-performance liquid chromatography (RP-HPLC) has been developed for the purification of biosynthetic human insulin (BHI). The RP-HPLC procedure has been successfully integrated into the multimodal chromatographic production process used to purify kilogram quantities of BHI. Axial compression column technology was used in the scale-up process. The RP-HPLC procedure yields an insulin product having high chemical purity and full biological activity.

INTRODUCTION

Recombinant DNA technology has provided the means for preparing virtually unlimited quantities of therapeutically important peptide and protein products. A recent example of the successful use of this technology is the production of the peptide hormone human insulin, using *Escherichia coli*[1–7]. While genetic engineering and associated fermentation technology provides the initial protein product, the protein must be extensively purified and processed before it can be formulated into a final dosage form. A purification process based on multimodal chromatography, which exploits differences in molecular charge, size, and hydrophobicity, is typically used to isolate the human insulin[6–8]. Such a purification scheme must be capable of efficiently isolating the insulin product from the very complex fermentation matrix. In addition, the insulin purification process should be capable of reducing the levels of insulin-like components, that is, those components resulting from minor modifications of the insulin molecule itself. The reduction of these components can be particularly challenging, since in many cases the insulin-like substances differ in the modification of only a single amino acid residue.

We have investigated the use of reversed-phase high-performance liquid chro-

* Present address: Chiron, Emeryville, CA 94608, U.S.A.
** Present address: Prochrom, Brownsburg, IN 46112 U.S.A.

0021-9673/89/$03.50

matography (RP-HPLC) as an integral step in the multimodal chromatographic purification of biosynthetic human insulin (BHI). RP-HPLC is a logical choice, since its selectivity and high resolving capabilities have been previously exploited in the field of insulin analysis. For example, insulin species which differ by a single amino acid residue have been successfully resolved using a wide variety of stationary and mobile phases[1,9–17]. It has been demonstrated that the technique can be very useful for the separation and quantitation of a variety of insulin-like components[11–20]. Modified forms, such as desamido, carbamoyl, formyl, and insulin polymers, have been successfully separated from the parent insulin molecule. RP-HPLC has also proven to be an invaluable tool for monitoring the quality and quantity of insulin throughout the isolation and purification process[20]. In addition, important chemical intermediates such as A- and B-chain S-sulfonates, and proinsulin and its S-sulfonate have been characterized by RP-HPLC[16,20,21].

The isolation and purification of insulin and insulin derivatives has also been investigated by preparative RP-HPLC. In these studies, analytical-scale columns were employed to isolate micro- to milligram quantities of the desired product. The purification of iodinated insulins, commonly used as tracers in radioimmunoassays and receptor assays, has been reported by a number of groups[16,22,23]. In these studies, [^{125}I]insulin isomers were successfully separated and isolated in a single run. Genetic variants of insulin have been detected and isolated from blood samples of diabetics by RP-HPLC[24]. Proinsulin, the biological precursor to insulin, has also been purified by this technique. The RP-HPLC procedure was used to purify the bovine proinsulin present in the high-molecular-weight fraction obtained from size-exclusion chromatography of insulin[25]. In another study, a variant of bovine proinsulin was isolated by reversed-phase chromatography[26]. In a recent report, the levels of proinsulin associated with preparations of bovine and porcine insulins were reduced by RP-HPLC displacement chromatography[27]. In this study, up to 500 mg of insulin were purified on analytical columns of Nucleosil C_8, using centrimide as a displacing agent.

In the current paper, we will discuss the use of preparative RP-HPLC for purifying production scale quantities of BHI. We will examine the critical chromatographic operating parameters, the scale-up of the process, and the practical aspects of integrating this procedure into a multimodal purification scheme.

EXPERIMENTAL

Equipment

Laboratory scale purification studies were conducted with either a Varian (Walnut Creek, CA, U.S.A.) 5000 gradient HPLC system equipped with a Du Pont (Wilmington, DE U.S.A.) variable-wavelength detector set at 280 nm, or a Pharmacia (Piscataway, NJ, U.S.A.) FPLC system composed of an LCC 500 controller, two P-500 pumps, and a UV-2 detector system with lamp and filters for detection at 280 nm. The column effluent from both systems was fractionated using a Pharmacia Frac-100 fraction collector.

A Rainin (Woburn, MA, U.S.A.) Rabbit gradient system, composed of two model HP pumps fitted with 100-ml preparative heads and controlled with an Apple 2E computer system, was used for studies with the 50 × 5.0 cm I.D. column.

Pilot-plant and production-scale purification studies were conducted on LC 150 VE, LC 300, or LC 450 axial compression columns, available from Prochrom (Nancy, France). All units were equipped with dual-head high-pressure solvent delivery pumps and automation units for producing gradients. The columns were fitted with 2-μm frits (Mott Metallurgical, Farmington, CT, U.S.A.).

Materials

The stationary phases evaluated for the purification studies were obtained directly from the manufacturers as prepacked analytical columns or as bulk packings. The 10-μm Zorbax Process Grade C_8, used for the pilot-plant and production-scale purification studies was obtained from DuPont.

The partially purified human insulin zinc crystals used in the purification studies were prepared at Eli Lilly and Company (Indianapolis, IN, U.S.A.). The human insulin derivatives were prepared in the Lilly Research Laboratories Human insulin reference standard lots P99843 and RS0026 were used for the HPLC and for the biopotency assays.

All reagents used in these studies were of reagent grade quality or better and were obtained from a variety of suppliers.

Procedures

Packing of fixed-bed columns. Columns for the initial laboratory studies were packed with the desired stationary phase, using a high-pressure, non-balanced slurry-packing technique[28]. Columns and packing reservoir (HT Chemical, St. Louis, MO, U.S.A.) were fitted to a Model DSTV 72C Haskel pump (Burbank, CA, U.S.A.). The desired stationary phase was slurried in acetonitrile at a ratio of 1 g of packing per 2 ml of solvent. Morpholine at a concentration of 0.02% was added to prevent agglomeration of the particles. The slurry was sonicated for approximately 10 min and loaded into the packing reservoir; acetonitrile was then pumped through the system at a flow-rate high enough to generate 3000 p.s.i. (5000 p.s.i. for columns having internal diameters $\leq$ 1.0 cm).

Packing of axial compression columns. The stationary phase of choice was slurried with acetonitrile in a ratio of 1 kg of packing per 2 l of acetonitrile. Typically, 5-kg, 25-kg, and 50-kg quantities of packing were slurried for the 15-cm, 30-cm and 45-cm I.D. axial compression columns, respectively. The hydraulic piston of the column was lowered to a level to accommodate the volume of the slurry. The slurry was transferred to the column by means of an air diaphragm pump, the top flange was replaced, and the piston was raised, displacing the acetonitrile. The packed column was maintained at a pressure of 750 p.s.i. by the piston during column operation.

Evaluation of packed columns. The efficiency of the packed columns was evaluated with methyl benzoate as a test probe. The columns were equilibrated with 60% aqueous acetonitrile at a flow-rate of 3 cm/min. Flow was maintained in the direction of packing. A solution of 90% aqueous acetonitrile containing 130 μg of uracil and 30 μl of methyl benzoate per ml was introduced into the column with a loop injector (5–15 ml for the preparative columns and 20 μl for analytical columns). The chromatogram was recorded and the plate count was determined, using the half height procedure[28]. Plate counts of 30 000–40 000 plates/m were obtained for the fixed-bed columns, and 45 000–55 000 plates/m were common for the axial compression columns.

Purification studies. The column to be tested was equilibrated in 0.25 *M* acetic acid–acetonitrile (90:10). The BHI zinc insulin crystals to be purified were dissolved in the column equilibration buffer at a concentration of 15 mg/ml. The insulin solution was loaded onto the column at a flow-rate of 1.5 column volumes/h. (Note that unless otherwise stated, the term column volume (CV) refers to the volume of the *empty* column). Columns were typically loaded with 12–15 mg of insulin/ml of CV. After loading, the column was washed with 1 CV of the initial equilibration buffer and the gradient of choice was run, using 0.25 *M* acetic acid as eluent A and 60% aqueous acetonitrile as eluent B. During elution, 0.1-CV fractions were collected. The fractions were assayed with the analytical HPLC systems described below, and the desired fractions were pooled. During pilot-plant and production-scale studies, insulin was recovered from the mainstream pool by means of a variation of the zinc crystallization procedure described previously[29]. Briefly, the concentration of insulin is adjusted to 2 g/l with 0.25 *M* acetic acid, the pH is adjusted to 5.9 with ammonium hydroxide, and a 1.8 molar excess of zinc chloride over BHI is added. The zinc insulin crystals formed are isolated by filtration.

Analytical characterization of BHI

Analytical HPLC. Several analytical RP-HPLC systems were used to evaluate the quality and quantity of BHI throughout the purification process. Mobile phases containing the ion-pair reagents pentanesulfonic acid (PSA) or octanesulfonic acid (OSA) were used to characterize the BHI at the RP-HPLC purification step[30]. The PSA mobile phase was composed of 20 m*M* PSA in acetonitrile–Milli Q water (31:69) (pH 2.1, adjusted with phosphoric acid). The OSA mobile phase consisted of 20 m*M* OSA and 33m*M* phosphoric acid, in Milli Q water–acetonitrile (57:43) (pH 2.0, adjusted with phosphoric acid). Chromatography was conducted on a Hewlett-Packard (Palo Alto, CA, U.S.A.) Model 1090 liquid chromatograph fitted with two Zorbax C_8 (Du Pont), 150-Å columns (15 cm × 0.45 cm I.D., connected in series), thermostatted to 30°C and operated at a flow-rate of 0.8 ml/min. An alternative column system employed two Zorbax C_8 Reliance cartridge columns (connected in series), thermostatted to 35°C and operated at a flow-rate of 0.8 ml/min. The column effluent for all of the systems was monitored at 214 nm, and 20-μl injection volumes were typical. The detector output was analyzed by a chromatographic data-handling system, based on a Hewlett-Packard Series 1000 computer. The insulin concentration was determined by comparing the insulin peak area response of the sample to that of a standard, while the insulin purity was determined by comparing the area of the insulin peak to the total peak area in the chromatogram, disregarding the solvent front.

The RP-HPLC gradient system used to characterize the final BHI crystals has been reported previously[12].

E. coli polypeptides (ECPs). The radioimmunoassay system for detecting ECPs has been described previously[31]. The limit of detection is approximately 4 ppm.

Determination of bonded phase in BHI crystals. Final BHI crystals were checked for the presence of reversed-phase breakdown products (siloxanes) using a gas chromatographic assay procedure. Insulin (1 g) was extracted with 5 ml of dichloromethane for 30 min. The insulin was filtered, and 1 μl of the dichloromethane extract was injected into a Hewlett-Packard Model 5890 gas chromatograph, fitted with a

15 m × 0.53 mm I.D. Megabore DB-5 column (J. and W. Scientific, Folsom, CA, U.S.A.). The injection temperature was set to 200°C, and the temperature of the flame-ionization detector was set to 250°C. The column temperature was maintained at 45°C for 2 min, followed by a temperature program of 12°C/min for 12 min. The final column temperature of 200°C was held for an additional 8 min. Potential bonded phase breakdown products were obtained from Petrarch Systems (Bristol, PA, U.S.A.) and were dissolved in dichloromethane. These compounds included: *n*-octyldimethylsiloxane; 1,3-bis(*n*-octyl)-tetramethyldisiloxane; *n*-octylpentamethyldisiloxane; and hexamethylcyclotrisiloxane. The limit of detection for these compounds in final insulin crystals is approximately 10 ppm.

Biopotency assay of final zinc crystals. The hypoglycemic potency of final BHI zinc crystal lots was determined by the USP rabbit assay.

Limulus amebocyte lysate (LAL) assay. The assay has been described previously[32].

RESULTS AND DISCUSSION

In designing and implementing a reversed-phase purification step for BHI, a number of practical goals and objectives were considered. First, the procedure must be capable of producing a high-quality insulin product in good yields. Purities of >97.5% (RP-HPLC) with mainstream yields of ⩾75% served as minimum acceptable goals. Second, the process should be capable of generating high-purity insulin derived from different feed sources. The level of insulin-like components present in these feeds could range from 6 to 20%, depending upon the nature of the feed source. Third, the operational parameters must be compatible with physicochemical properties of the insulin molecule. The conditions must provide for good solubility, without subjecting the insulin either to extremes in pH or to conditions that would cause irreversible denaturation. Fourth, the process should complement the other steps in process. That is, it should enhance the multimodal purification scheme as well as produce a product that can be easily taken into the next phase of purification. Fifth, the process must be capable of being implemented in a production environment. The process, along with any necessary ancillary equipment, should be readily scalable. It must also be capable of operating in a very reproducible manner. Finally, the procedure must be economically viable. This necessitates good process yields and good packing lifetime. Additionally, the procedure should be able to replace conventional chromatography steps and/or purify material which otherwise could not be purified by conventional procedures.

Production of BHI

The production of biosynthetic human insulin (BHI) can be accomplished by either the A- and B-chain[1,5–7] or the proinsulin[2,5–7] processes described in Fig. 1. In the chain process, the A- and B-chains which comprise the insulin molecule, are separately fermented, isolated, and purified in the form of stable S-sulfonate derivatives. The chains are then combined to form the insulin molecule which is subjected to conventional ion-exchange and size-exclusion chromatography. During the course of the chromatographic purification, fractions are generated that contain appreciable quantities of insulin but which are not pure enough to be included in the mainstream.

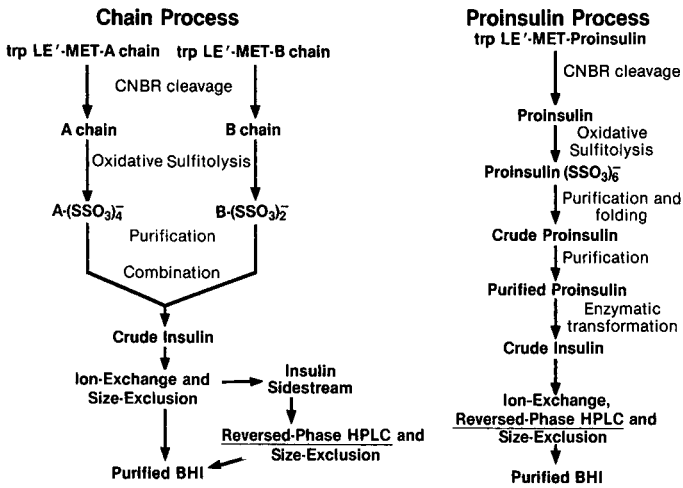

Fig. 1. Production of BHI by chain and proinsulin processes.

In particular, the levels of insulin-like components are enriched in these sidestream fractions. The quantity of purified insulin obtained by recycling the sidestreams through the original process is not great enough to make recycling feasible. These insulin sidestreams are therefore excellent candidates for the high resolving capability of RP-HPLC.

The proinsulin route, which is the current method of choice for producing human insulin, includes RP-HPLC as a routine step in the overall purification scheme. The proinsulin route has proven to be a more efficient method for preparing BHI, since only a single fermentation isolation scheme is necessary. In this procedure, the S-sulfonate derivative of proinsulin is isolated and chromatographically purified. The S-sulfonate is then folded to form proinsulin, which is further purified before being enzymatically transformed to BHI. The resulting BHI is purified by ion-exchange chromatography and is crystallized. The redissolved crystals serve as the charge material for the reversed-phase procedure. Following reversed-phase purification, the insulin is purified by size-exclusion chromatography and crystallization.

In both of the synthetic routes, placement of the reversed-phase step within the overall purification scheme was based on a number of practical and procedural considerations. First, it is the insulin molecule itself which is to be purified by HPLC. This requires that the reversed-phase step be placed after either the combination of the chains or the enzymatic conversion of proinsulin to insulin. Second, by inserting the step late in the overall process, we can take advantage of the fact that the majority of the *E. coli*-derived impurities, which arise from the bacterial host system, have been removed by the preceding steps. It is necessary to minimize these impurities since they reduce the effective lifetime of the stationary phase by physically and/or chemically fouling the packing due to low solubility or irreversible binding[20]. This is critical, since the silica-based packings have pH limitations which preclude the use of pH extremes for clean-up and regeneration. Third, the HPLC procedure is designed to be a "polishing" step. It is intended to reduce the level of insulin-like components which

are generated early in the isolation purification scheme and which are difficult to remove by conventional chromatographic procedures. In addition, the reversed-phase step complements the ion-exchange step that precedes it and the size-exclusion step which follows. Insulin is therefore subjected to three different modes of purification. Finally, because every purification process incurs progressive yield losses, a smaller amount of material will need to be processed through later steps than through the initial steps. For the reversed-phase procedure, this translates into fewer runs and smaller amounts of packing material.

Chromatographic parameters

A variety of chromatographic parameters was evaluated and optimized on small columns (15 × 0.94 cm I.D.), using laboratory equipment, before scale-up of the process was undertaken. A brief summary of the critical operational parameters follows.

Stationary phase. A number of stationary phases (C_4, C_8, C_{18}) produced by a variety of manufacturers (Du Pont, Vydac, Amicon, Synchrom) were initially evaluated for their ability to purify insulin. In general, $\leq$12-μm silica particles, derivatized with C_8 or C_{18}, yielded the best results. Pore sizes of 120 to 150 Å were ideal for this application, since they were large enough to permit efficient mass transfer of the insulin in and out of the pores, yet small enough to provide sufficient surface area for this preparative application. In addition, the large-pore silicas ($\geq$300 Å) proved to be more fragile than the smaller-pore materials. Greater care was required in packing these particles, since they were more friable and, hence, gave rise to "fines", which caused excessive pressures. While there were a number of commercial packings which possessed the desired chemical and physical properties for this application, the need for large quantities of packing material limited our available options. The 10-μm Zorbax Process Grade C_8 was available in large supplies and met our chromatographic criteria. By working closely with the manufacturer and designing a laboratory scale preparative evaluation system, we were assured of lot to lot reproducibility. More recently, other manufacturers have begun to produce small-particle, reversed-phase stationary phases in large bulk quantities, and these packings could prove suitable for similar production scale applications.

Mobile-phase pH and buffer. Analytical studies with a variety of reversed-phase systems, have shown that an acidic mobile phase can provide excellent resolution of insulin from structurally similar insulin-like components[10–19]. Minor modifications in the insulin molecule resulting in monodesamido (A-21) formation, or derivatization of amines via carbamoylation or formylation, result in insulin derivatives which have significantly increased retention[12,13]. Derivatives of this nature are typical of the kind of insulin-like components that are found in the charge stream going into reversed-phase purification. Fig. 2 shows the elution order of these common derivatives under both acid and alkaline mobile-phase pH conditions. Note that in the mildly alkaline pH elution scheme, the derivatives are eluted on either side of the parent insulin peak. By contrast, under acidic elution conditions, all of the derivatives are eluted after the insulin peak. The ideal elution scheme should uniformly concentrate and elute the insulin-like components on one side of the insulin peak. Additionally, the yield of purified insulin is expected to be maximized if insulin is eluted *ahead* of the components to be removed[33]. Thus, the acidic mobile phase is the better choice here.

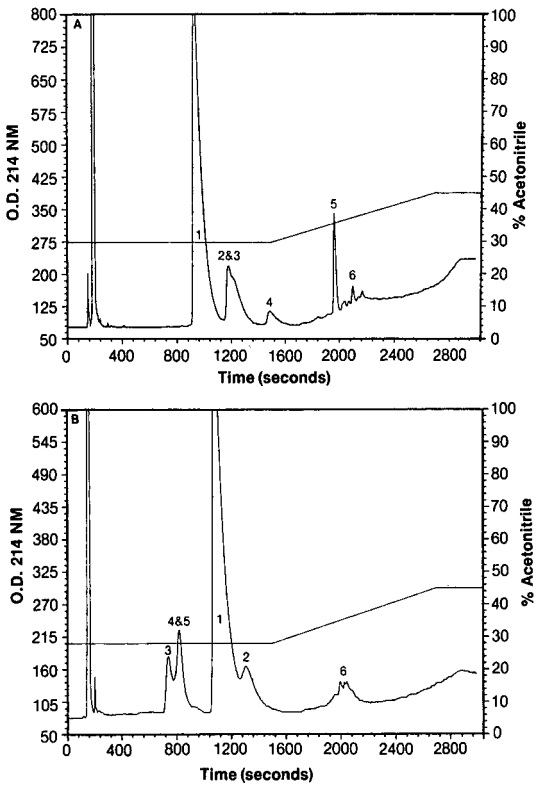

Fig. 2. Elution of BHI and BHI derivatives in RP-HPLC with (A) acid and (B) alkaline mobile phases. Column, Zorbax C_8, 150 Å (25 × 0.45 cm I.D.), thermostatted to 35°C; flow-rate, 1.0 ml/min; sample load, 7.5 μg BHI and 1.3 μg of BHI derivatives. Solutes: 1 = BHI, 2 = desamido A-21 BHI, 3 = N-carbamoyl-Gly BHI, 4 = N-formyl-Gly BHI, 5 = N-carbamoyl-Phe BHI, 6 = BHI dimers. Mobile phases: (A) eluent A = 0.1 *M* phosphate (pH 2.1), eluent B = eluent A–acetonitrile (1:1); (B) eluent A = 0.1 *M* phosphate (pH 7.3), eluent B = eluent A–acetonitrile (1:1).

An ideal pH for insulin purification is in the region of 3.0–4.0, since this pH range is far enough below the isoelectric pH of 5.4 to provide for good insulin solubility. Under acidic conditions, insulin can deamidate to generate monodesamido (A-21) insulin[34]. However, because the RP-HPLC procedure can be conducted within a matter of hours, and the resulting insulin can be removed from the acidic environment via zinc crystallization, deamidation is not a significant problem. Additionally, the mildly acidic conditions will minimize the formation of monodesamido (B-3) insulin, which can be generated at pH 7 or slightly above[34,35]. The mildly acidic mobile phase is also compatible with the pH limitations of the stationary phase (2.0–8.0), as it is low enough to prevent dissolution of the silica support and high enough to minimize hydrolysis of the alkyl chain[36]. Stationary phase stability is critical in both preventing contamination of the insulin with these potential breakdown products and insuring a reasonable column lifetime.

The type of acidic buffer used in the mobile phase is also important in this application. Insulin can undergo self-association and aggregate. This, in turn, can

lead to gel formation and precipitation[37,38]. Gel formation is accelerated when insulin is present in high concentrations at low pH and high electrolyte concentrations. The presence of organic solvents can aggravate this problem. Thus, the mobile phase buffer should be capable of maintaining a stable pH without the addition of salts. The buffer of choice must also be compatible with downstream processing. In this instance, zinc crystallization of the reversed-phase mainstream was the method of choice, since it provides an efficient and convenient means of concentrating and holding the insulin before further processing.

The buffers evaluated for this application included sodium phosphate, formic, acetic, and propionic acids. Acetic acid, at a concentration of 0.25 *M* in eluent A, meets all of the operational criteria. It is compatible with the chromatography and provides good insulin solubility. It buffers in the vicinity of pH 3 without the need for other salts; and, insulin can be readily crystallized from the acetic acid containing mobile phase by the addition of zinc chloride. Acetic acid-containing mobile phases have also been widely used for the size-exclusion chromatography of insulins[13,18,26,27,29,39,40]. In addition to allowing insulin concentrations to exceed 50 g/l, it serves to dissociate the insulin hexamer into a monomer, which is more suitable for chromatography.

Organic modifier. The organic modifier used to elute insulin from the stationary phase should provide both the desired chromatographic selectivity and good insulin solubility. It should have a low viscosity in order to minimize the back pressure in the system, and should be readily available in large quantities. A variety of solvents, including: ethanol and isopropanol, acetonitrile and acetone were considered. Ethanol and isopropanol gave poor resolution of the insulin-like components from insulin and resulted in mainstream yields of only 50–60%. In addition, the solubility of insulin was low in the isopropanol-containing mobile phase and isopropanol gave rise to back pressures *ca.* 1.2–1.5 times greater than for ethanol. Acetone resulted in very poor mainstream yields ($< 50\%$), due to poor insulin solubility. Acetone furthermore precludes monitoring of the process stream at 280 nm. Acetonitrile was the best solvent for this process, as it provides good chromatographic selectivity, insulin solubility, and results in lower operating back pressures than isopropanol. The use of acetonitrile as an organic modifier for analytical and semi-preparative insulin separations has been widely documented[1,2,9–26]. Preparative studies with acetonitrile demonstrated that mainstream yields on the order of 75–85% could be readily obtained (see *Insulin purification*). Acetonitrile can be obtained in bulk quantities from a variety of suppliers and, if desired, can be recovered by distillation. In addition, insulin can be readily recovered from the mobile phase by the addition of zinc chloride and acetic acid, since the presence of acetonitrile at levels $\leq 10\%$ does not interfere with the formation of zinc insulin crystals.

Loading and elution scheme. A chromatographic procedure in which insulin is initially loaded onto the stationary phase in a water-rich mobile phase, followed by gradient elution with acetonitrile, was determined to be ideal for this application. This type of load and elution scheme allows the insulin to be concentrated on the column and then eluted in a volume of solution equivalent to one column volume (empty) or less. By contrast, insulin loaded and eluted under isocratic conditions was typically eluted in 2 or more CV. The small volume of solution resulting from the gradient elution conditions, makes handling and processing of the insulin much easier.

The capacity of the stationary phase for insulin was determined to be approximately 85 mg of BHI/ml of packing. This was determined by loading the insulin charge solution onto a 15 × 0.94 cm I.D. column (10.4 ml) at a flow-rate of 1.5 CV/h (*ca.* 0.3 ml/min) and monitoring the column effluent for insulin concentrations ≥ 0.1 mg/ml. The capacity was defined as being the total quantity of insulin on column at the point of breakthrough, divided by the volume of packing (10.4 ml). For purification studies, loadings comparable to approximately 18% of the capacity of the packed column were used.

Insulin elution was accomplished with a linear gradient, typically ranging from 15 to 30% acetonitrile. Gradient elution was found to be superior to stepwise elution. While stepwise gradients are easier to generate and are therefore preferred for large-scale applications, it was impossible to find a concentration of acetonitrile that would provide a high quality product ($\geq 97\%$) with good recovery ($\geq 75\%$) in a manageable volume (≤ 1 CV). The overload condition under which this procedure is operating gives rise to a non-linear adsorption isotherm. Under this condition, a continuous gradient elution scheme was necessary to produce the desired results of high purity with good mainstream yield. The gradient volume was found to have a significant effect on product quality, mainstream recovery, and volume. A gradient of 15 to 30% acetonitrile running over 8 CV yielded the best results. This represents a gradient slope of approximately 2% acetonitrile/CV.

Regeneration. After elution of the insulin, it is necessary to regenerate the column in order to remove any strongly retained components. The regeneration process reduces the potential for column fouling and helps to increase column lifetime. Effective elution of these strongly retained components is accomplished by increasing the organic modifier concentration to 60%, and by increasing the pH of mobile phase to 7.4 by using a 50 m*M* ammonium phosphate buffer. It is important to note that both the increase in organic modifier concentration and the change in mobile phase pH are necessary to regenerate the column effectively. Detailed regeneration studies indicate that the alkaline buffer is necessary in order to elute a small portion of insulin and other components which are retained by secondary silanol interactions. Elution is further enhanced by increasing the organic modifier concentration. With this regeneration procedure, quantitative recovery ($\geq 97\%$) of insulin and total protein can be obtained.

Insulin purification. With the parameters discussed above, a series of laboratory-scale purification studies were conducted before scale-up was pursued. Fig. 3 shows a typical elution profile for the preparative purification of BHI. The charge for this study was derived from the proinsulin process. The loading and elution conditions are outlined in the legend and are similar to those discussed above. The overload condition does not permit resolution of the various components as judged from the UV profile. However, when the collected fractions are subjected to analytical RP-HPLC, separation of insulin-like components from the insulin becomes very clear. Fractions having a purity of $>96\%$ were included in the mainstream. Fig. 4 shows the analytical chromatograms for the column charge and purified mainstream. In addition, a profile for the sidestream is included. It is interesting to note that while the insulin-like components are eluted after the main peak in the preparative system (at higher acetonitrile concentrations and during the column regeneration), these components eluted on either side of the insulin peak in the analytical system. The ion-pairing reagent,

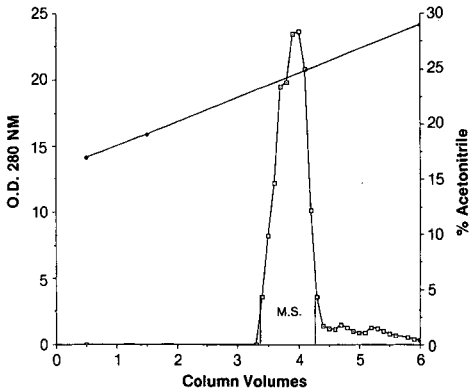

Fig. 3. Preparative chromatogram for BHI. Column, 10-μm Zorbax Process Grade C_8 (15 × 0.94 cm I.D.); load, 153 mg of BHI derived from proinsulin process; gradient, 17 to 29% acetonitrile in 0.25 *M* acetic acid, in 6 CV; flow-rate, 0.3 ml/min. Fractions 3.3 to 4.3 column volumes were pooled (mainstream). Fractions 3.2, 4.4–5.4, and the protein eluted in column regeneration (not shown) were combined (sidestream).

present in the mobile phase of the analytical system, affects the elution order of these components relative to the main insulin peak[30]. The purity of the mainstream in this case is 98.7% compared to *ca.* 91.5% for the starting material. The average mainstream insulin yield for five such preparative experiments was 82%, an additional 15% being present in the sidestream and regeneration solutions, giving an overall insulin yield of 97%.

Scale-up of the purification process

Having optimized the parameters for the insulin purification process on small laboratory columns, we increased column sizes in a series of scale-up experiments. Table I summarizes the column sizes used in these studies. As we progressed through

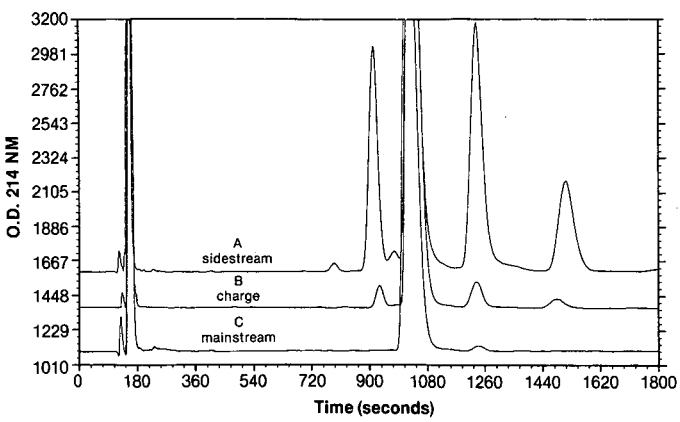

Fig.4. Analytical characterization of BHI purified by RP-HPLC (Fig. 3). Analysis conducted on a Zorbax C_8 column (30 × 0.45 cm I.D.) with pentanesulfonic acid as the mobile phase. Chromatograms: (A) BHI sidestream (purity = 50%), (B) BHI charge (purity = 91.0%), (C) BHI mainstream (purity = 98.7%).

TABLE I

COLUMN SIZES USED FOR SCALE-UP STUDIES

Column size (cm)	*Internal volume (l)*	*Type*	*Insulin load (g)**
15 × 0.94	0.010	Fixed	0.15
30 × 2.2	0.114	Fixed	1.7
50 × 5.0	0.59	Fixed	8.9
45 × 15	8.00	Axial	120
50 × 30	35.0	Axial	525
50 × 45	80.0	Axial	1200

* Assuming 15 g/l.

this series of columns, we could systematically test and modify the column packing procedures as well as the ancillary equipment required for the chromatographic operation. As the column size was increased, the quantity of insulin loaded on column was maintained at approximately 14–15 g/CV. When changing column sizes, the flow-rate and gradient volume were also changed in proportion to the volume of the column. Thus, flow-rates of 1.5 CV/h and gradient slopes of 2%/CV were used as a first approximation. Table II summarizes typical elution conditions and purification results obtained for three different column sizes using chain-derived insulin as the charge material (purity *ca.* 83%). Mainstream purities, recoveries, and volumes were consistent as the process was transferred from the lab to the pilot plant and eventually into the production facility. Minor changes in the gradient slope were necessary to obtain the desired level of purification and mainstream recovery. However, we suppose that these minor changes are due in large part to variations in the type of equipment that is being used for each scale, as well as to subtle changes in the packing, since these studies were carried out with several different lots of packing material.

Throughout the early phases of this project, we realized that if this procedure was to be implemented in a production setting, it would be necessary to purify 400–500 g of insulin in a single run. Given the loadings discussed above, a 30-l column would be required. The complexities of efficiently and reproducibly packing columns

TABLE II

SUMMARY OF SCALE-UP STUDIES

Column size (cm)	*Operation type*	*Operation conditions*			*Mainstream*		
		Flow-rate (CV/h)	*Gradient range (% acetonitrile/CV)*	*Loading*	*Purity (%)*	*Yield (%)*	*Volume (CV)*
15 × 0.94 (10 ml)*	Lab	1.6	17 to 30% (2.2%)	13 mg/ml	98.5	82	1
35 × 15 (6.2 l)	Pilot plant	1.5	13 to 30% (2%)	15 g/l	98.6	79	0.8
57 × 30 (40 l)	Production	1.4	15 to 28% (2.1%)	15 g/l	98.6	83	1.2

* Column volume

of this size with 10-μm particles are considerable. The alternative which we elected was the use of "self-packing", axial compression columns. The advantages of these systems for large-scale chromatography have been discussed previously[41–43]. Of greatest importance to us is that they provide the user with the ability to pack the columns reproducibly with chromatographic media of his/her choice. Since the units are available in a variety of sizes, initial evaluation of the process in a laboratory or pilot plant setting is possible before it is transferred to a production facility. The ease of packing and unpacking the column also makes the system attractive for pilot plant operations, where a variety of products, requiring different chromatographic media, may be processed. In both the pilot plant and production environments, we found that personnel experienced with the equipment and the packing procedure could reproducibly pack columns having over 40 000 plates/m.

Examples of production scale purification. Reversed-phase HPLC purification of BHI, derived from both the chain and proinsulin routes has been successfully conducted in a production environment. The resolving power of this procedure is perhaps best exemplified by the purification of chain-derived insulin, since it contains a number of structurally related components which can amount to 20% of the protein in the preparation. Fig. 5 shows the analytical chromatograms obtained for both the charge and the mainstream. The major insulin-like components have been identified in the charge chromatogram. The purification was accomplished on a 48 × 30 cm I.D. column, with a gradient of 17 to 30% acetonitrile over 6 CV and a flow-rate of 1.4 CV/h (0.8 l/min). The column was loaded with 500 g of BHI. The reduction in insulin-like components in this step is dramatic; the mainstream purity being 98.5% *vs.* 80% in the charge solution, with the mainstream yield being *ca.* 82%. More than 30 lots could be purified using the same packed column. Attempts to isolate insulin, at a similar level of high purity by a combination of intermediate-performance cation- and anion-exchange steps, were unsuccessful. A significant reduction in the levels of ECPs was also obtained in the RP-HPLC step. The ECP content of the charge material is typically in the range of 500–1000 ppm, while the level of ECPs in the reversed-

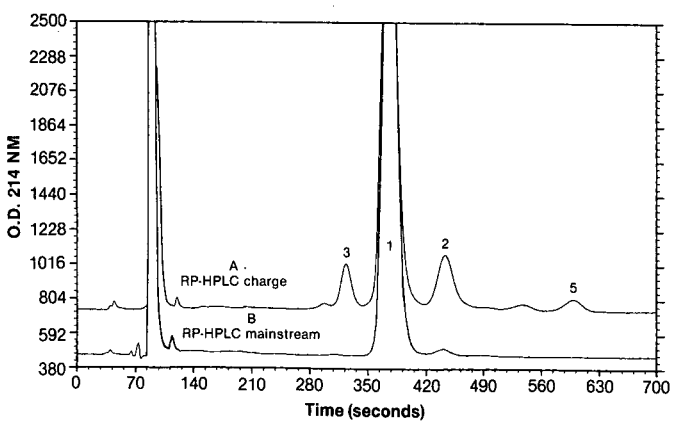

Fig. 5. Analytical characterization of chain-derived BHI, purified on a 30-cm I.D. RP-HPLC column. Analysis conducted on a Zorbax C_8 Reliance cartridge column (8 × 0.4 cm I.D.) with pentanesulfonic acid mobile phase. Chromatograms: (A) BHI charge (purity = 80.0%), (B) BHI mainstream (purity = 98.5%).

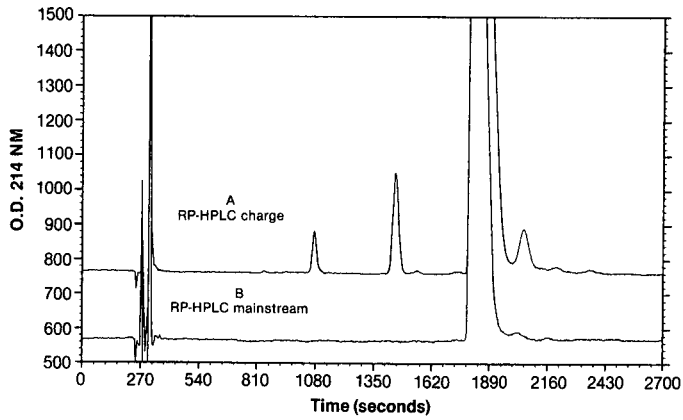

Fig. 6. Analytical characterization of proinsulin-derived BHI, purified on a 30-cm I.D. RP-HPLC column. Analysis conducted on a Zorbax C_8 Reliance cartridge column (8 × 0.4 cm I.D.) with octanesulfonic acid mobile phase. Chromatograms: (A) BHI Charge (purity = 91.5%), (B) BHI mainstream (purity = 99.1%).

phase mainstream is $\leqslant 10$ ppm. A further reduction in ECP levels is accomplished in the subsequent size-exclusion and final crystallization steps.

Proinsulin-derived BHI has also been successfully purified by RP-HPLC on a production scale. Fig. 6 shows the analytical chromatograms for a typical reversed-phase charge and mainstream. The insulin-like components present in the charge are similar to those from the chain process, but they are present at lower levels. In this example, the charge purity is *ca.* 91% and the mainstream is $\geqslant 99\%$. The purification was achieved using a 45 × 30 cm I.D. column, loaded with 500 g of BHI. The elution gradient was from 18 to 29% acetonitrile and was run over 6 CV at a flow-rate of 1.5 CV/h (0.8 l/min).

Insulin purification studies conducted with a 45-cm I.D. axial compression column have given comparable results. The use of the larger-diameter column allows over 1 kg of BHI to be processed in a single run.

Analytical characterization of final insulin crystals. Both chain- and proinsulin-derived RP-HPLC crystals were further purified by size-exclusion chromatography and zinc crystallization before being subjected to a series of assays. The key assay results for typical lots of BHI, derived from both the chain- and proinsulin-processes are summarized in Table III. Data for lots of chain-derived BHI, purified by conventional chromatographic procedures, are also included. The tests indicate a high degree of chemical purity, as evidenced by the excellent HPLC purity, and the low level of potential impurities such as ECPs and endotoxins. Note the improvement in the HPLC purity for the RP-HPLC-purified, chain-derived BHI compared to that from the conventional process. This is especially dramatic in light of the fact that this material was derived from sidestream fractions which were more highly enriched in insulin-like components prior to the reversed-phase purification step.

The final crystals were also found to be free of any siloxane products, which can result from the breakdown of the stationary phase. The presence of siloxanes in preparations of iodinated insulins, purified by RP-HPLC, has been implicated in the

TABLE III

ANALYTICAL CHARACTERIZATION OF BHI

Process	*Purification method*	*Lot*	*Biopotency (units/mg, anhydrous basis)*	*HPLC purity** *(%)*	*ECP*	*Endotoxins (E.U./mg)*	*Siloxanes (ppm)*
Chain	Conventional chromatography	A	28.4	96.1	< 4	< 0.13	–
		B	29.5	95	< 4	0.13	–
	RP-HPLC	C	30.0	98.8	< 4	< 0.18	< 10
		D	27.4	98.7	< 4	< 0.36	< 10
Proinsulin	RP-HPLC	E	28.6	99.0	< 4	< 0.13	< 10
		F	29.0	99.0	< 4	0.13	< 10

* Gradient RP-HPLC[12].

reduced biological activity observed for these preparations[25]. In the present study, the size-exclusion and final crystallization steps could remove these products from the RP-HPLC purified insulin. With this in mind, crystals obtained immediately after RP-HPLC were also analyzed for siloxane products. No siloxanes were detected in these lots during the lifetime of the packed column.

The biological potency shows that there is no difference between the activity of insulin subjected to reversed-phase purification and that obtained from the more conventional procedure. This demonstrates that with careful selection of operational conditions, insulin can be subjected to RP-HPLC purification without adversely effecting its biological potency. Successful clinical trials with insulin derived from the proinsulin process, also indicate its high degree of purity and efficacy[44].

CONCLUSIONS

The studies discussed here indicate that RP-HPLC can be an effective method for the purification of insulin. A high purity, fully active product is obtained in good yields. RP-HPLC serves as a complement to the ion-exchange and size-exclusion steps, thereby lending itself to the multimodal approach to chromatographic purification. By careful integration into the overall purification process, RP-HPLC yields a product which can be readily processed through the remaining purification steps. The process can be effectively scaled up from the laboratory, to the pilot plant, and eventually to a production environment, where multikilogram-quantities of material are produced.

ACKNOWLEDGEMENTS

We wish to thank the many Lilly associates who made significant contributions to this work; in particular, the members of the biosynthetic development, technical service, engineering, pilot plant, and production groups. We would like to acknowledge the contributions of F. S. Schmid to this work. We are also indebted to Dr. E. L. Smithwick for his advice and support throughout the course of this work.

REFERENCES

1 R. E. Chance, J. A. Hoffmann, E. P. Kroeff, M. G. Johnson, E. W. Schirmer, W. W. W. Bromer, M. J. Ross and R. Wetzel, in D. H. Rich and E. Gross (Editors), *Peptides: Synthesis-Structure-Function, Proceedings of the Seventh American Peptide Symposium*, Pierce Chemical Company, Rockford, IL, 1981, pp. 721–728.
2 B. H. Frank, J. M. Pettee, R. E. Zimmerman and P. J. Burck, in D. H. Rich and E. Gross (Editors), *Peptides: Synthesis-Structure-Function, Proceedings of the Seventh American Peptide Symposium*, Pierce Chemical Company, Rockford, IL, 1981, pp. 729–737.
3 M. J. Ross, in J. L. Gueriguian (Editor), *Insulins, Growth Hormone, and Recombinant DNA Technology*, Raven Press, New York, 1981, pp. 33–48.
4 I. S. Johnson, *Science*, 219 (1983) 632–637.
5 J. P. Burnett, in M. Inouye (Editor), *Experimental Manipulation of Gene Expression*, Academic Press, New York, 1983, pp. 259–277.
6 B. H. Frank and R. E. Chance, *Munch. Med. Wschr.*, 125 (Suppl. 1) (1983) 14–20
7 B. H. Frank and R. E. Chance, *Therapeutic Agents Produced by Genetic Engineering "Quo Vadis?" Symposium, Sanofi, May 29–30, Toulouse-Labège* 1985, pp. 138–146.
8 R. D. Johnson, *Fluid Phase Equilibria*, 29 (1986) 109–123.
9 A. Dinner and L. Lorenz, *Anal. Chem.*, 51 (1979) 1872–1873.
10 R. E. Chance, E. P. Kroeff, J. A. Hoffmann and B. H. Frank, *Diabetes Care*, 4 (1981) 147–154.
11 L. F. Lloyd and P. H. Corran, *J. Chromatogr.*, 240 (1982) 445–454.
12 E. P. Kroeff and R. E. Chance, in J. L. Gueriguian, E. D. Bransome and A. S. Outschoorn (Editors), *Proceedings of the FDA-USP Workshop on Drug and Reference Standards for Insulins, Somatropins, and Thyroid-axis Hormones*, The United States Pharmacopeial Convention, Rockville, MD, 1982, pp. 148–162.
13 B. S. Welinder and F. H. Andersen, in J. L. Gueriguian, E. D. Bransome and A. S. Outschoorn (Editors), *Proceedings of the FDA-USP Workshop on Drug and Reference Standards for Insulins, Somatropins, and Thyroid-axis Hormones*, The United States Pharmacopeial Convention, Rockville, MD, 1982, pp. 163–177.
14 J. Rivier and R. McClintock, *J. Chromatogr.*, 268 (1983) 112–119.
15 A. McLeod and S. P. Wood, *J. Chromatogr.*, 285 (1984) 319–331.
16 D. Kalant, J. C. Crawhall and B. I. Posner, *Biochem. Med.*, 34 (1985) 230–240.
17 D. J. Smith, R. M. Venable, and J. Collins, *J. Chromatogr. Sci.*, 23 (1985) 81–90.
18 K. H. Jorgensen, O. Hallund, L. G. Heding, B. Tronier, K. Falholt, U. Damgaard, L. Thim and J. Brange, in J. L. Gueriguian, E. D. Bransome and A. S. Outschoorn (Editors), *Proceedings of the FDA-USP Workshop on Drug and Reference Standards for Insulins, Somatropins and Thyroid-axis Hormones*, The United States Pharmacopeial Convention, Rockville, MD, 1982, pp. 139–147.
19 A. Peter, G. Szepesi, L. Baláspiri and K. Burger, *J. Chromatogr.*, 408 (1987) 43–52.
20 R. D. DiMarchi, H. B. Long, E. P. Kroeff and R. E. Chance, in W. S. Hancock (Editor), *High Performance Liquid Chromatography In Biotechnology*, Wiley, New York, in press.
21 O. Ladrón De Guevara, G. Estrada, S. Antonio, X. Alvarado, L. Guereca, F. Zamudio and F. Bolívar, *J. Chromatogr.*, 349 (1985) 91–98.
22 B. H. Frank, M. J. Beckage and K. A. Willey, *J. Chromatogr.*, 266 (1983) 239–248.
23 S. Linde, B. S. Welinder, B. Hansen and O. Sonne, *J. Chromatogr.*, 369 (1986) 327–339.
24 S. Seino, A. Funakoshi, Z. Fu and A. Vinik, *Diabetes*, 34 (1985) 1–7.
25 A. Ü. Parman and J. M. Rideout, *J. Chromatogr.*, 256 (1983) 283–291.
26 B. H. Frank, A. H. Pekar, J. M. Pettee, E. M. Schirmer, M. G. Johnson and R. E. Chance, *Int. J. Peptide Protein Res.*, 23 (1984) 506–515.
27 G. Vigh, Z. Varga-Puchony, G. Szepesi and M. Gazdag, *J. Chromatogr.*, 386 (1987) 353–362.
28 L. R. Snyder and J. J. Kirkland, *Introduction to Modern Liquid Chromatography*, Wiley, New York, 1979, pp. 202–245.
29 R. L. Jackson, E. W. Shuey, E. L. Grinnan and R. M. Ellis, *Diabetes*, 18 (1969) 206–211.
30 In preparation.
31 J. W. Ross, R. S. Baker, C. S. Hooker, I. S. Johnson, J. R. Schmidtke and W. C. Smith, in J. L. Gueriguian, E. D. Bransome and A. S. Outschoorn (Editors), *Proceedings of the FDA-USP Workshop on Drug and Reference Standards for Insulins, Somatropins, and Thyroid-axis Hormones*, The United States Pharmacopeial Convention, Rockville, MD, 1982, pp. 127–139.

32 *United States Pharmacopeial, USP XXI*, The United States Pharmacopeial Convention, Rockville, MD, 1985, p. 1165.
33 S. Ghodbane and G. Guiochon, *J. Chromatogr.*, 440 (1988) 9–22.
34 J. Brange, *Galenics of Insulin, The Physico-chemical and Pharmaceutical Aspects of Insulin and Insulin Preparations*, Springer-Verlag, Berlin, 1987, p. 54.
35 A. A. Kossiakoff, *Science*, 240 (1988) 191–194.
36 L. R. Snyder and J. J. Kirkland, *Introduction to Modern Liquid Chromatography*, Wiley, New York, 1979, pp. 269–322.
37 D. F. Waugh, *J. Am. Chem. Soc.*, 68 (1946) 247–250.
38 D. F. Waugh, D. F. Wilhelmson, S. L. Commerford and M. L. Sackler, *J. Am. Chem. Soc.*, 75 (1953) 2592–2600.
39 D. F. Steiner, O. Hallund, A. Rubinstein, S. Cho and C. Bayliss, *Diabetes*, 17 (1968) 725–736.
40 R. E. Chance, M. A. Root and J. A. Galloway, *Acta Endocrinologica*, 83 (1976) 185.
41 H. Colin, *Sep. Sci. Techol.*, 22 (1987) 1851–1856.
42 E. Godbille and P. Devaux, *J. Chromatogr. Sci.*, 12 (1974) 564–569.
43 F. W. Karasek, *Res. Dev.*, 228 (1977) 32–36.
44 Eli Lilly and Co., unpublished results.

Journal of Chromatography, 461 (1989) 63–72
Elsevier Science Publishers B.V., Amsterdam — Printed in The Netherlands

CHROMSYMP. 1498

ANALYTICAL PERFORMANCE OF PROCESS-SCALE LIQUID CHROMATOGRAPHY COLUMNS

T. J. GENTILUCCI*, S. I. SIVAKOFF and G. B. COX
E. I. du Pont de Nemours & Co., Inc., Medical Products Department, Glasgow Site, Mailbox 122, Wilmington, DE 19898 (U.S.A.)
and
S. D. STEARNS and M. W. HUTCHINSON
Valco Instruments Co. Inc., P.O. Box 55603, Houston, TX 77255 (U.S.A.)

SUMMARY

The design of process columns with efficiencies equal to those of analytical columns is discussed, including advantages of the use of the same packing material in both. A new design in column hardware has been developed which allows process columns of 50 mm internal diameter to be packed with 10-μm, silica-based materials and to be routinely produced with reduced plate heights of 2.5 or less, yielding column efficiencies of $>$ 40 000 plates/m in 25-cm-long columns. A description of the column design, focused on flow distribution and high-pressure safety considerations is presented. The scale-up from analytical to process chromatography is facilitated by the use of high-efficiency chromatographic materials.

INTRODUCTION

Recent advances in biotechnology, specifically recombinant DNA technology, have given impetus to the production of highly desirable drugs on the gram and kilogram scale. As these products are mostly peptides and proteins, the problems of their purification are complex. This is especially true with regard to the stringent purity requirements imposed upon products of recombinant DNA. As a result, there is an increasing need for high-resolution separation techniques of peptide and protein purification. In many cases, the final purification of these compounds requires the high resolving power of liquid chromatography.

Recent advances in the theory of preparative liquid chromatography have obviously focused on analytical efficiency[1]. For the optimum production rate of a given component in a mixture, it has been demonstrated by Knox and Pyper[1] that the analytical efficiency of the process column should be three times the number of plates required for the preparative separation at the optimum sample load. Thus, for relatively easy separations the efficiency requirements of preparative columns are modest. When more complex separations with small selectivities between the components of interest are considered, the requirement for high plate counts becomes increasingly important. In order to provide this resolving power and to keep column

0021-9673/89/$03.50

dimensions within reasonable bounds[1], it is necessary to use particle sizes in the 5–10-μm range. Such materials are capable of producing high-performance, high-efficiency columns with at least 40 000 theoretical plates/meter.

Although the operating pressures required for large-scale columns, packed with 10-μm particles can be modest, it is often possible to increase the throughput of such columns by operating them at very high flow-rates, trading off their intrinsic high efficiency for speed[2]. In addition, the requirements for packing process columns efficiently dictate the redesign of the hardware to improve the pressure resistance in both packing and operational use of these columns. The maximum pressure tolerance of the currently available hardware is 2000 p.s.i.g. High-performance silica packings routinely require loading pressures in excess of 6000 p.s.i.g.

A cooperative arrangement was set up between E. I. du Pont de Nemours & Co. and Valco Instruments to develop column hardware which meets these requirements. This paper describes the results of that collaboration to develop process-scale columns.

EXPERIMENTAL

Materials and methods

HPLC columns. The analytical and semi-preparative liquid chromatography columns (25 cm × 4.6 mm, 9.4 mm, and 21.2 mm I.D.) were obtained from DuPont (Wilmington, DE, U.S.A.).

The 25 cm × 50 mm I.D. column hardware were manufactured by Valco Instruments (Houston, TX, U.S.A.). These tubes were packed by a proprietary high-pressure slurry technique. A 25 cm × 50 mm I.D. Modcolumn™ was obtained from H. T. Chemicals (St. Louis, MO, U.S.A.). All tubes were packed with two reversed-phase materials, Zorbax® PRO-10 C_8, and Zorbax® PRO-10/300 Protein Plus (C_3) packings. The particle size of both packing materials is 10 μm. These materials were obtained from DuPont. The same lot of packing material was used for all columns of the same type.

Size-exclusion chromatography was performed on Zorbax BioSeries GF-250 columns from DuPont. The columns used were GF-250 (25 cm × 9.4 mm) and GF-250 XXL (25 cm × 50 mm). The GF-250 columns were packed with 4.5-μm, 150-Å PSM-150 Diol material.

HPLC procedure. The reversed-phase C_8 columns were evaluated with a standard test sample of uracil, phenol, 4-chloronitrobenzene, and toluene. The chromatography was performed isocratically with a mobile phase of 80% aq. methanol. Theoretical plates and skew were calculated from the last peak (toluene). The flow-rate of the 4.6-mm column and the 50-mm column were 1.0 ml/min and 90 ml/min, respectively.

The reversed-phase Protein PLUS columns were evaluated for toluene only, with 100% methanol as the mobile phase. The flow-rates of the 4.6-mm column and 50-mm columns were 1.2 ml/min and 110 ml/min, respectively.

Size-exclusion chromatography was performed on the GF-250 columns with 0.2 *M* sodium phosphate buffer (pH 7.0) as the mobile phase in all cases. The flow-rates were 1 ml/min for the 9.4-mm-I.D. column, 4 ml/min for the 21.2-mm-I.D. column, and 18 ml/min for the 50-mm-I.D. column. The injection volumes were varied from 10 μl for the analytical column to 1.5 ml for the process column. The protein test mixture

consisted of thyroglobulin, immunoglobulin G (IgG), bovine serum albumin (BSA), ovalbumin, and ovalbumin, and myoglobin, and it contained sodium azide. The calculated column efficiency was based on the next-to-last peak, myoglobin.

Instrumentation

Chromatography at flow-rates in excess of 40 ml/min was performed on a Varex PSLC-100 (Rockville, MD, U.S.A.) instrument.

Size-exclusion chromatography on the 50-mm-I.D. columns was performed on a DuPont 8800 or SM 80 liquid chromatograph, equipped with a 4X prep-head assembly, capable of flow-rates up to 40 ml/min. The system included a DuPont variable-wavelength detector and a Rheodyne 7125 injection valve (Rheodyne, Cotati, CA, U.S.A.).

Chromatography at flow-rates up to 10 ml/min was performed on a DuPont 8800 liquid chromatograph, equipped with a Rheodyne 7125 injector, a DuPont variable-wavelength detector, and a DuPont 2-pen recorder. A second system, consisting of a LKB (Gaithersburg, MD, U.S.A.) GTI 2150 pump, 2158 LKB detector, Rheodyne 7125 injector, and a LKB 2210 2-pen recorder was also used.

All detector analog data were digitized and archived by a Nelson Analytical (Cupertino, CA, U.S.A.) data system, using software modified in house to generate theoretical plate and skew measurement.

Reagents

Reference proteins were purchased from Sigma (St. Louis, MO, U.S.A.). All other chemicals were reagent-grade or HPLC-grade materials, purchased from J. T. Baker (Phillipsburg, PA, U.S.A.). The reference samples and reagents were used as received, unless otherwise stated.

RESULTS AND DISCUSSION

The decision to make a high-pressure (8000 p.s.i.g. ASME [American Society of Mechanical Engineers] designed) column, which was easy to seal and could mimic the characteristics of an analytical column, was pursued after a thorough review of the available process-scale hardware. The products offered were limited in pressure resistance to 2000 p.s.i.g. These columns also exhibited some or all of the following: recessed frits, double frits, metal or Teflon™ O-rings, poor surface finish, and welded-on flanges. Columns of these types were tested and found to be difficult to use. The Teflon O-rings were easily pinched, and recessed frits made cleaning the end after column packing extremely difficult. A summary of available column hardware is shown in Table I[3].

The safe use of these columns at high pressures for loading and operation in laboratory or plant environments was of the utmost importance. Emphasis on this design was placed in several areas. The sealing mechanism and the wall thickness dictared the pressure ratings. The inlet design, frit thickness, frit placement, and sample distribution were carefully evaluated to optimize column performance. These aspects will be examined in further detail below.

The basic concept of the new column design originated from the oil and gas industry[4]. The Grayloc™ hub is a high-pressure fitting, designed to make joints

TABLE I

COLUMN HARDWARE COMPARISON

	DuPont analytical column	*H.T. Chemicals*	*Amicon*	*DuPont Valco*
Inlet distribution	Cone	Double frit	Dispersion plate	1° Cone
Frit thickness	0.032	0.120	–	0.062
Frit position	Tube end	Recessed	–	Tube end
Pressure rating	8000	2000	3000	4000–8000
ASME design	N/A	No	Yes	Yes
Sealing mechanism	Ferrule	Teflon O-ring	–	Metal taper

between pipes leakproof at pressures in excess of 8000 p.s.i.g. It consists of two shaped collars which are pressed together by a formed clamp. The joint is rendered leakproof by a metal taper seal, machined on the tube of the hub body (see Fig. 1). A backup seal ring of PEEK (polyetheretherketone) is provided to ensure proper sealing.

The first trial involved the use of an externally threaded tube onto which the hub was threaded and capped with a blind hub, containing the frit and end-fitting of the column. This design was tested and found to have adequate sealing capabilities but lacked the precision required for holding the packed bed in place. The high pressures used in loading caused stresses in the threads, which allowed the end hub (cap) to pull away from the frit. Small amounts of packing then escaped from the tube and became lodged between the tube end and the frit and, subsequently, caused column voids and failure.

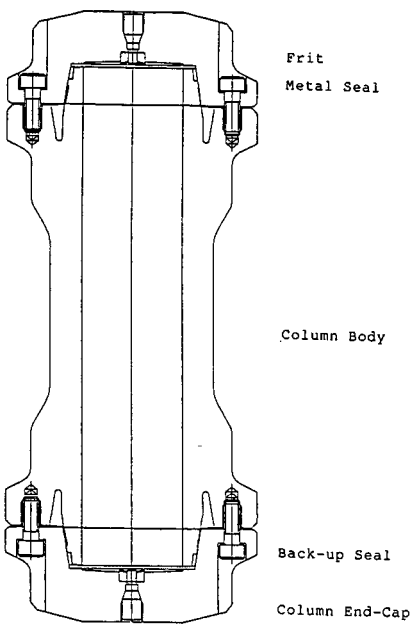

Fig. 1. Drawing of 25 cm × 50 mm I.D. column.

The final design of the ASME high-pressure column consists of a column end-cap, nozzle assembly, flow-distributor plate, 2-μm frit, sealing ring, and tube. The end cap is constructed of 316 stainless steel and designed to withstand pressures of 8000 p.s.i.g. per ASME design codes. The inlet to the end cap is designed to be used with 0.25-in. O.D. tubing with a male nut and ferrule assembly during the high-pressure packing of the column. For chromatography, the 0.25-in. inlet is then converted to 0.125-in. O.D. tubing in order to keep band spreading to a minimum with an internal reducing distribution nozzle assembly.

The distribution nozzle was designed to spread the eluent and sample uniformly to the 2-in. I.D. column. Extensive experimentation on early prototypes showed that jets of mobile phase passing through the frit deformed the packing bed at the top of the column and degraded the column performance. The nozzle has an I.D. of 0.07 in. and directs the flow 65° from the inlet flow through six evenly spaced ports of 0.03 in. I.D. This design effectively prevents the mobile phase from forming jets through the frit and disturbing the packing.

The flow distributor is sandwiched between the column end cap and the frit and is used to distribute the eluent and sample uniformly to the head of the column. The flow distributor was designed to support the frit and keep it flat with respect to the column end. A 1° cone is formed in the distributor to minimize the dead-volume and to mimic the distribution cone commonly used in the Valco 1-in. column end-fittings. Column efficiency, measured as a function of the sample load injected into the column is shown in Fig. 2A and B. These data indicate that the entire cross-section of the 50-mm-I.D. column is being utilized.

The frit used in this column is 0.062 in. thick and sits on the end of the column tube. The frit is compressed between the tube end and the flow-distributor end-cap. The sealing force is sufficient to mark the frit with the impression of the tube end, as is commonly seen in analytical columns. The frit is sufficiently thin to minimize band spreading. The ratio of the thickness to diameter is 0.031 compared to 0.177 for a 4.6-mm analytical column.

The wall thickness of the column tube was selected per ASME code to sustain a pressure of 8000 p.s.i.g. The column seal is made on the metal taper of the end of the tube. This paper seal behaves like the tubing ferrule used in the analytical columns. The column is held together with bolts and clamps to sustain the maximum pressure of 8000 p.s.i.g. The column weight can be reduced by 42 lb by removing the clamps. It can then be used with the bolts only at pressures up to 4000 p.s.i.g., which is more than most current instrument pumps are capable of delivering. The inside wall of the column is polished to a 15 μm RMS (root mean square) finish.

The final inlet design was reached through extensive experimentation. The original design had a straight in-flow through a 1/8-in. tube. The eluent entered the column at a cone-shaped space above the frit. Many columns were loaded and tested, but their performance rapidly declined.

A nozzle was designed with six equally spaced ports to distribute the force of the flow 65° from incoming eluent path. With this inlet design, consistently stable columns were produced.

The distribution of sample across the column was investigated by comparison of the 50-mm column tubes with narrower column tubes under conditions of sample overload. The performance of preparative columns has been extensively evaluated[2] in

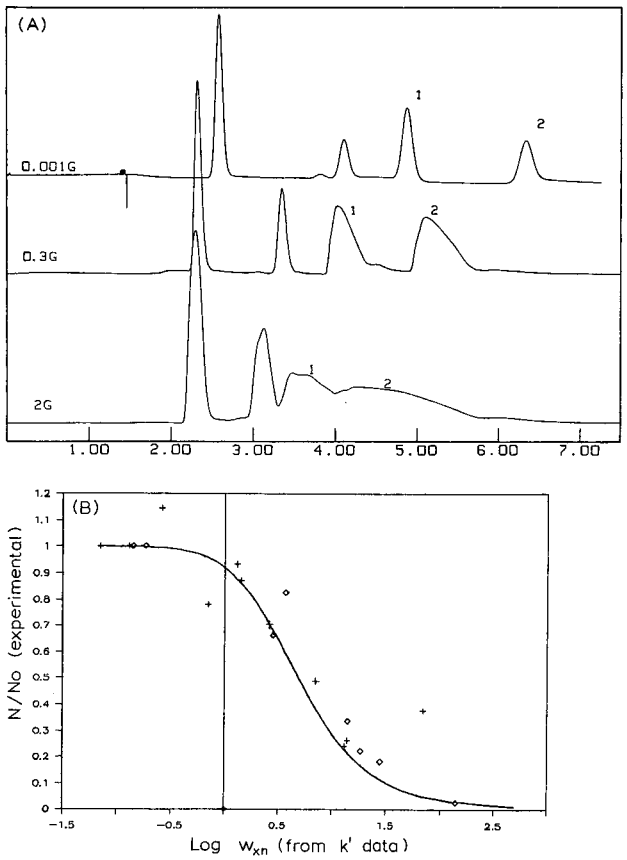

Fig. 2. (A) Comparison of sample loading for 2-phenylethanol (1) and 3-phenylpropanol (2) at sample loads of 0.001 g, 0.3 g and 2.0 g on a PRO-10 C_8 250 mm × 50 mm column. The eluent was 60% aq. ethanol at 145 ml/min. (B) Plot of predictive loading on column with experimental loading for the 50-mm Pro-10 C_8 column used for Fig. 4.

the course of the development of theories relating column performance with sample loads in the domain of non-linear chromatography. That work showed that it is possible to predict the efficiency and retention time of a component in a given column, provided the analytical retention and efficiency are known, as well as the saturation capacity of the column for the particular solute. The latter parameter, usually derived from chromatographic experiments at analytical and preparative loads, is the value of maximum uptake of solute by the column and corresponds to a monolayer of solute molecules on the surface of the packing. In addition, normalizing factors have been found, which allow plotting of all data from columns of quite different sizes on axes of the same scale. For the efficiency, for example, it was shown that the ratio of plate number for the overloaded peak to the analytical plate number was given by the equation

$$\frac{N}{N_0} = \frac{1}{1 + w_{xn}}$$

where

$$w_{xn} = N_0[k'_0/(1 + k'_0)]^2 wx/ws$$

and wx is the sample load, ws the saturation capacity of the column and, N_0 and k'_0 are the analytical efficiency and capacity factor for the peak, respectively. Plotting the plate number ratio against log w_{xn} yields a graph which is normalized such that data from all columns fit the same curve. Hence, if the sample introduced into the preparative column is not well distributed across the cross-section of the column, the points from loading experiments will show a premature overloading effect with a consequent decrease in column efficiency. Alternatively, a good distribution of sample should show a normalized performance close to that of the smaller column sizes.

In order to investigate this aspect of performance, a mixture of two aromatic alcohols, 2-phenylethanol and 3-phenylpropanol, was used as a sample. Columns of 25 cm in length and of 4.6, 9.4, 21.2, and 50 mm in I.D. were used with a range of sample loads. Fig. 2 shows the chromatograms obtained with various loads on the 50-mm column. Data from these experiments were compared with extensive data derived from columns of different dimensions and with different samples. A plot of the ratio of preparative to analytical efficiencies against log w_{xn} is shown in Fig. 2B. It is clear from this plot that the plate numbers for the components under overload conditions are slightly higher for the 50-mm column than for the narrower columns. This implies that the sample is, in fact, spread fully over the diameter of the column. The higher efficiency is probably due to a reduction in the interference by the column walls, the so-called wall effects, on the wider-diameter-column[5].

The analytical performance of the 50-mm-I.D. column was determined for several varieties of silica-based packings and was compared with that of conventional analytical columns, packed with the same batches of packing material. The 50-mm-I.D. columns displayed efficiencies similar to or higher than the equivalent analytical columns operated at the same linear velocity. Thus, it can be concluded that these

TABLE II

COLUMN PERFORMANCE

Column type	*I.D. (mm)*	*Flow-rate (ml/min)*	*Plates*	*Skew*	*h*
PRO-10 C_8	4.6	1.0	10 496	1.05	2.4
PRO-10 C_8	50.0	90.0	13 335	0.19	1.8
PRO-10/300 C_3	4.6	1.0	10 712	1.03	2.4
PRO-10/300 C_3	50.0	90.0	14 238	0.06	1.7
GF-250 Diol	9.4	1.0	17 628	0.58	2.8
GF-250 Diol	50.0	18.0	16 108	0.76	3.1

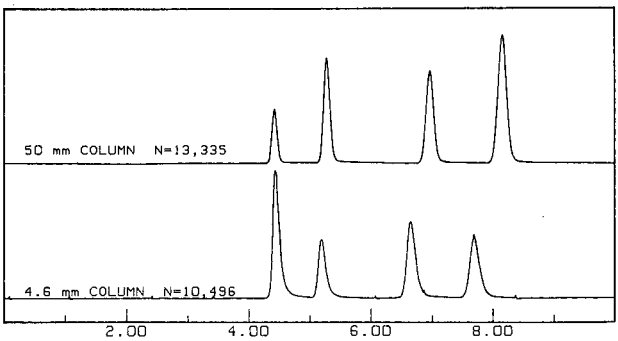

Fig. 3. Scale-up from 250 × 4.6 mm to 250 × 50 mm PRO-10 C_8 columns. Chromatographic conditions as previously described in Experimental.

columns are packed at least as well as, and in some cases, much better than the 4.6-mm-I.D. columns. This equivalence of performance enables simple scale-up of preparative chromatograms from exploratory experiments with small columns to the 50-mm-I.D. columns for large-scale purifications. A summary of the column performance, for columns of 25 cm in length, is shown in Table II.

Fig. 3 shows a direct scale-up separation of PRO-10 C_8, 4.6-mm-I.D. and 50-mm-I.D. columns utilizing a common, small-molecule test sample. The columns were eluted with a mobile phase of 80% aq. methanol at a rate of 0.7 ml/min and 90 ml/min, respectively. The 50-mm-I.D. column efficiency (N) for toluene was in excess of 50 000 plates/m.

The column geometry was tested on a second type of packing to show that the analytical performance of a 50-mm-I.D. column could be used for scaling up from an analytical column of similar performance. A gel column (GF-250), containing a 5-μm, 150-A° pore-size, Diol-bonded silica-based packing, was used to purify a protein mixture. Fig. 4 shows the direct scale-up of a protein separation from a 9.4-mm-I.D. column to a 50-mm-I.D. column. The proteins used for this separation were thyroglobulin, immunoglobulin, bovine serum albumin (BSA), ovalbumin, and

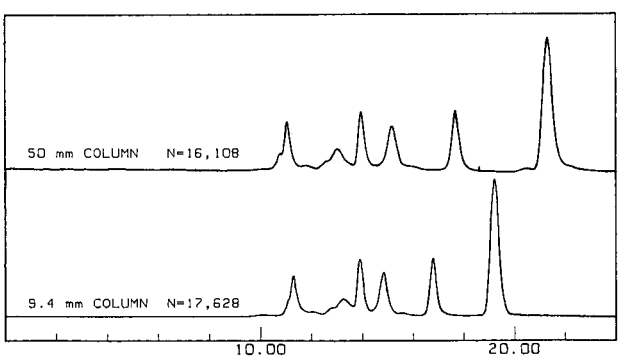

Fig. 4. Scale-up from 25 cm × 9.4 mm to 25 cm × 50 mm GF-250 columns. Chromatographic conditions as previously described in Experimental.

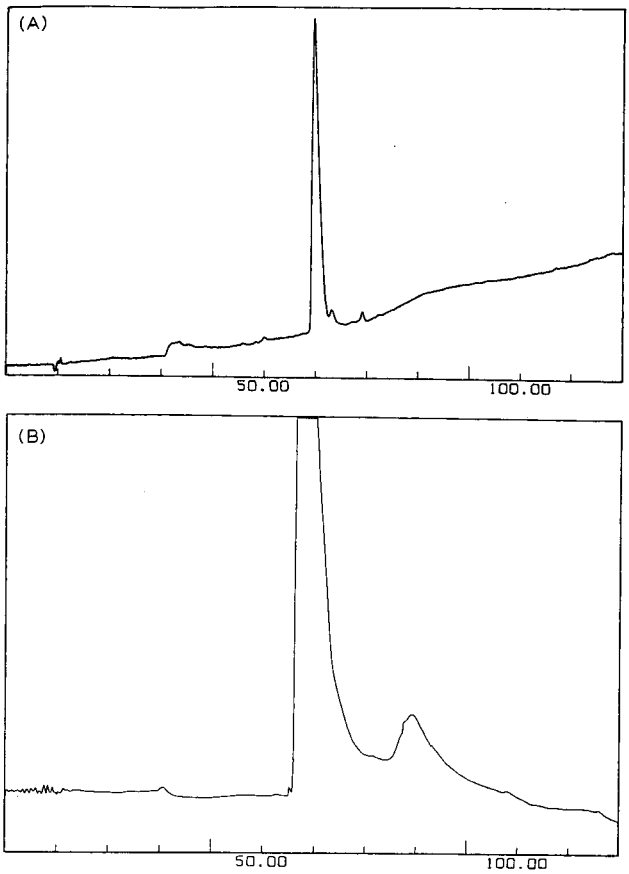

Fig. 5. (A) Analytical chromatogram for purification of bovine insulin (0.01 mg) on a 250 × 4.6 mm PRO-10 C_8 column. Eluent A, 0.1% aq. trifluoroacetic acid (TFA); eluent B, 0.1% TFA in acetonitrile; flow-rate 0.33 ml/min; linear gradient, 18% B to 80% B in 110 min. (B) Process chromatogram for purification of 5.4 g of bovine insulin on a 250 × 50 min PRO-10 C_8 column. Eluent A, 0.1% aq. TFA; eluent B, 0.1% TFA in acetonitrile; flow-rate, linear gradient, 18% B to 80% B in 110 min.

myoglobin. A small molecule, sodium azide, was used as a permeation volume marker. The packing lots were different for the two sizes of columns used in this experiment and account for the difference in relative retention times of the small molecule.

A bovine insulin scale-up under overload condition was performed on a 50-mm-I.D. PRO-10 C_8 column. The analytical chromatogram is shown in Fig. 5A and the preparative chromatogram is depicted in Fig. 5B. The bovine insulin sample was eluted with a 110-min linear gradient of acetonitrile, containing 0.1% trifluoroacetic acid (TFA). The scale-up was accomplished by simply increasing the flow-rate from 0.33 ml/min for the 4.6-mm-I.D. column to 37 ml/min for the 50-mm-I.D. column.

ACKNOWLEDGEMENTS

The authors wish to thank the following people from DuPont, Medical Products: C. J. Janes for the verification of the HPLC gel filtration data, as well as C.

A. DeRose, D. I. Bailey, C. B. Belles, and J. C. Wright. We also thank Dr. Lloyd Snyder from L. C. Resources, Inc. A special thanks to Valco Instrument Co., Inc. for their cooperation; specifically to J. McGee for his painstaking mechanical work.

REFERENCES

1 J. H. Knox and H. M. Pyper, *J. Chromatogr.*, 363 (1986) 1.
2 L. R. Snyder, G. B. Cox and P. E. Antle, *Chromatographia*, 24 (1987) 82.
3 S. I. Sivakoff, T. J. Gentilucci, G. B. Cox, C. A. DeRose, C. B. Belles and D. I. Bailey, presented at the *2nd International Symposium on Preparative and Up-Scale Liquid Chromatography, Baden-Baden, Feb. 1–3, 1988.*
4 Grayloc^{TM} Products Catalog, Gray Tool Company, Houston, TX, August, 1981.
5 J. H. Knox, G. R. Laird and P. A. Raven, *J. Chromatogr.*, 122 (1976) 129.

Journal of Chromatography, 461 (1989) 73–87
Elsevier Science Publishers B.V., Amsterdam — Printed in The Netherlands

CHROMSYMP. 1481

APPLICATION OF AN ASYMMETRICAL FLOW FIELD-FLOW FRACTIONATION CHANNEL TO THE SEPARATION AND CHARACTERIZATION OF PROTEINS, PLASMIDS, PLASMID FRAGMENTS, POLYSACCHARIDES AND UNICELLULAR ALGAE

K.-G. WAHLUND* and A. LITZÉN
Department of Analytical Pharmaceutical Chemistry, University of Uppsala Biomedical Center, Box 574, S-751 23 Uppsala (Sweden)

SUMMARY

The asymmetrical flow field-flow fractionation channel has been improved by introduction of a different sample loading method, downstream central injection, which reduces sample relaxation and focusing time considerably and allows the concentration of material in the channel, thereby enabling the loading of very large sample volumes. The performance of the channel was demonstrated by the separation of a protein from its dimer, retention of nucleic acids, *i.e.*, plasmids and enzymatically cleaved plasmids, hyaluronate and unicellular algae.

INTRODUCTION

Flow field-flow fractionation (flow FFF) is the most universally applicable method among the various modes of FFF techniques[1]. Like all other FFF modes, it is usually performed in a thin, ribbon-like, open channel, through which the flow of a liquid carrier is maintained. When some external force field is applied perpendicular to the channel walls, it may interact with sample molecules or particles and drive them to one of the walls, the accumulation wall, where they will accumulate at some defined distance from that wall. Due to the parabolic velocity profile between the channel walls, samples which are present at different distances from the accumulation wall will obtain different velocities when they migrate with the carrier stream down the channel. This differential migration causes the separation.

In flow FFF the force field is a secondary flow of carrier (cross-flow) through the channel walls, which therefore have to be porous. The universality of the method stems from the fact that the cross-flow interacts with any sample molecule or particle in the channel. One limiting factor, however, is the pore size of the semipermeable membrane used as the accumulation wall. This membrane must be permeable to the carrier but not to the sample, and that sets a lower limit for the molecular weights of samples that can be retained in the channels.

Flow FFF has already been shown to separate macromolecular and particulate water-soluble materials of widely different natures, such as proteins[2], viruses[3],

0021-9673/89/$03.50

polystyrene sulphonates[4] and silica sols[5]. Those separations were, however, quite time-consuming, often requiring many hours.

Recent interest in high-speed separations has led to much shorter elution times through the optimization of the flow-rates[6]. The elution times for sulphonated polystyrenes[6] were much reduced and the modernized techniques were used for size fractionation of humic acids and fulvic acids[7]. Most striking has been the very rapid particle separations obtained by flow/steric FFF of polystyrene latex beads in the size range from 2 to 50 μm in diameter[8,9].

The results presented in this paper were obtained in an "asymmetrical" flow FFF channel[10] which was developed in order to simplify the construction of flow FFF channels and to facilitate studies of their properties. This is possible partly because the asymmetrical channel permits the use of a glass wall which makes the channel contents visible. The theory of the operation of the channel was developed[10] and it was shown that under certain conditions the asymmetrical channel can be operated much like a normal "symmetrical" channel but that sample introduction tends to be more cumbersome, requiring a focusing and relaxation procedure that became very time-consuming for high-molecular-weight samples.

In the present study, the asymmetrical channel has been modified by moving the sample loading point from the inlet end to some point downstream and central in the channel. This downstream central injection serves to decrease the sample focusing and relaxation time, but it also permits the loading of much larger sample volumes. In the previous paper on the asymmetrical channel[10], actual separation was demonstrated only for a mixture of three proteins. In the present paper, results are given for a broader range of sample types. The channel was operated both in normal FFF mode and in steric FFF mode. The latter permits the separation of particles, taking advantage of an hyperlayer effect, which originates in hydrodynamical lift forces acting on the particles[8,9,11].

The performance of the modified channel design will be illustrated by its application to the rapid and efficient elution of a protein and its dimer, retention of plasmids, separation of plasmid fragments, obtained after cleavage by restriction enzymes, size fractionation of an high-molecular-weight polysaccharide (sodium hyaluronate) and size fractionation of unicellular fresh-water algae.

EXPERIMENTAL

The flow FFF channel was of the asymmetrical design recently described[10], which has a porous frit mounted in a Lucite block. The frit is covered in sequence by a semipermeable membrane, a PTFE (polytetrafluoroethylene) spacer, a glass plate and a Lucite block. Bolts are used to clamp the assembly together. Two porous frit (porous ceramics P-6-C; Coors Ceramics, Golden, CO, U.S.A.) mountings were a generous gift from Dr. J. C. Giddings, at the Department of Chemistry at the University of Utah, Salt Lake City. The semipermeable membranes were a cellulosic material (Diaflo Ultrafiltration Membrane Type YM; Amicon, Danvers, MA, U.S.A.). A cut, 28.5 cm long and 1.0 cm wide, with triangular ends was made in the PTFE spacers.

Three channels with different membranes, and of different thicknesses, were assembled. They are numbered I, II and III, and have the following characteristics:

I and II had a YM 10 membrane (nominal molecular weight cut-off of 10 000 for globular molecules), and III had a YM 30 membrane (cut-off at 30 000). Channel I had a nominal spacer thickness of 0.032 cm, giving a nominal volume of 0.86 ml, II had a nominal spacer thickness of 0.030 cm and a nominal volume of 0.81 ml and III had a nominal spacer thickness of 0.050 cm and a volume of 1.4 ml. The void volume of channels I and II were determined by injection of copper sulphate as described earlier[10], and was found to be 0.86 and 0.79 ml, respectively. Inlet and outlet holes in the glass plate (made of float-glass) were positioned at a distance of 28.50 cm from each other and fitted with PTFE tubing, as described earlier[10]. The inlet tubing was 1 mm I.D., and the outlet tubing was 0.3 mm I.D. and 8 cm long. The channels were positioned vertically in order to avoid gravitational sedimentation from contributing to the retention of particles.

Sample loading was made through a third hole, positioned 4.0 cm downstream from the inlet hole. It was fitted with PTFE tubing (8 cm × 0.3 mm I.D.) and connected to a Model 7125 sample injection valve (Rheodyne, Cotati, CA, U.S.A.) coupled to an LKB 2150 HPLC pump (Pharmacia LKB Biotechnology, Bromma, Sweden). Sample loops were from 10 to 500 μl in volume. The total hold-up volume between the sample loop and the channel was about 35 μl. The carrier inlet flow was delivered from a Beckman 114M Solvent Delivery System or an Altex 110A Pump (both from Beckman Instruments, Berkeley, CA, U.S.A.). Fluorometric detection of the eluate was performed on-line by a Schoeffel FS 970 L.C. Fluorometer (Kratos Analytical, Ramsey, NJ, U.S.A.). It was equipped with a xenon lamp FSA 170 and a xenon lamp power supply FSA 190 (Kratos Analytical), which were kindly loaned from Pharmacia Therapeutics (Uppsala, Sweden). Absorptiometric detection was performed by a SpectroMonitor III spectrophotometric detector (LDC, Riviera Beach, FL, U.S.A.), set at 280 nm for proteins, 260 nm for plasmids and 420 nm for the algae. The main detector response from the algae is believed to be due to light scattering by the algal cells. The three-way and four-way manual switching valves (see Fig. 1) were of Types SRV-3 and SRV-4 (Pharmacia, Uppsala, Sweden). The needle valve N1 was a Micro Metering valve SS-22RS2 (Whitey, Highland Heights, OH, U.S.A.). The needle valves N2 and N3 were Fine Metering valves SS-SS1 (Nupro, Willoughby, OH, U.S.A.).

The operating procedures followed those given previously[10] with exceptions due to the introduction of the new sample loading procedure. With valves V1 and V3 (Fig. 1) set for the relaxation/focusing mode, sample loading was effected by having pump 2 work at a flow-rate usually of 0.05 ml/min except for large volume samples (> 100 μl) when it was 0.25 ml/min. The flow from pump 2 was maintained for a time sufficient to load the complete sample into the channel. This usually required a volume of twice the loop volume and the hold-up volume. Sample volumes greater than 500 μl were obtained by repeated filling of the loop.

Fig. 2 illustrates the flow patterns in the channel.

Human serum albumin (HSA) Fraction V was from Sigma (St. Louis, MO, U.S.A.). The plasmids were kindly supplied by the Department of Pharmaceutical Microbiology (University of Uppsala, Uppsala) and Pharmacia Biotechnology. Dextran and sodium hyaluronate, tagged with fluorescein, were kindly supplied by Pharmacia Ophthalmics (Uppsala, Sweden). They were reported to have weight-average molecular weights of $\approx 150\,000$ and 79 500 daltons respectively. Samples of

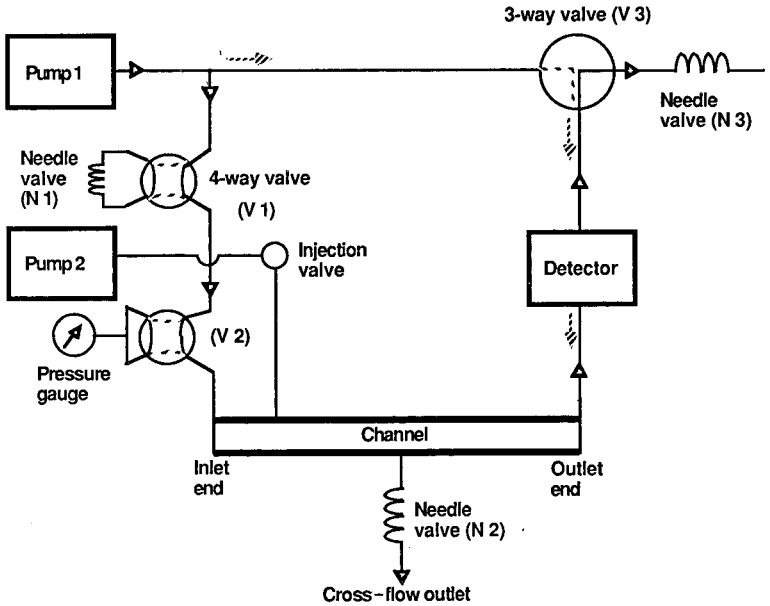

Fig. 1. Schematic drawing of apparatus for flow FFF with asymmetrical channel. The flow directions indicated are used for elution. The dashed lines and arrows show the flow directions during sample loading, relaxation and focusing. Simultaneous switching of valves V1 and V3 is used to shift between focusing/relaxation and elution mode. By switching valve V2 the pressure in the channel can be read. The needle valve N1 is used to adjust the focusing point. Adjustment of N2 and N3 determines the ratio between the cross-flow-rate and channel outlet flow-rate.

various species of algae were kindly donated by the Department of Limnology (University of Uppsala, Uppsala) and were suspended in a culture medium or resuspended in the carrier. The carrier was a Tris–HNO_3 buffer (pH 7.4), ionic strength 0.1, containing 0.02% sodium azide with the addition of 1 m*M* EDTA for the plasmid experiments.

RESULTS AND DISCUSSION

The data treatment follows that of ref. 10 and the following symbols are used: z' = focusing point (distance from inlet end), $\dot{V}_c'$ = cross-flow-rate during relaxation, $\dot{V}_c'$ = cross-flow-rate during elution, $\dot{V}_{out}$ = flow-rate at channel outlet end, t^0 = void time and t_R = retention time.

Downstream central sample injection

The previous study[10] of the asymmetrical channel showed that sample relaxation is done best by a so-called opposing-flow relaxation which involves focusing of the sample to a point some distance (a few cm) down the channel. To obtain a narrow starting zone of the sample, it is then required that it migrates from the sample loading point at the inlet end down to the focusing point. It was shown

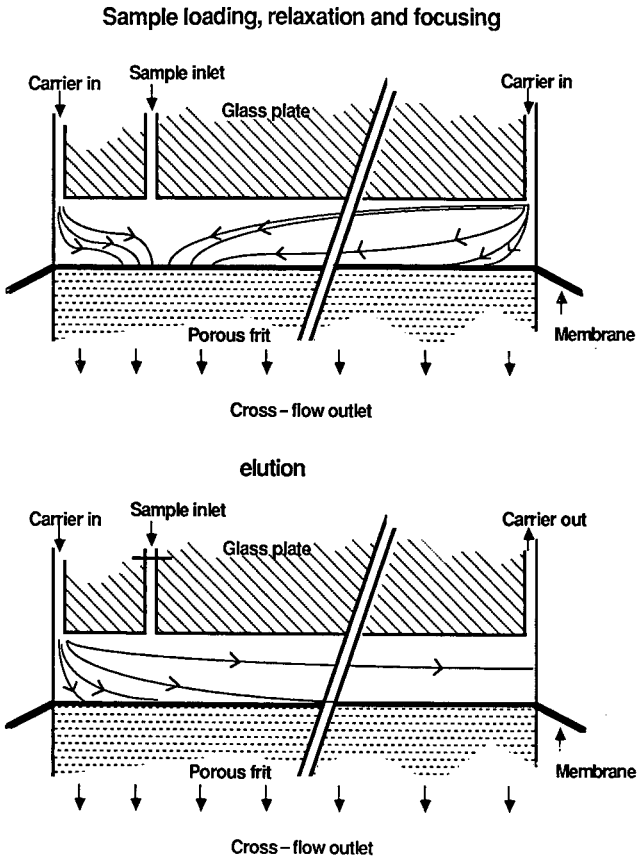

Fig. 2. Illustration of the function of the asymmetrical flow FFF channel in sample loading, relaxation/focusing mode and in elution mode. Streamlines are only approximate.

theoretically[10] that this would require an inconveniently long time for high-molecular-weight samples having a low diffusion coefficient and therefore a low migration velocity. The obvious way to reduce focusing time is to load the sample directly at the predetermined focusing point. This was done by inserting a sample loading tube into the glass plate a few cm downstream from the channel inlet end and on the centre line of the channel. Sample loading is then accomplished while the flowstreams in the channel are in the opposing-flow relaxation mode. The focusing point, regulated by the relative magnitude of the two opposing flowstreams, is preferably located a few mm downstream from the sample loading point. This is done in order to prevent the sample-loading flowstream from flushing away sample material, already loaded, from the focusing point. Experiments with a coloured sample (Blue dextran) showed that the visible zone length of the starting zone became about 5 mm. The zone length will depend on the magnitude of the sample loading flow-rate relative to the opposing flow-rates. The loaded sample exhibited a more or less elliptical zone shape. With this new sample loading technique, the total time for loading, focusing and relaxation of

small-volume samples can be kept below 2.5 min, even for high-molecular-weight samples, as demonstrated in the following paragraphs.

The downstream central injection has two more advantages.

(1) It will allow the loading of large sample volumes, because they will be compressed in the focusing procedure. Very large sample volumes may require long loading times because the sample-loading flow-rate must be sufficiently low in relation to the opposing flows in order to keep the starting zone small. As much as 5 ml of a sample have been loaded in a channel having a void volume of only 0.8 ml.

(2) The other advantage is that the sample is loaded on the central line of the channel and may not reach the edges of the channel, even during the elution. Therefore, the influence of adverse "edge effects"[12] may be decreased.

Separation of protein monomer and dimer

The separation of proteins by flow FFF has been demonstrated a number of times. Early efforts[13,14] were very time-consuming (often several hours), and the resolution was always limited by higher-than-predicted plate heights, H (ref. 14). When flow optimization similar to that in ref. 6 is used in order to obtain rapid elution, in combination with high efficiency, the plate height still appears high for the three proteins separated[10]. The flow optimization is based on the concomitant increase in longitudinal flow velocity and cross-flow velocity[6] so that the increased longitudinal velocity is balanced by an increased retention level. Because the non-equilibrium plate height decreases with the square of the channel thickness, w^2, at constant retention degree[6], it was thought that the 0.03-cm thick channel used in this work would lead to improved plate heights, as compared to the 0.05-cm thick channel used in the previous work[10].

The fractogram in Fig. 3 shows the elution of a sample of HSA under flow conditions that give rapid elution and very high retention, corresponding to 29 void times for the main peak, which is the albumin monomer. The second peak, well resolved from the monomer, is thought to be the dimer of albumin. This fractogram also appears to represent one of the most efficient elutions by flow FFF; the number of plates, calculated for the monomer peak, is 518, which corresponds to an average plate height, $\bar{H}$, of 0.47 mm. In some other, more optimized experiments, even higher plate numbers, 700, were obtained. The longitudinal velocity decreases linearly from the inlet end to the outlet end[10] resulting in a decreased local plate height. Still, it can be shown that the observed plate height is very much above the expected non-equilibrium plate height, even if this is calculated for the longitudinal velocity valid at the inlet.

It is expected that conditions similar to that of Fig. 3 can be used to separate and detect higher aggregates of proteins, perhaps using flow programming to optimize the elution time of the higher aggregates.

Retention of plasmids and separation of plasmid fragments

In working with plasmids and other nucleic acids there is often a need to fractionate the material according to size. The dominating fractionating procedure is agarose gel electrophoresis, involving, first, the electrophoretic separation in the gel, and then the extraction of the separated zones from the gel by, *e.g.*, isotachophoresis[15]. Such procedures, although requiring relatively simple equipment, tend to be rather time-consuming. Separation would be much faster with flow FFF, which has the

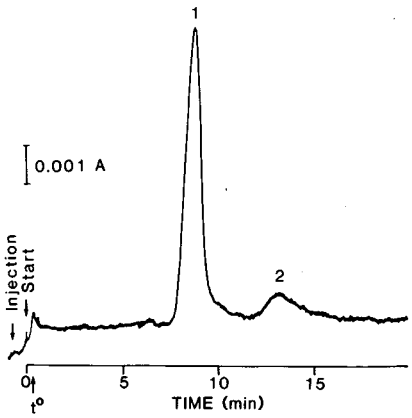

Fig. 3. Separation of the monomer and dimer of HSA (channel II). Peaks: 1 = monomer; 2 = dimer. Sample: 10 mg/ml HSA, ≈1 μl. Relaxation/focusing: focusing point (distance from inlet; z' = 4.1 cm, $\dot{V}_c'$ = 4 ml/min; elution, $\dot{V}_c$ = 5.37 ml/min, $\dot{V}_{out}$ = 0.72 ml/min, t^0 = 0.30 min. Observed diffusion coefficient for peak 1 is $5.8 \cdot 10^{-7}$ cm^2/s.

further advantage that the material can be kept in any suitable aqueous solution and that the procedure is easily handled or automated. Another advantage is that simply by manipulating the flow-rates one can apply the method to materials over a very broad size range. The resolution of flow FFF may not be as high as that of electrophoresis, and the method seems therefore most suitable for the fractionation of material showing relatively large differences in molecular weight. Separations of plasmids and other DNA material have been demonstrated by Kirkland and co-workers[16] by sedimentation FFF, which is capable of higher separation selectivity than flow FFF. However, the sedimentation FFF apparatus is much more complex and expensive.

Figs. 4 and 5 demonstrate the retention of two different plasmids. The elution time of each of them was easily adjusted by chosing flow-rates based on an approximate estimation of their diffusion coefficients. The retention ratios were 0.077 and 0.050, respectively. When higher retention levels were chosen, the peaks tended to show some fronting.

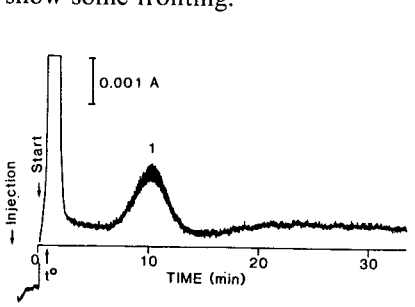

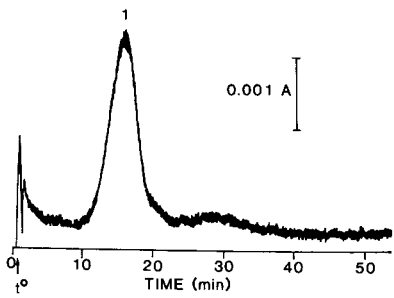

Fig. 4. Isolation of the plasmid pGL 101 (2390 base pairs) by flow FFF (channel II). Sample: 0.5 μg/μl pGL 101, 4 μl. Relaxation/focusing: z' = 4.1 cm, $\dot{V}_c'$ = 4 ml/min. Elution: $\dot{V}_c$ = 0.27 ml/min, $\dot{V}_{out}$ = 0.75 ml/min, t^0 = 0.78 min.

Fig. 5. Isolation of the plasmid pBR 322 (4360 base pairs) by flow FFF (channel II). Sample: 0.5 μg/μl pBR 322, 2 μl. Other conditions as in Fig. 4.

One obvious application of flow FFF would be the isolation of, *e.g.*, small fragments from the large fragments that are obtained upon cleavage of plasmids with restriction enzymes. Such experiments are illustrated in Fig. 6. A plasmid, pTL 830, was cleaved by three different enzymes or enzyme combinations in order to give fragments of the sizes given in the Figure legend. The elution curves correspond very well with predictions regarding both the position and the relative area of the peaks obtained from the two fragments. The resolution of the two peaks increases with increasing difference in the number of base pairs and the peak-area ratio changes approximately in proportion to the ratio of the number of base pairs in each fragment. The poor shape of the large fragments may be due to the very high retention of these peaks, in one case corresponding to 65 void times. Flow programming[6] can easily be used to speed up the elution of highly retained peaks.

The large response sometimes occurring close to the void time was also seen in blank experiments; it is perhaps caused by pressure pulses. In some cases, such as the fractogram at the bottom right, an extra response close to the void time but not occurring in the blank was obtained; this is possibly caused by some impurity in the sample and requires further study.

Positive identifications of the small fragments were obtained by agarose gel electrophoresis for peaks 1 in the two top fractograms. The third case was not tested. The purity and identity of the large fragment in the top right fractogram was tested by collecting a 5-ml fraction. It was reinjected and eluted under the same conditions as for the parent fractogram. As expected, peak 1 had now disappeared, and the area of the

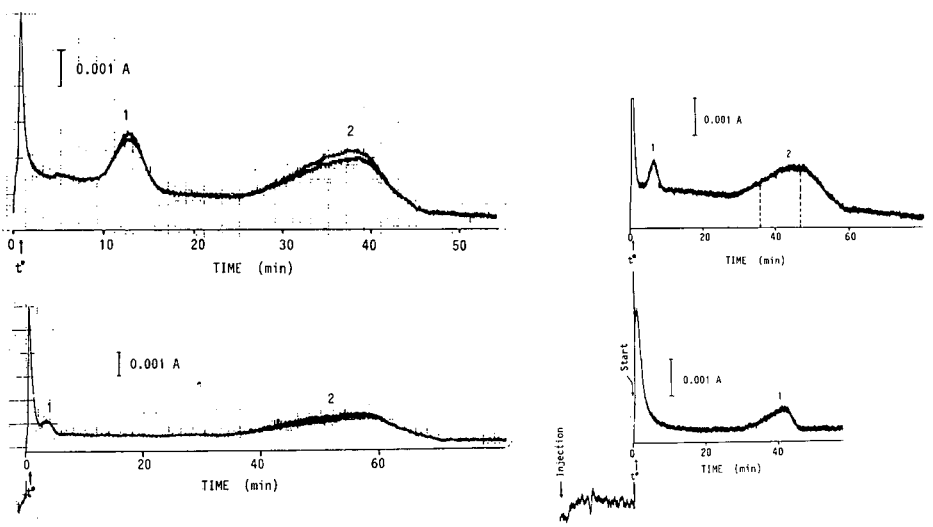

Fig. 6. Fractograms of pTL 830 (5300 base pairs) after cleavage with different restriction enzymes. Reinjection of collected large-volume fraction (channel II). Sample at top and bottom left, and top right: digests of 0.4 μg/μl pTL 830, 4 μl. Relaxation/focusing; $z' = 4.7$ cm, $\dot{V}_c' = 4$ ml/min. Elution; $\dot{V}_c = 0.33$ ml/min, $\dot{V}_{out} = 0.66$ ml/min, $t^0 = 0.85$ min. Left top: cleavage with EcoR1 (1200 base pairs + 4100 base pairs). Left bottom: cleavage with BamH1 and Bg1II (200 base pairs + 5100 base pairs). Right top: cleavage with PstI and Bg1II (700 base pairs + 4600 base pairs). Right bottom: reinjection of a 5-ml fraction, collected from peak 2 of the right top fractogram, as indicated by the dashed lines. Injection flow: 0.25 ml/min for 21 min.

reinjected peak corresponds reasonably well to the area of the fraction collected. This procedure demonstrates perfectly how very large sample volumes can be loaded in the asymmetrical flow FFF channel.

These results show the great potential of the application of flow FFF to the size fractionation of nucleic acids.

Size fractionation of hyaluronate

The study of the size distribution of macromolecules is often an important step in their characterization. The traditional method for this has been size-exclusion chromatography (SEC). However, the pore size of the packing material sets a limit to the upper value for the molecular weight of samples that can be retained in such a column.

With flow FFF one can fractionate, on an analytical scale, macromolecules and particles ranging from molecular weights as low as about 1000 to particle sizes of about 50 μm[1]. Thus, flow FFF can be not only a complement to SEC but can also be used to perform macromolecular fractionations in the high-molecular-weight range where SEC has limited applicability. Sodium hyaluronate is used in eye surgery due to its viscoelastic properties. Its molecular weight can vary greatly, but the material used for medical work usually has an average molecular weight of about $5 \cdot 10^6$ daltons. Fractionation of such material by SEC tends to be very time-consuming due to the high molecular weights which usually require low flow-rates. Also, the elution times tend to vary with sample concentration[17] and it is known that the diffusion coefficient is concentration-dependent[18].

Since natural sodium hyaluronate has a low detection sensitivity in UV absorption and refractive index measurements we had to use sodium hyaluronate tagged with fluorescein for this study. This can be detected at low concentrations by a fluorescence detector. The weight-average molecular weight (MW) of this sample was 79 500 daltons. The properties of the native, and often more high-molecular-weight, sodium hyaluronate may be different from those of the tagged sodium hyaluronate, but the latter may nevertheless serve as a model compound in an initial study of the possibilities and problems in using flow FFF for an high-molecular-weight polysaccharide. Application to native sodium hyaluronate will require the development of more sensitive detection techniques.

Effect of sample amount

Since the parameter that governs retention in flow FFF is the diffusion coefficient of the sample[4], which can be calculated from the elution time[10], we studied the observed diffusion coefficients as a function of the sample amount (Fig. 7). We found that less than 6 μg of hyaluronate must be injected in order to obtain diffusion coefficients that are independent of sample amount. Such low amounts require very sensitive detection, which was provided by the fluorescence detector. With the dextran sample, the limiting sample amount was 2 μg.

Fractionation and reinjection

Hyaluronate is a polydisperse material, exhibiting a broad range of molecular weights. If such a sample is eluted through the flow FFF channel, its contents will be fractionated along the elution time axis, the smallest molecules being eluted first. The

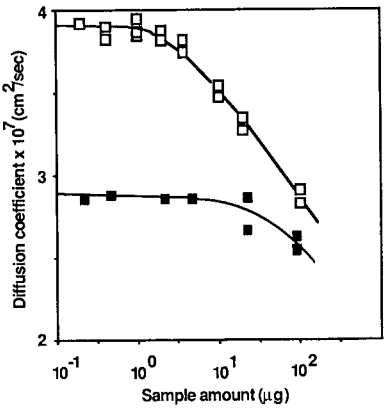

Fig. 7. Sample concentration effects on the observed diffusion coefficient. □ = Fluorescein-tagged dextran, weight-average MW ≈150 000 daltons. Relaxation/focusing: $z' = 4.3$ cm, $\dot{V}_c' = 2.5$ ml/min. Elution: $\dot{V}_c = 0.95$ ml/min, $\dot{V}_{out} = 0.53$ ml/min, $t^0 = 0.89$ min, $t_R = 6.9$–8.8 min (channel I). ■ = Fluorescein-tagged sodium hyaluronate, weight-average MW = 79 500 daltons. Relaxation/focusing: $z' = 4.2$ cm, $\dot{V}_c' = 4$ ml/min. Elution: $\dot{V}_c = 0.80$ ml/min, $\dot{V}_{out} = 0.44$ ml/min, $t^0 = 0.95$ min, $t_R = 7.8$–9.4 min (channel II).

resulting elution profile will be a more or less broad peak. Peak broadening is also caused by non-equilibrium processes during the elution, and it needs to be shown that the observed peak width is the result of the fractionation process. This can be done by isolating small fractions and reinjecting them into the channel[19]. The elution profiles resulting from the injection of such fractions should then occur at elution times identical to those at which each fraction was collected. Such experiments are summarized in Fig. 8.

The reinjected fractions all occur at elution times that coincide well with the collection time. This shows that a true size fractionation of the hyaluronate has been obtained.

Measurement of the diffusion coefficient

Since the diffusion coefficient is the property of the sample that determines the retention and it may be necessary to compare the results of fractionations obtained

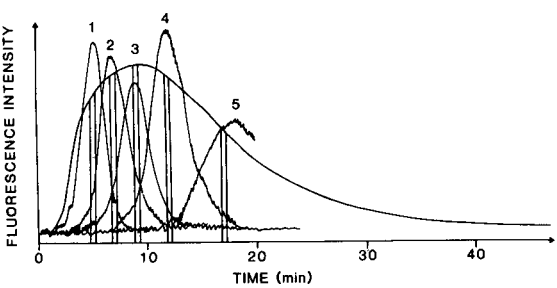

Fig. 8. Fractionation of sodium hyaluronate, followed by reinjection of collected fractions. The broad curve is from the parent sample from which five narrow fractions, 0.25 min wide, were collected (indicated by the vertical lines) and reinjected. The five fractions were analyzed under the same conditions as for the parent sample. Parent sample: hyaluronate tagged with fluorescein (4.5 μg in 98 μl). Relaxation/focusing: $z' = 4.3$ cm, $\dot{V}_c' = 4$ ml/min. Elution: $\dot{V}_c = 0.80$ ml/min, $\dot{V}_{out} = 0.47$ ml/min, $t^0 = 0.89$ min (channel II).

under different flow conditions which may give different retention levels, it may be advantageous to transform the elution time curves into a frequency distribution of diffusion coefficients. Such results are demonstrated in Fig. 9. Each fractogram was digitized and the abscissa was transferred to give diffusion coefficients using the known quantitative relationships between elution time and diffusion coefficient[10]. The ordinate values were multiplied by $\Delta t_R/\Delta D$, where Δt_R is the difference in elution time for consecutive digitized points and ΔD the corresponding difference in diffusion coefficient. Each distribution was normalized so that the area under the curve equalled unity. This transformation ensures that the correct proportionality between the sample mass and the area under the curve is maintained (*cf.*, refs. 7 and 20). One of the curves was obtained with large sample load (92 μg, *i.e.*, above the limit in Fig. 7) and the other two with smaller loads (<2 μg, *i.e.*, below the limit). The distribution curve for the large amount deviates, because the above mentioned limit of sample amount was exceeded. Experiments made with loads lower than 6 μg gave distribution curves that coincided irrespective of the flow conditions in the channel. However, deviations were observed for very high and low retention levels. This shows that conditions can be found under which consistent values of diffusion coefficients can be obtained. These results indicate that flow FFF may be used for size fractionation of relatively high-molecular-weight water-soluble polysaccharides.

Fractionation of unicellular fresh-water algae

The principle of steric FFF can be used to separate particles in the size range 1–100 μm[21,22]. The resolution in steric FFF depends directly on the particle radius because the particles are driven by the cross flow to contact the accumulation wall, and their equilibrium level above the wall is thus determined by their own physical size. Successful separations of human and animal cells, which have sizes in the range mentioned, were demonstrated by the use of sedimentation/steric FFF[23]. Extremely

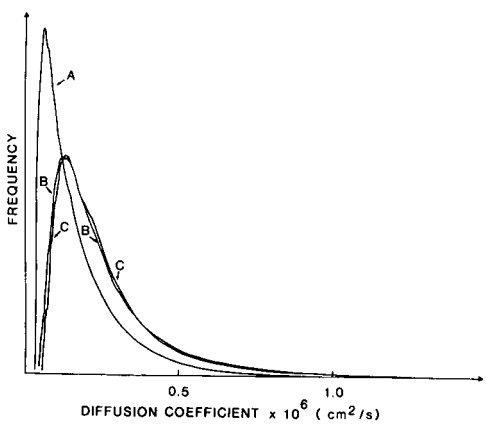

Fig. 9. Distribution of the observed diffusion coefficient of hyaluronate, tagged with fluorescein. Effect of sample amount (channel II). Relaxation/focusing: $z' = 4.3$ cm (B+C) and 4.6 cm (A), $\dot{V}_c' = 4$ ml/min. (A) Sample amount, 92 μg; elution, $\dot{V}_c = 0.82$ ml/min, $\dot{V}_{out} = 0.43$ ml/min, $t^0 = 0.93$ min. (B) Sample amount, 2.2 μg; elution, $\dot{V}_c = 0.80$ ml/min, $\dot{V}_{out} = 0.42$ ml/min, $t^0 = 0.97$ min. (C) Sample amount, 0.92 μg; elution, $\dot{V}_c = 0.55$ ml/min, $\dot{V}_{out} = 0.37$ ml/min, $t^0 = 0.20$ ml/min.

rapid fractionation of polystyrene particles with sedimentation/steric FFF at very high flow-rates, in combination with high field strength, showed[11] that the separation process is influenced by a hydrodynamical lift force which tends to focus the particles at some distance from the accumulation wall which is greater than the particle radius. Such a situation fulfils the requirements for hyperlayer FFF[24] which was also termed focusing FFF[25,26]. The hyperlayer mode is also operational in flow/steric FFF, resulting in very rapid separations of polystyrene beads in the range of 2–50 μm in diameter[8,9].

It is of interest to attempt the application of this principle to the separation of biological cells having sizes in the range mentioned. One such application might be the size fractionation of unicellular fresh-water algae. In limnology one is often faced with the problem of obtaining a size fractionation of natural water samples as a means of indicating the variations in cell size of algae. It is known, *e.g.*, that zooplankton feed on unicellular algae and that different species of zooplankton prefer different species of algae, depending on algal cell size.

A few different species of algae were chosen for study. The experiments followed the principles given earlier for the operation of flow/steric FFF[8,9], with the channel positioned vertically to avoid the influence of gravity on the retention[9]. However, the previous studies were made in the symmetrical flow FFF channel, where the cross-flow velocity is uniform over the channel thickness. In the present work, with the asymmetrical channel, the decreasing cross-flow velocity obtained on going from the accumulation wall to the "upper" wall[10] makes the balance between the presumed lift forces and the cross-flow-induced drift towards the accumulation wall different from that in the symmetrical channel. When the equilibrium distance of the particles from the accumulation wall is greater than 0.06 of the channel thickness, they are in a region of changing cross-flow velocity gradient[10]. This would correspond to a retention ratio [the elution time, t^0, of an unretained component (void time) divided by the elution time of the retained sample, t_R] of >0.35, *i.e.*, very weak retention (corresponding to about <3 void times). It is above this retention ratio that different results are expected in the two types of channels. However, none of the results presented below was obtained under such conditions.

Table I shows the different species of algae used for this study together with their approximate sizes. The size distribution of these algae may be rather broad resulting in relatively wide elution profiles. Moreover, the real cell size may be somewhat different from the value given. The results obtained are rather preliminary, and a more detailed study would require much more work to characterize the original samples with respect to cell shape, size and size distribution.

TABLE I
SPECIES OF UNICELLULAR FRESH-WATER ALGAE STUDIED

Species (and abbreviation)	*Approximate average size (μm)*
Chlorella sp. (Csp)	2.5
Chlorella homosphaera (Ch)	5.3
Haematococcus capensis var. *borealis* (Hcb)	15
Haematococcus droebackiensis (Hd)	21

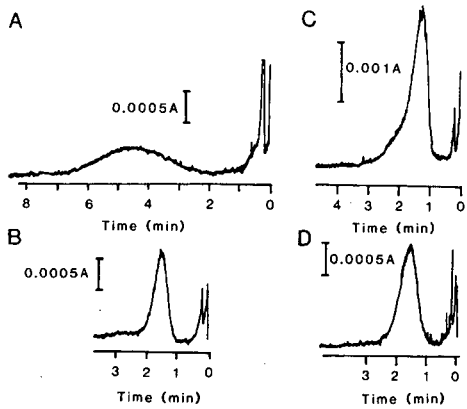

Fig. 10. Fractograms of the four different species of unicellular algae of Table I (channel III). Relaxation/focusing: $z' = 4.3$ cm, time = 3 min, $\dot{V}_c' = 3.0$ ml/min. (A) Csp, $\dot{V}_c = 0.43$ ml/min, $\dot{V}_{out} = 5.06$ ml/min, $t^0 = 0.23$ min;(B) Ch, $\dot{V}_c = 0.29$ ml/min, $\dot{V}_{out} = 7.32$ ml/min, $t^0 = 0.16$ min; (C) Hcb, $\dot{V}_c = 0.29$ ml/min, $\dot{V}_{out} = 6.98$ ml/min, $t^0 = 0.17$ min; (D) Hd, $\dot{V}_c = 0.34$ ml/min, $\dot{V}_{out} = 7.06$ ml/min, $t^0 = 0.17$ min.

Fig. 10A–D show fractograms of the individual samples. The adjustment of retention times for each species was based on the experience gained in the previous study[8,9]. Larger cells would be eluted before smaller cells, and this is the expected elution order in steric FFF. Increases in retention time can be obtained by either increasing the "field strength", *i.e.*, the cross-flow rate, $\dot{V}_c$, or decreasing the longitudinal flow-rate ("channel flow-rate"), as measured at the outlet of the channel, $\dot{V}_{out}$. An increased cross-flow rate increases the retention degree, whereas the main effect of decreasing the channel flow-rate is to decrease the longitudinal carrier velocity. The flow conditions were adjusted so that the elution times of the various samples of algae fell below *ca.* 5 min.

Rather well shaped peaks were obtained from each population of algae. Data in Fig. 10B–D were obtained under similar conditions and the separation of the three species was slight. They all were eluted at approximately the same time, although their sizes range from 5 to 21 μm. However, they were clearly retained, because the void time was only a fraction of a minute under the conditions used. Thus, efforts to separate mixtures of these species failed. Much more detailed studies are needed in order to find the reason for the low resolution. However, the smallest species (Csp) shows a much longer elution time than the others, and when it is mixed with the largest species (Hd) the two populations can be partially fractionated, as shown in Fig. 11. The decrease in elution time of Csp on going from Fig. 10 to Fig. 11 depends on the change in flow-rates. The lower cross-flow rate decreases the retention degree (increases the retention ratio), while the higher channel flow-rate speeds up elution.

The identity of the zones obtained was checked in only one case by optical microscopy. A collected fraction of Hcb contained cells of algae of the same size and shape as that in the original sample, and there is no reason to believe that the other response curves obtained would be caused by anything else than the respective sizes of algae. The fractogram of Fig. 11 was reproduced several times with the same result.

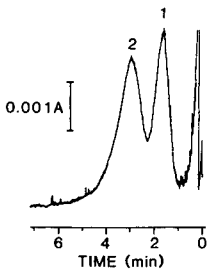

Fig. 11. Fractogram of a mixture of two populations of unicellular algae (channel III). Peaks: 1 = Hd (21 μm); 2 = Csp (2.5 μm). Relaxation/focusing: z' = 4.4 cm, time = 3 min, $\dot{V}_c'$ = 3.0 ml/min. Elution: $\dot{V}_c$ = 0.30 ml/min, $\dot{V}_{out}$ = 7.06 ml/min, t^0 = 0.17 min.

The successful and rapid separation in Fig. 11 gives hope that flow/steric FFF eventually can be developed into a new method of analyzing the size distribution of cells.

ACKNOWLEDGEMENTS

We gratefully acknowledge the help of Drs. R. Bell and L. Bern (Department of Limnology at the University of Uppsala) for the gift of samples of algae and many fruitful discussions. Dr. G. Swedberg (Department of Pharmaceutical Microbiology, University of Uppsala) kindly provided cleaved plasmids and performed the electrophoretic identification. Dr. P. Månsson (Pharmacia Ophtalmics, Uppsala) kindly supplied the dextran and hyaluronate.

REFERENCES

1 J. C. Giddings, *Sep. Sci. Technol.*, 19 (1984–1985) 831.
2 J. C. Giddings, F. J. Yang and M. N. Myers, *Anal. Biochem.*, 81 (1977) 395.
3 J. C. Giddings, F. J. Yang and M. N. Myers, *J. Virol.*, 21 (1977) 131.
4 J. C. Giddings, G. C. Lin and M. N. Myers, *J. Liq. Chromatogr.*, 1 (1978) 1.
5 J. C. Giddings, G. C. Lin and M. N. Myers, *J. Colloid Interface Sci.*, 65 (1978) 67.
6 K.-G. Wahlund, H. S. Winegarner, K. D. Caldwell and J. C. Giddings, *Anal. Chem.*, 58 (1986) 573.
7 R. Beckett, Z. Jue and J. C. Giddings, *Environ. Sci. Technol.*, 21 (1987) 289.
8 J. C. Giddings, X. Chen, K.-G. Wahlund and M. N. Myers, *Anal. Chem.*, 59 (1987) 1957.
9 X. Chen, K.-G. Wahlund and J. C. Giddings, *Anal. Chem.*, 60 (1988) 362.
10 K.-G. Wahlund and J. C. Giddings, *Anal. Chem.*, 59 (1987) 1332.
11 T. Koch and J. C. Giddings, *Anal. Chem.*, 58 (1986) 994.
12 J. C. Giddings and M. R. Schure, *Chem. Eng. Sci.*, 42 (1987) 1471.
13 J. C. Giddings, F. J. Yang and M. N. Myers, *Science (Washington, D.C.)*, 193 (1976) 1244.
14 J. C. Giddings, F. J. Yang and M. N. Myers, *Anal. Chem.*, 48 (1976) 1126.
15 L.-G. Överstedt, K. Hammarström, N. Balgobin, S. Hjerten, U. Pettersson and J. Chattopadhyaya, *Biochem. Biophys. Acta*, 782 (1984) 120.
16 L. E. Schallinger, J. E. Gray, L. W. Wagner, S. Knowlton and J. J. Kirkland, *J. Chromatogr., Biomed. Appl.*, 342 (1985) 67.
17 C. Abad, L. Braco, V. Soria, R. Garcia and A. Campos, *Br. Polymer J.*, 19 (1987) 501.
18 T. C. Laurent, M. Ryan and A. Pietruszkiewicz, *Biochim. Biophys. Acta*, 42 (1960) 476.
19 J. C. Giddings and F.-S. Yang, *J. Colloid Interface Sci.*, 105 (1985) 55.
20 J. C. Giddings, M. N. Myers, F. J. F. Yang and L. K. Smith, in M. Kerker (Editor), *Colloid and Interface Science*, Vol. IV, Academic Press, New York, 1976, p. 381.

21 J. C. Giddings and M. N. Myers, *Sep. Sci. Technol.*, 13 (1978) 637.
22 M. N. Myers and J. C. Giddings, *Anal. Chem.*, 54 (1982) 2284.
23 K. D. Caldwell, Z.-Q. Cheng, P. Hradecky and J. C. Giddings, *Cell Biophysics*, 6 (1984) 233.
24 J. C. Giddings, *Sep. Sci. Technol.*, 18 (1983) 765.
25 J. Janča and J. Chmelík, *Anal. Chem.*, 56 (1984) 2481.
26 J. Janča, *Makromol. Chem., Rapid Commun.*, 8 (1987) 233.

Journal of Chromatography, 461 (1988) 89–93
Elsevier Science Publishers B.V., Amsterdam — Printed in The Netherlands

CHROMSYMP. 1459

GRADIENT ELUTION IN HOLLOW-FIBRE FLOW FIELD-FLOW FRACTIONATION

ALF CARLSHAF* and JAN ÅKE JÖNSSON
Department of Analytical Chemistry, University of Lund, P.O. Box 124, S.221 00 Lund (Sweden)

SUMMARY

The scope of the technically simple hollow-fibre version fo field-flow fractionation has been extended to gradient elution. An arrangement of two liquid chromatographic pumps and a gradient controller permits sample introduction, relaxation and elution under gradient conditions to be conveniently performed. The retention times experimentally found can be theoretically explained. The technique was applied to model separations of polystyrene latex beads and plasmids.

INTRODUCTION

In a previous paper[1] we presented a novel version of flow field-flow fractionation (FFF) in which the classical parallel-plate channel is exchanged for a circular hollow fibre. This configuration appears to have several advantages, such as better mechanical properties and easier connection to liquid chromatographic equipment. Also, the flow-rates can be more precisely controlled. This, in addition to providing higher accuracy, also permits the application of gradient elution techniques.

In gradient elution techniques, the temperature or solvent composition is continuously varied in order to extend the number of components that can be separated within a given time. In the various FFF techniques, the external force field is varied to obtain the corresponding effect[2]. In sedimentation FFF, the gravity field, *i.e.*, the centrifuge speed is varied during elution. This is now a standard technique[3,4]. In thermal FFF the temperature difference between the plates is varied[5,6], while the parameter varied in flow FFF is the lateral flow-rate. This has been described for the parallel-plate system by Wahlund *et al.*[7].

In this paper we present a simple method for creating gradients in the hollow-fibre flow FFF system. The hollow-fibre unit is connected to a commercially available liquid chromatographic system, designed for gradient operation. The computerized, independent control of pump speeds facilitates the application of gradient techniques to this type of FFF.

EXPERIMENTAL

Materials

The hollow-fibre flow FFF system was previously described in detail[1]. Briefly, it

0021-9673/89/$03.50

is based on the FPLC™ range of liquid chromatographic equipment (Pharmacia LKB, Uppsala, Sweden). The hollow fibre, either a Model H10-P100-20 or H5-P100-43 with inner diameters of 500 and 1100 μm, respectively (Amicon, Danvers, MA, U.S.A.) was encapsulated in an empty, modified column tube (Model C 16, Pharmacia), see Fig. 1. The sample was injected with an injection valve (internal volume 5 μl, Model 7410; Rheodyne, Cotati, CA, U.S.A.), equipped with a pneumatic control unit.

The detector was a fixed wavelength (254 nm) UV detector (UV-1, Pharmacia). The axial and the radial liquid flows were created by two syringe pumps (Model P-500, Pharmacia), connected to the fibre. The pumps were further connected to a computerized control unit (LCC-500, Pharmacia), which was programmed to control the pumps independently as well as the injection valve.

The gradient elution technique in the hollow-fibre system was tested with polystyrene latex beads, 0.09, 0.30 and 0.80 μm in diameter (Sigma, St. Louis, MO, U.S.A.) and the plasmid PUC-8 from the Molecular Biology Division, Pharmacia.

A buffer solution of 0.01 *M* Tris–HCl containing 1 m*M* EDTA, 100 m*M* sodium chloride, 0.04% sodium azide and 0.1% Triton X-100 at pH 7.0 served both as diluent for the latex beads and as a carrier in the separation. The same buffer, without Triton X-100, was used for the PUC-8.

Methods

In Fig. 2 the pumping sequence for sample introduction, relaxation, restoration and gradient elution is shown. The principle is the same as that described in the previous paper[1], except that the cross-flow, F_2, was now decreased during Phase IV.

Briefly, the sample was introduced into the fibre (Phase I) with the axial flow, F_1 (the flow pumped by pump P_1) at a constant rate (typically 30 or 80 μl/min). During Phase II (the relaxation period), F_1 was decreased to about 20 μl/min. During this time, the sample was allowed to migrate to its equilibrium distance from the fibre wall and was axially compressed. In Phase III, F_1 was increased to the flow-rate used in elution. The radial flow, F_2, which was controlled by pump P_2, was kept constant during Phases I–III and decreased successively during Phase IV. Thus, components with a wide range of particle sizes can be separated with optimum resolution. It is possible to use an initial radial flow that is considerably higher than under isocratic conditions, and this speeds up the relaxation process.

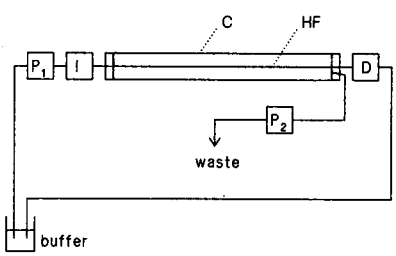

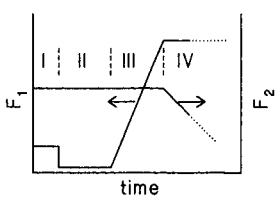

Fig. 1. Experimental set-up, including pumps P_1 and P_2, injection valve I, photometric detector D, porous hollow fibre HF and column tube C. For details, see the text.

Fig. 2. Pumping sequence for the pumps P_1 (creating the axial flow, F_1) and P_2 (creating the radial flow, F_2). The phases of the operation are: sample introduction (I), relaxation (II), restoration (III) to gradient elution condition (IV).

THEORETICAL

The general theory for hollow-fibre flow FFF was developed previously[1] for isocratic conditions and is here modified for gradients. The retention is governed by the Péclet number, Pé, which is defined as:

$$\text{Pé} = \frac{u_r(R) \cdot R}{D} \tag{1}$$

In eqn. 1, $u_r(R)$ is the radial flow-velocity component at the fibre wall, *i.e.*, at the distance R from the centre of the fibre, R being the radius of the fibre and D the diffusion coefficient of the sample particles to be separated. Assuming (a) that $u_r(R)$ is constant along the fibre and with time, and (b) that Pé > 50, the retention time, t_R, is given by (eqn. 14 in ref. 1)

$$t_R = \frac{1}{R_f} \cdot \frac{L}{\bar{u}_z} = \frac{\text{Pé}}{4} \cdot \frac{L}{\bar{u}_z} \tag{2}$$

where L is the length of the fibre and R_f is the retention ratio, *i.e.*, the velocity of the particles in question relative to $\bar{u}_z$ which is the axial flow velocity, averaged over the fibre cross-section.

The retention volume under gradient conditions is found as the solution of the following integral equation[2]

$$L = \int_0^{t_R} R_f \cdot \bar{u}_z \cdot dt = \int_0^{t_R} \frac{4}{\text{Pé}} \cdot \bar{u}_z \cdot dt \tag{3}$$

where $u_r(R)$ and, thus, Pé vary with time. A simple, linear gradient with a constant, initial period is expressed by:

$$u_r(R) = u_0 \qquad 0 < t < t_1 \tag{4}$$

$$u_r(R) = u_0 + b(t - t_1) \qquad t > t_1$$

With this, an explicit expression for t_R is readily obtained for the case where $t_R > t_1$

$$t_R = \frac{u_0}{b} \exp\left[\frac{\left(L - \frac{t_1 \cdot 4 \cdot \bar{u}_z}{\text{Pé}(0)} \right) \text{R} \cdot \text{b}}{4 \cdot \text{D} \cdot \bar{u}_z} \right] - 1 + t_1 \tag{5}$$

where Pé(0) is the initial Péclet number (at $t < t_1$). The case where $t_R < t_1$ is equivalent to isocratic (non-programmed) conditions and consequently trivial.

From eqn. 5, the expected retention times can be estimated. The use of eqn. 2 instead of more elaborate equations[1], which remove the restrictions necessary for eqn. 2, leads to an underestimation of the retention time in the isocratic mode. Thus,

also eqn. 5 may be expected to underestimate t_R. For more accurate calculations, numerical calculations are necessary.

RESULTS AND DISCUSSION

To evaluate the potential of gradient elution, polystyrene latex beads with different particle diameters (0.09 and 0.30 μm) were separated. Linear gradients from 40 to 0 μl/min in 15, 30 and 45 min and from 70 to 0 μl/min in 30 and 45 min were used. Baseline separation was obtained in all cases. In Fig. 3 two examples are shown.

Retention times, calculated with eqn. 5, agree fairly well with experimentally obtained values. The agreement is best (all differences < 1 min) if the value used for the fibre radius, R, is 300 μm in the cases where $u_0 = 40$ μl/min and 330 μm when $u_0 = 70$ μl/min. The nominal radius of the fibre used was 250 μm. Also, in the previous work[1] it was necessary to use a fibre radius larger than the nominal one in the calculations. Consequently, it seems as if the fibre expanded due to the pressure difference between the inside and the outside, which is created by the radial flow pump (P_2). This assumption was further substantiated by the observation that the dead (hold up) time also increased with the radial flow[1].

A time-optimized separation of three types of latex beads (0.09, 0.30 and 0.80 μm) with a three-segment gradient is shown in Fig. 4. The total time needed for elution was 45 min.

A separation of these components under isocratic conditions would require approximately 160 min (calculated as the sum of the relaxation time and the retention time of the largest particles with the lowest practical flow-rate of pump P_2).

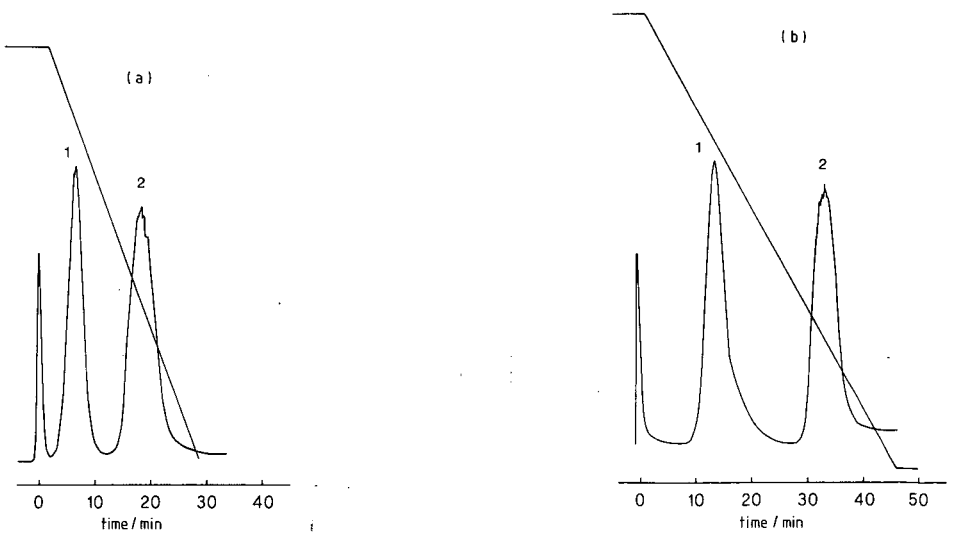

Fig. 3. Separation of polystyrene latex beads, 0.09 μm (peak 1) and 0.30 μm (peak 2) in diameter. Fibre radius: 250 μm. $F_1 = 200$ μl/min. (a) F_2 = gradient from 40 to 0 μl/min in 30 min; (b) F_2 = gradient from 70 to 0 μl/min in 45 min.

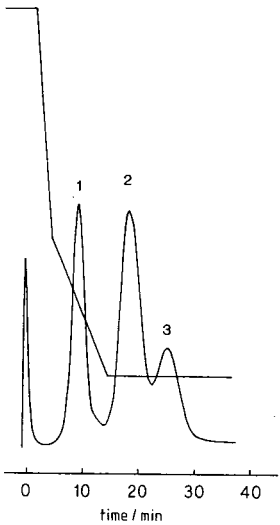

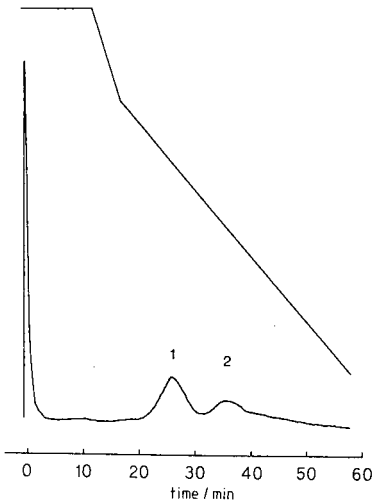

Fig. 4. Separation of polystyrene latex beads, 0.09, 0.30 and 0.80 μm in diameter (peaks 1–3). Fibre radius: 250 μm. F_1 = 200 μl/min; F_2 = 70 μl/min (initially), decreased as shown to the final value of 14 μl/min.

Fig. 5. Separation of the monomer (peak 1) and dimer (peak 2) of the plasmid PUC-8. Fibre radius: 550 μm. F_1 = 500 μl/min; F_2 = 100 μl/min (initially), decreased as shown to the final value of 20 μl/min.

As an application of the system described, we optimized a gradient separation of the monomer and dimer of the plasmid PUC-8, as shown in Fig. 5. Baseline separation was obtained in *ca.* 45 min. A similar separation of the plasmid PBR-325 was published by Kirkland and Yau[8], who used the technique of time-delayed exponential-sedimentation FFF. Using the technically much simpler hollow-fibre flow FFF technique, comparable results are obtained.

ACKNOWLEDGEMENT

We thank the Swedish Board of Technical Development (STU) and Pharmacia LKB AB for generously supporting this work.

REFERENCES

1 J. Å. Jönsson and A. Carlshaf, *Anal. Chem.*, 61 (1989) 11.
2 J. C. Giddings and K. D. Caldwell, *Anal. Chem.*, 56 (1984) 2093.
3 J. J. Kirkland, S. W. Rementer and W. W. Yau, *Anal. Chem.*, 53 (1981) 1730.
4 J. C. Giddings, P. S. Williams and R. Beckett, *Anal. Chem.*, 59 (1987) 28.
5 J. C. Giddings, L. K. Smith and M. N. Myers, *Anal. Chem.*, 48 (1976) 1587.
6 J. J. Kirkland, S. W. Rementer and W. W. Yau, *Anal. Chem.*m 60 (1988) 610.
7 K.-G. Wahlund, H. Winegarner, K. D. Caldwell and J. C. Giddings, *Anal. Chem.*, 58 (1986) 573.
8 J. J. Kirkland and W. W. Yau, *Science (Washington, D.C.)*, 218 (1982) 121.

Journal of Chromatography, 461 (1989) 95–101
Elsevier Science Publishers B.V., Amsterdam — Printed in The Netherlands

CHROMSYMP. 1447

FOCUSING COUNTERPARTS OF ELECTRICAL FIELD FLOW FRACTIONATION AND CAPILLARY ZONE ELECTROPHORESIS

ELECTRICAL HYPERLAYER FIELD FLOW FRACTIONATION AND CAPILLARY ISOELECTRIC FOCUSING

WOLFGANG THORMANN*,*, MILLICENT A. FIRESTONE, MARK L. DIETZ, TED CECCONIE and RICHARD A. MOSHER

Center for Separation Science, University of Arizona, Building 20, Tucson, AZ 85721 (U.S.A.)

SUMMARY

Efforts are currently being undertaken to develop electrical hyperlayer field flow fractionation (EHFFF) and capillary isoelectric focusing (CIEF) as fully instrumental approaches for the analysis of amphoteric samples, such as peptides and proteins. In these techniques a pH gradient parallel to an applied electric force field is employed for sample discrimination according to differences in isoelectric points. EHFFF is performed in a thin ribbon-like channel containing a mobile phase with the electric field perpendicular to the flow direction, whereas CIEF utilizes a quiescent solution with the electric field parallel to the column axis. The principle of EHFFF, the design of EHFFF instrumentation and first results are discussed together with the differences and similarities between EHFFF and CIEF.

INTRODUCTION

Efforts are currently being undertaken in our laboratory to develop electrical hyperlayer field flow fractionation (EHFFF) and capillary isoelectric focusing (CIEF) as fully instrumental approaches for the analysis of amphoteric samples, such as peptides and proteins. EHFFF and CIEF represent the focusing counterparts of electrical field flow fractionation (EFFF) and capillary zone electrophoresis (CZE), respectively[1,2]. CZE[3–7] is conducted in a continuous buffer where the samples are the only discontinuities present. Under the influence of an electric field, sample zones migrate without exhibiting any steady state behavior and, thus, their shape and position continuously change with time (Fig. 1a). In this technique, separation is based upon differences in net mobility. In CIEF[8–12], sample components are sorted according to their isoelectric points in an equilibrium gradient. Typically, a mixture of carrier ampholytes is exposed to an electric field in order to establish a gradient of pH

* Present address: Department of Clinical Pharmacology, University of Bern, Murtenstrasse 35, CH-3010 Bern, Switzerland.

0021-9673/89/$03.50

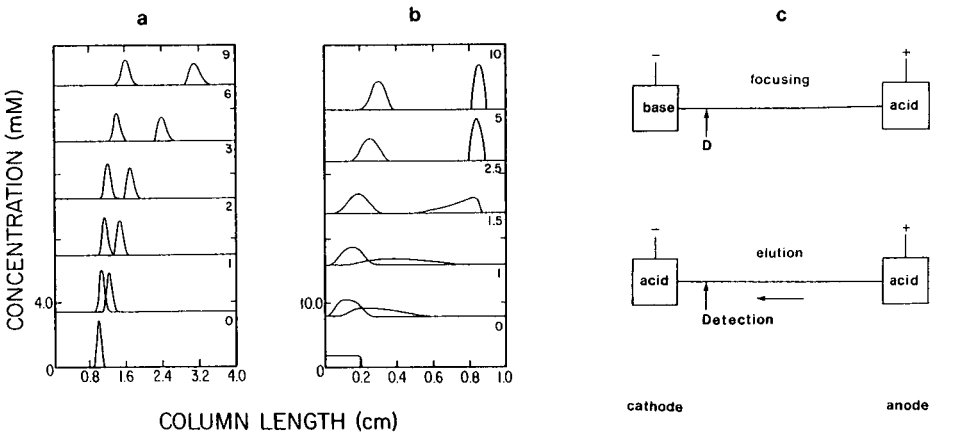

Fig. 1. Schematic representation of the separation dynamics of two sample components in CZE (a) and CIEF (b), together with the two sequential stages in CIEF, focusing and elution (c). D = detector. Computer simulated concentration profiles of two sample components in CZE (a) and CIEF (b) are shown at the time point indicated in the upper righthand corner of each plot. Each successive time point is offset from the previous one by a constant amount for presentation purposes.

increasing from anode to cathode. Proteins and other amphoteric compounds can be separated in this gradient provided their isoelectric points are sufficiently different. Unlike CZE, CIEF sample zones attain a stationary steady state (Fig. 1b). Thus, for detection by an on-column sensor placed toward the column end, the separative pattern must be mobilized [*e.g.* electromobilized (Fig. 1c)] after focusing.

The development of field flow fractionation (FFF) in the last two decades represents an important contribution to the separation of macromolecules and particles[13–15]. FFF is based on the simultaneous influence of an external force field and a flow velocity profile on the constituents undergoing separation. In EFFF, for example, an electric field applied perpendicular to the flow direction acts as the differential retarding force (Fig. 2a)[16–21]. This force causes charged solute molecules to accumulate in layers of distinct thickness near one channel wall. Each solute is then transported by flow along the channel at a rate determined by the mean thickness of its layer. In hyperlayer field flow fractionation (HFFF) separation is based on partitioning by the concomitant presence of an applied force field and an equilibrium gradient[2,22]. In contrast to regular FFF methods, most of the focused solutes in HFFF do not reach the walls of the channel, thereby excluding interactions between the sample components and the column walls. In EHFFF a pH gradient is used in addition to the electric field, the same gradient combination as in CIEF. Amphoteric samples are condensed in layers away from the walls, where the pH value equals their isoelectric point, as is illustrated in Fig. 2b. To date, sedimentation HFFF[2,22–26], in which a density gradient is used in addition to the sedimentation field, and flow HFFF[27], have been discussed. In this paper, the use of an electrically produced pH gradient across the thin dimension of an FFF ribbon-like channel is described. The design of EHFFF instrumentation and first results are discussed together with the differences and similarities between EHFFF and CIEF.

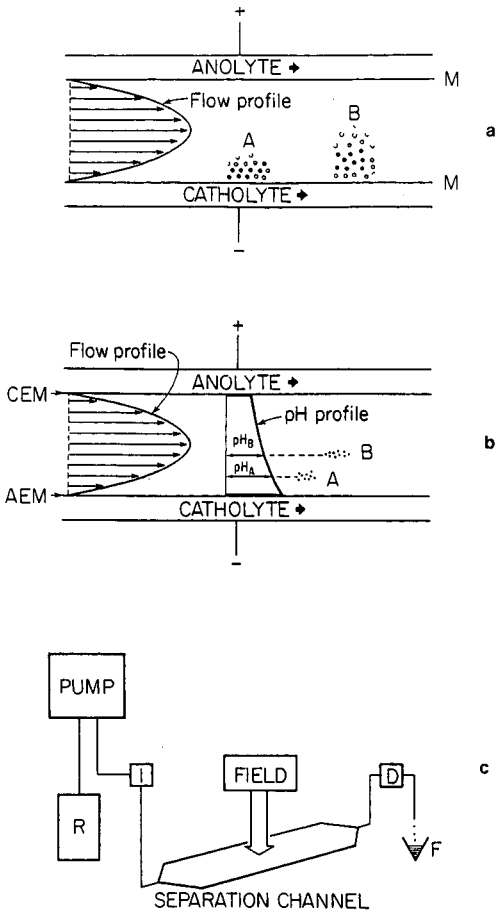

Fig. 2. Schematic representation of (a) EFFF, (b) EHFFF and (c) an FFF apparatus. M = dialysis membrane; CEM = cation-exchange membrane; AEM = anion-exchange membrane; R = buffer reservoir; I = sample injection port; D = detector; F = fraction collector.

EXPERIMENTAL

CIEF experiments were performed with the Tachophor 2127 (LKB, Bromma, Sweden), as described in detail elsewhere[9]. The Tachophor features an air-cooled PTFE capillary of 0.5 mm I.D. and 10 cm length, mounted between the dual detection block (LKB 2127-140) and a laboratory-built electrode compartment. A syringe was employed to insert the mixture of sample and carrier components into the focusing capillary. The cathode was on the detection side (leading electrolyte compartment of Tachophor). After focusing, the cathodic solution was replaced by the anolyte permitting electromobilization of the separative pattern past the detection block. Conductivity and absorbance measurements were continuously made during both the focusing and elution stages. The experiments were run at either constant current or constant voltage, provided by a Spellman RHR 30P30/CR/FG high-voltage d.c. power supply (2 mA max; 30 kV).

A schematic representation of an EHFFF apparatus is depicted in Fig. 2c. The relation to a high-performance liquid chromatography (HPLC) system in which the chromatographic column is replaced by the FFF trough is obvious. The EHFFF separation cell construction was similar to that used for EFFF by Giddings *et al.*[15]. It features a ribbon-like channel (2 × 20 × 0.025 cm) formed by a PTFE spacer which is sandwiched between ion-exchange membranes (Ionics, Watertown, MA, U.S.A.) by use of two Plexiglass blocks (Fig. 3). These blocks contain the electrode reservoirs, as well as fittings for sample, carrier buffer, catholyte and anolyte insertion and drain. A Model 2150 HPLC pump, a Model 2158 Uvicord absorbance monitor with an 8-μl HPLC flow cell, a Model 2195 pH/ion monitor and, for application of anolyte and catholyte, a Model 2132 Microperpex peristaltic pump (all from LKB) were the peripheral instruments (Fig. 2c). Samples were injected with a microliter syringe. A Kepco APH 2000 M power supply was employed for application of the electric force field. The setup was used in the flow-injection mode with and without an applied electric field, as well as in a stopped-flow mode for focusing in quiescent solution, followed by elution of the focused solutes.

The simple buffer mixtures used in this study consisted of three amino acids,

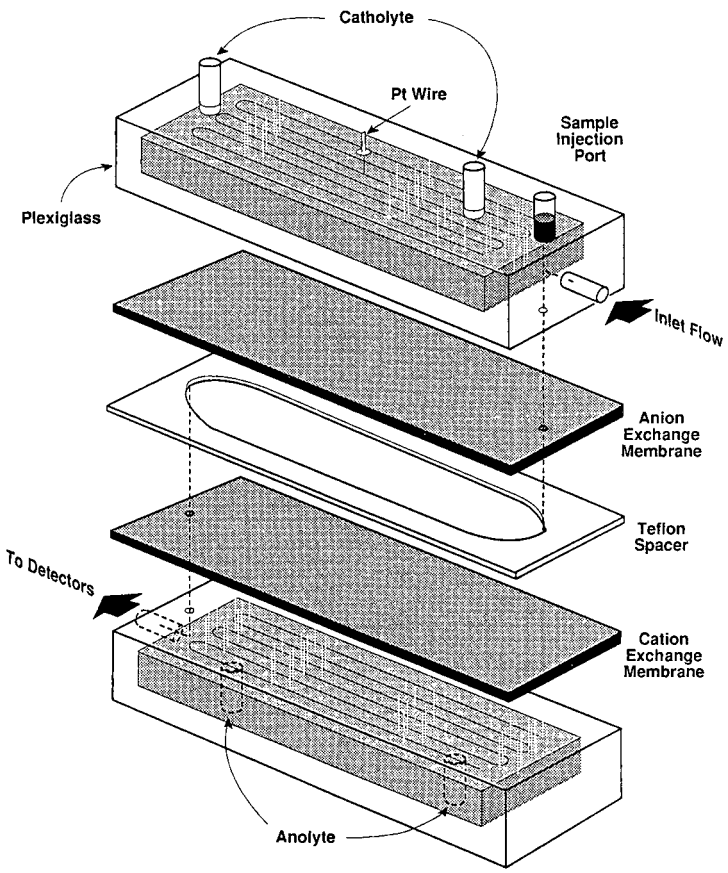

Fig. 3. Exploded assembly of the EHFFF separation cell.

glutamic acid (Fisher Scientific, West Haven, CT, U.S.A.), cycloserine (Sigma, St. Louis, MO, U.S.A.) and arginine (Sigma). The synthetic carrier ampholytes employed were 3.5–10 pH range Ampholine (LKB). Model protein mixtures were prepared from any number of the following: bovine albumin (Alb, Miles Laboratories, Elkhart, IN, U.S.A., pI = 4.9), canine hemoglobin (Hb, isolated locally, pI = 7.3), bovine ribonuclease A (Sigma, pI = 9.6), and equine cytochrome c (Sigma, pI = 10.3). Solutions of phosphoric acid (anolyte) and sodium hydroxide (catholyte), 100 mM each, were employed as electrode buffers for CIEF and EHFFF. Hydroxypropylmethyl cellulose (HPMC) was from Sigma.

RESULTS AND DISCUSSION

The generation of the lateral pH gradient in EHFFF is analogous to the establishment of natural pH gradients in isoelectric focusing. Based on theoretical and practical considerations, the advantages of EHFFF compared to CIEF are manyfold, but the following two are especially important. Firstly, the voltage applied in EHFFF is effectively multiplied by the ratio of column length to width. Because the pH gradient is generated across the smallest channel dimension, much lower applied potentials produce field strengths equivalent to those present in CIEF. Secondly, EHFFF avoids the difficulties of detection in CIEF associated with the production of a stationary steady state. Without the use of scanning or array detectors, the focused proteins in CIEF must be mobilized in order to pass them across a sensor. Fig. 4 shows

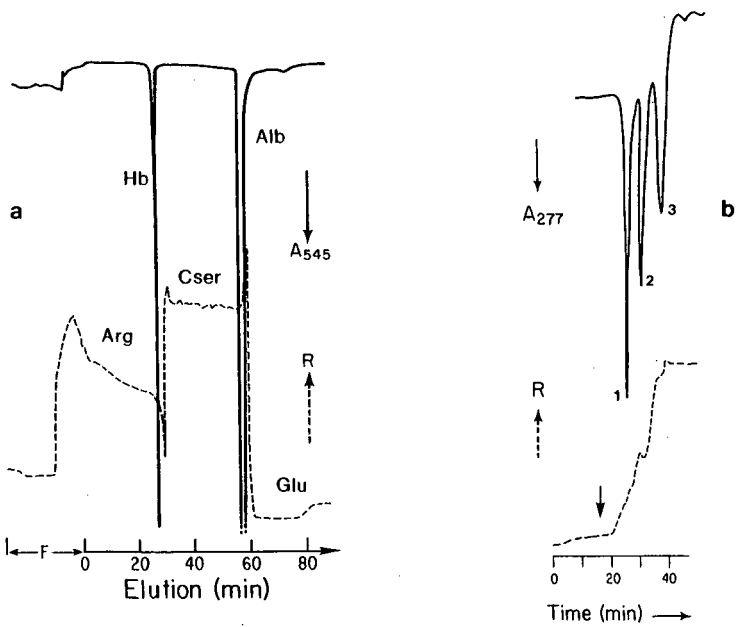

Fig. 4. (a) CIEF conductivity data (expressed as resistance, R) and absorbance data at 545 nm of Hb and Alb focused in a three-component buffer comprising glutamic acid (Glu, 5 mM), cycloserine (Cser, 5 mM) and arginine (Arg, 30 mM) and (b) corresponding CIEF conductivity (R) and absorbance (277 nm) data of cytochrome c (0.18 mg/ml; 1), ribonuclease A (0.36 mg/ml; 2) and Hb (0.08 mg/ml; 3) in 1% Ampholine, 8 mM arginine and 1% HPMC. Focusing occurred (a) within 20 min at 3 kV and (b) within 17 min at 2 kV. The arrow in the latter pherogram marks the beginning of elution.

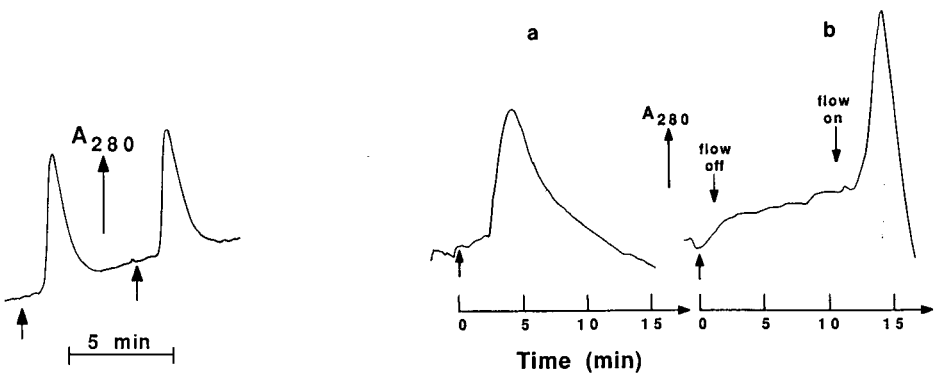

Fig. 5. Flow-injection peaks of 1 μl of 50 mg/ml albumin in a three-component buffer composed of glutamic acid, cycloserine and arginine (10 m*M* each) obtained with the EHFFF apparatus without applied electric field. The data of two consecutive experiments is shown to illustrate reproducibility. The flow-rate was 1.0 ml/min. The arrows mark the time of sample injection. The channel dead volume was about 1 ml.

Fig. 6. Effect of focusing on peak shape in the stopped-flow EHFFF mode. The flow-rate was 0.1 ml/min. The sample and the buffer were the same as for Fig. 5. The flow-injection peak without any electric field is shown in Fig. 6a, and the eluted peak after a focusing period of 10 min without buffer flow is presented in Fig. 6b.

pherograms obtained for the CIEF separation of two model systems of proteins. For detection, the zone structures were electromobilized by replacement of the base (100 m*M* sodium hydroxide) in the cathodic electrode compartment with acid (100 m*M* phosphoric acid) (Fig. 1c) and application of a constant current of 100 μA. This mobilization step significantly prolongs the analysis and might sacrify resolution. EHFFF overcomes this problem by its inherent nature as an elution technique.

The EHFFF apparatus was first tested in the flow-injection mode without application of an electric field. Typical UV responses obtained by injecting 1-μl aliquots of 50 mg/ml albumin into a carrier buffer composed of glutamic acid, cycloserine and arginine (10 m*M* each) are shown in Fig. 5. The buffer flow-rate was 1 ml/min. A ten-fold reduction in the flow-rate produced a broader and more asymmetric peak (Fig. 6a). The asymmetry present in both Figs. 5 and 6a indicates the presence of solute interaction with the channel walls (membranes). Application of the electric field (2.8 V, 2 mA) did not significantly change the elution times of the sample front, the peak maximum and the peak shape. This was true for a flow-rate range of 0.1–0.3 ml/min. Neither could any evidence of separation of proteins be observed. Both results suggested that the length of the separation channel was insufficient.

One way to lengthen the separation channel effectively is to employ a stopped-flow mode of operation. In this mode the sample was first injected without buffer flow, then swept into the beginning of the channel. The electric field was then applied for a specified time without any buffer flow. This allowed focusing to occur before elution was started. The effect on the eluted sample shape, for a focusing time of 10 min at a current of 2 mA (about 2.72 V) followed by an elution in the continued presence of the field at a flow-rate of 0.1 ml/min, is shown in Fig. 6b. The protein sample was found to be eluted as a much sharper zone, indicating a substantial reduction or even exclusion of interactions between the macromolecules and the walls. To our

knowledge, this contribution constitutes the first experimental demonstration of the impact of a lateral pH gradient on the EFFF sample zone. Moreover, these results suggest that EHFFF has the potential of overcoming many of the difficulties encountered in protein analysis by electrical and other FFF techniques, in CZE and in CIEF. Investigations directed toward the exploration of EHFFF as a separation methodology for amphoteric compounds and toward the development of improved separation channels, featuring various types of membranes and non-gassing electrode assemblies, are now underway in our laboratory.

ACKNOWLEDGEMENTS

The authors would like to acknowledge the generous donation of the Tachophor 2127 by its manufacturer, LKB, Bromma, Sweden. This work was partly supported by NASA grant NAGW-693 and by Pharmacia-LKB AB, Sweden (EHFFF project).

REFERENCES

1 J. C. Giddings and K. Dahlgren, *Sep. Sci.*, 6 (1971) 345.
2 J. C. Giddings, *Sep. Sci. Technol.*, 18 (1983) 765.
3 F. E. P. Mikkers, F. M. Everaerts and Th. P. E. M. Verheggen, *J. Chromatogr.*, 169 (1979) 1.
4 J. W. Jorgenson and K. D. Lukacs, *Science (Washington, D.C.)*, 222 (1983) 266.
5 W. Thormann, *Electrophoresis*, 4 (1983) 383.
6 A. S. Cohen, S. Terabe, J. A. Smith and B. L. Karger, *Anal. Chem.*, 59 (1987) 1021.
7 S. Hjertén, *J. Chromatogr.*, 270 (1983) 1.
8 W. Thormann, A. Tsai, J.-R. Michaud, R. A. Mosher and M. Bier, *J. Chromatogr.*, 389 (1987) 75.
9 M. A. Firestone and W. Thormann, *J. Chromatogr.*, 436 (1988) 309.
10 S. Hjertén and M.-D. Zhu, *J. Chromatogr.*, 348 (1985) 265.
11 S. Hjertén, F. Kilár, L. Liao and M. Zhu, in M. Dunn (Editor), *Electrophoresis '86*, VCH Verlagsgesellschaft, Winheim, 1986, pp. 451.
12 S. Hjertén, J. Liao and K. Yao, *J. Chromatogr.*, 387 (1987) 127.
13 J. C. Giddings, *Anal. Chem.*, 53 (1981) 1170A.
14 J. C. Giddings, *Sep. Sci. Technol.*, 19 (1984-85) 831.
15 J. C. Giddings, M. N. Myers, K. D. Caldwell and S. R. Fisher, in D. Glick (Editor), *Methods of Biochemical Analysis*, Vol. 26, Wiley, New York, 1980, pp. 79.
16 K. D. Caldwell, L. F. Kesner, M. N. Myers and J. C. Giddings, *Science (Washington, D.C.)*, 176 (1972) 296.
17 L. F. Kesner, K. D. Caldwell, M. N. Myers and J. C. Giddings, *Anal. Chem.*, 48 (1976) 1834.
18 J. C. Giddings, G. Lin and M. N. Myers, *Sep. Sci.*, 11 (1976) 553.
19 H. L. Lee, J. F. G. Reis, J. Dohner and E. N. Lightfoot, *AIChE J.*, 20 (1974) 776.
20 A. S. Chiang, E. H. Kmiotek, S. M. Langan, P. T. Noble, J. F. G. Reis and E. N. Lightfoot, *Sep. Sci. Technol.*, 14 (1979) 453.
21 J. M. Davies, F. R. F. Fan and A. J. Bard, *Anal. Chem.*, 59 (1987) 1339.
22 J. Janča and J. Chmelík, *Anal. Chem.*, 56 (1984) 2481.
23 M. R. Schure, K. D. Caldwell and J. C. Giddings, *Anal. Chem.*, 58 (1986) 1509.
24 J. Chmelík and J. Janča, *J. Liq. Chromatogr.*, 9 (1986) 55.
25 J. Janča and N. Nováková, *J. Liq. Chromatogr.*, 10 (1987) 2869.
26 J. Janča, *J. Chromatogr.*, 404 (1987) 23.
27 J. C. Giddings, X. Chen, K. Wahlund and M. N. Myers, *Anal. Chem.*, 59 (1987) 1957.

Journal of Chromatography, 461 (1989) 103–110
Elsevier Science Publishers B.V., Amsterdam — Printed in The Netherlands

CHROM. 1413

SEDIMENTATION FIELD-FLOW FRACTIONATION OF COLLOIDAL METAL HYDROSOLS

LARRY E. OPPENHEIMER* and GREGORY A. SMITH
Photographic Research Laboratories, Photographic Products Group, Eastman Kodak Company, Rochester, NY 14650 (U.S.A.).

SUMMARY

Sedimentation field-flow fractionation can be readily used to characterize the particle size distributions in metal hydrosols with particle diameters extending well below 0.01 μm. Processes that change the size distribution, such as particle growth or coagulation, can be investigated by this method. For materials such as silver, where the optical properties of the hydrosol depend on the particle shape, sedimentation field-flow fractionation can be combined with detection by diode array spectrophotometry to obtain data that allow inferences to be made about the non-spherical nature of the dispersed material.

INTRODUCTION

Dispersions of metal particles in aqueous media have been investigated by colloid chemists for many years. A century ago Carey Lea[1] described procedures that are still in use for producing silver hydrosols. Recently there has been an increase in interest in these sols because of their utility as substrates for surface-enhanced Raman scattering experiments. As with other uses for colloidal systems, the relevant properties of the sol depend on the size, shape, and/or specific surface area of the metal particles[2]. Jolivet *et al.*[3] demonstrated that silver sols are subject to particle growth and aggregation when no protective colloid is present. Characterization of these materials has generally been done by electron microscopy. Unfortunately, the information about the state of aggregation of a sol contained in micrographs is often ambiguous because it is difficult to tell if the sample has been aggregated, or deaggregated, in preparation for microscopy. Also, quantitative information about systems of non-spherical particles is difficult to obtain by electron microscopy. In a recent publication[4] we described the use of sedimentation field-flow fractionation (SFFF) for the characterization of particle size distributions in metal sols containing both spherical and filamentary particles and have found it to be both fast and accurate as well as sensitive to the state of aggregation of the sample.

While measurement of the distribution of particle masses, or diameters for spherical particles, by SFFF is straightforward, obtaining shape information about sols containing non-spherical particles is much more difficult. An example of such a

system is filamentary silver, which is often the product of photographic development of silver halide particles[5]. SFFF allows the separation of particles from a dispersion of silver filaments according to their mass without regard to particle shape[6]. Detection with a diode array spectrophotometer can then be used to generate spectra of the effluent of the SFFF system. The results are a series of spectra for fractions of increasing particle mass. The spectra of silver particles vary considerably with the axial ratio of the particles[2,7]. This property makes it possible to derive particle shape information from the fractogram and spectra. Similarly, silver spheres in the early stages of aggregation have the optical properties of ellipsoids and show the optical effects of non-spherical particles[2].

EXPERIMENTAL

Instrumentation

Separations were performed on a SF[3]1000 particle fractionator produced by the Clinical & Instrument Systems Division of DuPont (Wilmington, DE, U.S.A.). The device has a 0.025-cm channel width and an integral DuPont Instruments 860 absorbance detector that was operated at 254 nm. It is similar to devices described in the literature[8]. Experiments were performed using a time-delayed exponential-decay programmed field[8,9] with initial rotor speeds between 10 000 and 15 000 rpm, which correspond to fields of 10 647 and 23 957 g, respectively. In all experiments the field decay constant was 4 min, the relaxation time was 2 min, and the flow-rate was 2 ml/min. A 0.1% aqueous solution of FL-70 surfactant (Fischer Scientific, Fair Lawn, NJ, U.S.A.) was used as the eluent.

Spectra were obtained with an HP 8452 diode array spectrophotometer (Hewlett Packard, Palo Alto, CA, U.S.A.) equipped with a 30-μl flow cell. Typically, spectra were collected at 2-min intervals during peak elution over the wavelength range 300–820 nm.

Dispersions

Filamentary silver was made by photographic development of chemically fogged silver halide in gelatin[5]. An electron micrograph of such a sol appears in Fig. 1.

Silver sols containing spherical particles were made by reduction of silver oxide with dextrin or by the reduction of silver nitrate with iron(II) sulfate in the presence of sodium citrate[10–12]. For storage, 10% (by weight) gelatin was added to the dispersions.

RESULTS

The output of the SFFF system for each experiment, a curve of extinction *versus* time, was used to generate a particle size distribution by applying an equation of the form $t = 3\tau \ln (D / \beta)$ to the time axis[9]. This relationship between elution time t and D, the diameter for spherical particles or equivalent spherical diameter for non-spherical particles, is valid for time-delayed exponential-decay programmed field SFFF when t is greater than the time constant for rotor speed decay, τ. Here β contains the sample and eluent densities and instrumental parameters. The absorb-

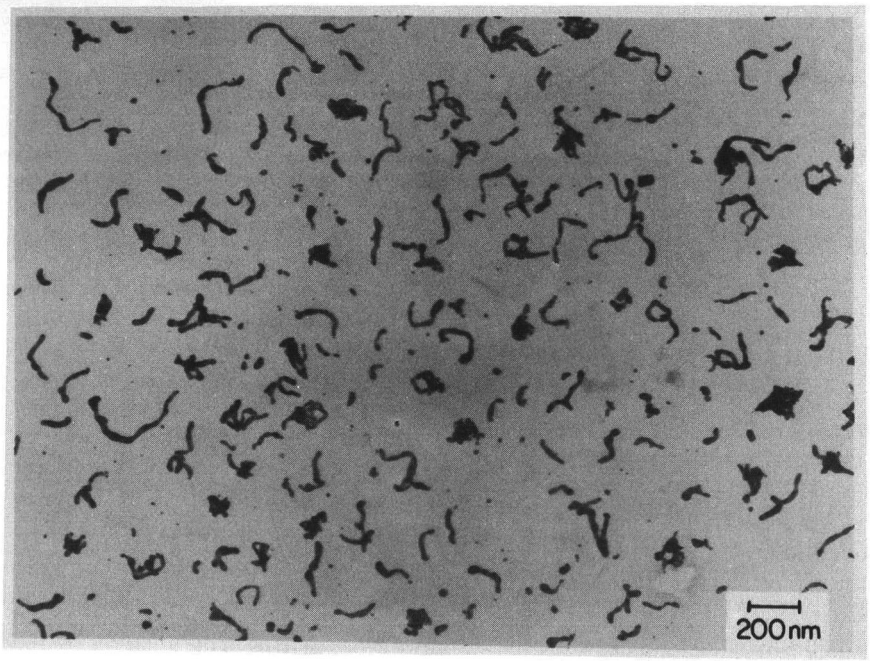

Fig. 1. Electron micrograph of particles in a filamentary silver sol.

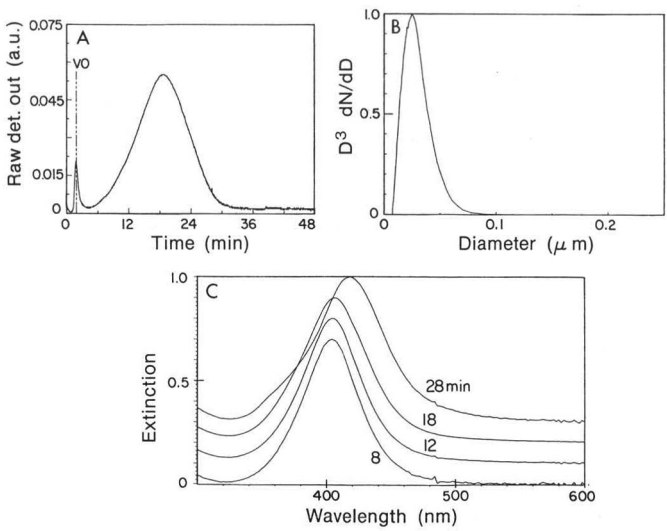

Fig. 2. Results for a sol containing spherical silver particles that were stabilized with gelatin. (A) Raw SFFF data. (B) Particle size distribution. (C) Spectra taken of the eluent at the indicated elution times (*cf.* A).

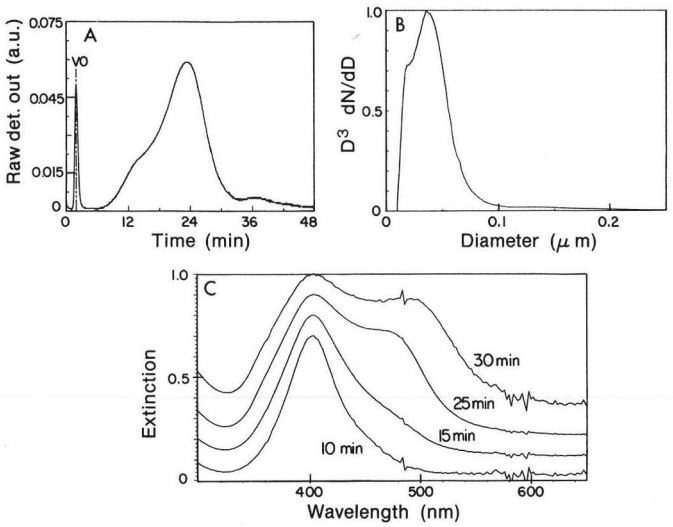

Fig. 3. Results for the sol described in Fig. 2 after coagulation. (A) Raw SFFF data. (B) Particle size distribution. (C) Spectra taken of the eluent at the indicated elution times (*cf.* A).

ance at each time was related to the mass frequency of particles by dividing by the calculated diameter, as explained in our earlier paper[4], to yield a value proportional to $D^3\,\mathrm{d}N/\mathrm{d}D$. In this manner a mass distribution was obtained for each sample. The raw data and corresponding size distributions are shown in Fig. 2A and B–4A and B. In addition, four of the spectra obtained in the course of each experiment, normalized to the same height in each case, are included in Figures 2C–4C.

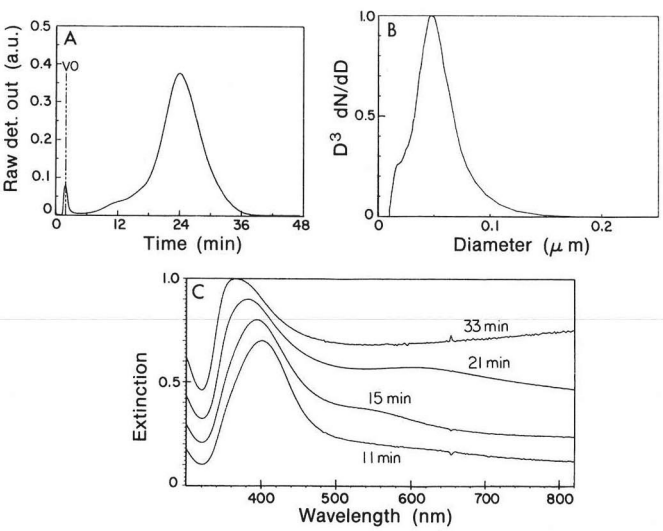

Fig. 4. Results for a sol containing filamentary silver particles that were stabilized with gelatin. (A) Raw SFFF data. (B) Particle size distribution. (C) Spectra taken of the eluent at the indicated elution times (*cf.* A).

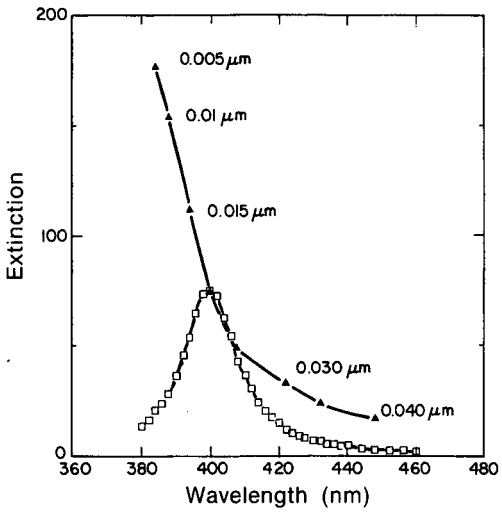

Fig. 5. Calculated extinction spectrum for 0.02 μm silver spheres (□) and the locus of the peak positions as a function of particle diameter (▲).

DISCUSSION

Optical absorption by colloidal dispersions of silver is known to depend on both the size and shape of the dispersed particles[2,7]. The extinction spectra of these materials are, in principle, readily calculated using the Mie equations for spherical particles or the Rayleigh-Gans approximation for ellipsoidal particles (see ref. 13). However, the calculations require a knowledge of the complex refractive index of the particles as a function of wavelength. There are several sets of refractive index data for silver in the literature, with significant variations among them[14]. We have chosen to use the data of Johnson and Christy[15] because they give a clear indication of the

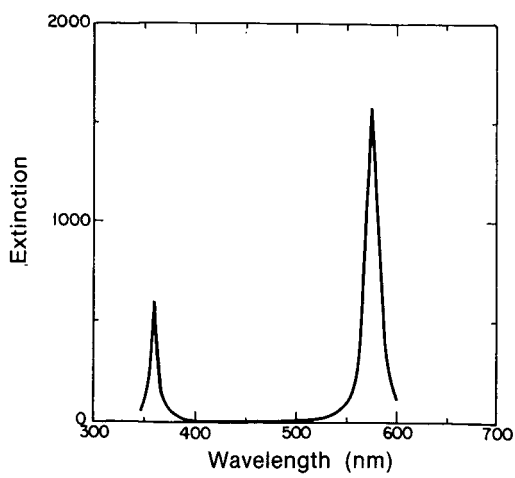

Fig. 6. Calculated extinction spectrum for silver ellipsoids with minor axis 0.02 μm and axial ratio 3.0.

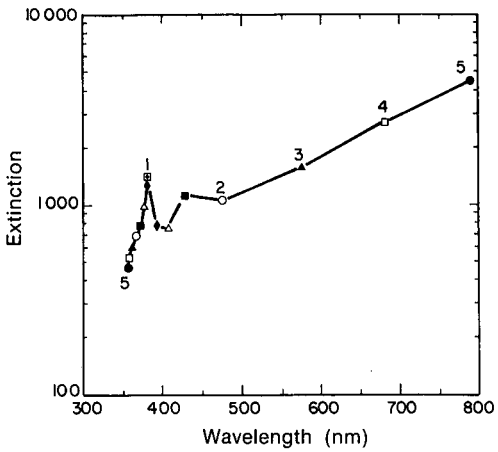

Fig. 7. Locus of peak positions calculated for extinction by silver ellipsoids with minor axis 0.02 μm as a function of axial ratio.

trends we expect to find as the particle size and shape vary and they have been used by other investigators for similar studies.

Fig. 5 shows the extinction behavior of spherical silver particles as a function of diameter. The spectrum is shown for particles 0.02 μm in diameter along with the locus of the peak extinction for varying diameter. Note that the peak moves to longer wavelengths as the diameter increases. When we consider ellipsoidal particles, we find that the extinction spectrum splits into two peaks, as shown in Fig. 6 for an axial ratio of 3.0. The locus of the peaks is plotted as a function of axial ratio in Fig. 7 for constant minor axis of 0.02 μm. The long wavelength peak moves to longer wavelengths and the short wavelength peak to shorter wavelengths as the axial ratio increases with the minor axis held constant. Kerker[2] reported similar results for calcu-

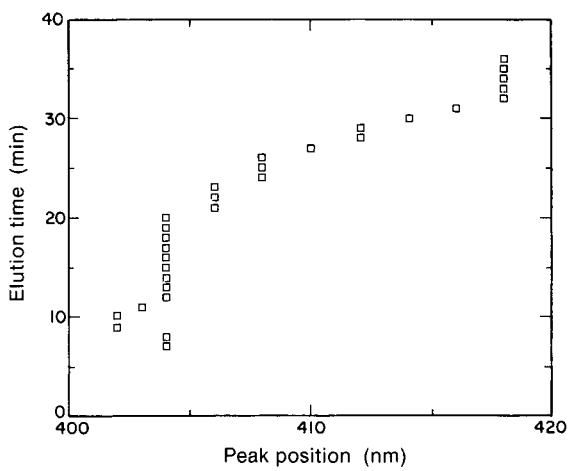

Fig. 8. Peak position as a function of elution time for SFFF of the silver sol containing spherical particles.

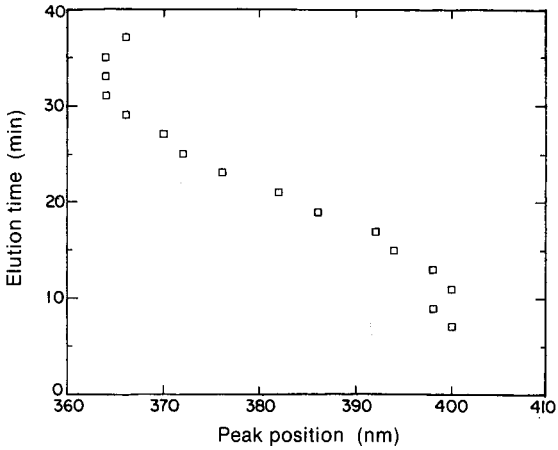

Fig. 9. Position of the short wavelength peak as a function of elution time for SFFF of the silver sol containing filamentary particles.

lations performed for particles at different axial ratios with the particle volume held constant. The changes in peak position and magnitude predicted in these graphs can be observed experimentally, while the peaks are broader than predicted by the Rayleigh-Gans theory.

Given this background we can attempt to understand the results of SFFF with diode array detection on three different samples samples of colloidal silver. Fig. 2 contains results for a sample of spherical colloidal silver protected from aggregation by absorbed gelatin. We have shown earlier[4] that the gelatin itself has no effect on the SFFF results. The spectra are similar, the main feature being a single peak close to 400 nm. As predicted in Fig. 5, the position of the peak moves to longer wavelengths as the particle size increases while the peak shape remains unchanged. The peak position is plotted as a function of elution time in Fig. 8. The discontinuous appearance of this plot, and of Fig. 9, is due in large measure to the limited wavelength resolution of the diode array detection, 2 nm in our case.

Fig. 3 contains SFFF results and spectra for a sample of the same sol which had been destabilized by the addition of a proteolytic enzyme 1 h prior to the experiment. The enzyme destroyed the gelatin, allowing the particles to aggregate. On visual observation it was noted that the color of the sol changed from yellow to red-orange. The particle size distribution has changed in the manner we might expect for an aggregating sol, with a shoulder remaining at small particle sizes corresponding to the original, unaggregrated, particles as well as the appearance of a shoulder at larger sizes corresponding to the appearance of large particles, *i.e.*, aggregates. The spectra clearly reflect the ellipsoid-like behavior of these particles. For the smaller particles the spectra are similar to those in Fig. 2. As larger particles were examined, a shoulder formed on the long wavelength side of the peak, which eventually evolved into a distinct, if poorly resolved, second peak. The wavelength of the second maximum is somewhat less than 500 nm, as predicted for ellipsoids with an axial ratio of about 2. We expect this since the main cause of the peak is most likely the presence of doublets in the dispersion. The position of the short wavelength peak is constant across the

fractogram, showing neither the shift to longer wavelengths associated with increasingly large spherical particles or the shift to shorter wavelengths of ellipsoids. This is probably the result of a fortuitous combination of both these phenomena occurring simultaneously.

Fig. 4. contains the results for a filamentary silver sol. The results are not nearly as dramatic as those in Fig. 3, but the formation of the second peak, which moves to longer wavelengths as the particle mass increases, can be seen. The position of this peak is beyond the 820 nm limit of our detector for the largest particles present here. For this sample, where there are relatively few spherical particles, the short wavelength peak does move to shorter wavelengths as the particle mass increases, as shown in Fig. 9. The broadness of the peak for this sample is not unexpected because of the polydispersity of the sample with respect to axial ratio and the wide deviations from ellipsoidal particle shape of some of the particles.

In conclusion then, SFFF can be used to determine particle size (or mass) distributions in metal hydrosols without regard to the particle shape. When combined with spectrophotometric detection using a diode array detector, SFFF can be used to obtain particle shape information for dispersions of non-spherical particles when the absorption spectrum of the dispersed phase is a function of the particle shape. We have demonstrated this using silver dispersions consisting of unaggregated and aggregated spherical particles and of filamentary particles.

REFERENCES

1 M. Carey Lea, *Am. J. Sci.*, 37 (1889) 476.
2 M. Kerker, *J. Colloid Interface Sci.*, 105 (1985) 297.
3 J.P. Jolivet, M. Gzara, J. Mazieres and J. Lefebvre, *J. Colloid Interface Sci.*, 107 (1985) 429.
4 L.E. Oppenheimer and G.A. Smith, *Langmuir*, 4 (1987) 144.
5 T.H. James (Editor), *The Theory of the Photographic Process*, Macmillan, New York, 4th ed., 1977.
6 J.J. Kirkland, L.E. Schallinger and W.W. Yau, *Anal. Chem.*. 57 (1985) 2271.
7 D.C. Skillman and C.R. Berry, *J. Chem. Phys.*, 48 (1968) 3297.
8 J.J. Kirkland, S.W. Rementer and W.W. Yau, *Anal. Chem.*, 53 (1981) 1730.
9 W.W. Yau and J.J. Kirkland, *Sep. Sci.*, 16 (1981) 577.
10 G. Frens and J.Th.G. Overbeek, *Kolloid-Z.*, 233 (1969) 922.
11 *Gmelins Handbuch der anorganischen Chemie*, Vol. 61 A3, Verlag Chemie, Weinheim, 1977, p. 196.
12 Luppo-Cramer, *Kolloid-Z.*, 13 (1913) 180.
13 M. Kerker, *The Scattering of Light and Other Electromagnetic Radiation*, Academic, New York, 1969.
14 M. Kerker, *J. Opt. Soc. Am. B*, 2 (1985) 1327.
15 P.B. Johnson and R.W. Christy, *Phys. Rev. B*, 6 (1972) 4370.

Journal of Chromatography, 461 (1989) 111–120
Elsevier Science Publishers B.V., Amsterdam — Printed in The Netherlands

CHROMSYMP. 1532

ANALYSIS OF STEROIDS BY CAPILLARY SUPERCRITICAL FLUID CHROMATOGRAPHY WITH PHOSPHORUS-SELECTIVE DETECTION

P. A. DAVID and M. NOVOTNY*
Department of Chemistry, Indiana University, Bloomington, IN 47405 (U.S.A.)

SUMMARY

Steroids were derivatized with dimethylthiophosphinic chloride to produce steroidal thiophosphinic esters. A catalyst, 4-dimethylaminopyridine, was used to promote quantitative and reproducible thiophosphinic ester formation at low reaction temperatures. The derivatives were analyzed by capillary supercritical fluid chromatography (SFC) with phosphorus thermionic detection.

The phosphorus thermionic detector exhibited linearity over 3–4 orders of magnitude. A sensitivity of 120 fg P/s was obtained for the dithiophosphinic ester of pregnanediol at a signal-to-noise ratio of 3. The efficiency of capillary SFC and the excellent sensitivity of the phosphorus thermionic detector were demonstrated by the analysis of steroids isolated from both human urine and plasma.

INTRODUCTION

During the last several years, supercritical fluid chromatography (SFC) has been demonstrated as an effective separation method for non-volatile and thermally labile compounds. Capillary SFC has been particularly successful in the analysis of relatively non-polar mixtures of synthetic oligomers and petrochemicals which are readily soluble in the commonly used SFC mobile phases (carbon dioxide, nitrous oxide). Unfortunately, polar compounds exibit limited solubility in the preferred SFC mobile phases. For continuous growth and popularity, SFC needs more applications to polar substances, such as those encountered in biochemical and pharmaceutical analysis.

Among several ways to extend the scope of SFC toward polar solutes, sample derivatization has been attractive as a means of increasing the sample solubility in carbon dioxide or nitrous oxide. This has now been demonstrated with silylated oligosaccharides[1] and biological conjugates of steroid metabolites and bile acids[2]. An additional benefit can be realized through the use of chemical derivatization. Selection of a derivatization reagent that incorporates a heteroatom-containing moiety into the derivatized molecule allows the use of sensitive and highly selective thermionic detection. This has been recently demonstrated through the analysis of quinoxalinols, originated from α-ketoacids, by capillary SFC with nitrogen thermionic detection[3].

This communication deals with the sensitive analysis of steroids by capillary SFC with phosporus-selective detection. Steroid hydroxy groups are derivatized with

0021-9673/89/$03.50

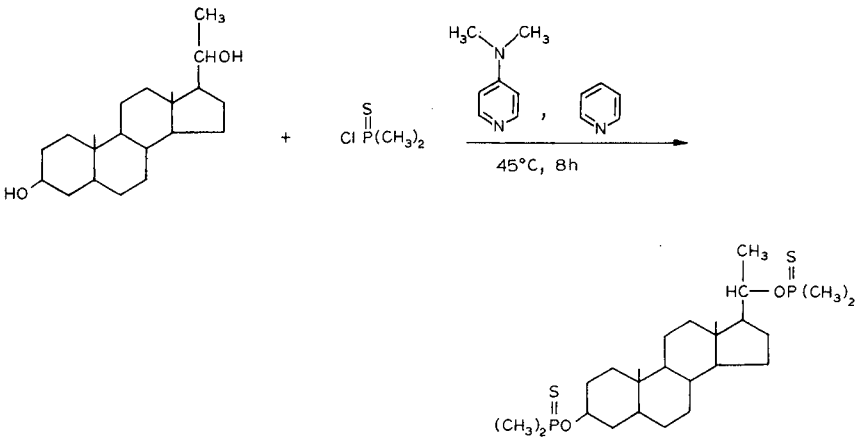

Fig. 1. Formation of a steroid thiophosphinic ester. Model steroid: pregnanediol. Catalyst: DMAP. Solvent: pyridine.

dimethylthiophosphinic chloride to form the corresponding steroid thiophosphinic esters (Fig. 1). This derivatization scheme was initially reported for the gas chromatographic (GC) analysis of monohydroxysteroids[4], but found little practical use because of the need for relatively high column temperatures. We have introduced here a nucleophilic catalyst, 4-(dimethylamino)pyridine[5], to allow this reaction to be generally applicable to all hydroxysteroids. The requirements for a derivatization reagent are somewhat less stringent in SFC than in GC. For successful SFC application the derivatization must be reproducible, but full coverage of all polar functionalities is not required. The inert capillary columns and solvating ability of the mobile phase allow for the efficient SFC analysis of solutes containing a few underivatized polar groups. In capillary GC, chromatographic efficiency is severely compromised by the presence of underivatized polar functionalities.

The further purpose of this article is to demonstrate the excellent sensitivity possible with the phosphorus thermionic detector coupled to capillary SFC. To illustrate this point, steroids were isolated from physiological fluids (blood and urine) and converted to thiophosphinic esters prior to SFC analysis.

EXPERIMENTAL

Chromatographic equipment

The supercritical fluid chromatograph was a home-made instrument as described previously[6]. Mobile phase delivery and pressure control were accomplished with a Brownlee Labs. micropump with software version G (Applied Biosystems, Santa Clara, CA, U.S.A.). The mobile phase employed was SFC grade nitrous oxide (Scott Specialty Gases, Plumsteadville, PA, U.S.A.). The nitrous oxide cylinder was charged with 1500 p.s.i. of helium-head space pressure to facilitate rapid filling of the pump without externally cooling the pump heads. Injection was accomplished via an electrically actuated high-pressure valve with an internal sample loop volume of 0.06 μl (Valco Instruments, Houston, TX, U.S.A.). Split injection was used for all analyses,

with a split ratio of 5:1. The capillary column used was 10 m × 50 μm I.D. The fused-silica surface was deactivated prior to coating through treatment with polymethylhydrosiloxane (85 cSt) (Petrarch Systems, Bristol, MA, U.S.A.). The column was statically coated at 65°C with a 40 mg/ml solution of SE-33 in Freon 11 to produce a 0.50-μm film[8]. The stationary phase was crosslinked three times with azo-*tert.*-butane (Alfa Products, Danvers, MA, U.S.A.).

The pressure restriction required for the operation of a flame-based detector was accomplished by forming an integral restrictor[10] directly at the end of the coated column. The detector was a modified Perkin-Elmer Sigma 3 nitrogen–phosphorus detector. The detector modification consisted of machining a brass detector base containing a centered 1/8 in. swagelok union (Crawford Fitting, Salon, OH, U.S.A.). The detector flame jet was firmly held in the union with a graphite ferrule. The flame jet was a 2 cm × 1 mm I.D. × 3 mm O.D. quartz tube with a conical stainless-steel flame jet tip crimped at the end. The tip outlet orifice was 0.010 in. Polarization voltage and signal amplification were provided by Perkin-Elmer stand-alone nitrogen–phosphorus detection (NPD) electrometer (Perkin-Elmer, Norwalk, CT, U.S.A.). The rubidium silicate thermionic source was prepared according to the procedure of Lubkowitz *et al.*[11]. Beads containing 1.8% B_2O_3, 12.6% Na_2O, 73.3% SiO_2 and 12.2% Rb_2O exhibited optimum sensitivity and 1–2 month lifetime. Typical detector operating conditions were: 300°C heating block temperature, −260 V polarizing voltage, 25 ml/min hydrogen flow, 275 ml/min air flow.

Chemicals

Steroid standards were obtained from Sigma (St. Louis, MO, U.S.A.). Dimethylthiophosphinic chloride was received from Alpha Products. 4-(Dimethylamino)pyridine (DMAP) (Aldrich, Milwaukee, WI, U.S.A.) was employed as a catalyst, and was purified prior to use by alumina column chromatography using diethyleter as the eluent. Pyridine (MCB Manufacturing Chemists, Cincinnati, OH, U.S.A.) was distilled over potassium hydroxide prior to use and stored in glass vials over potassium hydroxide pellets.

Preparation of standard steroids

Microgram amounts of standard steroids were dissolved in 0.2 ml of dry pyridine. Under a dry nitrogen purge, 1.5 μl of neat dimethylthiophosphinic chloride and 10 μl of a 0.1 *M* DMAP solution in dry pyridine were added. The reaction vial was tightly sealed and placed in a heating block at 45°C for 8 h. After the reaction was completed, the reaction mixture was taken to dryness under a stream of nitrogen. To the residue, 50 mg of sodium bicarbonate and 0.2 m of methanol were added. The mixture was heated at 50°C for 1 h to react any remaining dimethylthiophosphinic chloride. The mixture was again taken to dryness under a stream of dry nitrogen. The residue was dissolved in 0.3 ml of methanol and transferred to a syringe attached to a Sep-Pak C_{18} cartridge (Waters Assoc., Milford, MA, U.S.A.). The methanol solution was mixed with 0.7 ml of water and passed through the Sep-Pak cartridge. Excess reagent and reaction by-products (mainly dimethylthiophosphinic anhydride) were eluted with 20 ml methanol–water (30:70, v/v). The derivatized steroids were recovered with 5 ml of methanol, take to dryness, and reconstituted in 0.1 ml of methanol.

Preparation of urine sample

A 10-ml aliquot of a 24-h collection of human pregnancy urine was processed according to the procedure described by Axelson *et al.*[12]. Briefly, the urine was filtered through a Sep-Pak C_{18} cartridge and the steroids were eluted with methanol. After a cation-exchange step (SP- Sephadex, H^+ form), the steroid conjugates were fractionated on a TEAP-LH-20, strong anion-exchange column in the hydroxide form[12]. Three fractions were collected: (1) unconjugated neutral and phenolic steroids, (2) glucuronide conjugated steroids, and (3) mono- and disulphate conjugated steroids The glucuronide conjugates were enzymatically hydrolyzed by β-glucuronidase (Sigma) at 37°C for 24 h. After hydrolysis, Sep-Pak C_{18} and TEAP-LH-20 steps were employed to purify the liberated steroids. Steroid sulfates were cleaved by solvolysis with acidified tetrahydrofuran for 1 h at 50°C. The neutral and phenolic steroids were purified through anion exchange with the TEAP-LH-20 material.

All three fractions were taken to dryness under a stream of nitrogen and reconstituted in 0.2 ml of dry pyridine. Under a nitrogen purge, 3 μl of neat dimethylthiophosphinic chloride and 10 μl of 0.1 *M* DMAP in pyridine were added. The reaction proceeded at 45°C for 12 h. After completion, each fraction was processed in an identical fashion as described in the preparation of standard derivatives. Finally, both fractions 1 and 3 were brought to a final volume of 25 μl with methanol. Fraction 2 was reconstituted to 50 μl with methanol.

Preparation of plasma sample

A 5-ml sample of heparinized human male plasma was processed according to the procedure of Axelson and Sahlberg[13]. The plasma was diluted to 15 ml total volume with distilled water. This solution was heated to 60–64°C for 10 min and passed through a Sep-Pak C_{18} cartridge also held at 64°C. The cartridge was washed with 5 ml of water at 64°C, and steroids were eluted with 8 ml of methanol at room temperature. The Sep-Pak extraction was performed at elevated temperatures to minimize steroidal-protein interactions. Silanized glassware was used throughout the plasma steroid preparation to prevent losses due to irreversible adsorption of conjugated steroids to glass surfaces.

The steroids were fractionated via ion-exchange procedures identical to the urinary steroid preparation. However, the unconjugated plasma steroid fraction was not analyzed, since this fraction contained lipids with unconjugated steroids as minor components. The majority of the plasma steroids are known to exist as either glucuronides or sulfate conjugates. The conjugated fractions were derivatized with dimethylthiophosphinic chloride as described for the urinary steroids. Both fractions were reconstituted to a final volume of 15 μl with methanol.

RESULTS AND DISCUSSION

A reaction temperature of 45°C was chosen for the formation of steroid thiophosphinic esters to allow this derivatization scheme to be generally applicable to all classes of steroids. It was observed that reaction temperatures of 70°C or greater caused decomposition of the labile corticosteroids. The reaction time for the thiophosphinic ester formation was optimized using 5α-pregnane-3β,20β-diol as the model steroid (Fig. 2). At reaction times of less than 8 h, a mixture of products was

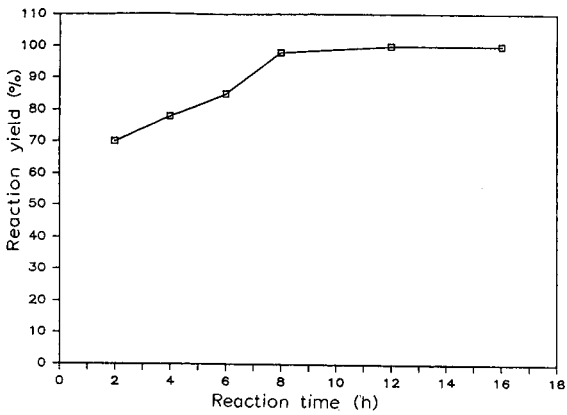

Fig. 2. Reaction time optimization. Model steroid: pregnanediol. Reaction temperature: 45°C.

obtained. This was determined by the appearance of three peaks in the SFC run for pregnanediol. Two early-eluting peaks corresponded to a single-ester formation at either the 3 and 20 positions, respectively, and a later-eluting peak corresponded to the fully derivatized diester of pregnanediol. At reaction times of 8 h or greater, the test chromatogram for pregnanediol contained only one peak, with a retention time matching that for the fully derivatized steroid. To ensure reproducible reaction of more complex steroids, reaction times of 12 h were used for all steroid isolated from physiological fluids.

The linearity and sensitivity of the phosphorus thermionic detector were examined using two representative steroid probes, androstrone and pregnanediol (Fig. 3A and B). All points on the curves were the average of five peak area measurements at each concentration. All peak area measurements had a relative standard deviation (R.S.D.) of 5% or less. Fig. 3A is the calibration curve for the thiophosphinic ester of androsterone (And-PS). The response was linear over 3–4 orders of magnitude with a slope of 0.97 and a minimum detectable quantity (MDQ) of 60 pg And-PS. This corresponds to a sensitivity of 250 fg P/s. with a peak to peak signal-to-noise ratio of 3. Fig. 3B is the calibration curve for the dithiophosphinic ester of pregnanediol (Preg-PS). The detector response was linear over 3–4 orders of magnitude, with a slope of 1.03 and a MDQ of 20 pg Preg-PS. Sensitivity for Preg-PS was 120 fg P/s at a signal-to-noise ratio of 3. As expected, the phosphorus thermionic detector exhibits twice the response for Preg-PS which contains twice the amount of phosphorus as compared to And-PS. Therefore, multiply derivatized steroids should afford even greater sensitivity.

To determine the reproducibility of the thiophosphinic ester reaction, several standard pregnanes (C_{21} steroids) and estrogens were analyzed. Fig. 4 is the standard chromatogram of various pregnane derivatives. The three peaks after 30 min all correspond to doubly derivatized steroids. Compound 3, a pregnanetetrol, reacts at the 3 and 20 positions, while compound 4, β-cortolone, reacts at the 3 and 21 positions. The sterically hindered 11β position and the tertiary hydroxyl group at the 17 position do not react under these circumstances. From these results, ester formation at sterically favorable primary and secondary hydroxyl groups can be predicted with a fair

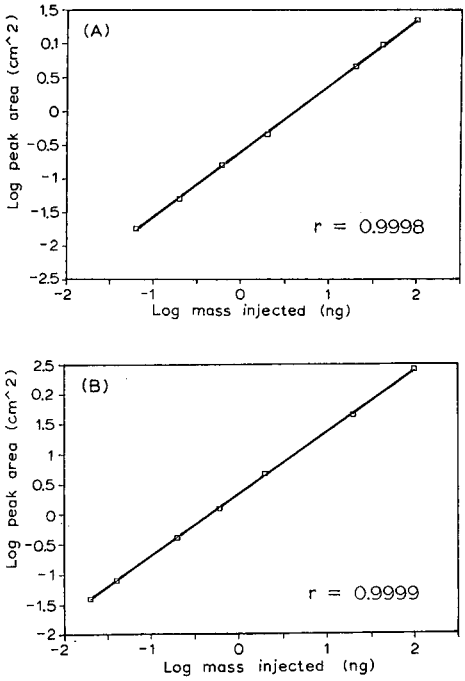

Fig. 3 Linearity of thermionic detection response. (A) androsterone; (B) pregnanediol.

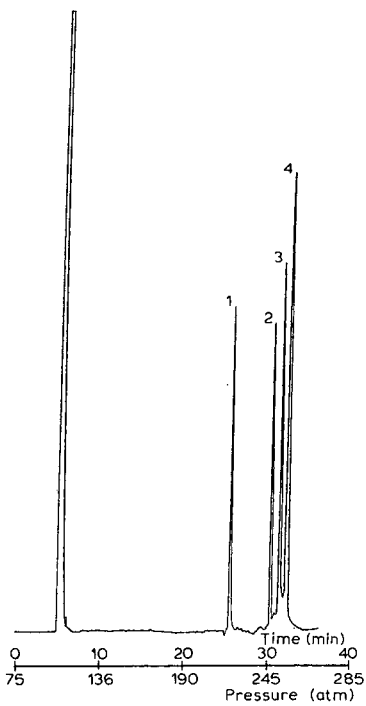

Fig. 4. Standard chromatogram of pregnanes. Peak identifications: 1 = androsterone; 2 = pregnanediol; 3 = 5β-pregnane 3α,11β,17α,20β-tetrol; 4 = 5β-pregnane 3α,17α,20β,21-tetrol-11-one (β-cortolone). Mobile phase: nitrous oxide. Column temperature: 100°C. Pressure ramp: 8 atm/min.

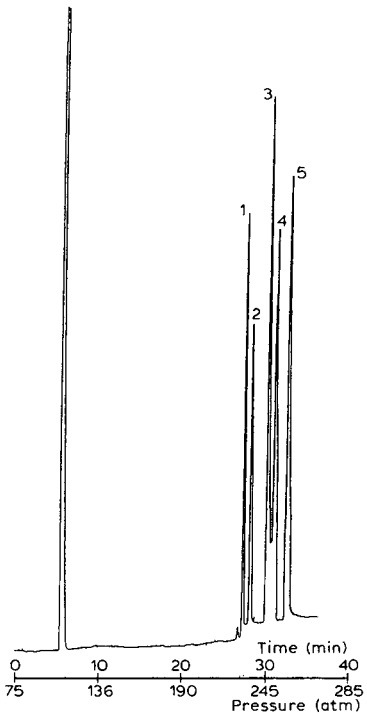

Fig. 5. Standard chromatogram of estrogens. Peak identificatons: 1 = 6-dehydroestrone, 2 = estrone, 3 = estradiol, 4 = 6-ketoestradiol, 5 = estriol. Mobile phase: nitrous oxide. Column temperature: 100°C. Pressure ramp: 8 atm/min.

degree of confidence. All derivatized steroids elute with fairly symmetric peak profiles, indicating that the underivatized hydroxyl groups do not degrade chromatographic efficiency. Fig. 5 is a chromatogram of several standard estrogens. Dimethylthiophosphinic chloride is an excellent reagent for estrogens, in that all the standards steroids were reproducibly and fully derivatized and separated efficiently.

Fig. 6A–C demonstrate chromatograms of the unconjugated, glucuronide, and sulfate steroid fractions, respectively, isolated from human pregnancy urine. All the fractions were spiked at the 10-ng level with androsterone or the respective conjugated androsterone compound as an internal standard. A few steroids have been tentatively identified by retention time comparisons with standard steroids (see figure captions). All the chromatograms were obtained using split injection with a 5:1 split ratio. The steroids in the glucuronide fraction were roughly twice as concentrated as those in the remaining fractions. Consequently, the glucuronide fraction was diluted to twice the final volume of the other fractions to maintain similar chromatographic resolution.

The excellent sensitivity of the phosphorus thermionic detector was demonstrated by the analysis of plasma steroids (Fig. 7A and B). Each fraction was spiked at the 5-ng level with the respective conjugated androsterone compound. Again, the sample introduction method was a split injection with a 5:1 split ratio. Steroids are generally present at ng per ml levels in plasma; therefore, the smaller peaks in the chromatograms correspond to low- or sub-nanogram amounts of steroid thio-

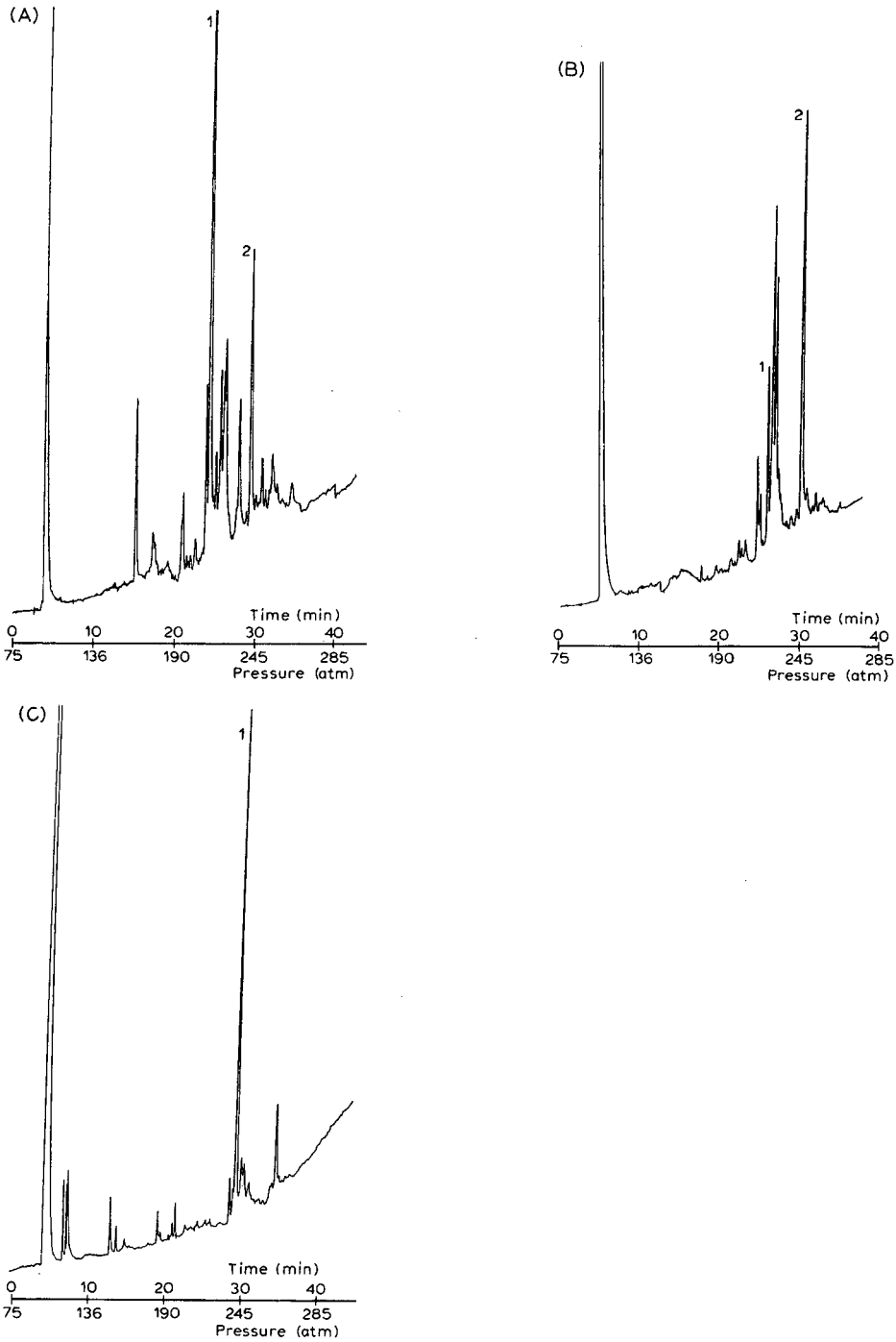

Fig. 6. Chromatograms of urinary steroids. (A) Unconjugated fraction: 1 = androsterone (spike); 2 = estradiol. (B) Glucuronide fraction: 1 = androsterone (spike); 2 = estriol. (C) Sulfate fraction: 1 = 5-androsten-3β-ol-17-one (spike). Chromatographic conditions as in Figs. 4 and 5.

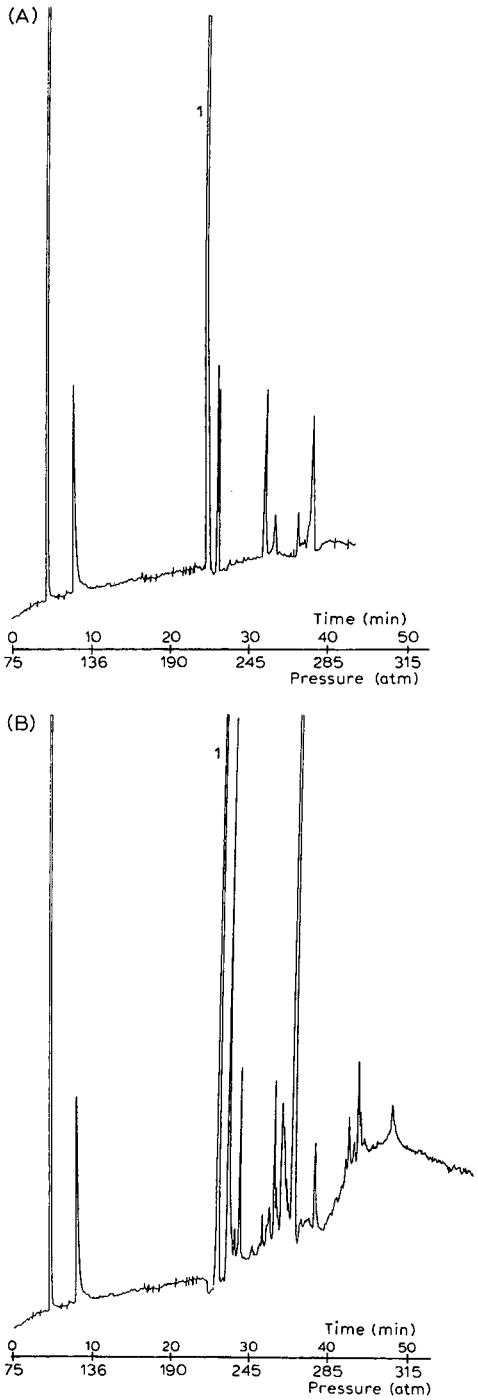

Fig. 7. Chromatograms of plasma steroids. (A) Glucuronide fraction: 1 = androsterone (spike). (B) Sulfate fraction: 1 = 5-androsterone-3β-ol-17-one (spike). Electrometer setting: $2 \cdot 10^{-12}$ A. Other chromatographic conditions as in Fig. 6.

phosphinic esters. These chromatograms serve to illustrate that, under commonly used SFC pressure programming conditions, high sensitivity thermionic detection can be obtained with minimal baseline noise and drift.

Chemical derivatization has been demonstrated as a viable solution to improving the solubility of polar compounds in the common SFC mobile phases carbon dioxide, nitrous oxide. When the derivatization also incorporates a heteroatom-containing moiety into the molecules, highly sensitive thermionic detection can be utilized. The phosphorus mode of the thermionic detector exhibits sufficient sensitivity to permit the analysis of steroids at ppb levels. Capillary SFC provides excellent efficiency for the analysis of these compounds isolated from complex physiological matrices. The capillary SFC analysis of other hydroxy- or amine-containing[14] biochemically important compounds is considerably more attractive when the dimethylthiophosphinic chloride derivatization scheme is utilized in conjunction with phosphorus thermionic detection.

ACKNOWLEDGEMENTS

We thank Dr. Donald Wiesler for his helpful suggestions concerning the reactivity of dimethylthiophosphinic chloride. We also acknowledge Karen Chandler of the Indiana University Student Health Service for assistance in collection of the plasma sample. This research was supported by Grant No. CHE 8605935 from the National Science Foundation and a grant-in-aid from Dow Chemical Company.

REFERENCES

1 T. L. Chester and D. P. Innis, *J. High Resolut. Chromatogr. Chromatogr. Commun.*, 9 (1986) 209–212.
2 C. Borra. F. Andreolini and M. Novotny, *Anal. Chem.*, in press.
3 P. A. David and M. Novotny, *J. Chromatogr.*, 452 (1988) 623–629.
4 K. Jacob and W. Vogt, *J. Chromatogr.*, 150 (1978) 339–344.
5 G. Höfle, W. Steglich and H. Vorbrüggen, *Angew. Cem. Int. Ed. Engl.*, 17 (1978) 569–583.
6 M. Novotny and P. David, *J. High Resolut. Chromatogr. Chromatogr. Commun.*, 9 (1986) 647–651.
7 C. L. Wooley, R. C. Kong, B. E. Ritcher and M. L. Lee, *J. High Resolut. Chromatogr. Chromatogr. Commun.*, 7 (1984) 329–332.
8 C. L. Wooley, B. J. Tarbet, K. E. Markides, M. L. Lee and K. D. Bartle, *J. High Resolut. Chromatogr. Chromatogr. Commun.*, 11 (1988) 113–118.
9 B. W. Wright, P. A. Peaden, M. L. Lee and T. J. Stark, *J. Chromatogr.*, 248 (1982) 17–34.
10 E. J. Guthrie and H. E. Schwartz, *J. Chromatogr. Sci.*, 24 (1986) 236–241.
11 J. A. Lubkowitz, B. P. Semonian, J. Galobardes and L.B. Rogers, *Anal. Chem.*, 50 (1978) 672–676.
12 M. Axelson, B.-L. Sahlberg and J. Sjövall, *J. Chromatogr.*, 224 (1981) 355–37.
13 M. Axelson and B.-L. Sahlberg, *J. Steroid Biochem.*, 18 (1983) 313–321.
14 K. Jacob, C. Falkner and W. Vogt, *J. Chromatogr.*, 167 (1978) 67–75.

Journal of Chromatography, 461 (1989) 121–127
Elsevier Science Publishers B.V., Amsterdam — Printed in The Netherlands

CHROMSYMP. 1501

ENANTIOMER RESOLUTION OF D- AND L-α-AMINO ACID DERIVATIVES BY SUPERCRITICAL FLUID CHROMATOGRAPHY ON NOVEL CHIRAL DIAMIDE PHASES WITH CARBON DIOXIDE

AKIRA DOBASHI, YASUO DOBASHI, TAMAMI ONO and SHOJI HARA*
Tokyo College of Pharmacy, 1432-1 Horinouchi, Hachioji, Tokyo 192-03 (Japan)
and
MUNEO SAITO, SAKAE HIGASHIDATE and YOSHIO YAMAUCHI
Japan Spectroscopic Co. Ltd., 2967-5 Ishikawa-cho, Hachioji, Tokyo 192 (Japan)

SUMMARY

The rapid resolution of racemic N-4-nitrobenzoylamino acid isopropyl esters was accomplished without the loss of enantioselectivity by supercritical fluid chromatography (SFC) on novel chiral valine–diamide phases with carbon dioxide and a polar methanol modifier. In each stationary phase, a chiral moiety was anchored to the silica gel surface by a long decamethylene spacer. The enantioselectivity in SFC was comparable to that in liquid chromatography using 2-propanol–*n*-hexane. The time required for analysis was less than 5 min, and the range of enantiomer resolution (R_s) was 10.8–1.25. On using 2-propanol in place of methanol the separation was improved, but was accompanied by a decrease in column efficiency. The end-capping effect of the remaining surface silanols on enantiomer resolution is discussed.

INTRODUCTION

The liquid chromatographic (LC) resolution of enantiomers offers an intriguing approach to the solution of various stereochemical problems and facilitates the assessment of different metabolic processes that occur between enantiomers in drugs[1,2]. Recent progress in LC, especially with chiral stationary phases (CSPs), clearly demonstrates the variety of applications of this approach. Supercritical fluid chromatography (SFC)[3] should find more general acceptance for more rapid resolution, considering the longer time required for the performance of LC than gas–liquid chromatography[4,5]. Using SFC, the rapid resolution of enantiomers on various kinds of CSPs can be carried out without loss of enantioselectivity, owing to the fast solute diffusion[6–9].

Mourier *et al.*[6] have demonstrated that when used in conjunction with various alcohols as polar modifiers, a super- and subcritical carbon dioxide mobile phase can be used to effect the rapid resolution of racemic phosphine oxide on a classical Pirkle stationary phase. They also discussed a mechanism for the retention of achiral solutes in SFC with carbon dioxide[7]. We have conducted experiments to accelerate the resolution of racemic N-acylated amino acid esters through use of a combination of

0021-9673/89/$03.50

carbon dioxide and a polar modifier (methanol, acetonitrile and diethyl ether) with a chiral diamide phase (N-formyl-L-valylamino)propylsilica[8]. Carbon dioxide, with a polarity close to that of *n*-hexane, is an efficient mobile phase component in which diastereomeric hydrogen-bond associations occur. The separations thus effected occur in less than 4 min. Differences in the action of polar modifiers in SFC and LC resolution were also examined[8].

Novel CSPs used in this study contain a chiral valine–diamide moiety, anchored to the silica gel surface by a long decamethylene spacer (Fig. 1). On the remaining surface silanols, two different CSPs were made; one is exhaustively trimethylsilylated so as to remove bare silanols (CSP 1) and the another is not trimethylsilylated (CSP 2). The long spacer provides good accessibility for solute enantiomers to the chiral moiety without interaction with the silica surface. The CSPs depend entirely on two amide functionalities for entrapping enantiomers through hydrogen bonds and for the outstanding capacity they demonstrate in separating a wide range of enantiomers in LC[10]. On using the CSPs in SFC with polar modifiers, such as methanol and 2-propanol, more rapid enantiomer analysis of amino acid derivatives was achieved while maintaining the high enantioselectivity under LC conditions. The effects due to surface modification with trimethylsilylation on enantiomer resolution and the successful application of SFC resolution are discussed below.

EXPERIMENTAL

SFC was carried out with a Jasco Super-100 SF chromatograph, equipped with a Multi-320 multichannel UV detector, as described previously[8]. The chiral columns (25 cm × 4.6 mm I.D.), each packed with CSP 1 and 2 (Fig. 1), were prepared according to a recently reported procedure[10]. Liquid carbon dioxide was pumped into the column at a flow-rate of 5 ml/min. This flow-rate was measured at −5°C and corresponded to a column inlet pressure of 260 bar. Methanol and 2-propanol were used as polar modifiers and were delivered into the liquid carbon dioxide flow at flow-rates ranging from 10 to 200 μl/min. The column temperature was maintained at 40°C in a column oven. The carbon dioxide density was controlled through regulation of the column outlet pressure from 96 to 200 bar. Mobile phase equilibration was completed within 10 min under these conditions. All other chromatographic conditions were the same as previously reported[8]. The samples to be resolved were also the same as those in previous work[11].

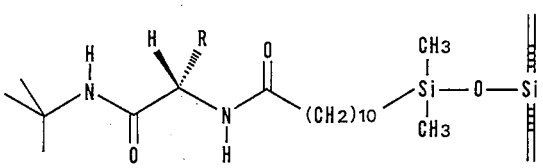

Fig. 1. Chiral diamide-bonded silica (R = isopropyl). The remaining surface silanols on CSP 1 were exhaustively trimethylsilylated. CSP 2, packing not trimethylsilylated.

RESULTS AND DISCUSSION

A series of racemic N-4-nitrobenzoylamino acid isopropyl esters were found to be completely resolved on CSP 1 with a carbon dioxide–methanol mixture, as shown in Table I. LC data obtained with a 2-propanol–*n*-hexane mixture are also included in Table I for comparison with those obtained by SFC. The enantioselectivity in SFC was comparable to that in LC. In the previous study, the enantioselectivity was found to be not so markedly diminished as that in LC when polar methanol was used as a modifier (LC with a possible methanol–*n*-hexane mixture virtually failed to provide any enantiomer resolution of the amino acid derivatives on the classical chiral diamide phase[8]). In LC, maximum enantiomer separability could be induced by separating the chiral moiety from the silica gel surface via a long spacer and by exhaustive trimethylsilylation of the remaining surface silanols[10,12]. Only in this way can diastereomeric hydrogen-bond association in the chiral moiety assume a significant role in determining the enantioselectivity and retentivity of a solute enantiomer[7]. Stated differently, solute retention is determined by the particular degree of hydrogen-bond

TABLE I

COMPARISON OF SFC AND LC WITH ALCOHOL MODIFIERS IN THE RESOLUTION OF RACEMIC N-4-NITROBENZOYLAMINO ACID ISOPROPYL ESTERS ON CSP 1

SFC conditions: liquid carbon dioxide delivery rate, 5 ml/min; column outlet pressure, 200 bar; column temperature, 40°C; methanol modifier delivery rate, 20 μl/min, except for the tryptophan derivative (100 μl/min); column, 25 × 0.46 cm I.D.; detection, UV at 255 nm. LC conditions: mobile phase, 1% (v/v) 2-propanol in *n*-hexane; column temperature, ambient (*ca.* 24°C); flow-rate, 1 ml/min; detection, UV at 254 nm.

Amino acid	*SFC (carbon dioxide–methanol)*				*LC (2-propanol–n-hexane)*		
	t_{RD}*	k'_D**	α***	R_s§	t_{RD}*	k'_D**	α***
Leu	2.69	1.99	2.32	10.75	8.32	1.15	2.69
Val	1.71	0.90	1.69	4.26	6.30	0.64	2.02
Ala	2.00	1.22	1.94	6.54	9.46	1.48	1.89
Phe	2.64	1.93	1.85	7.39	7.96	1.08	2.12
Ile	1.83	1.03	1.74	4.67	5.94	0.67	2.04
Asp	1.55	0.72	1.24	1.25	6.00	0.69	1.29
Glu	2.16	1.40	1.74	5.53	7.50	1.12	1.74
Ser	4.10	3.56	1.34	3.38	20.43	4.15	1.25
Thr	3.17	2.52	1.32	3.78	12.17	2.43	1.30
Tyr	5.37	4.97	1.83	8.02	12.22	2.45	1.80
Cys	5.31	4.90	1.37	4.14	15.40	3.33	1.29
Met	2.99	2.32	1.94	7.90	11.99	1.95	1.93
Trp	11.44	11.71	1.42	6.30	54.08	13.99	1.69

* t_{RD} = Retention time of the first-eluted D-enantiomer.

** k' = Capacity factor for SFC (calculated with nominal hold-up time, determined by the frontal solvent peak, which was a constant 0.89 min under the above SFC conditions).

*** α = separation factor (k' of the L-enantiomer/k' of the D-enantiomer).

§ R_s = resolution $[2\Delta T/(W_D + W_L)]$, where Δt is the difference between t_{RD} and t_{RL} (retention time of the L-enantiomer) and W is the peak width in units of time measurement].

association and therefore, for certain cases of weak hydrogen-bonding solutes, it is difficult to vary the solute retention in response to changes in modifier concentration in LC. In SFC, however, the physical state of carbon dioxide can be adjusted so as to facilitate the retention of less polar solute enantiomers. In this separation study, the column temperature was decreased from 60 to 40°C and the rate of application of methanol modifier from 500 to 20 μl/min, in contrast to the conditions used in the previous SFC study[8]. The time required for enantiomer analysis was less than 5 min, except for the tryptophan derivative, which showed the highest retention of all the amino acid derivatives, being 11.44 min for the first eluted D-enantiomer, even at a methanol flow-rate of 100 μl/min in SFC. Fig. 2a illustrates a typical chromatogram of a racemic N-4-nitrobenzoylleucine isopropyl ester with a high resolution (R_s = 10.8), and Fig. 2b is a chromatogram obtained with a very short analysis time (less than 2 min). In all SFC experiments, the D-enantiomer was always eluted before the L-enantiomer, as in LC.

Mourier and co-workers[6,7] found that 2-propanol, being less polar than methanol, acts more effectively as a modifier in a supercritical carbon dioxide mobile phase, at least with respect to the magnitude of the separation factor. The use of 2-propanol instead of methanol on CSP 1 resulted in a greater separation factor. Resolution data for neutral amino acid derivatives with the 2-propanol modifier are listed in Table II. For instance, at a 2-propanol flow-rate of 40 μl/min, which gave essentially the same retention of the first eluted D-enantiomer as did methanol, the separation factor of the valine derivative was increased from 1.69 to 2.15. Such an effect appears reasonable considering the possibly more competitive association of the more polar methanol compared with the less polar 2-propanol for hydrogen bonds between the chiral moiety and solute enantiomers. With the polar methanol, the column efficiency was greater. The valine derivative indicated an HETP value of 0.165 mm for SFC under the above conditions and 0.076 mm on using the methanol modifier. The average HETP value for all amino acid derivatives resolved was 0.07 mm with the

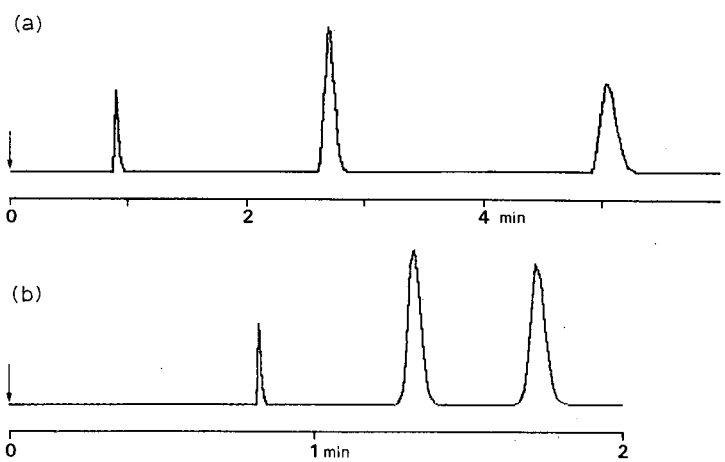

Fig. 2. Optical resolution of racemic N-4-nitrobenzoylleucine isopropyl ester with supercritical carbon dioxide containing methanol as the modifier. (a) SFC conditions as in Table I; (b) SFC on CSP 2 at a methanol flow-rate of 200 μl/min. Other conditions as in Table I.

TABLE II

SFC WITH 2-PROPANOL MODIFIER FOR RESOLUTION OF NEUTRAL N-4-NITROBENZOYLAMINO ACID ISOPROPYL ESTERS ON CSP 1

SFC conditions as in Table I, although the modifier and delivery rate are different.

Amino acid	*Modifier delivery rate (μl/min)*								
	40			*70*			*100*		
	t_{RD}	k'_D	α	t_{RD}	k'_D	α	t_{RD}	k'_D	α
Val	1.68	0.88	2.15	1.63	0.78	1.33	1.54	0.71	1.16
Ala	1.93	1.11	2.02	1.84	1.04	1.90	1.76	0.96	1.83
Phe	2.43	1.78	1.81	2.33	1.58	1.88	2.17	1.40	1.84
Leu	2.49	1.87	2.36	2.37	1.63	2.31	2.22	1.50	2.16

methanol modifier. It is therefore evident that the resolution of a series of enantiomers of the amino acid derivatives can be achieved with the carbon dioxide–methanol mixture. The enantiomer resolution (R_s) exceeded 3.4, except for the aspartic acid derivative (R_s = 1.25). The largest R_s, 10.8, was obtained with the leucine derivative.

Fig. 3 shows the influence of the 2-propanol content on the retention of the first eluted D-enantiomer of the (a) leucine and (b) alanine derivatives and on the separation factors of these derivatives. Comparison of trimethylsilylated CSP 1 with non-trimethylsilylated CSP 2 in Fig. 3 indicates that CSP 2 causes a greater increase in retention with decreasing 2-propanol content. In both instances a greater enantiomer retention initially led to a slight increase in the separation factor, and then a marked decrease ensued. In contrast, CSP 1 caused less change in the retention and separation factors. It is particularly significant that no marked decrease in the separation factor occurred in a region of lower 2-propanol content for CSP 1. With CSP 1, the supercritical mobile phase gave fairly symmetrical peaks, whereas CSP 2 gave a larger peak asymmetry factor, *i. e.*, a greater degree of peak tailing, with an increase in enantiomer retention. Peak asymmetry factors[13], as determined from the first eluted peak, are given in Fig. 3. The retention behaviour of the two enantiomeric derivatives with changing methanol content were similar to those observed with changing 2-propanol content, as can be seen from Fig. 4. The retention enhancement with a decrease in the modifier content was, however, smaller with methanol than with 2-propanol as the modifier. At methanol flow-rates exceeding 50 μl/min, either derivative provided greater separation factors on CSP 2 than on CSP 1. Fig. 2b shows rapid resolution of the leucine derivative on CSP 2 at a flow-rate of 200 μl/min.

The results of a previous LC study on CSP 1 clearly demonstrate that the separation factor becomes larger after trimethylsilylation of the remaining surface silanols of the CSPs[10,12]. However, under SFC conditions, the separation factor decreased rather than increased with trimethylsilylation in experiments with higher modifier contents. This tendency was more pronounced with the leucine than the alanine derivative when the 2-propanol modifier was used. As reported by Mourier *et al.*[7], the retention effect, as discussed in connection with non-polar–non-polar chromatography[14], may contribute at least to some extent to SFC when using the CSP discussed here. When conducting non-polar–non-polar chromatography with octade-

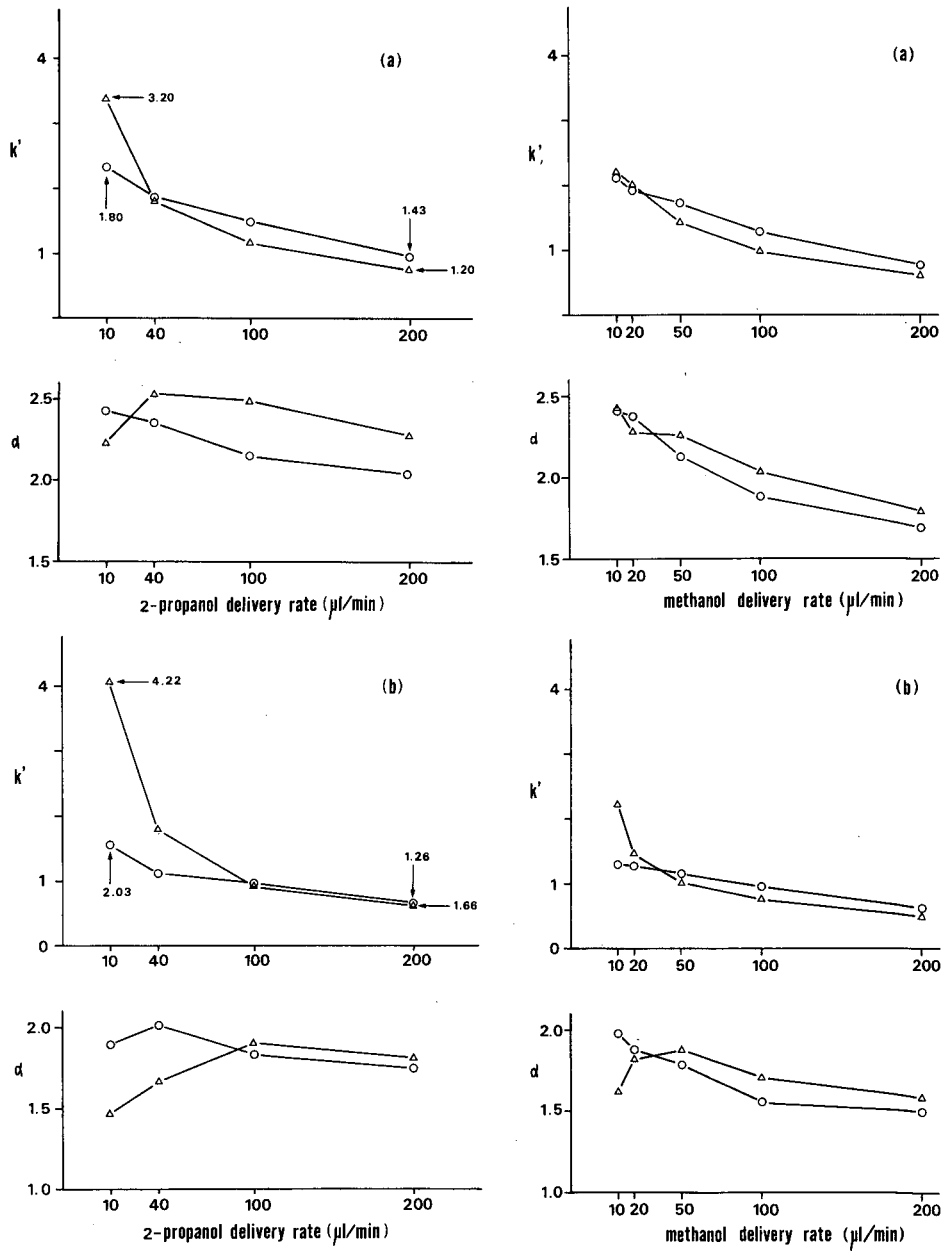

Fig. 3. Influence of 2-propanol delivery rate on k' of the first-eluted D-enantiomer of racemic (a) leucine and (b) alanine derivatives and on α. SFC conditions as in Table I, but with different modifier and delivery rate. ○, For CSP 1, trimethylsilylated packing; △, for CSP 2, packing not trimethylsilylated. Peak asymmetry factors (A_s), calculated from the first-eluted peak, are indicated by arrows.

Fig. 4. Influence of methanol delivery rate on k' of the first-eluted D-enantiomer of racemic (a) leucine and (b) alanine derivatives and on α. SFC conditions as in Table I, but with different delivery rate. ○, For CSP 1; △, for CSP 2.

cylsilica as the stationary phase and *n*-hexane as the mobile phase, the solute retention increases with decrease in the concentration of polar alcohol modifier in the mobile phase. Should the above contribution of the non-polar–non-polar interaction to the enantiomer retention become apparent on the trimethylsilylated surface of CSP 1, this would possibly lead to greater increase in retention than that observed on CSP 2 and a decrease in the separation factor through intervention of a non-chiral retention process other than the aforementioned hydrogen-bond association. The leucine derivative, having an isobutyl side-chain, would probably exert a greater influence on CSP 1 than the alanine derivative with only a methyl side-chain. This influence of surface modification on retention and enantioselectivity will be examined in further detail.

REFERENCES

1 S. Hara and J. Cazes (Editors), *Optical Resolution by Liquid Chromatography, J. Liq. Chromatogr.*, Special Issue, 9, Nos. 2 and 3 (1986).
2 L. J. Crane and M. Zief (Editors), *Chromatographic Chiral Separations*, Marcel Dekker, New York, 1987.
3 M. Novotny, S. R. Springston, P. A. Peaden, J. C. Fjeldstad and M. L. Lee, *Anal. Chem.*, 53 (1981) 407A.
4 V. Schurig, in J. D. Morrison (Editor) *Asymmetric Synthesis*, Vol. 1, Academic Press, London, 1983, p. 59.
5 W. A. Koenig, *The Practice of Enantiomer Separation by Capillary Gas Chromatography*, Hüthig, Heidelberg, 1987.
6 P. A. Mourier, E. Eliot, M. H. Caude, R. H. Rosset and A. G. Tambute, *Anal. Chem.*, 57 (1985) 2819.
7 P. Mourier, P. Sassiat, M. Caude and R. Rosset, *J. Chromatogr.*, 353 (1986) 61.
8 S. Hara, A. Dobashi, K. Kinoshita, T. Hondo, M. Saito and M. Senda, *J. Chromatogr.*, 371 (1986) 153.
9 P. Macaudiere, M. Caude, R. Rosset and A. Tambute, *J. Chromatogr.*, 405 (1987) 135.
10 A. Dobashi, Y. Dobashi, K. Kinoshita and S. Hara, *Anal. Chem.*, 60 (1988) 1985
11 A. Dobashi and S. Hara, *Anal. Chem.*, 55 (1983) 1805.
12 Y. Dobashi and S. Hara, *J. Org. Chem.*, 52 (1987) 2490.
13 L. R. Snyder and J. J. Kirkland, *Introduction to Modern Liquid Chromatography*, Wiley, New York, 2nd ed., 1979, p. 222.
14 C.-G. Wu and S. N. Deming, *J. Chromatogr.*, 302 (1984) 79.

Journal of Chromatography, 461 (1989) 129–137
Elsevier Science Publishers B.V., Amsterdam — Printed in The Netherlands

CHROMSYMP. 1484

COMPUTATIONAL CHEMICAL STUDIES OF CHIRAL STATIONARY PHASE MODELS

COMPLEXES OF METHYL N-(2-NAPHTHYL)ALANINATE WITH N-(3,5-DINITROBENZOYL)LEUCINE *n*-PROPYLAMIDE

SID TOPIOL* and MICHAEL SABIO
Department of Medicinal Chemistry, Berlex Laboratories Inc., 110 East Hanover Avenue, Cedar Knolls, NJ 07927 (U.S.A.)

SUMMARY

Recent computational chemical studies on (*S*)-methyl N-(2-naphthyl)alaninate with (*S*)- and (*R*)-N-(3,5-dinitrobenzoyl)leucine *n*-propylamide were further refined by using semi-empirical quantum-chemical methods for determining structural and energetic parameters. These results confirm the earlier prediction that the same three primary interactions ("contact points") that others have proposed for the *SS* complex can also be achieved by the less stable *SR* complex without significant additional energy. Thus, a classical three-point mechanism for chiral recognition is not expected to be operative in this interaction model. We have verified earlier predictions that the computationally determined repulsive nature of the π interaction could become attractive through the use of more refined calculations, while still maintaining the equality between the *SS* and *SR* complexes.

INTRODUCTION

It is becoming increasingly evident, in areas such as drug design, that it is often critically important to separate enantiomers[1]. One approach, which is being widely developed, is stereoselective synthesis. Alternatively, methods are being developed for chiral separations after synthesis, typically by means of some resolving agent[2–7]. One of the most widely used approaches to the separation of enantiomers is chromatography on the chiral stationary phases developed by Pirkle and co-workers[7–10]. A model for the molecular interactions responsible for chiral separation has been suggested for some of these systems[7–10]. In order to aid in their analysis, computational chemical studies have been undertaken on models of these systems. For instance, Lipkowitz and co-workers[11–15] have used molecular mechanical and semi-empirical quantum-chemical methods to optimize the conformations of models for the isolated analytes and stationary phases. These workers have also studied intermolecular interactions of these models by using a rigid monomer approximation. Similar studies, based on molecular mechanical methods, have been reported by Norinder and Sundholm[16].

0021-9673/89/$03.50

Recently, we have also reported studies[17] on the model complex of (*S*)-methyl N-(2-naphthyl)alaninate (NAP) with (*S*)- and (*R*)-N-(3,5-dinitrobenzoyl)leucine *n*-propylamide (DNB; *SS* and *SR* complexes), where the former was used as a model for the stationary phase and the latter as the analyte. In these studies, all the geometric parameters of the complexes were fully optimized by molecular mechanical methods. Interaction energies for the complexes and model fragments were then evaluated by semi-empirical and *ab initio* quantum-chemical methods. In this way, the interaction model proposed by Pirkle and co-workers for the complex of the *S* enantiomers of NAP and DNB (*i.e.*, the *SS* complex; see Fig. 1) was examined.

In this model, three primary interactions are responsible for stabilization of the complex: a π–π interaction and two hydrogen bonds (see Fig. 1). Loss of one of these interactions has been suggested as responsible for the lesser stability of the (*S*)-NAP–(*R*)-DNB complex[7–10]. We therefore also investigated the interaction of (*S*)-NAP with (*R*)-DNB. Analysis of the results showed that the *SS* complex is stable in the form suggested by Pirkle and co-workers, but that the *SR* complex is able to maintain the same three interactions without any significant conformational strain. This led to the conclusion that the proposed model is not responsible for chiral recognition through a classical three-point interaction mechanism (we shall hereafter refer to such primary interactions as "contact points"). A classical three-point interaction required the participation of atoms or groups along three different bonds at the chiral center. The model proposed by Pirkle and co-workers, which involves three primary interactions between (*S*)-NAP and (*S*)- or (*R*)-DNB, can be considered a pseudo-two-point interaction scheme because the three contact points lie along only two of the bonds of the chiral center (see the Results and Discussion).

In a previous study[17], we found that the total interaction energies for the *SS* and *SR* complexes were similar to each other when assessed by the molecular mechanics-derived structures in semi-empirical quantum-chemical AM1 calculations[18],

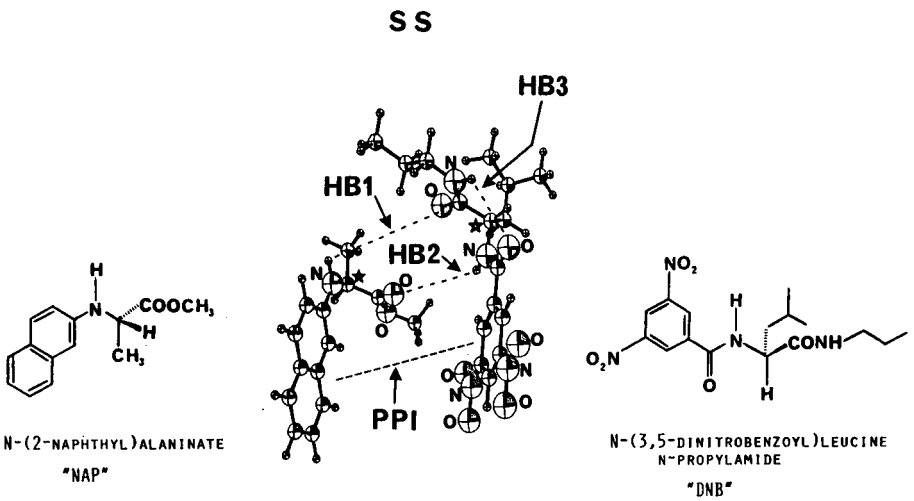

Fig. 1. Schematic representation of the interaction model for (*S*)-NAP with (*S*)-DNB. HB1 and HB2 represent the two intermolecular hydrogen bonds, and HB3 represents the intramolecular hydrogen bond in DNB. PPI denotes the interaction of the π systems of NAP and DNB.

i.e., AM1//MMFF (see ref. 17 for details of the calculations and see the Experimental section for an explanation of this notation). In addition, when these three interactions were modeled separately as small fragments, the interaction energies for the *SS* and *SR* models were also similar and, when added to each other, they approximately reproduced the total interaction energy of the respective complex. This suggested that these three interactions are indeed the dominant interactions of these complexes. It was also found that both hydrogen bonds were predicted to be stabilizing, HB2 (see Fig. 1) being more stable. This result was consistent with the NOE data of Pirkle and Pochapsky[8–10]. On the other hand, while the two (*SS* and *SR*) π interactions were found to be nearly equal to each other and therefore not expected to be responsible for chiral recognition, they were found to be slightly repulsive. Similar conclusions from experimental data for related systems have been reported by Wainer and Alembik[19]. Although chiral recognition could only be a function of the inequality of *SS* and *SR* interactions and does not depend on whether they are stabilizing or destabilizing, it was speculated that these destabilizing interactions could become stabilizing on further refinement of the calculations. Therefore, it seemed worthwhile to explore this aspect further. We report below more sophisticated quantum-chemical calculations on these systems, aimed at refining the question of the stability of the π interactions.

EXPERIMENTAL

Completely relaxed geometries of the complexes of (*S*)-NAP with the *R* and *S* enantiomers of DNB were obtained by using the semi-empirical quantum-chemical AM1[18] method, as implemented in AMPAC (Version 1.00)[20]. Substructures derived from the fully optimized complexes were generated in CHEM-X[21] in order to model the important interactions of the complexes. AM1 energies of interaction were calculated for the AM1 completely relaxed geometries of the complexes and frozen fragments thereof. In this paper, energy calculations using method "X" for structures derived from method "Y" are denoted X//Y. For example, AM1//MMFF signifies that an AM1 energy calculation was performed for a structure optimized by the MMFF method.

RESULTS AND DISCUSSION

In a previous study[17] the structures of the model complexes were fully optimized with the MMFF molecular-mechanics method. The local minimum investigated for the *SS* complex was that based on the model proposed by Pirkle and coworkers[7–10]. As described[17], a similar minimum was found for the SR complex. These structures are shown in Fig. 2 (upper structures). Full reoptimization of all the structural parameters for both complexes by means of the semi-empirical quantum-chemical AM1 method has now also been performed. These structures are also shown in Fig. 2 (lower structures). Some of their interesting features are evident. Once again, both the *SS* and the *SR* complexes maintain all three primary interactions. Also, the two structures are again strikingly similar to each other. The primary difference is in the reversal of the hydrogen atom and *sec.*-butyl group on the chiral center of (*R*)- *vs.* (*S*)-DNB. As pointed out previously[17], these groups sit outside the region of

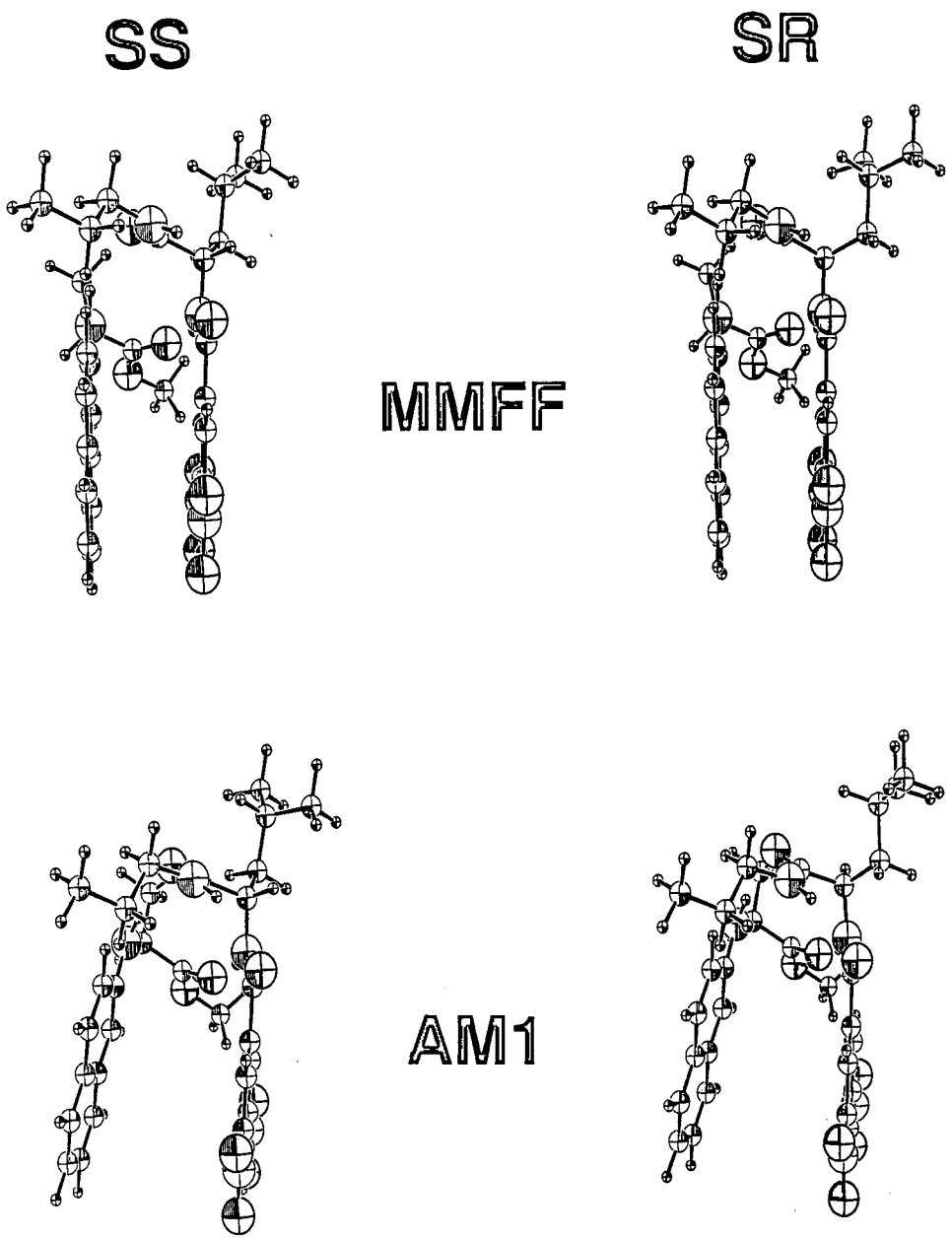

Fig. 2. Structures of the *SS* and *SR* complexes fully optimized with the MMFF molecular mechanics (see ref. 17) and the semi-empirical AM1 methods. See Fig. 1. for details.

the primary interactions and could only exert a differential effect in the form of through-space field interactions. Of course, it is possible that these differences could lead to chiral recognition. This could be illustrated with the recently proposed dis-

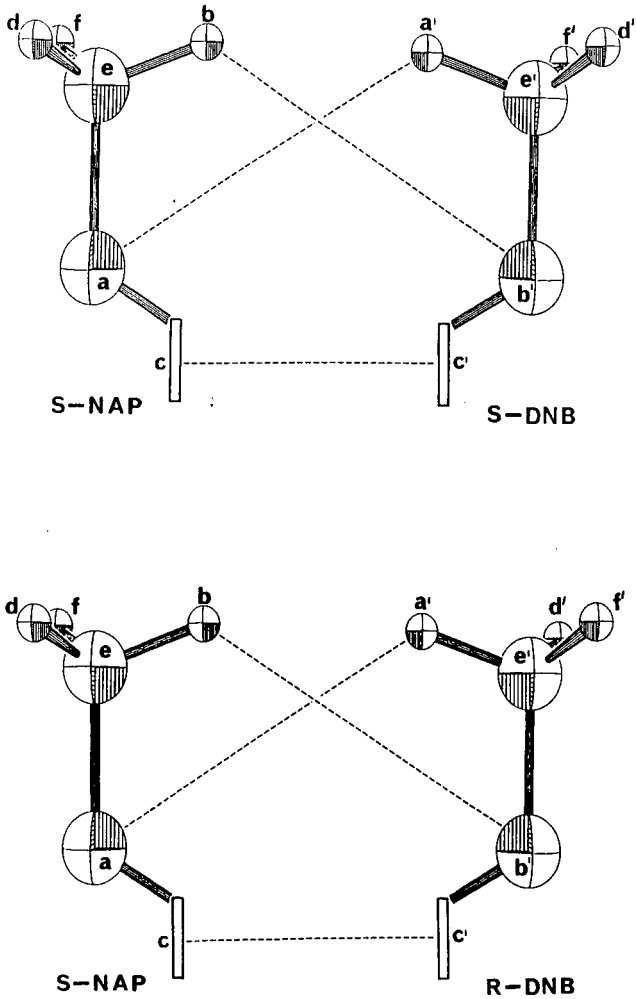

Fig. 3. Schematic representation of the primary interactions in the *SS* and *SR* complexes of NAP and DNB. a---a′ and b---b′ represent the two hydrogen bonds and c---c′ represent the π–π interaction (see Fig. 1).

tance-matrix analysis[22]. Nevertheless, it is clear that a classical three-contact-point mechanism is not responsible for chiral recognition here. This is because the three contact points lie along only two of the bonds of the chiral centers. Thus, in terms of classical point-of-interaction schemes, these may be thought of as pseudo-two-point interactions (see Fig. 3).

It is also evident from the structures shown in Fig. 2 that the aromatic systems of the π interactions are not as close in space when optimized with the AM1 method. Hence the repulsive nature of the π interactions when the MMFF structures are used for AM1 calculations are likely to be a result of having too small a separation between the dinitrobenzoyl and naphthyl groups.

TABLE I

GEOMETRY OF COMPLEXES OF (*S*)-METHYL N-(2-NAPHTHYL)ALANINATE (NAP) WITH N-(3,5-DINITROBENZOYL)LEUCINE *n*-PROPYLAMIDE (DNB)

Parameter	*Geometry*			
	S(NAP)–S(DNB) complex		*S(NAP)–R(DNB) complex*	
	MMFF*	AM1*	MMFF*	AM1*
Geometric parameter**:				
HB1 (Å)	2.217	2.153	2.225	2.152
HB2 (Å)	2.341	2.081	2.302	2.073
HB3 (Å)	2.365	2.276	2.226	2.187
Naphthyl (NAP) and phenyl (DNB) rings:				
Distance between centroids (Å)	3.384	4.959	3.388	5.069
Measure of angle between normals (degrees)	2.4	11.5	2.1	14.0

* Method of geometry optimization. See the Experimental sections here and in ref. 17 for details.
** See Fig. 1.

Quantitatively, Tables I and II show that the structures and energies of the *SS* and *SR* complexes are indeed very close to each other for the AM1 optimized structures. Based on a comparison of the AM1 total energies of the AM1-derived (or molecular mechanics-derived) geometries of the complexes, the *SS* complex is 0.83 (or 0.89) kcal/mol more stable than the *SR* complex (see the bottom of Table II); this difference represents a combination of both the differential through-space field effects (see above) and conformational strain energy. As described more fully in ref. 17, while total energies may not be very reliable, energy differences, which are used as indicators of separability, may be more reliable. We note that energy differences of *ca.*

TABLE II

ENERGETICS OF COMPLEXES OF (*S*)-METHYL N-(2-NAPHTHYL)ALANINATE [NAP] WITH N-(3,5-DINITROBENZYL)LEUCINE *n*-PROPYLAMIDE [DNB]

*Structure***	*Parameter*	*S(NAP)–S(DNB) complex*		*S (NAP)–R(DNB) complex*	
		AM1//MMFF*	AM1//AM1*	AM1//MMFF*	AM1//AM1*
PHB1	Interaction energy	−2.94	−2.85	−2.91	−2.81
PHB2	(kcal/mol)***	−5.20	−6.70	−4.97	−6.64
PPI-SM		3.70	−0.84	3.66	−0.82
PPI		3.61	−1.04	3.69	−1.01
Complex		−5.19	−11.22	−4.96	−11.37
Complex	Difference in total energy (kcal/mol)	−0.89	−0.83		

* Method of energy calculation. See the Experimental section for a definition of the notation and see ref. 17 of the details of the AM1//MMFF calculations.
** See Fig. 4 and the Experimental section.
*** See the Results and Discussion section for a note about the accuracy of the interaction energies.

0.5 kcal/mol correspond to separability factors in the range of 1.0–1.5, whereas differences of 2–4 kcal/mol correspond to factors of 100–200.

The interaction energies of the complexes, and those based on the model fragments for the three primary interactions shown in Fig. 4, are very similar for the AM1 structures (see Table II). The substructures of the complexes were taken from the fully relaxed geometries of the complexes. The geometries of the isolated substructures were not subsequently relaxed. Hence the interaction energies of the complexes and the various substructures in Table II are calculated less accurately than the total energy of either complex. For example, with full relaxation permitted for all geomet-

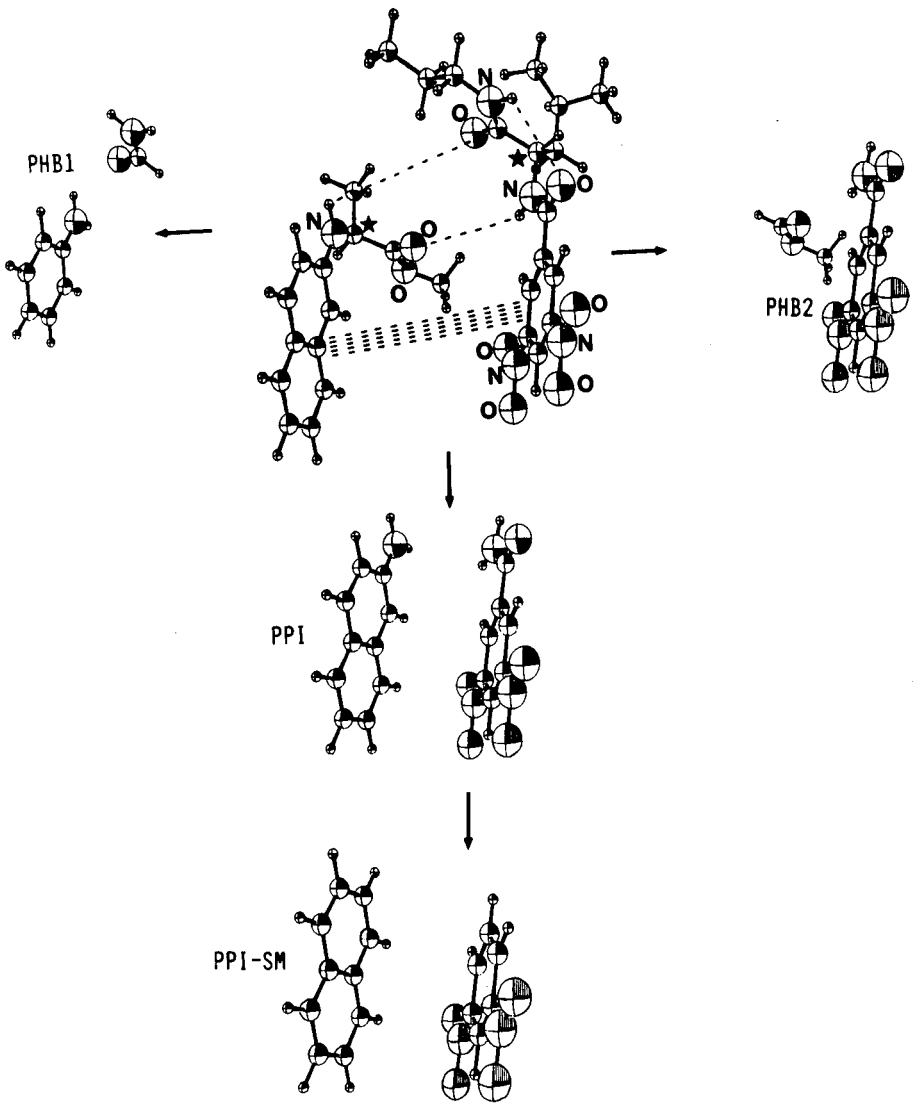

Fig. 4. Schematic representation of the model fragments of the NAP–DNB complex.

ric parameters of NAP and DNB (or analogously for the substructures), each as an isolated entity, the differences in the interaction energy of the *SS* and *SR* complexes would be equivalent in magnitude and direction to the difference in the total energies of the complexes due to the energetic equivalence of the two enantiomers of DNB.

The qualitative nature of the two hydrogen bonds remains the same for the AM1 structures, although the hydrogen bond HB2 is *ca.* 1.5 kcal/mol more stable here than with the MMFF structure. On the other hand, the π interactions for the *SS* and *SR* complexes remain similar to each other but are lowered in energy by *ca.* 4.5 kcal/mol so that they now contribute slightly to the stabilization of the complexes. It is apparent that a separation of the dinitrobenzoyl and naphthyl groups which is greater than that of the molecular mechanics-derived structures is required for the π interaction to become stabilizing (see above).

CONCLUSIONS

Further investigations of the proposed model for the interaction of the *SS* complexes of NAP and DNB based on the semi-empirical AM1 optimized results are in basic qualitative agreement with earlier findings that the same three contact points may be achieved by the *SR* complex also. This is because the three contact points, in classical terms, form a pseudo-two-point interaction mechanism. Hence this interaction scheme cannot be reponsible for chiral recognition through a classical three-point-interaction mechanism, requiring either the loss of one of these contact points for the less stable *SR* complex or inaccessible strain energy. If this interaction model is the energetically dominant one for both the *SS* and *SR* complexes, chiral recognition could be achieved via through-space field effects. These effects could be understood through the use of the distance-matrix analysis scheme recently proposed for chiral recognition[22] Alternatively, other mechanisms must be responsible for chiral recognition. For example, it may be that chiral recognition is achieved through the composite of many low-energy conformations of the complexes. Approaches for treating such mechanisms have recently been proposed[23,24]. Another possible factor is the dimerization of the analytes. Recent experimental findings by Pirkle and Pochapsky[8] support such a possibility.

ACKNOWLEDGEMENT

We are grateful to Walton Caldwell for valuable discussions.

REFERENCES

1 E.J. Ariens, *Trends Pharmacol. Sci.*, 7 (1986) 200, and references cited therein.
2 D.W. Armstrong, *Anal. Chem.*, 59 (1987) 84A.
3 D.W. Armstrong, *J. Liq. Cromatogr.*, 7 (S-2) (1987) 353.
4 Y. Okamoto, *Chemtech*, 17 (1987) 176.
5 S. Allenmark, *J. Biochem. Biophys. Methods*, 9 (1984) 1.
6 V.A. Davankov, A.R. Kurganov and A.S. Bochkov, *Adv. Chromatogr.*, 22 (1948) 71.
7 W.H. Pirkle and J. Finn, in J.D. Morrison (Editor), *Asymmetric Synthesis*, Academic Press, New York, 1983, pp. 87–124.
8 W.H. Pirkle and T.C. Pochapsky, *J. Am. Chem. Soc.*, 109 (1987) 5975.
9 W.H. Pirkle and T.C. Pochapsky, *J. Am. Chem. Soc.*, 108 (1986) 5627.

10 W.H. Pirkle and T.C. Pochapsky, *J. Am. Chem. Soc.*, 108 (1986) 352.
11 K.B. Lipkowitz, D.A. Demeter, J.M. Landwer, C.A. Parish and T. Darden, *J. Comput. Chem.*, 9 (1988) 63.
12 K.B. Lipkowitz, D.A Demeter, C.A. Parish, J.M. Landwer and T. Darden, *J. Comput. Chem.*, 6 (1987) 753.
13 K.B. Lipkowitz, J.M. Landwer and T. Darden, *Anal. Chem.*, 58 (1986) 1611.
14 K.B. Lipkowitz, D.J. Malik and T. Darden, *Tetrahedron Lett.*, 27 (1986) 1759.
15 K.B. Lipkowitz, D.A. Demeter and C.A. Parish, *Anal. Chem.*, 59 (1987) 1731.
16 U. Norinder and E.G. Sundholm, *J. Liq. Chromatogr.*, 10 (1987) 2825.
17 S. Topiol, M. Sabio, J. Moroz and W.B. Caldwell, *J. Am. Chem. Soc.*, 110 (1988) 8367.
18 M.J. Dewar, E.G. Zoebisch, E.F. Healy and J.J.P. Stewart, *J. Am. Chem. Soc.*, 107 (1985) 3902.
19 I.W. Wainer and M.C. Alembik, *J. Chromatogr.*, 367 (1986) 59.
20 J.J.P. Stewart, *AMPAC, Version 1.00,* Quantum Chemistry Program Exchange, Program No. 506, 1986.
21 *CHEM-X,* Copywrite 1986, 1987, 1988, Chemical Design, Oxford.
22 S. Topiol, Chirality, 1 (1989) in press.
23 R.E. Boehm, D. Martire and D.W. Armstrong, *Anal. Chem.*, 60 (1988) 522.
24 K.B. Lipkowitz, D.A. Demeter, R. Zegarra, R. Larter and T. Darden, *J. Am. Chem. Soc.*, 110 (1988) 3446.

Journal of Chromatography, 461 (1989) 139–147
Elsevier Science Publishers B.V., Amsterdam — Printed in The Netherlands

CHROMSYMP. 1475

RETENTION MECHANISMS ON METALLIC STATIONARY PHASES

BARBARA J. BASSLER*, ROMAN KALISZAN** and RICHARD A. HARTWICK*
Department of Chemistry, Rutgers University, Piscataway, NJ 08854 (U.S.A.)

SUMMARY

An electron-rich, porous graphitic carbon stationary phase for high-performance liquid chromatography has been shown to act as an electron-pair acceptor of solutes under non-polar conditions. The application of delocalized electron bands as chromatographic substrates was extended to other conductors, namely a palladium metal stationary phase, which also interacted by an electron donor–acceptor mechanism. Quantitative structure–retention relationships are presented as indicators of chromatographic retention mechanisms.

INTRODUCTION

Despite the widespread use of chromatography as an analytical tool, relatively little is known about chromatographic mechanisms at the molecular level. In the course of studying various non-polar stationary phases for use in retention prediction, porous graphitic carbon, which was expected to behave as an "ideal reversed phase"[1], produced retention behavior anomalous for classical reversed phases[2].

Upon closer examination, retention on graphite should not be governed by only dispersive (electrostatic) interactions, particularly under non-polar solvent conditions where solvophobic phenomena[3] are minimized. The uniqueness of porous graphitic carbon compared to hydrocarbonaceous stationary phases is due to its delocalized band of electrons[4], available for electronic interactions, specifically donor–acceptor (charge transfer) interactions and direct π-electron overlap[5,6]. Using the tools of quantitative structure–retention relationships (QSRRs)[7], *i.e.*, linear free-energy relationships, the chromatographic column becomes a "free-energy transducer"[8], translating differences in chemical potentials of solutes, arising from differences in structure, to chromatographic retention. If such electronic interactions, in addition to the expected London forces, are governing retention on porous graphitic carbon, then solute descriptors reflecting electron donor–acceptor properties and/or orbital energies should be highly correlated to solute retention.

Furthermore, if the delocalized electron band of graphite contributes sub-

* On educational leave from Hoechst-Roussel Pharmaceuticals, Somerville, NJ 08876, U.S.A.
** Present address: Department of Biopharmaceutics and Pharmacodynamics, Medical Academy, 80-416 Gdansk, Poland.

0021-9673/89/$03.50

stantially to its selectivity, then an entire class of substrates possessing similar electronic structures, *i.e.*, metals and conductive polymers, should also exhibit similar characteristics as chromatographic stationary phases. Metal ions have previously been used in chromatography to alter and improve retention properties of conventional stationary phases through the formation of discrete metal complexes[9–15]. However, reduced metal or metal-like surfaces have not been widely studied as chromatographic phases.

The experiments described in this report were designed to (1) determine whether the delocalized bands of electrons in porous graphitic carbon participate in solute–substrate interactions under non-polar solvent conditions, and (2) determine whether selected metals behave in a similar fashion, demonstrating a new class of stationary phases based on solute–[conduction-band] interactions.

EXPERIMENTAL

Materials

Porous graphitic carbon was obtained from Professor John Knox (University of Edinburgh, Edinburgh, U.K.). Palladium spheres (nominal diameter 8 μm) were lent by Platina Laboratories (Piscataway, NJ, U.S.A.). Solvents were of high-performance liquid chromatography (HPLC) grade and were purchased from Fisher (Pittsburgh, PA, U.S.A.). Solutes (Table I) of the highest available purity were purchased from various sources and used without further purification.

TABLE I

SOLUTE SET FOR CHROMATOGRAPHIC ANALYSES

1	Benzene	C_6H_6
2	Toluene	$C_6H_5CH_3$
3	Acetophenone	$C_6H_5COCH_3$
4	Chlorobenzene	C_6H_5Cl
5	Methyl benzoate	$C_6H_5COOCH_3$
6	Nitrobenzene	$C_6H_5NO_2$
7*	Aniline	$C_6H_5NH_2$
8	Anisole	$C_6H_5COCH_3$
9	Benzyl alcohol	$C_6H_5CH_2OH$
10	Phenol	C_6H_5OH
11	*p*-Cresol	$C_6H_4OHCH_3$
12	4-Ethylphenol	$C_6H_4OHC_2H_5$
13	4-*n*-Propylphenol	$C_6H_4OHC_3H_7$
14	4-*sec.*-Butylphenol	$C_6H_4OHCH(CH_3)(CH_2CH_3)$
15	4-*tert.*-Butylphenol	$C_6H_4OHC(CH_3)_3$
16	Carvacrol	C_6H_3OH-*o*-CH_3-*m*-$CH(CH_3)_2$
17	Thymol	C_6H_3OH-*m*-CH_3-*o*-$CH(CH_3)_2$
18	2-Isopropylphenol	$C_6H_4OHCH(CH_3)_2$
19	2-*tert.*-Butylphenol	$C_6H_4OHC(CH_3)_3$
Additional solutes		
20	Pyridine	C_5H_5N
21	3-*tert.*-Butylphenol	$C_6H_4OHC(CH_3)_3$
22	2-*sec.*-Butylphenol	$C_6H_4OHCH(CH_3)(CH_2CH_3)$

* Not included in correlations.

Chromatographic apparatus and conditions

The chromatographic system was comprised of a Model 8500 syringe pump (Varian, Walnut Creek, CA, U.S.A.), a Model 834 autosampler (DuPont, Wilmington, DE, U.S.A.), a Model 7013 injection valve with 1-μl loop (Rheodyne, Cotati, CA, U.S.A.) and a Model 757 UV detector, 210 nm, with 0.5-μl flowcell (Kratos Analytical, Ramsey, NJ, U.S.A.). A temperature-controlled chamber, made from R-10 foam insulation and thermostated with 3 m of 1 cm diameter copper tubing containing circulating temperature-controlled water, housed 0.5 m of mobile phase equilibration tubing, the injection valve and the column. A 30 cm × 1 mm glass-lined, stainless-steel column blank (previously silanized with trimethylchlorosilane) was packed with a slurry of porous graphitic carbon in heptane at 3000 p.s.i. for 1 h. A 50 cm × 1 mm glass-lined, stainless-steel column blank (also silanized) was dry-packed with palladium spheres. Heptane-dissolved solutes were chromatographed with neat heptane eluent at 2 ml/h for porous graphitic carbon or 4 ml/h for palladium and 23°C with detection at 210 nm. The column void volume was determined by refractive index change of an injection of pentane in heptane. Chromatographic data were collected with MAXIMA™ chromatography software (Dynamic Solutions, Ventura, CA, U.S.A.). The first statistical moments (retention times) of the peaks were calculated by summation of at least 50 time slices, by downloading the data from MAXIMA™ to Lotus 123™ (version 2.01; Lotus Development, Cambridge, MA, U.S.A.) where the moment analyses were completed.

Molecular descriptors and statistical analysis

QSRRs were constructed by statistical correlation of matrices[7]: (1) $m \cdot n$, where m = solute and n = various numerical molecular descriptors, and (2) $m \cdot l$, where l = solute retention, expressed as log k'. Molecular descriptors [heat of formation (H_f), total energy (E_{tot}), E_{homo}, E_{lumo}, dipole moment and excess atom charge] were calculated for each solute by using MNDO3[16] on molecular coordinate files obtained from the Cambridge Crystallographic Database[17]. Calculations were performed on a VAX 780 computer with an array processor.

Submolecular polarity parameters, Δ, were calculated from excess atomic charges[18]. Values of pK were obtained from the literature[19]. Statistical models were constructed by stepwise linear regression by means of Asystant+™ software (version 1.0; Macmillan Software, New York, NY, U.S.A.). The suitability of retention models was determined by correlation coefficients and statistical significance.

Surface analysis of phases

Scanning Auger spectroscopy was performed on the palladium powder to determine surface characteristics (presence of oxidation or contaminants).

RESULTS AND DISCUSSION

Retention mechanisms under normal-phase conditions

Experimental conditions were chosen (heptane eluent, substituted aromatic solutes, see Table I) to maximize the occurrence of chemical interactions that might be masked under the solvophobic environment conditions normally encountered in reversed-phase chromatography. Typical chromatograms are shown in Figs. 1 and 2.

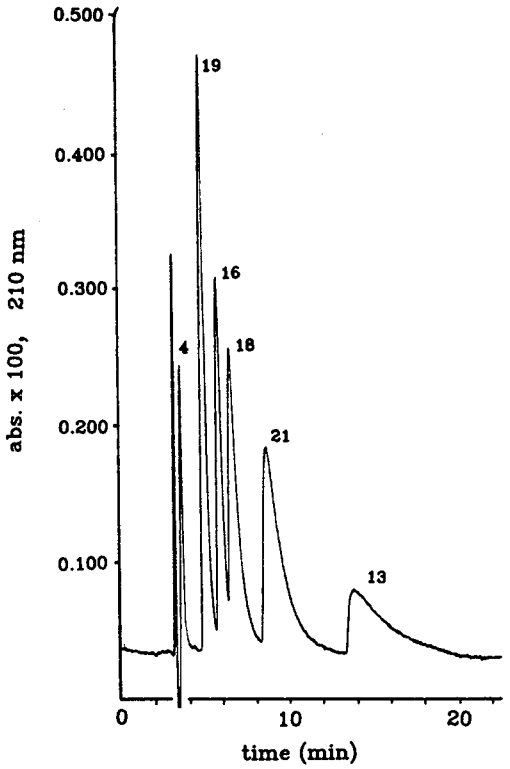

Fig. 1. Typical retention of substituted benzenes on porous graphitic carbon eluted with heptane. Solute labels correspond to Table I.

Our initial hypothesis pictured the substrate electron band participating in direct π–π orbital overlap between the aromatic ring of the solutes and the substrate (stationary phase). Had this idea been correct, good correlation between solute retention and the energies of the available π-bonding orbitals, E_{homo} and E_{lumo}, would

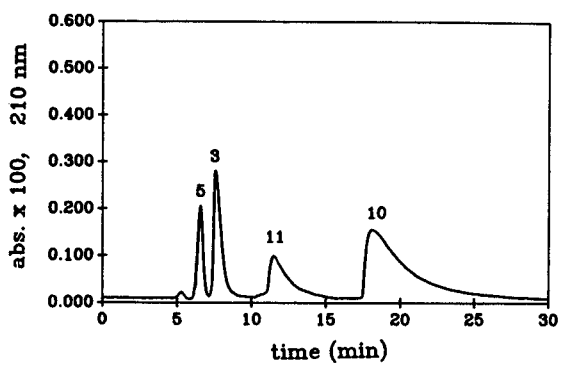

Fig. 2. Typical retention of substituted benzenes on palladium spheres eluted with heptane. Solute labels correspond to Table I.

have been expected. However, in the case of retention on porous graphitic carbon, we found the solute retention to be correlated only weakly to E_{homo} and E_{lumo}, with a stronger correlation to the submolecular polarity parameter, Δ, a measure of the localized or concentrated dipole of a molecule. The strongest correlation observed is that shown in eqn. 1:

$$\log k' = 2.10\Delta - 1.01 \quad (1)$$
$$n = 21 \quad r = 0.800 \quad F\text{-value} = 33.7 \quad \text{significance} = 1.37 \cdot 10^{-5}$$

It was found that improved correlation equations could be obtained by separating the phenols from other substituted benzenes as shown in eqns. 2 and 3:

For substituted benzenes

$$\log k' = 1.57\Delta - 0.277\, E_{homo} - 3.49 \quad (2)$$
$$n = 11 \quad r = 0.972 \quad F\text{-value} = 69.3 \quad \text{significance} = 8.86 \cdot 10^{-6}$$

For phenols

$$\log k' = -39.4\Delta - 2.45\, E_{lumo} + 17.9 \quad (3)$$
$$n = 10 \quad r = 0.907 \quad F\text{-value} = 16.3 \quad \text{significance} = 0.00230$$

While the majority of the correlations was attributed to the submolecular polarity parameter, Δ, alone ($r = 0.923$ and -0.747, sig. $= 5.02 \cdot 10^{-5}$ and 0.0131, for benzenes and phenols, respectively) better models were formed by including the contributions of E_{homo} and E_{lumo} (above).

These and other analyses indicated that a localized polar segment of the molecule was responsible for retention rather than the π-orbitals of the aromatic ring, reflected by E_{homo}. Equivalent studies on the palladium metal substrate produced similar results, in that retention was best correlated to a localized segment of the solute molecule, reflected by Δ, rather than to the π-orbital energies alone. The equations observed for palladium are shown in eqns. 4 and 5:
For the entire solute set

$$\log k' = -2.79\Delta + 1.05 \quad (4)$$
$$n = 15 \quad r = 0.610 \quad F\text{-value} = 7.70 \quad \text{significance} = 0.058$$

For phenols only

$$\log k' = -45.0\Delta - 2.75\, E_{lumo} + 20.2 \quad (5)$$
$$n = 10 \quad r = 0.826 \quad F\text{-value} = 7.53 \quad \text{significance } 0.018$$

Again, primary correlation was achieved with Δ alone ($r = -0.685$, significance $=$ 0.895), with the complement of E_{lumo}.

Furthermore, alkyl- and halogen-substituted benzenes were unretained on the palladium stationary phase and only very weakly retained on porous graphitic carbon. Solutes containing oxygen or nitrogen (n-electron donors) were retained more strongly

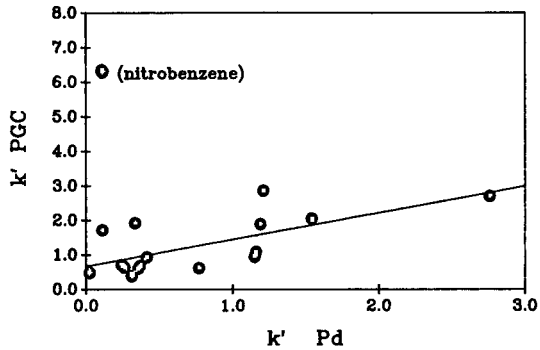

Fig. 3. Comparison of retention, k', of substituted benzenes and phenols between porous graphitic carbon (PGC) and palladium (Pd). Regression line does not include nitrobenzene.

on both phases. With the exception of nitrobenzene, good correlations between the retention properties of palladium and porous graphitic carbon were observed under non-polar solvent conditions (Fig. 3).

On a "perfect reversed-phase", where only dispersive interactions could take place, very little solute retention would be expected with non-polar eluents. It was difficult to find such a material to serve as the control stationary phase. An exhaustively coated alumina/cross-linked polybutadiene phase[20], used under similar non-polar conditions, exhibited strong retention towards a number of solutes, presumably due to unshielded accessible aluminol sites or oxidized sites on the butadiene. However, no similarity in retention properties to the metallic phases was observed. Polystyrene-based materials were not suitable as control stationary phases, due to their aromatic nature.

Upon closer examination of solute retention on porous graphitic carbon and palladium, the polar substituent on the solute ring was further implicated in retention. Positional isomers of substituted phenols showed a decrease in retention for *tert.*-butyl-substituted phenol when the substituent was moved from the *para-* to the *meta-* and finally to the *ortho*-position. Inductive and resonance effects on the solute ring could be ruled out due to the dissimilar behavior of the *ortho-* and *para-*substituents. In addition, as the bulkiness of the *ortho*-substituent increased, retention decreased on both porous graphitic carbon and palladium, further highlighting the activity of the hydroxyl group in the retention of phenols on porous graphitic carbon and palladium (Fig. 4).

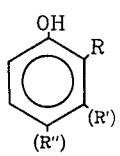

	k'	
	PGC	Pd
R = i-Pr	0.68	0.37
= s-Bu	0.60	0.36
= t-Bu	0.38	0.31
R' = t-Bu	0.93	0.42
R''= Methyl	2.9	1.2
= Ethyl	1.9	1.2
= s-Bu	1.1	1.2
= t-Bu	0.95	1.1

Fig. 4. Retention of phenol isomers on porous graphitic carbon (PGC) and palladium (Pd) as a function of substituent size and ring position. i = iso; s = *sec.*; t = *tert.*; Bu = butyl; Pr = propyl.

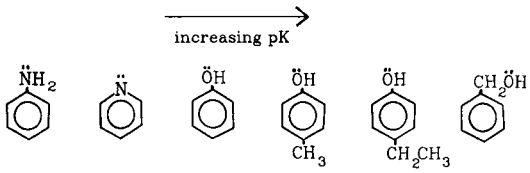

		k'				
PGC	)10	3.49	2.76	2.86	1.89	0.772
Pd	)10	---	2.70	1.21	1.19	0.615

Fig. 5. Solute basicity and retention. PGC = Porous graphitic carbon; Pd = palladium.

The ability of the polar group to donate a lone pair of electrons to the substrate was indicated by observing retention trends and basicity of the polar group lone pair (Fig. 5). Specifically, where pK values were available for solutes, a linear trend of pK to solute retention was apparent (Fig. 6), even though the number of data points was limited.

The correlation of retention with basicity and the loss of retention when access to the unshared pair of electrons on basic solutes was hindered, in addition to the poor retention characteristics of solutes unable to function as n-electron donors on porous graphitic carbon and palladium, offered strong evidence that the dominant retention mechanism of the substituted aromatic molecules studied was an electron-pair donor–acceptor interaction.

To a first approximation, ultra-high vacuum studies of metallic surfaces support the types of solute–substrate interactions encountered in HPLC on electron-band substrates. For example, studies of solute adsorption on palladium metal in ultra-high vacuum[21] support the idea of an n–σ donor–acceptor interaction of the lone electron pair governing adsorption of pyridine, as opposed to the adsorption of benzene or xylene which is dominated by π-electron transfer. As a result, the aromatic ring, which is normally adsorbed parallel to the metal surface, is adsorbed polar-end-down when a lone electron pair, as in pyridine, phenol, or aniline, is present.

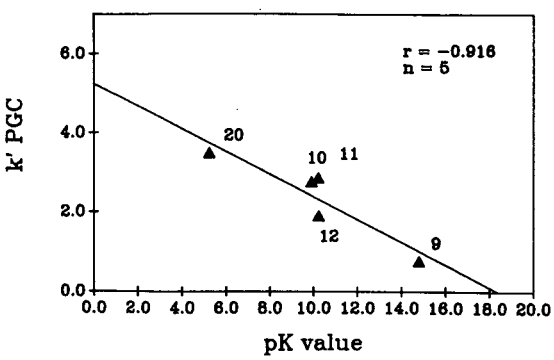

Fig. 6. Dependence of retention on solute pK on porous graphitic carbon (PGC). Solute labels correspond to Table I.

Additional support of such a mechanism is found in argentation chromatography, where silver ions are incorporated into the mobile or stationary phase of a reversed-phase system to increase selectivity of various unsaturated hydrocarbons and azaheterocycles[9,10,12,13]. While the delocalized electron bands of porous graphitic carbon and palladium do not form the same discrete metal–ligand complexes found with metal ions, their selectivity and bond strength follow the same order under similar solvent conditions[12], based on the basicity and spatial environment of solute lone-electron pairs.

Surface analysis of palladium

Scanning Auger spectroscopy showed the palladium spheres used as HPLC substrates to be essentially free of surface oxide and foreign metal contamination, as demonstrated by the characteristic shape and separation of the palladium $3d_{3/2}$ and $3d_{5/2}$ peaks. Extensive analyses indicated that the palladium surface was chemically clean.

CONCLUSION

A porous graphitic carbon stationary phase for HPLC was demonstrated by statistical approaches to behave primarily as an electron pair acceptor for substituted aromatic solutes capable of n-donation under non-polar solvent conditions. The retention order of the solutes closely followed the basicity of the lone electron pair on various solutes. Diminished retention of solutes with sterically hindered lone pairs was also consistent with this interpretation. Palladium metal exhibited trends qualitatively similar to graphite under normal-phase conditions.

Due to strong adsorption of water to the palladium surface, it was not possible to compare porous graphitic carbon materials with palladium under reversed-phase conditions. It was also found that palladium was easily "poisoned" by solutes which had very high affinities for the stationary phase. Work is in progress to examine other metals, in particular gold, to determine whether changes in retention levels and orders follow that predicted from the known band properties of these two metals. It is possible that the electronic properties observed can be attenuated through coverage of the metal with a thin aromatic polymer film, and/or by the use of semi-conductive polymers.

Regardless of these practical problems, the development of efficient, electrically conductive chromatographic surfaces should permit several interesting new experiments, such as the use of a chromatographic sorbent as an electrode, in an attempt to modulate retention as a function of potential[22,23]. They may also function as improved charge-transfer-type materials. Research is currently underway to investigate these applications.

ACKNOWLEDGEMENTS

The generous loan of precious metals from Platina Labs. is gratefully acknowledged. Special thanks to Dr. Len Spaulding, Platina Labs., and Dr. Eric Garfunkel, Rutgers University, for numerous conversations and to Dr. Robert Caraciolla, Rutgers University, for surface analyses of phases. Support for this

research was provided by grants from the PQ Corporation, and the Petroleum Research Fund.

REFERENCES

1 J. H. Knox, B. Kaur and G. R. Millward, *J. Chromatogr.*, 352 (1986) 3.
2 S. H. Hsu, *PhD. thesis*, Rutgers University, 1986, p. 162.
3 C. Horváth, W. Melander and I. Molnár, *J. Chromatogr.*, 125 (1976) 129.
4 C. Priester, G. Allan and J. Conard, *Phys. Rev. B*, 26 (1982) 4680.
5 L. Nondek, *J. Chromatogr.*, 373 (1986) 61.
6 W. Holstein and H. Hemetsberger, *Chromatographia*, 15 (1982) 251.
7 R. Kaliszan, *Quantitative Structure-Chromatographic Retention Relationships*, Wiley, New York, 1987.
8 R. Kaliszan, *Chromatography*, June (1987) 19.
9 G. Schomburg and K. Zegarski, *J. Chromatogr.*, 114 (1975) 174.
10 S. P. Wasik and R. L. Brown, *Anal. Chem.*, 48 (1976) 2218.
11 G. A. Eiceman and F. A. Janecka, *J. Chromatogr. Sci.*, 21 (1983) 555.
12 R. Vivilecchia, M. Thiébaud and R. W. Frei, *J. Chromatogr. Sci.*, 10 (1972) 411.
13 B. Vonach and G. J. Schomburg, *J. Chromatogr.*, 149 (1978) 417.
14 L. A. d'Avila, H. Colin and G. Guiochon, *Anal. Chem.*, 55 (1983) 1019.
15 R. M. Smith, S. J. Bale, S. G. Westcott and M. Martin-Smith, *Analyst (London)*, 112 (1987) 1209.
16 M. J. S. Dewar, *QCPE*, 11 (1975) 279.
17 *Cambridge Crystallographic Database*, Cambridge Crystallographic Data Centre, University Chemical Laboratory, Cambridge, U.K., 1979.
18 K. Ośmialowski, J. Halkiewicz, A. Radecki and R. Kaliszan, *J. Chromatogr.*, 346 (1985) 53.
19 D. D. Perrin, B. Dempsey and E. P. Serjeant, *pK_a Prediction for Organic Acids and Bases*, Chapman and Hall, London, 1981.
20 U. Bien-Vogelsang, A. Deege, H. Figge, J. Kohler and G. Schomburg, *Chromatographia*, 19 (1984) 1970.
21 F. P. Netzer and J. U. Mack, *J. Chem. Phys.*, 79 (1983) 1017.
22 R. F. Antrim, R. A. Scherrer and A. M. Yacynych, *Anal. Chim. Acta*, 164 (1984) 283.
23 R. F. Antrim, R. A. Scherrer and A. M. Yacynych, *Anal. Lett.*, 21 (1988) 1085.

Journal of Chromatography, 461 (1989) 149–163
Elsevier Science Publishers B.V., Amsterdam — Printed in The Netherlands

CHROMSYMP. 1472

MEASUREMENT OF STATISTICAL MOMENTS OF RESOLVED AND OVERLAPPING CHROMATOGRAPHIC PEAKS*

MARK S. JEANSONNE and JOE P. FOLEY*
Department of Chemistry, Louisiana State University, Baton Rouge, LA 70803-1804 (U.S.A.)

SUMMARY

A method for the accurate calculation of statistical moments, excess and skew is described. Based on peak width, asymmetry and peak height measurements this method is applicable to both fully resolved and overlapping chromatographic peaks. It is also useful for the deconvolution of overlapping chromatographic peaks. The advantages of this method over the traditional approach to measuring peak statistical moments, excess and skew are discussed.

INTRODUCTION

The importance of statistical moment analysis to the chromatographer cannot be overemphasized because a large amount of information can be derived from such an analysis. Statistical moment analysis cannot only be used to measure directly parameters such as area (zeroth moment), peak centroid (first statistical moment) and variance (second statistical moment), but other important parameters can be calculated indirectly as well. For example, column efficiency can be calculated from $N = M_1^2/M_2$, where N is the column efficiency, M_1 is the first statistical moment and M_2 is the variance. Other parameters, such as the third and fourth statistical moments give information on peak asymmetry and peak flattening, respectively. Peak skew and excess are parameters related to statistical moments and provide a measure of the deviation of the chromatographic peak from a Gaussian peak profile.

Traditionally, statistical moments for digitally represented chromatographic peaks have been approximated by the simple summation of the magnitude of the peak signal at each data point between the peak start and stop limits, as shown in Fig. 1a. However, any approach based on summation for the calculation of statistical moments has several shortcomings when applied to real chromatographic data.

First, it has been shown that the accuracy and precision of the summation method is directly affected by the amount of noise present in the chromatogram[1,2]. The noise level has been shown to affect peak start/stop assignments, and this affects the limits of summation and, consequently, the value of the statistical moments calculated[3].

* Presented in part at the *Pittsburgh Conference and Exposition in New Orleans, LA, February 1988*, paper No. 088.

0021-9673/89/$03.50

(a)

$$M_0 = \text{area} = \int_{-\infty}^{\infty} h(t)\,\mathrm{d}t \approx \sum_{\text{start}}^{\text{stop}} h(t)\,\Delta t$$

$$M_1 = \text{retention time} = \int_{-\infty}^{\infty} t \cdot h(t)\,\mathrm{d}t \approx \sum_{\text{start}}^{\text{stop}} t \cdot h(t)\,\Delta t$$

$$M_2 = \text{variance} = \int_{-\infty}^{\infty} (t - M_1)^2 \cdot h(t)\,\mathrm{d}t \approx \sum_{\text{start}}^{\text{stop}} (t - M_1)^2 \cdot h(t)\,\Delta t$$

$$M_3 = \int_{-\infty}^{\infty} (t - M_1)^3 \cdot h(t)\,\mathrm{d}t \approx \sum_{\text{start}}^{\text{stop}} (t - M_1)^3 \cdot h(t)\,\Delta t$$

$$M_4 = \int_{-\infty}^{\infty} (t - M_1)^4 \cdot h(t)\,\mathrm{d}t \approx \sum_{\text{start}}^{\text{stop}} (t - M_1)^4 \cdot h(t)\,\Delta t$$

γ_S = skew = $M_3/{M_2}^{3/2}$
γ_E = excess = $M_4/{M_2}^2 - 3$

(b)

$$\sigma_G = \frac{W}{f_1(b/a)}$$

$M_2 = W^2 \cdot f_2(b/a)$
$M_1 = t_r + W \cdot f_3(b/a)$

$$\tau = \sqrt{M_2 - \sigma_G^2}$$

$M_3 = 2\,\tau^3$
$M_4 = 3\,\sigma_G^4 + 6\,{\sigma_G}^2\tau^2 + 9\,\tau^4$
$\gamma_S = M_3/M_2^{3/2}$
$\gamma_E = M_4/M_2^2 - 3$

Fig. 1. Equations used for calculation of statistical moments and other peak parameters by (a) the summation method and by (b) the width-asymmetry method. t_r = retention time. $h(t)$ = chromatographic peak profile.

Secondly, the accuracy of the summation method (equations shown in Fig. 1a) deteriorates rapidly as the peaks begin to overlap. We have recently shown[4] that errors in peak area can exceed 100% when the summation approach (perpendicular drop algorithm) is applied to overlapping peaks. As we shall show later in this report, errors in the higher moments calculated via the summation method are usually much larger under the same circumstances.

A final drawback of the summation method is that it is computationally intensive, requiring numerous calculations (see Fig. 1a) for every data point in the peak

of interest. This is particularly true for the higher moments and related parameters. Although this problem has been alleviated somewhat by the advances in computer technology (faster computations), the summation method remains noticeably time-consuming on many commercial chromatographs with microcomputer-based data systems.

Most, if not all, of the problems associated with the measurement of statistical moments can be reduced or eliminated if one has an accurate model for the chromatographic peaks of interest. A model that has been reported to be accurate for most chromatographic peaks[5–7] is the Exponentially Modified Gaussian (EMG) function, which is the convolution of a Gaussian and an exponential decay function. Recently, we introduced[8] a convenient procedure for determining whether or not the use of the EMG model is appropriate. This procedure utilizes empirical equations for calculating peak area based on peak width, asymmetry and peak height measurements. Once the validity of the EMG model for a given set of peaks has been confirmed, these equations can also be used for the accurate measurement of peak areas of overlapping chromatographic peaks[4]. Note that this method relies on the measurement of peak width and asymmetry for the less distorted peak of the overlapped pair (the first peak) at a point above the valley where distortion from the second peak is low.

Although some of the problems associated with the traditional measurement of statistical moments can be reduced or eliminated via the use of a variety of sophisticated, curve-fitting/deconvolution procedures, these procedures also have numerous drawbacks. First, they are nearly always even more time-consuming than the traditional summation approach. In many cases a final summation step is required after the preliminary curve-fitting/deconvolution procedures. Secondly, some of the procedures require multi-channel detection which is not always available. Thirdly and most importantly, for a variety of reasons the curve-fitting/deconvolution approaches have not yet proven to be sufficiently reliable. For example, with iterative procedures, lack of convergence is frequently observed. In general, these and other disadvantages have dissuaded most, if not all, commercial manufacturers from implementing the curve-fitting/deconvolution approaches into their chromatographic data systems.

The purpose of this paper is to report an alternative to both the traditional and least squares/deconvolution methods for the measurement of statistical moments. Our present approach utilizes empirical equations (Fig.1b) similar to those we already reported for peak area[7], but also includes a very simple deconvolution procedure for a pair of overlapping peaks. The derivation of these equations will not be included here, as this topic will constitute a separate paper[9]. For the remainder of this report, we will refer to our method of statistical moment measurement as the width-asymmetry method.

EXPERIMENTAL

Both an Apple Macintosh Plus and an IBM PC-AT were utilized for simulated peak generation and other calculations. All programs were written in either Microsoft BASIC or TRUE BASIC.

EMG peak generation

All peaks generated were based on the EMG function[5] expressed as

$$\mathrm{EMG}(t) = \frac{A}{\tau} \cdot \exp\left[\frac{1}{2}\left(\frac{\sigma_G}{\tau}\right)^2 - \frac{t - t_G}{\tau}\right] \int_{-\infty}^{z} \frac{\exp\left(\frac{-y^2}{2}\right)}{\sqrt{2\pi}} \, dy \qquad (1)$$

where A is the peak area, t_G is the retention time, σ_G is the standard deviation of the Gaussian function, τ is the time constant of the exponential decay function convoluted with the Gaussian function and $Z = (t - t_G)/\sigma_G - \sigma_G/\tau$. As the τ/σ_G ratio increases, the peak in question will become more skewed, and as it decreases, the peak approaches a Gaussian shape.

Single chromatographic peaks at τ/σ_G ratios of 0, 0.5, 1, 2, 3 and 4, with σ_G a constant at 0.1 min, were generated for this study, using a sampling rate of three points per second. As shown in Fig. 2 ($\tau/\sigma_G = 2$), about 30 points per peak measured from 10% peak height to 10% peak height were needed for $\leqslant 2\%$ error.

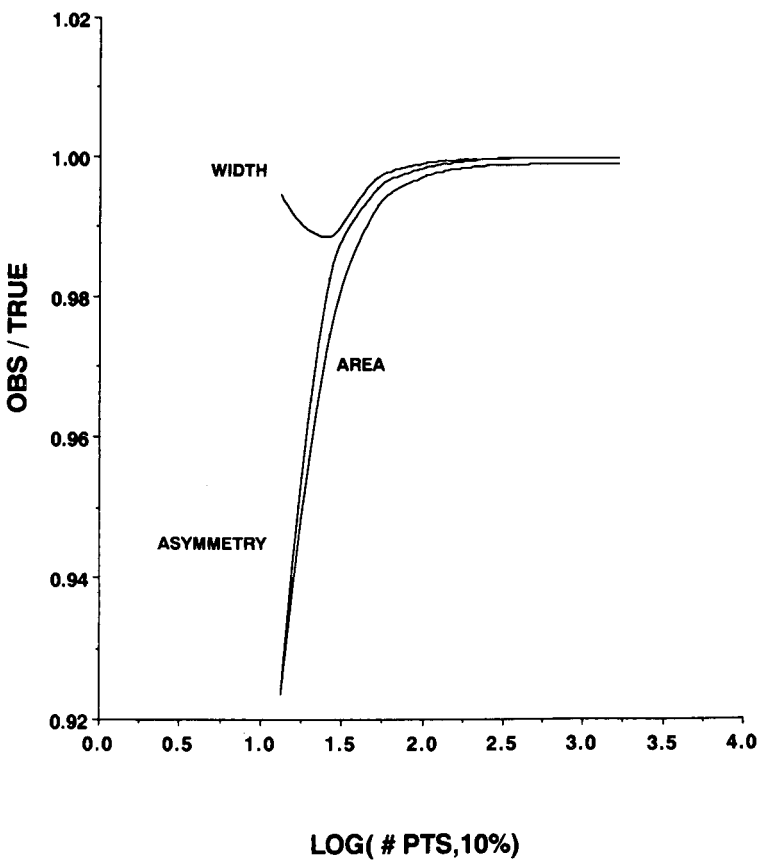

Fig. 2. Effect of the data sampling rate on the measurement of peak width, asymmetry and peak area.

Overlapped chromatographic peaks at τ/σ_G ratios of 0.5, 1, 2, 3 and 4 were generated at resolution values of 0.625, 0.75, 0.875, 1, 1.125, 1.25, 1.375 and 1.5 by using the same sampling rate as the single peaks. Resolution was defined as $\Delta t_G/4(\text{variance})^{1/2}$, where $\Delta t_G = t_{G,2} - t_{G,1}$, and variance was defined as $\sigma_G^2 + \tau^2$ for an exponentially modified Gaussian peak. The peaks were overlapped by adding two individual, simulated peaks of equal area and τ/σ_G value. However, the degree of peak overlap will be reported here as the percent valley due to the inadequacy of the resolution parameter for fully describing tailed overlapped peaks[4]. Percent valley was defined as $h_v/h_p \cdot 100\%$, where h_v and h_p are shown in Fig. 3.

Real chromatographic peak generation

Real single and overlapped pairs of peaks were generated on a Series 400 liquid chromatograph (Perkin-Elmer, Norwalk, CT, U.S.A.), using pyrene as the analyte. The mobile phase composition was 75% aqueous acetonitrile at a flow-rate of 1.5 ml/min. The column used was a Vydac pH-stable C_8 column. A Model V[4] variable wavelength ultraviolet absorption detector (Isco, Lincoln, NB, U.S.A.), set at 330 nm was used to detect pyrene. An Omega-2 data system (Perkin-Elmer) utilizing an IBM AT computer was used for storage of the chromatograms.

Overlapped peaks were obtained from precise, rapid duplicate injections of a standard solution of pyrene. This single-standard, rapid, duplicate-injection approach has many advantages over a two-component standard solution method which would require changing conditions to obtain different degrees of overlap. First, it allows the degree of peak overlap to be easily controlled by simply varying the length of time between injections. Secondly, this method avoids any relative change in the molar absorptivities of two analytes in the mixture as mobile-phase conditions are changed to obtain different degrees of overlap. Thirdly, it permits a single peak to be obtained under the same conditions as the overlapped peaks, thus allowing the statistical moments measured by the summation and width-asymmetry methods for the isolated peak to be compared with those measured for the overlapped peak pair without any concern about changes in the peak shape and/or concentration. Finally,

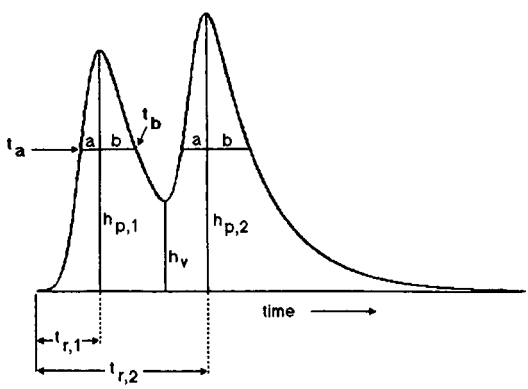

Fig. 3. Measurement of graphic parameters for an overlapping pair of chromatographic peaks. t_r and h_p are the retention time and peak height of respective peaks, and h_v is the height of the valley. Peak width at the desired peak height fraction is given by $t_a - t_b$.

one can be confident that the true area ratio of the overlapped peaks is unity, since equal amounts of the same compound are being injected.

Two pairs of tailed, overlapping peaks with percent valleys of 40 and 67% were generated. A single control peak with the same amount of peak tailing as the overlapping peaks was also generated. The amount of peak tailing was adjusted by adding or removing dead-volume ahead of the column.

Peak parameter measurement

The equations given in Fig. 1a, for determining the zeroth through fourth statistical moments by summation, were applied to both simulated and real peaks. For the simulated peaks, start/stop assignments (limits of integration) for isolated peaks were taken as the point where the peak was determined to be "on baseline", which depended on the "baseline level" being used for the peak. Baseline levels of $1 \cdot 10^{-9}$ and $3 \cdot 10^{-3}$ were used, which corresponded to approximately 0.00 and 0.1% of the peak height, respectively. The lower baseline was used as an ideal baseline in order to obtain a maximum level of accuracy for purposes of comparison. The ideal baseline was chosen to be slightly above zero, since the value of Z in eqn. 1 necessary to give a zero baseline would result in an overflow condition. This ideal baseline was used only for peaks in which no noise was present, since noise affects peak/start assignments in real chromatograms.

For overlapped peak pairs, the starting point for the first peak and stopping point for the second peak were chosen as for isolated peaks. The peak stop for the first peak and the peak start for the second peak were taken as the intersection of the baseline being used and a perpendicular line, drawn to the minimum of the valley between the peaks (see Fig. 3). This method for dealing with overlapped peaks is commonly referred to as the perpendicular drop algorithm.

For the real chromatographic peaks, the baseline level and the start/stop assignments were determined by the data system, the perpendicular drop method being employed for overlapped peaks. The peak detection algorithms in the data system were optimized for the types of real peaks that were generated.

The widths of the peaks at 10, 25, 50 and 75% relative peak height were determined by utilizing a four point least squares fit where four points on each side of the peak, symmetric about the particular height, was used and the difference in time between the two points ($t_a - t_b$) was taken as the peak width (see Fig. 3). Four points were used, since the accuracy of the value obtained for peak width did not increase when more points were fit.

Peak height was obtained by subtracting the baseline value being used from the peak maximum obtained via a quadratic least-squares curve fit of the seven highest points in the peak. The seven-point group was selected so that the middle point had the highest value. The time at which the maximum was calculated from the quadratic fit was used as the retention time of the peak. Seven points were used, since this number represented a compromise between the optimum number of points for a peak with a τ/σ_G ratio of 1 (mildly skewed) and a peak with a τ/σ_G ratio of 4 (heavily skewed) for the data sampling rate used. This compromise was selected so that the quadratic fit could be used for peaks for which the value of τ/σ_G was not known, as in real chromatograms. The asymmetry of the peak was taken as the value of b/a, where a and b were determined as shown in Fig. 3 at the appropriate peak heights.

RESULTS AND DISCUSSION

Simulated peaks without noise

The values for the area and the variance obtained by the summation and width-asymmetry methods for simulated peaks and an ideal baseline are compared in Fig. 4 as a function of the percent valley between the peaks. For only slightly tailed peaks ($\tau/\sigma_G = 1$, Fig. 4a), it appears that the summation method for peak area and variance is fairly accurate for the noiseless peaks used in this study. However, for moderately tailed peaks ($\tau/\sigma_G = 2$, Fig. 4b), the area of the second peak and the variance of the first peak have become much less accurate relative to the same parameters measured by using the width-asymmetry method. This trend continues in Fig. 4c for $\tau/\sigma_G = 4$. Thus, the width-asymmetry method can be used to measure accurately both the area and variance for the left peak of a highly skewed and overlapped pair of peaks, while the same parameters cannot be measured as accurately for either peak when the summation method is used.

Fig. 5 illustrates the same results for peak area and variance as Fig. 4c, but with a less ideal baseline. Here, the variance for the first peak, as measured by the summation method, is very inaccurate. This is due to a significant portion of the tail of the first peak being truncated by the higher baseline, and shows the sensitivity of the variance to baseline errors when measured by the summation method. However, the variance measured by our width-asymmetry method does not show this sensitivity.

The errors in the higher moments, skew and excess are compared in Fig. 6 for an overlapped pair of highly skewed peaks ($\tau/\sigma_G = 4$) and an ideal baseline. Since an ideal baseline was simulated, the moments measured for the right peak by the summation method (see Fig. 6a) show a fair accuracy up to a high percent valley for these noiseless peaks. However, results this accurate cannot be expected for real chromatographic peaks, due to the problems outlined in the introduction for the summation method. As expected, the higher moments, skew and excess, measured by the summation method for the left peak, show greater sensitivity to the truncation of the peak tail than do the area and variance for the left peak, measured by the summation method.

However, the higher moments, skew and excess measured by the width-asymmetry method for the left peak do not show this sensitivity (see Fig. 6b). In fact, the accuracy for these parameters, measured by the width-asymmetry method, is much better than that obtained by the summation method for the right peak. This shows that the width-asymmetry method is better overall for measuring the higher statistical moments, excess and skew for at least one peak of an overlapped pair of peaks.

Table I shows the maximum percent valleys (maximum overlap) for which the two methods described here are in error by less than 5%. As seen there, for most of the moments calculated by the width-asymmetry method for the left peak, the maximum overlap that can be tolerated is higher. However, for the right peak, some of the moments calculated by the summation method are more accurate. These results were expected, since the tail for the right peak is fully included in the limits of integration. Peak overlap of the peaks prevents the tail of the left peak from being included in the summation method. This confirms the well-known results that the tail of a skewed peak is especially important in calculating the higher moments by the summation method. Also, the results show that the degree of distortion in the left peak is low for two overlapped EMG peaks. Overall, these results indicate that all the statistical

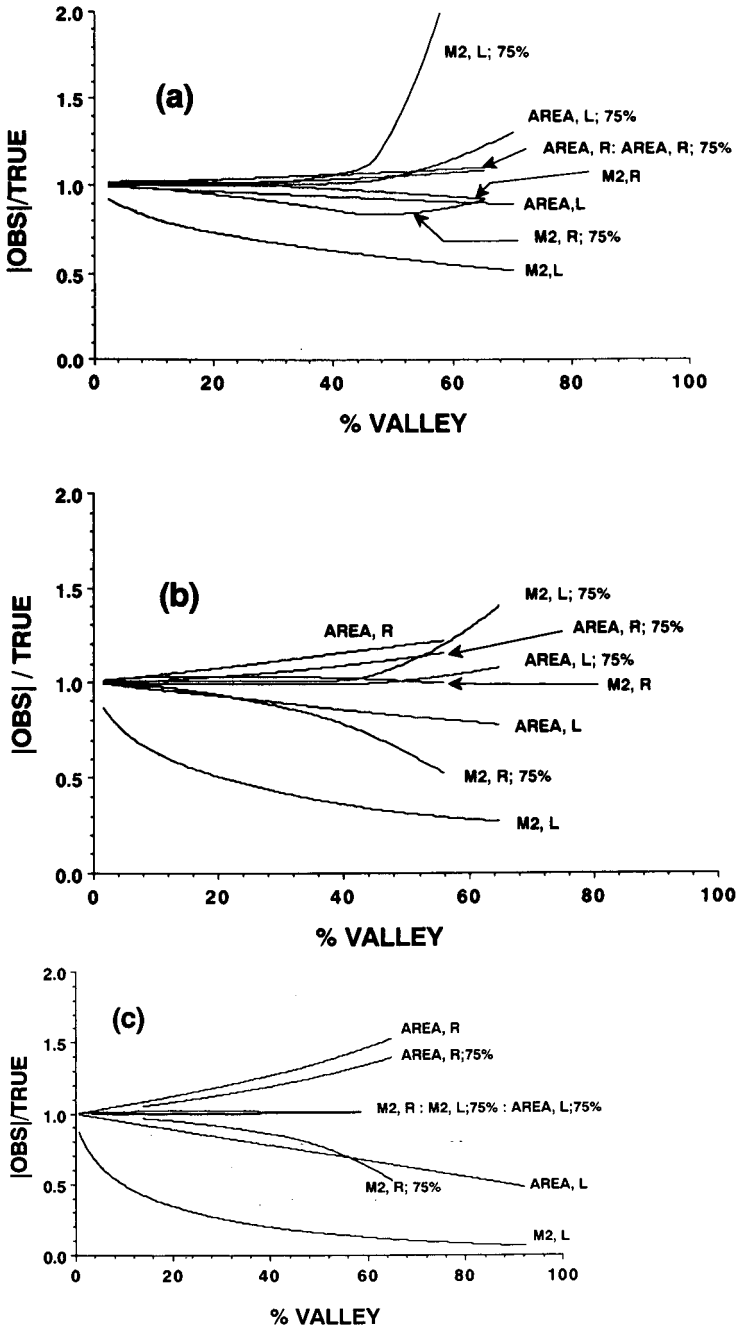

Fig. 4. Comparison of the errors in peak area and variance occurring in the summation and width-asymmetry methods as a function of peak overlap (percent valley) for: (a) $\tau/\sigma_G = 1$; (b) $\tau/\sigma_G = 2$ and (c) $\tau/\sigma_G = 4$. Labels in the plot refer to: (a) the parameter; (b) the peak (first, L, or second, R) for which a parameter was obtained and (c) the relative peak height at which the width and asymmetry were measured (width-asymmetry only). For example, "M2, L; 75%" refers to the variance measured for the first peak of the overlapped pair at 75% of the peak height, while "M2, R" refers to the variance of the second peak measured by the summation method.

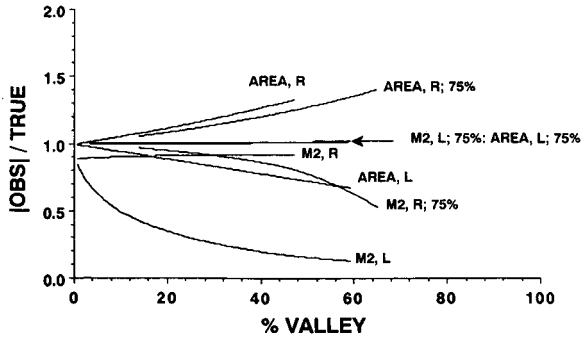

Fig. 5. Comparison of the errors in peak area and variance occurring in the summation and width-asymmetry methods as a function of peak overlap for a highly skewed pair of peaks ($\tau/\sigma_G = 4$) with a less than ideal baseline level (0.1%). Conditions as in Fig. 4.

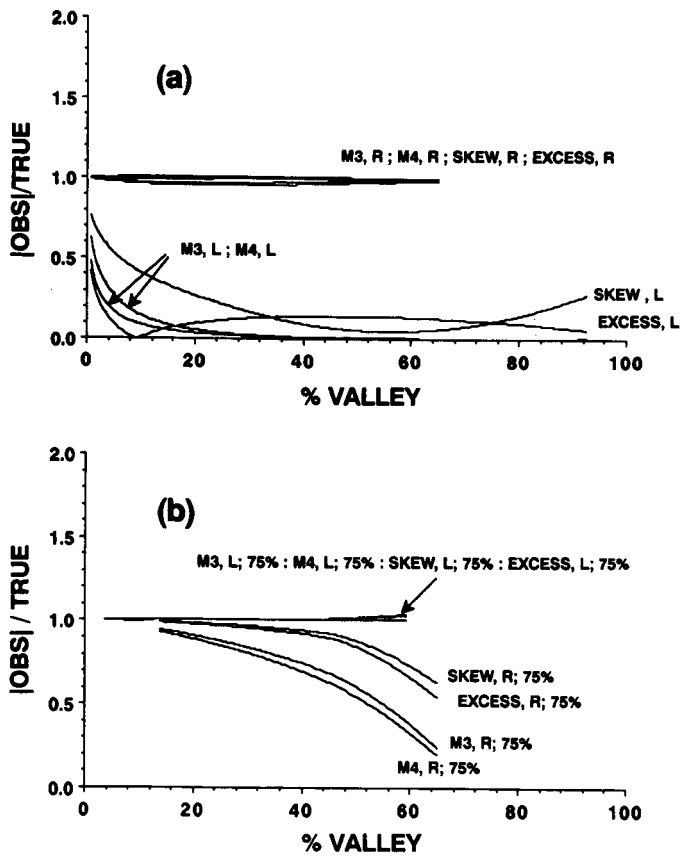

Fig. 6. Comparison of the errors in peak parameters other than peak area and variance for overlapped peak pairs with $\tau/\sigma_G = 4$ occurring in: (a) summation method and (b) width-asymmetry method. Conditions as in Fig. 4.

TABLE I

MAXIMUM PEAK OVERLAP (PERCENT VALLEYS) THAT CAN BE TOLERATED BY THE WIDTH-ASYMMETRY AND SUMMATION METHODS FOR A GIVEN ACCURACY ($\leqslant$ 5% ERROR)

	Peak	*Area*	M_2	M_3	M_4	*Skew*	*Excess*
Width-asymmetry method	First	47	34	16	24	17	15
	Second	4	17	8	8	8	7
Summation method/ ideal baseline*	First	9	<2	<2	<2	<2	<2
	Second	8	34	5	11	5	2
Summation method/ non-ideal baseline**	First	8	<2	<2	<2	<2	<2
	Second	9	24	9	<2	9	<2

* Peak start/stop corresponds to points where signal is $5 \cdot 10^{-8}$% of maximum.
** Peak start/stop correspond to points where signal is 0.1% of maximum.

moments, including excess and skew can be measured accurately for peaks that are moderately overlapped, the more skewed peaks giving the best results. This latter trend is due primarily to the percent valley parameter, which tends to underestimate peak overlap for symmetrical peaks and to overestimate peak overlap for skewed peaks. (However, this measure of peak overlap is no worse than any other parameter, and is more practical than most other measures of peak overlap for skewed peaks[4].) Of course, Figs. 4–6 also show that for those overlapped peaks which are not highly skewed the summation method may occasionally give better results.

Although the summation method appears to be fairly accurate for the higher moments of the second peak of a moderately to highly skewed overlapping peak pair, it will generally be very inaccurate with real chromatographic data (peaks with noise). In modern chromatographic integrators and data systems, much of the tail of even a mildly skewed peak is often not included in the summation, due to baseline errors occurring when the algorithm used detects a peak stop before the actual end of the peak is reached. Many data systems rely on the first derivative, second derivative or similar tests to detect peak end with a slope sensitivity setting which depends on the degree of noise in the chromatogram[10]. The slope sensitivity is set at a level higher than what might be expected for the baseline drift. However, this setting may frequently also be higher than the slope on the tail of a skewed chromatographic peak. On overlapped pairs of peaks, the premature peak end would affect the second peak almost exclusively, therefore disallowing the use of the second peak in accurate computation by the summation method of the higher statistical moments for that peak, and often of the area and the second moment as well. In contrast, the width-asymmetry method is relatively unaffected by this type of truncation error[11]. Furthermore, in this example, the width-asymmetry method, which is applied to the first peak of an overlapped pair, would be entirely unaffected by the premature peak stop on the trailing edge of the second peak.

Results for real chromatographic peaks

Table II shows the results for an isolated, real chromatographic peak, obtained under ideal conditions [high signal-to-noise (S/N) ratios, no overlap, baseline

resolution, etc.]. As seen in Table II, the zeroth through fourth statistical moments, along with peak excess and skew for the single peak, were found to be similar for the width-asymmetry and summation methods. Under less ideal conditions, with a much smaller S/N ratio, the summation method would probably give results very different from the width-asymmetry method, due to the limitations of the summation method mentioned in the Introduction.

The appropriateness of the EMG model for this real chromatographic peak is demonstrated by the agreement obtained for the various peak parameters at different relative peak heights. Although the agreement is not exact, the spread in peak parameters is small (usually $< 5\%$) compared to the error encountered when using the summation method on most real peaks, the latter due to the problems outlined in the Introduction.

The advantage of the width-asymmetry method over the summation method for real peaks becomes apparent when overlapping peaks are examined. Table III gives the results for the summation and width-asymmetry methods for two pairs of peaks that overlap by different amounts. As seen for the 40% valley case, the summation method gave relative areas of 39.5% for the left peak and 60.5% for the right peak. Since the true relative areas of the peaks are 50%, the error in peak area for each peak is 10.5% when using the summation method and perpendicular drop algorithm. In contrast, the width-asymmetry method gave relative areas of 50.0% for each peak, *i.e.*, exactly the correct result.

For the more heavily overlapped peak pair (67% valley), the errors associated with the summation method increased, whereas the width-asymmetry method again gave results very close to the correct result (areas measured for the single peak shown in Table II). The relative areas for the left and right peaks, determined by the summation method, were in error by 17% for each peak, whereas the relative areas measured by the width-asymmetry method were in error by only 1%. The other statistical moments, including skew and excess for the left peak, show a large difference between those calculated by the width-asymmetry and summation methods. Also, a comparison of these parameters measured for the left peak by using the width-asymmetry method to those for the single, isolated peak (see Table II) shows that the width-asymmetry method gave very good results.

TABLE II

COMPARISON OF SUMMATION AND WIDTH-ASYMMETRY METHODS FOR AN ISOLATED REAL CHROMATOGRAPHIC PEAK

	Height (%)	*Peak area (mV · s)*	M_1	M_2	M_3	M_4	*Skew*	*Excess*
Summation method	Not applicable	5449.6	1.718	0.0424	0.0186	0.0216	2.146	8.974
Width-asymmetry method	10	5370.0	1.722	0.0410	0.0149	0.0138	1.794	5.191
	25	5530.7	–	0.0440	0.0167	0.0159	1.807	5.242
	50	5870.8	1.892	0.0468	0.0184	0.0181	1.817	5.278
	75	5802.7	–	0.0500	0.0205	0.0208	1.828	5.321

TABLE III

COMPARISON OF SUMMATION AND WIDTH-ASYMMETRY METHODS FOR TWO SETS OF OVERLAPPING, REAL PEAKS

Overlapping peaks generated from rapid, duplicate injections of pyrene (see Experimental section). Therefore, values for all the parameters except M_1 should be the same for all peaks within experimental error.

	Height (%)	*Peak area (mV · s)*	M_1	M_2	M_3	M_4	*Skew*	*Excess*
Summation method								
*40% Valley**								
Left peak	Not applicable	4481.4	1.633	0.0093	$3.7 \cdot 10^{-5}$	$1.9 \cdot 10^{-4}$	−0.795	0.042
Right peak	Not applicable	6866.8	2.101	0.0501	0.0319	0.0469	2.839	15.669
*67% Valley**								
Left peak	Not applicable	3733.6	1.609	0.0061	$-6.13 \cdot 10^{-5}$	$5.1 \cdot 10^{-5}$	−1.626	−0.130
Right peak	Not applicable	7347.5	1.997	0.0416	0.0175	0.0179	2.067	7.340
Width-asymmetry method								
*40% Valley**								
Left peak	50	5672.7	–	0.0405	0.0140	0.0130	1.720	4.907
	75	5676.8	–	0.0419	0.0150	0.0141	1.744	5.000
Right peak**	50	5675.5	–	0.0371	0.0118	0.0105	1.654	4.656
	75	5671.4	–	0.0354	0.0113	0.0098	1.690	4.794
*67% Valley**								
Left peak	50	–	–	–	–	–	–	–
	75	5694.2	–	0.0454	0.0170	0.0166	1.761	5.063
Right peak**	50	–	–	0.0218	0.0024	0.0020	0.746	1.612
	75	5386.9	–	0.0258	0.0062	0.0047	1.483	4.025

* Valley height relative to left (first) peak.

** Areas calculated as $A_R = (A_L + A_R)_{summation} - A_L$; other parameters calculated using the width-asymmetry equations in Fig. 1b. Width-asymmetry equations should normally not be employed for the more distorted peak of an overlapping pair of peaks. Results are shown here for purposes of comparison only.

Modified width-asymmetry method for true peak deconvolution

In order to determine relative areas, the width-asymmetry method requires knowledge of the total area of the two overlapping peaks, as measured by the summation method. The total area cannot be calculated by the width-asymmetry method, because the distortion of the right peak by the tail of the left peak causes an erroneous contribution to the total area. Thus, the width-asymmetry method, as employed until now, is not a true peak deconvolution method, since parameters other than the peak area are not additive and therefore cannot be determined for the second peak by subtraction. However, the width-asymmetry method can be modified and used to deconvolve an overlapping pair of peaks as follows: first, the first peak of the overlapping pair is calculated point by point via eqn. 1 over an appropriate time interval from values of σ_G, τ and A that are estimated from peak width, asymmetry and peak-height (area only) measurements by using equations described elsewhere[5]. Next, t_G is estimated from $M_1 - \tau$ and then adjusted so that the maxima of the calculated peak coincides exactly with the maxima of the first peak in the overlapping pair of real peaks. Finally, the second peak of the overlapped pair is obtained by subtracting, point by point, the calculated values of the first peak from the total chromatographic signal.

The accuracy of the width-asymmetry deconvolution method is evident from Table IV for real chromatographic peaks. As Tables III and IV show, both the original width-asymmetry method and the modified width-asymmetry/deconvolution method give accurate results for all parameters for the first peak of the overlapped pair. Note, however, that the original width-asymmetry method uses values of peak height, width and asymmetry obtained directly from the actual chromatogram (at 75% relative peak height), whereas the width-asymmetry/deconvolution method uses the same values from an artificially constructed peak.

Fig. 7 illustrates the results of the width-asymmetry deconvolution method, applied to the chromatogram of overlapped peaks with the 40% valley (relative to the left peak); superimposed on the real chromatogram are the two simulated peaks, obtained from the width-asymmetry deconvolution method. As seen, the deconvoluted first peak falls directly on the actual first peak of the overlapped pair. This was expected, since there is little distortion of the first peak in the overlapped pair from the second peak. The distortion of the second peak in the overlapped pair, caused by the tail of the first peak, is readily apparent, though, as the difference in both height and area of the second peak and its corresponding deconvoluted peak is large. This distortion is the reason that the perpendicular drop method underestimates the area of the first peak and overestimates the area of the second peak in an overlapped pair of peaks. It is also why, as mentioned above and shown here, the width-asymmetry method cannot be applied directly to the second peak of an overlapped pair of peaks.

Computational time

As stated in the Introduction, one problem with the summation method is that every point in the chromatographic peak must be involved in moment calculations. However, when the width-asymmetry method is used, most of the points in a peak of interest do not have any calculations performed on them. When the two methods were timed against each other, the width-asymmetry method was found to be about twice as fast for single-peak chromatograms and up to ten times faster for multiple-peak chromatograms.

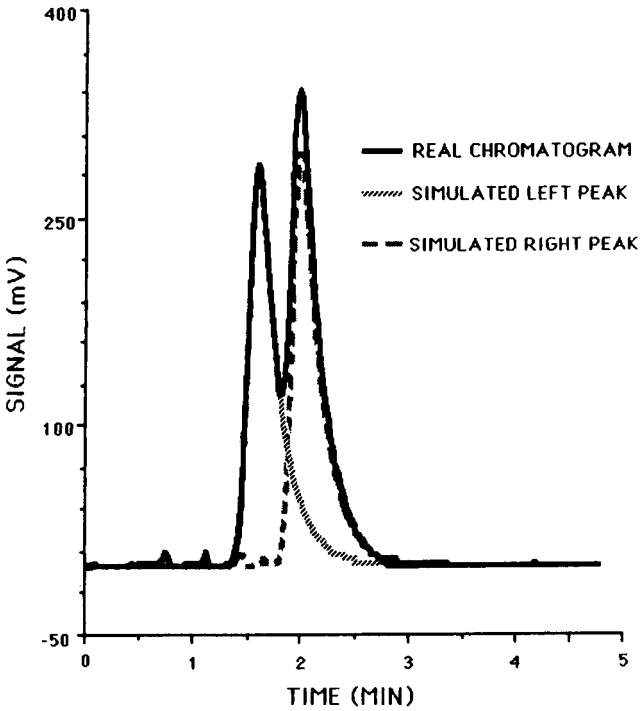

Fig. 7. Visual interpretation of the width-asymmetry/deconvolution method. The solid black line indicates the real overlapping chromatographic peaks, while the lighter lines show the individual peaks that are predicted by the width-asymmetry/deconvolution method.

TABLE IV

RESULTS FOR MODIFIED WIDTH-ASYMMETRY/DECONVOLUTION METHOD FOR TWO SETS OF OVERLAPPING, REAL PEAKS

Conditions as in Table III. Values for each parameter were calculated from width-asymmetry equations at 10, 25, 50 and 75% relative peak height. The values obtained were then averaged for this table. The spread of values for any parameter never exceeded 5% for the left peak and 10% for the right peak.

	Peak area *(mV · s)*	M_1	M_2	M_3	M_4	*Skew*	*Excess*
40% Valley							
Left peak	5654.4	1.798	0.0415	0.0147	0.0138	1.738	4.976
Right peak	5598.1	2.197	0.0411	0.0150	0.0139	1.804	5.229
67% Valley							
Left peak	5676.4	1.827	0.0450	0.0168	0.0164	1.755	5.042
Right peak	5272.2	2.090	0.0356	0.0120	0.0104	1.780	5.138

ACKNOWLEDGEMENTS

We gratefully acknowledge the support of this work by the Computer-Aided Chemistry Department of the Perkin-Elmer Corporation and the National Oceanographic and Atmospheric Administration (NOAA). Mark S. Jeansonne also thanks Jeffrey Crow for his helpful discussion on this topic.

REFERENCES

1 S. N. Chesler and S. P. Cram, *Anal. Chem.*, 43 (1971) 1922–1933.
2 T. Petitclerc and G. Guiochon, *J. Chromatogr. Sci.*, 14 (1976) 531–535.
3 E. Grushka, M. N. Myers and P. D. Schettler, *Anal. Chem.*, 41 (1969) 889–892.
4 J. P. Foley, *J. Chromatogr.*, 384 (1987) 301–313.
5 J. P. Foley and J. G. Dorsey, *J. Chromatogr. Sci.*, 22 (1984) 40–46.
6 R. E. Pauls and L. B. Rogers, *Anal. Chem.*, 49 (1977) 625–628.
7 E. Grushka, *Anal. Chem.*, 44 (1972) 1733–1738.
8 J. P. Foley, *Anal. Chem.*, 59 (1987) 1984–1987.
9 J. P. Foley and M. S. Jeansonne, manuscript in preparation.
10 A. L. Colmsjo, *Chromatographia*, 23 (1987) 257–260.
11 D. P. Anderson and R. R. Walters, *J. Chromatogr. Sci.*, 22 (1984) 353–359.

Journal of Chromatography, 461 (1989) 165–176
Elsevier Science Publishers B.V., Amsterdam — Printed in The Netherlands

CHROMSYMP. 1464

GENERALIZED TREATMENT OF SPATIAL AND TEMPORAL COLUMN PARAMETERS, APPLICABLE TO GAS, LIQUID AND SUPERCRITICAL FLUID CHROMATOGRAPHY

I. THEORY

DANIEL E. MARTIRE
Department of Chemistry, Georgetown University, Washington, DC 20057 (U.S.A.)

SUMMARY

Starting with Darcy's law, rearranged and expressed in terms of the local carrier *density* at a given temperature, general equations are derived for the spatial and temporal density distribution functions, average densities and column profiles of the mobile-phase fluid, and the observed (column-averaged) capacity factor(s) and column profiles of the solute component(s). These more direct, exact and tractable equations are applied to gas, liquid and supercritical fluid chromatography, and the results are discussed.

INTRODUCTION

In all chromatographic systems there is necessarily a pressure (or density) gradient of the mobile phase along the column. A fundamental problem, especially in packed-column supercritical fluid chromatography, where the mobile phase is both non-ideal and highly compressible, and column pressure drops may be substantial[1–7], is accurately relating an observed solute retention parameter (*e.g.*, the capacity factor, k') to the column inlet and outlet conditions and appropriate column-averaged quantities. Therefore, the ultimate goal of the present study is to provide a generalized solution to this basic problem by formulating sufficiently exact and numerically tractable integral equations, applicable to gas (GC), liquid (LC) and supercritical fluid (SFC) chromatography.

Starting with Darcy's law under isothermal conditions and neglecting what are normally minor temperature-gradient effects in analytical SFC[7], LC[8] and GC[9], general equations are derived for the spatial and temporal distribution functions in a column (packed or capillary), in terms of the local density, isothermal compressibility coefficient and viscosity of the mobile phase, where the last two properties depend on the local density as well. The spatial and temporal distribution functions, which essentially describe how the mobile-phase density varies with its position and residence time, respectively, in the column, are then applied to obtain general expressions for the spatial and temporal average densities, and the related column profiles, for prescribed

0021-9673/89/$03.50

inlet and outlet conditions. Similarly, starting with an expression for the solute capacity factor in terms of the local carrier density, the observed (or column-averaged) capacity factor is related to temporal averages involving the mobile-phase density. It is shown that the derived equations yield both new and familiar results for GC and LC. Their application to SFC, which will be covered in some detail in the seond part of this investigation[10], is also briefly considered. (Note that alternative approaches for SFC, treating some of the same aspects as the present study, are developed in refs. 3, 6 and, most noteworthy, 7.)

It should be emphasized that the isothermal distribution functions are ultimately expressed in terms of density, rather than pressure, where the former is the more convenient and natural state variable. There are three compelling reasons for this outcome. First, application of the condition of conservation of mass flow to Darcy's equation introduces a density factor which, in general, cannot be directly replaced by a term or terms involving pressure, using an equation of state that is both manageable and realistic (this is especially true for SFC). This would lead to cumbersome numerical evaluations and/or unnecessary (and, perhaps, invalid) approximations. Second, according to a recently developed, unified molecular theory of absorption[11,12] and adsorption[13,14] chromatography, solute retention (*e.g.*, k') is predicted to be a universal function of the reduced temperature and density (*not* pressure) of the mobile phase. Third, the isothermal viscosity of the mobile-phase fluid is a better behaved function of density and, according to theory, is more sensibly represented in terms of density[15].

THEORY

According to Darcy's law, at constant column temperature and for apparent Reynolds numbers within an acceptable upper limit[8], the linear velocity of the mobile phase, u, is related to the pressure gradient in the column, $\mathrm{d}P/\mathrm{d}x$, and the viscosity of the mobile phase, η, by

$$u = -(B/\eta)\,(\mathrm{d}P/\mathrm{d}x) \tag{1}$$

where B is the specific permeability coefficient of the column. In general, u, η and $\mathrm{d}P/\mathrm{d}x$ are local values, *i.e.*, they are all functions of x, the distance from the inlet of the column, at which $x = 0$ (and, at the outlet, $x = L$, the column length). Multiplying the numerator and denominator on the right-hand side of eqn. 1 by $\mathrm{d}\rho$, where ρ denotes the local mobile-phase density, and rearranging, one has

$$\mathrm{d}x = -(B/\eta u)\,(\delta P/\delta\rho)_T \mathrm{d}\rho \tag{2}$$

where the partial derivative is introduced to affirm the isothermal condition. Eqn. 2 relates a differential spatial element to a differential density element and is used to describe how the carrier density varies with the distance along the column. It also follows that u, η and $(\delta P/\delta\rho)_T$ may be expressed as functions of ρ.

Conservation of mass flow requires that, through any cross-sectional area of the column,

$$u\rho = u_o\rho_o = \text{constant} \tag{3}$$

where the subscript o refers to the column outlet. Combining eqns. 2 and 3, one finds

$$dx = -(C/\eta)\rho\,(\delta P/\delta\rho)_T d\rho = -CD_x(\rho)d\rho \tag{4}$$

where $C = B/u_o\rho_o$, and where

$$D_x(\rho) = \eta^{-1}\rho\,(\delta P/\delta\rho)_T = (\eta\beta)^{-1} \tag{5}$$

is the unnormalized, spatial distribution function and $\beta = \rho^{-1}\,(\delta\rho/\delta P)_T$ is the isothermal compressibility coefficient of the carrier fluid.

The unnormalized, temporal distribution function, $D_t(\rho)$, which is used to describe how the mobile-phase density varies with its residence time in the column, is formulated by applying the usual definition of u as the time derivative of distance ($\dot{x}$):

$$u = \dot{x} = dx/dt \tag{6}$$

Eqns. 3–6 combine to give

$$dt = -ED_t(\rho)d\rho \tag{7}$$

which relates a differential temporal element to a differential density element, where $E = C/u_o\rho_o = B/(u_o\rho_o)^2$ and where

$$D_t(\rho) = \eta^{-1}\rho^2(\delta P/\delta\rho)_T = \rho(\eta\beta)^{-1} = \rho D_x(\rho) \tag{8}$$

Note that eqns. 4 (with 5) and 7 (with 8) have a common "core", *viz.*, $\eta^{-1}(\delta P/\delta\rho)_T$.

The mobile-phase density, averaged over the length of the column, *i.e.*, the spatial average density, $\langle\rho\rangle_x$, is simply

$$\langle\rho\rangle_x = \int_o^L \rho\,dx \Big/ \int_o^L dx \tag{9}$$

From eqns. 4 and 9,

$$\langle\rho\rangle_x = \int_{\rho_o}^{\rho_i} \rho D_x(\rho)\,d\rho \Big/ \int_{\rho_o}^{\rho_i} D_x(\rho)\,d\rho \tag{10}$$

where $D_x(\rho)$ is given by eqn. 5 and $\rho = \rho_i$ (inlet density) at $x = 0$ and $\rho = \rho_o$ (outlet density) at $x = L$.

The mobile-phase density averaged over the residence time in the column, *i.e.*, the temporal average density, $\langle\rho\rangle_t$, is simply

$$\langle\rho\rangle_t = \int_o^{t_u} \rho\,dt \Big/ \int_o^{t_u} dt \tag{11}$$

where t_u denotes the total residence time of typical mobile-phase molecules, or the migration time for truly unretained solute molecules (peak-maximum value). From eqns. 7 and 11,

$$\langle \rho \rangle_t = \int_{\rho_o}^{\rho_i} \rho D_t(\rho)\, d\rho \Big/ \int_{\rho_o}^{\rho_i} D_t(\rho)\, d\rho \tag{12}$$

where $D_t(\rho)$ is given by eqn. 8 and $\rho = \rho_i$ at $t = 0$ ($x = 0$) and $\rho = \rho_o$ at $t = t_u$ ($x = L$).

To determine numerical values for the integral limits in eqns. 10 and 12, ρ_o and ρ_i, at the column operating temperature, T, and the respective pressures, P_o and P_i, one needs reliable equation-of-state information for the mobile-phase fluid being studied (gas, liquid or supercritical fluid). Evaluation of these integral equations (as well as subsequent relationships) also requires a knowledge of $\eta(\rho)$ at T (*e.g.*, by fitting tabulated viscosity data[15]) and $\beta(\rho)$ at T (again, from equation-of-state data), over the density range ρ_o to ρ_i.

Before considering a retained solute component, let us first derive other useful equations for averaged mobile-phase or unretained-solute quantities. In general, it follows from eqns. 10 and 12 that the average value of the nth power of the carrier density, $\langle \rho^n \rangle_j$, where $j = x$ or t, is given by

$$\langle \rho^n \rangle_j = \int_{\rho_o}^{\rho_i} \rho^n D_j(\rho)\, d\rho \Big/ \int_{\rho_o}^{\rho_i} D_j(\rho)\, d\rho \tag{13}$$

where $n = 1, 2, 3, 4, \ldots$. Also, the average linear velocity of the mobile phase, $\langle u \rangle$, is obtained from

$$\langle u \rangle = L/t_u = \int_0^L dx \Big/ \int_0^{t_u} dt \tag{14}$$

Using eqns. 4, 7–10 (with $E = C/u_o\rho_o$) and 14, one finds

$$\langle u \rangle = L/t_u = u_o\rho_o/\langle \rho \rangle_x \tag{15}$$

where $\langle \rho \rangle_x$ is given by eqn. 10. Multiplying eqn. 15 by the effective cross-sectional area of the column, A_{eff} (assumed to be constant throughout the column), where $LA_{eff} = V_v$ is the void volume of the column, and rearranging, one obtains

$$V_v\langle \rho \rangle_x = (u_o\rho_o A_{eff})t_u = \dot{m}t_u = G_u \tag{16}$$

where, with units of ml for V_v, g/ml for $\langle \rho \rangle_x$ and minutes for t_u, $\dot{m} = u_o\rho_o A_{eff}$ is then the observed mass flow-rate of the mobile phase in units of grams per minute. Furthermore, $V_v\langle \rho \rangle_x$ or $\dot{m}t_u$ represents the total mass of mobile-phase fluid required to sweep typical carrier molecules or unretained solute molecules from the inlet to the

outlet of the column. This "void mass" is designated as G_u. Eqn. 16 suggests two possible methods for determining G_u: (a) measurement of V_v and computation of $\langle\rho\rangle_x$; (b) measurement of $\dot{m}$ and t_u.

Turning now to a retained solute component (subscript s) and comparing its linear velocity with that of the mobile phase or an unretained solute component (subscript u) one has

$$u = \dot{x} = \mathrm{d}x/\mathrm{d}t = \mathrm{d}x/\mathrm{d}t_u \tag{17}$$

$$u_s = \dot{x}_s = \mathrm{d}x/\mathrm{d}t_s = u/(1 + k') \tag{18}$$

where k' is the local capacity factor of the solute, *i.e.*, the value at column position x, corresponding to a local density ρ. Therefore, from eqns. 3–5, 7, 8, 17 and 18, one obtains the following equations for the observed (peak-maximum) retention times, t_u and t_s, and the observed or temporal-averaged capacity factor, $\langle k'\rangle_t$

$$t_u = \int_0^L (1/u)\,\mathrm{d}x = E\int_{\rho_o}^{\rho_i} D_t(\rho)\,\mathrm{d}\rho \tag{19}$$

$$t_s = \int_0^L [(1 + k')/u]\,\mathrm{d}x = E\int_{\rho_o}^{\rho_i} (1 + k')\,D_t(\rho)\,\mathrm{d}\rho \tag{20}$$

$$\langle k'\rangle_t = (t_s - t_u)/t_u = \int_{\rho_o}^{\rho_i} k' D_t(\rho)\,\mathrm{d}\rho \Big/ \int_{\rho_o}^{\rho_i} D_t(\rho)\,\mathrm{d}\rho \tag{21}$$

It also follows from eqns. 16 and 21 that the net retention mass, $\langle G_n\rangle$, defined by

$$\langle G_n\rangle = G_s - G_u = \dot{m}(t_s - t_u) \tag{22}$$

where G_s is the mass of mobile phase at T required to sweep the retained solute component from the inlet to the outlet of the column, is related to $\langle k'\rangle_t$ by

$$\langle G_n\rangle = \dot{m}(t_s - t_u) = \dot{m}t_u\langle k'\rangle_t = V_v\langle\rho\rangle_x\langle k'\rangle_t = \langle\rho\rangle_x\langle V_n\rangle \tag{23}$$

where $\langle V_n\rangle = V_v\langle k'\rangle_t$ is the observed net retention volume. Eqn. 23 should prove to be particularly useful in SFC.

The local capacity factor in fluid-absorption chromatography[11,12] is predicted to have the general form

$$k' = k'_e \exp(a\rho + b\rho^2) \tag{24}$$

where $a < 0$, $b > 0$ and $k' \to k'_e$ as $\rho \to 0$. Inserting eqn. 24 into eqn. 21, one obtains

$$\langle k'\rangle_t = k'_e\,\langle\exp(a\rho + b\rho^2)\rangle_t \tag{25}$$

It is important to note that $\langle k' \rangle_t$ is proportional to the temporal average of the exponential in eqn. 25, which, in general, cannot be rigorously replaced by an exponential involving temporal averages of powers of the density. However, if $(\rho_i - \rho_o)/\rho_o$ is sufficiently small with respect to unity, a reasonable approximation is possible. Rewriting eqn. 24 as

$$k' = k_e' \exp[a\langle\rho\rangle_t + b\langle\rho^2\rangle_t] \cdot \exp[a(\rho - \langle\rho\rangle_t) + b(\rho^2 - \langle\rho^2\rangle_t)] \tag{26}$$

expanding the second exponential in eqn. 26 as a power series in ρ, and applying eqns. 13 (with $j = t$) and 21, one obtains

$$\langle k' \rangle_t = k_e' (\exp[a\langle\rho\rangle_t + b\langle\rho^2\rangle_t]) [1 + a^2(\langle\rho^2\rangle_t - \langle\rho\rangle_t^2)/2 + ab(\langle\rho^3\rangle_t - \langle\rho\rangle_t\langle\rho^2\rangle_t) + b^2(\langle\rho^4\rangle_t - \langle\rho^2\rangle_t^2)/2 + \ldots] \approx k_e' \exp[a\langle\rho\rangle_t + b\langle\rho^2\rangle_t] \tag{27}$$

It can be shown that if $a\rho + b\rho^2 < 0$, then $\langle \exp(a\rho + b\rho^2) \rangle \geq \exp(a\langle\rho\rangle_t + b\langle\rho^2\rangle_t)$, thus establishing an upper limit on this approximation.

Finally, let us obtain the salient equations for generating the various column profiles. The local mobile-phase density, ρ, at a fractional distance x/L from the column inlet is, from eqn. 4,

$$x/L = \int_0^x \mathrm{d}x \Big/ \int_0^L \mathrm{d}x = \int_\rho^{\rho_i} D_x(\rho)\, \mathrm{d}\rho \Big/ \int_{\rho_o}^{\rho_i} D_x(\rho)\, \mathrm{d}\rho \tag{28}$$

As ρ is inversely proportional to u, eqn. 28 may also be used to construct u/u_o *vs.* x/L profiles. The local density, ρ, when the carrier or an unretained solute has spent the fractional time τ_u/t_u on the column is, from eqns. 7 and 17,

$$\tau_u/t_u = \int_0^{\tau_u} \mathrm{d}t \Big/ \int_0^{t_u} \mathrm{d}t = \int_\rho^{\rho_i} D_t(\rho)\, \mathrm{d}\rho \Big/ \int_{\rho_o}^{\rho_i} D_t(\rho)\, \mathrm{d}\rho \tag{29}$$

which, with eqn. 28, also permits the construction of τ_u/t_u *vs.* x/L profiles. The local mobile-phase density, ρ, corresponding to the fractional solute migration time τ_s/t_s on the column is, from eqns. 7 and 18,

$$\tau_s/t_s = \int_0^{\tau_s} \mathrm{d}t_s \Big/ \int_0^{t_s} \mathrm{d}t_s = \int_\rho^{\rho_i} (1 + k')D_t(\rho)\, \mathrm{d}\rho \Big/ \int_{\rho_0}^{\rho_i} (1 + k')D_t(\rho)\, \mathrm{d}\rho \tag{30}$$

which, with eqn. 28, may also be used to construct τ_s/t_s *vs.* x/L profiles.

APPLICATIONS AND DISCUSSION

Let us begin by examining gas–liquid chromatography (GLC) with, in general,

a non-ideal mobile phase. The equation of state for a non-ideal carrier gas under fairly high, but not extreme, inlet-pressure conditions ($P_i < 10$ atm), is well represented by[16]

$$(PM_c/RT) = \rho[1 + (B_{cc}\rho/M_c)] \approx \rho[1 + (B_{cc}P/RT)] \tag{31}$$

where R is the gas constant, T is the column temperature, and M_c and B_{cc} denote the molar mass and second virial coefficient, respectively, of the neat carrier gas. From eqn. 31,

$$\rho(\delta P/\delta\rho)_T = (RT/M_c)\,\rho\,[1 + (2B_{cc}\rho/M_c)] \tag{32}$$

From published viscosity data[15] and, according to theory[9], the viscosity of the carrier gas within the stated pressure limit is well represented by

$$\eta^{-1} = \eta_e^{-1}\,[1 + \alpha_c\rho] \tag{33}$$

where $\alpha_c < 0$ is a constant (for a given carrier gas and temperature) and $\eta \rightarrow \eta_e$ as $\rho \rightarrow 0$. Through second power in density, eqns. 5, 32 and 33 yield

$$D_x(\rho) = I\rho\,(1 + A_c\rho) \tag{34}$$

where $I = \eta_e^{-1}\,(RT/M_c) =$ constant, and

$$A_c = (2B_{cc}/M_c) + \alpha_c \tag{35}$$

From eqns. 10 and 34, the spatial average density, $\langle\rho\rangle_x$, for a non-ideal carrier gas is then

$$\langle\rho\rangle_x/\rho_o = J_2^3(\rho) \cdot [1 + \Delta_x] \tag{36}$$

where

$$J_n^m(\rho) = (n/m)\,[(\Gamma^m - 1)/(\Gamma^n - 1)] \tag{37}$$

$$1 + \Delta_x = [1 + A_c\rho_o J_3^4(\rho)]/[1 + A_c\rho_o J_2^3(\rho)] \tag{38}$$

and where $\Gamma = \rho_i/\rho_o$, and $\Delta_x \ll 1$ is a small correction term (see below). Applying eqns. 35–38 to carbon dioxide at 310 K, where $\alpha_c = -0.786$ ml/g[15], $B_{cc} = -114$ ml/mol[17] and, hence, $A_c = -5.967$ ml/g, and letting $P_i = 5$ atm and $P_o = 1$ atm (from eqn. 31, $\rho_i = 8.850 \cdot 10^{-3}$ g/ml, $\rho_o = 1.738 \cdot 10^{-3}$ g/ml and, hence, $\Gamma = 5.092$), one calculates

$$\langle\rho\rangle_x/\rho_o = 3.4916 \tag{39}$$

where $J_2^3(\rho) = 3.5039$ and $\Delta_x = -0.0036$. Therefore, the correction term is trivially small and $\langle\rho\rangle_x/\rho_o$ under the chosen conditions is very well approximated by $J_2^3(\rho)$. (For more common GC carrier gases, such as helium, hydrogen and nitrogen, which have much smaller B_{cc} values[17] and, hence, A_c values, the correction term would be one order of magnitude smaller.)

It is of practical interest, for the accurate determination of net retention volumes, to compare $\langle\rho\rangle_x/\rho_o$ from eqn. 39 with the value which one would obtain by assuming ideal-gas behavior:

$$\langle\rho\rangle_x/\rho_o = \langle P\rangle_x/P_o = J_2^3(P) \tag{40}$$

where

$$J_2^3(P) = (2/3)\,[(P_i/P_o)^3 - 1]/[(P_i/P_o)^2 - 1] \tag{41}$$

is the reciprocal of the well known Martin–James compressibility factor, $J_3^2(P)$. With $P_i/P_o = 5$, eqns. 40 and 41 give

$$\langle P\rangle_x/P_o = 3.4444 \tag{42}$$

If the volumetric flow-rate of the carrier gas is determined at $T = 310$ K and $P_o = 1$ atm, and is denoted by $\dot{V}(T, P_o)$, then the more exact treatment gives the following result for the net retention volume, $\langle V_n\rangle$, at T and $\langle P\rangle_x$

$$\langle V_n\rangle = (t_s - t_u)\,\dot{V}(T, \langle P\rangle_x) = (t_s - t_u)\,(\rho_o/\langle\rho\rangle_x)\,\dot{V}(T, P_o) \tag{43}$$

while the ideal-gas assumption would give

$$\langle V_n\rangle = (t_s - t_u)\,(P_o/\langle P\rangle_x)\,\dot{V}(T, P_o) \tag{44}$$

where $\dot{V} = \dot{m}/\rho$. From eqns. 39 and42–44 it is seen that, with carbon dioxide as the carrier gas and under these experimental conditions, the ideal-gas assumption would lead to an error of $+1.37\%$ in the determination of $\langle V_n\rangle$. Fortunately, with the more commonly used carrier gases, the error would be one order of magnitude smaller[16].

Turning to the temporal average density and proceeding as before, eqns. 8, 12 and 34 give

$$D_t(\rho) = I\rho^2(I + A_c\rho) \tag{45}$$

$$\langle\rho\rangle_t/\rho_o = J_3^4(\rho) \cdot [1 + \Delta_t] \tag{46}$$

where

$$1 + \Delta_t = [1 + A_c\rho_o J_4^5(\rho)]/[1 + A_c\rho_o J_3^4(\rho)] \tag{47}$$

and where A_c and $J_n^m(\rho)$ are given by eqns. 35 and 37, respectively. For carbon dioxide and under the same experimental conditions, one calculates values of $\Delta_t = -0.0025$ (again, a trivial correction), $\langle\rho\rangle_t/\rho_o = 3.8328$ and $\langle P\rangle_t/P_o = J_3^4(P) = 3.7742$, where the former average is 1.55% higher than the latter. Also, provided the inlet pressure is not extreme ($P_i < 10$ atm.), GC column profiles based on density distributions should be within a few percent of those based on pressure distributions.

Concluding the discussion of GC by considering a retained solute component, the local k' through the first power in density is[11,12]

$$k' = k'_e \exp[(2B_{cs} - \bar{V}_s^\infty)\rho/M_c] \tag{48}$$

where B_{cs} is the carrier gas–solute interaction second virial coefficient and $\bar{V}_s^\infty$ is the infinite-dilution partial molar volume of the solute in the stationary liquid. Expanding the exponential in eqn. 48 as a power series in ρ, applying eqns. 13 and 21 and taking the logarithm of the result, one obtains, through the first power in density,

$$\ln \langle k' \rangle_t = \ln k'_e + [(2B_{cs} - \bar{V}_s^\infty)\rho_o/M_c]\,[\langle \rho \rangle_t/\rho_o] \tag{49}$$

where $\langle \rho \rangle_t/\rho_o \approx J_3^4(\rho)$. Replacing ρ_o/M_c by P_o/RT (with negligible error) and approximating $\langle \rho \rangle_t/\rho_o$ by $\langle P \rangle_t/P_o = J_3^4(P)$ (with up to a few percent error; see above), one finds

$$\ln \langle k' \rangle_t \approx \ln k'_e + [(2B_{cs} - \bar{V}_s^\infty)P_o/RT] \cdot J_3^4(P) \tag{50}$$

which is a more approximate, but familiar, result[9].

Using the present density formalism, treatment of averages in liquid chromatography is even more straightforward. Analysis of equation-of-state information[8] and viscosity data[15] for dense fluids indicates that $D_x(\rho)$ follows the form

$$D_x(\rho) = c\rho^r \tag{51}$$

where c is a constant and $r > 0$ may be as large as 4. Accordingly, from eqns. 8, 10, 12 and 37,

$$\langle \rho \rangle_x/\rho_o = J_{r+1}^{r+2}(\rho) \tag{52}$$

$$\langle \rho \rangle_t/\rho_o = J_{r+2}^{r+3}(\rho) \tag{53}$$

Further, as it is unlikely that, under normal LC operating conditions, the outlet and inlet densities will differ by more than 5% ($1.00 < \rho_i/\rho_o \leqslant 1.05$), it follows that

$$\langle \rho \rangle_x \approx \langle \rho \rangle_t \approx (\rho_i + \rho_o)/2 \tag{54}$$

with a maximum error of about 0.1%. Also, if the local k' can be described by eqn. 24, then, from eqn. 27,

$$\ln \langle k' \rangle_t \approx \ln k'_e + a\langle \rho \rangle_j + b\langle \rho \rangle_j^2 \tag{55}$$

where $j = x$ or t, $\langle \rho^2 \rangle_j \approx \langle \rho \rangle_j^2$ and $\langle \rho \rangle_j \approx (\rho_i + \rho_o)/2$, the arithmetic-mean value. Note that, for liquids, ρ_i and ρ_o may be calculated, with acceptable accuracy, using the Tait equation of state[8] and knowledge of P_i and P_o at T.

SFC, on the other hand, is by no means as straightforward. The mobile phase is

very non-ideal (in contrast to GC) and highly compressible (in contrast to LC). As a result, $D_x(\rho)$ and $D_t(\rho)$ are more complex analytical functions of ρ. Although the second part of this investigation[10] treats applications to SFC in great detail, the utility of the present approach in SFC will, nevertheless, be illustrated here.

The Jacobsen–Stewart modification of the Benedict–Webb–Rubin (BWR) equation of state yields exceptionally reliable PVT data, over very wide ranges of pressure and temperature, for low-molar-mass, non-polar fluids[18,19]. Using this BWR equation of state and tabulated viscosity data[15], the "core" of $D_x(\rho)$ and $D_t(\rho)$, $\eta^{-1} \cdot (\delta P/\delta\rho)_T$, can be readily and accurately generated as an analytical function of ρ, at the desired temperature, for carbon dioxide and light hydrocarbons[10,19]. For carbon dioxide an excellent fit to $\eta^{-1}\ (\delta P/\delta\rho)_T$ is obtained with a seventh-order polynomial in ρ[10]:

$$\eta^{-1}\ (\delta P/\delta\rho)_T = \sum_{l=0}^{7} c_l \rho^l \tag{56}$$

It follows from eqns. 5 and 8 that

$$D_x(\rho) = \sum_{l=0}^{7} c_l \rho^{l+1} \tag{57}$$

$$D_t(\rho) = \sum_{l=0}^{7} c_l \rho^{l+2} \tag{58}$$

from which the various mobile-phase averages and column profiles may be calculated, once the c_l values have been determined.

Table I gives some numerical results for an SFC (packed) column, with carbon dioxide as the mobile phase at 320 K, having an inlet pressure of $P_i = 120$ bar and an outlet pressure of $P_o = 100$ bar, with respective densities of $\rho_i = 0.6331$ and $\rho_o =$

TABLE I

NUMERICAL RESULTS FOR SFC COLUMN PROFILES WITH CARBON DIOXIDE AT 320 K

Column inlet: $P_i = 120$ bar; $\rho_i = 0.6331$ g/ml. Column outlet: $P_o = 100$ bar; $\rho_o = 0.4497$ g/ml.

ρ/ρ_o	x/L	τ_u/t_u	u/u_o
1.408	0.000	0.000	0.710
1.367	0.165	0.185	0.732
1.326	0.308	0.340	0.754
1.285	0.432	0.470	0.778
1.245	0.541	0.581	0.803
1.204	0.636	0.675	0.831
1.163	0.722	0.757	0.860
1.122	0.799	0.828	0.891
1.082	0.870	0.891	0.925
1.041	0.937	0.948	0.961
1.000	1.000	1.000	1.000

0.4497 g/ml. Listed in the first column are local densities, given as ρ/ρ_o, in ten equally spaced decrements from ρ_i to ρ_o (note that these ρ values can be easily converted to P values using the extended BWR equation of state[10]). For the purpose of examining mobile-phase profiles, the values in the second (fractional distance, from eqn. 28), third (fractional residence time, from eqn. 29) and fourth (relative velocity, from eqn. 3) columns are computed. Note also that the arithmetic mean of ρ/ρ_o is 1.204, whereas $\langle\rho\rangle_x/\rho_o = 1.241$ (from eqn. 10) and $\langle\rho\rangle_t/\rho_o = 1.252$ (from eqn. 12). The result for the temporal average density, for example, reveals that the mobile phase is spending relatively more time in the high-density, inlet region of the column, where it is moving with a relatively slower velocity.

From Table I it is seen that the arithmetic-mean density is reached when typical mobile-phase molecules have passed through 63.6% of the column length and have spent 67.5% of their residence time in the column. Therefore, the initial (inlet) rate of change of ρ/ρ_o with x/L or τ_u/t_u is smaller than the final (outlet) rate. At both the spatial and temporal midpoints ($x/L = 0.5$ and $\tau_u/t_u = 0.5$) the local density is greater than the arithmetic-mean density. It is also apparent that a typical carrier molecule requires over half of its total residence time to reach the positional midpoint of the column.

Fairly exact and detailed calculations and analyses, such as those outlined above, for both the mobile phase and retained solutes[10], are therefore possible for SFC. At this stage, the procedure is limited to carbon dioxide or a light hydrocarbon as the neat mobile phase. Also, the theory, in its present form, is not applicable to density-programmed SFC.

CONCLUSIONS

The equations derived here permit a more tractable and exact approach to obtaining and analyzing average densities and column profiles of gas, liquid and supercritical fluid mobile phases. They also provide a more direct means of relating observed solute retention quantities to temporal density averages ($\langle\rho^n\rangle_t$), which is of practical importance in packed-column SFC[10,20].

ACKNOWLEDGEMENTS

This material is based on work supported by the National Science Foundation under Grant CHE-8305045. The author is also grateful to R. E. Boehm, T. J. Bruno, A. Hussam, D. P. Poe and R. L. Riester for helpful discussions.

REFERENCES

1 D. R. Gere, R. Board and D. McManigill, *Anal. Chem.*, 54 (1982) 736.
2 P. J. Schoenmakers and F. C. C. J. G. Verhoeven, *J. Chromatogr.*, 352 (1986) 315.
3 A. Wilsch and G. M. Schneider, *J. Chromatogr.*, 357 (1986) 239.
4 P. A. Mourier, M. H. Caude and R. H. Rosset, *Chromatographia*, 23 (1987) 21.
5 P. J. Schoenmakers and L. G. M. Uunk, *Chromatographia*, 24 (1987) 51.
6 M. Perrut, *J. Chromatogr.*, 396 (1987) 1.
7 P. J. Schoenmakers, P. E. Rothfusz and F. C. C. J. G. Verhoeven, *J. Chromatogr.*, 395 (1987) 91, and references cited therein.
8 M. Martin, G. Blu and G. Guiochon, *J. Chromatogr. Sci.*, 11 (1973) 641, and references cited therein.

9 J. R. Conder and C. L. Young, *Physicochemical Measurements by Gas Chromatography*, Wiley, Chichester, 1979, Ch. 2 and 8.
10 D. E. Martire, R. L. Riester, T. J. Bruno, A. Hussam and D. P. Poe, in preparation.
11 D. E. Martire and R. E. Boehm, *J. Phys. Chem.*, 91 (1987) 2433.
12 D. E. Martire, *J. Liq. Chromatogr.*, 10 (1987) 1569.
13 D. E. Martire, *J. Chromatogr.*, 452 (1988) 17.
14 D. E. Martire, *J. Liq. Chromatogr.*, 11 (1988) 1779.
15 K. Stephan and K. Lucas, *Viscosity of Dense Fluids*, Plenum Press, New York, 1979.
16 D. E. Martire and D. C. Locke, *Anal. Chem.*, 37 (1965) 144.
17 J. H. Dymond and E. B. Smith, *The Virial Coefficients of Pure Gases and Mixtures*, Clarendon Press, Oxford, 1980.
18 R. T. Jacobsen and R. J. Stewart, *J. Phys. Chem. Ref. Data*, 2 (1973) 757.
19 J. F. Ely, *Proceedings of the 63rd Gas Processors Association Annual Convention*, Gas Processors Association, Tulsa, OK, 1984, pp. 9–22.
20 X. Zhang, D. E. Martire and R. G. Christensen, in preparation.

Journal of Chromatography, 461 (1989) 177–191
Elsevier Science Publishers B.V., Amsterdam — Printed in The Netherlands

CHROMSYMP. 1417

MODELING OCTANOL–WATER PARTITION COEFFICIENTS BY REVERSED-PHASE LIQUID CHROMATOGRAPHY

DOUGLAS J. MINICK*, DAVID A. BRENT and JOHN FRENZ
Wellcome Research Laboratories, 3030 Cornwallis Drive, Research Triangle Park, NC 27709 (U.S.A.)

SUMMARY

The dynamic range of a polycratic reversed-phase liquid chromatographic (RPLC) method for measuring hydrophobicity constants (log k'_w) for non-ionic, organic molecules was examined. Evidence is presented that indicates that the differential hydrogen bonding effect present in most RPLC methods has been minimized by selection of appropriate stationary and mobile phase conditions. Thus, values of log k'_w determined for compounds of different net hydrogen bonding properties (non-congeners) can be compared directly. Results indicate that non-congeners with hydrophobicities varying between $-0.20 \leqslant \log k'_w \leqslant 5.27$ can be measured by this procedure. Additionally, the net hydrogen bonding property of any solute molecule can be predicted from the chromatographic experiment. Finally, the suppression of hydrogen-bonding discrimination effects in this method is shown to be a result of the low levels of octanol and alkylamine added to the mobile phase.

INTRODUCTION

Octanol–water partition coefficients (log $P_{o/w}$) have been used successfully in correlations with biological activities for a large number of structurally diverse organic compounds[1,2]. However, the shake-flask technique that is used to measure log $P_{o/w}$ is prone to errors and experimental problems[3], and alternative methods for estimating this important physical parameter, including chromatographic ones, have been investigated. Reversed-phase liquid chromatography (RPLC) has been used most often to estimate values of log $P_{o/w}$. Good correlations are generally found between chromatographic retention data and log $P_{o/w}$ for structurally similar compounds[3–5]. Dissimilar compounds (non-congeners) usually yield poorer results when log $P_{o/w}$ constants are correlated with RPLC retention data in comparison to those obtained by subdividing the set into structurally similar classes and regressing the data in each class independently[6–11]. The inability to describe these correlations by a single regression equation is due to a differential hydrogen bonding effect that is qualitatively similar to that observed when octanol–water partition coefficients are correlated with alkane–water partition coefficients for a set of non-congeners[12]. The usual RPLC and alkane–water systems exhibit greater hydrogen bonding selectivity than does the octanol–water system.

0021-9673/89/$03.50

A number of methods have been reported by investigators attempting to suppress hydrogen bonding discrimination in the chromatographic system. As early as 1976, Mirrlees *et al.*[13] obtained a good correlation between log $P_{o/w}$ and RPLC retention for a set of non-congeners. They were able to successfully model octanol–water partitioning by using octanol-saturated Kieselguhr as the stationary phase and octanol-saturated water as the eluent. Later, Unger *et al.*[14] obtained similar results using octanol-saturated octadecyl silica gel as the stationary phase. In more recent studies, Terada[15] and Miyake *et al.*[16] obtained good correlations between log $P_{o/w}$ and capacity factors (log k') for sets of non-congeners by including hydrogen bonding indicator variables in their regression equations. The inclusion of these variables improved regression results by partially compensating for the hydrogen bonding properties inherent in their chromatographic data. RPLC systems with methanol as the organic component of the eluent have been shown to model octanol–water partitioning well[8,17]. Valkó[18] has reported a method for estimating log $P_{o/w}$ when acetonitrile is used as the organic component in the eluent. Under these conditions, values of log $P_{o/w}$ for a set of non-congeners were accurately predicted by a multiple regression equation containing two parameters derived from chromatographic data. The parameters obtained for each compound were the slope and intercept of the linear regression of log k'_φ *vs.* φ_{ACN} data (ACN stands for acetonitrile), where log k'_φ is the capacity factor measured at a number of different volume fractions of organic modifier (φ_{ACN}). Extrapolation of data measured at several eluent strengths in this manner is termed "polycratic", from the Greek kratos or "strength". The parameters derived by polycratic methods generally yield hydrophobicity constants which correlate better with log $P_{o/w}$ than retention data obtained under monocratic conditions, as discussed by Braumann[17].

Recently, we reported a polycratic procedure[19] for estimating hydrophobicity constants by RPLC that largely eliminates the discrimination arising from differences in hydrogen bonding capacity of non-congeners. This method used mixtures of aqueous buffer, methanol, octanol and *n*-decylamine as eluents and octyl-modified silica as the stationary phase to obtain extrapolated capacity factors (log k'_w). log k'_w is the intercept of the linear regression of log k'_φ and φ_{MeOH}, defined analogously to φ_{ACN}, above. Unlike a previously reported method for estimating hydrophilicity with varying mobile phase composition[20], this new approach included trace amounts of octanol and alkylamine in the eluent, and showed little differential hydrogen bonding effects, presumably owing to enrichment of these components in the stationary phase. In addition, log k'_w was shown to be relatively independent of the value measured for the column dead-time (t_0) and was chosen as the chromatographic parameter for constructing a hydrophobicity scale. This has the advantage that log k'_w results from different research groups can be compared without complications which may arise from differences in procedures used to estimate t_0. Finally, this method does not require converting chromatographic data to the octanol–water scale in order to compare compounds of varying hydrophilicity. Instead, values of log k'_w are considered to be *a priori* hydrophobicity constants[17] that reflect the same molecular properties which control partitioning in the octanol–water system.

In this paper, we wish to report additional results obtained by using the recently published method. First, the range of hydrophobicities measurable by this method was evaluated. In this study, log k'_w values were determined for two sets of non-congeners.

The first set contained compounds that were relatively hydrophobic ($0.95 \leqslant \log P_{o/w} \leqslant 5.5$), and was used to evaluate the upper range of the chromatographic method. The second set contained compounds that were relatively hydrophilic ($-0.65 \leqslant \log P_{o/w} \leqslant 2.26$), and was used to assess the lower range. Data from both experiments were correlated with measured ($\log P_{o/w}$) and calculated (CLOGP) octanol–water partition coefficients in order to demonstrate that $\log k'_w$ varied linearly with these parameters over the range examined. In addition, since the compounds comprising these sets are non-congeneric, these results confirm that the hydrogen bonding selectivity present in most chromatographic systems has been effectively suppressed under these RPLC conditions. An octadecyl-derivatized polymeric stationary phase was examined as a possible alternative to octyl-modified silica gel in the analysis of hydrophilic analytes, and should provide greater column stability at the relatively high mobile phase pH employed. The results also show that the net hydrogen bonding properties of solutes can be predicted from the same chromatographic data used to determine hydrophobicity constants ($\log k'_w$) in which this information was suppressed. This capability is demonstrated for the two sets of non-congeners. Finally, chromatographic data are presented which help to explain why the conditions chosen for this method overcome the differential hydrogen bonding effect.

EXPERIMENTAL

Chromatographic equipment

All chromatographic data were obtained using a Waters Assoc. (Milford, MA, U.S.A.) Model 840 chromatographic system equipped with two Model 590 pumps, a WISP 712 autoinjector, and a Model 450 variable-wavelength detector, operated at 220 nm and 0.2 a.u.f.s. This system utilizes a Professional 380 computer (Digital Equipment Corporation, Maynard, MA, U.S.A.) to control hardware, acquire and store data, and estimate retention times.

Stainless-steel columns (15 cm × 4.5 mm, I.D.) packed with 5-μm octyl-modified silicas were purchased from ES Industries (Marlton, NJ, U.S.A.). A stainless-steel column (15 cm × 4.6 mm, I.D.) packed with octadecyl-modified Macrophase MP-1 was supplied by Interaction Chemicals (Mountain View, CA, U.S.A.). A silica saturator column (5 cm × 4.5 mm, I.D.) positioned between the pumps and the autoinjector was filled with Partisil 20/400 silica gel from Whatman (Clifton, NJ, U.S.A.). A Rheodyne (Cotati, CA, U.S.A.) column inlet filter containing a 0.5-μm filter element was positioned between the autoinjector and the analytical columns in order to prevent blockage.

Materials

HPLC-grade methanol, analytical-grade 1-octanol, and solutions of 1 *M* sodium hydroxide and 1 *M* hydrochloric acid were purchased from Fisher Scientific (Pittsburgh, PA, U.S.A.).

4-Morpholinopropanesulfonic acid (MOPS), *n*-decylamine (99%), and all test solutes were obtained from Aldrich (Milwaukee, WI, U.S.A.). The water used to prepare the mobile phases was purified using a Milli-Q Water System from Millipore (Bedford, MA, U.S.A.). Deuterated methanol was obtained from MSD Isotopes (Montreal, Canada).

Procedures

The flow-rate was 2.0 ml/min for all the experiments in which silica-based packings were used. For the experiment with the polymer-based packing, a flow-rate of 1.0 ml/min was used. All eluents were filtered through a 0.45-μm Durapore filter (Millipore) prior to use, and purged continuously with helium during use to prevent problems associated with the build-up of dissolved gases in the eluent.

Capacity factors were measured in duplicate at each eluent composition. Dead-times (t_0) for the silica-based packings were estimated from the retention of deuterated methanol in a pure methanol eluent. For the polymeric packing, the dead-time could not be estimated at $\varphi_{MeOH} = 1$ due to the restricted eluent ranges recommended for this packing. Consequently, this parameter was approximated by the retention time of the solvent disturbance peak measured from injections of pure methanol at an eluent composition of $\varphi_{MeOH} = 0.75$. Although it is unlikely that the latter estimate of t_0 rigorously defines the column dead-volume, we have shown previously that the derivation of log k'_w was insensitive to the exact value of t_0 used[19].

For experiments with silica-based packings, mobile phases consisted of different volume fractions of organic and aqueous solutions which were mixed from separate pumps. Variations in the volume fraction of organic modifier in the eluent were accomplished by the pump control capabilities of the chromatographic system. The organic portion contained methanol and 1-octanol (0.25%, v/v), while the aqueous portion contained MOPS buffer (0.02 *M*) and *n*-decylamine (0.15%, v/v) and was adjusted to pH 7.4 by additions of 1 *M* sodium hydroxide or 1 *M* hydrochloric acid. For the experiments wih the polymeric packing, solutions containing 80% (v/v) and 20% (v/v) of the organic portion of the eluent were blended before use. Different volume fractions of organic modifier were then formed by pumping the amounts of these solutions needed to achieve the desired volume fraction. The organic portion contained methanol and 1-octanol (0.25%, v/v), while the aqueous portion contained MOPS buffer (0.02 *M*). The aqueous portion was adjusted to pH 7.4 prior to blending with the organic portion.

Chromatographic retention data were measured at 0.1-increments of φ_{MeOH} for $0.25 \leqslant \varphi_{MeOH} \leqslant 0.75$ for all eluites except thymine and adenine, and these data used in eqn. 1 to derive values of log k'_w and S (the slope parameter). Thymine and adenine were unretained at $\varphi_{MeOH} \geqslant 0.45$, and additional retention data were required at $\varphi_{MeOH} = 0.30$ and $\varphi_{MeOH} = 0.27$ in order to decrease the uncertainty in estimates of log k'_w and S for these compounds. The correlation coefficients, r, from the log k'_φ *vs.* φ_{MeOH} regressions were >0.990 for all compounds except camphorquinone where $r > 0.983$, indicating that log k'_φ varies linearly with φ_{MeOH} within the range of organic compositions examined. Values of CLOGP were calculated using the MedChem Software, (Pomona, CA, U.S.A.), and the correlations between chromatographic results and octanol–water partition coefficients were analyzed using the linear regression program in the RS/1 statistical package (Cambridge, MA, U.S.A.).

RESULTS AND DISCUSSION

Establishment of the dynamic range

The set of non-congeners used to investigate the upper limit of the dynamic range is shown in Table I. These solutes were selected on the basis of both hydrophobic and

TABLE I

COMPOUNDS AND VALUES OF SLOPE, LOG k'_w, LOG $P_{o/w}$. AND CLOGP USED TO INVESTIGATE THE UPPER LIMIT OF DYNAMIC RANGE

Compound	*Classification**	Slope	log k'_w	*log* $P_{o/w}$**	CLOGP***
Phenol	d	2.46	1.16	1.46	1.48
4-Methoxyphenol	d	2.33	1.02	1.34	1.58
Acetophenone	a	2.34	1.40	1.58	1.58
Naphthalene	a	3.98	3.00	3.30	3.32
2-Hydroxynaphthalene	d	3.35	2.15	2.70	2.65
1,4-Dihydroxynaphthalene	d	2.79	1.32	na	1.98
N-phenyl-1-naphthylamine	d	5.11	3.97	na	4.79
4-Bromoaniline	a	3.16	2.01	2.26	2.08
4-Methoxyaniline	a	1.61	0.62	0.95	1.02
Camphorquinone	a	2.11	1.23	1.52	0.46
1-Phenylhexane	a	6.19	5.27	5.52	5.44
Anthracene	a	4.77	3.94	4.45	4.49
9-Methylanthracene	a	5.01	4.26	5.07	5.14
9-Anthracene carboxaldehyde	a	4.17	3.44	na	3.84
9-Anthracenemethanol	d	4.08	2.99	na	3.45
Anthraquinone	a	3.56	2.91	3.39	2.72
1,8-Dichloroanthraquinone	a	3.96	3.27	na	4.19
9-Acetylanthracene	a	4.40	3.42	na	3.93
1-Aminoanthraquinone	a	3.61	2.93	na	2.15
1-Amino-4-hydroxyanthraquinone	m	3.28	2.50	na	1.80
4-Biphenylmethanol	d	3.89	2.74	na	2.99
2-Biphenylmethanol	d	3.82	2.62	na	2.99
4-Biphenylcarboxaldehyde	a	3.97	2.98	na	3.38
Carbazole	d	4.15	3.03	3.72	3.53
Quinoline	a	2.72	1.93	2.03	2.05
Phenanthadine	a	3.65	3.00	na	3.22
Acridine	a	3.56	2.87	3.40	3.43
Benz(a)anthracene-7,12-dione	a	4.74	4.26	na	3.89
4,5-Diphenylimidazole	d	4.34	3.25	na	4.15
Phenanthrene	a	4.81	3.94	4.46	4.49
Fluoranthene	a	4.96	4.21	na	4.95
Pyrene	a	4.96	4.26	4.88	4.95

* d = net hydrogen bond donor, a = net hydrogen bond acceptor, m = mixed net hydrogen bonding properties.

** Values were taken from ref. 1.

*** Values calculated by using MedChem software.

net hydrogen bonding characteristics. Net hydrogen bonding classifications were made according to the general scheme reported by Leo *et al.*[12], and values of log $P_{o/w}$ were taken from ref. 1. Values of log k'_w and S were obtained by linear regression using

$$\log k'_\varphi = \log k'_w - S\varphi_{MeOH} \quad (1)$$

where φ_{MeOH} = volume fraction of methanol in the eluent, log k'_φ = the logarithm of the capacity ratio measured at each φ_{MeOH}, S = the slope parameter, and log k'_w = chromatographic hydrophobicity constant. Values of log k'_w were correlated with log $P_{o/w}$ and CLOGP, and the regression results reported in Table II. Graphs of

TABLE II

UPPER LIMIT STUDY: LINEAR REGRESSION EQUATIONS FOR LOG $P_{o/w}$ *vs.* LOG k'_w AND CLOGP *vs.* LOG k'_w

n = Number of data points; r = correlation coefficient, S.D. = overall standard deviation of the regression. The standard deviations in the slope and intercept are shown in parentheses.

(i) log $P_{o/w}$ = 1.076 (0.032) log k'_w + 0.216 (0.095)			
n = 17	r = 0.9933	S.D. = 0.175	
(ii) CLOGP = 1.008 (0.051) log k'_w + 0.386 (0.161)			
n = 29	r = 0.9673	S.D. = 0.313	

the log $P_{o/w}$ *vs.* log k'_w and CLOGP *vs.* log k'_w regressions are shown in Fig. 1a and b, respectively, where data are plotted according to the net hydrogen bonding classifications reported in Table I. In the graph of log $P_{o/w}$ *vs.* log k'_w, the data show only minimal systematic deviations arising from the differential hydrogen bonding effect and demonstrate that hydrophobicity constants for non-ionic non-congeners can be estimated up to at least log $P_{o/w}$ = 5.5 without any serious deviations arising from this effect. In the graph of CLOGP *vs.* log k_w, the calculated values for camphorquinone, 1-aminoanthraquinone and 1-amino-4-hydroxyanthraquinone were considered incor-

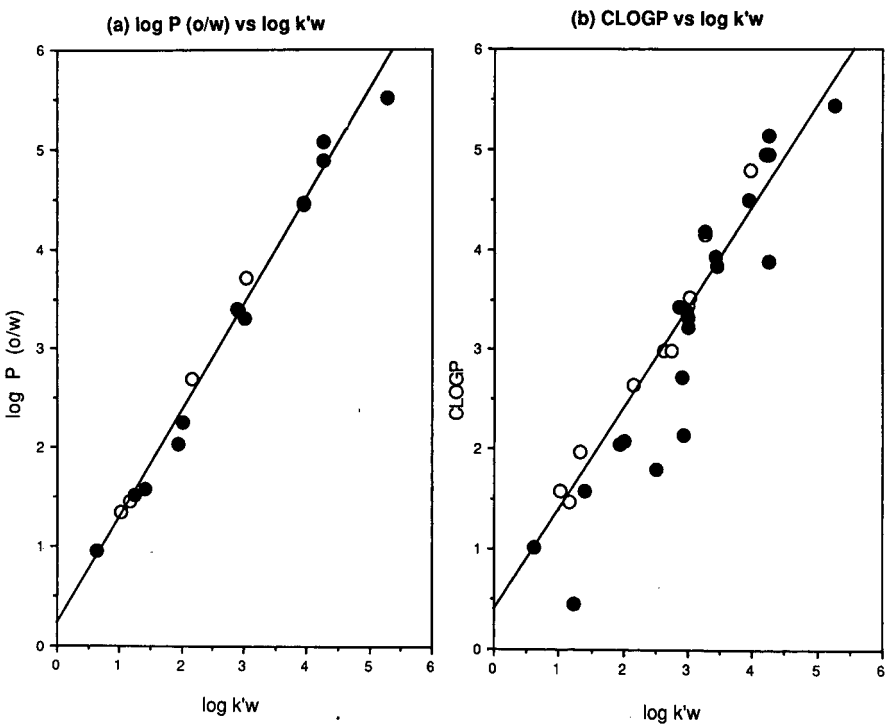

Fig. 1. Relationship between chromatographic hydrophobicity constants (log k'_w) and (a) measured octanol–water partition coefficients (log $P_{o/w}$), and (b) calculated octanol–water partition coefficients (CLOGP) for a relatively hydrophobic series of non-congeners. Solutes have been graphed according to the net hydrogen bonding classifications in Table I. The two solute classes are designated by ○ = donors and ● = acceptors. These log k_w data were determined on C_8-modified silica.

rect and were omitted from the regression reported in Table II for this correlation. A comparison between log $P_{o/w}$ and CLOGP for camphorquinone (1.52 and 0.46, respectively) indicates that the calculated value is incorrect. For the other two compounds, no log $P_{o/w}$ values are available to compare with the CLOGP values. However, these compounds are both capable of forming intramolecular hydrogen bonds, and it has been our experience that this type of effect is not well predicted by CLOGP. The formation of these bonds reduces the availability of acceptor and donor groups to form intermolecular hydrogen bonds with water molecules, resulting in measured log $P_{o/w}$ values which are higher than predicted from a calculation based upon the additive properties of isolated groups. Although log k'_w cannot be completely ruled out as the source of the error observed here, the expected hydrogen bonding characteristics for these solutes were predicted exactly from the slope *vs.* log k'_w data (see discussion below), suggesting that these solutes behaved normally under these RPLC conditions. Regardless of these considerations, the good correlation between log $P_{o/w}$ and log k'_w in contrast to the relatively poor correlation between CLOGP and log k'_w serves to illustrate potential inaccuracies in the calculated data. More importantly, the correlation between log k'_w and CLOGP illustrates that, even for a relatively large set of data, hydrogen bonding discrimination is minimal in this chromatographic system.

The set of non-congeners used to investigate the lower limit of the dynamic range is reported in Table III. Some variations were observed for values of log k'_w for the test compounds measured in both experiments, particularly for phenol. The origin of these variations is unclear and is currently being examined. As before, this set was selected on the basis of both the hydrophilic and net hydrogen bonding properties of these solutes. CLOGP and log $P_{o/w}$ data were both correlated with log k'_w, and the results

TABLE III

COMPOUNDS AND VALUES OF SLOPE, LOG k'_w, LOG $P_{o/w}$, AND CLOGP USED TO INVESTIGATE THE LOWER LIMIT OF DYNAMIC RANGE

Compound	*Classification*	*Slope*	*log k'_w*	*log $P_{o/w}$**	*CLOGP***
Phenol	d	2.59	1.26	1.46	1.48
4-Methoxyphenol	d	2.38	1.07	1.34	1.58
Aniline	a	1.94	0.86	0.98	0.92
4-Methoxyaniline	a	1.67	0.68	0.95	1.02
4-Bromoaniline	a	3.24	2.09	2.26	2.08
Camphorquinone	a	2.20	1.29	1.52	0.46
Acetophenone	a	2.34	1.40	1.58	1.58
Naphthalene	a	4.20	3.14	3.30	3.32
Resorcinol	d	2.12	0.50	0.80	0.81
Hydroquinone	d	1.91	0.19	0.55	0.81
Pyridine	a	1.35	0.74	0.65	0.67
4-Acetylpyridine	a	1.19	0.47	0.54	0.44
Pyrazole	a	1.11	0.088	0.26	0.26
Adenine	a	0.44	−0.20	−0.09	−0.34
Thymine	a	–	–	−0.65	error

* Values taken from ref. 1.

** Values calculated by using MedChem software.

TABLE IV

LOWER LIMIT STUDY: LINEAR REGRESSION EQUATIONS FOR LOG $P_{o/w}$ *vs.* LOG k'_w AND CLOGP *vs.* log k'_w

n = Number of data points; r = correlation coefficient; S.D. = overall standard deviation of regression. The standard deviations in the slope and intercept are shown in parentheses.

(i) log $P_{o/w}$ = 1.010 (0.075) log k'_w + 0.176 (0.063)		
n = 12	r = 0.9737	S.D. = 0.126
(ii) CLOGP = 0.982 (0.141) log k'_w + 0.237 (0.113)		
n = 11	r = 0.9180	S.D. = 0.222

reported in Table IV. As before, camphorquinone was omitted from the CLOGP *vs.* log k'_w regression. Thymine, the most hydrophilic compound in this study, was unretained under these experimental conditions. Also, data for naphthalene and 4-bromoaniline were omitted from the correlation in order not to skew the results away from the hydrophilic region. These results indicate that values of log k'_w can be estimated for solutes with measured log $P_{o/w}$ values below zero. Graphs illustrating

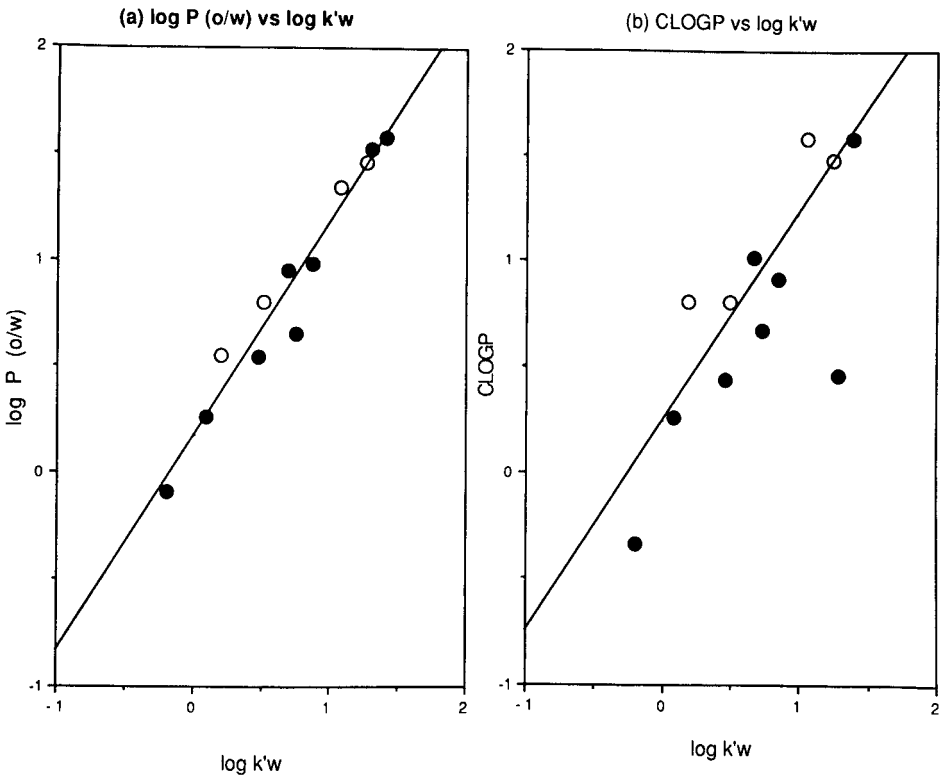

Fig. 2. Relationship between chromatographic hydrophobicity constants (log k'_w) and (a) measured octanol–water partition coefficients (log $P_{o/w}$), and (b) calculated octanol–water partition coefficients (CLOGP) for a relatively hydrophilic series of non-congeners. Solutes have been graphed according to the net hydrogen bonding classifications in Table III. The two solute classes are designated by ○ = donors and ● = acceptors. These log k_w data were determined on C_8-modified silica.

these correlations are shown in Fig. 2. Although the presence of some hydrogen bond discrimination is suggested in this figure, this effect appears to be slight.

In an attempt to lower the dynamic range further, an octadecyl-derivatized polymeric stationary phase was investigated. The increased phase ratio for this packing should allow relatively hydrophilic compounds that are unretained on the C_8 silica-based packing to be measured. Using the polymeric packing, log k'_w for thymine was estimated, indicating that the hydrophobicity index could be extended to include solutes with log $P_{o/w}$ values as low as -0.65. The correlation between log $P_{o/w}$ and log k'_w values measured on this column is illustrated in Fig. 3. The regression statistics are included in the figure legend. The data for thymine were omitted from the regression so that results could be compared directly with those derived from the C_8 packing. The statistical results are slightly poorer than those reported for eqn. 1 in Table IV. The deviation in the slope of this regression from unity indicates that the physical processes involved in retention on this column are not identical to those governing retention on the octyl-silica column. Equations correlating log $P_{o/w}$ and log k'_w data represent linear free-energy relationships in which the slope is an estimate of how closely the free

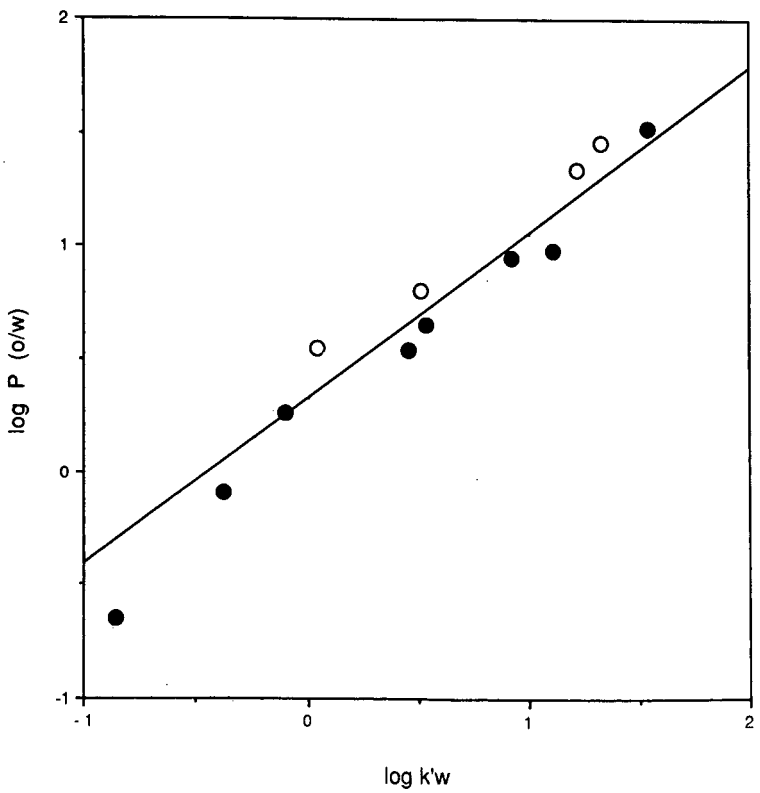

Fig. 3. Relationship between measured octanol–water partition coefficients (log $P_{o/w}$) and chromatographic hydrophobicity constants (log k'_w) determined using an octadecyl-derivatized polymeric stationary phase. The regression equation fit to this data is: log $P_{o/w}$ = 0.730 (0.058) × log k'_w + 0.324 (0.058), where the standard deviations in the slope and intercept are shown in parentheses. For this regression, n = 11, r = 0.9702 and S.D. = 0.134. Solute classes are designated by ○ = donors and ● = acceptors.

energies of the processes compare[21]. A unit slope in such a plot indicates that the two processes are "homoenergetic"[21], *i.e.*, the free energy changes are identical. However, the slope of the regression equation relating log $P_{o/w}$ with log k'_w values derived from the polymeric C_{18} phase is 0.730, indicating that these two processes are "homeoenergetic"[21], or energetically similar, since there is a linear correlation between the two, but not identical. Although more pronounced hydrogen bonding discrimination has been reported for C_{18} phases than for C_8 phases[19], the relatively large deviation from unity in the slope may also be due to solute interactions with the polymeric backbone of this packing.

The log $P_{o/w}$ and log k'_w data in Tables I and III were combined to produce an overall regression equation. For solutes measured in both experiments, log k'_w values used in this correlation were obtained from averaged k'_w. This correlation is shown in Fig. 4, where the regression results are reported in the legend. As expected, these results indicate that the values of log k'_w for these non-congeners vary linearly with log $P_{o/w}$ data over the entire range and that hydrogen bonding discrimination is minimal.

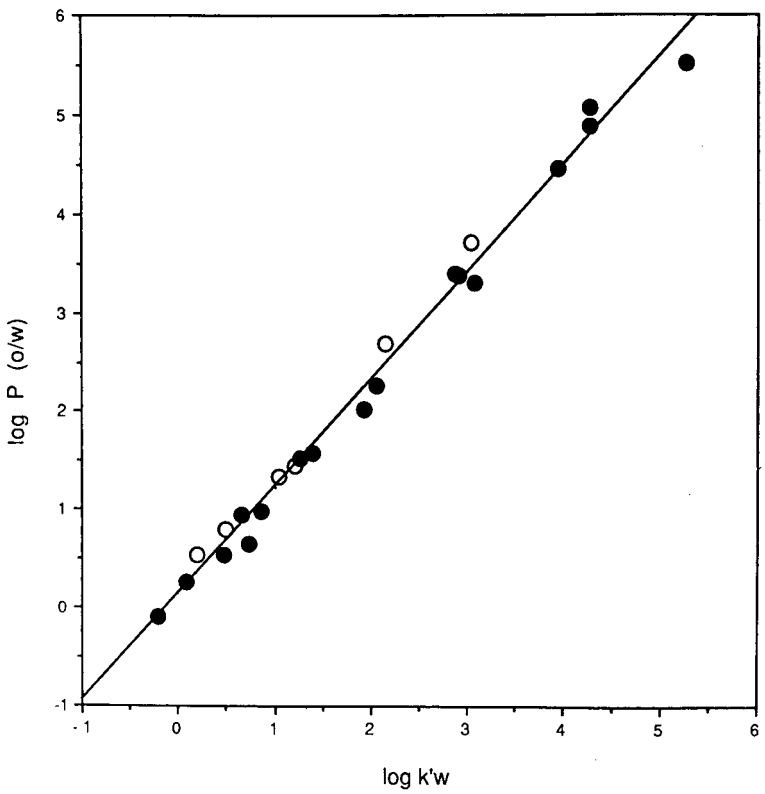

Fig. 4. The overall relationship between all of the chromatographic hydrophobicity constants (log k'_w) and measured octanol–water partition coefficients reported in Tables I and III. The regression equation fit to this data is: log $P_{o/w}$ = 1.090 (0.023) × log k'_w + 0.146 (0.058), where the standard deviations in the slope and intercept are shown in parentheses. For this regression, n = 24, r = 0.9951 and S.D. = 0.172. Solute classes are designated by ○ = donors and ● = acceptors.

Determination of hydrogen-bonding tendency

A distinct advantage of this RPLC method over the standard measurement of octanol–water partition coefficients is the ability to derive qualitative hydrogen bonding information from the same chromatographic data used to derive hydrophobicity constants. In the course of this work, the differential hydrogen bonding effect was observed to vary inversely in correlations between log $P_{o/w}$ and either log k'_w or S, where S is the slope constant derived from eqn. 1. Consequently, as chromatographic conditions were varied to minimize this effect between log $P_{o/w}$ and log k'_w data, it became more pronounced between log $P_{o/w}$ and S. This observation indicated that a parameter containing hydrogen bonding information could be obtained simultaneously from the same RPLC experiment designed to obtain hydrophobicity constants in which hydrogen bonding differences were attenuated.

To illustrate this, a graph of the S *vs.* log k'_w data from Tables I and III is shown in Fig. 5, where compounds were graphed according to net hydrogen bonding. In Fig. 5, compounds for which the net hydrogen bonding properties can be unambiguously assigned (*e.g.*, phenols = donors, ketones = acceptors) fall on different but approximately parallel lines. The lines shown here were fit by using a limited number of

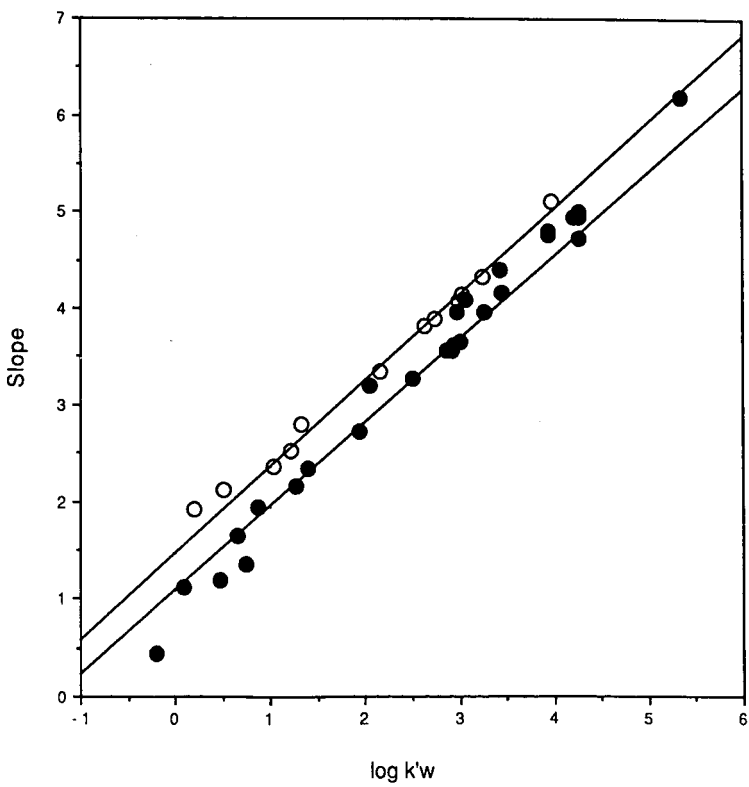

Fig. 5. Relationship between the chromatographic hydrophobicity constants, log k'_w and S, derived from eqn. 1. Data are graphed according to the net hydrogen bonding classifications shown in Tables I and III such that ○ = donors and ● = acceptors. Fitted lines were included for illustrative purposes and do not represent lines fit by regressing all S *vs.* log k'_w data from these tables.

S *vs.* log k'_w data ($n = 6$ data points in both cases), and were included primarily for illustration purposes. The results generally support the classifications reported in Tables I and III, including the classification of di-N-substituted aromatic amines (carbazole, N-phenyl-1-naphthyl amine, and 4,5-diphenylimidazole) as donors, and other aromatic amines (anilines) and ring-N compounds as acceptors, along with ketones and aldehydes. Fused-ring aromatics were uniformly found to lie between the donor and acceptor lines, and although this class of solutes was grouped as acceptors by Leo *et al.*[12], the data here suggest that these solutes might be more accurately classified as neutral compounds. The point corresponding to 1-aminoanthraquinone lies on the acceptor line, while that corresponding to 1-amino-4-hydroxyanthraquinone lies between the donor and acceptor lines. Since aminoanthraquinone contains only acceptor groups, the point for this compound should lie close to the line describing other strong acceptors. In the second compound, the presence of the hydroxyl group would be expected to contribute donor properties to the overall hydrogen bonding characteristics, resulting in a weaker net acceptor. This behavior is predicted exactly, and illustrates how these RPLC results can be used to qualitatively predict the net hydrogen bonding property of a solute containing both donor and acceptor functional groups, and may facilitate structure elucidation of unknown compounds.

The only aromatic amine observed to deviate significantly from the scheme of Leo *et al.*[12] was 4-bromoaniline, which lies between the donor and acceptor lines. This location indicates that this compound acts more like a weak acceptor or neutral than a strong acceptor, in contrast to the behavior of the other two anilines investigated here. The classification of this solute as a weak acceptor may be explained in part by considering the pK_a values of these compounds. The pK_a reported for 4-bromoaniline is low (3.82) in comparison to aniline (4.60) and 4-methoxyaniline (5.31)[22]. Since the pK_a is a measure of the proton accepting strength of a solute, this compound would be predicted to behave as a weaker acceptor than the other compounds. Two additional compounds showing deviations from expected behavior were 9-acetylanthracene and 4-biphenylcarboxaldehyde, which were both located between the donor and acceptor lines, instead of on the acceptor line. It is unclear why this behavior was observed, but the results suggest that these solutes may have undergone chemical reactions, such as the formation of a hemiacetal or hemiketal, which produced a change in their net hydrogen bonding properties.

The results shown in Fig. 5 demonstrate that two different molecular properties are obtainable from a single experiment, when the chromatographic conditions described here are used. Values of log k'_w can be used to estimate hydrophobicity quantitatively without an overlapping effect arising from variations in hydrogen bonding between different classes of solutes. Concomitantly, S appears to reflect both hydrophobic and hydrogen bonding properties and can be correlated with log k'_w to classify solutes qualitatively according to net hydrogen bonding. Since the slope parameter does exhibit hydrogen-bonding discrimination, S may be useful as an alternative estimate of hydrophobicity in correlations with biological activity that are better modeled by alkane–water partition coefficients. The parallel nature of the lines describing strong donors and strong acceptors suggests that this scheme might be useful in quantifying net hydrogen bonding properties of solutes from a general knowledge of the strengths of hydrogen bonds.

TABLE V

CORRELATION OF LOG $P_{o/w}$ WITH LOG k'_w DATA DETERMINED FROM THE MODIFIER COMPONENTS STUDY

n = Number of data points; r = correlation coefficient; S.D. = overall standard deviation of regression. The standard deviations in the slope and intercept are shown in parentheses.

(a) Methanol (no octanol)/MOPS (no amine)
log $P_{o/w}$ = 1.094 (0.227) log k'_w − 0.157 (0.423)
n = 7 r = 0.9069 S.D. = 0.359

(b) Methanol + octanol (0.25%, v/v)/MOPS (no amine)
log $P_{o/w}$ = 1.005 (0.092) log k'_w + 0.105 (0.166)
n = 7 r = 0.9796 S.D. = 0.171

(c) Methanol (no octanol)/MOPS + n-decylamine (0.15%, v/v)
log $P_{o/w}$ = 1.162 (0.123) log k'_w − 0.216 (0.223)
n = 7 r = 0.9731 S.D. = 0.196

(d) Methanol + octanol (0.25%, v/v)/MOPS + n-decylamine (0.15%, v/v)
log $P_{o/w}$ = 0.947 (0.026) log k'_w + 0.297 (0.046)
n = 7 r = 0.9980 S.D. = 0.053

Chromatographic conditions influencing the suppression of hydrogen bonding

Trace modifiers in the eluent were varied in order to determine what properties of the mobile phase were responsible for suppressing the differential hydrogen bonding effect. Results from these experiments indicated that the combination of these trace components produces suppression of this effect. The set of test compounds used in this study had been proposed earlier for comparing the hydrophobic properties of different columns[4] and included: phenol and 4-methoxyphenol (strong donors); 4-methoxyaniline, acetophenone, and camphorquinone (strong acceptors); 4-bromoaniline and naphthalene (weak acceptors). The eluent conditions were varied as follows: (a) methanol as the organic component (no octanol) and MOPS buffer as the aqueous phase (no amine); (b) methanol + octanol, but MOPS buffer only in the aqueous phase; (c) methanol only, but MOPS + amine in the aqueous phase; (d) methanol + octanol, and MOPS buffer + amine (the standard mobile-phase operating conditions). Values of log k'_w data derived from each set of eluent conditions were correlated with the values of log $P_{o/w}$ reported in Table I. The results of these correlations are reported in Table V and illustrated in Fig. 6, where log $P_{o/w}$ *vs.* log k'_w data are graphed according to the net hydrogen bonding properties of the solutes. These results show that the differential hydrogen bonding effect is greatest when the eluent contains no octanol or amine, but is still present when either but not both of these trace components is present in the eluent. However, it is clear from Fig. 6d that maximum suppression of this effect is observed only when both of these components are present. These results suggest that octanol and n-decylamine in the eluent alter properties of the stationary phase synergistically, producing a net desolvation–solvation process in this system that models closely the desolvation–solvation process occurring in the octanol–water system.

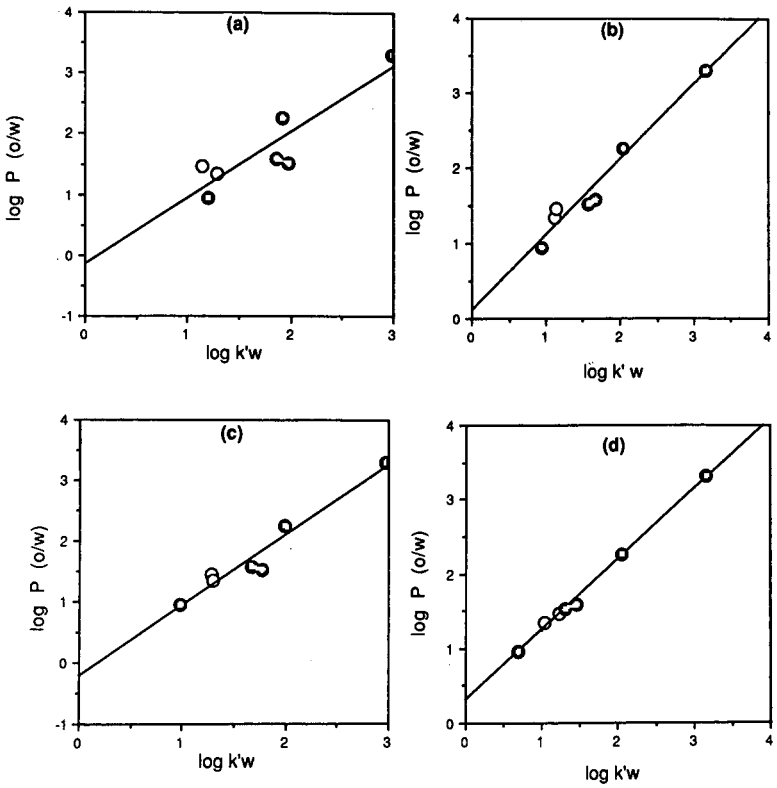

Fig. 6. Graphs illustrating the effect of trace components in the eluent. These graphs indicate the synergistic effect of octanol and decylamine upon the properties of the chromatographic system which result in accurate modeling of the octanol–water liquid–liquid partitioning system. Solutes have been graphed according to net hydrogen bonding: ○ = donors and ● = acceptors.

CONCLUSIONS

The dynamic range of a recently published method for measuring hydrophobicity constants has been investigated. Results indicate that this method is capable of estimating these constants within the range $-0.20 \leqslant \log k'_w \leqslant 5.27$, corresponding to a range $-0.09 \leqslant \log P_{o/w} \leqslant 5.52$ in the $\log P_{o/w}$ scale. As discussed by Braumann[17], values of $\log k'_w$ determined by extrapolation appear to form an *a priori* scale of hydrophobicities. Comparisons between $\log k'_w$ and $\log P_{o/w}$ demonstrate that this chromatographic method yields hydrophobicity constants for non-ionic solutes which closely estimate the same molecular properties estimated by octanol–water liquid–liquid partition coefficients. However, the RPLC experiment is more information-rich than the shake-flask experiment used to measure $\log P_{o/w}$, for in addition to providing hydrophobicity constants ($\log k'_w$) devoid of hydrogen bonding information, a second hydrophobicity constant (the S constant) containing information about hydrogen bonding tendencies is obtained simultaneously. The RPLC experiment is faster and more readily automated than the shake-flask method used to measure $\log P$, and is not

dependent on the purity of the sample, as is the spectrophotometric determination of log *P*.

Finally, the role of octanol and *n*-decylamine in the eluent was examined, and results were presented which suggest that it is the combination of these modifiers in the eluent which is responsible for minimizing the differential hydrogen bonding effect.

REFERENCES

1 C. Hansch and A. Leo, *Substituent Constants for Correlation Analysis in Chemistry and Biology*, Wiley-Interscience, New York, 1980.
2 F. Helmer, K. Kiehs and C. Hansch, *Biochemistry*, 7 (1968) 2858.
3 D. A. Brent, J. J. Sabatka, D. J. Minick and D. J. Henry, *J. Med. Chem.*, 26 (1983) 1014.
4 S. E. Krikorian, T. A. Chorn and J. W. King, *Quant. Struct.-Act. Relat.*, 6 (1987) 65.
5 F. Gaspari and M. Bonati, *J. Pharm. Pharmacol.*, 39 (1987) 252.
6 C. V. Eadsforth, *Pest. Sci.*, 17 (1986) 311.
7 J. E. Haky and A. M. Young, *J. Liq. Chromatogr.*, 7 (1984) 675.
8 T. Braumann, G. Weber and L. H. Grimme, *J. Chromatogr.*, 261 (1983) 329.
9 W. E. Hammers, G. J. Meurs and C. L. de Ligny, *J. Chromatogr.*, 247 (1982) 1.
10 J. J. Sabatka, D. J. Minick, T. K. Shumaker, G. L. Hodgson Jr. and D. A. Brent, *J. Chromatogr.*, 384 (1987) 349.
11 K. Miyake and H. Terada, *J. Chromatogr.*, 240 (1982) 9.
12 A. Leo, C. Hansch and E. Elkins, *Chem. Rev.*, 71 (1971) 525.
13 M. J. Mirrlees, S. J. Moulton, C. T. Murphy and P. J. Taylor, *J. Med. Chem.*, 19 (1976) 615.
14 S. H. Unger, J. R. Cook and J. S. Hollenberg, *J. Pharm. Sci.*, 67 (1978) 1364.
15 H. Terada, *Quant. Struct.-Act. Relat.*, 5 (1986) 81.
16 K. Miyake, N. Mizuno and H. Terada, *J. Chromatogr.*, 439 (1988) 227.
17 T. Braumann, *J. Chromatogr.*, 373 (1986) 191.
18 K. Valkó, *J. Liq. Chromatogr.*, 7 (1984) 1405.
19 D. J. Minick, J. Frenz, M. A. Patrick and D. A. Brent, *J. Med. Chem.*, in press.
20 J. E. Garst and W. C. Wilson, *J. Pharm. Sci.*, 73 (1984) 1616.
21 W. Melander, J. Stoveken and Cs. Horváth, *J. Chromatogr.*, 199 (1980) 35.
22 A. Albert and E. P. Serjeant, *The Determination of Ionization Constants*, Chapman and Hall, London, U.K., 1971.

Journal of Chromatography, 4610 (1989) 193–207
Elsevier Science Publishers B.V., Amsterdam — Printed in The Netherlands

CHROMSYMP. 1482

RETENTION MECHANISMS IN REVERSED-PHASE CHROMATOGRAPHY

STATIONARY PHASE BONDING DENSITY AND SOLUTE SELECTIVITY

KAREN B. SENTELL* and JOHN G. DORSEY*
Department of Chemistry, University of Florida, Gainesville, FL 32611 (U.S.A.)

SUMMARY

Chromatographic selectivity for small, non-polar solutes has been determined as a function of monomeric octadecyl stationary phase bonding density over the range 1.74–4.07 μmol/m^2. Phenyl or shape selectivity increases with increasing bonding density, whereas methylene selectivity remains approximately constant. These findings are in agreement with the mean field statistical thermodynamic theory of Dill, which predicts that increased stationary phase chain density should lead to increased anisotropic chain ordering and increased solute-shape selectivity. These studies provide further evidence that partitioning, not adsorption, is the dominant mode of retention for small, non-polar molecules in reversed-phase liquid chromatography.

INTRODUCTION

Chromatographic selectivity (α) is an important experimental probe in studies of the solute retention process. It reflects the difference between two solutes in the Gibbs free energy of transfer from the mobile phase to the stationary phase:

$$\alpha = k'_a/k'_b \text{ and } \ln \alpha = -\Delta(\Delta G)/RT$$

where k'_a and k'_b are capacity factors for solutes a and b, ΔG is the Gibbs free energy, R is the gas constant and T is the absolute temperature. Unlike differences in solute capacity factors, intercolumn selectivity differences cannot be due to different column phase ratios. If the same mobile phase composition is used when comparing different stationary phases, mobile phase contributions to the free energy of transfer are equivalent, cancelling each other in the selectivity ratio. In such a case, selectivity is indicative of differences in the different stationary phases[1]; this implies that very fundamental aspects of the stationary phase retention contribution can be studied via selectivity behavior.

The role of the stationary phase in reversed-phase liquid chromatographic (RPLC) selectivity has had much prior consideration. Many workers have examined

* Present address: Department of Chemistry, Cook Physical Science Building, University of Vermont, Burlington, VT 05405, U.S.A.

0021-9673/89/$03.50

the relationship between bonded-phase chain length and selectivity. Although some have reported little or no change in selectivity with stationary phase chain length[2,3], it has been reported by others that methylene selectivity increases as a function of chain length[4–7]. Others have observed increasing selectivity of benzene derivatives[8–10], styrene oligomers[11] and polynuclear aromatic hydrocarbons (PAHs)[12–15] with stationary phase chain length. The work of Hennion *et al.*[12] is especially significant, as the phases compared were prepared to have the same bonded-group surface coverage. Tchapla *et al.*[16] examined methylene selectivity for C_1, C_6, C_8, C_{14} and C_{18} monomeric bonded phases as a function of solute carbon number. They found that the selectivity continuously decreases up to a certain carbon number, at which a large step decrease in selectivity occurs. Their explanation of this phenomenon is that the stationary phase bonded chains solvate the alkyl chains of the solute molecule and, so long as the length of the solute alkyl chain is less than that of the bonded phase, increasing the number of methylene groups in the solute causes a constant stationary phase contribution to selectivity. Once the length of the solute alkyl chain exceeds that of the bonded phase, the remaining solute methylene groups no longer penetrate the chains; they undergo weaker dispersive interactions than those which penetrate, causing a sharp drop in selectivity. This behavior was not observed with the C_1 bonded phase, as solutes will not penetrate it. Lochmuller and Wilder[13] used a similar argument to explain increasing PAH selectivity as a function of bonded-chain length.

Correlations between selectivity and bonded-phase carbon loading have also been made[17–21]. However, early in the history of bonded phases Unger *et al.*[22] cautioned that carbon content alone is misleading because of differences in the surface area of the original silica, which result in different surface densities of the bonded alkyl groups. This concern makes the interpretation of many of the previous studies difficult. Engelhardt and Ahr[5] correlated selectivity for PAHs and phenylalkanes on monomeric and polymeric octadecyl phases with bonded-group surface coverage, noting that PAHs, being more "rigid", were especially affected by surface coverage. Tanaka *et al.*[23] observed increased hydrophobic selectivity as a function of monomeric octyl surface coverage. Hennion *et al.*[12] noted that the selectivity of their polymeric octadecyl phases increased up to 15% carbon, and subsequently leveled off; these results would also hold true for surface coverage, as the same silica substrate and silane reagent were used to produce all of these phases.

Comparison of the selectivity behavior of stationary phases prepared with different reagents, alkyl chain lengths and/or silica substrates adds these variables to an already complex situation and may explain the inconsistencies among conclusions drawn by different groups. Sander and Wise[24], Staroverov *et al.*[25], and Van den Driest and Ritchie[26] observed differences in selectivity as a function of silica substrate pore size and pretreatment which were especially marked for polymeric phases. Rather than solute size-exclusion effects, Sander and Wise attributed these differences to changes in the makeup of the bonded-phase structure as a consequence of these substrate parameters.

Antle and co-workers[27,28] stated that there are two types of reversed-phase (RP) column selectivity, solvophobic and chemical. Solvophobic selectivity arises from hydrophobic interactions between the solute molecules and the stationary phase. Tanaka *et al.*[23] and Jandera[29] noted from experimental evidence that hydrophobicity is the most important RP stationary phase selectivity parameter for non-polar solutes;

this has been confirmed by chemometric analyses, using cluster and principal components analysis[30] and factor analysis[31]. Chemical selectivity comes about from strong interactions (for example, hydrogen bonding or complexation) between the solute molecules and specific active sites, such as silanol groups or trace metal contaminants on the silica surface[27,29]; this effect is relatively unimportant for non-polar solutes.

A third type of selectivity, shape selectivity, can also be exhibited by chemically bonded phases. Some researchers[1,5,32–34] have examined selectivity for rigid molecules, such as PAHs, polyphenyls and cycloaliphatics, on bonded phases with various ligand structures. They found that these types of solutes were preferentially retained by alkylphenyl, alkylnaphthyl, alkylpyrenyl, cycloalkyl, cycloalkenyl and octadecyl stationary phases over other alkyl phases. They concluded that steric considerations were crucial in the retention of rigid or planar molecules. As octadecyl phases consist of lengthy alkyl chains bonded to the silica surface, the conformation of the bonded chains plays an important role in retention.

Wise and co-workers[24,35–38] and Van den Driest *et al.*[39] compared PAH selectivities on monomeric and polymeric octadecyl-bonded phases. Polymeric phases exhibit superior selectivity; moreover, selectivity increases as a function of polymeric surface coverage. Selectivities shown by monomeric phases are more like those of polymeric phases as the bonded-chain length increases; selectivities for polymeric phases become more "monomeric" with decreasing chain length[14]. Sander and Wise[14] explained these trends as being controlled by the overall thickness of the stationary phase.

Martire and Boehm[40], using a liquid crystal model of the stationary phase, proposed the first statistical mechanical theory to address explicitly the effects of chain organization on solute retention and selectivity. More recently, Dill[41,42] proposed a lattice-interphase model of the bonded-phase surface and described the equilibrium partition coefficient for a solute from the chemical potentials of the solute in the mobile phase system and in the bonded-chain interphase. The molecular details of the retention process involve (i) the creation of a solute-sized cavity in the stationary phase, (ii) the transfer of the solute from the mobile to the stationary phase and (iii) the closing of the solute-sized cavity in the mobile phase. In this retention model, non-polar solute partitioning and selectivity will be strongly affected by the surface density of the bonded alkyl chains.

We are investigating experimentally the molecular mechanism of retention, as described by Dill[41,42]. He proposed that two driving forces dominate retention and selectivity: (i) the chemical differences of the contacts of the solute with surrounding molecular neighbors in the stationary and mobile phase and (ii) the partial ordering of the grafted stationary phase chains. This, at sufficiently high bonding density, leads to an entropic expulsion of solute from the stationary phase relative to that which would be expected in a simpler, amorphous oil–water partitioning process. At low densities, partitioning should increase linearly with the bonded-phase surface coverage as the surface becomes more fully covered by the hydrocarbon chains and therefore less polar. Partitioning should reach a maximum at the point at which neighbor interactions among chains become important. At higher surface densities, partitioning decreases owing to increasing entropic expulsion of solute by the grafted chains[41–43]. We have tested with an extensive database of almost 350 sets of experiments and

found, in agreement with theory, that the mobile phase contribution to retention can be described by the binary interaction constants of solutes with solvents[44]. We have also examined the effects of alkyl chain bonding density on the partitioning and retention of small, non-polar solutes[45], and have found that experimental partitioning behavior for non-polar solutes mirrors the predicted behavior, a maximum in partition coefficients being found at a stationary phase chain density of about 3.0 μmol/m^2. In this work we have tested this further by examining the effects of alkyl chain bonding density on selectivities of non-polar solutes.

EXPERIMENTAL

Monomeric, silica-bonded phases with surface coverages ranging from 1.74 to 4.07 μmol/m^2 were prepared as described previously[46] from 20–30-μm Davisil (W. R. Grace, Baltimore, MD, U.S.A.) with a pore diameter of 147 Å. The liquid chromatographic system used for the selectivity measurements has also been described previously[45]. Toluene (Eastman Organic Chemicals, Rochester, NY, U.S.A.), ethylbenzene (Fisher Scientific, Fair Lawn, NJ, U.S.A.), propylbenzene (Alfa Products, Danvers, MA, U.S.A.), butylbenzene (Eastman) and pentylbenzene (Alfa) standards were prepared in high-performance liquid chromatographic (HPLC)-grade methanol for methylene selectivity studies. Benzene (Mallinckrodt, Paris, KY, U.S.A.), biphenyl (Eastman), recrystallized three times from ethanol, and *p*-terphenyl (Sigma, St. Louis, MO, U.S.A.) standards in methanol comprised the phenyl selectivity test solutes. The Column Evaluation Test Mixture 1 (PAH) of the National Bureau of Standards (NBS, Gaithersburg, MD, U.S.A.) was used to measure the overall selectivity for PAHs; this mixture contains benzo[*a*]pyrene (BaP), 1,2:3,4:5,6:7,8-tetrabenzonaphthalene (TBN) and phenanthro[3,4-*c*]phenanthrene (PhPh). Their structures are shown in Fig. 1.

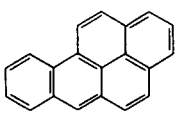

Benzo[a]pyrene (BaP)

Phenanthro [3,4-c] phenanthrene (PhPh)

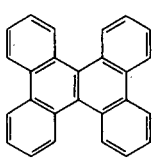

1,2:3,4:5,6:7,8-Tetrabenzonaphthalene (TBN)

Fig. 1. Structures of the solutes in the NBS Column Evaluation Test Mixture No. 1 (PAH).

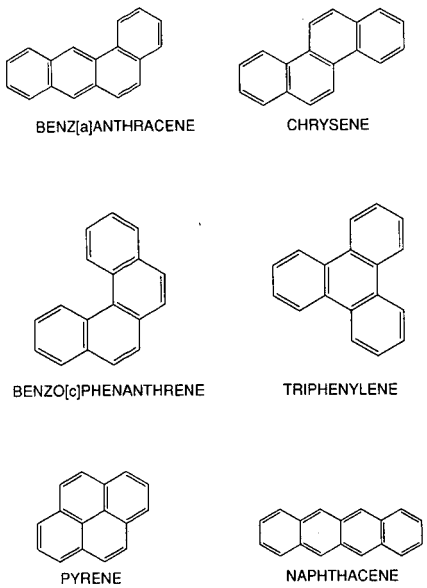

Fig. 2. Structures of the four-ring PAH test solutes.

PAH selectivity was also examined with the four-ring PAHs chrysene, benz[*a*]-anthracene, benzo[*c*]phenanthrene, naphthacene, triphenylene (all of mol.wt. 228.28) and pyrene (mol.wt. 202.26), shown in Fig. 2. The four-ring PAHs [Aldrich, Milwaukee, WI, U.S.A., except for naphthacene (Eastman)] were prepared in HPLC-grade acetonitrile. Methylene and phenyl selectivity studies were conducted at 35.0°C with methanol–water (55:45) and acetonitrile–water (85:15) as mobile phases. Owing to their limited methanol solubility, the four-ring PAHs were evaluated at 35.0°C with only acetonitrile–water (85:15) as the mobile phase. The NBS test mixture was also evaluated with acetonitrile–water (85:15), but at ambient temperature (25.0–29.0°C) so as to replicate better the conditions of Wise and Sander[36]. The mobile phase flow-rate was 1.5 ml/min in all instances; capacity factors were measured from triplicate chart-recorder tracings for each solute.

RESULTS AND DISCUSSION

The chromatographic selectivity was examined as a function of monomeric octadecyl stationary phase bonding density. When the same mobile-phase compositions are used to compare selectivities on different stationary phases, mobile phase contributions to selectivity are equivalent, and changes in selectivity are attributable to stationary phase contributions[1]. Although Wise and co-workers[24,35–37] have extensively examined the effect of polymeric alkyl bonding density on selectivity for PAHs, monomeric phases have not been exhaustively examined. Monomeric stationary phases, used here, can only result in monomeric layers on the silica surface, giving a relatively well characterized surface. For polymeric phases, surface density numbers should be viewed only as a rough indication of true chain density. As the degree of polymerization is almost never known, Sander and Wise[35] stated that "the

use of surface coverage values to calculate interchain distances is probably not justified for polymeric phases". Methylene and phenyl selectivities as a function of octadecyl bonding density for methanol–water (55:45) and acetonitrile–water (85:15) are listed in Tables I and II. As these selectivity values are calculated from the slopes of plots of ln k' *versus* homologue unit number for each stationary phase, the least-squares linear regression coefficients of correlation for each of these plots are included to verify linear behavior. Colin *et al.*[7] stated that a linear relationship exists between ln k' and the homologue unit number only for unit numbers above three to five. This number of units, termed the critical carbon number, results from the fact that the effect of an additional homologue unit should only become constant when it is sufficiently removed from the basic functional group. Thus, for homologues below the critical carbon number, the plot of ln k' *versus* homologue unit number is expected to exhibit curvature. However, this departure from linearity is generally small for RPLC systems, causing a very limited influence on the average slope of the plot[7]. This expected curvature was not found for either mobile phase system, as all of the correlation coefficients are greater than or equal to 0.991.

Methylene selectivity *versus* octadecyl bonding density for the homologous methylene series toluene, ethylbenzene, propylbenzene, butylbenzene and pentylbenzene is plotted in Fig. 3 for the methanol–water (55:45) system and in Fig. 4 for the acetonitrile–water (85:15) system. The average methylene selectivity value $\pm$ one standard deviation for the methanol–water mobile phase is 1.96 $\pm$ 0.03 and that for the acetonitrile–water system is 1.34 $\pm$ 0.07. Using methanol–water (55:45) as the mobile phase and octadecyl columns, Colin *et al.*[7] and Karger *et al.*[47] reported methylene selectivity values of 2.14 and 2.0, respectively. For octadecyl columns and acetonitrile–water (85:15), Colin *et al.*[7], Karger *et al.*[47] and Krstulovic *et al.*[6] reported values of 1.40, 1.3 and 1.4, respectively; our reported methylene selectivity values are

TABLE I

METHYLENE AND PHENYL SELECTIVITIES AT 35.0°C AS A FUNCTION OF OCTADECYL BONDING DENSITY FOR METHANOL–WATER (55:45) AS THE MOBILE PHASE

C_{18} *bonding density* (μmol/m^2)	*Methylene selectivity*	*Methylene correlation coefficient**	*Phenyl selectivity*	*Phenyl correlation coefficient***
1.74	1.92	0.9993	7.27	0.9997
1.98	1.96	0.9997	7.05	1.0000
2.07	1.92	0.9994	7.38	0.9996
2.09	1.97	0.9999	7.20	1.0000
2.75	1.94	0.9993	7.61	0.9999
3.06	1.99	0.9996	7.83	0.9999
3.24	1.97	0.9995	7.94	0.9999
3.34	1.97	0.9994	8.13	0.9997
3.56	1.93	0.9994	7.96	0.9998
3.60	1.96	0.9997	8.17	0.9997
4.07	2.00	0.9996	8.18	0.9994

* Correlation coefficient for the plot of ln k' *versus* carbon number; the slope of this line is ln(methylene selectivity).

** Correlation coefficient for the plot of ln k' *versus* phenyl number; the slope of this line is ln(phenyl selectivity).

TABLE II

METHYLENE AND PHENYL SELECTIVITIES AT 35.0°C AS A FUNCTION OF OCTADECYL BONDING DENSITY FOR ACETONITRILE–WATER (85:15) AS THE MOBILE PHASE

C_{18} bonding density (μmol/m^2)	*Methylene selectivity*	*Methylene correlation coefficient**	*Phenyl selectivity*	*Phenyl correlation coefficient**
1.74	1.29	0.9991	1.90	0.9996
1.98	1.28	0.9993	1.92	0.9994
2.07	1.21	0.9935	1.94	1.0000
2.09	1.31	0.9994	1.95	0.9999
2.75	1.53	0.9906	2.00	0.9995
2.84	1.35	0.9983	2.04	0.9999
3.06	1.34	0.9988	2.04	0.9997
3.15	1.34	0.9974	2.01	0.9995
3.24	1.35	0.9990	2.03	0.9992
3.34	1.36	0.9943	2.02	0.9992
3.56	1.35	0.9995	2.03	0.9995
3.60	1.36	0.9999	2.11	0.9997
4.07	1.36	0.9960	2.12	0.9971

* See Table I

comparable to these values for both mobile phase systems. It is not surprising that methylene selectivities are approximately constant in either system; methylene selectivity is a type of solvophobic selectivity, due solely to non-specific hydrophobic interactions between the solute molecules and the stationary phase, and it is therefore unaffected by the greater chain ordering resulting from increasing octadecyl bonding density. This observation is supported by the work of Lochmuller and Wilder[13], who found that methylene selectivities for small solutes on octadecyl columns compare favorably with liquid–liquid partition selectivities. It has also been predicted that solute-methylene selectivities should be unaffected by the molecular organization of the interphase[41].

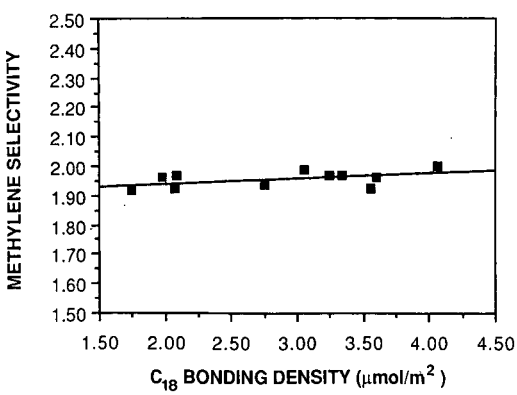

Fig. 3. Methylene selectivity *versus* octadecyl bonding density at 35.0°C for methanol–water (55:45) as the mobile phase.

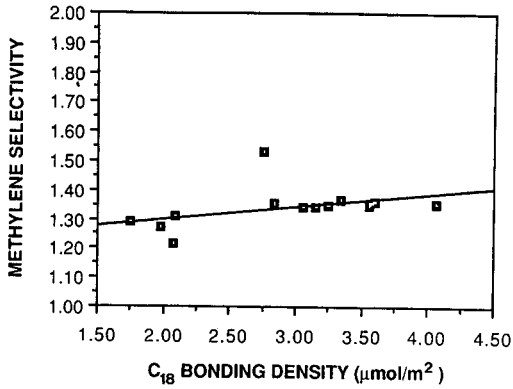

Fig. 4. Methylene selectivity *versus* octadecyl bonding density at 35.0°C for acetonitrile–water (85:15) as the mobile phase.

The relationship between phenyl selectivity and bonding density for the phenyl homologous series benzene, biphenyl and *p*-terphenyl is shown in Figs. 5 and 6 for methanol–water (55:45) and acetonitrile–water (85:15), respectively. Phenyl selectivity increases with increasing octadecyl bonding density in an approximately linear fashion with least-squares linear regression slopes of 0.508 and 0.0871 and correlation coefficients (r) of 0.955 and 0.941 for the methanol–water and acetonitrile–water systems, respectively. This correlation between phenyl selectivity and octadecyl bonding density can be attributed to shape selectivity. Martire and Boehm[40] predicted that solute selectivity should decrease as a function of solute shape in the order rod-like > planar > chain-like. This behavior was also observed by Lochmuller *et al.*[1], and this effect has been explained in terms of increased ordering of the bonded RP chains[1,6,40].

Wise and co-workers[24,35–37] examined the PAH selectivity of monomeric and polymeric octadecyl phases with bonding density ranges of 1.8–3.2 and 2.7–7.3 μmol/m^2, respectively. Wise and Sander[36] found that for polymeric phases with high bonding densities (greater than about 5.1 μmol/m^2) non-planar solutes were eluted before planar solutes and that non-linear solutes were eluted before linear solutes, even

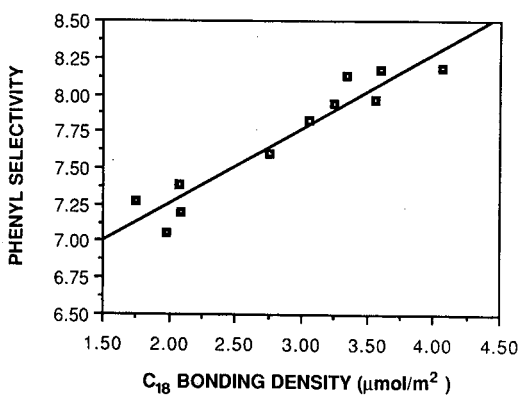

Fig. 5. Phenyl selectivity *versus* octadecyl bonding density at 35.0°C for methanol–water (55:45) as the mobile phase.

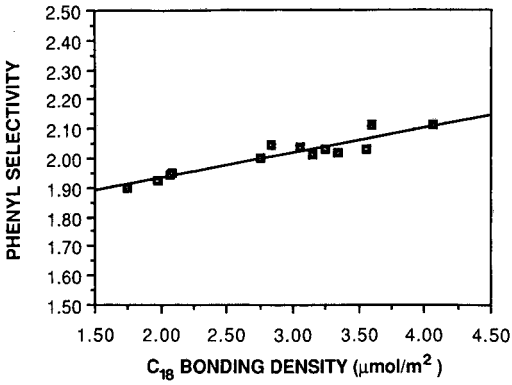

Fig. 6. Phenyl selectivity *versus* octadecyl bonding density at 35.0°C for acetonitrile–water (85:15) as the mobile phase.

if the solutes compared had similar molecular weights, overall shapes and molecular dimensions. Additionally, they found that the selectivity between planar–non-planar and linear–non-linear PAHs increases with increasing degree of non-planarity and non-linearity. Their "slot model" postulates that non-planar solutes have a greater "thickness", hindering penetration of the solute into the narrow slots between the bonded alkyl chains[36]. The situation is analogous for linear molecules, which would show greater retention than non-linear molecules. This also corresponds with Martire and Boehm's theory[40], which predicts that shape selectivity is greater for rigid-rod solutes than for globular solutes, especially when the stationary phase chains are fully extended or more rigid. Wise and Sander[36] argued that polymeric phases with higher alkyl densities are more extended and rigid than polymeric phases with low densities or monomeric phases.

The trend of greater phenyl selectivity with increasing octadecyl bonding density shown here is not surprising. The Dill interphase model[41,42] predicts that, as alkyl surface densities increase, the corresponding configurational constraints are also increased, creating a more rigid and ordered chain-packing structure. This anisotropy of the bonded chains gives rise to additional shape selectivity among solute molecules, as molecules which can most effectively align themselves with the chains are those which are most effectively retained. In this model, the driving force for retention is the creation of a solute-sized cavity in the stationary phase. As the bonding density and, consequently, chain ordering are increased, the free energy required for cavity formation also increases. It costs more free energy to insert solute substructures that are parallel to the silica–bonded chain interface than for substructures that align themselves with the chains and normal to the interface. Therefore, selectivity for linear and planar molecules will increase with increasing alkyl bonding density, as predicted by this theory and as shown by the results of our experiments.

It is interesting to compare the slope of the acetonitrile–water (85:15) phenyl selectivity plot (0.0871) with that for methanol–water (55:45) (0.508). One explanation of this disparity is the structural difference between the solvation layers of the bonded phase in the two very different mobile phase systems. The acetonitrile–water (85:15) solvation layer is relatively robust; at any of the bonded-phase alkyl densities the

stationary phase surface will be well solvated and the chains ordered. This means that the relative retention will only be affected to a small extent by changes in bonding density; chain ordering will increase little with increased packing constraints, as the chains are already relatively ordered. In methanol–water (55:45), the chains are not as well solvated and are rather disordered. Thus, shape selectivity will be affected by bonding density to a much greater extent in the methanol–water system; this is exhibited by the larger slope of the phenyl selectivity plot.

Sorption isotherm data[48] indicate that reversed-phase stationary phases become saturated with acetonitrile at fairly low volume fractions of acetonitrile and therefore these stationary phases maintain a relatively constant acetonitrile composition over the entire mobile phase composition range. Stalcup *et al.*[49] noted a relative insensitivity in PAH net retention volumes as a function of mobile phase composition in acetonitrile–water mobile phases. They explained this with a microphase formation model. In this model, non-polar solutes experience an acetonitrile-rich mobile-phase environment and a stationary phase environment that is essentially unaffected by changes in mobile phase composition. In contrast, Stalcup *et al.*[49] observed that PAH retention in methanol–water mobile phase systems increases with increasing mobile phase water content. For methanol–water mobile phases, sorption isotherm data[50] indicate that the methanol concentration in the stationary phase increases slightly with increasing amount of methanol in the mobile phase. The smaller slope of our acetonitrile–water selectivity plot is in agreement with the observations and conclusions of Stalcup *et al.*[49].

Sander and Wise[35] devised a simple, empirical, chromatographic test to gauge the relative monomeric or polymeric nature of a bonded phase. They found that the elution order of a three-component PAH test mixture of PhPh, TBN and BaP at ambient temperature with acetonitrile–water (85:15) is dependent on the type of stationary phase and surface coverage. For monomeric phases (bonding densities up to about 3.2 μmol/m^2), the elution order is BaP $\leqslant$ PhPh $<$ TBN; for oligomeric phases (bonding densities of 3.3 to about 4.2 μmol/m^2) the elution order is PhPh $<$ BaP $<$ TBN. Polymeric phases (bonding density $>$ 4.3 μmol/m^2) give the elution order PhPh $<$ TBN $<$ BaP. Each type of phase also results in a different narrow range of values for TBN–BaP selectivity. By examining the elution order of the compounds in the test mixture, the PAH selectivity of any RP column can be quickly predicted.

The selectivity behavior of the PAH test mixture of Sander and Wise on our monomeric columns, compiled in Table III, further confirms that shape selectivity increases with increasing alkyl bonding density. For bonding densities of 1.74–3.56 μmol/m^2 the TBN–BaP selectivity is about 1.7 and the elution order is BaP = PhPh $<$ TBN. At 3.60 and 4.07 μmol/m^2, the elution order changes to PhPh $<$ BaP $<$ TBN and the TBN–BaP selectivities are 1.56 and 1.63, respectively. The planar BaP molecule is now retained longer than the helical PhPh. Although this was classified as "oligomeric"-type behavior by Sander and Wise[35], this stationary phase was prepared from the monochlorosilane, as opposed to the trichlorosilane reagent used by Sander and Wise to prepare the oligomeric bonded phases. The oligomeric bonded phases are actually polymeric-type phases the bonding density (or "thickness") of which has been controlled by sequential polymerization.

The selectivities for the four-ring PAHs were also correlated with stationary-phase bonding density. The selectivity for every possible pairing of these compounds

TABLE III

TETRABUTYLNAPHTHALENE (TBN)–BENZO[*a*]PYRENE (BaP) SELECTIVITY AS A FUNCTION OF OCTADECYL BONDING DENSITY FOR ACETONITRILE–WATER (85:15) AS THE MOBILE PHASE

C_{18} bonding density ($\mu mol/m^2$)	*TBN–BaP selectivity**	*Stationary phase behavior***
1.74	1.68	Monomeric
1.98	1.68	Monomeric
2.07	1.72	Monomeric
2.09	1.70	Monomeric
2.75	1.73	Monomeric
2.84	1.72	Monomeric
3.06	1.75	Monomeric
3.15	1.73	Monomeric
3.24	1.72	Monomeric
3.34	1.70	Monomeric
3.56	1.69	Monomeric
3.60	1.56	Oligomeric
4.07	1.63	Oligomeric

* Ratio of k'_{TBN} to k'_{BaP}.

** Stationary phase characterization based on the classification system of Sander and Wise[35]. If the elution order is BaP $\leqslant$ PhPh $<$ TBN, the stationary phase is considered to be monomeric; an elution order of PhPh $<$ BaP $<$ TBN is considered to be due to an oligomeric stationary phase.

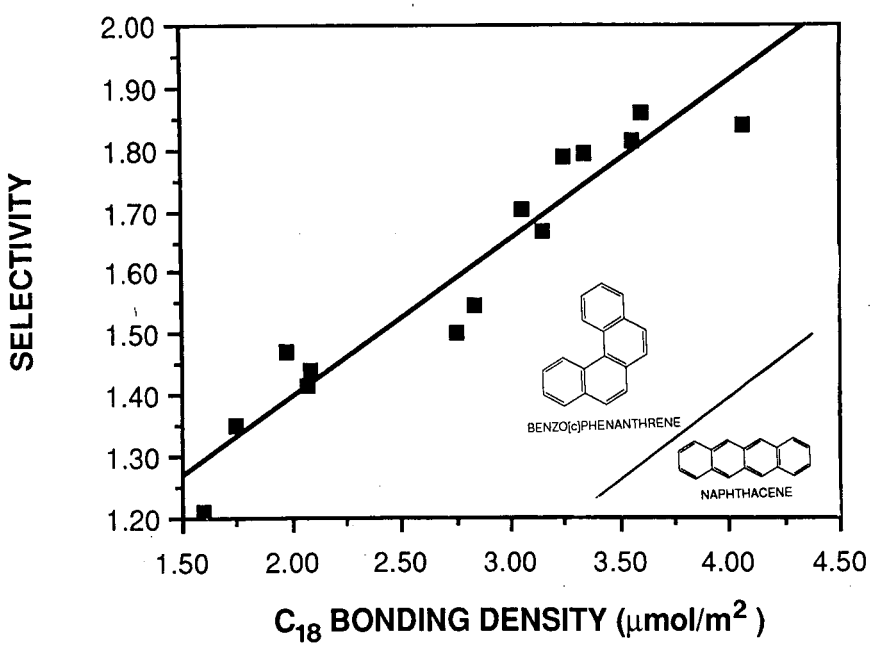

Fig. 7. Benzo[*c*]phenanthrene–naphthacene selectivity *versus* octadecyl bonding density at 35.0°C for acetonitrile–water (85:15) as the mobile phase.

TABLE IV

FOUR-RING PAH SELECTIVITIES AT 35.0°C AS A FUNCTION OF OCTADECYL BONDING DENSITY FOR ACETONITRILE–WATER (85:15) AS THE MOBILE PHASE

Bonding density ($\mu mol/m^2$)	*Benz[a]anthracene–naphthacene*	*Chrysene–naphthacene*	*Benzo[c]phenanthrene–naphthacene*
1.60	1.21	1.16	1.21
1.74	1.37	1.37	1.35
1.98	1.46	1.52	1.47
2.07	1.44	1.41	1.42
2.09	1.44	1.43	1.44
2.75	1.51	1.48	1.50
2.84	1.61	1.58	1.55
3.06	1.76	1.70	1.70
3.15	1.70	1.71	1.67
3.24	1.80	1.81	1.79
3.34	1.89	1.86	1.79
3.56	1.86	1.89	1.81
3.60	1.93	1.92	1.86
4.07	1.92	1.92	1.84

	Benzo[c]phenanthrene–triphenylene	*Triphenylene–pyrene*	*Benz[a]anthracene–chrysene*
1.60	1.02	1.11	1.05
1.74	1.00	1.13	1.00
1.98	1.06	1.14	0.96
2.07	1.03	1.16	1.03
2.09	1.04	1.12	1.01
2.75	1.06	1.13	1.02
2.84	1.06	1.11	1.02
3.06	1.08	1.08	1.03
3.15	1.07	1.10	1.00
3.24	1.11	1.09	1.00
3.34	1.06	1.11	1.01
3.56	1.07	1.11	0.99
3.60	1.08	1.11	1.00
4.07	1.08	1.09	1.00

on each of the monomeric octadecyl columns is compiled in Table IV. Selectivity was also plotted *versus* octadecyl bonding density, as shown for benzo[*c*]phenanthrene and naphthacene in Fig. 7. For most of the pairs, except triphenylene–pyrene and benz[*a*]anthracene–chrysene, a distinct correlation between selectivity and bonding density was observed. This is the same sort of behavior which Wise and co-workers[24,35–37] have reported for polymeric bonded phases. Linear behavior (coefficients of correlation $\geqslant 0.95$) was found for all the PAHs when paired with naphthacene; correlation coefficients $\geqslant 0.80$ were obtained for the benz[*a*]-anthracene–triphenylene, chrysene–triphenylene, benz[*a*]anthracene–pyrene and benzo[*c*]phenanthrene–triphenylene solute pairs. Except for naphthacene, in all

Triphenylene–naphthacene	*Pyrene–naphthacene*	*Benz[a]anthracene–triphenylene*	*Chrysene–triphenylene*	*Benz[a]anthracene–pyrene*
1.19	1.07	1.02	0.97	1.13
1.35	1.19	1.01	1.01	1.15
1.39	1.22	1.05	1.09	1.20
1.38	1.19	1.05	1.02	1.21
1.38	1.23	1.04	1.03	1.17
1.42	1.26	1.06	1.04	1.20
1.47	1.32	1.10	1.07	1.22
1.58	1.46	1.12	1.08	1.21
1.56	1.42	1.09	1.09	1.19
1.61	1.48	1.12	1.13	1.22
1.70	1.53	1.11	1.10	1.24
1.69	1.53	1.10	1.11	1.22
1.73	1.56	1.12	1.11	1.24
1.70	1.57	1.13	1.13	1.23

Benz[a]anthracene–benzo[c]phenanthrene	*Chrysene–benzo[c]phenanthrene*	*Chrysene–pyrene*	*Benzo[c]phenanthrene–pyrene*
1.00	0.95	1.08	1.13
1.01	1.01	1.15	1.13
0.99	1.03	1.25	1.20
1.02	0.99	1.18	1.19
1.00	0.99	1.16	1.17
1.00	0.98	1.18	1.20
1.04	1.02	1.19	1.17
1.03	1.00	1.17	1.17
1.02	1.02	1.20	1.17
1.01	1.01	1.23	1.21
1.05	1.04	1.22	1.17
1.03	1.04	1.24	1.19
1.04	1.03	1.23	1.19
1.04	1.04	1.22	1.18

instances in which a positive correlation between selectivity and bonding density was observed, the solute elution order corresponded with increasing length to breadth ratio (L/B), again concurring with the results of Wise and co-workers[35,37]. For the naphthacene solute the converse is true. For triphenylene–pyrene a negative correlation between selectivity and bonding density is exhibited and the solute elution order corresponds with decreasing L/B. Benz[*a*]anthracene and chrysene are poorly resolved and have a selectivity ratio of *ca.* 1 in every instance; this is not surprising, as this separation is notoriously difficult[37].

The fact that our monomeric phases exhibit the same PAH selectivity as the lower density polymeric phases of Sander and Wise is strong evidence that PAH and/or

shape selectivities are not a function of the degree of stationary phase polymerization or thickness but rather are a function of alkyl chain ordering. The trends in the observed enthalpic and relative entropic contributions to retention as a function of mobile phase composition reported by Stalcup *et al.*[49] also support this conclusion. Carbon-13 NMR studies of reversed-phase packings[51–53] are indicative that there is an increasing amount of bonded chain interaction with increasing alkyl surface density. The correlation of phenyl selectivity with alkyl bonding density further supports this conclusion. The overall results of our selectivity studies lend further credence to Dill's molecular mechanism of RPLC retention[41,42] and again indicate that partitioning is the dominant mode of RPLC retention for small, hydrophobic molecules.

CONCLUSIONS

Our studies significantly further our understanding of retention and selectivity processes in reversed-phase liquid chromatography. It is now clear that selectivity differences among different commercial columns are due not only to differences in the starting silica material, but also to differences in the chain density of the bonded alkyl phase. It is further clear that higher chain densities should lead to improved chromatographic selectivity, providing impetus for further studies of bonding reactions that can produce such high-density phases. It is also possible that this better understanding of solute selectivity will lead us closer to the development of a useful liquid chromatographic retention index system.

ACKNOWLEDGEMENTS

The authors gratefully acknowledge many helpful discussions with Ken A. Dill and thank Lane C. Sander for providing samples of the NBS Column Evaluation Test Mixture. Support of this work by NIH GM33382 and support for K.B.S. from an ACS Analytical Division fellowship, sponsored by the Procter and Gamble Company, are also gratefully acknowledged.

REFERENCES

1 C. H. Lochmuller, M. L. Hunnicut and J. F. Mullaney, *J. Phys. Chem.*, 89 (1985) 5770.
2 H. Colin, A. M. Krstulovic, M.-F. Gonnord, G. Guiochon, Z. Yun and P. Jandera, *Chromatographia*, 17 (1983) 9.
3 W. R. Melander and Cs. Horváth, *Chromatographia*, 15 (1982) 86.
4 H. J. Isaaq, *J. Liq. Chromatogr.*, 4 (1981) 1917.
5 H. Engelhardt and G. Ahr, *Chromatographia*, 14 (1981) 227.
6 A. M. Krstulovic, H. Colin, A. Tchapla and G. Guiochon, *Chromatographia*, 17 (1983) 228.
7 H. Colin, G. Guiochon, Z. Yun, J. C. Diez-Masa and J. Jandera, *J. Chromatogr. Sci.*, 21 (1983) 179.
8 K. Jinno and K. Kawasaki, *Chromatographia*, 18 (1984) 103.
9 K. Jinno and K. Kawasaki, *Chromatographia*, 18 (1984) 499.
10 H. Hemetsberger, M. Kellermann and H. Ricken, *Chromatographia*, 10 (1977) 726.
11 J. J. Lewis, L. B. Rogers and R. E. Pauls, *J. Chromatogr.*, 299 (1984) 331.
12 M. C. Hennion, C. Picard and M. Caude, *J. Chromatogr.*, 166 (1978) 21.
13 C. H. Lochmuller and D. R. Wilder, *J. Chromatogr. Sci.*, 17 (1979) 574.
14 L. C. Sander and S. A. Wise, *Anal. Chem.*, 59 (1987) 2309.
15 N. Tanaka, K. Sakagami and M. Araki, *J. Chromatogr.*, 199 (1980) 327.

16 A. Tchapla, H. Colin and G. Guiochon, *Anal. Chem.*, 56 (1984) 621.
17 B. Shaikh and J. E. Tomaszewski, *Chromatographia*, 17 (1983) 675.
18 A. L. Colsmjo and M. W. Ericsson, *J. Liq. Chromatogr.*, 9 (1986) 2825.
19 P. Spacek, M. Kubin, S. Vozka and B. Porsch, *J. Liq. Chromatogr.*, 3 (1980) 1465.
20 A. P. Goldberg, *Anal. Chem.*, 54 (1982) 342.
21 R. P. W. Scott and P. Kucera, *J. Chromatogr.*, 142 (1977) 213.
22 K. K. Unger, N. Becker and P. Roumeliotis, *J. Chromatogr.*, 125 (1976) 115.
23 N. Tanaka, H. Goodell and B. L. Karger, *J. Chromatogr.*, 158 (1978) 233.
24 L. C. Sander and S. A. Wise, *J. Chromatogr.*, 316 (1984) 163.
25 S. M. Staroverov, A. A. Serdan and G. V. Lisichkin, *J. Chromatogr.*, 364 (1986) 377.
26 P. J. van den Driest and H. J. Ritchie, *Chromatographia*, 24 (1987) 324.
27 P. E. Antle and L. R. Snyder, *LC, Liq. Chromatogr. HPLC Mag.*, 2 (1984) 840.
28 P. E. Antle, A. P. Goldberg and L. R. Snyder, *J. Chromatogr.*, 321 (1985) 1.
29 P. Jandera, *J. Chromatogr.*, 352 (1986) 91.
30 M. F. Delaney, A. N. Papas and M. J. Walters, *J. Chromatogr.*, 410 (1987) 31.
31 J. R. Chrétien, B. Walczak, L. Morin-Allory, M. Dreux and M. Lafosse, *J. Chromatogr.*, 371 (1986) 253.
32 K. Jinno, T. Nagoshi, N. Tanaka, M. Okamoto, J. C. Fetzer and W. R. Biggs, *J. Chromatogr.*, 392 (1987) 75.
33 N. Tanaka, Y. Tokuda, K. Iwaguchi and M. Araki, *J. Chromatogr.*, 239 (1982) 761.
34 H. Hemetsberger, P. Behrensmeyer, J. Henning and H. Ricken, *Chromatographia*, 12 (1979) 71.
35 L. C. Sander and S. A. Wise, *Anal. Chem.*, 56 (1984) 504.
36 S. A. Wise and L. C. Sander, *J. High Resolut. Chromatogr. Chromatogr. Commun.*, 8 (1985) 248.
37 S. A. Wise and W. E. May, *Anal. Chem.*, 55 (1983) 1479.
38 S. A. Wise, W. J. Bonnett, F. R. Guenther and W. E. May, *J. Chromatogr. Sci.*, 19 (1981) 457.
39 P. J. van den Driest, H. J. Ritchie and S. Rose, *LC · GC, Liq. Chromatogr. Gas Chromatogr. Mag.*, 6 (1988) 124.
40 D. E. Martire and R. E. Boehm, *J. Phys. Chem.*, 87 (1983) 1045.
41 K. A. Dill, *J. Phys. Chem.*, 91 (1987) 1980.
42 K. A. Dill, J. Naghizadeh and J. A. Marqusee, *Annu. Rev. Phys. Chem.*, 39 (1988) 425.
43 J. G. Dorsey and K. A. Dill, *Chem. Rev.*, (1989) in press.
44 P. T. Ying, J. G. Dorsey and K. A. Dill, *Anal. Chem.*, submitted for publication.
45 K. B. Sentell and J. G. Dorsey, *Anal. Chem.*, submitted for publication.
46 K. B. Sentell, K. W. Barnes and J. G. Dorsey, *J. Chromatogr.*, 455 (1988) 95.
47 B. L. Karger, J. R. Gant, A. Hartkopf and P. H. Weiner, *J. Chromatogr.*, 128 (1976) 65.
48 P. L. Zhu, *Chromatographia*, 21 (1986) 229.
49 A. M. Stalcup, D. E. Martire and S. A. Wise, *J. Chromatogr.*, 442 (1988) 1.
50 R. P. W. Scott and C. F. Simpson, *Faraday Symp. Chem. Soc.*, 15 (1980) 69.
51 R. K. Gilpin and M. E. Gangoda, *Anal. Chem.*, 56 (1984) 1470.
52 P. Shah, L. B. Rogers and J. C. Fetzer, *J. Chromatogr.*, 388 (1987) 411.
53 E. Bayer, A. Paulus, B. Peters, G. Laupp, J. Reiners and K. Albert, *J. Chromatogr.*, 364 (1986) 25.

Journal of Chromatography, 461 (1989) 209–227
Elsevier Science Publishers B.V., Amsterdam — Printed in The Netherlands

CHROMSYMP. 1478

RETENTION BEHAVIOUR OF LARGE POLYCYCLIC AROMATIC HYDROCARBONS IN REVERSED-PHASE LIQUID CHROMATOGRAPHY ON A POLYMERIC OCTADECYLSILICA STATIONARY PHASE

K. JINNO* and T. IBUKI
School of Materials Science, Toyohashi University of Technology, Toyohashi 440 (Japan)
N. TANAKA
Kyoto Institute of Technology, Kyoto 606 (Japan)
M. OKAMOTO
Gifu Prefectural Tajimi Hospital, Tajimi 506 (Japan)
J. C. FETZER and W. R. BIGGS
Chevron Research Company, Richmond, CA 94501 (U.S.A.)
and
P. R. GRIFFITHS and J. M. OLINGER
Department of Chemistry, University of California, Riverside, CA 92521 (U.S.A.)

SUMMARY

Fourier transform infrared spectroscopy, nuclear magnetic resonance spectroscopy and differential scanning calorimetry experiments were performed in order to study the retention mechanism in reversed-phase liquid chromatography for large polycyclic aromatic hydrocarbons. The effects of changing the mobile phase composition and column temperature were evaluated. The results suggest that a change in mobile phase composition from pure methanol to pure dichloromethane induces further non-planarity in non-planar solutes and also slightly changes the conformation of a polymeric octadecyl stationary phase. Conversely, a change to higher column temperatures drastically changes the structure of the stationary phase from solid-like to liquid-like, with only a small change of non-planar solutes to more non-planar conformations.

INTRODUCTION

The influence of the size and shape of polycyclic aromatic hydrocarbons (PAHs) on their retention in reversed-phase liquid chromatography (RPLC) has been widely investigated[1–10] because the compounds have mutagenic and carcinogenic activity. This makes it important to determine their levels in the environment. For PAHs containing less than six rings, it is clear that retention in RPLC is controlled by their size and two-dimensional shape. With certain stationary phases in non-aqueous RPLC[9,10], in contrast, some large PAHs, such as the peropyrene-type PAHs, show anomalous elution behavior apparently not controlled simply by the size and shape of

0021-9673/89/$03.50

the molecule. Non-planar solutes that are larger in size than smaller, planar solutes are eluted earlier with higher concentrations of dichloromethane in the mobile phase on particular chemically bonded stationary phases. In systematic studies to investigate this point we found that the elution behavior of large PAHs appears to be controlled by two main factors: (1) the orderliness of the chemically bonded stationary phases and (2) the degree of solute planarity. With a polymeric, derivatized octadecylsilica (P-ODS) as the stationary phase rather than a monomerically derivatized octadecylsilica, the tendency to recognize the molecular planarity of PAHs has been found to increase[11,12]. Wise and Sander[13] have concluded that the structure of P-ODS is more rigid and slit-like (the "slot model") than that of monomeric ODS. Thus, P-ODS cannot retain or interact well with non-planar PAHs because of its slit-like structure, while planar solutes can be retained more strongly, because they more easily enter the slits. The results of our experiments also indicate that P-ODS is preferable to various bonded phases[11,14,15] for retaining planar PAHs. If the column temperature is lower than 45°C or if there is an high dichloromethane concentration (in methanol), the recognition ability for molecular planarity increases. As an explanation of these results, we have proposed a mechanism in which the temperature and mobile-phase composition induce a structural change in P-ODS. However, a more detailed description of the mechanism was impossible because direct confirmatory evidence was lacking.

A number of attempts to understand the function of the stationary phase in RPLC have been reported in which spectroscopic techniques were used, such as nuclear magnetic resonance (NMR) spectrometry[16–24], Fourier-transform infrared spectrometry (FT-IR)[25,26] and thermal analysis[27]. However, those reports concerned mainly characteristics including conformational studies of the starting silane materials and stationary phases other than octadecyl chains and sometimes no distinction was made between monomeric and polymeric ODS phases. A deficiency of those publications is also that they do not relate these data to chromatographic retention data obtained with the stationary phases. Greater understanding of RPLC retention mechanisms will come from the interpretation of chromatographic data related to the characteristics of stationary phases examined by supplemental spectroscopic techniques.

In this paper, as an extension of our previous work, the retention mechanism for large PAHs in non-aqueous RPLC with P-ODS has been investigated by spectroscopic techniques in addition to chromatographic techniques to explain the anomalous chromatographic retention behaviour observed for some PAHs in previous studies.

EXPERIMENTAL

A micro-LC system comprised of an MF-2 microfeeder (Azuma Electric, Tokyo, Japan) and an Uvidec-100-III detector (Jasco, Tokyo, Japan) was used. A microloop injector 7619 (Rheodyne, Cotati, CA, U.S.A.) was used for sample introduction. The column was a fused-silica capillary (30 cm × 0.53 mm I.D.) packed with Vydac 201 TPB5 P-ODS (Separations Group, Hesperia, CA, U.S.A.) which from our earlier work appears to be made from a trifunctional silane[15].

The peropyrene-type PAHs used as sample probes (Fig. 1), were synthesized by procedures described elsewhere[9,10]. Their purity was checked by HPLC with

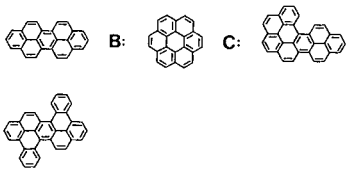

Fig. 1. Structures of peropyrene-type PAHs used in this work. A = Dibenz[*cd,lm*]perylene; B = coronene; C = benzo[*lm*]phenanthro[4,5,6-*abcd*]perylene; D = tetrabenzo[*a,cd,j,m*]perylene.

monitoring of their UV spectra using a Jasco MULTI-320 photodiode array detector, and by comparison with literature spectra[28,29]. The mobile phases were mixtures of methanol and dichloromethane or methanol and chloroform. The flow-rate was typically 4 μl/min.

Diffuse-reflectance infrared spectra were obtained on a FTS-20 instrument (Digilab, MA, U.S.A.) equipped with a temperature controller. The Vydac material was analyzed as 10% dilutions in potassium chloride which had been ground for 5 min. The depth of the sample was approximately 2.3–2.4 mm. The sample was packed by careful mounting inside the sample cup and then pressed with a flat object to pack it down. A Nichrome wire, wrapped around the detection cell, was used to increase the temperature by applying a direct current of varying voltage. Spectra were obtained at room temperature (*ca.* 20°C), as well as at 30, 40, 45, 50 and 60°C. The sample was held at the selected temperature for approximately 3 min before starting spectral collection. Spectra were the ensemble average of 256 scans taken at a resolution of 4 cm^{-1}. An MCT (mercury–cadmium–telluride) detector was used. Boxcar apodization was applied to the interferograms. Once obtained, the single-beam spectrum (between 4000 and 1000 cm^{-1}) of the sample was ratioed to the single-beam spectrum of potassium chloride at the same temperature. These reflectance data were transferred for treatment by SpectraCalc software (Galactic, Nashua, NH, U.S.A.). Once in SpectraCalc, the spectra were baseline-corrected, using either a two-point or a four-point baseline correction in the C–H stretching region. The Kubelka-Munk spectrum was then calculated from the baseline-corrected portion (between 3400 and 2600 cm^{-1}). SpectraCalc was performed on a IBM-AT-compatible computer.

The high-resolution ^{13}C NMR spectra of the suspensions of P-ODS and mobile-phase solvents, and the ^{1}H NMR spectra of coronene and tetrabenzo-[*a,cd,j,lm*]perylene, dissolved in the mobile phase solvents, were recorded with a JNM-GX270 FT-NMR spectrometer (JEOL, Tokyo, Japan). The spectra were obtained at two different temperatures, 27 and 50°C. For ^{13}C NMR, the experiments were conducted on 0.2 g of P-ODS, which was weighed directly into a 10-mm NMR tube and about 5–6 ml of the desired mixture of solvents ([^{2}H]methanol–[^{2}H]-dichloromethane or [^{2}H]methanol–[^{2}H]chloroform) were added[30]. The tube was hand-shaken until proper mixing was obtained. A ^{13}C NMR spectrum of this suspension was recorded as described in ref. 30. For the ^{1}H NMR spectra, the samples were dissolved in mixtures of [^{2}H]methanol, [^{2}H]dichloromethane and [^{2}H]-chloroform. The cross-polarization magic-angle solid-state (CP-MAS) ^{13}C NMR spectra of Vydac material were obtained with the same NMR spectrometer. The experimental conditions are as follows: observation frequency, 5600 Hz; observation

point, 8192; frequency width, 27 027 Hz; scans, 5000; acquisition time, 0.038 s; pulse delay, 6 s; pulse width, 4.5 μs; irradiation frequency, 5400 Hz; standard shift, 29.5 ppm for adamantane; broadening factor, 3.00 Hz; receiver gain, 23–26; measurements at room temperature, 30, 40, 45 and 50°C.

Thermal analysis (differential scanning calorimetry, DSC) was performed with a SSC-5000 and DSC-200 thermal analyzer (Seiko Denshi, Tokyo, Japan). The measurement range was between 20 and 200°C, and the temperature programming rate was 10°C/min.

Although the stationary phase is in the presence of mobile phase during chromatography, for convenience and because of difficult technical problems, DSC and FT-IR measurements were carried out in the dry state.

Molecular structure graphics were generated by using a MV6000 System II computer (Data General, Tokyo, Japan), loaded with TUTORS[31] software which has been developed in the Chemometrics Center of Toyohashi University of Technology.

RESULTS AND DISCUSSION

Elution order change with changing mobile phase composition

The chromatographic elution orders of peropyrene-type PAHs with different mobile phase compositions were reported in our previous paper[14] but were measured again with P-ODS. The results are illustrated in Fig. 2. The mobile phase compositions ranged between 20 and 50% dichloromethane in methanol. The typical behavior shown in Fig. 2 can be interpreted to mean that the elution order of large PAHs mainly depends upon their sizes and planarity. In contrast, it has been confirmed for small PAHs that their retention is generally controlled by their sizes and shapes[8,11]. In the current work, tetrabenzo[*a,cd,j,lm*]perylene (nine rings) is always eluted earlier than dibenzo[*cd,lm*]perylene (seven rings). At higher dichloromethane concentrations the solute was eluted even earlier than coronene, the smallest molecule used in this work. This is due to the non-planarity of tetrabenzo[*a,cd,j,lm*]perylene. The non-polarity of tetrabenzo[*a,cd,j,lm*]perylene in the solid state has been confirmed by a computerized molecular display technique based on the crystal structure data obtained by X-ray

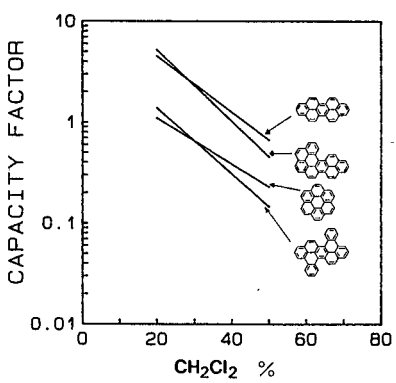

Fig. 2. Plots of log *k'* of four peropyrene-type PAHs *vs.* dichloromethane concentration in methanol as the mobile phase.

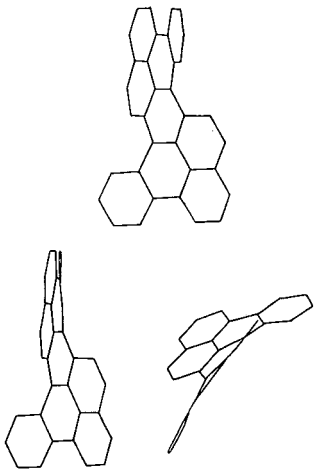

Fig. 3. Three-dimensional structure of tetrabenzo[*a,cd,j,lm*]perylene drawn by computer graphics.

diffraction[32]. The structure is shown in Fig. 3, where the distortion of this molecule appears to be very large. The contribution of dichloromethane to this exclusion-like retention behavior of the non-planar PAHs may be caused by the facts that, with changing mobile-phase composition, the structure of P-ODS is changing or the solute planarity is changing or both.

In order to determine which factor is dominant in non-aqueous RPLC, NMR measurements were performed. In Fig. 4, ^{13}C NMR spectra of P-ODS, suspended in

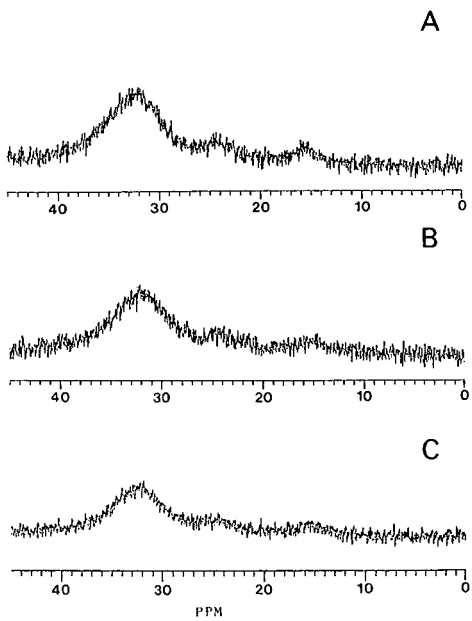

Fig. 4. ^{13}C NMR spectra of Vydac 201 TPB5 in various solvents: (A) 100% [$^2H_2$]dichloromethane; (B) [$^2H_2$]dichloromethane–[$^2H_4$]methanol (50:50); (C) 100% [$^2H_4$]methanol.

different compositions of [^{2}H]methanol–[^{2}H]dichloromethane, are shown. It has been proposed by Yonker *et al.*[33] and McNally and Rogers[34] that the width at half-height of the bulk $-CH_2$ peaks at 33 ppm[30] can be used as a measure of the liquid-like nature of the bonded alkyl chains. Wider peaks are a result of less freedom of movement due to interactions of the bonded-phase chain with the surface, including other bonded-phase chains and unreacted silanols. As seen in Fig. 4, only small changes occur with increasing dichloromethane concentration. It appears that, as the solvent is changed from pure methanol to pure dichloromethane, the peak width and intensity increase for the peak at 33 ppm as well as for the peaks at 24 ppm (assigned to β-CH_2) and 15 ppm (assigned to terminal methyl groups[30]). These small changes might mean there is a solvent effect on this P-ODS. The work of Shah *et al.*[30] indicates that in 100% dichloromethane the difunctional polymeric octadecyl alkyl chain is moving relatively freely and interacts with the solvent. Although Fig. 4 does not show this clearly, it is reasonable to consider that, as the percentage of methanol increases, the molecular motion of the bonded-alkyl chain becomes more restricted, but not so much as was observed for a difunctional polymeric phase by Shah *et al.*[30].

As solute structure changes seem to be more reasonable in the sense of solution chemistry, ^{1}H NMR spectra were collected for representative solutes, coronene (as a planar PAH) and tetrabenzo[*a,cd,j,lm*]perylene (as a non-planar PAH), at three different [^{2}H]dichloromethane concentrations (20, 50 and 100% in [^{2}H]methanol). The results are shown in Fig. 5. The signals of tetrabenzo[*a,cd,j,lm*]perylene at 9.2 ppm were drastically shifted to higher magnetic field when the dichloromethane concentration in the mobile phase was increased from 20 to 50%. No difference in spectra was observed between 50 and 100% dichloromethane. The signals at 9.2 ppm with 20% dichloromethane showed four lines, but with 50 and 100% only two lines remained and two lines were shifted to higher field. The signals at 9.2 ppm can be assigned to two protons in the A-region of the molecular structure shown in Fig. 5. The shift of the signals to 9.05 ppm might mean that the environment of the protons has changed to be similar to those in the B-region in the structure. In contrast, the signal of coronene at 8.95 ppm did not show any shift with changing solvent composition. It is possible that tetrabenzo[*a,cd,j,lm*]perylene becomes more non-planar with increasing dichloromethane concentration. Evidence in support of this is provided by the UV spectrometric studies of Fetzer and Biggs[10]. This planarity change is the main cause of the anomalous chromatographic retention behavior. The structure change of the stationary phase seems to be a second factor contributing to the phenomena. Because the signal change in the NMR measurements in the molecular planarity study is more drastic than that observed for the stationary phase when the mobile phase compositions are changed, solute-planarity changes dominate the elution behaviour.

Elution behaviour with changing column temperature

Our previous paper[15] showed that the column temperature is an important factor in controlling the retention of large PAHs. Lower temperatures are preferable for planarity recognition. We also indicated that thermal analysis data (DSC) can be used to find out whether the structure change of P-ODS with changing temperature causes the improved recognition ability between planar and non-planar PAHs. In this work, we give more information in support of this conclusion.

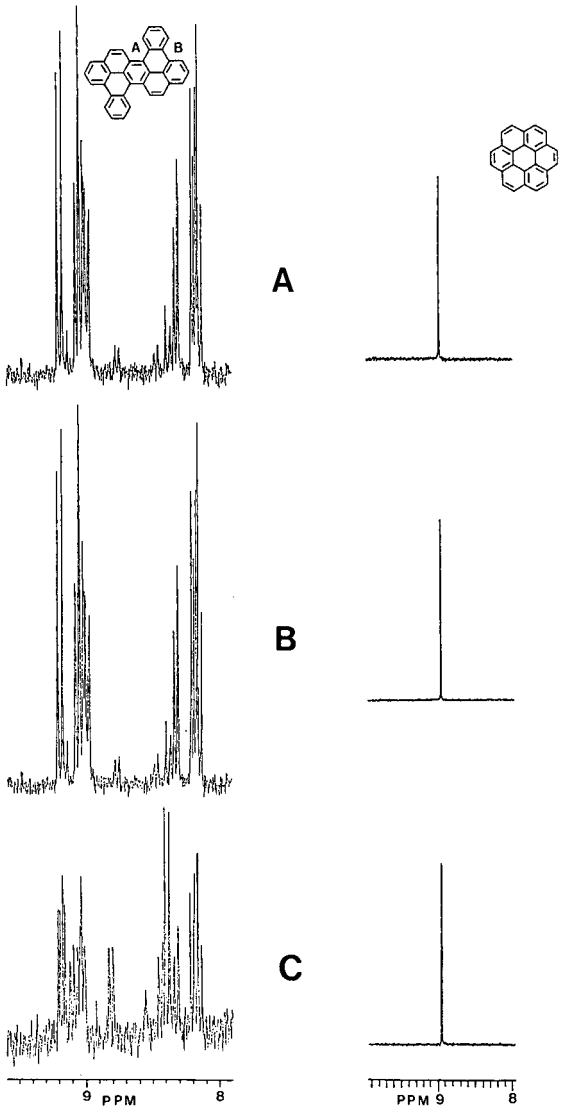

Fig. 5. ^{1}H NMR spectra of tetrabenzo[*a,cd,j,lm*]perylene and coronene in various solvents: (A) and (B) as in Fig. 4; (C) [$^{2}H_2$]dichloromethane–[$^{2}H_4$]methanol (20:80).

In Fig. 6, the DSC chart of P-ODS[15] is shown. The data clearly indicate that P-ODS undergoes a drastic change around 45°C, above the melting point of octadecane (29–30°C). Monomeric ODS (laboratory-made) has a weak transition at 35°C, as determined by similar DSC measurements. The DSC results indicate that a transition of P-ODS occurred at about 45°C and this may be caused by a phase transition from a solid-like to a liquid-like structure. The retention data for PAHs at various column temperatures also show large changes in behavior at about 45°C. Fig. 7 shows the Van 't Hoff plots for two planar and non-planar PAHs in the solvent

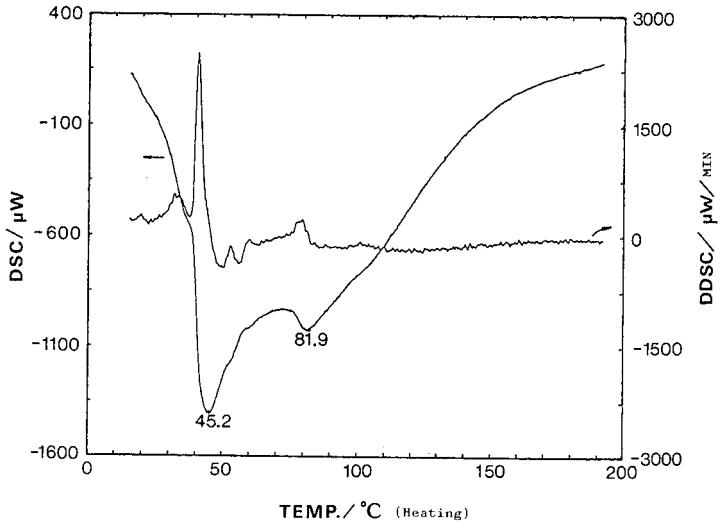

Fig. 6. DSC chart of Vydac 201 TPB5[15]. DDSC = Differential of DSC curve.

methanol–chloroform (50:50). The plots should be linear for a normal chromatographic process if the retention mechanism is constant. However, in this case, two linear relationships were found between $\log k'$ and $1/T$ (where k' = capacity factor and T = temperature), and the critical points in the Figure are at about 45°C. This indicates that the transition found in the DSC measurements causes this anomalous retention behavior of the large PAHs. The retention ratio, *i.e.*, separation factor of coronene and tetrabenzo[*a,cd,j,lm*]perylene was calculated for each column temperature and plotted as shown in Fig. 8. Planarity recognition between coronene and tetrabenzo[*a,cd,j,lm*]perylene changed with column temperature because the ratio is smaller, and increasing temperature decreased recognition ability. The critical point again seems to be between 40 and 50°C. Similar observations were reported in our previous paper[15], where different PAHs were used as the sample probes. The data shown above suggest that a critical point exists between 40 and 50°C, and this may be

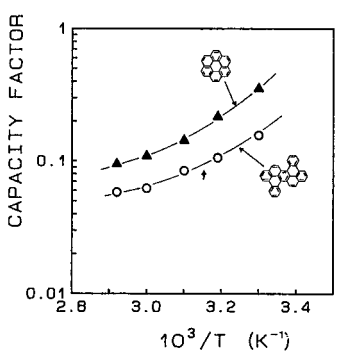

Fig. 7. Van 't Hoff plots for coronene and tetrabenzo[*a,cd,j,lm*]perylene with methanol–chloroform (50:50) as the mobile phase. The arrow indicates the critical point.

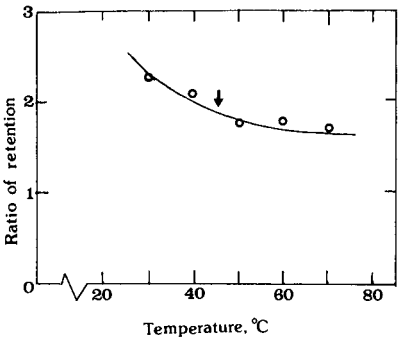

Fig. 8. Retention ratio of coronene and tetrabenzo[*a,cd,j,lm*]perylene *vs.* temperature. The arrow indicates the critical point.

explained by the existence of phase transitions of the P-ODS between these temperatures.

In order to estimate the characteristics of the transition of P-ODS at 45°C, several spectroscopic investigations were performed. First, FT-IR spectra of the stationary phase itself were collected, using the diffuse-reflectance spectroscopic technique. The spectra obtained (Fig. 9) showed an obvious change with temperature, a shift of 2 cm^{-1} in the band at 2850 cm^{-1}. Fig. 10C shows the center of gravity at the band at 2850 cm^{-1} plotted *versus* the temperature. This plot can be considered to be

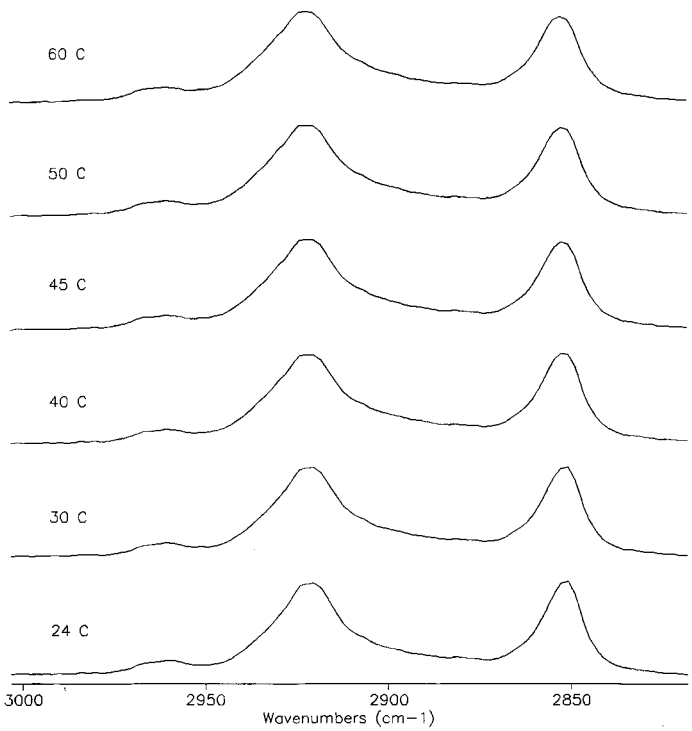

Fig. 9. Diffuse-reflectance infrared spectra of Vydac 201 TPB5 at various temperatures.

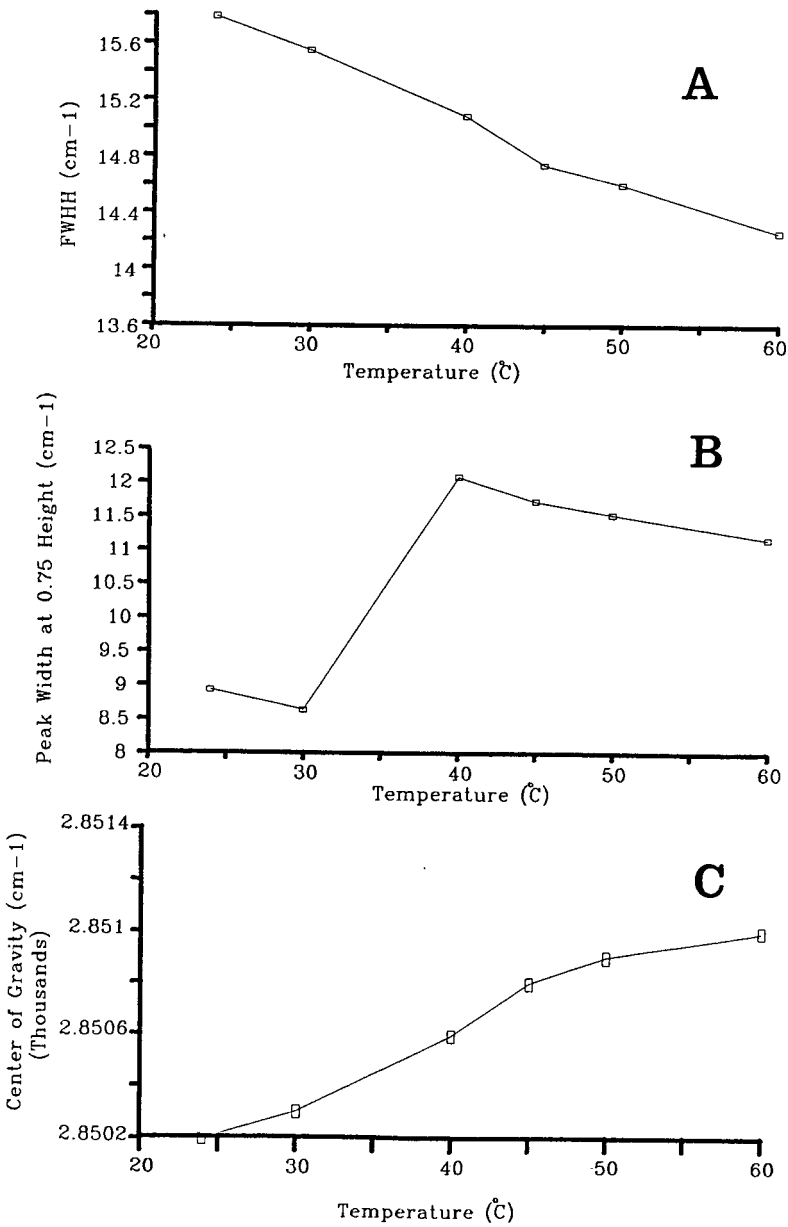

Fig. 10. Interpretation of FT-IR spectra of Vydac 201TPB5. (A) FWHH *vs.* temperature; (B) peak width at 0.75 height *vs.* temperature; (C) center of gravity *vs.* temperature.

sigmoidal, centered near 45°C. Then we tried to determine the full width of the peak. Fig. 10A shows the full width at half-height *versus* temperature. This is unusual, because the band width usually increases with temperature if the absorption is due to a single structural functionality. It is reasonable to rationalize this result in terms of

two highly overlapped bands, separated by less than the full width at half-height (FWHH). The band at higher wavenumber would correspond to the more liquid-like region and that at lower wavenumber to the more solid-like region as reported for alkanes by Casal *et al.*[35]. If this type of behaviour actually describes what is happening in practice, one might expect the width at, for example, 75% height to be more likely to show temperature effects. As shown in Fig. 10B, a distinct break was found between 30 and 45°C. Therefore, it is concluded that IR spectrometric information appears to indicate some transitional structure change with increasing temperature up to 50°C. This corresponds well with the thermal transition (around 45°C) observed by DSC. Therefore, one may conclude that at 45°C some transition occurs in the CH_2 chains of the octadecyl groups.

NMR measurements gave a clearer interpretation of the transition of P-ODS. They were performed in the solid state, because CP-MAS-NMR should be more useful in understanding the conformational change of CH_2 chains. The NMR spectra are shown in Fig. 11A and B for room temperature and 50°C, respectively. Three distinct peaks are seen at 12, 22 ppm and 30 ppm (the strongest). The assignments of these signals are roughly as follows

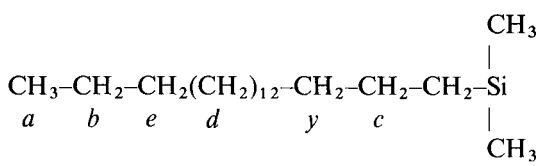

where $a = 12$ ppm, $b = 21.5$ ppm, $c = 22$ ppm, d, e and $y = 30$–33 ppm[30]. The absence of signals at 0 ppm indicates that this bonded phase is of the polymeric type, and the absence of signals at 18 and 34 ppm indicates the rigid location of this carbon chain. The details of the NMR spectral changes with temperature are summarized in Fig. 12. The most drastic change is seen at 30 ppm for the bulk $-CH_2$ signal. At room temperature, the peak has two maxima, but with increasing temperature they merge, and above 45°C the maxima at 32 ppm disappear and become a shoulder. This tendency is much clearer in Fig. 13, where the peak deconvolution procedure has been applied to three different spectra at room temperature (A), 40°C (B) and 50°C (C), respectively. The numerical data are summarized in Table I. The peak at 32 ppm shifted toward 30.8 ppm with increasing temperature. This situation is reminiscent of the case of monomeric and low-loaded polymeric ODS phases. The NMR spectrum at 50°C is very similar to that of Vydac 218 TP5 reported by Shah *et al.*[30]. Vydac 218 is a low-loaded polymeric phase and the distance between alkyl chains on the surface may be larger than that of Vydac 201. From the NMR spectra, which indicate the existence of different types of $-CH_2$ chains in the bulk, one can assume that the polymeric alkyl chain at room temperature exhibits the ordered phase suggested by Sander *et al.*[25] or "fold" like structure[16] and with increasing column temperature it becomes disordered, adopting various conformations and becoming freely mobile. Therefore, the NMR signal at 30 ppm becomes unified and similar to those of monomeric and low-loaded polymeric phases. Further studies are required in comparison with other types of ODS phases such as monomeric ones or monomeric phases with endcapping. However, the CP-MAS data suggest that the transition

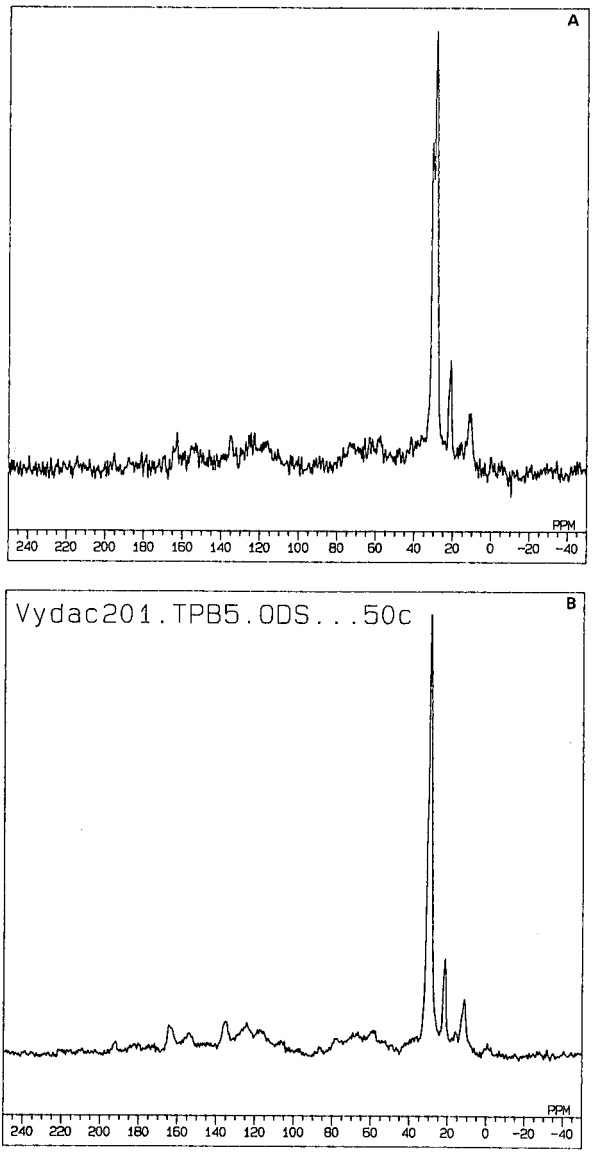

Fig. 11. CP-MAS-^{13}C NMR spectra of Vydac 201 TPB5 at room temperature (A) and 50°C (B).

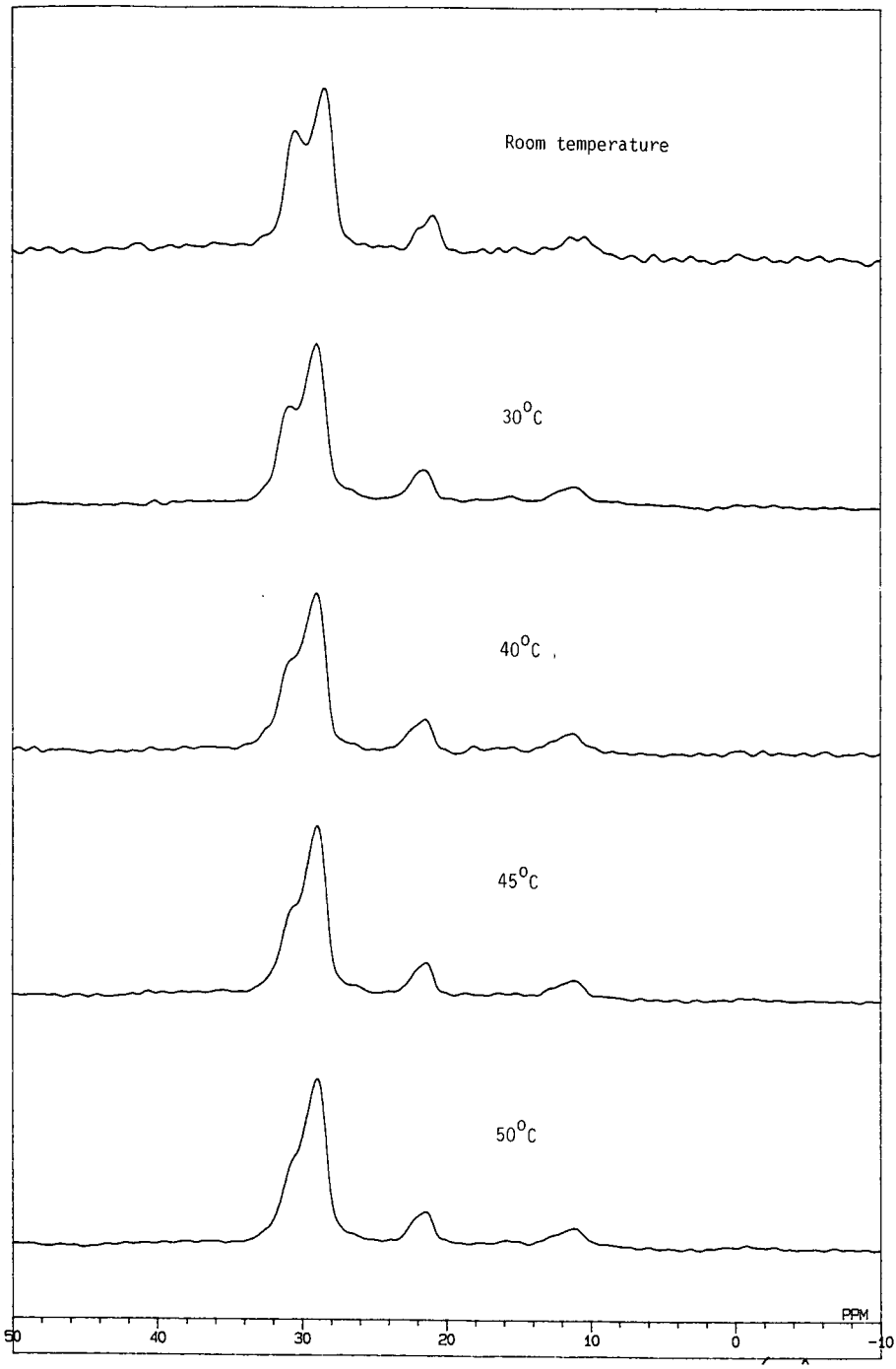

Fig. 12. CP-MAS-^{13}C NMR spectra of Vydac 201 TPB5 at various temperatures.

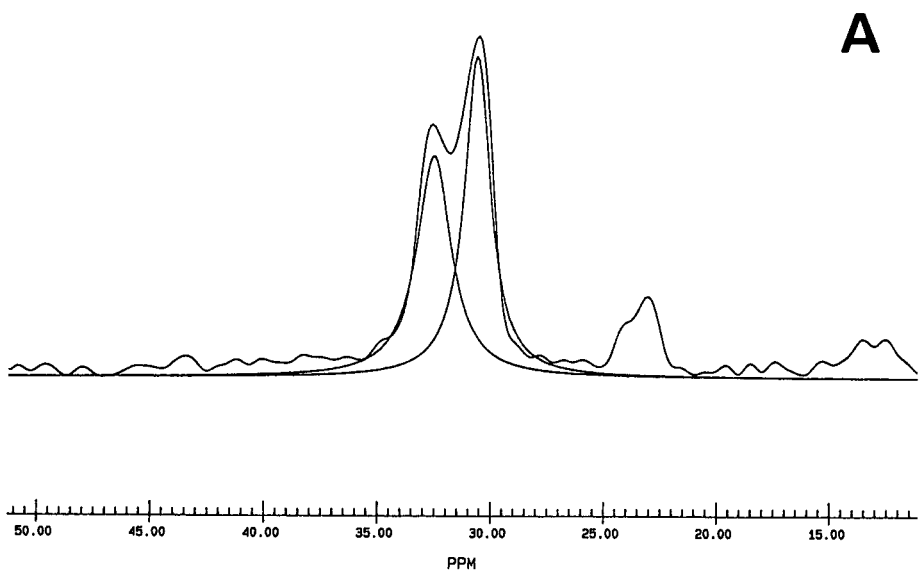
A
50.00
45.00
40.00
35.00
30.00
25.00
20.00
15.00
PPM

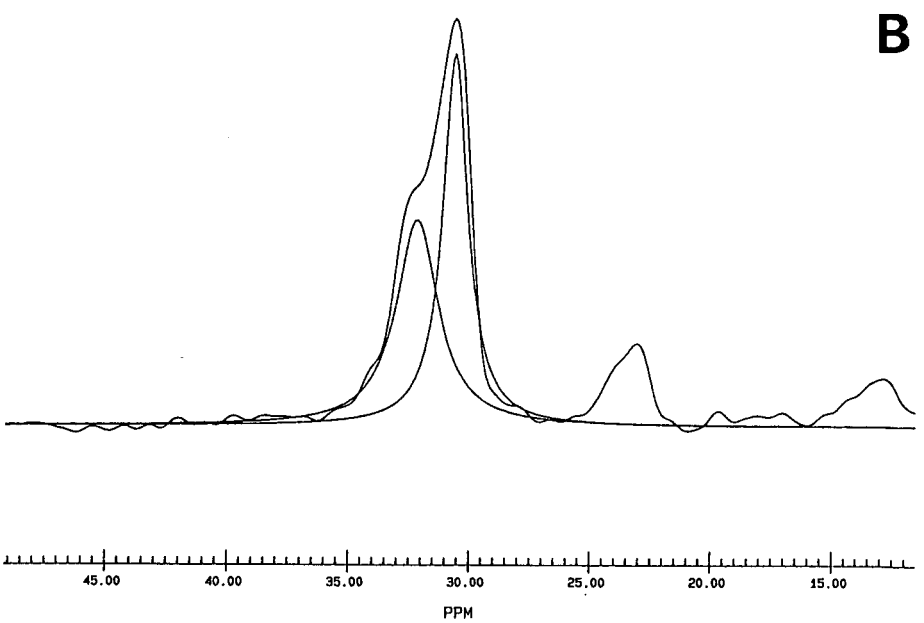
B
45.00
40.00
35.00
30.00
25.00
20.00
15.00
PPM

Fig. 13.

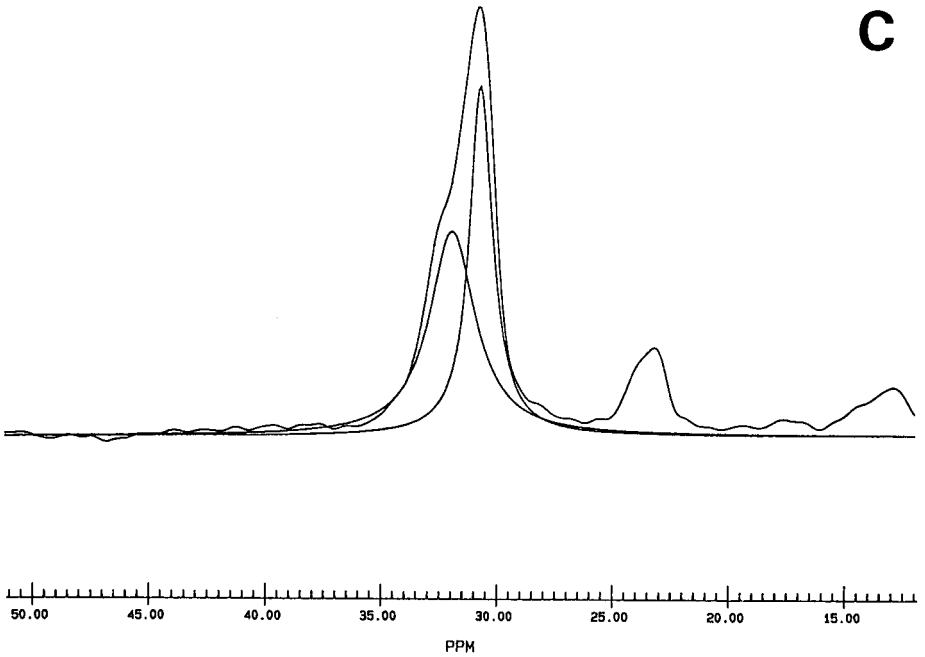

Fig. 13. Peak deconvolution for the signal at the 30 ppm at room temperature (A), 40°C (B) and 50°C (C).

around 45°C is a kind of melting from a solid-like to a liquid-like structure in the dry state stationary phase.

Fig. 14 shows the ^{13}C NMR spectra of suspended P-ODS, measured at 27 and 50°C. In this case, [^{2}H]chloroform was substituted for [^{2}H]dichloromethane, which was used in the study of the mobile phase effects on the conformation of P-ODS, because NMR measurements at temperatures higher than the boiling point of dichloromethane were not possible over long periods. The figures provide evidence to support the assumption that the structure of P-ODS changes from solid-like to liquid-like between 27 and 50°C, because the signal intensities for $-CH_2$ and bulk $-CH_2$ increase relatively, while the peak widths decreased with increasing temperature.

TABLE I

RESULTS OF PEAK DECONVOLUTION FOR CP-MAS-NMR SPECTRA OF VYDAC 201

	Ambient		*40°C*		*50°C*	
	1	*2*	*1*	*2*	*1*	*2*
Chemical shift (ppm)	32.8	30.8	32.4	30.8	32.0	30.8
Peak height	69.3	100	55.5	100	58.7	100
Peak width (Hz)	123.2	94.7	141.1	85.5	161.5	81.9
Area ratio	90.1	100	91.7	100	100	86.4

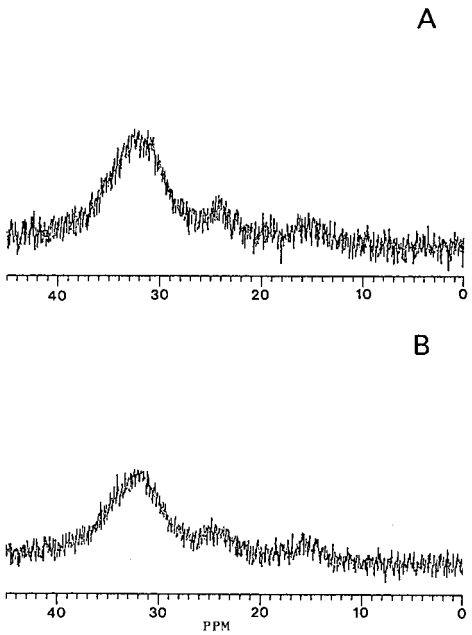

Fig. 14. ^{13}C NMR spectra of Vydac 201 TPB5 at 50°C (A) and 27°C (B).

Fig. 15 shows the NMR spectra of tetrabenzo[*a,cd,j,lm*]perylene dissolved in [^{2}H]chloroform–[^{2}H]methanol (50:50) at 50°C (A) and at 27°C (B) in 20% [^{2}H]chloroform in [^{2}H]methanol at 27°C (C), respectively. The change in mobile phase composition produced a drastic shift of the signals around 9.2 ppm. As previously discussed, the solvents of higher [^{2}H]dichloromethane concentration shifted two lines in the region of 9.2 ppm, which showed four lines at lower [^{2}H]dichloromethane concentrations. A similar tendency, but less than in the case of [^{2}H]dichloromethane, was seen with [^{2}H]chloroform. This is seen in spectrum C in Fig. 15, where two split signals appeared. By increasing the [^{2}H]chloroform concentration, a pair of signals at 9.2 ppm were shifted to higher magnetic field. Fig. 15B shows the four sharp lines observed when the [^{2}H]chloroform concentration was changed from 20 to 50% in [^{2}H]methanol. A change in temperature also gave a directionally similar, but smaller, signal shift at 9.2 ppm. This behaviour is identical to that observed when the [^{2}H]dichloromethane or [^{2}H]chloroform concentration in the mobile phase was increased. As discussed previously, increasing the [^{2}H]dichloromethane concentration in the solvent induced distortion of the molecular structure of tetrabenzo[*a,cd,j,lm*]-perylene. An increase in column temperature also induced such distortion. At higher temperatures the non-planarity of the solute is increased but to a smaller extent than when the solvent is changed.

The data shown and discussed above are evidence that changing the mobile phase composition causes a drastic change in solute conformation and a small change in P-ODS conformation to a more freely mobile state. From the solid-state NMR data, it is seen that the change to higher column temperature causes a drastic change in the

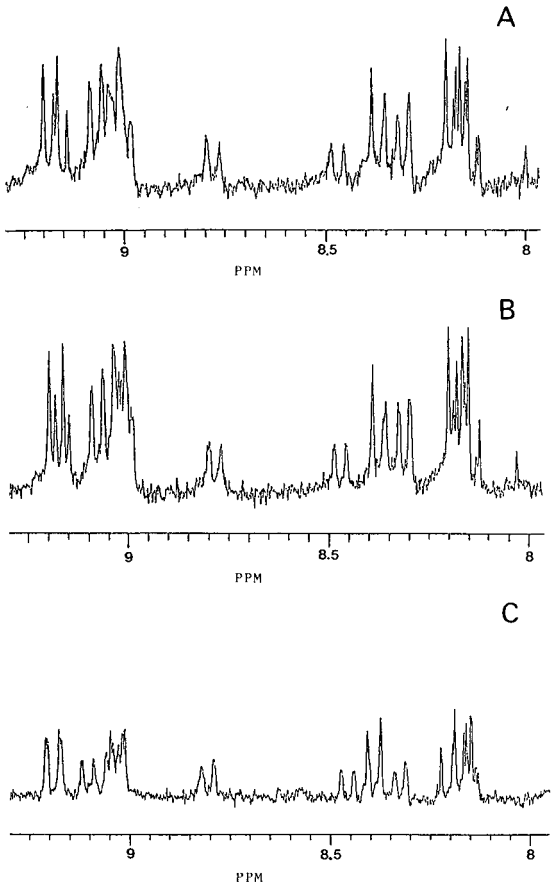

Fig. 15. ^{1}H NMR spectra of tetrabenzo[*a,cd,j,lm*]perylene at different mobile phase compositions and temperatures: (A) [$^2H_2$]dichloromethane–[$^2H_4$]methanol (50:50) at 0°C; (B) as (A) but at 27°C; (C) as (B) but solvent ratio 20:80.

dry stationary phase from solid-like to liquid-like (the critical temperature is about 45°C) and the solution NMR data indicate only a small change in the solute conformation. Although the suspension NMR data did not give clear information on the environment close to the actual chromatographic process, it is possible to say that the solid-like P-ODS phase is preferable for retaining planar PAHs more strongly than non-planar PAHs, and the liquid-like structure has less planarity recognition ability compared to the former state. These characters of the polymeric phase are very similar to those of bonded liquid crystalline phases[36–40]. The data shown here indicate that the ordering of the polymeric phase in the solid-like state is large enough to recognize the planarity of molecules like those of the liquid crystalline phases. This suggests that the very great influence of steric factors make the slot model[13] appropriate for the polymeric phase. The Dill[41] interphase model predicts that as alkyl surface densities increase, the corresponding configurational constraints are also increased, creating a more rigid and ordered chain packing structure. This anisotropy of the bonded

chains gives rise to additional shape selectivity among solute molecules, since the molecules which can most effectively align with the chains are those which are most effectively retained. In this model, the driving force for retention is the creation of a solute-sized cavity in the stationary phase. As the bonding density and consequently chain ordering are increased the free energy required for cavity formation also increases. Greater free energy is required to insert solute substructures which are parallel to the silica–bonded chain interface than for substructures which align with the chains and are normal to the interface, therefore the selectivity for linear and planar molecules will increase with alkyl bonding density, as predicted by this theory and as shown by our experiments. However, more precise and informative suspension NMR data are required and works is in progress in our laboratory using a 400-MHz NMR instrument.

ACKNOWLEDGEMENTS

The authors thank Dr. H. Nagashima of School of Materials Science, Toyohashi University of Technology, for his assistance and useful discussions on NMR measurements. K.J. and P.R.G. are grateful for support by the Japan–U.S. Joint Project from the Japan Society for Promotion Sciences and the National Science Foundation. This work has been partially financed by a Grant-in-Aid for General Research (Grant No. 630550564) from the Ministry of Education and Culture of Japan.

REFERENCES

1 S. A. Wise, in A. Bjorseth (Editor), *Handbook of PAH*, Marcel Dekker, New York, 1983, pp. 183–256.
2 A. L. Colmjo and J. C. MacDonald, *Chromatographia*, 13 (1980) 350.
3 A. Radecki, H. Lamparczyk and R. Kaliszan, *Chromatographia*, 12 (1979) 595.
4 K. Ogan, E. Katz and W. Salivin, *Anal. Chem.*, 51 (1979) 1315.
5 R. Kaliszan, *J. Chromatogr.*, 220 (1981) 71.
6 E. Katz and K. Ogan, *J. Liq. Chromatogr.*, 3 (1980) 1151.
7 S. A. Wise and W. E. May, *Anal. Chem.*, 55 (1983) 1479.
8 S. A. Wise, W. J. Bonnett, F. R. Guenther and W. E. May, *J. Chromatogr. Sci.*, 19 (1981) 457.
9 J. C. Fetzer and W. R. Biggs, *J. Chromatogr.*, 295 (1984) 161.
10 J. C. Fetzer and W. R. Biggs, *J. Chromatogr.*, 322 (1985) 275.
11 K. Jinno, T. Nagoshi, N. Tanaka, M. Okamoto, J. C. Fetzer and W. R. Biggs, *J. Chromatogr.*, 386 (1987) 123.
12 K. Jinno, T. Nagoshi, N. Tanaka, M. Okamoto, J. C. Fetzer and W. R. Biggs, *J. Chromatogr.*, 392 (1987) 75.
13 S. A. Wise and L. C. Sander, *J. High Resolut. Chromatogr. Chromatogr. Commun.*, 8 (1985) 248.
14 K. Jinno, N. Anazawa, M. Okamoto, N. Tanaka, J. C. Fetzer and W. R. Biggs, *J. Chromatogr.*, 402 (1987) 173.
15 K. Jinno, T. Nagoshi, N. Tanaka, M. Okamoto, J. C. Fetzer and W. R. Biggs, *J. Chromatogr.*, 436 (1988) 1.
16 R. K. Gilpin, *Anal. Chem.*, 57 (1985) 1465A.
17 D. W. Sindorf and G. E. Marciel, *J. Am. Chem. Soc.*, 105 (1983) 1848.
18 D. W. Sindorf and G. E. Marciel, *J. Am. Chem. Soc.*, 105 (1983) 3767.
19 R. K. Gilpin and M. E. Gangoda, *J. Magn. Reson.*, 64 (1985) 408.
20 R. K. Gilpin and M. E. Gangoda, *J. Chromatogr. Sci.*, 21 (1983) 352.
21 R. K. Gilpin and M. E. Gangoda, *Anal. Chem.*, 56 (1984) 1470.
22 E. Bayer, A. Paulus, B. Peters, G. Laupp, J. Reiners and K. Albert, *J. Chromatogr.*, 364 (1986) 25.
23 M. Gangoda, R. K. Gilpin and B. M. Fung, *J. Magn. Reson.*, 74 (1987) 134.

24 E. Bayer, K. Albert, J. Reiners, M. Nieder and D. Müller, *J. Chromatogr.*, 264 (1983) 197.
25 L. C. Sander, J. B. Callis and L. R. Field, *Anal. Chem.*, 55 (1983) 1068.
26 D. E. Leyden, D. S. Kendall, L. W. Burgraf, F. J. Pern and M. DeBello, *Anal. Chem.*, 54 (1982) 101.
27 D. Morel, K. Tabar, J. Serpinet, P. Claudy and J. M. Letoffe, *J. Chromatogr.*, 395 (1987) 73.
28 E. Clar, *Polycyclic Hydrocarbons*, Vol. 2, Springer, London, 1964.
29 J. C. Fetzer, *Adv. Chem.*, 217 (1988) 326.
30 P. Shah, L. R. Rogers and J. C. Fetzer, *J. Chromatogr.*, 388 (1987) 411.
31 Y. Takahashi, K. Hosokawa, F. Yoshida, M. Ozaki and S. Sasaki, *Anal. Chim. Acta*, in press.
32 Y. Kohno, M. Konno, Y. Saito and H. Inokuchi, *Acta Crystallogr., Sect. B*, 31 (1975) 2076.
33 C. R. Yonker, T. A. Zwier and M. F. Burke, *J. Chromatogr.*, 241 (1982) 257.
34 M. E. McNally and L. B. Rogers, *J. Chromatogr.*, 331 (1985) 23.
35 H. L. Casal, D. G. Cameron and H. H. Mantsch, *Can. J. Chem.*, 61 (1983) 1736.
36 S. A. Wise, L. C. Sander, H.-Ch. K. Chang, K. E. Markides and M. L. Lee, *Chromatographia*, 25 (1988) 473.
37 L. C. Sander and S. A. Wise, *Adv. Chromatogr. (N.Y.)*, 25 (1986) 139.
38 M. L. Lee, R. C. Kong, C. L. Woolley and J. S. Bradshaw, *J. Chromatogr. Sci.*, 22 (1984) 136.
39 B. A. Jones, J. S. Bradshaw, M. Nishioka and M. L. Lee, *J. Org. Chem.*, 49 (1984) 4947.
40 J. S. Bradshaw, C. Schregenberger, K. H. C. Chang, K. E. Markides and M. L. Lee, *J. Chromatogr.*, 358 (1986) 95.
41 K. A. Dill, *J. Phys. Chem.*, 91 (1987) 1980.

Journal of Chromatography, 461 (1989) 229–242
Elsevier Science Publishers B.V., Amsterdam — Printed in The Netherlands

CHROMSYMP. 1510

SOLUTION PROPERTIES OF POLYELECTROLYTES

IV. USE OF A NEW HYDROPHILIC SIZE-EXCLUSION CHROMATOGRAPHIC PACKING FOR THE SEPARATION OF ANIONIC AND CATIONIC POLYIONS

E. PÉREZ-PAYÁ and L. BRACO*

Departament de Bioquímica i Biologia Molecular, Facultades de Ciencias, Universitat de Valencia, 46100 Burjassot (Valencia) (Spain)

A. CAMPOS and V. SORIA

Departament de Química Física, Facultades de Ciencias, Universitat de Valencia, 46100 Burjassot (Valencia) (Spain)

and

C. ABAD*

Departament de Bioquímica i Biologia Molecular, Facultades de Ciencias, Universitat de Valencia, 46100 Burjassot (Valencia) (Spain)

SUMMARY

The chromatographic behaviour of sodium polystyrenesulphonate in Ultrahydrogel aqueous size-exclusion chromatographic packings was analysed under different experimental conditions. Three types of mobile phases (salt-free water, sodium nitrate solution and buffers of different pH) were investigated in order to characterize the elution mechanisms and to optimize the separation. Several parameters, such as sample concentration, injection volume, eluent pH and ionic strength were considered. Finally, a "universal" calibration graph was obtained under simple, mild, optimized conditions of the mobile phase (0.2 *M* acetate buffer, pH 4.0), which is congruent for both polyanions and polycations and also for uncharged polymers.

INTRODUCTION

The high-performance liquid chromatography of charged macromolecules in aqueous media has undergone a great evolution in the last few years, mainly owing to the advent of commercially available hydrophilic stationary phases for high-performance size-exclusion chromatography (SEC)[1]. There are a number of SEC effects inherent in polyelectrolytes which arise from both ionic interactions between the

* Present address: Department of Chemistry, Massachusetts Institute of Technology, Cambridge, MA 02139, U.S.A.

0021-9673/89/$03.50

polyion and the packing (*e.g.*, Donnan equilibrium ion inclusion and ion exclusion) and from changes in the dimensions of the polymer molecules in solution, controlled by concentration, pH and ionic strength. These effects and ways of minimizing them have been discussed in detail elsewhere[2–6]. In this context, two recent contributions deserve to be mentioned: Dubin *et al.*[7] reported a study of the resolution of electrostatic and steric factors for sodium polystyrenesulphonate on controlled-pore glass and Potschka[8] eluted a set of native proteins, having well defined structures, on rigid resins in a variety of aqueous buffers differing in composition, pH and ionic strength. It was concluded that the unperturbed dimensions of a polyelectrolyte can be determined by SEC, taking into account the surrounding diffuse double layer and any other interactions of the solvent. However, in practice, the existence of electrostatic interactions between the eluite and the surface of the packing is still problematic, as it causes deviations towards higher or lower elution volumes when the elution volume of uncharged polymers of the same molecular weight is taken as a reference. In order to minimize or even prevent this effect, the use of a support bearing a relatively small number of ionizable groups may be of great interest, in addition to both the design of a suitable composition of the mobile phase (pH and ionic strength) and the optimization of other experimental parameters, such as sample concentration and injection volume.

In this paper, we report a preliminary study of the influence of the aforementioned variables on the elution of sodium polystyrenesulphonate (NaPSS) from Ultrahydrogel[9]. This packing is based on hydroxylated polymethacrylate with a low content of residual carboxylic groups, which confer upon it *a priori* some advantages over the silica-based supports by minimizing the electrostatic interactions with the polyelectrolyte. The elution behaviour was characterized in terms of the log $M[\eta]$ *vs.* elution volume calibration (where M is the molecular weight and $[\eta]$ the intrinsic viscosity) for each of the mobile phases tested. This allowed the selection of optimum experimental conditions for the analysis of NaPSS with these columns.

The recommended conditions were later applied to the chromatography of several polycations, such as poly(2-vinylpyridine) (P2VPy), poly(4-vinylpyridine) (P4VPy) and poly-L-lysine (PLys). According to the symmetry and positions of the peaks in the chromatograms, it appears that the frequently observed secondary adsorption effects do not occur to a significant extent and that the elution mechanism approaches that of pure SEC[10]. Finally, a universal calibration, suitable for uncharged polymers, polyanions and polycations is presented.

EXPERIMENTAL

A Waters liquid chromatograph (Waters Chromatography Division, Millipore, Milford, MA, U.S.A.) equipped with an M-45 solvent delivery system, a U6K universal injector and an R-410 refractive index detector, coupled to a SP 4290 automatic recorder (Spectra-Physics, San José, CA, U.S.A.), was used.

Two Waters Ultrahydrogel columns packed with hydroxylated polymethacrylate-based gel of 250 and 500 Å nominal pore size were used. These columns will be referred to as UHG-250 and UHG-500, respectively. They have been reported to perform over a broad pH range (from 2 to 12) and are compatible with eluents containing a high percentage of organic solvents[9].

Three different types of mobile phases were used: Waters Milli-Q-quality pure water, sodium nitrate solution and acetate and phosphate buffers with several pH and ionic strength values. All salts used were of analytical-reagent grade from Merck (Darmstadt, F.R.G.). The eluents were always filtered and degassed through a 0.45-μm Micro Filtration Systems regenerated cellulose filter (Millipore) prior to use. The columns were equilibrated for at least 12 h before the start of an experiment. The polymer solutions were always prepared with the corresponding mobile phase as solvent. The flow-rate was 0.8 ml/min. Each sample was injected three times as a check on the reproducibility.

The following dextran samples were obtained from Pharmacia (Uppsala, Sweden): 10T, 20T, 40T, 70T, 150T and 500T, having weight-average molecular weights of $10 \cdot 10^3$, $17.7 \cdot 10^3$, $40.0 \cdot 10^3$, $83.3 \cdot 10^3$, $170 \cdot 10^3$ and $500 \cdot 10^3$, respectively. NaPSS standards were narrow-distribution ($M_w/M_n < 1.1$ in all instances), dialysed fractions, purchased from Pressure Chemical (Pittsburg, PA, U.S.A.), with nominal molecular weights of $1.6 \cdot 10^3$, $4 \cdot 10^3$, $16 \cdot 10^3$, $31 \cdot 10^3$, $88 \cdot 10^3$, $177 \cdot 10^3$ and $354 \cdot 10^3$. Poly(ethylene oxide) (PEO) samples (MW 2000 and 4000) were obtained from Fluka (Buchs, Switzerland). Narrow fractions of poly(2-vinylpyridine) (P2VPy) (MW $2.9 \cdot 10^3$, $7.0 \cdot 10^3$, $10.5 \cdot 10^3$ and $28.0 \cdot 10^3$, were from Pressure Chemical. A poly(4-vinylpyridine) (P4VPy) sample was obtained by ultrafiltration of a commercial sample of nominal MW $4 \cdot 10^4$, supplied by Polyscience (Warrington, PA, U.S.A.). Ultrafiltration was carried out with a Millipore 142-mm diameter HI-FLUX UF cell. Finally, two poly-L-lysine (PLys) samples from Sigma (St. Louis, MO, U.S.A.) of average MW $3.8 \cdot 10^3$ and $5.8 \cdot 10^3$ were also used as polycations.

Viscosity measurements were made with a modified Ubbelohde viscometer thermostated at 25.0 $\pm$ 0.1°C. Flow-times were determined to 0.01 s; the flow-time of the pure solvent was always higher than 110 s. Kinetic energy corrections were included in the calculations of specific viscosities. The viscometric equations used for the uncharged polymers in all instances were $[\eta]_{dextran} = 97.8 \cdot 10^{-3} M^{0.50}$ (ref. 11) and $[\eta]_{PEO} = 2.0 + 0.016 M^{0.76}$ (ref. 12) because, as has been previously indicated, the influence of salt on the viscosity of non-ionic polymers, such as those mentioned above, may be neglected[10].

RESULTS AND DISCUSSION

In this paper, the elution volume, referred to as $V(c_p,c_s)$, is a function of two variables: the injected polyion concentration, c_p, and the concentration of salt in the eluent, c_s.

Numerous studies on the SEC of polyelectrolytes have been carried out with derivatized silica gel packings[2,13] in order to minimize the undesirable polymer–support interactions. We used high-performance SEC Ultrahydrogel columns[9], packed with a soft or semi-rigid non-derivatized gel, for the chromatography of different classes of polyions. It is well known that soft or semi-rigid gels must be used at low pressures, and this makes separations more time consuming. Further, the particles are larger and less uniform, causing a slight reduction in column efficiency. However, these apparent drawbacks may be largely compensated for in this instance by the clear advantages of bypassing the need for derivatization and especially the diminished polyelectrolyte–support interactions owing to the low residual charge density in the

gel. Our aim was to determine the extent to which and the conditions under which these advantages can make the use of this packing for the chromatography of polyions particularly appropriate. Different factors and variables that directly influence the SEC separation were investigated and optimized in order to obtain a calibration graph applicable to both polyanions and polycations and also to uncharged polymers by use of a common mobile phase.

It must be pointed out that, in general, the chromatography of polycations has been carried out with derivatized silica gels and eluents specifically designed for this type of polyelectrolyte[13]. We used three different types of mobile phases, in the following order: (a) salt-free water, (b) sodium nitrate solution and (c) phosphate and acetate buffers with different pH and ionic strength values.

Salt-free water

The use of pure water as a mobile phase allowed us to check the extent of the contribution of the residual surface charge density of the support to undesirable interactions with the polymer, and to characterize the behaviour of the system and the influence of several experimental variables under the less favourable conditions for the chromatography of polyions. It is well known that NaPSS in salt-free water adopts a concentration-dependent more or less stretched conformation, owing to the electrostatic repulsion between the charges of the monomeric units (see, for example, the values for the persistence length of this polymer in pure water in Table 4 in ref. 14). In fact, the more dilute the sample is, the more stretched are the chains. Therefore, if the interactions of the polyions with the gel were relatively strong (as is usually the case for other types of supports), a pronounced ion-exclusion effect should be observed,

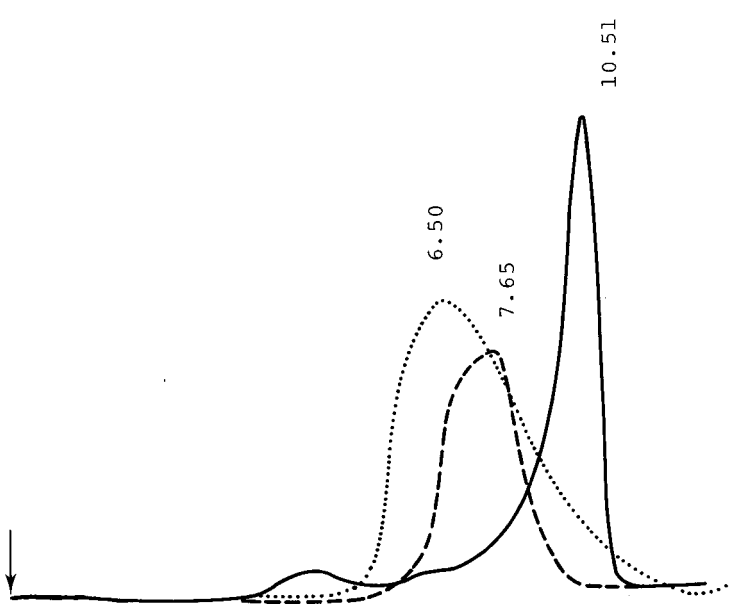

Fig. 1. Elution profiles of NaPSS for UHG-500, eluted with salt-free water. Flow-rate, 0.8 ml/min; injection volume, 100 μl; NaPSS concentration, 10 g/l. NaPSS molecular weight: (· · ·) 177; (– – –) 31; (———) 1.6 kDa.

preventing a reasonable separation of NaPSS samples of different molecular weight. However, as will be shown later in detail, a satisfactory (although evidently not optimized) resolution can be obtained, even with salt-free water as eluent, if certain simple experimental conditions are met. As an example, Fig. 1 shows the separation of three NaPSS samples of MW 177, 31 and 1.6 kDa on UHG-500, eluted with pure water, the elution volumes being 6.50, 7.65 and 10.51 ml, respectively. Moreover, this behaviour may be a real advantage, especially when for any given reason (*e.g.*, to minimize hydrophobic interactions between polymers and gel), salt-containing eluents of very low concentration must be used.

In order to verify these assumptions and to characterize and optimize the elution behaviour of NaPSS with salt-free water, a systematic study was carried out, using UHG-250 and UHG-500 independently, and including c_p and the injection volume V_i, as variables. V_i was considered on the basis of the following assumption: because (i) in pure water the conformation of the polyion is strongly dependent on concentration and (ii) the actual dilution of the sample through the column will increase as the volume injected decreases, it is to be expected that the conformation of NaPSS will vary to a different extent during elution, depending on the volume injected. Thus, for a given c_p value, the lower is V_i the more stretched the polyion chains are and, therefore, the smaller is the observed elution volume. This assumption proved to be correct, as shown in Fig. 2A, where, as an example, $V(c_p, 0)$ on UHG-250 is plotted as a function of V_i at constant c_p (10 g/l) for two different NaPSS molecular weights. Note that the variation is not linear; $V(p_p, 0)$ increases with increasing V_i up to about 50 μl and then the effect is attenuated, especially for the higher molecular weight. This trend was also observed for all the other molecular weights used (not shown). Interestingly, when only 1–5 μl are injected, the dilution of the sample is so dramatic that all NaPSS are eluted close to the column void volume. Under these conditions, the chains are presumably eluted in a very stretched (rod) conformation. Therefore, the range 50–100 μl and, in particular, a V_i value of 100 μl seems to be the most appropriate, because any error in the measurement of V_i will have a much smaller repercussion on $V(c_p, 0)$. On the other hand, significantly higher V_i values, such as 150–200 μl, cannot be recommended because of overloading effects (see below).

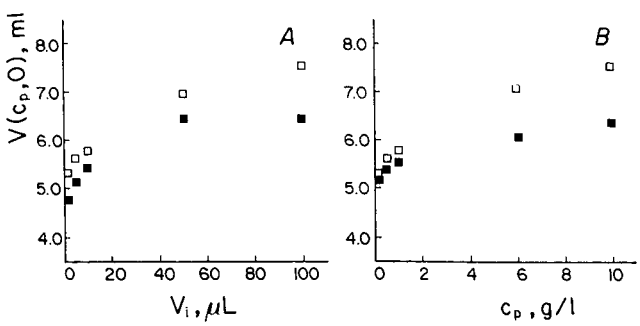

Fig. 2. Dependence of the elution volume, $V(c_p, 0)$, of NaPSS on (A) the injection volume, V_i, at a constant c_p (10 g/l) and (B) polyion concentration, c_p, at constant V_i (100 μl), for UHG-250 and salt-free water as eluent in both instances. NaPSS molecular weight: (A) (□) 1.6 and (■) 354 kDa; (B) (□) 1.6 and (■) 31 kDa.

Fig. 2B shows, as an example, the variation of $V(c_p, 0)$ on UHG-250 as a function of c_p [at constant V_i (100 μl)] for two different NaPSS molecular weights. This dependence also is not linear, similarly to the behaviour of NaPSS with salt-free water and a Waters I-250 protein column[14], as opposed to the behaviour obtained for uncharged polymers with organic solvents[15–18]. A similar trend to that in Fig. 2B was observed for all the other molecular weights tested. However, note that the shift in the elution volume with c_p increases as the molecular weight of the sample decreases, in contrast with the behaviour observed for uncharged polymers in organic media[16], where the concentration effect is almost negligible below 40 kDa. Although the efficiency of this column increases with increasing c_p when pure water is used as the eluent, it is evident that it is still poor.

A similar test was carried out with UHG-500 in order to establish a comparison under the same experimental conditions. Fig. 3 shows the effect of c_p on $V(p_p, 0)$ [at constant V_i (100 μl)] for NaPSS samples of 1.6, 31 and 177 kDa. Again, the functionality observed is similar to that found for UHG-250, but in this instance the separation achieved for $c_p > 2$ g/l is much better. Hence the higher average pore size of the UHG-500 column clearly provides a more appropriate sieve for the stretched NaPSS chains to be permeated in salt-free water. On the other hand, an increase in the shift of the elution volume with increasing c_p can be observed for this packing as the molecular weight decreases, as opposed to the behaviour for uncharged polymers in organic solvents. In a similar way to Fig. 2B, the injection of the polyelectrolyte at very low concentrations causes the resolution to be completely lost, this early elution being due to both coil expansion and charge repulsion. In addition to c_p, the influence of V_i on $V(c_p, 0)$ was also studied; the same trend as in Fig. 2A was observed for all the molecular weights used (not shown). Again, the highest $V(c_p, 0)$ value for a given sample at a given c_p was obtained for $V_i = 100$ μl.

The elution volumes for $V_i = 200$ μl were essentially the same as for 100 μl when the sample was dilute. However, when 200 μl were injected for $c_p > 2$ g/l, overloading effects[3,19,20] occurred, distorting the chromatogram. Hence, of all the conditions tested so far with salt-free water, an injection volume of 100 μl and a polyion

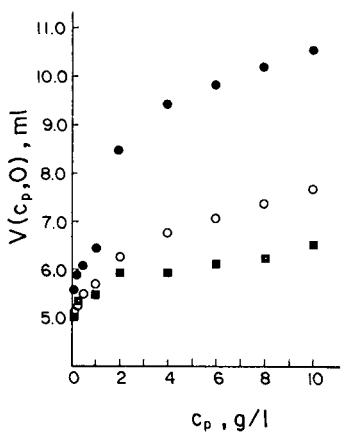

Fig. 3. Dependence of $V(c_p, 0)$ on NaPSS concentration at constant V_i (100 μl) for UHG-500, eluted with salt-free water. NaPSS molecular weight: (●) 1.6; (○) 31; (■) 177 kDa.

concentration of 10 g/l seem to be optimal for both UHG-500 and UHG-250. Further, as far as c_p is concerned, a value of 10 g/l should not be exceeded in the range of molecular weights examined, for two reasons:

(i) in order to prevent the appearance of viscous fingering[19] and macromolecular crowding[20], widely studied for both uncharged and charged polymers in organic and aqueous media respectively; these effects cause a distortion of the chromatogram, making it impossible to obtain any reliable data;

(ii) from a quantitative point of view, the upper threshold for c_p must correspond to the lower limit between dilute and semi-dilute concentrations[21]. Hence, this threshold would be determined by the relationship $c_p[\eta] < 1$ according to Doi's theory[22,23], because for $c_p[\eta]$ values higher than unity entanglement occurs, the polyion chains no longer remaining an individual entity. In this instance, the chromatographic column would not be able to achieve a good separation, and preliminary dilution of the sample would be need to suppress entanglement.

A more detailed analysis of the elution behaviour of NaPSS with UHG-500 and pure water was next carried out in terms of the log $M[\eta]$ *vs.* elution volume calibration for the different experimental conditions tested. This type of plot allows a better understanding and interpretation of the elution mechanisms[14,15,24,25] (including polyelectrolyte–support interactions) and will be used for the study of the remainder of the mobile phases in this work.

Fig. 4 depicts the different log $M[\eta]_{p,c_p}$ *vs.* $V(c_p, 0)$ calibration graphs for NaPSS for salt-free water, obtained as a function of c_p [at constant V_i (100 μl)], for a range of polyion concentrations from 0.1 to 10 g/l. $[\eta]_{p,c_p}$ has been defined previously[14]; it refers to the intrinsic viscosity of the polymer at finite concentration in pure water; its values have been reported elsewhere[14]. The reference calibration for uncharged polymers (dextrans and PEO), obtained at infinite dilution by extrapolation of at least four concentrations, is also included. The general pattern of the variation of the graphs is similar to that corresponding to NaPSS for salt-free water and the Waters I-250 protein column (see Fig. 7 in ref. 14). However, in this instance, the calibration graph at

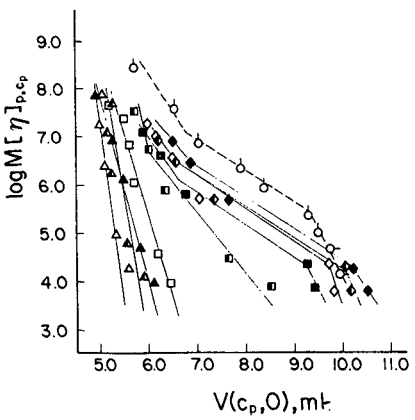

Fig. 4. Calibration graphs for NaPSS on UHG-500, eluted with salt-free water, at constant V_i = 100 μl, as a function of the polyion concentration. c_p: (△) 0.1; (◢) 0.25; (▲) 0.5; (□) 1.0; (◧) 2.0; (◨) 4.0; (◇) 6.0; (◆) 8.0 and (◆) 10.0 g/l. Also included is the calibration graph for uncharged polymers: (○) dextran and (○–) PEO.

the highest c_p is much closer to the reference graph and, interestingly, their slopes are almost identical. In addition to the set of graphs in Fig. 4, another set was obtained on plotting $\log M[\eta]_{p,c_p}$ *vs.* $V(c_p, 0)$ as a function of V_i [at constant c_p (10 g/l)] for a range of injection volumes from 1 to 100 μl (not shown). A very similar trend was observed, the calibration graphs approaching that for the uncharged polymers as V_i increased.

In order to summarize the results from both plots, Fig. 5 shows the variation of the slopes of the calibration graphs as a function of (A) c_p and (B) V_i. The dotted lines correspond to the slope of the reference calibration graph (dextran and PEO). It is evident that in both instances the slopes show a typical "polyelectrolytic behaviour", which must be basically governed by the conformation-dependent conformational changes of the poly-ion. As the actual concentration of the sample on the column increases, the differences between the slopes for NaPSS and uncharged polymers become smaller. In fact, some interesting conclusions concerning the polymer–substrate interactions arise from the analysis of Figs. 4 and 5. If the reference calibration is taken as that corresponding to a pure SEC elution mechanism, then the calibration graph obtained under the experimental conditions, c_p = 10 g/l and V_i = 100 μl, reveals a satisfactory resolution for the "very inadequate" eluent (salt-free water) used. This, in turn, supports the assumption that the interaction between the polyelectrolyte and the residual charges on the support is indeed diminished when compared with the behaviour reported for other types of hydrophilic gels, where the solute–substrate electrostatic interactions cause considerable secondary effects. In fact, the deviation in Fig. 4 towards higher elution volumes can be attributed to both (i) a not completely reached totally folded (Gaussian) conformation of the chains because

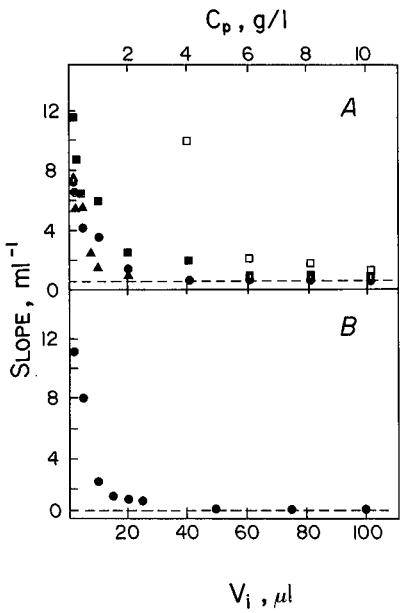

Fig. 5. Variation of the slope of the calibration graphs for NaPSS on UHG-500, eluted with salt-free water as a function of (A) c_p, at constant V_i = (●) 100 μl; (■) 50 μl; (□) 25 μl; and (▲) 200 μl; and (B) V_i, at constant c_p (10 g/l). The dotted lines correspond to the value of the slope for the uncharged polymers in both instances.

the concentration is not high enough and (ii) a residual, but definitely small, repulsive interaction between NaPSS and the carboxylic groups of the gel.

Sodium nitrate solution

UHG-250 was used for all the experiments involving salt-containing mobile phases because its pore size proved to be more suitable for the analysis once the chains approach the Gaussian coil conformation owing to the screening of poly-ion charges by counter ions. The ionic strength of the eluent is an important factor, as it strongly determines the conformation of the polyelectrolytes in solution[5,8,24–26]. Recently, a correlation between eluent ionic strength and size of the diffuse double layer around polyelectrolytes at infinite dilution was established in deriving a theory on the elution mechanisms of SEC of poly-ions[8]. In this way, counter ions in a polyelectrolyte solution can be classified into three categories[27]: counter ions freely moving outside the region occupied by macro-ions, those bound but mobile in this region and those bound to individual charged groups of the macro-ion. The equilibrium between free counter ions and bound but mobile counter ions is most important in determining the conformation or size and shape, the main factor governing SEC. Thus, the poly-ion conformation will now depend on both c_p and c_s. When c_s increases at constant c_p, the Gaussian coil $\rightleftharpoons$ rod simplified equilibrium is shifted to the left as a result of the screening of the macro-ion charges, causing a decrease in the repulsion between different chain segments and facilitating the folding. From the chromatographic point of view, it can be assumed that (i) the charge screening will decrease even further the repulsive interactions between the polymer sulphonate and the residual carboxylic groups on the support and (ii) the accessibility of the NaPSS to the pores will be improved by the chain folding.

Fig. 6 shows the calibration graphs for NaPSS in UHG-250 when either a very dilute (c_s = 0.002 *M*, Fig. 6A) or a moderately concentrated (c_s = 0.1 *M*, Fig. 6B) sodium nitrate solution is used as eluent. The calibrations at two c_p values are shown, corresponding to the maximum and minimum poly-ion concentrations used in the previous section. The calibration graph for uncharged polymers (dextran and PEO) is also included. The values for the intrinsic viscosity of NaPSS at finite poly-ion concentration, at a given salt concentration, $[\eta]_{p,c_s,c}$, were obtained from ref. 25 and are summarized in Table I. As can be seen in Fig. 6A, the extent of screening by counter ions and, hence, of chain-folding is too limited for the macro-ions to penetrate the pores of the gel, so that elution takes place mainly through the interstices of the packing, making a chromatographic separation under these conditions impracticable. On the other hand, at this very low c_s, a concentration effect can still be observed on the calibration graphs. In contrast, at a salt concentration of 0.1 *M* (Fig. 6B) a calibration graph almost identical for NaPSS and uncharged polymers is obtained, which indicates that the repulsive polyelectrolyte–gel interactions have been substantially cancelled and that the hydrodynamic volume is now that corresponding to Gaussian coils.

Buffers of different pH values

Another important factor influencing the SEC separations of polyelectrolytes is the pH. It is important in determining whether a solute is ionized or not, and to regulate the degree of ionization of the surface functional groups on the support.

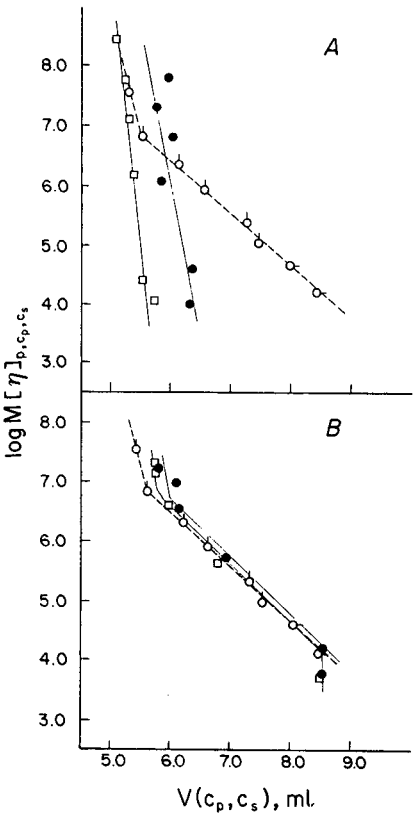

Fig. 6. Calibration graphs for NaPSS on UHG-250, eluted with sodium nitrate solutions. V_i = 100 μl in all instances. c_p: (□) 0.1 and (●) 10 g/l. Sodium nitrate concentration: (A) 0.002 and (B) 0.1 *M*. Also included are the calibration graphs for uncharged polymers: (○) dextran and (○–) PEO.

TABLE I

INTRINSIC VISCOSITY, $[\eta]_{p,c_p,c_s}$(ml/g) OF NaPSS IN SODIUM NITRATE SOLUTIONS[25]

Sodium nitrate concentration · 10⁻³ (g/mol)	c_s = 0.002 *M*		c_s = 0.10 *M*	
	c_p = 10 g/l	c_p = 0.1 g/l	c_p = 10 g/l	c_p = 0.1 g/l
354	176.8	799.1	51.4	54.9
177	108.4	313.7	58.5	81.8
88	68.9	147.6	38.7	45.6
31	36.0	49.0	16.3	14.6
4	11.4	11.9	4.5	3.6
1.6	6.4	7.0	3.8	3.5

Hence the mobile phase must be selected so as to minimize the remaining net charges without undesirable perturbations of the system or damaging of the gel. In addition, operating at lower pH may in some instances[5,7] contribute to a reduction in sample viscosity.

In order to establish the influence of pH on the elution behaviour of NaPSS for UHG-250, the following mobile phases were compared: 0.02 *M* phosphate buffer of pH 7.0 and 5.9 and 0.02 and 0.2 *M* acetate buffers of pH 4.0. As styrenesulphonic acid is strongly acidic, it is to be expected that variations of pH in the range 7.0–4.0 will not significantly affect the degree of ionization of the polyelectrolyte. However, as the pH decreases (approaching 4.0), the degree of protonation of the residual carboxylic groups on the support will increase, thus contributing to further deactivation of the gel surface and to a diminution of the polymer–substrate repulsive interactions. Fig. 7 shows the calibration graphs obtained for NaPSS for all the eluents tested. The corresponding $[\eta]_{p,c_p,c_s}$ values are summarized in Table II. As expected, the graphs approach the calibration for uncharged polymers as the pH decreases. Moreover, it is interesting that, at pH 4.0, even at low salt concentration (0.02 *M*), the resolution is moderately satisfactory. With both a low pH and a moderate ionic strength (0.2 *M*), slight shifts towards higher elution volumes occur. This shift in the elution volume could be attributed to hydrophobic and/or adsorption effects between the poly-ion and the packing. A similar behaviour for NaPSS has been observed at high ionic strength[28]. Conditions where apparently the undesirable secondary effects were therefore selected as being optimal for further study.

Finally, the analysis of the chromatographic behaviour of polyelectrolytes on UHG-250 was extended to the chromatography of polycations. It is well known that the chromatography of polycations presents some particularly difficult problems[29].

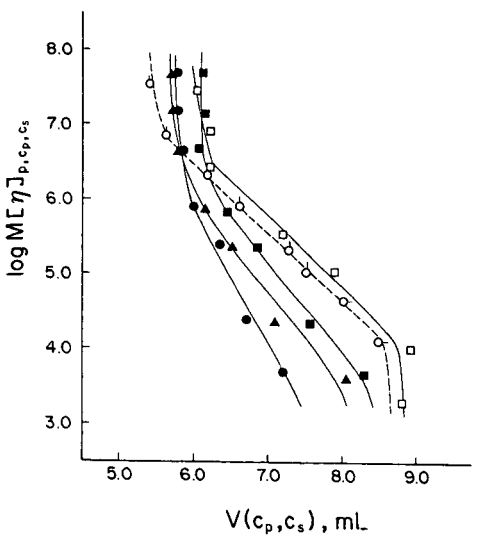

Fig. 7. Calibration graphs for NaPSS on UHG-250, eluted with buffers of different pH and ionic strength values. c_p = 10 g/l and V_i = 100 µl in all instances. Eluents: 0.02 *M* phosphate buffer at pH (●) 7.0 and (▲) 5.9; (■) 0.02 and (□) 0.2 *M* acetate buffer at pH 4.0. (○) Dextran and (○–) PEO.

TABLE II

INTRINSIC VISCOSITY, $[\eta]_{p,c_p,c_s}$ (ml/g) OF NaPSS IN DIFFERENT BUFFERS

c_p = 10 g/l in all instances.

Buffer	*NaPSS molecular weight · 10^{-3} (g/mol)*						
	1.6	*4*	*16*	*31*	*88*	*177*	*354*
0.02 *M* phosphate (pH 7.0)	3.1	5.9	15.6	24.4	52.4	81.5	134.3
0.02 *M* phosphate (pH 5.9)	2.8	5.3	14.2	22.3	49.0	75.9	126.4
0.02 *M* acetate (pH 4.0)	3.0	5.7	13.7	24.0	52.5	79.4	132.1
0.2 *M* acetate (pH 4.0)	1.3	2.6	7.3	11.7	29.9	42.9	77.8

Several mechanisms accounting for non-steric interactions between cationic polyelectrolytes and porous packing materials have been proposed, involving electrostatic adsorption, electrostatic exclusion and hydrophobic partitioning[13]. In order to verify the existence of a common mobile phase for the satisfactory elution of both polyanions and polycations, which would corroborate a "universal" behaviour for this packing, a number of polycations were examined under the above-mentioned seleccted chromatographic conditions (0.2 *M* acetate buffer, pH 4.0). Fig. 8 depicts, as an example, three elution profiles, corresponding to P2VPy, P4VPy and PLys samples with molecular weights of 10.5, 40 and 3.8 kDa, respectively. Also included for comparison is the chromatogram for a 40-kDa dextran sample. Although the solutions injected were prepared from the eluents, "salt" peaks always appeared. This is believed to be a result of ion inclusion[6]. In all instances, the position of these peaks is far enough from the polymer peak not to disturb it. If the polyelectrolyte samples adsorbed on the gel matrix (because of the opposite charge), severely distorted elution profiles (sharp start-up and tailing) would be observed. However, as these features do not appear in any of the chromatograms in Fig. 8, it can be reasonably assumed that all the samples are eluted essentially in terms of their molecular size, without significant secondary

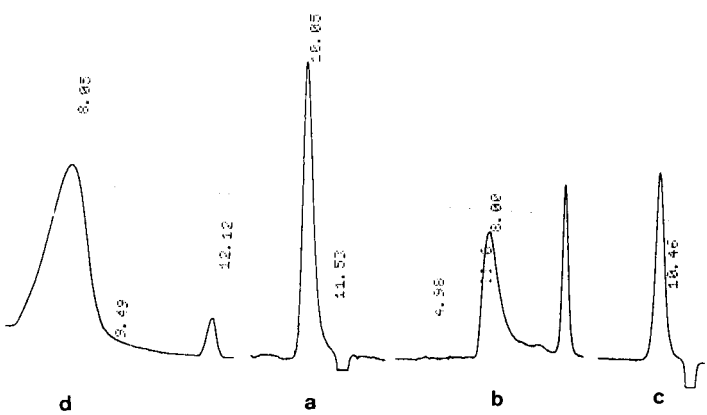

Fig. 8. Elution profiles of several polycations on UHG-250, eluted with 0.2 *M* acetate buffer (pH 4.0). (a) P2VPy, 10.5 kDa; (b) P4VPy, 40 kDa; (c) PLys, 3.8 kDa; (d) also included for comparison is a 40-kDa dextran sample.

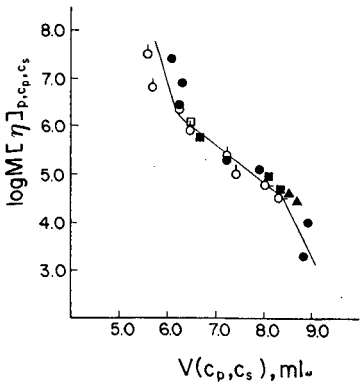

Fig. 9. Universal calibration graphs for both polyanions and polycations and also for uncharged polymers, obtained on UHG-250, eluted with 0.2 *M* acetate buffer (pH 4.0). c_p = 10 g/l and V_i = 100 μl in all instances. (●) NaPSS; (■) P2VPy; (□) P4VPy; (▲) PLys. (○) Dextran and (○–) PEO.

TABLE III

MARK–HOUWINK CONSTANTS FOR DIFFERENT POLYELECTROLYTES IN 0.2 *M* ACETATE BUFFER (pH 4.0)

Sample	$K \cdot 10^3$ *(ml/g)*	*a*	*Ref.*
NaPSS	0.803	0.940	This work
P2VPy	11.30	0.730	30
P4VPy	22.00	0.687	31
PLys	2.58	0.844	32

adsorption effects. Apparently, the combined effect of a low pH with a moderate ionic strength on the residual carboxylic groups of the support seems to cancel the electrostatic attractive interactions to a satisfactory extent, thus suppressing adsorption. This is further supported by the results in Fig. 9, which shows an optimized, general "universal" calibration graph for UHG-250 under the above-mentioned conditions of pH and ionic strength, including both anionic (NaPSS) and cationic (P2VPy, P4VPy and PLys) polyelectrolytes, and also uncharged polymers (dextran and PEO). The intrinsic viscosity values for the different poly-ions are summarized in Table III.

CONCLUSION

An analysis of the chromatographic behaviour of NaPSS with Ultrahydrogel packing has been carried out under different experimental conditions and an optimized composition of the mobile phase (pH and ionic strength) has been elucidated, allowing us to minimize polymer–substrate interactions. For the range of molecular weights studied, a common, "universal" calibration graph at a finite concentration of sample injected has been obtained for UHG-250 in the chromatography of both polyanions and polycations.

ACKNOWLEDGEMENT

This work was supported in part by Grant No. PB87-0996 from the Dirección General de Investigación Científica y Técnica (DGICYT) (Spain).

REFERENCES

1 K. K. Unger, R. Janzen and G. Jilge, *Chromatographia*, 24 (1987) 144.
2 H. G. Barth, *J. Chromatogr. Sci.*, 192 (1980) 409.
3 H. G. Barth and F. E. Regnier, *J. Chromatogr.*, 192 (1980) 275.
4 Y. Kato, K. Komiya, H. Sasaki and T. Hashimoto, *J. Chromatogr.*, 193 (1980) 311.
5 A. R. Cooper and D. S. Van Derveer, *J. Liq. Chromatogr.*, 1 (1978) 693.
6 B. Seenlund, *Adv. Chromatogr.*, 14 (1976) 37.
7 P. L. Dubin, C. M. Speck and J. I. Kaplan, *Anal. Chem.*, 60 (1988) 895.
8 M. Potschka, *J. Chromatogr.*, 441 (1988) 239.
9 Waters Chromatography Division, Millipore, *Polym. Notes*, 2, No. 1, July (1987).
10 P. L. Dubin and I. J. Levy, *J. Chromatogr.*, 235 (1982) 377.
11 F. R. Senti, N. N. Hellman, N. H. Ludwing, G. E. Babcock, R. Tobin, C. A. Class and B. L. Lamberts, *J. Polym. Sci.*, 17 (1955) 527.
12 H. G. Elias, *Kunst.-Plast.*, 4 (1961) 1.
13 E. V. Patton and D. M. Wonnacott, *J. Chromatogr.*, 389 (1987) 115.
14 C. Abad, L. Braco, V. Soria, R. Garcia and A. Campos, *Br. Polym. J.*, 19 (1987) 489.
15 S. Mori, in J. Janca (Editor), *Steric Exclusion Liquid Chromatography of Polymers* (*Chromatographic Science Series*, Vol. 25), Marcel Dekker, New York, 1984, p. 192.
16 R. Tejero, V. Soria, A. Campos, J. E. Figueruelo and C. Abad, *J. Liq. Chromatogr.*, 9 (1986) 711.
17 R. Tejero, V. Soria, B. Celda and A. Campos, *J. Chem. Soc., Faraday Trans. I*, 82 (1986) 2781.
18 T. Bleha, D. Bakos and D. Berek, *Polymer*, 18 (1977) 897.
19 J. C. Moore, *Sep. Sci.*, 5 (1970) 723.
20 L. H. Tung and J. C. Moore, in L. H. Tung (Editor), *Fractionation of Synthetic Polymers*, Marcel Dekker, New York, 1977, p. 619.
21 P. G. de Gennes, *Scaling Concepts in Polymer Physics*, Cornell University Press, New York, 1974.
22 M. Doi, *J. Polym. Sci., Polym. Phys. Ed.*, 19 (1981) 229.
23 H. Enomoto, Y. Einaga and A. Teramoto, *Macromolecules*, 18 (1985) 2695.
24 C. Abad, L. Braco, V. Soria, R. Garcia and A. Campos, *Br. Polym. J.*, 19 (1987) 501.
25 V. Soria, R. Garcia, A. Campos, L. Braco and C. Abad, *Br. Polym. J.*, 20 (1988) 115.
26 M. Rinaudo, J. Desbrieres and C. Rochas, *J. Liq. Chromatogr.*, 4 (1981) 1297.
27 F. Oosawa, in *Polyelectrolytes*, Marcel Dekker, New York, 1981, Ch. 2.
28 A. Bose, J. E. Rollings, J. M. Caruthers, M. R. Okos and G. T. Tsao, *J. Appl. Polym. Sci.*, 27 (1982) 795.
29 P. L. Dubin, *Sep. Purif. Methods*, 10 (1981) 287.
30 S. Arichi, *Bull. Chem. Soc. Jpn.*, 39 (1976) 439.
31 J. B. Berkowitz, M. Yamin and R. M. Fuoss, *J. Polym. Sci.*, 28 (1958) 69.
32 A. Yaron and A. Berger, *Biochim. Biophys. Acta*, 69 (1963) 397.

Journal of Chromatography, 461 (1989) 243–258
Elsevier Science Publishers B.V., Amsterdam — Printed in The Netherlands

CHROMSYMP. 1448

ROLE OF UNREACTED SILANOLS IN THE ADSORPTION PROPERTIES OF DERIVATIZED SILICA

GYÖRGY FÓTI, CRISTINA MARTINEZ and ERVIN sz. KOVÁTS*
Laboratoire de Chimie Technique de l'École Polytechnique Fédérale de Lausanne, CH-1015 Lausanne (Switzerland)

SUMMARY

The adsorbents studied were samples of a precipitated silica, covered with a dense layer of (3,3-dimethylbutyl)dimethylsiloxy-, (5-cyano-3,3-dimethylpentyl)-dimethylsiloxy- and tetradecyldimethylsiloxy- substituents. Deuteration of unreacted silanols across the graft was investigated, using dilute solutions of hydroxy-deuterated water, methanol and ethanol in acetonitrile. Excess adsorption isotherms of the solutes were also determined. The results suggest that access to all silanols is sterically hindered by the surface substituents but to different extents. They are accessible in a time average through occasional holes in the graft, formed by the lateral vibrational motion of the substituents.

INTRODUCTION

At the interface between silica, covered with an organyl-dimethylsiloxy monolayer that is as dense as possible, and a dilute solution of water in acetonitrile, the protons of the unreacted silanols have been shown to be easily accessible for isotope exchange across the graft[1,2]. This has been demonstrated by performing breakthrough experiments with water and deuterium oxide solutions on a chromatographic column packed with the grafted silica[1]. Based on the theory of the chromatographic process[3], the results permit the calculation of the surface concentration of the silanols accessible for H/^{2}H exchange. Using a silica modified with the same grafts as in this work, it has been shown that the extent of H/^{2}H exchange is independent of the linear flow-rate of the mobile phase at values $u_\mu < 0.6$ cm/s, and at these flow-rates it is also independent of the temperature between 20 and 80°C[2]. It has therefore been concluded that under normal experimental conditions ($u_\mu \approx 0.3$ cm/s; $T_c = 20.0$°C) all silanols exchange across the graft.

The sum of the surface concentration of reacted and unreacted silanols was the same on all adsorbents, amounting to

$$\Gamma_{OH,u} + \Gamma_{sox} = 8.44 \pm 0.10\ \mu mol/m^2 \quad (1)$$

where $\Gamma_{OH,u}$ is the surface concentration of unreacted silanols and Γ_{sox} is that of the

0021-9673/89/$03.50

organyl-dimethylsiloxy graft. This result is considered to be representative of the surface concentration of silanols on precipitated silicas. (The term "precipitated silica" refers to samples prepared in the usual way by acidification of a water-glass solution; see ref. 4, p. 554.) Eqn. 1 shows that on adsorbents usually applied in liquid–solid chromatography (Γ_{sox} = 3.6–4.2 μmol/m^2) an amount of about $\Gamma_{OH,u} \approx 4.5$ μmol/m^2 of unreacted silanols is present at the surface under the graft.

The same experiments also permitted the evaluation of points on the adsorption isotherm of water at low water concentrations. It has been repeatedly reported that water is preferentially adsorbed in this domain by grafted silicas[5–7]. In fact, at low volume fractions, $\varphi_w < 0.01$, the isotherm is characterized by a positive water adsorption, which already increases to a saturation value at $100\varphi_w = 0.2$–0.3% (v/v)[2]. Therefore, it has been proposed that on the non-polar surface there are specific adsorption sites, one site accommodating one water molecule. Application of the Everett–Klinkenberg[8,9] equation to the description of the isotherm gave $\Gamma_{Siol} = 0.7$ μmol/m^2 for water adsorption on silicas covered by the densest organyl-dimethylsiloxy layer; the subscript Siol refers to the hypothesis that these sites are silanols available for the adsorbate.

In summary, it has been shown that about 15% of the unreacted silanols are active for water adsorption. These silanols could be at particular positions with easy accessibility for components capable of forming hydrogen bonds. In a second extreme picture, every silanol might be accessible 15% of the time, owing to the vibrational motion of the graft.

In this paper, the accessibility of silanols for H/^{2}H exchange and for adsorption in dilute solutions of methanol and of ethanol is examined. It will be shown that the results are compatible with a model where the unreacted silanols are all sterically hindered so that their adsorption activity largely depends on the size of the adsorbate. Only a negligible proportion of the silanols is accessible without being sterically hindered.

The same chemically modified adsorbents were applied as in ref. 2 (see Fig. 1), grafted on two different batches of the same precipitated silica. The first adsorbent was covered by a dense layer of (3,3-dimethylbutyl)dimethylsiloxy (DMB) groups. The

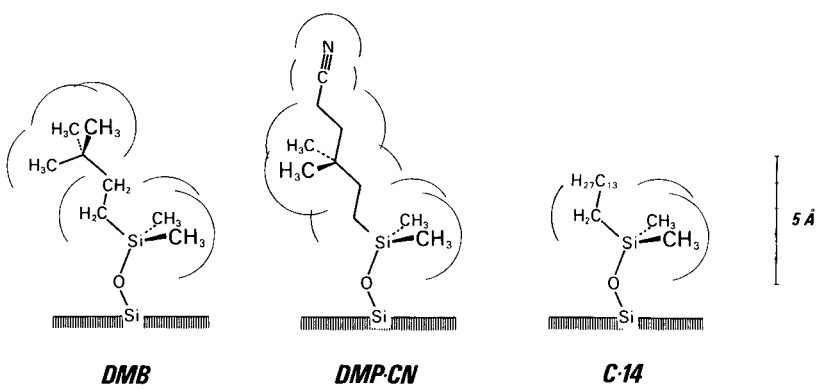

Fig. 1. The (3,3-dimethylbutyl)dimethylsiloxy (DMB), (5-cyano-3,3-dimethylpentyl)dimethylsiloxy (DMP · CN) and tetradecyldimethylsiloxy (C · 14) substituents.

surface of this adsorbent was shown to be non-polar and non-swellable; in the dense layer the dimethylmethylene base and the *tert.*-butyl head doubly shield the underlying matrix. The second adsorbent was a derivative of the DMB substituent. At the surface, covered by the (5-cyano-3,3-dimethylpentyl)dimethylsiloxy (DMP · CN) substituents, cyano groups are exposed. The surface is efficiently shielded by groups of bulky substituents, similar to the case with the DMB group. Finally, a tetradecyldimethylsiloxy (C · 14)-modified surface was chosen as an example of a long-chain covered surface. The C · 14-covered silica was preferred to the widely used C · 18-graft, because the latter shows a phase transition at about 15 ± 10°C; hence the graft is not in a well defined state at 20°C, the temperature often used in our experiments[10,11]. All adsorbents were covered with as dense a layer as possible[12–14], in contrast to the work reported in ref. 2, where the DMP · CN coverage was only about 92% of the maximum density. For surface concentrations, see Table I.

CALCULATIONS

The surface concentration of accessible unreacted silanols and that of the excess adsorption isotherm at low protic solute concentrations in acetonitrile is based on a series of breakthrough experiments. The underlaying theory is outlined in ref. 3 and is discussed in detail in ref. 2. In summary, on a chromatographic column packed with the grafted silica, first the breakthrough volume of a dilute solution of the protic solute was measured on the column containing dry acetonitrile, $V_R^{(0)}$ then, after equilibrium, the breakthrough volume of a dilute solution of the hydroxy-deuterated solute was determined to give V_R^*. The volume of the protic solute having the same number of exchangeable protons as those which were accessible at the surface for H/^{2}H exchange was calculated with the equation

$$V_{\kappa,\mathrm{exch}}\,(\mathrm{su}) = \varphi_{\mathrm{su}}[V_R^*(\mathrm{su}) - V_R^{(0)}(\mathrm{su})] \tag{2}$$

where $V_{\kappa,\mathrm{exch}}$ (su) is called the exchange capacity and φ_{su} is the volume fraction of the solute in acetonitrile. The surface concentration of the protons accessible by the protic solute for H/^{2}H exchange is given by

$$\Gamma_{\mathrm{OH,acc}}\,(\mathrm{su}) = zV_{\kappa,\mathrm{exch}}(\mathrm{su})/v_{\mathrm{su}}S \tag{3}$$

where z is the number of exchangeable protons in the solute ($z = 1$ for CH_3OH and C_2H_5OH and $z = 2$ for H_2O), v_{su} is the partial molar volume of the solute and S is the surface area of the adsorbent in the column.

The experiments were completed by determining the breakthrough volume of labelled acetonitrile on the column filled with acetonitrile. This retention volume was assumed to measure the hold-up volume, $V_{\mu/\mathrm{vNA}}$, of the system, where the subscript vNA refers to the specific Gibbs convention "*N*othing is *A*dsorbed in terms of *v*olumes", defined in the equation

$$\Psi_{\mathrm{su}} + \Psi_{\mathrm{AN}} = 0 \tag{4}$$

where Ψ is the adsorption in terms of volume per unit surface area and the subscripts su

and AN represent solute and acetonitrile, respectively[3]. Points on the adsorption isotherm were calculated with the equation

$$S\Psi_{su/vNA} = \varphi_{su}[V_R^{(0)}(su) - V_{\mu/vNA}] \tag{5}$$

If the Everett–Klinkenberg equation:

$$\Psi_{su/vNA} = \frac{\varphi_{su}\varphi_{AN}}{b + c\varphi_{su}} \tag{6}$$

is applicable (specific sites with strong adsorption affinity for the solute), the constants b and c can be determined from the linear plot of the equation

$$S\varphi_{AN}/[V_R^{(0)}(su) - V_{\mu/vNA}] = b + c\varphi_{su} \tag{7}$$

From eqn. 6, is seen that $1/b$ is the slope of the isotherm at $\varphi_{su} = 0$ and that $1/c$ is the limiting adsorption capacity of the surface for the solute where all sites accommodate a solute molecule. These sites will be identified as silanols accessible for solute adsorption. Their surface concentration in terms of moles per unit surface area is given by

$$\Gamma_{Siol} = 1/cv_{su} \tag{8}$$

where v_{su} is the partial molar volume of the solute.

In eqns. 2–8, a knowledge of the partial molar volume of the solute at high dilution, v_{su}, and the surface area of the adsorbent in the column, S, is necessary. The partial molar volume is nearly constant in the experimental domain investigated and can be calculated from the molar volume of the pure solute, v_{su}^0, as follows:

$$v_{su} = f_{su/AN}\, v_{su}^0 \qquad \text{for } \varphi_{su} \to 0 \tag{9}$$

The value of $f_{H_2O/AN} = 0.933$ was taken from ref. 15; the factors for methanol ($f_{CH_3OH/AN} = 0.988$) and ethanol ($f_{C_2H_5OH/AN} = 0.999$) were determined experimentally. These values, valid at 20.0°C, were used at all temperatures. The surface area of the adsorbent in the column was calculated on the basis of results reported in ref. 16. It has been shown that the surface area of grafted silica is nearly the same as that of the silica part in the adsorbent. The surface area of the adsorbent is therefore calculated from the molar volume of the pure solute, v_{su}^0, as follows:

$$S = m(SiO_2)s \tag{10}$$

where s is the specific surface area of the precipitated silica used as starting material. The mass of the silica in the column was calculated with the equation

$$m(SiO_2) = m\theta\{1 + 10^{-6}\,\Gamma_{sox}s[M(R) - corr]\}^{-1} \tag{11}$$

TABLE I

CHARACTERISTICS OF THE STATIONARY PHASES AND COLUMNS USED

The symbol Γ_{sox} represents the surface concentration of the organyl-dimethylsiloxy substituent, $m(SiO_2)$ is the weight of the silica part of the stationary phase, S is the surface area of the adsorbent in the column and $V_{\mu vNA}$ is the void volume, identified as the breakthrough volume AN → AN*. The DMB- and C · 14-covered adsorbents were prepared with batch 1 (s = 298 m^2/g) and the DMP · CN-covered sample with batch 2 (s = 291 m^2/g) of LiChrosorb Si 100. Standard deviations are given in the bottom row.

Stationary phase		*Column*			
Graft	Γ_{sox} ($\mu mol/m^2$)		$m(SiO_2)$ (g)	S (m^2)	$V_{\mu vNA}$ (ml)
DMB	3.90	A	1.162	346	5.11
		B	1.137	339	5.37
DMP · CN	3.96	A	1.257	366	5.28
		B	1.259	366	5.20
C · 14	4.08	A	1.172	349	5.02
		B	1.169	348	5.14
S.D.	0.02		0.002	4	0.02

where $m\theta$ is the mass of the grafted adsorbent in the column, Γ_{sox} ($\mu mol/m^2$) is the surface concentration of the graft, M(R) is the molecular weight of the organyl-dimethylsilyl radical and $corr$ = 2.5 is a correction for adsorbed water on the original silica lost and for proton substituted during silylation. The characteristics of the columns used in this study are listed in Table I.

EXPERIMENTAL

General

Silicon dioxide samples were stored and handled in a dry box (< 1 ppm of oxygen and water). Elemental analyses were made with a Perkin-Elmer Model 240 B apparatus. Nitrogen adsorption isotherms were measured with a slightly modified Sorptomatic 1800 apparatus from Carlo Erba (Milan, Italy)[17]. For further details, see refs. 2 and 18.

Materials

The precipitated silica used as starting material was batches 1 and 2 of LiChrosorb Si 100 from Merck (Darmstadt, F.R.G.) with a nominal grain diameter d_{gr} = 10 μm. BET evaluation of the nitrogen adsorption isotherm in the domain $0.05 < P_e/P_o < 0.23$ gave a specific surface area of 298 ± 3 m^2/g for batch 1 and 291 ± 3 m^2/g for batch 2. Nitrogen for adsorption experiments (99.999%) and liquid nitrogen for thermostating (99.8%) were obtained from Carbagas (Lausanne, Switzerland). The silylating agents, N-[(3,3-dimethylbutyl)dimethylsilyl]-N,N-dimethylamine, N-[(5-cyano-3,3-dimethylpentyl)dimethylsilyl]-N,N-dimethylamine and N-(tetradecyldimethylsilyl)-N,N-dimethylamine, were synthesized in our laboratory[12].

Eluent

Commercial high-performance liquid chromatographic (HPLC)-grade acetonitrile (AN) from Ammann Technik (Kölliken, Switzerland) was refluxed with phosphorus pentoxide (5.5 g for 1.5 l of acetonitrile) for 30 min and then distilled, discarding the first and last fractions of 10%. Karl Fisher titration of the distilled product gave a water content of $-0.0017 \pm 0.0065\%$ (w/w), corresponding to a maximum water content of 0.0048% ($100\varphi_W = 0.0038$).

Doubly distilled water was prepared by distilling deionized water over potassium permanganate. HPLC-grade methanol from Ammann Technik, research-grade ethanol from Fluka (Buchs, Switzerland), research-grade ^2H_2O, CH_3O^2H, $C_2H_5O^2H$ and C^2H_3CN from Chemische Fabrik Uetikon (Uetikon, Switzerland) (isotope purity > 99.5%) were used without purification.

Eluents of the appropriate composition were prepared by weighing. The volume fractions of solution pairs for isotope-exchange experiments with labelled and unlabelled solute did not differ by more than $100\Delta\varphi \approx 0.002$. Labelled acetonitrile was prepared by dissolving about 1.0% (w/w) [$^2H_3$]acetonitrite in acetonitrile. All eluents were degassed immediately before use in the bottle connected to the pump inlet by bubbling helium through the mixture. During the experiments, the mixture was kept under a slight helium overpressure (0.07 bar).

Chromatographic columns

Column materials were prepared by allowing vacuum-dried LiChrosorb Si 100 to react with the appropriate R-dimethyl(dimethylamino)silane at 180°C for 100 h, following the procedure in ref. 12. The DMB- and C · 14-covered adsorbents were prepared with batch 1 and the DMP · CN-covered sample with batch 2. For surface concentrations, Γ_{sox}, calculated from elemental analysis, see Table I.

The preparation of the columns is described in details in ref. 18. The columns were stainless-steel tubes (25.0 cm × 4.00 mm I.D.) and were packed by the slurry method (slurry in 2-propanol), then the column bed was compacted with pure methanol (C · 14) or with methanol containing 1% (w/w) of potassium bromide at 500 bar for 45 min. Two columns were packed with each adsorbent. The columns were dried after preparation at 120°C in an argon stream, and the mass of the stationary phase in the column, m_θ, was determined by weighing. The mass of silica in each column, $m(SiO_2)$, calculated with eqn. 11, is listed in Table I.

Apparatus

The solvent selector inlet of a Model 510 pump from Waters Assoc. (Milford, MA, U.S.A.) was connected to three eluent reservoirs, A, B and C. In this arrangement, solvent A could be switched to B or C by manipulating the solvent selector valve without perturbing the pressure at the pump outlet/column inlet. The pump outlet was connected to the column assembly, consisting of six columns in parallel, mounted in a thermostated bath (Model TX9 thermostat from Tamson, Zoetermeer, The Netherlands) between two Model 7060 six-way valves (Rheodyne, Cotati, CA, U.S.A.). The outlet of the column system was connected to a Model 401 differential refractometer detector of cell volume 10 μl (Waters Assoc.). The column temperature was measured as the temperature of the thermostating bath; the

long-term stability was ± 0.05 K. The flow-rate of the eluent was calculated from the time necessary to fill a calibrated glass tube, thermostated at 20.0 $\pm$ 0.1°C. The reproducibility of the flow measurement was ± 0.005 ml/min; the long-term stability of the flow-rate was $\pm 0.2\%$.

Experimental parameters

The mean column pressure, P_c, was calculated with the equation

$$P_c = P_i/2 \tag{12}$$

where P_i is the pressure at the column inlet. Typical values of P_c were 15–25 bar at a flow-rate of $\dot{V} = 1.0$ ml/min. The flow-rate, $\dot{V}$, was measured at the temperature (20.0°C) and pressure (atmospheric) of the flow meter. The retention times, t_R (= breakthrough times), were calculated from the integral average retention distances on the chart, determined by the graphical method described below. Retention volumes were calculated as

$$V_R = t_R \dot{V} \tag{13}$$

The eluent composition as a mass fraction was given by the method of preparation. The volume fraction was calculated by using the partial volume of the solute, which was calculated with eqn. 9.

Definition of the breakthrough volume, $V_R^*(su)$

When using CH_3O^2H and $C_2H_5O^2H$ as solutes, the exchange of surface protons for deuterons across the graft was never complete and depended on the time of the experiment. Therefore, for the determination of V_R^*(su), every experiment was stopped after having pumped a volume of $V_{\mu/vNA}$ + 10.0 ml of the solution of the hydroxy-deuterated solute through the column, which displaced the solution of the unlabelled solute ($\varphi_{su} = \varphi_{su*}$). After this volume, the incoming concentration of the labelled solute, $\varphi_{su*}^{(in)}$ was not attained, as seen in Fig. 2 (typical values of $\varphi_{su*}^{(out)}$ were 93–96% of $\varphi_{su*}^{(in)}$). The amount of protons exchanged in this experiment is equivalent to the volume of labelled solute, calculated as the shadowed area in Fig. 2. The volume $V_R^{(0)}$(su) was determined in a previous experiment as the breakthrough volume AN $\rightarrow$ su/AN. The evaluation was made as follows. First, the integral average retention volume, V_R^*(su), was determined by a graphical evaluation. The exchange capacity, $V_{\kappa,exch}$, calculated with eqn. 2, is then equivalent to the shadowed area. Note that, by exchanging all surface protons during the experiment (this is the case when water is used as a solute), a limiting value of V_R^*(su) would be attained. This limit is also shown in Fig. 2.

The average contact time of exchange was approximated as follows. In the actual experimental setup, the holdup volume, $V_{\mu/vNA}$, was the sum of a large holdup volume before the column, designated $V_\mu^{(pump)}$, and the effective holdup volume of the column, $V_{\mu/vNA}^{(col)}$ (typically around 2.3 ml).

$$V_{\mu/vNA} = V_\mu^{(pump)} + V_{\mu/vNA}^{(col)} \tag{14}$$

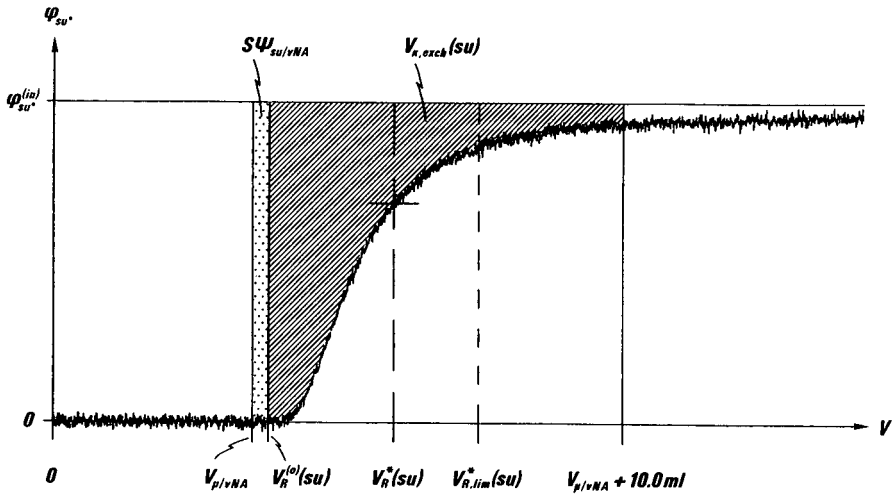

Fig. 2. Example of the graphical evaluation of a breakthrough experiment. Experimental conditions: displacement of a CH_3OH solution by CH_3O^2H solution; T_c = 40.0°C; $100\varphi_{su} = 100\varphi_{su^*} = 0.99$; $\dot{V}$ = 1.89 ml/min (see Table II). For a description of the evaluation, see text.

The experiment was conducted during the time t_{exp}:

$$t_{exp} = (V_{\mu/vNA} + 10.0)/\dot{V} \tag{15}$$

The inlet of the column was in contact with the labelled solute during the time $t_{exp} - t_{\mu}^{(pump)}$, but the effect of the exchange is observed in the detector only $t_{\mu/vNA}^{(col)} = V_{\mu/vNA}^{(col)}/\dot{V}$ later. The contact time at the end of the column with su* is $t_{exp} - t_R^*(su)$, and the effect of the exchange is seen immediately afterwards in the detector. Therefore, the average contact time of the adsorbent is approximately

$$\bar{t} = t_{exp} - \frac{1}{2}[t_{\mu/vNA} + t_R^*(su)] = \frac{1}{\dot{V}}\{10.0 - \frac{1}{2}[V_R^*(su) - V_{\mu/vNA}]\} \tag{16}$$

Experiments

In a first series of experiments, the breakthrough volumes, $V_R^{(0)}$ (AN → su/AN) and V_R^* (su/AN → su*/AN), were determined (su = methanol and ethanol) on the DMB-covered surface at constant eluent flow-rate ($\dot{V} \approx$ 1.9 ml/min) and different temperatures, ranging from 20.0 to 80.0°C. The void volume, $V_{\mu/vNA}$, was also determined (breakthrough volume AN → AN*). The exchange capacity, $V_{\kappa,exch}$, was calculated with eqn. 2; the surface concentration of protons accessible for $H/^2H$ exchange was calculated with eqn. 3. For the experimental conditions and results, see Table II.

In a second series of experiments, the breakthrough volumes, $V_R^{(0)}$ and V_R^*, were measured on the DMB-covered adsorbent with methanol and ethanol as solutes at 20.0 ± 0.1°C and different eluent flow-rates, ranging from $\dot{V}$ = 1.9 to 5.6 ml/min. For the results, see Table III.

TABLE II

SURFACE CONCENTRATION OF PROTONS ACCESSIBLE ACROSS THE DMB GRAFT FOR H/^{2}H EXCHANGE FROM DILUTE SOLUTIONS OF METHANOL AND ETHANOL IN ACETONITRILE AS A FUNCTION OF TEMPERATURE

Experimental conditions: surface area of the adsorbent, $S = 346 \pm 4$ m^2 (for other characteristics of column A, see Table I); volume fraction of the unlabelled and labelled solute in acetonitrile, $100\varphi_{CH_3OH} = 100\varphi_{CH_3OH^*} = 0.992 \pm 0.002$ and $100\varphi_{C_2H_5OH} = 100\varphi_{C_2H_5OH^*} = 0.998 \pm 0.002$. T_c = Column temperature; $\dot{V}$ = flow-rate of the eluent at 20.0 $\pm$ 0.1°C and atmospheric pressure; $V_R^{(0)}$ = breakthrough volume of a solution of methanol or ethanol in acetonitrile for a column filled with pure acetonitrile, *i.e.*, AN → su/AN, V_R^* is that for su/AN → su*/AN; $V_{\kappa,exch}$ = exchange capacity, calculated with eqn. 2; $\bar{t}$ = average contact time, calculated with eqn. 16; $\Gamma_{OH,acc}$ = surface concentration of protons accessible for H/^{2}H exchange, calculated with eqn. 3. Standard deviations are given in the bottom row.

su	T_c (°C)	$\dot{V}$ (ml/min)	$V_R^{(0)}$ (ml)	V_R^* (ml)	$V_{\kappa,exch}$ (μl)	$\bar{t}$ (min)	$\Gamma_{OH,acc}$ (μmol/m^2)
Methanol	20.0	1.912	5.51	8.03	25.0	4.48	1.81
	40.0	1.887	5.48	8.76	32.5	4.33	2.35
	60.0	1.910	5.44	9.27	38.0	4.15	2.75
	80.0	1.899	5.34	10.06	46.8	3.96	3.38
Ethanol	20.0	1.884	5.28	7.20	19.2	4.75	0.95
	40.0	1.881	5.28	8.07	27.8	4.53	1.38
	60.0	1.896	5.21	9.09	38.7	4.23	1.92
	80.0	1.885	5.15	10.69	55.3	3.83	2.74
S.D.	0.1	0.005	0.02	0.06	0.6	0.03	0.03

TABLE III

SURFACE CONCENTRATION OF PROTONS ACCESSIBLE ACROSS THE DMB GRAFT FOR H/^{2}H EXCHANGE FROM DILUTE SOLUTIONS OF METHANOL AND ETHANOL IN ACETONITRILE AS A FUNCTION OF FLOW-RATE

$T_c = 20.0 \pm 0.1$°C; other experimental conditions, column characteristics and symbols as in Table II

su	$\dot{V}$ (ml/min)	$V_R^{(0)}$ (ml)	V_R^* (ml)	$V_{\kappa,exch}$ (μl)	$\bar{t}$ (min)	$\Gamma_{OH,acc}$ (μmol/m^2)
Methanol	1.912	5.51	8.03	25.0	4.48	1.81
	2.786	5.49	7.57	20.6	3.15	1.49
	3.702	5.48	7.18	16.9	2.42	1.22
	4.568	5.53	7.09	15.5	1.97	1.12
	5.450	5.51	6.88	13.6	1.67	0.98
Ethanol	1.884	5.28	7.20	19.2	4.75	0.95
	2.765	5.30	6.85	15.5	3.30	0.77
	3.665	5.25	6.63	13.8	2.52	0.68
	4.647	5.27	6.43	11.6	2.01	0.57
	5.591	5.30	6.39	10.9	1.67	0.54
S.D.	0.005	0.02	0.06	0.6	0.03	0.03

TABLE IV

POINTS ON THE ADSORPTION ISOTHERM OF WATER, $\Psi_{W/vNA}$, ON THE DMP · CN-COVERED ADSORBENT FROM DILUTE SOLUTIONS OF WATER IN ACETONITRILE AS A FUNCTION OF THE VOLUME FRACTION OF WATER, $100\varphi_w$

For characteristics of the column DMP · CN/A, see Table I; for the symbol $V_R^{(0)}$, see Table II. Results ± standard deviations.

$100\varphi_W$	$V_R^{(0)}$ (ml)	$\Psi_{W/vNA}$ (nl/m^2)
0.142 ± 0.002	7.50 ± 0.13	8.6 ± 0.5
0.280 ± 0.002	6.53 ± 0.07	9.6 ± 0.6
0.463 ± 0.002	6.07 ± 0.04	10.0 ± 0.6
0.922 ± 0.002	5.69 ± 0.02	10.3 ± 0.7

In a third series of experiments, the breakthrough volumes, $V_R^{(0)}$, were measured on the DMP · CN-covered adsorbent with dilute solutions of water in acetonitrile at constant flow-rate ($\dot{V} \approx 1.9$ ml/min) and temperature ($T = 20.0$°C) but different water concentrations, ranging from $100\varphi_W = 0.14$ to 0.92%. The void volume, $V_{\mu/vNA}$, was also determined. Points on the adsorption isotherm, $\Psi_{su/vNA}$, were calculated with eqn. 5. For the results, see Table IV.

In a last series of experiments, the breakthrough volumes, $V_R^{(0)}$, were measured with methanol and ethanol as solutes on all adsorbents listed in Table I at constant flow-rate ($\dot{V} \approx 1.9$ ml/min) and temperature ($T_c = 20.0$°C) but different solute concentrations, ranging from $100\varphi_{su} = 0.14$ to 1.95%. The void volumes, $V_{\mu/vNA}$, were also determined. For the results, see Table V.

RESULTS AND DISCUSSION

Unreacted silanols under a triorganylsiloxy graft can be deuterated across the graft on contact with dilute solutions of hydroxy-deuterated solutes in organic solvents. There was a striking difference between deuteration with deuterium oxide solutions and that with solutions of hydroxy-deuterated methanol and ethanol. A complete isotopic exchange was achieved by using deuterium oxide at volume percentages $100\varphi_W < 1.0$ in chromatographic experiments[1,2], whereas for methanol and ethanol solutions of the same concentration the exchange was only partial and depended on the flow-rate in the chromatographic column and on the temperature of the breakthrough experiment.

In a series of experiments, a constant volume of the solution of the hydroxy-deuterated alcohol was pumped at different flow-rates through a column packed with DMB-covered adsorbent. The amount of unreacted protons exchanged for deuterons was determined from the breakthrough signal, as explained under Experimental. The results are listed in Table III. Let us now assume that there are two sorts of unreacted silanols. One sort is in a sterically unhindered position and its protons exchange easily, at a rate that can be considered to be instantaneous in the breakthrough experiment. The surface concentration of these protons is identified with that of relatively free-standing silanols, $\Gamma_{OH,free}$. A second sort of proton is found on sterically hindered silanols. These protons exchange slowly if the graft is in contact with the solution of the

TABLE V

POINTS ON THE ADSORPTION ISOTHERM OF THE SOLUTES METHANOL AND ETHANOL, $\Psi_{su/vNA}$, ON ADSORBENTS LISTED IN TABLE I, FROM DILUTE ACETONITRILE SOLUTIONS AS A FUNCTION OF THE VOLUME FRACTION OF THE SOLUTE, $100\varphi_{su}$

$T_c = 20.0 \pm 0.1°C$; $\dot{V} \approx 1.9$ ml/min. For the meaning of $V_R^{(0)}$, see Table II. Standard deviations: S.D. $(100\varphi_{su}) = 0.002$; S.D. $[V_R^{(0)}] = 0.02$ ml; the values of S.D. $(\Psi_{su/vNA})$ given in the table are valid for all series at similar compositions.

Graft	*su = methanol*			*su = ethanol*		
	$100\varphi_{su}$	$V_R^{(0)}$ *(ml)*	$\Psi_{su/vNA}$ *(nl/m²)*	$100\varphi_{su}$	$V_R^{(0)}$ *(ml)*	$\Psi_{su/vNA}$ *(nl/m²)*
DMB	*Column B:*			*Column B:*		
	0.137	6.01	2.6	0.149	5.68	1.4 ± 0.1
	0.286	5.90	4.5	0.297	5.58	1.8 ± 0.2
	0.492	5.82	6.5	0.493	5.56	2.8 ± 0.4
	0.977	5.77	11.5	0.984	5.55	5.2 ± 0.8
	1.458	5.72	15.1	1.469	5.52	6.5 ± 1.2
	1.933	5.67	17.1	1.947	5.52	8.6 ± 1.6
DMP · CN	*Column B:*			*Column A:*		
	0.137	5.87	2.5	0.149	5.56	1.1
	0.286	5.75	4.3	0.297	5.53	2.0
	0.492	5.70	6.7	0.493	5.50	3.0
	0.977	5.63	11.5	0.984	5.46	4.8
	1.458	5.58	15.1	1.469	5.46	7.2
	1.933	5.55	18.5	1.947	5.44	8.5
C · 14	*Column A:*			*Column B:*		
	0.137	5.69	2.6	0.149	5.44	1.3
	0.286	5.53	4.2	0.297	5.40	2.2
	0.492	5.50	6.8	0.493	5.35	3.0
	0.977	5.44	11.8	0.984	5.32	5.1
	1.458	5.38	15.0	1.469	5.30	6.8
	1.933	5.34	17.7	1.947	5.27	6.3

protic solute. The surface concentration of such silanols is designated $\Gamma_{OH,hin}$. The sum of the concentration of these protons is obviously equal to that of the unreacted silanols under the graft:

$$\Gamma_{OH,free} + \Gamma_{OH,hin} = \Gamma_{OH,u} \tag{17}$$

If such a grafted adsorbent were in contact with an infinite volume of a solution of the deuterated solute and if all sterically hindered protons exchanged with the same first-order rate, the time dependence of the surface concentration of protons exchanged in this experiment would be given by

$$\Gamma_{OH,acc} = \Gamma_{OH,free} + \Gamma_{OH,hin}(1 - e^{-kt}) \tag{18}$$

where k is the rate constant and t is the contact time. By plotting the logarithm of the non-deuterated fraction of the surface protons, $\ln[(\Gamma_{OH,u} - \Gamma_{OH,acc})/\Gamma_{OH,u}]$, as a function of the contact time, t, the linear plot obtained permits the determination of the constants in eqn. 18. In our breakthrough experiments, the restricted volume of the mobile phase can certainly not be considered as an infinite deuteron reservoir. Also, the real contact time is unknown. The average contact time, $\bar{t}$, calculated with eqn. 16 (see Experimental) is believed to be proportional to the true contact time. Fig. 3 shows the logarithmic plot of the non-deuterated fraction of the surface silanols as a function of the average contact time, $\bar{t}$, after the adsorbent in the column was in contact with a standard amount of hydroxy-labelled alcohol solution. The concentration of unreacted silanols of $\Gamma_{OH,u} = 4.54$ μmol/m^2 was calculated with $\Gamma_{DMB} = 3.90$ μmol/m^2 in eqn. 1. From the resulting linear plot, an apparent rate constant, $k_{app}^{(20)}$, could be calculated, valid under the given experimental conditions (20°C, $100\varphi_{su} = 1.0\%$). This is believed to be parallel to the real rate constant. The apparent rate constants and the corresponding time necessary to deuterate the surface to an extent of 50% [$t_{1/2}^{(20)} = \ln 2/k_{app}^{(20)}$] are listed in Table VI. The dependence of the rate constant on the concentration of the contacting solution was not examined. Therefore, k_{app} is only defined for the specific concentration used in these experiments. It is probable that the

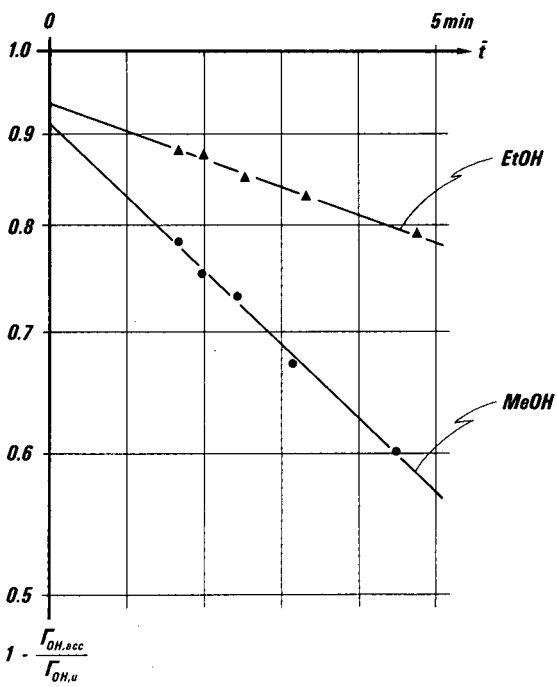

Fig. 3. Logarithmic plot of the molar fraction of the non-deuterated part of the unreacted silanols under the graft after contact with a standard amount of a dilute solution of the deuterated solute, CH_3O^2H and $C_2H_5O^2H$ ($\varphi_{su} = \varphi_{su*} = 0.010$) as a function of the average contact time, $\bar{t}$. The latter was calculated from the flow-rate with eqn. 16 (see Table III). EtOH = Ethanol; MeOH = methanol.

TABLE VI

SURFACE CONCENTRATION OF FREE-STANDING AND STERICALLY HINDERED SILANOLS, $\Gamma_{OH,free}$ AND $\Gamma_{OH,hin}$, ON DMB-COVERED SILICA, AS MEASURED BY H/^{2}H EXCHANGE

Data for water are from ref. 2. Also given are the apparent rate constants, $k_{app}^{(20)}$, and the corresponding half-life, $t_{1/2}^{(20)}$, of the exchange of the protons of the hindered silanols (under the experimental conditions T_c = 20°C and $100\varphi_{su}$ = 1.0; see Table III). The activation energies of the latter exchange, $\Delta E^{\ddagger}$, were calculated from data between 20 and 80°C (see Table II). Estimated errors (± values) are 95% confidence limits.

Solute	$\Gamma_{OH,free}$ *(μmol/m²)*	$\Gamma_{OH,hin}$ *(μmol/m²)*	$k_{app}^{(20)}$ *(min⁻¹)*	$t_{1/2}^{(20)}$ *(min)*	$\Delta E^{\ddagger}$ *(kcal/mol)*
Water	4.54 ± 0.10	0.0	–	–	–
Methanol	0.39 ± 0.16	4.15 ± 0.14	0.094 ± 0.013	7.3 ± 1.1	4.1 ± 0.4
Ethanol	0.30 ± 0.12	4.24 ± 0.06	0.036 ± 0.006	19.5 ± 3.8	6.3 ± 0.6

exchange rate is not linearly proportional to the bulk concentration but to that of the concentration of the solute in the physically adsorbed layer at the graft–solution interface. Therefore, the slower exchange with ethanol as solute might be partly due to its lower molar concentration at $100\varphi_{su}$ = 1.0 compared with methanol.

Extrapolation of the logarithmic plot in Fig. 3 to $\bar{t}$ = 0 (infinite flow-rate) gives the relative concentration of protons that do not exchange at a very short contact time, *i.e.*, the fraction of the hindered silanols $\Gamma_{OH,hin}/\Gamma_{OH,u}$. It is seen that this fraction constitutes the main part and that it is different for methanol and ethanol, being 91 and 94%, respectively. The corresponding remainder is the proportion of the "free-standing" silanols. In fact, if these silanols were really unhindered, their concentration should not depend on the size of the deuterating solute.

For the evaluation of the deuteration experiments at different temperatures it was assumed that the surface concentration of the "free silanols" seen by the individual solutes did not depend on temperature. The extent of deuteration by a constant amount of solution at one (about constant) flow-rate is listed in Table II. A knowledge of the surface concentration of $\Gamma_{OH,free}$ now allowed us to calculate apparent rate constants. These are plotted in Fig. 4 on a logarithmic scale as a function of the inverse of the absolute temperature. From the slope of the plot, an activation energy of $\Delta E^{\ddagger}$ = 4.1 and 6.3 kcal/mol was calculated for the deuteration across the graft with solutions of deuterated methanol and ethanol, respectively (see Table VI).

On the basis of these results, we conclude that the access to all unreacted silanols is sterically hindered by the dense graft. Also, there is no reason to postulate the presence of two sorts of silanols, free and hindered, as stated for the model which gave the starting picture for the evaluation of the kinetic results. Rather, it is probable that all the silanols are hindered but to different extents, and the apparent deuteration rates and activation energies are properties of an average silanol. The amplitude of the observed activation energy is of an order which might correspond to "making a hole" in the dense graft. By the vibrational motion of the substituents, access to a silanol is occasionally open. Consequently, almost every silanol is free at a certain but differing proportion of time.

In Fig. 5 are shown adsorption isotherms of methanol and ethanol from

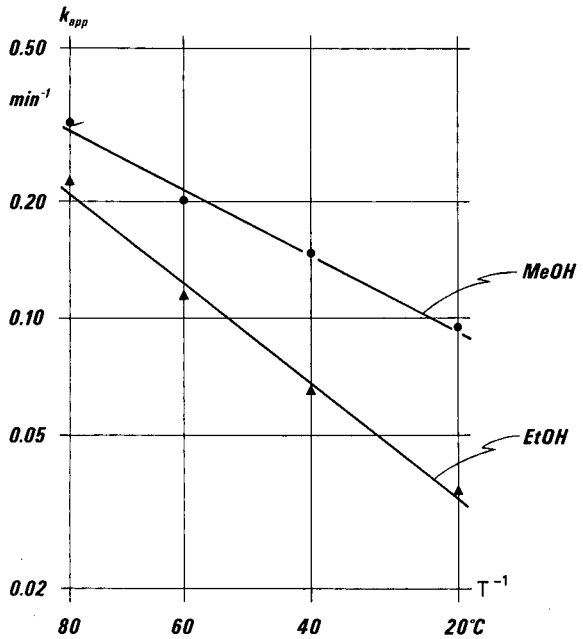

Fig. 4. Logarithmic plot of the apparent deuteration rate of the sterically hindered silanols as a function of the reciprocal of the absolute temperature. Rate constants were calculated from results in Table II.

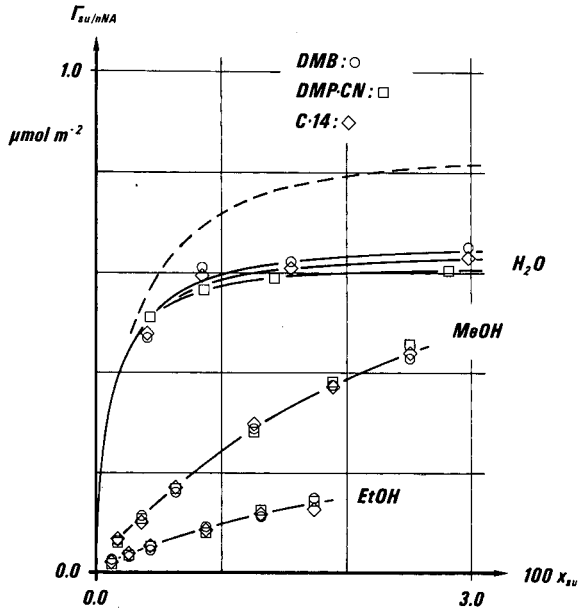

Fig. 5. Adsorption isotherms of water, methanol and ethanol from dilute solutions in acetonitrile on dense grafts of DMB, DMP · CN and C · 14 substituents on silica at 20.0°C. Isotherms, $\Gamma_{su/nNA}$, in units of μmol/m^2 were calculated from the isotherms $\Psi_{su/vNA}$ determined in units of μl/m^2. Traces of the water isotherm were calculated from the Everett–Klinkenberg representation of the adsorption and traces of the methanol and ethanol isotherms were drawn by eye. The broken line is the trace of the water adsorption isotherm on a DMP · CN graft 92% of the maximum density from ref. 2.

acetonitrile solutions at low concentrations in units of μmol/m^2. The conversion of the isotherms, determined as $\Psi_{su/vNA}$ in units of μl/m^2, was effected using eqn. 9 in ref. 2:

$$\Gamma_{su/nNA} = \Psi_{su/vNA} \cdot \frac{1}{v_\mu} \cdot \frac{x_{su}x_{AN}}{\varphi_{su}\varphi_{AN}} \tag{19}$$

where v_μ is the molar volume of the mixture of mole fraction x_{su}. For the sake of consistency, the isotherm Γ_{su} is referred to the nNA Gibbs convention "*N*othing is *A*dsorbed in terms of *n*umber of moles", defined by the equation

$$\Gamma_{su} + \Gamma_{AN} = 0 \tag{20}$$

The adsorption isotherms of water on the DMB- and C · 14-grafted silicas were taken from ref. 2. The broken line shows the trace of the description of the adsorption isotherm by the Everett–Klinkenberg equation on a DMP · CN-covered sample, where the graft was only 92% of the maximum density. The adsorption isotherm of water on a dense DMP · CN graft was determined in this work (see Tables V and VII). It is now of interest that the isotherms of different but dense grafts are very similar. For the description of the water isotherms, the following picture may be given. About 0.7 μmol/m^2 of the silanols appear as active sites for water adsorption; the sites are all occupied at water concentrations as low as $100\varphi_W \approx 0.3\%$. For the estimation of the molar surface concentration of the sites it was assumed that one site accommodates one water molecule. The adsorption isotherms of water on dense and loose DMP · CN grafts support this hypothesis. In fact, on the less dense graft (0.3 μmol/m^2), an additional amount of 0.3 μmol/m^2 of water is adsorbed at saturation.

The shape of the methanol and ethanol adsorption isotherms differs fundamentally from that of water. Because the excess adsorption is positive, it is probably that the presence of the unreacted silanols does contribute to the adsorption of the alcohols, but certainly to a lesser extent. In fact, if there were silanols without steric hindrance where the alcohols are retained by hydrogen bonds, the alcohol isotherms would be similar to that of water, *i.e.*, of the Everett–Klinkenberg type with saturation of active sites at low solute concentrations. Therefore, it can be concluded that the

TABLE VII

CONSTANTS OF THE EVERETT–KLINKENBERG EQUATION, b AND c (EQN. 6), FOR THE DESCRIPTION OF THE WATER ADSORPTION ISOTHERM, $\Psi_{W/vNA}$, FROM ACETONITRILE AT LOW VOLUME FRACTIONS ($100\varphi_W < 1.0$) ON DMP · CN-COVERED SILICAS

Data for the adsorbent covered with a loose DMP · CN-layer are from ref. 2 and those on the surface covered with a dense layer were calculated from data given in Table IV. The symbol $\Psi_{Siol} = 1/c$ is for the limiting surface concentration of water retained on specific adsorption sites; Γ_{Siol} is its molar equivalent. Errors (± values) are 95% confidence limits.

Layer	Γ_{sox} (μmol/m^2)	b (m^2/μl)	c (m^2/μl)	Ψ_{Siol} (nl/m^2)	Γ_{Siol} (μmol/m^2)
Loose	3.66 ± 0.04	0.057 ± 0.009	65 ± 10	15.4 ± 2.6	0.91 ± 0.14
Dense	3.96 ± 0.04	0.034 ± 0.004	92 ± 11	10.8 ± 1.3	0.64 ± 0.08

so-called "silanol effect" in the adsorption at the surface of grafted silicas shows a pronounced dependence on the steric environment of the proton donor/acceptor group of the adsorbate. For the adsorption of solutes from water–organic solvent mixtures, the situation might be slightly different. In fact, in these ternary systems, the water saturates the specific sites and displaces the solute molecules.

ACKNOWLEDGEMENT

This paper is part of a project supported by the Fonds National Suisse de la Recherche Scientifique.

REFERENCES

1 J. Goworek, F. Nooitgedacht, M. Rijkhof and H. Poppe, *J. Chromatogr.*, 352 (1986) 399.
2 G. Fóti and E. sz. Kováts, *Langmuir*, (1989) in press.
3 F. Riedo and E. sz. Kováts, *J. Chromatogr.*, 239 (1982) 1.
4 R. K. Iler, *The Chemistry of Silica*, Wiley, New York, 1979.
5 N. L. Ha, J. Ungvárai and E. sz. Kováts, *Anal. Chem.*, 54 (1982) 2410.
6 F. Köster, *Doctoral Thesis*, Ruhr-Universität Bochum, Bochum, 1984.
7 C. S. Koch, F. Köster and G. H. Findenegg, *J. Chromatogr.*, 406 (1987) 257.
8 D. H. Everett, *Trans. Faraday Soc.*, 60 (1964) 1803.
9 A. Klinkenberg, *Recl. Trav. Chim. Pays-Bas*, 78 (1959) 83.
10 G. Körösi and E. sz. Kováts, *Colloids Surfaces*, 2 (1981) 315.
11 D. Morel, J. Serpinet, J. M. Letoffe and P. Claudey, *Chromatographia*, 22 (1986) 103.
12 K. Szabó, N. L. Ha, Ph. Schneider, P. Zeltner and E. sz. Kováts, *Helv. Chim. Acta*, 67 (1984) 2128.
13 K. D. Lork, K. K. Unger and G. N. Kinkel, *J. Chromatogr.*, 352 (1986) 199.
14 D. Amati and E. sz. Kováts, *Langmuir*, 3 (1987) 687.
15 N. L. Ha and E. sz. Kováts, *Chromatographia*, 15 (1982) 61.
16 J. Gobet and E. sz. Kováts, *Adsorpt. Sci. Technol.*, 1 (1984) 285.
17 J. Gobet and E. sz. Kováts, *Adsorpt. Sci. Technol.*, 1 (1984) 77.
18 G. Fóti, M. L. Belvito and E. sz. Kováts, *J. Chromatogr.*, 440 (1988) 315.
19 D. Amati and E. sz. Kováts, *Langmuir*, 4 (1988) 329.

Journal of Chromatography, 461 (1989) 259–266
Elsevier Science Publishers B.V., Amsterdam — Printed in The Netherlands

CHROMSYMP. 1509

ISOCRATIC REVERSED-PHASE HIGH-PERFORMANCE LIQUID CHROMATOGRAPHY OF RIBONUCLEOTIDES, DEOXYNUCLEOTIDES, CYCLIC NUCLEOTIDES AND DEOXYCYCLIC NUCLEOTIDES

C. K. LIM* and T. J. PETERS
Division of Clinical Cell Biology, MRC Clinical Research Centre, Watford Road, Harrow, Middlesex HA1 3UJ (U.K.)

SUMMARY

An isocratic reversed-phase high-performance liquid chromatographic system is described for the separation of a relatively large number (>20) of ribonucleotides, deoxynucleotides, cyclic nucleotides and deoxycyclic nucleotides. A 25 cm × 5 mm ODS-Hypersil (5 μm particle size) column was used with methanol–triethylammonium phosphate buffer as eluent. The effects of methanol content, pH, and ionic strength of the buffer on retention and resolution of the nucleotides have been studied. The applicability of the system was demonstrated by the analysis of nucleotides in cells and tissue extracts.

INTRODUCTION

Since Horváth *et al.*[1] reported the separation of nucleotides on a pellicular ion-exchange column, much of the early high-performance liquid chromatographic (HPLC) separation of nucleotides has been based on ion-exchange chromatography[2–5]. The technique is still widely usd and has been considerably improved[6–12] with the development of microparticulate, chemically bonded anion-exchangers. Reversed-phase[13–25] and reversed-phase ion-pair chromatography[26–33] were introduced later as alternatives to ion-exchage chromatography. The nucleotides are usually separated by gradient elution chromatography and, although isocratic systems have been described, they were only for the separation of a limited number of compounds. We believe further improvement in column efficiency, resolution, and speed of analysis is possible, particularly with reversed-phase chromatography, by manipulation of the mobile phase. The present paper describes the development and application of an isocratic system, capable of simultaneously separating a relatively large number of ribonucleotides, deoxynucleotides, cyclic nucleotides and deoxycyclic nucleotides.

EXPERIMENTAL

Materials and reagents

Nucleotides were from Sigma (Poole, U.K.). Triethylamine, orthophosphoric

0021-9673/89/$03.50

acid, perchloric acid, potassium carbonate, potassium hydroxide, dipotassium hydrogenphosphate and *p*-toluenesulphonyl chloride were of AnalaR grade from BDH (Poole, U.K.). Triethylamine was redistilled over *p*-toluenesulphonyl chloride before use. Methanol was of HPLC grade from Rathburn (Walkerburn, U.K.).

Extraction of nucleotides from cells and tissues

Nucleotides were extracted from cell suspension or freeze-clamped tissue homogenate into ice-cold 20% (w/w) perchloric acid and centrifuged at 2000 *g* for 10 min. The supernatant was adjusted to pH 6.0–6.5 with an ice-cold mixture of 4 *M* potassium hydroxide and 1 *M* potassium hydrogenphosphate or a saturated solution of potassium carbonate.

High-performance liquid chromatography

A Varian Assoc. (Walnut Creek, CA, U.S.A.) Model 5000 liquid chromatograph was used with a variable-wavelength detector (Varian UV-100), set at 254 nm. The 254–280 nm wavelength ratios were measured using two detectors in series. The separation was carried out on a 25 cm × 5 mm ODS-Hypersil (5 μm particle size) column (Shandon Southern, Runcorn, U.K.) with methanol in triethylammonium phosphate buffer as eluent at a flow-rate of 1 ml/min. The buffer was prepared by adjusting the pH of orthophosphoric acid with redistilled triethylamine. Buffers of various molarity and pH were made. Sample injection was via a Rheodyne (Cotati, CA, U.S.A.) 7125 injector, fitted with a 100-μl loop.

RESULTS AND DISCUSSION

The simultaneous analysis of a wide range of nucleotides in biological materials, *e.g.*, nucleotide profile, requires gradient elution chromatography. However, in many biomedical and biochemical applications, relatively few nucleotides are measured. A highly efficient isocratic system, capable of resolving the compounds of interest from interferences, should therefore be adequate for such applications. An isocratic system is attractive, because apart from being more reproducible, it also overcomes the major problem of base-line drift common to gradient elution chromatography of nucleotides.

Of all the HPLC systems described for the separation of nucleotides, reversed-phase chromatography offers greater potential for further improvement, particularly by exploiting the solute–solvent–stationary phase interactions. The separation of a standard mixture of ribonucleotides and cyclic nucleotides on ODS-Hypersil with methanol–83.3 m*M* triethylammonium phosphate (pH 6.0) (4:96, v/v) as eluent is shown in Fig. 1. The same system was used for the separation of deoxy and deoxycyclic nucleotides (Fig. 2). The capacity ratio (k') values are shown in Table I. The speed, resolution, and the relatively large number of compounds separated clearly demonstrate the superiority of the system over other isocratic systems for nucleotides. The improvement is mainly attributed to the use of triethylammonium phosphase as the eluent buffer. Acidic amine phosphate buffers have been shown to possess properties, such as masking of residual silanol groups and acceleration of proton equilibrium, which are particularly favourable to reversed-phase chromatography[34]. The choice of triethylammonium phosphate was dictated by these considerations, as it is expected to have similar chromatographic properties. Triethylamine is, in fact, a well-known silanol-masking agent.

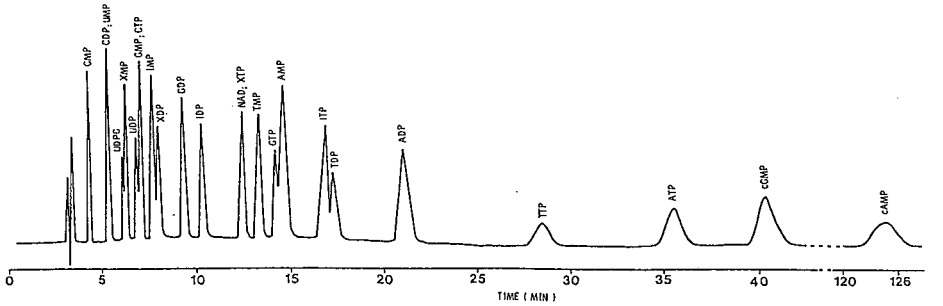

Fig. 1. Separation of a standard mixture of ribonucleotide and cyclic nucleotides. Column, ODS-Hypersil (25 cm × 5 mm I.D.); mobile phase, methanol–83.3 m*M* triethylamonium phosphate (4:96, v/v); flow-rate, 1 ml/min; detector, 254 nm.

The elution orders of cytidine < uridine < xanthosine < guanosine < inosine < thymidine < adenosine nucleotides and ribo < deoxyribo < deoxycyclic < cyclic nucleotides are in general consistent with the solvophobic theory proposed for reversed-phase chromatography with buffered eluents[35]. Thus, the more hydrophobic (less polar) nucleotides were retained longer than the less hydrophobic (more polar) ones. However, the elution order of nucleotide mono- < di- < tri-phosphates is the opposite of that expected and is similar to that observed for ion-exchange or ion-pair chromatography. This indicated a mixed retention mechanism. Ion pairing is more likely than ion-exchange chromatography, because triethylamine is an ion-pairing agent. Replacing triethylamonium phosphate with ammonium phosphate or ammonium acetate as the mobile phase buffer reverses the elution order to nucleotide tri- < di- < mono-phosphates.

Rapid separation of the more hydrophobic nucleotides can be achieved by increasing the organic modifier (methanol) content in the mobile phase (Fig. 3). The k' of cAMP, for example, was reduced from 38.2 to 8.2 when the methanol content was increased from 4 to 10% (v/v). The effect of methanol content on the k' of selected nucleotides is shown in Fig. 4. Increasing the methanol content does not necessarily imply a loss in resolution. Some nucleotide pairs, for example AMP and CTP, are actually better resolved at higher (6%) rather than lower (4%) methanol content. This is because, although increasing the methanol content decreases the k' of all nucleotides, the magnitude of this decrease is different for each nucleotide (Fig. 4), the triphosphate being more significantly affected than the di- and monophosphate nucleotides.

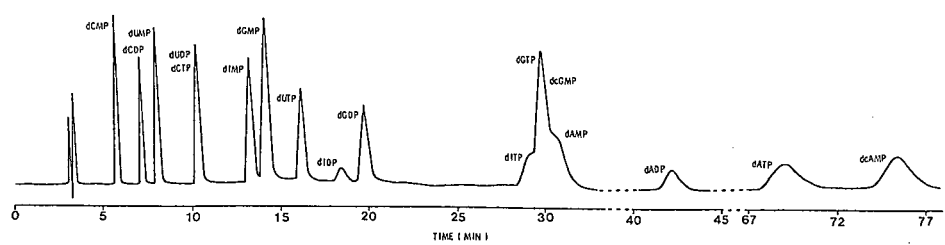

Fig. 2. Separation of a standard mixture of deoxynucleotides and deoxycyclic nucleotides. HPLC conditions as in Fig. 1.

TABLE I

CAPACITY RATIO (k') OF RIBONUCLEOTIDES, DEOXYNUCLEOTIDES, CYCLIC NUCLEOTIDES AND DEOXYCYCLIC NUCLEOTIDES ON 5-μm HYPERSIL-ODS WITH METHANOL–83.3 mM TRIETHYLAMMONIUM PHOSPHATE BUFFER (pH 6.0) (4:96, v/v) AS MOBILE PHASE

Compound	*Abbreviation*	*Capacity ratio (k')*
Cytidine 5'-monophosphate	CMP	0.4
Cytidine 5'-diphosphate	CDP	0.7
Uridine 5'-monophosphate	UMP	0.7
2'-Deoxycytidine 5'-monophosphate	dCMP	0.8
Uridine 5'-phosphoglucose	UDPG	0.9
Xanthosine 5'-monophosphate	XMP	1.0
Uridine 5'-diphosphate	UDP	1.2
2'-Deoxycytidine 5'-diphosphate	dCDP	1.2
Guanosine 5'-monophosphate	GMP	1.3
Cytidine 5'-triphosphate	CTP	1.3
Inosine 5'-monophosphate	IMP	1.4
2'-Deoxyuridine 5'-monophosphate	dUMP	1.5
Xanthosine 5'-diphosphate	XDP	1.5
Guanosine 5'-diphosphate	GDP	1.9
2'-Deoxyuridine 5'-diphosphate	dUDP	2.2
2'-Deoxycytidine 5'-triphosphate	dCTP	2.2
Inosine 5'-diphosphate	IDP	2.3
Nicotinamide adenine dinucleotide	NAD	2.9
Xanthosine 5'-triphosphate	XTP	2.9
Thymidine 5'-monophosphate	TMP	3.2
2'-Deoxyinosine 5'-monophosphate	dIMP	3.2
2'-Deoxyguanosine 5'-monophosphate	dGMP	3.4
Guanosine 5'-triphosphate	GTP	3.5
Adenosine 5'-monophosphate	AMP	3.6
2'-Deoxyuridine 5'-triphosphate	dUTP	4.1
Inosine 5'-triphosphate	ITP	4.3
Thymidine 5'-diphosphate	TDP	4.4
2'-Deoxyinosine 5'-diphosphate	dIDP	4.8
2'-Deoxyguanosine 5'-diphosphate	dGDP	5.2
Adenosine 5'-diphosphate	ADP	5.6
Thymidine 5'-triphosphate	TTP	8.0
2'-Deoxyinosine 5'-triphosphate	dITP	8.1
2'-Deoxyguanosine 5'-triphosphate	dGTP	8.3
2'-Deoxyguanosine 3':5'-cyclic monophosphate	dcGMP	8.3
2'-Deoxyadenosine 5'-monophosphate	dAMP	8.5
Adenosine triphosphate	ATP	10.1
Guanosine 3':5'-cyclic monophosphate	cGMP	11.6
2'-Deoxyadenosine 5'-diphosphate	dADP	12.3
2'-Deoxyadenosine 5'-triphosphate	dATP	20.7
2'-Deoxyadenosine 3':5'-cyclic monophosphate	dcAMP	22.6
Adenosine 3':5'-cyclic monophosphate	cAMP	38.2

The retention and resolution of the nucleotides may also be controlled by adjusting the pH of the buffer. Maximum retention and resolution of the purine nucleotides were between pH 4.5–6.0 (Fig. 5). The ionic strength of the buffer also affected retention and resolution (Fig. 6) but to a lesser extent than the pH. Buffers of between 80–85 mM are recommended for the present system.

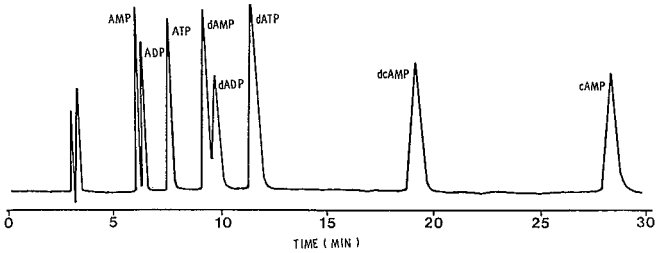

Fig. 3. Rapid separation of adenine nucleotides. Mobile phase, methanol–83.3 m*M* triethylammonium phosphate (pH 6.0) (10:90, v/v). Other HPLC conditions as in Fig. 1.

The applicability of the method is demonstrated by the analysis of nucleotides in cells and tissue extracts (Fig.7). The major nucleotides were clearly separated from impurities. The peaks were identified by chromatography after addition of standards and confirmed by absorbance ratio measurements at 254 and 280 nm.

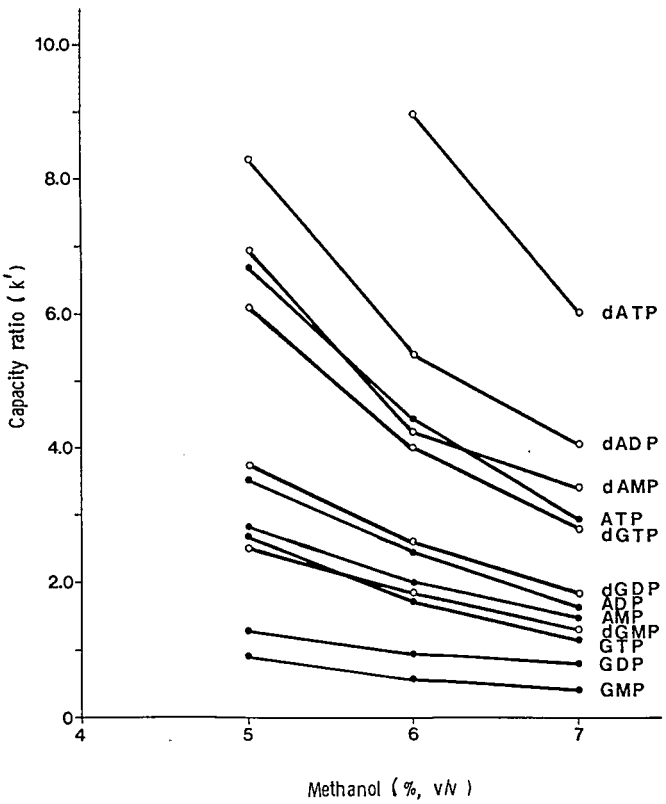

Fig. 4. Effect of methanol content on the retention and resolution of nucleotides. Mobile phase, methanol–83.3 m*M* triethylammonium phosphate (pH 5.0).

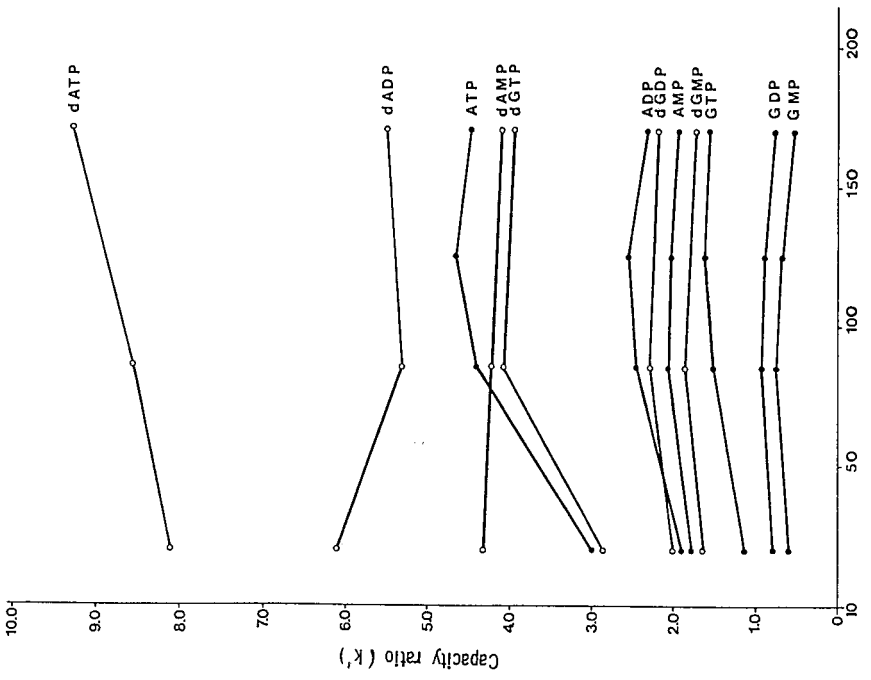

Fig. 5. Effect of pH on capacity ratios of nucleotides. Mobile phase, methanol–83.3 m*M* triethylammonium phosphate (6:94, v/v).

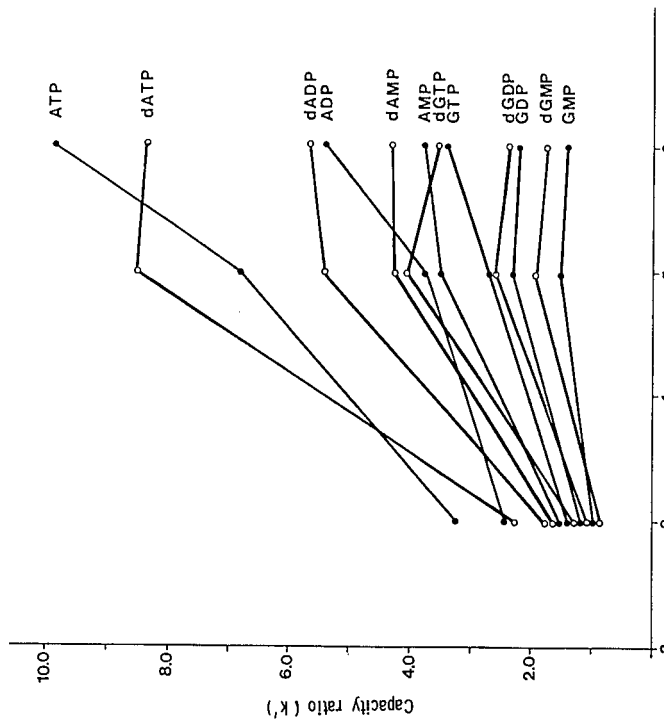

Fig. 6. Effect of triethylammonium phoshate buffer concentration on the retention of nucleotides. Mobile phase, methanol triethylammonium phosphate (pH 5.0) (6:94, v/v).

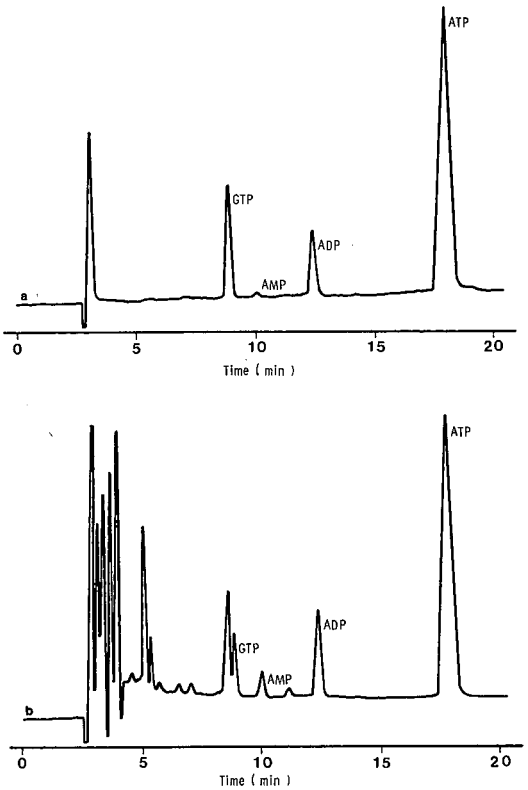

Fig. 7. Separation of nucleotides in (a) rat brown adipose tissue and (b) human lymphocytes. Column, ODS-Hypersil; eluent, methanol–83.3 m*M* triethylammonium phospate (pH 6.0) (6:94, v/v).

CONCLUSIONS

Triethylammonium phosphate is an excellent mobile phase buffer for reversed-phase chromatography of nucleotides. Isocratic systems with methanol in triethylammonium phosphate of controlled pH and ionic strength as mobile phases allowed rapid separation of more than twenty nucleotides without base-line drift. The retention mechanism is a mixed one, involving hydrophobic interaction and ion-pair formation. The system is suitable for a wide range of biomedical and biochemical applications.

ACKNOWLEDGEMENT

We are grateful to Mrs. Sheila Kingsley for secretarial assistance.

REFERENCES

1 Cs. Horváth, B. A. Preiss and S. R. Lipsky, *Anal. Chem.*, 39 (1967) 1422.
2 J. J. Kirkland, *J. Chromatogr. Sci.*, 8 (1970) 72.
3 P. R. Brown, *J. Chromatogr.*, 52 (1970) 257.
4 A. C. Burtis, M. N. Munk and F. R. McDonald, *Clin. Chem.*, 16 (1970) 667.

5 R. A. Henry, J. A. Schmit and R. C. Williams, *J. Chromatogr. Sci.*, 11 (1973) 358.
6 R. A. Hartwick and P. R. Brown, *J. Chromatogr.*, 12 (1975) 651.
7 M. McKeag and P. R. Brown, *J. Chromatogr.*, 152 (1978) 253.
8 D. Perrett, *Chromatographia.*, 16 (1982) 211.
9 R. A. De Abreu, J. M. Van Baal and J. A. Bakkeren, *J. Chromatogr.*, 227 (1982) 45.
10 E. G. Brown, P. R. Newton and N. W. Shaw, *Anal. Biochem.*, 123 (1982) 378.
11 P. D. Reiss, P. F. Zuurendonk and R. L. Veech, *Anal. Biochem.*, 140 (1984) 162.
12 H. Engelhardt and E. Schweinheim, *Chromatographia.*, 22 (1986) 425.
13 J. L. Hodge and E. F. Rossomando, *Anal. Biochem.*, 102 (1980) 59.
14 P. D. Schweinsberg and T. L. Loo, *J. Chromatogr.*, 181 (1980) 103.
15 M. Zakaria and P. R. Brown, *J. Chromatogr.*, 226 (1981) 267.
16 H. Martinez-Valdez, R. M. Kothari, H. V. Hershey and M. W. Taylor, *J. Chromatogr.*, 247 (1982) 307.
17 D. L. Ramos and A. M. Schoffstall, *J. Chromatogr.*, 261 (1983) 83.
18 P. R. Brown and A. M. Krstulovic, *Anal. Biochem.*, 99 (1979) 1.
19 M. Zakaria and P. R. Brown, *J. Chromatogr.*, 255 (1983) 151.
20 M. Zakaria, P. R. Brown and E. Grushka, *Anal. Biochem.*, 55 (1983) 457.
21 P. J. M. van Haastert, *J. Chromatogr.*, 210 (1981) 229.
22 P. J. M. van Haastert, *J. Chromatogr.*, 210 (1981) 241.
23 V. Stocchi, L. Cucchiarini, M. Magnani, L. Chiarantine, P. Palma and G. Crescentini, *Anal. Biochem.*, 146 (1985) 118.
24 C. L. Willis, C. K. Lim and T. J. Peters, *J. Pharm. Biomed. Anal.*, 4 (1986) 247.
25 J. Kehr and M. Charko, *Fresenius' Z. Anal. Chem.*, 325 (1986) 466.
26 N. E. Hoffman and J. C. Liao, *Anal. Chem.*, 49 (1977) 2231.
27 T. F. Walseth, G. Graff, M. C. Moos and N. D. Goldberg, *Anal. Biochem.*, 107 (1980) 240.
28 J. H. Knox and J. Jurand, *J. Chromatogr.*, 203 (1981) 85.
29 E. J. Jeungling and H. Kammermeier, *Anal. Biochem.*, 102 (1980) 358.
30 S. M. Payne and B. N. Ames, *Anal. Biochem.*, 123 (1982) 151.
31 J. P. Caronia, J. B. Crowther and R. A. Hartwick, *J. Liq. Chromatogr.*, 6 (1933) 1673.
32 J. Kehr and M. Chavko, *J. Chromatogr.*, 345 (1985) 267.
33 T. Kremmer, M. Boldizsár and L. Holczinger, *J. Chromatogr.*, 415 (1978) 53.
34 W. R. Melander, J. Stoveken and Cs. Horváth, *J. Chromatogr.*, 185 (1979) 111.
35 Cs. Horváth, W. Melander and I. Molnár, *J. Chromatogr.*, 125 (1976) 129.

Journal of Chromatography, 461 (1989) 267–270
Elsevier Science Publishers B.V., Amsterdam — Printed in The Netherlands

CHROMSYMP. 1455

DETERMINATION OF ELASTASE ACTIVITY BY REVERSED-PHASE HIGH-PERFORMANCE LIQUID CHROMATOGRAPHY

THEODORE A. STEIN*, JON R. COHEN, CHARLOTTE MANDELL and LESLIE WISE
**Department of Surgery, Long Island Jewish Medical Center, New Hyde Park, NY 11042 (U.S.A.), and State University of New York, Stony Brook, NY (U.S.A.)*

SUMMARY

The action of elastase on elastin was measured by high-performance liquid chromatography with on-line post-column derivatization. After alkaline hydrolysis, a 20-ml sample was injected into a ODS-2 gel column. An elastin-specific dipeptide, Val-Pro, and the internal standard, Gly-Leu, were eluted by a linear gradient of 0 to 10% of 1-propanol in 50 m*M* heptafluorobutyrate (pH 3) at a flow-rate of 1 ml/min. The eluent was reacted with fluorescamine, and the fluorescent products were measured. Retention times for Val-Pro and Gly-Leu were 17.33 and 23.54 min. The peak areas of 0.2–16 μg of Val-Pro gave a straight-line plot. Elastase activity was constant from 6 to 24 h and was 0.95 ± 0.02 (S.D.) μg/h. The method may be useful for the measurement of the elastolytic activity in some diseased tissues.

INTRODUCTION

Elastolytic activity has been identified in the pancreas, polymorphonuclear leukocytes, platelets, alveolar macrophages, fibroblasts, and several microorganisms[1–3]. In some tissues several isoenzymes of elastase also exist. The human and porcine pancreas contain two elastases and two proelastases[1,3]. Polymorphonuclear leukocytes from humans contain at least three isoenzymes[1]. The elastolytic activity measured in pathological specimens may thus be due to the combined effect of many different elastolytic proteases. In addition, the presence of other proteases, such as trypsin and chymotrypsin, will enhance the total elastolytic activity[1,4].

It has been suggested that alterations in elastin breakdown occur in such clinical entities as emphysema, abdominal aortic aneurysms, and pancreatitis[5–9]. Since the disease process may involve several elastases, the determination of the elastolytic activity in these specimens should be performed by solubilizing elastin. However, there have been some technical difficulties with the use of insoluble elastin for the measurement of elastase activity[1]. Gravimetric, nephelometric, and spectrophotometric methods of measuring the amount of soluble elastin have been inaccurate, and are at best semi-quantitative. In order to improve the assay, elastin has been derivatized with various dyes, fluorescent agents and radioactive isotopes[1,2]. However, the

0021-9673/89/$03.50

assays measure a group leaving from elastin and should not be considered elastolytic methods. Although there are several different structural types of elastin, based upon the amino sequence, some dipeptides occur in high frequency in hydrolysates of elastin[10]. One of these dipeptides is L-valyl-L-proline (Val-Pro), and 44 of these doublet sequences are present in 1000 amino acid units of bovine ligamentum nuchae elastin[11]. We report here a method by which the elastolytic activity of a biological specimen can be measured by determining the amount of Val-Pro solubilized from elastin.

EXPERIMENTAL

Materials

The high-performance liquid chromatographic (HPLC) system with an on-line post-column reaction device consisted of an automatic injector (Model 712), an automatic gradient controller (Model 680), two mobile-phase pumps (Models 510 and 501), a 250 × 4.6 mm I.D. Partisil ODS-2 column, two post-column pumps, two mixing T-pieces, two reaction coils, and a fluorescence detector (Model 420), all of which were purchased from the Waters Chromatography Division of Millipore (Milford, MA, U.S.A.).

Bovine ligamentum nuchae elastin, procine pancreatic elastase (Type IV), tris (hydroxymethyl)aminomethane (Tris), L-valyl-L-proline, glycyl-L-leucine, potassium hydroxide, sodium hydroxide, heptafluorobutyric acid, boric acid, sodium borate, and fluorescamine were obtained from Sigma (St. Louis, MO, U.S.A.), perchloric acid and hydrochloric acid from Mallinckrodt (St. Louis, MO, U.S.A.), 1-propanol from Burdick & Jackson Labs. (Muskegon, MI, U.S.A.), polypropylene test-tubes from Sarstedt (Princeton, NJ, U.S.A.), and a stainless-steel Swinney filter holder (13 mm) and nylon membranes (0.45 μm) from Rainin Instrument (Woburn, MA, U.S.A.).

Methods

Elastin (9 mg) was weighed out and suspended in 2 ml of sterile 0.2 *M* Tris–HCl buffer (pH 8.0). The hydrolysis of elastin was initiated by adding 28 units of the elastase, and incubating at room temperature. The final reaction volume was 2.2 ml. To obtain the zero time sample, the solution was mixed with a Vortex mixer before 0.5 ml of the reaction mixture was removed. This was immediately mixed with 0.5 ml of 0.4 *M* perchloric acid. At 6, 24, and 48 h, additional 0.5-ml portions of the reaction mixture were similarly withdrawn and added to the centrifuge tubes containing 0.5 ml of 0.4 *M* perchloric acid. After centrifugation at 3000 *g* for 10 min, the supernatant was decanted into 4 ml of 4 *M* potassium hydroxide, and incubated at 110°C for 18 h to obtain complete hydrolysis of the peptides, due to the elastolytic action. After neutralization with perchloric acid, the suspension was centrifuged as before, and the supernatant was decanted into another tube. The potassium perchlorate precipitate was washed twice with 0.5 ml of water and combined with the supernatant. The pooled solution was filtered through a 0.45-μm membrane to remove fine particles.

Standards

The internal standard, glycyl-L-leucine (Gly-Leu), and L-valyl-L-proline (Val-

Pro) were solubilized in water at a concentration of 1 mg/ml and were stored at –70°C. Dilutions with water for the assay were made daily. Val-Pro dilutions varied from 1 to 1000 μg/ml, and 100 μg/ml Gly-Leu were added to each standard. With an injection volume of 20 μl, 0.02–200 μg of Val-Pro, and 2 μg of Gly-Leu were injected into the column.

Chromatographic conditions

The method of Muramoto was modified, and an on-line post-column reaction was used to facilitate the collection of data[12]. The column was equilibrated at room temperature with 50 m*M* heptafluorobutyrate (pH 3.0) before each injection, at a flow-rate of 1 ml/min. After sample or standard injection, the dipeptides were separated by passing the equilibrating solution through the column for 5 min, and then adding 1-propanol to the mobile phase to produce a linear gradient of 0 to 10% of the alcohol in the initial solution over a period of 30 min. The post-column on-line derivatization of the dipeptides was obtained by mixing the mobile phase with 0.2 *M* borate buffer (pH 8.6) at af flow-rate of 50 μl/min. Fluorescamine, in a concentration of 0.2 mg/ml methanol, was then added at 75 μl/min. After mixing, the fluorescamine–Val-Pro reaction proceeded rapidly in the coil. The fluorescent products were determined at an excitation wavelength of 395 nm and with an emission filter with a 455-nm cutoff. Samples and standards were measured in triplicate. The column was again equilibrated with the initial mobile phase, and samples were injected at 50-min intervals.

Calculations

Alkaline hydrolysis of elastin produces a mixture of amino acids and the alkaline-resistant Val-Pro. However, during hydrolysis, the dipeptide has a tendency to cyclize and form a diketopiperazine[11]. Several investigators have demonstrated that

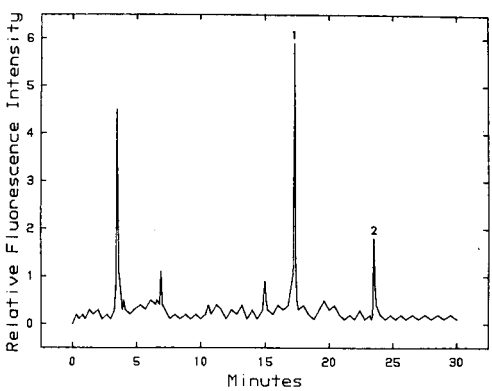

Fig. 1. Elution of 10 μg of L-valyl-L-proline (1) and 2 μg of glycyl-L-leucine (2) at retention times of 17.33 and 23.54 min, respectively. A 20-μl sample was injected into a ODS-2 gel column (250 × 4.6 mm I.D.). The dipeptides were eluted with 50 m*M* heptafluorobutyrate (pH 3) at a flow-rate of 1 ml/min for 5 min, and then by a linear gradient of 0 to 10% of 1-propanol in the heptafluorobutyrate for 30 min. Using two post-column pumps, mixing T-pieces, and reaction coils, the eluent was mixed with borate buffer (pH 8.6) and fluorescamine. The fluorescent products were measured at an excitation wavelength of 395 nm and with a 455-nm cutoff emission filter.

the two forms exist in a 1:1 ratio[10,13,14]. Since the diketopiperazine does not react with fluorescamine, only the Val-Pro peak was measured and used as the index of elastin hydrolysis. The arithmetic mean and standard deviation were calculated for each time period.

RESULTS

The retention times for Val-Pro and Gly-Leu were 17.33 and 23.54 min, respectively (Fig. 1). When the peak areas of the standards of Val-Pro were plotted against the concentrations, a straight line was obtained from 0.2 to 16 μg. The peak areas of the elastolytic products, which corresponded to the retention times of Val-Pro, were determined. The amount of Val-Pro released from elastin was calculated to be 0.95 ± 0.02 μg/h over the 48-h assay period. At 6 h, the rate was 1.00 μg/h, and at 48 h the rate was 0.94 μg/h.

DISCUSSION

Quantitation of elastolytic activity in biological specimens can be accomplished by measuring the breakdown of elastin, and determining the amount of Val-Pro which has been released. In this study, a "purified" porcine elastase, which contains elastase I, elastase II and trypsin activity, has been used to demonstrate the usefulness of the method. The rate of elastin hydrolysis is essentially constant from 6 to 48 h.

A chromatographic method comprising automatic injection, gradient elution, and on-line post-column derivatization permitted the assay of ten samples or standards in triplicate per 24 h. The elution of Val-Pro and Gly-Leu occurred in less than 25 min. In order to re-equilibrate the column, an additional 25 min was required before the next sample could be injected. This method may be useful in the measurement of the elastolytic activity of tissues and, in particular, specimens containing multiple proteolytic activities, such as the emphysematous lung, aneurysmal aorta, and septic pancreas.

REFERENCES

1 J. Bieth, in L. Robert (Editor), *Frontiers of Matrix Biology*, Vol. 6, S. Karger, Basel, 1978, p. 1.
2 B. S. Hartley and D. M. Shotton, in P. D. Boyer (Editor), *The Enzymes*, Vol. 3, Academic Press, New York, 3rd ed., 1971, Ch. 10, p. 323.
3 A. J. Barrett and J. K. McDonald, *Mammalian Proteases*, Vol. 1, Academic Press, New York, 1980, p. 32.
4 J. A. Foster, E. Bruenger, W. R. Gray and L. B. Sandberg, *J. Biol. Chem.*, 248 (1973) 2876.
5 J. S. Campa, R. M. Greenhalgh and J. T. Powell, *Atherosclerosis*, 65 (1978) 13.
6 T. T. Andreassen and H. Oxlund, *Acta Endocrinol. (Copenhagen)*, 115 (1978) 338.
7 M. Galdston, A. Janoff and A. L. Davis, *Am. Rev. Respir. Dis.*, 107 (1973) 718.
8 M. C. Geokhos, *Arch. Pathol.*, 86 (1968) 127.
9 R. W. Busuttil, H. Rinderbriecht, A. Flesher and C. Carmack, *J. Surg. Res.*, 32 (1982) 214.
10 G. Crombie, J. A. Foster and C. Franzblou, *Biochem. Biophys. Res. Comm.*, 512 (1973) 1228.
11 D. A. Keith, M. A. Paz and P. M. Gallop, *Biochem. Biophys. Res. Comm.*, 87 (1979) 1214.
12 K. Muramoto, J. Ramachandran, J. Hall, A. Hui and R. Stern, *Conn. Tiss. Res.*, 12 (1984) 307.
13 D. J. Cannon, *Ph.D. Dissertation*, Boston University, Boston, 1968.
14 P. V. Hauschka and P. M. Gallop, *Anal. Biochem.*, 92 (1979) 61.

Journal of Chromatography, 461 (1989) 271–275
Elsevier Science Publishers B.V., Amsterdam — Printed in The Netherlands

CHROMSYMP. 1476

Note

Purification of angiotensin-converting enzyme by gel high-performance liquid chromatography

QING CHENG MENG*, STEVEN J. KING and YIU-FAI CHEN
Hypertension Program of the Division of Cardiovascular Disease, Department of Medicine, University of Alabama at Birmingham, Birmingham, AL 35294 (U.S.A.)
LAWRENCE J. DELUCAS
Institute of Dental Research, Macromolecular Chrystallography and Department of Optometry, University of Alabama at Birmingham, Birmingam, AL 35294 (U.S.A.)
and
SUZANNE OPARIL
Hypertension Program of the Division of Cardiovascular Disease, Department of Medicine, University of Alabama at Birmingham, Birmingham, AL 35294 (U.S.A.)

Angiotensin-converting enzyme (ACE) (peptidyldipeptide hydrolase, E.C. 3.4.15.1) is a high-molecular-weight (*ca.* 150 kDa) glycosolated integral membrane protein, located on the luminal surface of the plasma membrane of endothelial cells and of other cell types, such as the epithelial cells of the kidney proximal tubules, seminiferous tubules of the testis, neurons and gut epithelial cells. Although ACE is an abundant membrane protein, it has proved difficult to isolate and purify.

Several approaches, including extensive chromatographic steps with DEAE-cellulose, Sephacryl, hydroxyapatite, phenyl-Sepharose and chromotofocusing, have been utilized to purify ACE[1,2]. These methods are time consuming and produce low yields of purified ACE, necessitating the use of large amounts of starting material. Affinity chromatography with active site directed inhibitors of ACE, such as lisinopril {N^{α}-[(*S*)-1-carboxy-3-phenylpropyl]-L-lysyl-L-proline}, has also been used to purify ACE[3–5]. Affinity chromatography is superior to conventional chromatographic methods in that it reduces the number of steps and the time required for purification of the enzyme. Further, the yield of purified enzyme is increased following purification by affinity chromatography, possibly owing to the time involved and/or reduced handling steps.

Previous work in our laboratory indicated that exposure of cultured porcine pulmonary artery endothelial cells to chronic normobaric hypoxia causes an increase in cell-associated ACE antigen without an increase in ACE activity[6]. This observation raises the possibility that an inactive form of ACE is synthesized by endothelial cells that are cultured under hypoxic conditions. Purification schemes based on active-site-directed affinity chromatography may therefore yield lower ACE levels than a scheme that does not require the binding of an affinity ligand to the active site of ACE.

The purification scheme illustrated in this study provides a rapid, quantitative method of isolating ACE from cultured endothelial cells. Further, this method

0021-9673/89/$03.50

provides a means of investigating ACE synthesis in small amounts of starting material, thus facilitating the study of regulation of the ACE synthesis.

EXPERIMENTAL

Cell culture

Porcine pulmonary artery endothelial cells were isolated and cultured as previously described[7]. Briefly, pulmonary arteries were dissected from intact porcine heart–lung combinations, obtained from a local slaughterhouse. The vessels were rinsed in Dulbecco's phosphate-buffered saline (DPBS) (pH 7.4) and then filled with 1% collagenase solution in DPBS. The collagenase filled vessels were incubated for 20 min at room temperature. Vessels were then massaged, and the released endothelial cells were removed by pipet and centrifuged at 500 *g* for 5 min at room temperature. Pellets were resuspended in complete medium [Medium 199 (GIBCO, Grand Island, NY, U.S.A.), 200 U/ml penicillin, 150 U/ml streptomycin, 4.76 mg/ml 4-(2-hydroxyethyl)-1-piperazinethanesulfonic acid (HEPES), 2.2 mg/ml sodium hydrogencarbonate, 0.29 mg/ml L-glutamine, 10% heat deactivated fetal calf serum (Armour Pharmaceutical, Tarrytown, NY, U.SA. (pH 7.4)] and seeded into 35-mm dishes, previously coated with fibronectin[8]. The medium was changed every other day, and cells were grown to confluence in an atmosphere of carbon dioxide–air (5:95) at 37°C.

Two days after the cultures reached confluence, two 35-mm dishes were harvested by scraping the cell sheets in 1.5 ml of DPBS (pH 7.4) and 50 U/ml of aprotinin and transferred into a 15-ml centrifuge tube. The dishes were washed with the same buffer and the washings were combined with the previous cell suspension. Cells were centrifuged at 500 *g* for 10 min at room temperature. The resulting pellet was resuspended in 250 μl of buffer, containing PBS (pH 7.4), 0.15 *M* sodium chloride, 1% bovine serum albumin (BSA), 0.5% Nonidet P-40 (Sigma, St. Louis, MO, U.S.A.) and 50 U/ml aprotinin. The cell suspension was kept on ice for 1 h with intermittent mixing, followed by centrifugation at 9000 *g* for 10 min at 4°C. The resulting supernatant was centrifuged at 28 000 *g* for 2 h at 4°C. After centrifugation, the supernatant was dialyzed (10 000 mol. wt. cutoff) overnight against 4 l of the mobile phase 0.041 *M* disodium hydrogenphosphate (Na_2HPO_4)–0.019 *M* sodium dihydrogenphosphate (NaH_2PO_4)–0.15 *M* sodium sulfate (Na_2SO_4), adjusted to pH 6.8 and then injected directly into the high-performance liquid chromatographic (HPLC) column.

Chromatography

HPLC experiments were performed with a Beckman 165 system (Model 165 variable-wavelength detector, operated at 280 nm, Model 112 solvent-delivery module, Kipp and Zonen BD 41 recorder, Rheodyne Model 340 injector). A Bio-Sil TSK-250 HPLC gel 30 × 7.5 mm I.D. column (Bio-Rad Labs., Richmond, CA, U.S.A.) was employed. Standard protein samples were obtained from Bio-Rad Labs. and included thyroglobulin (bovine), 670 kDa, γ-globulin (bovine), 158 kDa, ovalbumin (chicken), 44 kDa, myglobin (equine), 17 kDa and vitamin B_{12}, mol. wt. 1350. The mobile phase consisted of 0.041 *M* Na_2HPO_4–0.019 *M* NaH_2PO_4–0.15 *M* Na_2SO_4, adjusted to pH 6.8. All measurements were conducted at ambient temperature (25°C). The purity of the ACE was determined by sodium dodecylsulfate polyacrylamide gel electrophoresis (SDS-PAGE), Western blotting and HPLC.

Enzyme assay

Catalytically active ACE molecule were identified and quatitiated by measuring the binding of [^{125}I]351A [N$^{\alpha}$-(1-carbonyl-3-phenylpropyl)-L-lysyl-L-proline] (Merck, Sharp and Dohme Research Labs., West Point, PA, U.S.A.), a highly specific active-site-directed inhibitor of ACE, essentially as described by Tikkanen *et al.*[9]. To duplicate tubes, 100 μl of assay buffer (PBS, 100 μM zinc chloride, pH 7.4), 100 μl of sample and 20 μl of [^{125}I]351A stock solution (*ca.* 200 000 cpm) were added, and the samples were incubated at 37°C in a shaking water-bath for 2 h. After incubation, the tubes were placed on ice and 400 μl of ice-cold dextran-coated charcoal, kept in suspension by a magnetic stirrer, were added and kept on ice for 10 min. Ice-cold assay buffer (500 μl) was then added to each tube and the samples were mixed on a vortex mixer and centrifuged at 1000 *g* for 10 min at 4°C. The supernatants were transferred to clean tubes and their radioactivity was determined in a gamma counter. For the determination of non-specific binding, lisinopril (Merck, Sharp and Dohme) was added to the assay buffer at a final concentration of 1 μM. All other steps were as described above. Electrophoresis was performed in the presence of 0.1% SDS on a slab gel containing 7.5% acrylamide according to the method of Laemmli.[10] Protein was identified by silver staining or transfer to nitrocelluose by Western blotting and probing with a polyclonal antibody against porcine lung ACE.

RESULTS AND DISCUSSION

Fig. 1 is a representative HPLC trace of an extract of confluent porcine pulmonary artery endothelial cells obtained under the conditions described above. The equation for the resolution, R_s, is

$$R_s = 2 \cdot \frac{t_{R1} - t_{R2}}{W_1 + W_2}$$

where W_1 and W_2 are the band widths determined by the intersection of the tangents of the inflection points of the Gaussian peaks with the baseline and t_R is the retention time of a peak measured from the start. The resolution obtained by HPLC is 1.24, indicating satisfactory separation of ACE from other proteins. After collection of the peaks, the ACE activity was determined by using [^{125}I]351A as the ligand. Peak 2 was found to contain catalytically active ACE[3].

Silver stained SDS-PAGE of peak 2 shows a single major band with the same mobility as porcine lung ACE isolated using active-site-directed affinity chromatography. Peaks 1 and 3 show no ACE band by silver-stained SDS-PAGE analysis. Further Western blot analysis using polyclonal antibody against affinity purified ACE shows a single band corresponding to peak 2, which has the same electrophoretic mobility as affinity-purified porcine lung ACE. The molecular weight of the ACE band determined by SDS-PAGE analysis is 150–160 kDa. We obtained the molecular weight of the protein in peak 2 (Fig. 1) (catalytically active ACE) by constructing a calibration graph with proteins from 1350 to 670 000 kDa (Table I). The ACE-containing peak shows a retention volume of 7.40, corresponding to a molecular weight of 150–160 kDa, consistent with that found for ACE isolated using

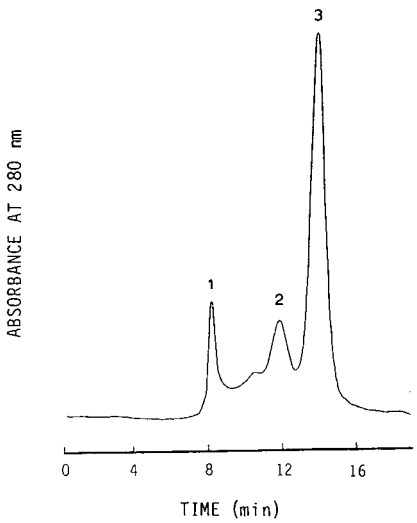

Fig. 1. Separation of angiotensin-converting enzyme (peak 2) from endothelial cells. Column: Bio-Sil TSK-250, 300 mm × 7.5 I.D.; eluent, 0.041 *M* Na_2HPO_4–0.019 *M* NaH_2PO_4–0.15 *M* Na_2SO_4 (pH 6.8); flow-rate, 0.6 ml/min; temperature, 25°C.

active-site-directed affinity chromatography in our laboratory and with the value reported in the literature for lung ACE.

The ACE purification scheme described in this paper provides a rapid, quantitative method of isolating ACE from cultured endothelial cells, although ACE is not purified to homogeneity by a single pass through the gel column. However, this method provides substantial enrichment of ACE, making possible studies of ACE synthesis and metabolism in small amounts of cultured endothelial cells. When combined with pulse labeling of the cultures with [^{35}S]methionine or [^{3}H]leucine, the method described provides a sample well suited for analysis by two-dimensional electrophoresis, followed by autoradiography. Application of this method appears to be limited to cultured endothelial cells. It is not applicable to use with tissue samples because of low yields, owing to the presence of a large proportion of non-ACE-containing cells.

TABLE I
STANDARD CURVE OF MOLECULAR WEIGHT AND RETENTION VOLUME

Substance	*Mol.wt.*	V_R*(ml)*
Thyroglobulin	670 000	4.66
γ-Globulin	158 000	7.38
Ovalbumin	44 000	8.98
Myoglobin	7000	10.24
Vitamin B_{12}	1350	13.13
ACE	150 000–160 000	7.40

ACKNOWLEDGEMENTS

The authors thank Ms. Charlane Crouse for her assistance in preparing the manuscript. [^{125}I]351A and lisinopril were generously supplied by Dr. Martin Hichens of Merck, Sharp and Dohme Research Labs. Endothelial cells were provided by Dr. Francois Booyse. This work was supported in part by NIH/NHLBI Grants HL-07457 and HL-22544.

REFERENCES

1 T. A. Stewart, J. A. Weare and E. G. Erdos, *Peptides*, 2 (1981) 145.
2 I. Y. Sakharov, E. A. Dukhanina and S. M. Danilov, *Biokhimiya*, 51 (1986) 946.
3 H. G. Bull, N. A. Thornberry and E. H. Cordes, *J. Biol. Chem.*, 260 (1985) 2963.
4 N. M. Hooper and A. J. Turner, *Biochem. J.*, 241 (1987) 625.
5 M. R. W. Ehlers, D. L. Maeder and R. E. Kirsch, *Biochim. Biophys. Acta*, 883 (1986) 361.
6 S. J. King, S. Oparil and F. M. Booyse, *Circulation*, 76 Suppl. IV (1987) IV-244.
7 F. M. Booyse, A. J. Quarfoot, S. Bell, D. N. Fass, J. C. Lewis, K. G. Mann and E. J. W. Bowie, *Proc. Natl. Acad. Sci. U.S.A.*, 74 (1977) 5702.
8 F. M. Booyse, A. J. Quarfoot, J. Chediak, M. B. Stemerman and T. Maciag, *Blood*, 58 (1981) 788.
9 I. Tikkanen, F. Fyhrquist and T. Forslund, *Clin. Sci.*, 67 (1984) 327.
10 U. K. Laemmli, *Nature (London)*, 227 (1970) 680.

Journal of Chromatography, 461 (1989) 277–280
Elsevier Science Publishers B.V., Amsterdam — Printed in The Netherlands

CHROM. 1466

DETERMINATION OF PHENYLALANINE IN RIVER WATER BY HIGH-PERFORMANCE LIQUID CHROMATOGRAPHY

P. J. RENNIE
River Dee Joint Organics Laboratory, Huntington W.T.W., Huntington, Chester CH3 6EA (U.K.)

SUMMARY

The use of *o*-phthalaldehyde derivatisation of phenylalanine followed by high-performance liquid chromatography with fluorescence detection as used for amino acid analysis in clinical laboratories was examined to assess its suitability for the monitoring of river pollution by the dairy industry by measuring the phenylalanine levels in river water. The method is described together with its statistical evaluation.

INTRODUCTION

Rivers are a major resource in the U.K. for water intended for potable use after suitable treatment. Pollution of rivers by the dairy industry (both industrial and farming) can cause problems other than oxygen deficiency in the water particularly if the river is being used as such a resource. During recent dairy product pollution incidents in the River Dee in recent years an off-flavour in the water was found after treatment. Subsequent gas chromatographic (GC)–mass spectrometric (MS) analysis of dichloromethane extracts of the treated water revealed the presence of various aldehydes: phenylacetaldehyde (hyacinthin), 2-methyl butyraldehyde and 3-methyl butyraldehyde[1]; all highly odoriferous compounds. These compounds were absent in the untreated water. Yoshioka *et al.*[2] reported the production of phenylacetaldehyde following chlorination of phenylalanine. This was later confirmed by laboratory investigations[1] which pointed to the effect of disinfection procedures (chlorination) on phenylalanine present in water following dairy pollution (milk and milk products contain high levels of phenylalanine, *e.g.*, skimmed milk contains 5% (w/v) phenylalanine). 2-Methyl butyraldehyde and 3-methyl butyraldehyde are likely to be the result of chlorination on leucine and isoleucine respectively.

At present monitoring river water for pollution by milk and milk products is difficult to achieve and the water analyst is left to monitor the odoriferous compounds in the potable supply by GC–MS. A method was thus required to assess phenylalanine levels in river water concentration $< 5\ \mu g\ l^{-1}$ to monitor dairy product pollution or farm spillage where phenylalanine present could result in off-flavour potable water.

One of the standard techniques available for the analysis of amino acids in the clinical laboratory is derivatisation with *o*-phthalaldehyde (OPA) followed by high-

performance liquid chromatography (HPLC) with fluorescence detection, this could achieve the detection limit required (low $\mu g\ l^{-1}$) without extensive pre-column concentration or extraction of the analyte. OPA reacts with primary amino groups in the presence of 2-mercaptoethanol to form highly fluorescent derivatives[3]; this reagent is highly specific and derivatisation takes place rapidly.

EXPERIMENTAL

OPA reagent was purchased ready prepared from Sigma (Poole, U.K.; product No. P-05332) and derivatisation was carried out as per the instructions accompanying the reagent, *i.e.*, equal volumes (0.5 ml) of reagent solution and sample were mixed together at room temperature. After 1 min 200 μl of the mixture were injected via a sample loop onto a LiChrosorb RP-18 column. Mobile phase was phosphate buffer (pH 7.0)–acetonitrile (70:30); flow-rate 1 ml min^{-1}. The fluorescence detector was optimised for the phenylalanine derivative, *i.e.*, excitation 341 nm, emission 444 nm.

Apparatus

HPLC pump. A dual reciprocating pump (Model 420; Kontron, Watford, U.K.) fitted with microbore heads and a Bourdon tube type pulse dampener was used.

Fluorescence detector. A Perkin-Elmer (Beaconsfield, U.K.) LS-3B fluorescence spectrometer used fitted with a HPLC flow cell (20 μl cell volume, 1.5 mm I.D.) was used.

Injector. A Rheodyne 7125 injector fitted with a 100-μl sample loop was applied.

Column. The column was LiChrosorb RP-18, 10 μm particles, 25 cm $\times$ 4 mm I.D.

Syringes. A 250-μl Rheodyne syringe (Hamilton 725SNR) and a 2-ml Luer tip fitted with a 7125 needle-port cleaner were used.

RESULTS AND DISCUSSIONS

To test the performance of the method, duplicate analyses were carried out on each of four days, of HPLC-grade water (blank), 10 $\mu g\ l^{-1}$ and 20 $\mu g\ l^{-1}$standards, river water from the River Dee at Huntington and River Dee water spiked with a 10 $\mu g\ l^{-1}$ phenylalanine addition (Fig. 1). The results of the last two samples were used to calculate the spiking recovery.

Statistical evaluation of the method was carried out according to the procedures given by Cheeseman and Wilson[4] (*viz.*, precision of standards and samples and spiking recovery). The results were analysed to derive the corresponding within-batch (s_w), between-batch (s_b) and total (s_t) standard deviations. The results are summarised in Table I, the numbers of degrees of freedom were derived from duplicate analyses on each of five days and are given in parentheses.

Analysis of variance showed that the 10 and 20 $\mu g\ l^{-1}$ phenylalanine standards showed no significant between-batch variability.

A limit of detection of 0.69 $\mu g\ l^{-1}$ of phenylalanine was calculated by using the

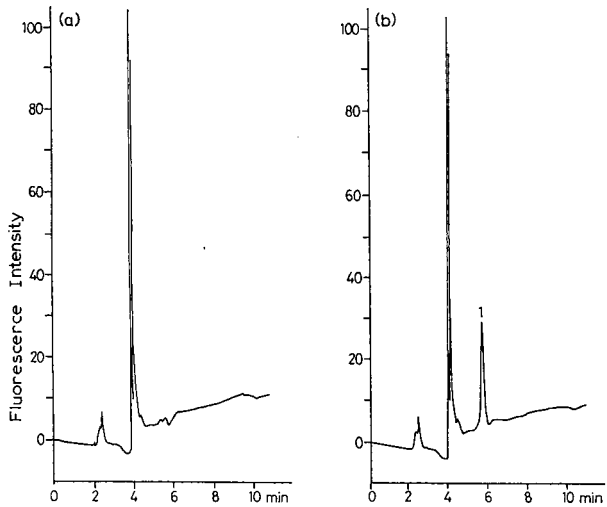

Fig. 1. Chromatograms of (a) River Dee water after OPA derivatisation and (b) River Dee water spiked with 10 $\mu g\ l^{-1}$ phenylalanine (1) after OPA derivatisation. Column: 25 cm × 4 mm I.D. LiChrosorb RP-18, 10 μm; mobile phase: Phosphate buffer (pH 7.0)–acetonitrile (70:30) at a flow-rate of 1 ml min^{-1}; detection: fluorescence, excitation wavelength 341 nm, emission wavelength nm.

formula $2t\sqrt{2}s_w$, where t is Student's single-sided t for a probability of 0.10 and s_w is the within-batch standard deviation of the blanks.

The spiking recovery of 89% was considered satisfactory.

CONCLUSIONS

The work showed that methods used in the clinical laboratory can be applied to environmental analysis with little or as in this case no changes. The selected method is simple, rapid and with satisfactory precision and detection limit.

TABLE I

PRECISION OF ANALYTICAL RESULTS

For chromatographic conditions, see text. Figures in parentheses are the degrees of freedom. N.S. indicates that the result is not statistically significant.

Solution	*Standard deviation ($\mu g\ l^{-1}$ phenylalanine)*			*Mean concentration found ($\mu g\ l^{-1}$ phenylalanine)*
	s_w	s_b	s_t	
Blank	0.17(4)	—	—	1.37**
10 $\mu g\ l^{-1}$ Phe	1.08(4)	N.S.(3)	1.08(5)	9.93***
20 $\mu g\ l^{-1}$ Phe	2.08(4)	N.S.(3)	2.08(5)	20.19***
River Dee water	0.34(40	N.S.(3)	0.57(4)	0.04***
River Dee water + 10 $\mu g\ l^{-1}$ phenylalanine	1.74(4)	N.S.(3)	01.74(5)	8.94***

** Value of blank in terms of $\mu g\ l^{-1}$ phenylalanine

*** All values corrected for blank.

ACKNOWLEDGEMENTS

The author thanks the Management Committee of the River Dee Joint Organics Laboratory for permission to publish this paper and Dr. P.J. Whittle for useful discussions.

REFERENCES

1 Investigatory Task Group Deepol, *Report No 35.85: Internal Report*, North West Water/Welsh Water, Shire Hall, Mold, Clwyd, U.K.
2 M. Yoshioka, F. Shimamura and Y. Shimizu, *Seikatsu Kagaku Kenkyusho Kenkyu Hokoku*, 13 (1980) 1–8.
3 B. N. Jones, S. Paabo and S. Stein, *J. Liq. Chromatogr.*, 4 (1981) 565.
4 R. V. Cheeseman and A. L. Wilson, *Manual on Analytical Quality Control for Water Industry*, Water Research Centre, Medmenham, 1978, TR66.

Journal of Chromatography, 461 (1989) 281–292
Elsevier Science Publishers B.V., Amsterdam — Printed in The Netherlands

CHROMSYMP. 1480

SOLVENT SELECTIVITY EFFECTS IN REVERSED-PHASE HIGH-PERFORMANCE LIQUID CHROMATOGRAPHY OF FLAVONOID COMPOUNDS

F. DONDI*

Analytical Chemistry Laboratory, Department of Chemistry, University of Ferrara, Via L. Borsari 46, I-44100 Ferrara (Italy)

Y. D. KAHIE

Analytical Chemistry, Faculty of Industrial Chemistry, Somali National University, P.O. Box 1081, Mogadishu (Somalia)

and

G. LODI, G. BLO, C. PIETROGRANDE and P. RESCHIGLIAN

Analytical Chemistry Laboratory, Department of Chemistry, University of Ferrara, Via L. Borsari 46, I-44100 Ferrara (Italy)

SUMMARY

The selectivity properties of methanol, acetonitrile and tetrahydrofuran as organic modifiers in the reversed-phase high-performance liquid chromatographic separation of flavonoid compounds was studied. Conditions for achieving separations between compound classes are described, in particular the possible separation of glycosides from aglycones in acetonitrile and tetrahydrofuran. Eleven retention contributions as $\Delta\log k'$ are reported, and their dependence on mobile-phase composition is described. Solvent strength values and useful gradient elution conditions are given.

INTRODUCTION

Flavonoid compounds are a large group of natural products based on a 2-phenylbenzopyrone structure[1–3]. Reversed-phase high-performance liquid chromatography (RP-HPLC) with isocratic and gradient elution with acid modifiers is a well established method in flavonoid analysis[4,5]. Some work has been carried out on methanol-containing systems[6]. In particular, compound pairs differing in the same substituent group exhibit constant retention differences expressed as $\Delta\log k'$ (= retention group contributions; k' = capacity factor). These retention group contributions are roughly independent of the column, acid modifier and mobile-phase composition[6]. In addition, a detailed study has been made of solvent strength values and their relevance to optimal gradient elution[7,8].

To date, with the exception of methanol, no systematic work has been carried out on the selectivity of organic modifiers, such as tetrahydrofuran (THF) and acetonitrile, which are widely employed in plant extract separations[4,9–12].

0021-9673/89/$03.50

In this work, the chromatographic behaviour of selected flavonoid compounds with these solvents was studied in an extended volume fraction (%,v/v) (φ%) range. This study will be useful for identification purposes and in defining the type and range of experimental variables within which to seek optimal separation conditions in isocratic and gradient elution.

EXPERIMENTAL

Capacity factors (k') for various fixed acetonitrile and THF φ% were determined for standard compounds with a Waters 600 multi-solvent system, equipped with a Rheodyne injection valve (20-μl sample loop), and a Waters 990 photodiode-array detector, coupled with an APC III personal computer (NEC).

All solvents and solutes were of HPLC grade (Rudi-Pont, Hetalab Chemical Corp., Parsippany, NJ, U.S.A.) and analytical-reagent grade, respectively. Acetonitrile, THF and water purified by a Norganic system (Millipore, Bedford, MA, U.S.A.) were the mobile phase solvents. The aqueous phase was buffered at pH 2–3 in 80 m*M* acetic acid–8 m*M* disodium hydrogenphosphate (Carlo Erba, Milan, Italy). Solvent mixtures were filtered through 0.2-μm Millipore filters and degassed with pure helium. The selected flavonoid standards were obtained from Sarsyntex (Merignac, France) and used as received. Standards (in ethanol) had a concentration of 10–100 ppm. The standards selected represent the classes flavones, flavonols, flavanones and glycosides (see Table I). The chromatographic column was a 30 cm × 3.9 mm I.D. 10-μm μBondapak C_{18} column (Waters Assoc., Milford, MA, U.S.A.) and was referred to as W3 in ref. 6. Retention data obtained with methanol taken from ref. 6 and considered here were obtained on a column quoted as Wl in that reference. Between these two columns a mean $\Delta\log k'$ value of 0.3 was observed[6].

RESULTS AND DISCUSSION

The retention data on THF and acetonitrile are presented in Tables I and II, respectively. The dependence of log k' on φ is nearly linear for THF but markedly deviates from linearity for acetonitrile, as observed previously for these solvents[13–18]. In this respect, THF behaves like methanol[7,8].

THF and methanol retention data were fitted with a linear equation and those for acetonitrile with a parabolic equation. The results of the best fit are reported in Tables III–V. The A data in these tables represent the log k' value extrapolated to aqueous buffer (log k'_w). The log k'_wvalues for the same solute, extrapolated from the three solvents, may differ because they reflect the different molecular environments prevailing in a particular solvent mixture and/or because the extrapolation procedure was imprecise. In Table VI the results of the correlation between log k'_w values obtained in solvent pairs are presented. It is remarkable that the slope and correlation between the log k'_w data for methanol and acetonitrile are close to those observed for other compounds in the same solvent systems[17]. For solvent pairs one may observe that linear dependences have intercepts near zero. These findings are good arguments for the coherence of the extrapolation procedure, and hence the mean log k'_w value for different flavonoid compounds can be taken as a measure of their lipophilicity[17,19–21].

For both isocratic and gradient elution applications the most interesting data

TABLE I

RETENTION (LOG k') OF SELECTED FLAVONOIDS ON A μBONDAPAK C_{18} COLUMN FOR φ(%) TETRAHYDROFURAN IN THE MOBILE PHASE (ACETIC ACID AS ACIDIC MODIFIER)

No.	*Compound*	*φ(%)*						
		20	*25*	*30*	*40*	*45*	*50*	*55*
1	Acacetin	–	–	1.48	0.74	0.58	0.26	0.09
2	Apigenin	–	–	1.20	0.62	0.40	0.14	–0.01
3	Apigenin 7-O-glucoside	1.18	0.80	0.52	–0.03	–0.22	–0.35	–
4	Apiin	1.05	0.67	0.42	–0.14	–0.32	–0.38	–
5	Chrysin	–	–	1.46	0.74	0.60	0.30	0.15
6	Chrysoeriol	–	–	1.18	0.54	0.35	0.10	–0.04
7	Eriodictyol	–	–	1.21	0.62	0.42	0.17	0.03
8	Galangin	–	–	1.69	0.95	0.80	0.46	0.27
9	Luteolin	–	–	1.05	0.48	0.33	0.08	–0.05
10	Luteolin 7-O-glucoside	1.08	0.70	0.43	–0.08	–0.26	–0.34	–
11	Morin	–	–	1.10	0.48	0.29	0.07	–0.10
12	Naringenin	–	–	1.33	0.72	0.51	0.24	0.08
13	Quercetagetin	0.91	0.61	0.32	–0.12	–0.25	–0.37	–
14	Quercetin	–	–	1.23	0.62	0.45	0.18	0.04
15	Quercitrin	1.29	0.92	0.67	0.05	–0.10	–0.25	–
16	Rutin	0.91	0.50	0.29	–0.22	–0.27	–0.34	–

TABLE II

RETENTION (LOG k') OF SELECTED FLAVONOIDS ON A μBONDAPAK C_{18} COLUMN FOR φ(%) ACETONITRILE IN THE MOBILE PHASE (ACETIC ACID AS ACIDIC MODIFIER)

No.	*Compound*	*φ%*						
		15	*20*	*25*	*30*	*40*	*45*	*50*
1	Acetin	–	–	–	1.34	0.85	0.67	0.48
2	Apigenin	–	–	1.08	0.80	0.35	0.21	0.07
3	Apigenin 7-O-glucoside	1.36	0.71	0.17	–0.05	–0.23	–	–
4	Apiin	0.81	0.62	0.06	–0.11	–0.21	–	–
5	Chrysin	–	–	–	1.27	0.80	0.63	0.45
6	Chrysoeriol	–	–	–	0.83	0.38	0.24	0.10
7	Eriodictyol	–	–	–	0.51	0.14	0.03	–0.07
8	Galangin	–	–	–	1.40	0.88	0.72	0.52
9	Luteolin	–	1.26	0.80	0.56	0.13	0.02	–0.10
10	Luteolin 7-O-glucoside	1.12	0.44	–0.03	–0.14	–0.24	–	–
11	Morin	–	–	–	0.45	0.05	–0.05	–0.15
12	Naringenin	–	–	–	0.78	0.36	0.23	0.07
13	Quercetagetin	0.75	0.15	–0.10	–0.21	–0.21	–	–
14	Quercetin	–	1.29	0.82	0.58	0.16	0.05	–0.05
15	Quercitrin	1.37	0.70	0.19	0.00	–0.22	–	–
16	Rutin	1.05	0.32	–0.16	–0.20	–0.22	–	–

TABLE III

LOG k' *VS.* φ LINEAR FITTING ACCORDING TO LOG $k' = A + B\varphi$ WITH METHANOL AS ORGANIC MODIFIER

μBondapak C_{18} column. $\sigma_{y \cdot x}$ = Standard error of regression; R = correlation coefficient.

No.	*Compound*	*A*	*B*	*R*	$\sigma_{y \cdot x}$
1	Acacetin	3.4 ± 0.1	−4.17 ± 0.14	1.00	0.04
2	Apigenin	3.21 ± 0.24	−4.68 ± 0.46	0.99	0.05
3	Apigenin 7-O-glucoside	2.56 ± 0.31	−4.70 ± 0.64	0.98	0.07
4	Apiin	2.13 ± 0.25	−4.06 ± 0.45	0.98	0.09
5	Chrysin	3.28 ± 0.46	−4.20 ± 0.92	0.98	0.07
6	Chrysoeriol	3.0 ± 0.3	−4.1 ± 0.5	0.99	0.04
7	Eriodictyol	2.57 ± 0.25	−4.52 ± 0.43	0.99	0.08
8	Galangin	3.53 ± 0.14	−4.73 ± 0.25	1.00	0.05
9	Luteolin	2.66 ± 0.17	−4.06 ± 0.31	0.99	0.06
10	Luteolin 7-O-glucoside	2.46 ± 0.20	−4.88 ± 0.40	0.99	0.06
11	Morin	2.74 ± 0.11	−4.66 ± 0.22	1.00	0.03
12	Naringenin	2.66 ± 0.26	−4.36 ± 0.50	0.99	0.06
13	Quercetagetin	1.87 ± 0.19	−4.24 ± 0.37	0.99	0.06
14	Quercetin	2.96 ± 0.27	−4.8 ± 0.6	0.99	0.06
15	Quercitrin	2.57 ± 0.14	−4.56 ± 0.26	1.00	0.03
16	Rutin	1.96 ± 0.14	−3.7 ± 0.3	1.00	0.02

TABLE IV

LOG k' *VS.* φ PARABOLIC FITTING ACCORDING TO LOG $k' = A + B\varphi + C\varphi^2$ WITH ACETONITRILE AS ORGANIC MODIFIER

μBondapak C_{18} column. $\varphi_{y \cdot x}$ = Standard error or regression; R = correlation coefficient.

No.	*Compound*	*A*	*B*	*C*	*R*	$\sigma_{y \cdot x}$
1	Acacetin	3.41 ± 0.26	− 8.5 ± 1.4	5.3 ± 1.7	1.00	0.02
2	Apigenin	3.07 ± 0.11	− 9.92 ± 0.64	7.87 ± 0.86	1.00	0.01
3	Apigenin 7-O-glucoside	2.47 ± 0.27	−13.2 ± 1.6	16.0 ± 2.2	1.00	0.02
4	Apiin	2.13 ± 0.48	− 9.7 ± 3.8	8.0 ± 7.0	0.99	0.09
5	Chrysin	3.28 ± 0.26	− 8.3 ± 1.4	5.3 ± 1.7	1.00	0.02
6	Chrysoeriol	3.07 ± 0.28	− 9.8 ± 1.4	7.7 ± 1.8	1.00	0.02
7	Eriodictyol	2.49 ± 0.20	− 8.8 ± 1.0	7.5 ± 1.3	1.00	0.01
8	Galangin	3.68 ± 0.53	− 9.6 ± 2.7	6.5 ± 3.4	1.00	0.03
9	Luteolin	2.68 ± 0.19	− 9.4 ± 1.0	7.8 ± 1.4	1.00	0.02
10	Luteolin 7-O-glucoside	2.52 ± 0.32	−13.9 ± 2.1	17.1 ± 3.2	0.99	0.05
11	Morin	2.7 ± 0.3	−10.2 ± 1.7	9.1 ± 2.1	1.00	0.02
12	Naringenin	2.63 ± 0.41	− 7.8 ± 2.1	5.4 ± 2.7	1.00	0.02
13	Quercetagetin	1.96 ± 0.33	−12.7 ± 2.5	18.0 ± 4.5	1.00	0.02
14	Quercetin	2.78 ± 0.35	−10.0 ± 2.1	8.7 ± 2.9	1.00	0.02
15	Quercitrin	2.53 ± 0.46	−13.3 ± 2.7	16.0 ± 3.8	0.99	0.04
16	Rutin	1.72 ± 0.15	− 8.35 ± 0.97	6.7 ± 1.5	1.00	0.02

TABLE V

LOG k' *VS.* φ LINEAR FITTING ACCORDING TO LOG $k' = A + B\varphi$ WITH TETRAHYDROFURAN AS ORGANIC MODIFIER

μBondapak C_{18} column. $\sigma_{y.x}$ = Standard error of regression; R = correlation coefficient.

No.	*Compound*	*A*	*B*	*R*	$\sigma_{y.x}$
1	Acacetin	3.24 ± 0.23	−6.0 ± 0.6	0.99	0.08
2	Apigenin	3.0 ± 0.04	−6.0 ± 0.1	1.00	0.01
3	Apigenin 7-O-glucoside	2.33 ± 0.09	−5.95 ± 0.32	1.00	0.05
4	Apiin	2.18 ± 0.09	−5.83 ± 0.31	1.00	0.05
5	Chrysin	3.15 ± 0.18	−5.73 ± 0.43	0.99	0.06
6	Chrysoeriol	2.95 ± 0.15	−5.94 ± 0.40	1.00	0.04
7	Eriodictyol	2.6 ± 0.2	−4.73 ± 0.42	0.99	0.08
8	Galangin	3.48 ± 0.17	−6.05 ± 0.41	1.00	0.06
9	Luteolin	2.46 ± 0.15	−4.79 ± 0.36	0.99	0.05
10	Luteolin 7-O-glucoside	2.36 ± 0.16	−6.5 ± 0.6	1.00	0.04
11	Morin	2.61 ± 0.17	−5.15 ± 0.41	0.99	0.06
12	Naringenin	2.8 ± 0.2	−5.04 ± 0.37	0.99	0.07
13	Quercetagetin	1.9 ± 0.1	−5.12 ± 0.30	1.00	0.04
14	Quercetin	2.78 ± 0.20	−5.25 ± 0.49	1.00	0.07
15	Quercitrin	2.48 ± 0.07	−6.1 ± 0.2	1.00	0.04
16	Rutin	1.94 ± 0.14	−5.46 ± 0.48	0.99	0.07

that can be obtained from the observed log k' *vs.* φ dependence are the location and the extent of $\Delta\varphi$ intervals, where the log k' values range between 1 and 0 ($k' = 10$ and $k' = 1$)[13,14]. Table VII reports the $\Delta\varphi$ data together with the mean solvent strength, $\bar{S}$. The $\bar{S}$ values reported in this table are equal to

$$\bar{S} = \Delta\log k'/\Delta\varphi \tag{1}$$

and, as $\Delta\log k' = 1$, they are simply equal to

$$\bar{S} = 1/\Delta\varphi \tag{2}$$

The $\bar{S}$ data for methanol differ from the S values reported in ref. 8. In that case, S was calculated as the slope of the linear portion of the log k' *vs.* φ function in the

TABLE VI

CORRELATION BETWEEN LOG k'_w DATA OBTAINED FROM DIFFERENT ORGANIC MODIFIER PAIRS, LOG $k'_{w,1} = A + B$ LOG $k'_{w,2}$

R = Correlation coefficient.

Modifier pairs (1,2)	*A*	*B*	*R*
Acetonitrile–methanol	−0.15 ± 0.10	1.04 ± 0.05	0.98
Acetonitrile–THF	−0.27 ± 0.12	1.12 ± 0.07	0.97
THF–methanol	0.18 ± 0.10	0.90 ± 0.05	0.98

TABLE VII

USEFUL φ(%) RANGES FOR GRADIENT ELUTION AND MEAN SOLVENT STRENGTHS OF SELECTED FLAVONOID COMPOUNDS IN THE RP C_{18} SYSTEM WITH ACETIC ACID AS THE ACID MODIFIER

Compound	*Methanol*			*THF*			*Acetonitrile*		
	φ ($k' = 10$)	φ ($k' = 1$)	S	φ ($k' = 10$)	φ ($k' = 1$)	S	φ ($k' = 10$)	φ ($k' = 1$)	S
Eriodictyol	39	55	4.9	34	56	4.5	17	46	3.4
Naringenin	34	61	3.1	35	58	4.3	25	53	3.6
Acacetin	49	82	3.0	33	58	4.0	35	63	3.6
Apigenin	46	74	3.2	34	55	4.8	26	53	3.7
Apigenin 7-O-glucoside	36	54	4.9	23	40	5.9	18	29	9.1
Apiin	37	53	5.4	21	38	5.9	17	27	10.0
Chrysin	56	80	4.2	34	59	4.0	34	63	3.4
Chrysoeriol	45	72	3.7	33	54	4.8	19	53	2.9
Luteolin	43	65	4.2	31	54	4.3	23	46	4.3
Luteolin 7-O-glucoside	33	52	4.5	21	39	5.6	16	25	11.1
Galangin	54	80	3.8	39	62	4.3	36	64	3.6
Morin	36	58	4.2	28	52	4.2	17	43	3.8
Quercetagetin	28	45	4.0	19	37	5.6	13	22	11.1
Quercetin	42	59	4.0	34	57	4.3	23	48	4.0
Quercitrin	38	56	4.9	23	42	5.3	18	30	8.3
Rutin	34	52	4.5	19	36	5.9	15	24	11.1
Common mean and S.D.			4.2 ± 0.7			4.9 ± 0.7			6.1 ± 3.3
Aglycone mean and S.D.			3.8 ± 0.6			4.3 ± 0.3			3.6 ± 0.4
Glycoside mean and S.D.			4.7 ± 0.5			5.7 ± 0.2			10.1 ± 1.2

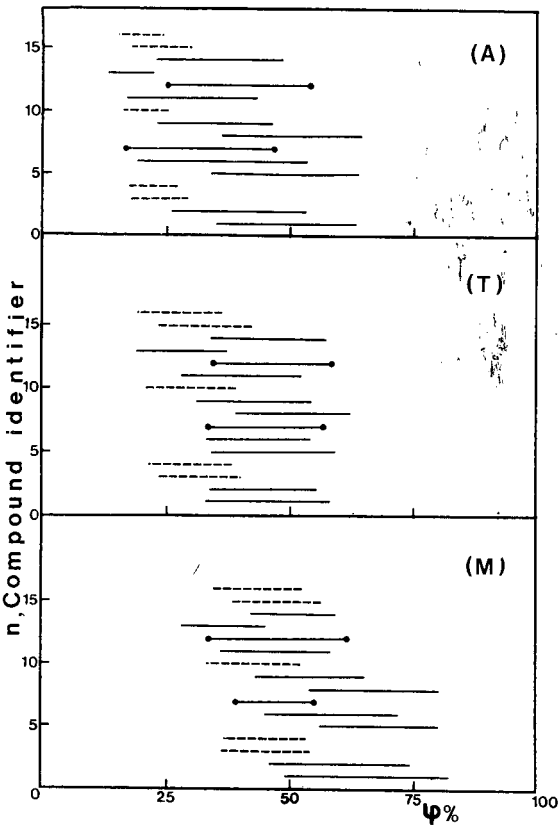

Fig. 1. Useful $\Delta\varphi$ elution range intervals for $1 < k' < 10$. For compound identification, see Table I. - - - = Glycosides; ●—● = flavanones; —— = flavones. A, T and M refer to acetonitrile, THF and methanol respectively.

range log k' = 1–0, whereas here $\bar{S}$ is the mean slope within the same range. This calculation was followed in order to have a common basis when the different solvents are compared.

An overview of the useful $\Delta\varphi$ pattern for gradient and isocratic elution with different solvents is present in Fig. 1. If the minimum φ value giving a k' value lower than 10 is taken as a criterion of elution power, the order is generally acetonitrile > THF > methanol.

Regarding the mean solvent strength, $\bar{S}$, glycosides generally exhibit higher values than aglycones, with the exception of quercitrin, where the extensive hydroxylation is responsible for its anomalous behaviour. Of the three solvents, the effect is more marked for acetonitrile, the most powerful of the series. These high $\bar{S}$ values are peculiar to these compounds and can be explained only by a specific interaction with acetonitrile. Another interesting factor that emerges for the data in Fig. 1 is that it is possible to separate glycosides and aglycones with either THF or acetonitrile. With the former, Snyder's linear solvent strength (LSS) gradient elution theory[13,14] will probably support the selection of a gradient with a nearly constant slope in the range

TABLE VIII

COMPARISON BETWEEN ΔLOG k' RETENTION GROUP CONTRIBUTIONS IN DIFFERENT SOLVENT

Group contribution	*Compounds*	*Δlog k' CH_3OH*	*(φ range)**	*Δlog k' CH_3CN*	*(φ range)**	*Δlog k' THF*	*(φ range)**	*Δlog k'_w***
3-OH	8– 5	0.01 ± 0.01	(0.55–0.70)	0.09 ± 0.06	(0.30–0.50)	0.18 ± 0.11	(0.30–0.55)	0.33 ± 0.07
3-OH	14– 9	–0.13 ± 0.15	(0.45–0.60)	0.03 ± 0.03	(0.30–0.50)	0.13 ± 0.09	(0.30–0.59)	0.24 ± 0.12
6-OH	13–14	–0.85 ± 0.06	(0.40–0.50)	–0.80 ± 0.77	(0.20–0.45)	–0.72 ± 0.36	(0.30–0.50)	–0.93 ± 0.14
3'-OH	9– 2	–0.22 ± 0.05	(0.45–0.60)	–0.22 ± 0.11	(0.25–0.50)	–0.09 ± 0.11	(0.30–0.55)	–0.49 ± 0.09
3'-OH	10– 3	–0.19 ± 0.02	(0.30–0.70)	–0.22 ± 0.26	(0.15–0.50)	–0.07 ± 0.07	(0.20–0.50)	–0.01 ± 0.08
3'-OH	7–12	–0.24 ± 0.12	(0.40–0.70)	–0.21 ± 0.13	(0.30–0.50)	–0.09 ± 0.07	(0.30–0.55)	–0.14 ± 0.05
4'-OH	2– 5	–0.29 ± 0.06	(0.45–0.70)	–0.43 ± 0.09	(0.30–0.50)	–0.18 ± 0.12	(0.30–0.55)	–0.14 ± 0.07
3'-OCH_3 (—HO)	6– 2	0.06 ± 0.02	(0.40–0.55)	0.03 ± 0.00	(0.30–0.50)	–0.05 ± 0.05	(0.40–0.55)	–0.09 ± 0.11
4'-OCH_3	1– 5	0.14 ± 0.02	(0.45–0.55)	0.05 ± 0.04	(0.30–0.50)	–0.02 ± 0.06	(0.30–0.55)	0.11 ± 0.02
2,3-Unsaturation	12– 2	–0.44 ± 0.04	(0.40–0.50)	0.01 ± 0.04	(0.30–0.50)	0.11 ± 0.04	(0.30–0.55)	–0.39 ± 0.18
2,3-Unsaturation	7– 9	–0.25 ± 0.07	(0.40–0.55)	0.02 ± 0.08	(0.30–0.50)	0.11 ± 0.08	(0.30–0.55)	–0.05 ± 0.16
3-Glycoside (rhamose)	15–14	–0.25 ± 0.03	(0.40–0.55)	–0.54 ± 0.25	(0.20–0.50)	–0.53 ± 0.12	(0.30–0.50)	–0.31 ± 0.07
3-Glycoside (rutinose)	16–14	–0.44 ± 0.03	(0.40–0.55)	–0.78 ± 0.60	(0.20–0.45)	–0.75 ± 0.42	(0.30–0.50)	–0.97 ± 0.11
7-Glycoside (glucose)	3– 2	–0.68 ± 0.04	(0.45–0.60)	–0.78 ± 0.33	(0.25–0.45)	–0.61 ± 0.19	(0.30–0.50)	–0.64 ± 0.04
7-Glycoside (glucose)	10– 9	–0.65 ± 0.03	(0.40–0.60)	–0.68 ± 0.46	(0.20–0.45)	–0.56 ± 0.16	(0.30–0.50)	–0.16 ± 0.05
7-Glycoside (apiosylglucose)	4– 2	–0.76 ± 0.06	(0.45–0.60)	–0.83 ± 0.46	(0.25–0.45)	–0.69 ± 0.26	(0.30–0.50)	–0.95 ± 0.13

* Mean data with their range values and mobile phase composition ranges are reported for the three organic solvents.

** Mean data with standard deviation are reported for Δlog k'_w with water.

$0.15 < \varphi < 0.60$; for acetonitrile, two slopes are indicated: first low ($0.10 < \varphi < 0.25$) and then three times steeper ($0.25 < \varphi < 0.70$). In addition, the marked positive curvatures of the log k' *vs.* φ plots (see Fig. 2) support convex gradient shapes. This, which requires an optimization procedure, will be the subject of further study.

The general pattern of structure retention relationships in these two solvents was compared with results obtained previously with methanol[6] by calculating the group contribution to the retention as $\Delta\log k'$ for various substitutions in the benzopyran ring. Only log k' data roughly in the range 1–0 were employed. The dependence on φ is presented in Figs. 2 and 3 for selected groups in the three solvents. A marked dependence of $\Delta\log k'$ on φ is often observed in THF and acetonitrile. The general independence of $\Delta\log k'$ from φ and also from other variables (*e.g.*, the chain length of the bonded phase and the type of acid modifier), as previously observed for methanol[6], must be considered peculiar to methanol. Another distinct feature of THF and acetonitrile is their levelling effect on the $\Delta\log k'$ contributions: negative $\Delta\log k'$ values increase with an increase in the organic content of the mobile phase, whereas positive values decrease. In Table VIII the mean $\Delta\log k'$ values are reported together with their ranges. It can be seen that both the $\Delta\log k'$ values and their ranges for glycosides are always higher for acetonitrile and THF than for methanol. Hence the fact that glycosides are eluted early by THF and especially by acetonitrile must be ascribed to specific, strong polar and/or hydrogen-bonding acceptor properties of these two solvents with respect to methanol. The same kind of strong specific interaction is observed for the 6-OH group in quercetagetin, thus explaining why this compound is eluted with the glycosides. Another specific behaviour strongly dependent on solvent type is the unsaturation contribution, which distinguishes flavones from

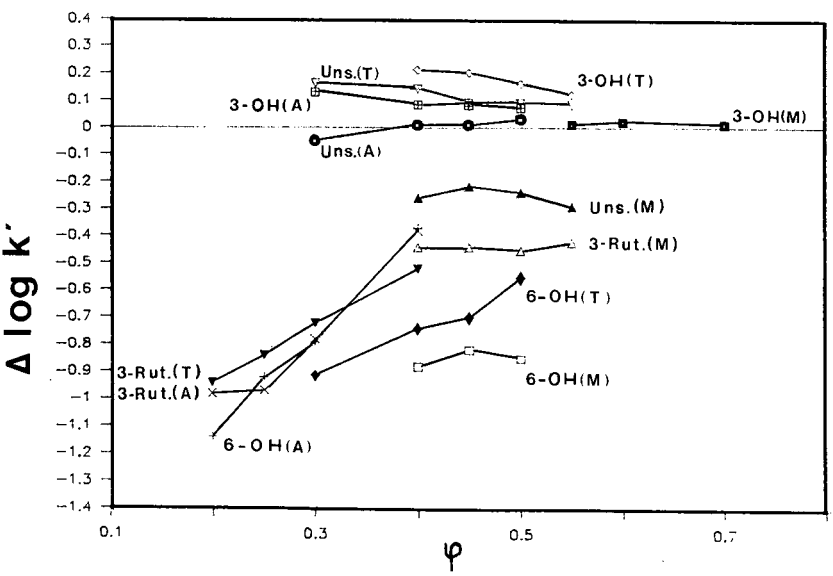

Fig. 2. Dependence of $\Delta\log k'$ group contributions on mobile phase composition. 3-OH refers to the pair of compounds 8 and 5; Uns. refers to the pair of compounds 7 and 9; 3-Rut refers to the pair of compounds 16 and 14; 6-OH refers to the pair of compounds 13 and 14 (see Table VIII). A, T and M as in Fig. 1.

flavanones. Despite the fact that there were differences in molecular structure, the flavones being planar and the flavanones partially planar, only in methanol is there a marked difference with a significant negative group contribution and early elution among glycoside compounds. This effect is lower for acetonitrile and reversed for THF (see Fig. 2). It is not easy to explain this behaviour, which is probably a combined effect of solvation enthalpy and entropy. The ordered solvent structure of the aqueous methanol system implies a larger solvation entropy for the planar flavones than for the non-planar flavanones[22]. This effect must be reversed in THF or other solvation processes must be operative.

The $\Delta\log k'$ data now discussed can be compared with the $\Delta\log k'_w$ data, which can be calculated by using $\log k_w'$ data obtained by extrapolation procedures (see Table VIII). No systematic differences are observed between the extrapolated values with water and those observed with various solvent mixtures as mobile phases. However, a significant negative $\Delta\log k'_w$ value for unsaturation, as in methanol, is observed. In addition, the decreased polarity effect of the 3-OH group, giving rise to an intramolecular hydrogen bond, appears strongest with water.

Let us now consider some practical applications for the selectivity properties of these three organic modifiers. It may be recalled that the $\Delta\log k'$ data reported in Table VIII and Figs. 2 and 3 are also the logarithms of the relative retentions. A difficult resolution, unobtainable with a particular organic modifier, may be obtained by simply changing it or by modifying the volume fraction. For example, the flavonol galangin (compound 8), which cannot be separated from the corresponding flavone chrysin (compound 5) in methanol, can be resolved with acetonitrile or even better with THF (see Fig. 2). Another, similar pair (quercetin *vs.* luteolin) is better separated in either THF or methanol (see Table VIII). It is relevant that the minor differences,

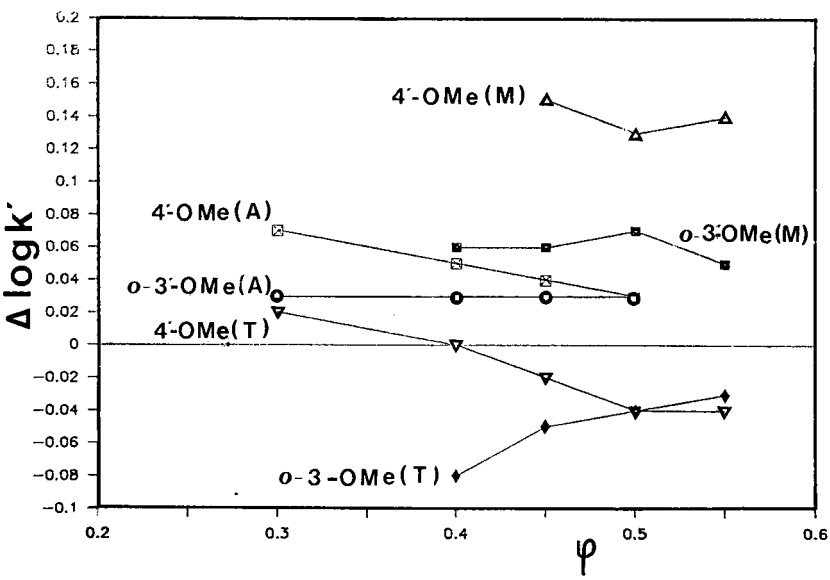

Fig. 3. Dependence of $\Delta\log k'$ group contributions on mobile phase composition (see Table VI). Me = Methyl. A, T and M as in Fig. 1.

from the same 3-OH group contribution, imply different chromatographic conditions. Other particularly difficult separation problems are compound pairs that differ in the occurrence of a OCH_3 group. An isolated OCH_3 [the 4'-OCH_3 group in the pair of compounds 1 and 5] clearly enhances the lipophilicity with a corresponding increase in retention (see Fig. 3). The latter is most pronounced for methanol and less so for acetonitrile, and inversion effects take place in THF. When an OH group is close to OCH_3 (*e.g.*, in the pair of compounds 6 and 2), the total lipophilicity of the molecule is lowered through the *ortho* effect, and separation can be achieved with both THF and methanol (see Fig. 3). Note that a $\Delta \log k'$ value of 0.05 means a retention difference of 12%. Finally, in acetonitrile and THF the general dependence of $\Delta \log k'$ on φ makes the mobile phase composition change a useful parameter in solving particularly difficult separation or identification problems.

CONCLUSION

The three organic modifiers considered exhibit significant selectivity peculiarities toward flavonoid compounds in RP-HPLC. The overall effect, derived by a careful analysis of group contributions to retention, is complex and probably the result of the many simultaneously acting factors (different specific and non-specific interactions, together with different solvophobic effects)[20–25]. For methanol[6], the group contributions are largely independent of solvent composition, which probably helps in understanding gradient elution behaviour. Nonetheless, as organic modifiers, THF and acetonitrile can be useful in facilitating the selective elution of different classes of compounds, such as glycosides and the parent aglycone, and in achieving particular resolutions and identifications. Minor changes in $\Delta \log k'$ values for the same substituent group likewise have important practical relevance, and a more extended study of different flavonoids may lead to additional insights into the secondary effects which may, nonetheless, play an important rôle in certain separations.

ACKNOWLEDGEMENTS

This work was supported by the Italian Ministry of Public Education (MPI), the Italian Ministry of Foreign Affairs (MAE) and the Somali National University.

REFERENCES

1 J. B. Harborne, T. J. Mabry and H. Mabry (Editors), *The Flavonoids*, Chapman and Hall, London, 1975.
2 J. B. Harborne, in V. Cody, E. Middleton, Jr. and J. B. Harborne (Editors), *Plant Flavonoids in Biology and Medicine*, A. R. Liss, New York, 1986, pp. 15–24.
3 K. R. Markham, *Techniques of Flavanoid Identification*, Academic Press, London, 1982.
4 J. B. Harborne, in E. Heftman, (Editor), *Chromatography – Part B: Applications (Journal of Chromatography Library*, Vol. 22B), Elsevier, Amsterdam, 1983, p. B407.
5 K. Hostettmann and M. Hostettmann, in J. B. Harborne and T. J. Mabry (Editors), *The Flavonoids: Advances in Research*, Chapman and Hall, London, 1982, pp. 1–18.
6 F. Dondi, G. Blo, Y. D. Kahie, G. Lodi, C. Pietrogrande and P. Reschiglian, *Chromatographia*, 25 (1988) 423.
7 F. Dondi, Y. D. Kahie, G. Lodi, M. Remelli, P. Reschiglian and C. Bighi, *Anal. Chim. Acta*, 191 (1986) 261.

8 F. Dondi, Y. D. Kahie, G. Lodi, P. Reschiglian, C. Pietrogrande, C. Bighi and G. P. Cartoni, *Chromatographia*, 23 (1987) 844.
9 I. McMurrough, *J. Chromatogr.*, 218 (1981) 683.
10 I. McMurrough and G. P. Hennigan, *J. Chromatogr.*, 258 (1983) 103.
11 R. L. Rouseff and S. V. Ting, *J. Chromatogr.*, 176 (1979) 75.
12 R. V. Tamma and G. C. Miller, *J. Chromatogr.*, 322 (1985) 236.
13 L. R. Snyder, J. W. Dolan and J. R. Gant, *J. Chromatogr.*, 165 (1979) 3.
14 J. W. Dolan, J. R. Gant and L. R. Snyder, *J. Chromatogr.*, 165 (1979) 31.
15 P. J. Schoenmakers, H. A. Billiet and L. de Galan, *J. Chromatogr.*, 185 (1979) 179.
16 P. J. Schoenmakers, H. A. Billiet and L. de Galan, *J. Chromatogr.*, 282 (1983) 107.
17 D. Reymond, G. N. Chung, J. M. Mayer and B. Testa, *J. Chromatogr.*, 391 (1987) 97.
18 P. L. Zhu, *Chromatographia*, 29 (1986) 229.
19 M. C. Pietrogrande, P. A. Borea and G. L. Biagi, *J. Chromatogr.*, 447 (1988) 404.
20 T. Braumann, *J. Chromatogr.*, 373 (1986) 191.
21 R. Kaliszan, *CRC Crit. Rev. Anal. Chem.*, 16 (1986) 323.
22 L. W. Wulf and C. W. Nagel, *J. Chromatogr.*, 116 (1976) 271.
23 L. R. Snyder, *J. Chromatogr. Sci.*, 16 (1978) 233.
24 Cs. Horváth, W. Melander and I. Molnár, *J. Chromatogr.*, 125 (1976) 129.
25 B. P. Johnson, M. G. Khaledi and J. G. Dorsey, *Anal. Chem.*, 58 (1986) 2354.

Journal of Chromatography, 461 (1989) 293–303
Elsevier Science Publishers B.V., Amsterdam — Printed in The Netherlands

CHROMSYMP. 1418

SEPARATION OF THIODIGLYCOL POLYETHERS AND RELATED COMPOUNDS BY REVERSED-PHASE HIGH-PERFORMANCE LIQUID CHROMATOGRAPHY

DOUGLAS E. DOSTER* and MELODEE ZENTNER
Morton Thiokol Inc., Morton Chemical Division, Research Center, 1275 Lake Avenue, Woodstock, IL 60098-7499 (U.S.A.)

SUMMARY

Low-molecular-weight (MW < 3000) thiodiglycolpolyether polymers were separated by reversed-phase high-performance liquid chromatography into as many as twenty oligomeric species. This separation was accomplished by using gradient elution with water and methanol on a semi-microbore ODS reversed-phase column. Detection was by the use of a diode-array UV detector. The method was also used in the separation of sulfur-containing cyclic compounds, polysulfur thiodiglycol compounds and polythiodiglycol formal oligomers. The separation of these compounds provides data that indicate that the separation mechanism for the thiodiglycolpolyether polymers is a combination of precipitation dissolution and sorption mechanisms. Structural proof of the polysulfur thiodiglycol compounds was obtained by NMR.

INTRODUCTION

At Morton Thiokol research is being conducted on the synthesis of low-molecular-weight (MW < 3000) thiodiglycolpolyether polymers. The object of the present investigation was to obtain both qualitative and quantitative information about the content of the oligomeric species in the polymer. These data were used to develop material with the desired end-use properties.

In the last several years there has been considerable interest in separating synthetic organic polymers into their oligomeric species by high-performance liquid chromatography (HPLC). Chromatographic separations of this type provide better insight into the composition of a polymer than data obtained from gel permeation chromatography. Work by Barka and Hoffmann [1] showed that polyethylene glycols (PEG) could be separated into as many as 110 oligomeric species by reversed-phase HPLC. In work cited by Kuo *et al.*[2], HPLC played a key role in characterizing the oligomeric species of resins used in coatings. Munteanu[3] used reversed-phase HPLC to separate the oligomers of bisphenol A glycidyl methacrylate.

Several researchers have speculated as to the type of mechanisms that are involved in these separations. Barka and Hoffman[1] theorized that the separation mech-

0021-9673/89/$03.50

anism for PEG included both sorption effects and molecular-size effects. Jinno and Sato[4] stated that both hydrophobic interaction effects and molecular size and shape played a role in the separation of polystyrene oligomers.

Work by Armstrong and Bul[5] demonstrated that various narrow-range molecular-weight polystyrene standards could be separated by a selective precipitation dissolution mechanism. Van den Berg and Clockner[6,7] found that copolymers of styrene–acrylonitrile and styrene–methyl methacrylate were separated into their various components by the combination of precipitation dissolution and sorption mechanisms. Mourey and Smith [8] and Mourey[9] also found that polystyrene oligomers were separated by a precipitation dissolution–sorption mechanism.

The reversed-phase HPLC separation of sulfur-containing compounds has been extensively studied by Mockel[10]. This work showed that *n*-aliphatic polysulfides R_2S_n (where $n = 2$–10) could be easily separated by reversed-phase HPLC. These species were separated according to the number of sulfur atoms in the molecule and to the length of the alkyl chains. Mockel also found that for non-cyclic and cyclic sulfur compounds the number and substitution pattern of the sulfur atoms were a major factor determining the separation of these compounds.

EXPERIMENTAL

The HPLC system consisted of a Hewlett-Packard (Avondale, PA, U.S.A.) 1090A chromatograph, equipped with a ternary solvent-delivery system, temperature-controlled column compartment, autosampler, diode-array detector, and HP (Hewlett-Packard) workstation. The column used for this work measured 150 mm × 2.0 mm I.D. and was packed with Phenomenex (Rancho Palos Verdes, CA, U.S.A.) Spherex (ODS) with a mean particle size of 3 μm.

The NMR was determined with a Varian VXR 300 (Varian Instrument Group 205 W. Touhy Avenue Park Ridge, IL, U.S.A.). The ^{13}C spectrum was run at 75 MHz with complete decoupling. Deuterated dimethylsulphoxide (DMSO) was used as the solvent and tetramethylsilane (TMS) as the reference.

Methanol, dichloromethane and water were purchased from EM Science (Cherry Hill, NJ, U.S.A), Omni Solv grade. The solvents were degassed with helium. The gradient elution programs used for the various separations are listed in Table I.

Samples

The thiodiglycolpolyether polymers $H[OCH_2CH_2SCH_2CH_2]_nOH$, polysulfur thiodiglycol compounds $[HOCH_2CH_2]_2S_n$, and the polythiodiglycolformal $H[OCH_2CH_2SCH_2CH_2OCH_2]_nOCH_2CH_2SCH_2CH_2OH$ were synthesized by the Morton Thiokol Woodstock Technical Center organic synthesis group. 2-Hydroxyethyl sulfide (thiodiglycol) (>99%), 2-hydroxyethyl disulfide (dithiodiglycol) (95%), 1,4-thioxane (98%), 1,4-dithiane (97%), and 1,3-dithiane (97%) were purchased from Aldrich (Milwaukee, WI, U.S.A.).

Sample preparation

The thiodiglycolpolyether samples were dissolved in dichloromethane unless otherwise indicated. All other samples were dissolved in methanol. The concentrations used for each sample are listed in the figures. A 3-μl amount of the diluted sample was injected into the column.

TABLE I

GRADIENT ELUTION PROGRAMS

Program	*Flow-rate (μl/min)*	*Time (min)*	*Water (%)*	*Methanol (%)*	*Dichloromethane (%)*
A	300	0	100	0	0
		1	100	0	0
		30	0	100	0
		35	0	100	0
		45	0	0	100
		50	0	0	100
		60	0	100	0
		65	0	100	0
		75	100	0	0
		85	100	0	0
B	350	0	70	30	0
		10	70	30	0
C	350	0	80	20	0
		30	0	100	0
		40	0	100	0
		45	80	20	0
		5	80	20	0
D	300	0	100	0	0
		1	100	0	0
		25	0	100	0
		40	0	100	0
		50	100	0	0
		60	100	0	0
E	350	0	80	20	0
		20	0	100	0
		30	0	100	0
		35	80	20	0
		45	80	20	0

Chromatograms

All of the chromatograms shown in this work, except for the polysulfur thiodiglycol, were obtained by setting the diode-array detector to 210 nm. At this wavelength, the solvent programs used showed a considerable increase in absorption as analysis time increased. The chromatograms presented here were obtained by recording a blank solvent run and then using the HP workstation to subtract the solvent absorption from the sample run.

RESULTS AND DISCUSSION

Figs. 1 and 2 illustrate the separation of two different thiodiglycolpolyether polymers (TDPEP) by means of gradient elution program A (Table I). The chromatograms show the separation of at least twenty oligomeric species. The peak at 5 min corresponds to the retention time of thiodiglycol. The other peaks correspond to an increase in length of the polymeric chain. The relative differences in the intensity of

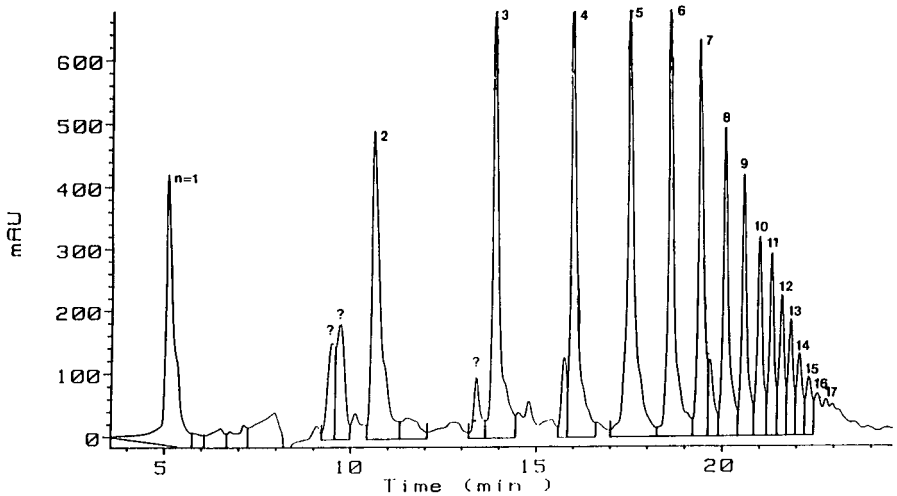

Fig. 1. Chromatogram of thiodiglycolpolyether polymer sample 1, 0.5 g in 10 ml dichloromethane. Gradient elution program A. The numbers (n) indicate the polymer chain length, $H(OCH_2CH_2SCH_2CH_2)_nOH$ for each peak.

higher-molecular-weight species peaks between these two samples are related to changes in the synthetic scheme.

Increase in system pressure are observed upon injection of these samples. Dichloromethane and long equilibration times are required to permit multiple injections without increase in back-pressure after a few injections. No further oligomeric species were eluted from the column when the eluent was at 100% dichloromethane. The

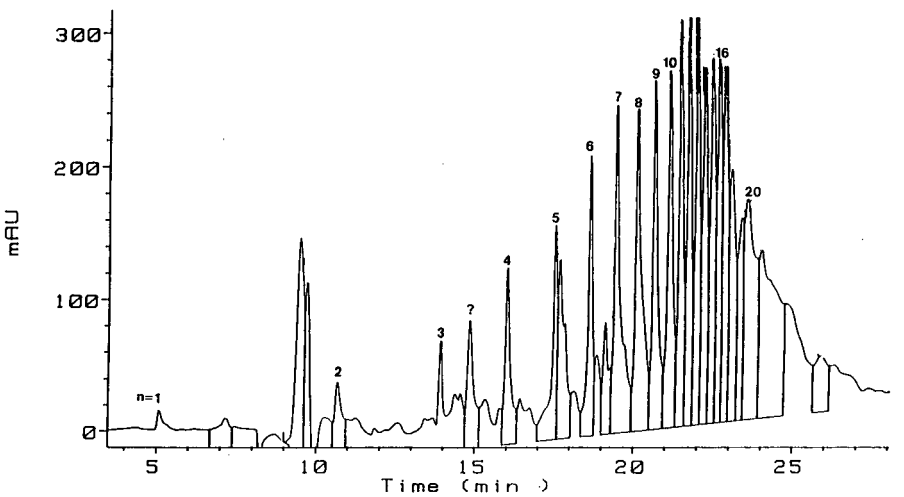

Fig. 2. Chromatogram of thiodiglycolpolyether polymer sample 2, 0.5 g in 10 ml dichloromethane. Gradient elution program A. The numbers (n) indicate the polymer chain length, $H(OCH_2CH_2SCH_2CH_2)_nOH$ for each peak.

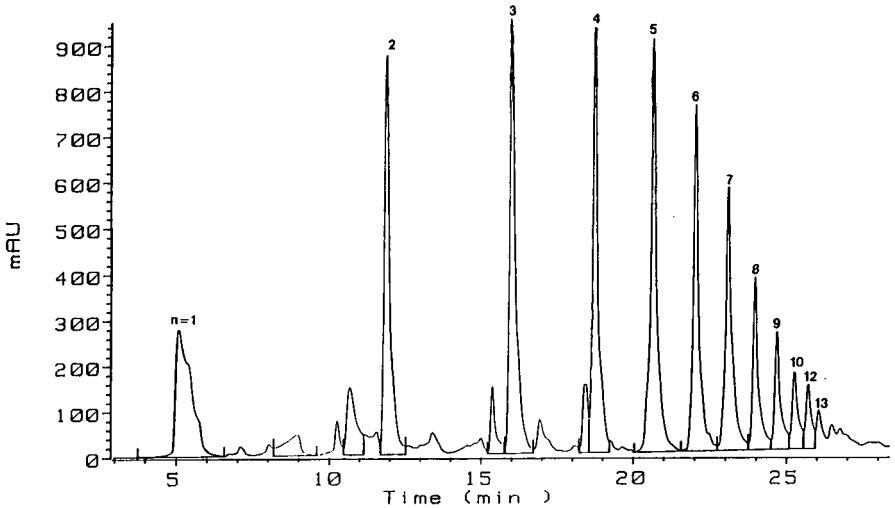

Fig. 3. Chromatogram of thiodiglycolpolyether polymer sample 1, 0.5 g in 10 ml methanol. Gradient elution program A. The numbers (n) indicate the polymer chain length, $H(OCH_2CH_2SCH_2CH_2)_nOH$ for each peak.

TDPEP samples are only partly soluble in methanol. Figs. 3 and 4 illustrate the separation observed when methanol extracts are chromatographed with gradient elution program A. The major change observed is the lower relative amount of the higher-molecular-weight species, which is due to their low solubility in methanol.

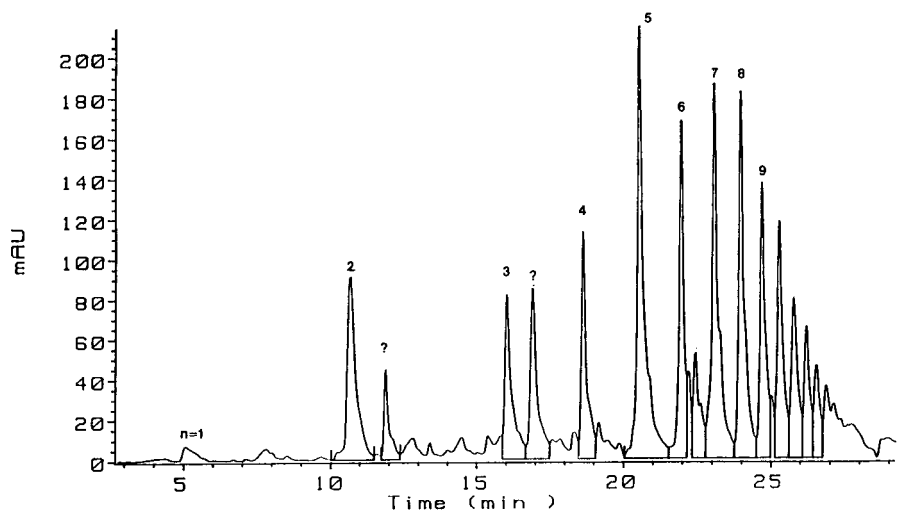

Fig. 4. Chromatogram of thiodiglycolpolyether polymer sample 2, 0.5 g in 10 ml methanol. Gradient elution program A. The numbers (n) indicate the polymer chain length, $H(OCH_2CH_2SCH_2CH_2)_nOH$ for each peak.

When samples dissolved in dichloromethane or methanol were diluted with water, precipitation occured. When samples are chromatographed with gradient elution program A, initially precipitation occured, resulting in a pressure increase. When the samples were chromatographed using 100% methanol, very little separation of the oligomers was observed. If the observed elution pattern of the oligomers is due solely to a precipitation dissolution mechanism, oligomeric species should be eluted with dichloromethane. However, all of the oligomeric species observed are eluted before the elution program reaches 100% methanol, indicating that the species are undergoing some type of hydrophobic interaction. Further evidence for this is provided by the narrow peak shape observed. This would not be expected if only precipitation dissolution occurred. Thus the data would seem to support both a precipitation dissolution mechanism and a sorption mechanism cooperating in the separation of these sulfur-containg species.

Further evidence that a sorption mechanism plays a role in separating these types of sulfur-containing compounds is the separation of a mixture of thiodiglycol (TDG), dithiodiglycol (DTDG), 1,4-thioxane, 1,3-dithiane, and 1,4-dithiane. Fig. 5 shows the separation of these compounds by means of elution program B. The separation of TDG and DTDG is consistent with the separation of polysulfides observed by Mockel[10] in that the retention time increases with the number of sulfur atoms. The separation of thioxane, 1,3-dithiane and 1,4-dithiane also agrees with the observations of Mockel[10].

Further evidence that increasing the number of sulfur atoms in these glycol compounds increases, the retention time is found in Fig. 6. Using elution program C, polysulfur thiodiglycol was resolved into nine species with 2–10 sulfur atoms. This chromatogram also shows that the retention time increases with the number of sulfur atoms. It is interesting that sulfur (S_8) was eluted after the other sulfur-containing species. This probably occured because sulfur is insoluble in water and precipitated

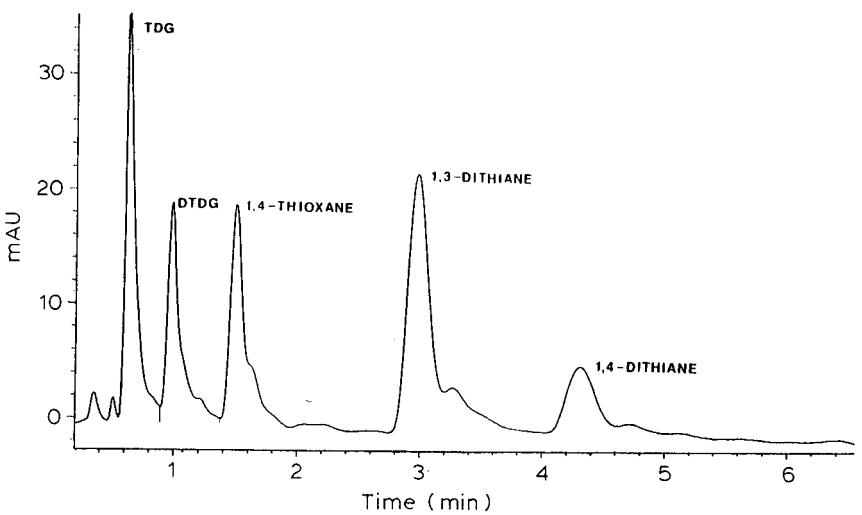

Fig. 5. Chromatogram of TDG, DTDG, 1,4-thioxane, 1,3-dithiane and 1,4-dithiane samples, *ca.* 400 ppm each in methanol. Gradient elution program B.

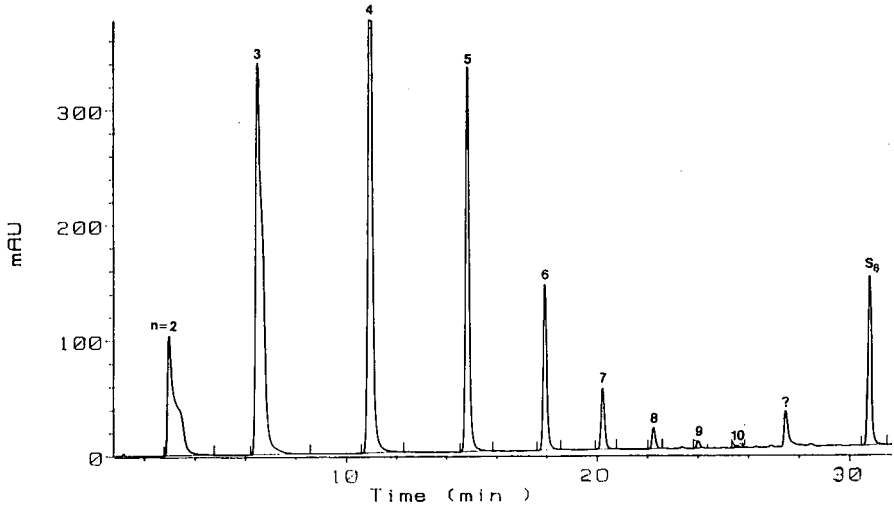

Fig. 6. Chromatogram of polysulfur thiodiglycol sample, 0.5 g in 10 ml methanol. Gradient elution program C. The numbers (n) indicate the sulfur chain length, $(HOCH_2CH_2)_2S_n$ for each peak.

initially on the column and then underwent a separation by a mechanism similar to that for TDPEP.

Supporting evidence for polysulfur species in the sample of polysulfur thiodiglycol was obtained by NMR. Fig. 7 shows the ^{13}C NMR spectrum of DTDG. It contains two peaks: the methylenes attached to sulfur atoms at 41.3 ppm and the hydroxyl-terminated methylenes at 59.6 ppm. Fig. 8 shows the ^{13}C NMR spectrum of the polysulfur thiodiglycol. It contains five peaks in the region of 41.1–42.1 ppm, instead of the single peak at 41.3. The extra peaks correspond to the higher rankings of sulfur linkages (S_3, S_4, S_5, etc.). Based on the relative intensities of the HPLC peaks and the NMR signals the following assignments have been made:

$-CH_2S_2$ 41.3 ppm
$-CH_2S_3$ 41.1 ppm
$-CH_2S_4$ 41.8 ppm
$-CH_2S_5$ 42.1 ppm
$-CH_2S_6$ 42.0 ppm

A four-peak separation was also visible for the hydroxyl-terminated methylenes in the 59.4–59.6 ppm region. A peak corresponding to sulfur S_6 species was not observed, possibly due to the number of bonds separating the methylenes in the 59.4–59.6 ppm region which cause overlap with the other peaks.

An interesting phenomenon was observed in the ^{13}C NMR spectrum of the polysulfur thiodiglycol sample (Fig. 8). The S_2 methylene was seen at 41.3 ppm and the S_3 methylene at 41.1 ppm, while the S_4 and S_5 methylenes were at 41.8 and 42.1 ppm, respectively. Some type of sulfur shielding effect may be producing the upfield

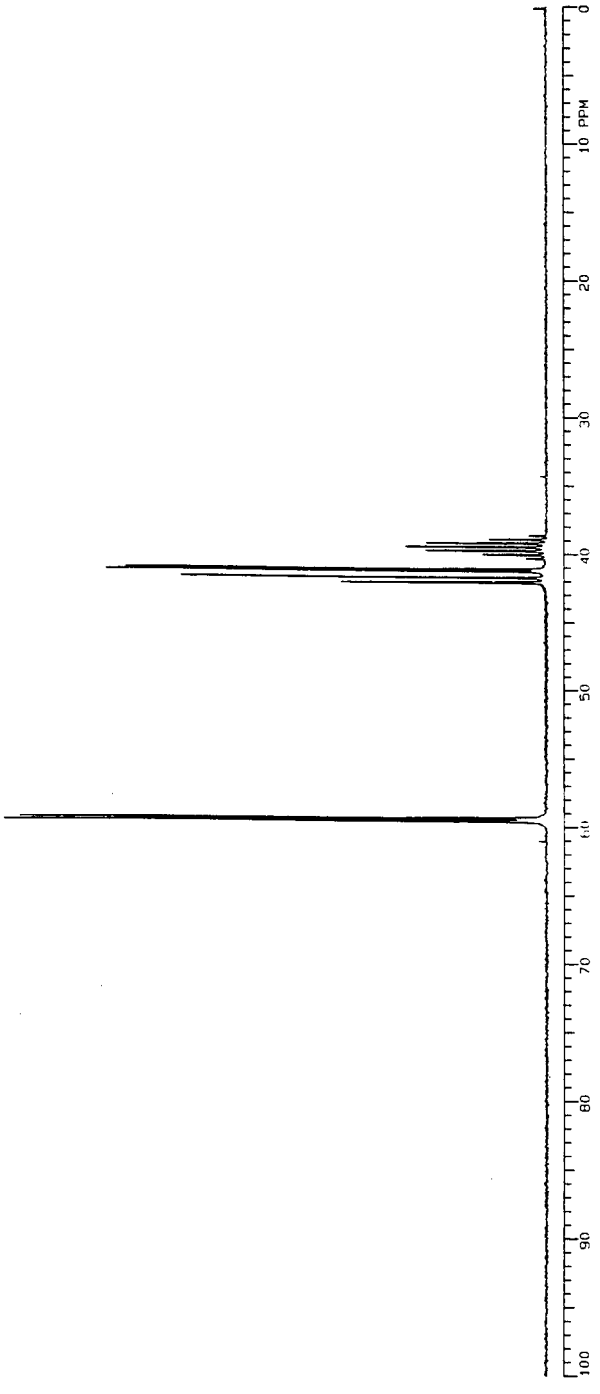

Fig. 7. ^{13}C NMR Spectrum of dithiodiglycol, $(HOCH_2CH_2)_2S_2$.

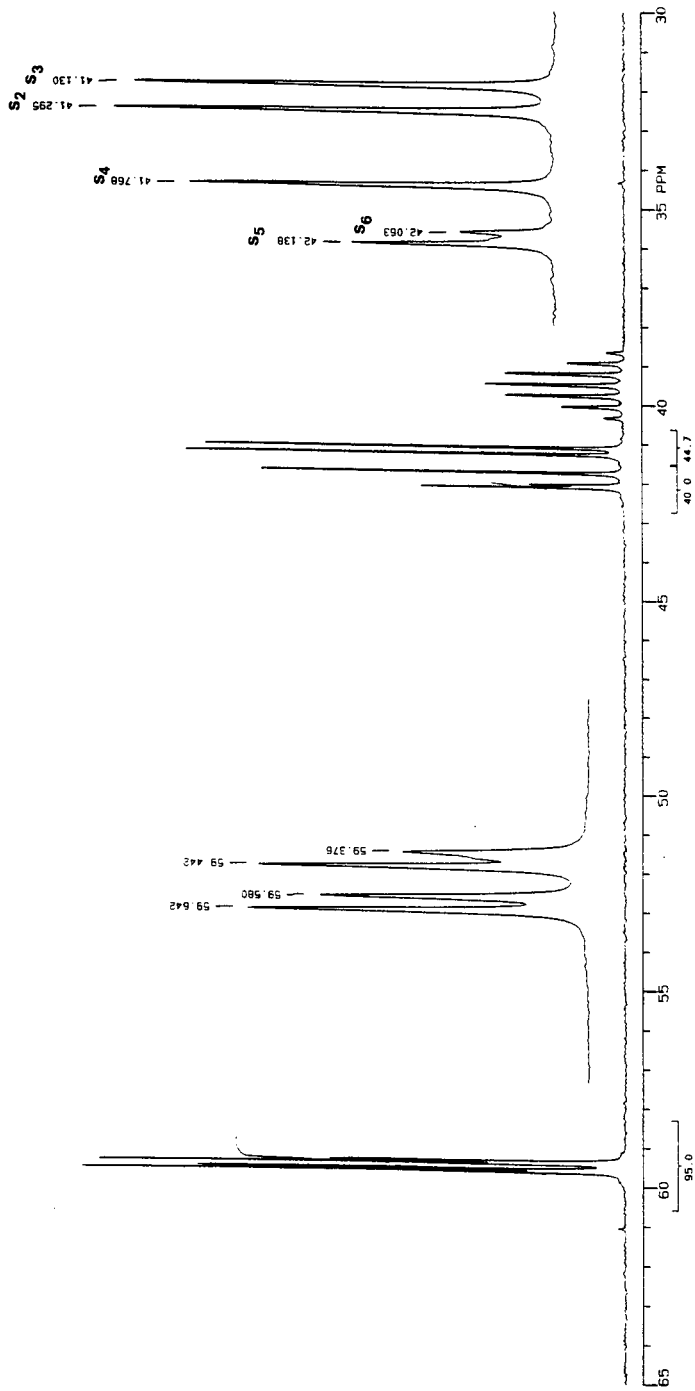

Fig. 8. ^{13}C NMR spectrum of polysulfur thiodiglycol ($HOCH_2CH_2)_2S_n$.

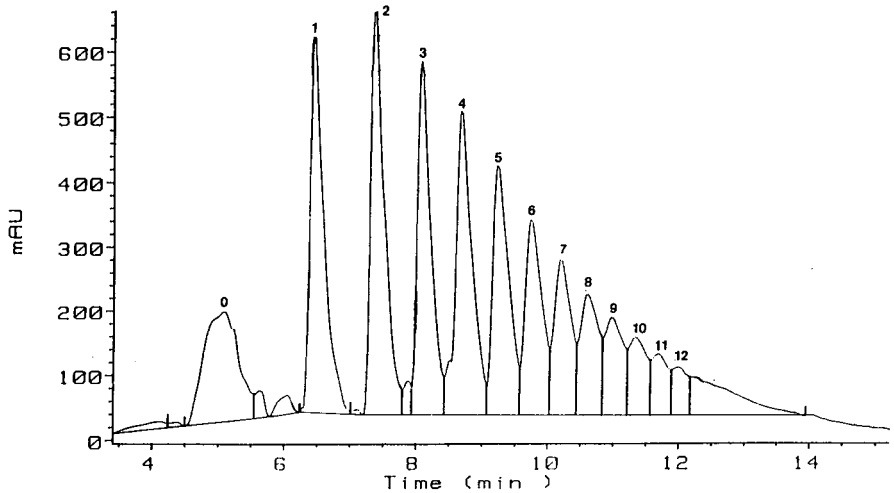

Fig. 9. Chromatogram of oxidized thiodiglycolpolyether polymer sample, 0.5 g in 10 ml methanol. Gradient elution program D. The numbers (n) indicate the polymer chain length, $H(OCH_2CH_2SOCH_2CH_2)_n$-OH for each peak.

shift of the $-CH_2S_3-$ while the higher rankings of sulfur (S_4, S_5, etc.) were shifted downfield, as expected.

A sample of polythiodiglycol polyethers was oxidized to the structure represented by $H(OCH_2CH_2SOCH_2CH_2)OH$. Fig. 9 shows the separation of this material by means of elution program D. The corresponding oxidized *vs.* unoxidized TDPEP

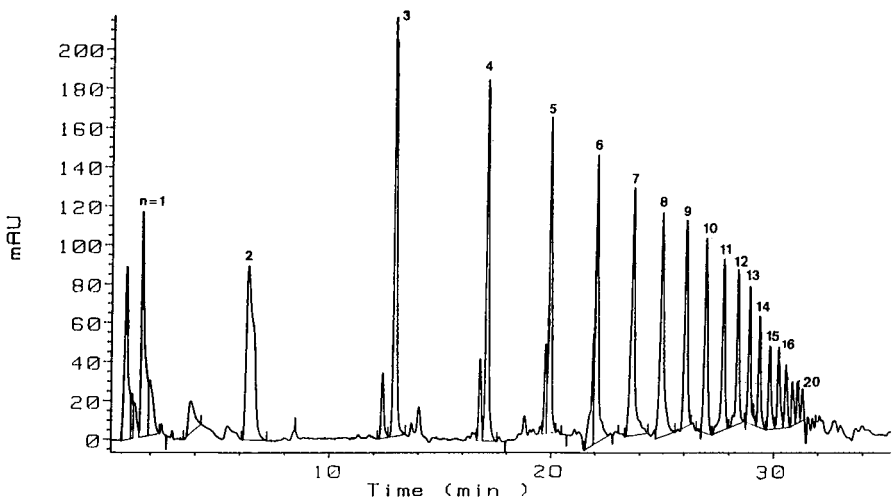

Fig. 10. Chromatogram of polythiodiglycol formal polymer sample, 0.5 g in 10 ml methanol. Gradient elution program E. The numbers (n) indicate the polymer chain length, $H(OCH_2CH_2SCH_2CH_2)_n$-$OCH_2CH_2SCH_2CH_2OH$ for each peak.

oligomeric species decrease in retention time dramatically. Since this material is soluble in water and methanol in all proportions, it does not precipitate on the column under these conditions. Thus, these oligomeric species were separated exclusively by a sorption mechanism. The large decrease in retention time may also be partly a result of the increase in oxygen content. This may be similar to the decrease in retention time observed by Mockel[10] when comparing alkyl ethers to the corresponding alkylthio ethers. Mockel speculated that this effect was due to the increase in hydrogen bonding with the eluent, due to the increase oxygen content.

Fig. 10 illustrates the separation of at least twenty polythiodiglycol formal oligomeric species by means of elution program E. A pressure increase was observed when this sample was injected. This was due to the material being only partly soluble in water and totally soluble in methanol, which resulted in precipitation on the column. If the resulting resolution of this material was due only to a sorption mechanism, the increase in oxygen content in these species should have decreased the retention time relative to corresponding TDPEP species. But the gradient program for this separation had to reach 100% methanol 10 min sooner than the solvent program for the corresponding TDPEP to obtain similar retention times. Thus, the corresponding formal oligomers were retained on the column more strongly than the TDPEP species. It can be argued that the increase in retention time could be a result of the increase in the alkyl chain length. Mockel[10] observed that the retention time of polysulfides increased as the alkyl chain length increased. Most likely, these compounds were separated by a combination of all of these mechanisms.

CONCLUSIONS

Semi-micro-bore reversed-phase HPLC has been shown to resolve effectively thiodiglycolpolyether polymers into at least twenty oligomeric species. It is apparent that these oligomeric species are separated by a sorption mechanism as well as a precipitation dissolution mechanism. Our separation scheme was applied to other compounds with similar structures.

ACKNOWLEDGEMENTS

We thank Dr. David Lankin of Varian Instruments for his help and permission to use the VXR 300 NMR spectrophotometer. Discussions with Dr. John G. Gilmore were helpful in the preparation this manuscript.

REFERENCES

1 G. Barka and P. Hoffmann, *J. Chromatogr.*, 389 (1987) 273.
2 C. Kuo, T. Provder and A. F. Kah, *Paint & Resin*, March/April (1983) 26.
3 D. Munteanu, A. Isfan and D. Bratu, *Crhomatographia*, 23 (1987) 412.
4 K. Jinno and T. Sato, *J. Liq. Chromatogr.*, 6 (1983) 1631.
5 D. W. Armstrong and K. H. Bul, *Anal. Chem.*, 54 (1982) 706.
6 G. Glockner, J. H. M. van den Berg, N. L. J. Meijerink, T. G. Scholte and R. Koningsveld, *Macromolecules*, 17 (1984) 962.
7 G. Glöckner and J. H. M. van den Berg, *J. Chromatogr.*, 352 (1986) 511.
8 T. H. Mourey and G. A. Smith, *Anal. Chem.*, 56 (1984) 1773.
9 T. H. Mourey, *Anal. Chem.*, 56 (1984) 1777.
10 H. J. Möckel, *J. Chromatogr.*, 317 (1984) 589.

Journal of Chromatography, 461 (1989) 305–313
Elsevier Science Publishers B.V., Amsterdam — Printed in The Netherlands

CHROMSYMP. 1524

ANALYTICAL STUDY OF NON-IONIC SURFACTANTS USED IN ENHANCED OIL RECOVERY

OPTIMIZATION OF ANALYTICAL CONDITIONS IN REVERSED-PHASE PARTITION CHROMATOGRAPHY

P. L. DESBENE*, B. DESMAZIERES and J. J. BASSELIER
P. and M. Curie University, Laboratory of Structural Organic Chemistry, UA 455, 4 Place Jussieu, 75230 Paris Cédex 05 (France)
and
A. DESBENE-MONVERNAY
Paris VII University, ITODYS, 1 rue Guy de la Brosse, 75005 Paris (France)

SUMMARY

The analysis of non-ionic polyoxyethylenic surfactants used in enhanced oil recovery was investigated by reversed-phase partition chromatography with UV detection. A systematic comparative survey of commercially available non-polar stationary phases (C_{18}, C_8, C_6, C_4, C_2, phenyl, cyano and diol) is presented. Various solvents miscible with water (methanol, acetonitrile, tetrahydrofuran, dioxane, acetone and 2-propanol) were tested as mobile phases. A good evaluation of the distribution *versus* the number of ethylene oxide groups in these surfactants was obtained with alkyl-bonded silica (C_{18} and C_8) by isocratic elution with tetrahydrofuran or acetonitrile as solvent additives. Peaks were identified by the simultaneous elution of pure standards.

INTRODUCTION

Various chromatographic methods have been proposed for the analysis of polyoxyethylenic surfactants similar to those used in enhanced oil recovery. Most of the studies have been performed by normal-phase high-performance liquid chromatography (HPLC). The literature[1–5] suggests that adsorption chromatography will not give a satisfactory analysis of surfactants that have a wide distribution of polyoxyethylene oxide units. The only HPLC technique that appears to offer promise for the analysis of surfactants in terms of their ethylene oxide distribution is normal-phase partition chromatography using amino-bonded silica[6–9], cyano-bonded material[10–13] and, more recently, diol-bonded packings[14–16]. In particular, we have previously reported the analysis of non-ionic surfactants (KL 6, KM 11 and KM 20) containing ethylene oxide units of various lengths condensed with long-chain (C_{16} and C_{18})

0021-9673/89/$03.50

aliphatic alcohols via normal-phase partition chromatography on diol-bonded silica[16,17]. The mean lengths of the polyoxyethylene chains in these compounds are 6.2, 11.4 and 19.8 ethylene oxide units (E.O.), respectively, according to the standard method AFNOR NFT 73403 (cloud point measure)[18]. These values are rounded off by the manufacturer to 6, 11 and 20 E.O., respectively. It is interesting that these values are in good agreement with the mean lengths of polyoxyethylene chain deduced from ^{1}H NMR measurements[19]. These complex mixtures also contain 2–3% of polyoxyethyleneglycol (PEG), determinated by the Weibull method[20,21]. They are finally characterized by the presence of various fatty alcohol chains that we have analysed by gas chromatography (GC) after cleavage in the presence of hydrobromic acid[22]. For KM 11 and KM 20, the repartition of fatty alcohol chains is saturated C_{16} chains 30% and saturated C_{18} chains 70%, and for KL 6 saturated C_{16} chains 30%, saturated C_{18} chains 35% and unsaturated C_{18} chains 35%.

We have previously analysed these surfactants in *n*-decane, as a model of a petroleum phase, and in brine[17]. In order to perform the analysis of these surfactants in crude oil phases, a specific and sensitive detection method, such as electrochemical detection, is required. As this detection method is difficult to carry out in normal-phase partition chromatography, we considered reversed-phase partition chromatography, already used in surfactant studies.

Non-ionic surfactants, such as phenyl derivatives of polyoxyethylene glycols[23,24] and ethylene oxide condensates with fatty alcohols[7,23,25–28], have been studied by reversed-phase partition chromatography. Various bonded alkyl silicas (C_2, C_8 and C_{18}) and various polar mobile phases (mainly methanol) have been used in isocratic elution[23,26,27] and gradient elution[25,29,30]. Previous work on the analysis of polyoxyethylene condensates of fatty alcohols showed that it was impossible to study the distribution of polyoxyethylene chains *versus* the ethylene oxide number with C_8 or C_{18} bonded silica and an aqueous methanol mobile phase[7,23,28]. Under these conditions, the separation obtained was a function of fatty chain length. The separation as a function of the number of ethylene oxide units was possible on C_2 bonded silica with acetonitrile as a solvent additive, provided that there was only one fatty alcohol chain[27]. We have found only one reference concerning the study of the distribution of polyoxyethylene chains in a mixture of surfactants obtained from C_{12} and C_{16} fatty alcohols[25]. A C_{18} bonded silica stationary phase was used, and the analysis was performed by gradient elution with water–methanol. Unfortunately, the overlap of the two distributions (corresponding to C_{12} and C_{16} alkyl chains) was too great and the interpretation of these distributions was difficult.

In order to obtain the distribution of polyoxyethylene chains in KL 6, KM 11 and KM 20 surfactants with both C_{16} and C_{18} fatty alcohol chains (and also an unsaturated C_{18} chain in KL 6), we have optimized the analysis. We tested the commercially available stationary phases used in reversed-phase partition chromatography (C_2, C_4, C_6, C_8, C_{18}, phenyl, cyano and diol) and various aqueous-organic mobile phases [methanol, tetrahydrofuran (THF), acetonitrile, dioxane, 2-propanol and acetone].

EXPERIMENTAL

Materials

The apparatus consisted of a PU 4003 dual-piston pump and associated controller (Philips Analytical, Cambridge, U.K.), a Model 7010 injector with a 10–100-μl sample loop (Rheodyne, Cotati, CA, U.S.A.) and a PU 4025 UV–VIS detector (Philips Analytical). The signal from the detector was displayed on a Kipp & Zonen (Delft, The Netherlands) recorder. A Hewlett-Packard (Palo Alto, CA, U.S.A.) terminal 1, level 4 integrator from an HP 5880A gas chromatograph was used to handle the data. A Gilson (Villiers-le-Bel, France) Model 202 fraction collector and an R 401 refractometric detector (Waters Assoc., Milford, MA, U.S.A.) were added to the system in order to prepare standards with various polyoxyethylene chain lengths.

The eight columns tested had the same inside diameter (4.6 mm) but different lengths. The 5-μm Nucleosil C_4 column (SFCC, Gagny, France) was 100 mm long, the 5-μm Nucleosil C_6 (SFCC), the 5-μm Ultraspher C_{18} (Beckman, Fullerton, CA, U.S.A.) and the 7-μm Nucleosil CN columns (the last was packed in our laboratory by the method reported by Coq *et al.*[31]) were 150 mm long and the 5-μm Nucleosil phenyl (SFCC), 7-μm LiChrospher diol (Merck, Darmstadt, F.R.G.), 5-μm Nucleosil C_8 and 5-μm LiChrosorb C_2 columns (the last two were packed in our laboratory by the Rocca method[31]) were 250 mm long.

All the organic solvents were of HPLC grade from Merck (Darmstadt, F.R.G.), BDH (Poole, U.K.), SDS (Ivry, France) and Prolabo (Paris, France). The water was made using Milli-Q and Milli-Ro systems (Millipore, Molsheim, France). The surfactant standards with six ethylene oxide units and either a C_{16} or a C_{18} moiety were purchased from Nikko Chemicals (Tokyo, Japan). The surfactants studied (KL 6, KM 11 and KM 20, from Marchon France, Saint Mihiel, France) were of technical grade; their characteristics are given in Table I. 3,5-Dinitrobenzoyl chloride (DNB) (RP grade) derivatization reagent was purchased from Prolabo.

An HP 5880A gas chromatograph (Hewlett-Packard) fitted with a 25 m × 0.25 mm I.D. CP Sil5 capillary column (Chrompack France, Les Ulis, France) was used for the determination of fatty alcohol chains in the different non-ionic surfactants.

TABLE I

CHARACTERISTICS OF THE THREE SURFACTANTS ANALYSED

Characteristic	*KL 6*	*KM 11*	*KM 20*
Mean number of E.O. units:			
According to AFNOR standard[18]	6.2	11.4	19.8
According to NMR[19]	6.4	12.1	19.0
PEG content* (%)	2.4	2.5	3.0
Repartition of fatty alcohol chains (%)**			
Saturated C_{16}	30 ± 2	30 ± 2	30 ± 2
Saturated C_{18}	35 ± 2	70 ± 2	70 ± 2
Unsaturated C_{18}	35 ± 2	–	–

* Determined by means of the Weibull method[20].

** PEG = polyethylene glycol; determined by GC analysis after treatement with hydrobromic acid–acetic acid[22].

Measures of molar absorptivity of the standards obtained by semi-preparative HPLC (after derivatization to the esters with DNB) were performed using an HP 8450A UV–VIS spectrophotometer (Hewlett-Packard).

Method

The water present in each sample was removed by Dean and Stark azeotropic distillation[32] with benzene. DNB was added in a stoichiometric amount, together with magnesium shavings to remove hydrochloric acid formed in the reaction. KL 6 and KM 11 required refluxing for 30 min; KM 20 required 1 h. After refluxing, the solution was cooled and filtered and the benzene was evaporated. The resulting ester was suitable for analysis by HPLC without further preparation.

The standards of polyethoxylated alcohols containing a fixed number of ethylene oxide units were obtained after semi-preparative separations of KM 11 components (derivatized to DNB esters) by normal-phase HPLC with diol-bonded silica using the previously described conditions[16].

RESULTS AND DISCUSSION

Two of the surfactants (KM 11 and KM 20) have no chromophoric group and cannot be detected by UV methods. We therefore derivatized the surfactants with DNB by the method of Nozawa and Ohnuma[27] to obtain absorption at 254 nm. Although KL 6 has a chromophoric group (unsaturation), it was also derivatized. We have verified with standards obtained from KM 11 by semi-preparative HPLC that, regardless of the polyoxyethylene chain length, and within experimental error, the molar absorptivity is constant ($\varepsilon_{254} = 8100$). This result is in agreement with those obtained by Ahel and Giger[9] for polyoxyethylated alkylphenols.

In order to optimize the separation of the polyoxyethylene chains of the surfactants, we undertook a comparative study of various available reversed-phase columns.

Whatever the bonded silica considered (diol, cyano or phenyl) and regardless of the nature of the added solvents (methanol, THF, acetonitrile, acetone, 2-propanol), these systems were not sufficiently selective and did not allow an acceptable resolution. This was particularly true with the diol and cyano phases, where no separation was observed as a function of number of ethylene oxide units. The phenyl phase was the most selective of the three moderately polar phases tested, but its resolution was still insufficient and did not allow the analysis of the surfactants as a function of number of ethylene oxide units.

From the literature data, the C_2 stationary phase appeared, among the commercial alkyl phases, to be the most promising[27]. Therefore, we first tested the efficiency of this phase. With different solvent additives (THF, mixtures of THF and 2-propanol and, mainly, acetonitrile), the chromatograms showed a better resolution of the most polar compounds in the complex mixtures analysed than the chromatograms obtained with the preceding phases of intermediate polarity. However, regardless of the nature of the mobile phase, their resolution was still insufficient.

For all non-ionic surfactants analyzed (KL 6, KM 11 and KM 20), the C_4 bonded silica, which is, in theory, more apolar than the preceding one, did not give improved resolution. Among the solvent additives, acetonitrile gave the best selectivity.

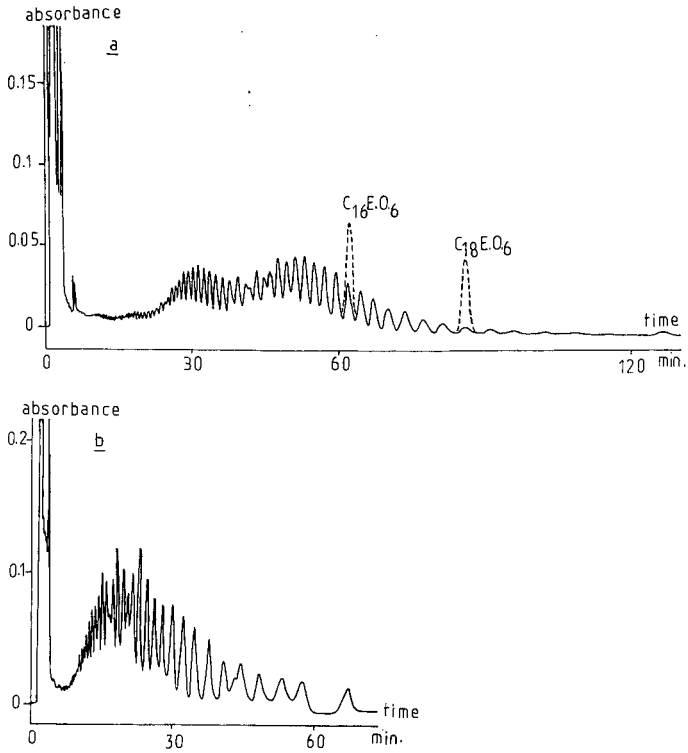

Fig 1. Chromatograms of non-ionic surfactants, derivatized with DNB, obtained with a C_6 stationary phase (Nucleosil C_6, d_p = 5 μm). Column, 15 × 0.46 cm I.D.; mobile phase, acetonitrile–water (60:40) or acetone–water (65:35); flow-rate, 1 ml/min; detection wavelength, 254 nm with acetonitrile and 340 nm with acetone as solvent additive. (a) KM 20 ester; (b) KM 11 ester.

With the more apolar C_6 bonded silica it was impossible to obtain a separation of the polyoxyethylene chains when methanol was used as the solvent additive, but the other additives (THF, acetone and acetonitrile) allowed a more or less satisfactory resolution, depending on the nature of the surfactant being analysed. Using acetonitrile or acetone as solvent additives, this stationary phase allowed an acceptable resolution of KM 20 (Fig. 1a). In fact, we observed under these conditions two distinct series of peaks. The first series, having the smallest capacity factor, corresponded to the polyoxyethylene chains condensed on a C_{16} fatty alcohol. The second series, which was observed at a higher elution volume, corresponded to the ethylene oxide condensates with a C_{18} fatty alcohol. The simultaneous elution of two standards, each with a polyoxyethylene chain of 6 units and with a C_{16} and a C_{18} fatty chain, showed that there was a shift of 7 ethylene oxide units between the two series. Unfortunately, the C_6 phase, which gave an acceptable analysis for surfactants with high ethylene oxide numbers (such as KM 20), was less suitable for the analysis of surfactants with shorter polyoxyethylene chains, such as KM 11 (Fig. 1b). These encouraging results led us to study more lipophilic stationary phases.

We also studied the influence of the solvent additives on selectivity and resolution with C_8 bonded silica. In agreement with literature data[7,23], methanol did

not allow a separation with respect to number of ethylene oxide units, but fatty alcohol chains were separated. Using dioxane, resolution as a function of the number of ethylene oxide units was not achieved. The other solvent additives (THF, THF–2-propanol, acetone, acetonitrile) gave a satisfactory resolution of KM 20 and KM 11. The addition of 2-propanol to THF did not modify the selectivity. Acetonitrile gave the best selectivity, as with C_2 and C_6 stationary phases, and allowed separation. As with the C_6 bonded silica, the presence of two series of peaks indicated of a further separation of the aliphatic chains. In order to obtain a correct determination of the number of ethylene oxide units for each peak, we performed the simultaneous elution of standard samples. The distance between the two alkyl chains, for the same number of ethylene oxide units, was 8 E.O. This shift was sufficient to allow the study of the distribution of KM 11 and KM 20 *versus* the number of ethylene oxide units. The relative abundances of the C_{16} and C_{18} fatty chains was known (30% and 70%, respectively; see Experimental), so it was possible to quantify the distributions by correcting for the partial overlap. The mean value of the number of ethylene oxide units ($\bar{n}$) could therefore be calculated for each surfactant. In fact, the plots of log k' *versus* n E.O for each fatty chain (C_{16} or C_{18}) are linear and parallel. Because of the peak broadening when the elution time increased and the partial overlapping of the two series of peaks, the chromatograms such as those given in Fig. 1 (KM 11 and KM 20) gave a distorted representation of the distribution of these surfactants as a function of their number of ethylene oxide units. To avoid these distorsions, we give the histograms of the distribution of KM 11 and KM 20 in Figs. 2 and 3. These histograms are easily obtained from the integration of chromatographic peaks, the molar absorptivity being constant, as mentioned above, regardless of the polyoxyethylene chain length. Therefore, all further chromatograms of the surfactants are presented in the form of histograms. The mean length of the polyoxyethylene chains was easily deduced from the histograms or was calculated. The following values were found: $\bar{n}_{exp.} = 12.9$ E.O. for KM 11 and $\bar{n}_{exp.} = 18.3$ E.O. for KM 20.

For KL 6, the selectivity obtained with this phase was not sufficient with THF or acetonitrile to allow the study of its distribution *versus* the number of ethylene oxide units. This important difference in chromatographic behaviour resulted from the greater complexity of the KL 6. This surfactant was obtained by condensing ethylene oxide on fatty alcohols with C_{16}, C_{18} and unsaturated C_{18} chains (see Experimental). The three series of distributions were not sufficiently separated to allow meaningful

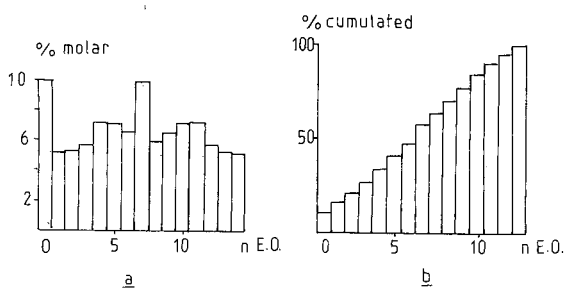

Fig. 2. Distribution histograms of KM 11 determined from the chromatographic data obtained with a C_8 stationary phase (Nucleosil C_8). Mobile phase, acetonitrile–water (60:40); flow-rate, 1 ml/min; detection wavelength, 254 nm. (a) Retention as a function of E.O.; (b) cumulated retention as a function of E.O.

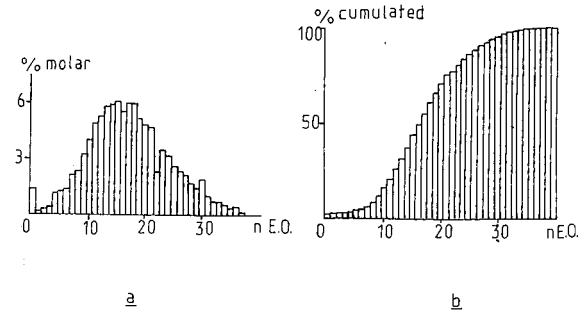

Fig. 3. Distribution histograms of KM 20 determined from the chromatographic data obtained with a C_8 stationary phase. Conditions as in Fig. 2.

corrections for overlapping peaks. In order to obtain the evaluation of the mean length of the polyoxyethylene chain of KL6, we used a more lipophilic phase.

C_{18} bonded silica allowed a good separation with KM 11 and KM 20 using acetonitrile, THF or acetone as solvent additive. No resolution was obtained using dioxane. In good agreement with literature data[25–28], methanol gave only a separation of the fatty chains. The study of the distributions of KM 11 and KM 20, as a function of their number of ethylene oxide units, with this stationary phase was performed using an acetonitrile–water mobile phase. The distance between the two alkyl chains, for the same number of ethylene oxide units, was 12 E.O. This greater selectivity allowed a better precision in the determination of ethylene oxide distributions because peak overlapping was less of a problem. The mean values of the number of ethylene oxide units are $\bar{n}_{exp}$ = 12.3 E.O. for KM 11 and $\bar{n}_{exp}$ = 18.5 E.O. for KM 20. Of course, this greater selectivity was obtained with a longer time of analysis. For KL 6, the association of acetonitrile as solvent additive with a C_{18} stationary phase allowed for the first time an almost acceptable resolution. The overlapping of the three series of peaks, corresponding to the three different fatty alcohol chain, was still complex but it was possible to obtain an evaluation of the distribution. We assumed that the ethylene oxide repartition was symmetrical. From the integration of the ten first peaks, a relatively satisfactory value was obtained (Fig 4.): $\bar{n}_{exp}$ = 6.6 E.O. for KL 6.

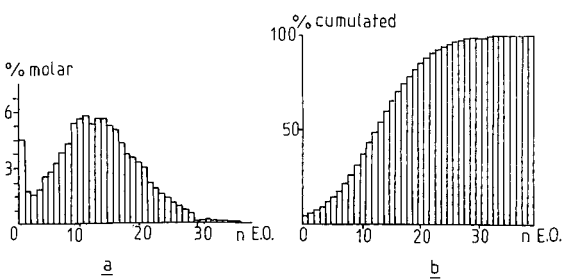

Fig. 4. Distribution histograms of KL 6 determined from the chromatographic data obtained with a C_{18} stationary phase (Ultraspher C_{18}). Mobile phase, acetonitrile–water (75:25); flow-rate, 1 ml/min; detection wavelength, 254 nm. (a) Retention as a function of E.O.; (b) cumulated retention as a function of E.O.

CONCLUSION

From this comparative survey of the various bonded phases available in reversed-phase partition chromatography, it appeared that only alkyl-bonded phases allowed the analysis of the distributions of ethylene oxide condensates of fatty alcohol mixtures as a function of the number of ethylene oxide units and alkyl chain lengths.

Methanol did not give a separation with respect to the number of ethylene oxide units. With this solvent additive, only fatty chains were separated. Dioxane did not allow a separation as a function of the number of ethylene oxide units, regardless of the nature of the alkyl-bonded silica (C_8 or C_{18}). Only three solvents, acetonitrile, THF and, to a lesser extent, acetone, gave the possibility of adapting the selectivity in order to obtain a satisfactory resolution of the non-ionic surfactants used in enhanced oil recovery as a function of their number of ethylene oxide units.

The C_{18} stationary phase gave the best performances, allowing a correct analysis regardless of the mean length of the polyoxyethylene chain. Unfortunately, this stationary phase, which gave the best selectivity, was characterized by long times of analysis.

The C_8 bonded phase afforded slightly shorter times of analysis and a satisfactory analysis of the two surfactants with longer polyoxyethylene chains (KM 11 and KM 20). For KL 6, the overlap of the three distributions did not allow the precise determination of the mean number of ethylene oxide units, but a global quantification was possible.

The selected systems, *i.e.*, C_8 or C_{18} bonded silica and THF–water or acetonitrile–water mobile phases, have been examined according to their compatibility with electrochemical detection in a further study which will be reported later[33].

REFERENCES

1 C. F. Allen and L. I. Rice, *J. Chromatogr.*, 110 (1975) 151.
2 M. C. Allen and D. E. Linder, *J. Am. Oil Chem. Soc.*, 58 (1981) 950.
3 J. D. McClure, *J. Am. Oil Chem. Soc.*, 59 (1982) 364.
4 A. Aserin, M. Frenkel and N. Garti, *J. Am. Oil Chem. Soc.*, 61 (1984) 805.
5 K. Nakamura and I. Matsumoto, *Nippon Kagaku Kaishi*, 8 (1975) 1342.
6 N. Cortesi, E. Moretti and E. Fredli, *Riv. Ital. Sostanze Grasse*, 57 (1980) 141.
7 B. F. Bogatzki and L. H. Lippmann, *Acta Polym.*, 34 (1983) 219.
8 M. Ahel and W. Giger, *Anal. Chem.*, 57 (1985) 1577.
9 M. Ahel and W. Giger, *Anal. Chem.*, 57 (1985) 2584.
10 A. C. Hayman and N. A. Parris, paper presented at the *1979 Pittsburgh Conference*, paper 24.
11 A. M. Rothman, *J. Chromatogr.*, 253 (1982) 283.
12 R. E. A. Escott, S. J. Brinkworth and T. A. Steedman, *J. Chromatogr.*, 282 (1983) 655.
13 J. A. Pilc and P. A. Sermon, *J. Chromatogr.*, 398 (1987) 375.
14 I. Zeman, J. Silha and M. Bares, *Tenside Deterg.*, 23 (1986) 4.
15 I. Zeman, *J. Chromatogr.*, 363 (1986) 223.
16 P. L. Desbène, B. Desmazières, V. Even, J. J. Basselier and L. Minssieux, *Chromatographia.*, 24 (1987) 857.
17 P. L. Desbène, B. Desmazières, J. J. Basselier and L. Minssieux, *Chromatographia.*, 24 (1987) 588.
18 *AFNOR Standard*, T 73-403, Paris, (1977).
19 P. L. Desbène, V. Even, B. Desmazières, J. J. Basselier and L. Minssieux, *Analusis*, 16 (1988) 55.
20 B. Weibull, *International Congress on Surface-Active Agents*, Cologne, 1960, Vol. 3, pp. 121–124.
21 ISO Standard, 2268, Paris, (1979).

22 B. G. Luke, *J. Chromatogr.*, 84 (1973) 43.
23 D. Thomas and J. L. Rocca, *Analusis*, 7 (1979) 386.
24 W. R. Melander, A. Nahum and C. Horváth, *J. Chromatogr.*, 185 (1979) 129.
25 H. Shiraishi, A. Otsuki and K. Fuwa, *Bull. Chem. Soc. Jpn.*, 55 (1982) 1410.
26 M. Kudoh, S. Konami, S. Fudano and S. Yamaguchi, *J. Chromatogr.*, 234 (1982) 209.
27 A. Nozawa and T. Ohnuma, *J. Chromatogr.*, 187 (1980) 261.
28 N. Parris and J. K. Weil, *J. Am. Oil Chem. Soc.*, 56 (1979) 775.
29 R. M. Cassidy, *J. Liq. Chromatogr.*, 1 (1978) 241.
30 F. P. B. van der Maeden, M. E. F. Biemond and P. C. G. M. Janssen, *J. Chromatogr.*, 149 (1978) 539.
31 B. Coq, C. Gonnet and J. L. Rocca, *J. Chromatogr.*, 106 (1975) 249.
32 A. I. Vogel, *Practical Organic Chemistry*, Longmans, London, 3rd, ed., 1961, p. 429.
33 P. L. Desbène, B. Desmazières, J. J. Basselier and A. Desbène-Monvernay, *J. Chromatogr.*, in press.

Journal of Chromatography, 461 (1989) 315–326
Elsevier Science Publishers B.V., Amsterdam — Printed in The Netherlands

CHROMSYMP. 1443

HIGH-PERFORMANCE LIQUID CHROMATOGRAPHIC SEPARATION OF RING-OXIDIZED METABOLITES OF NITRO-POLYCYCLIC AROMATIC HYDROCARBONS*

LINDA S. VON TUNGELN and PETER P. FU*
National Center for Toxicological Research, Food and Drug Administration, Jefferson, AR 72079 (U.S.A.)

SUMMARY

Nitro-polycyclic aromatic hydrocarbons (nitro-PAHs) are widespread genotoxic environmental pollutants, which require metabolic activation to exert their biological activities. Metabolism of nitro-PAHs generates ring-oxidized metabolites including epoxides, phenols, dihydrodiols and tetrahydrotetrols. Separation of the oxidized metabolites and related compounds of a series of isomeric nitro compounds derived from anthracene, benz[*a*]anthracene, benzo[*a*]pyrene and benzo[*e*]pyrene was studied by high-performance liquid chromatography (HPLC) of different types of columns (monomeric and polymeric; reversed-phase and normal-phase). In the reversed-phase HPLC system, the general elution order of these compounds is: parent nitro-PAHs > phenolic derivatives > epoxides > dihydrodiols > tetrahydrotetrols. Among the geometric isomers, *trans*-dihydrodiols with both hydroxyl groups at the quasiaxial positions were eluted earlier than those with the hydroxyl groups at the quasiequatorial positions. Orientation of the nitro substituent has also been found to be an important structural feature for determining the relative retention order. Among the geometric isomers of nitro-PAHs and *trans*-dihydrodiols, the isomers with their nitro groups perpendicular or nearly perpendicular to the aromatic rings were eluted faster than the analogues with their nitro groups parallel or nearly parallel to the aromatic rings. Normal-phase HPLC gave opposite retention order, but with different separability among some of the compounds. Therefore, combination of both reversed- and normal-phase HPLC provides efficient separation of the ring-oxidized derivatives of nitro-PAHs. Results are also presented to compare the separation efficiency among different types of columns used. The results suggest that the polarity of solutes is the principal factor for determining their HPLC retention time.

INTRODUCTION

Nitro-polycyclic aromatic hydrocarbons (nitro-PAHs) are genotoxic environmental pollutants formed by the incomplete combustion of organic material[1–4]. The

* The opinion or assertions contained herein are the private ones of the authors and are not to be construed as official or reflecting the views of the Food and Drug Administration.

0021-9673/89/$03.50

biological effects of these compounds are thought to arise from metabolic activation to reactive electrophiles by ring oxidation and/or reduction of the nitro functional group[1–4]. Recently, it has been found that some structural features of nitro-PAHs can affect metabolism, DNA-binding, mutagenic and tumorigenic potencies, and chemical properties of these types of compounds[5]. It is known that when a compound is eluted from a high-performance liquid chromatographic (HPLC) column, polarity and molecular size of the molecule are important factors in determining the HPLC retention time[6,7]. Polarity is largely related to the type, number, and location of the functional group(s) in a molecule. To date, the relationship between the structures of the ring-oxidized derivatives of nitro-PAHs and their HPLC retention times has not been reported. Consequently, a study of HPLC retention times of ring-oxidized derivatives of nitro-PAHs on different types of HPLC columns will help toward a better understanding of their structural features, and in turn, may be useful for correlating the structures and mutagenicity/tumorigenicity of these compounds.

In this report, a series of ring-oxidized derivatives of nitro-PAHs were used as substrates in an examination of the separating ability of several HPLC columns of different types (monomeric and polymeric; reversed-phase and normal-phase). The structures and abbreviations of the compounds used in this study are shown in Figs. 1 and 2. The analytical HPLC columns employed included: Zorbax ODS column (250 × 4.6 mm I.D.), Zorbax SIL column (250 × 4.6 mm I.D.) (DuPont Medical Products, Wilmington, DE, U.S.A.), Vydac ODS column (250 × 4.6 mm I.D.) (The Separations Group, Hesperia, CA, U.S.A.), Waters μBondapak C_{18} column (300 × 3. 9 mm I.D.) (Milford, MA, U.S.A.), Deltabond phenyl column (250 × 4.6 mm I.D.), and Deltabond C_8 column (250 × 4.6 mm I.D.) (Keystone Scientific, State College, PA, U.S.A.).

EXPERIMENTAL

Materials

1-Nitro-7,8,9,10-tetrahydrobenzo[*a*]pyrene (7,8,9,10-H_4-1-NBaP), 7,8,9,10-H_4-3-NBaP, 7,8,9,10-H_4-6-NBaP, 7-hydroxy-6-nitro-7,8,9,10-tetrahydrobenzo[*a*]pyrene (7-OH-7,8,9,10-H_4-6-NBaP), 6-nitro-9,10-dihydrobenzo[*a*]pyren-7(8H)-one (7-keto-7,8,9,10-H_4-6-NBaP), *cis*-5,6-dihydroxy-7-nitro-5,6-dihydrobenz[*a*]anthracene (7-NBA *c*-5,6-dihydrodiol), *cis*-5,6-diacetoxy-7-nitro-5,6-dihydrobenz[*a*]anthracene (7-NBA *c*-5,6-diacetate), *cis*-4,5-diacetoxy-6-nitro-4,5-dihydrobenzo[*a*]pyrene (6-NBaP *c*-4,5-diacetate), 11-hydroxy-7-nitrobenz[*a*]anthracene (11-OH-7-NBA), 7-hydroxy-6-nitrobenzo[*a*]pyrene (7-OH-6-NBaP) and 11-acetoxy-7-nitrobenz[*a*]anthracene (11-OAc-7-NBA) were synthesized as previously described[8–10]. 7-Keto-7,8,9,10-H_4-1-NBaP, 7-keto-7,8,9,10-H_4-3-NBaP, 7-OH-7,8,9,10-H_4-1-NBaP and 7-OH-7,8,9,10-H_4-3-NBaP were obtained as minor products from the nitration of 9,10-dihydrobenzo[*a*]pyren-7(8H)-one, followed by reduction. *cis*-11,12-Dihydroxy-6-nitro-11,12-dihydrochrysene (6-NC *c*-11,12-dihydrodiol) was synthesized according to the procedure of El-Bayoumy and Hecht[11]. *cis*-4,5-Dihydroxy-1-nitro-4,5-dihydrobenzo[*a*]pyrene (1-NBaP *c*-4,5-dihydrodiol) and *cis*-4,5-dihydroxy-3-nitro-4,5-dihydrobenzo[*e*]pyrene (3-NBeP *c*-4,5-dihydrodiol) were similarly prepared.

cis-11,12-Diacetoxy-6-nitro-11,12-dihydrochrysene (6-NC *c*-11,12-diacetate) and *cis*-4,5-diacetoxy-3-nitro-4,5-dihydrobenzo[*e*]pyrene (3-NBeP *c*-4,5-diacetate)

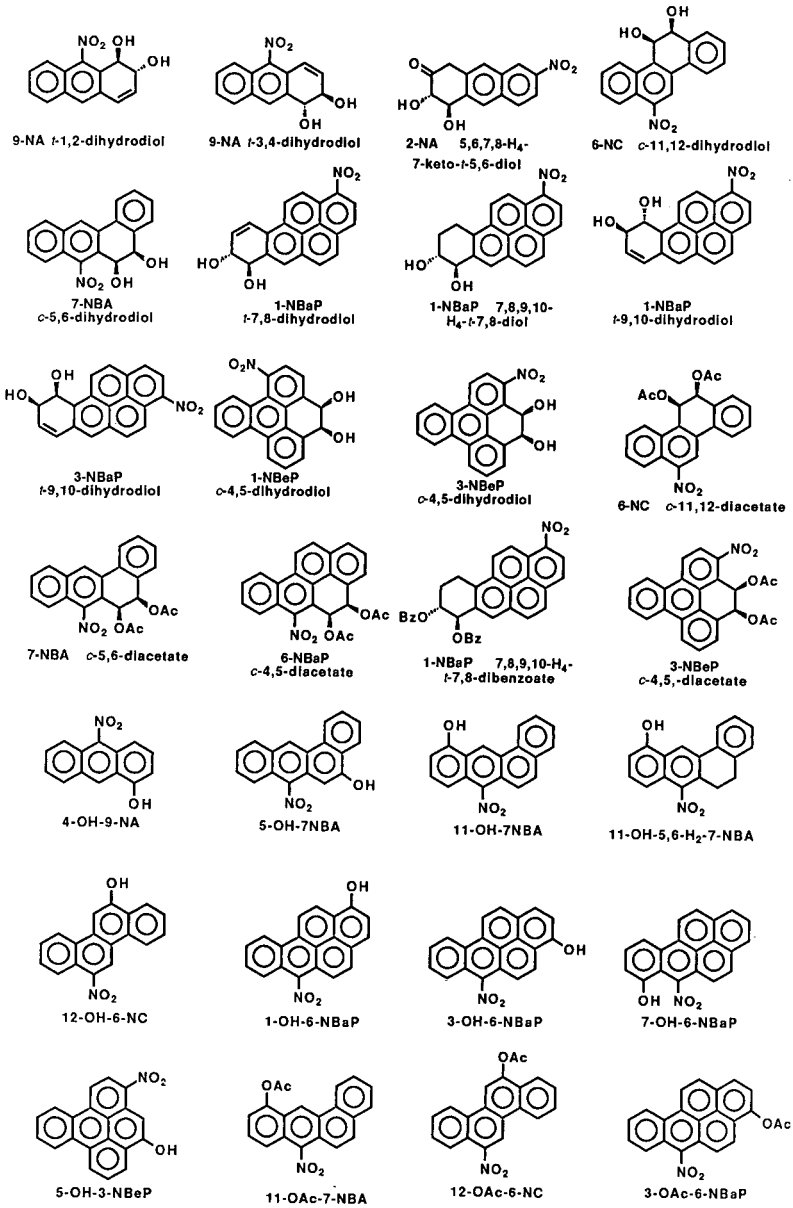

Fig. 1. Structures and abbreviations of nitro-PAH dihydrodiols, hydroxylated nitro-PAHs and their derivatives used in this study.

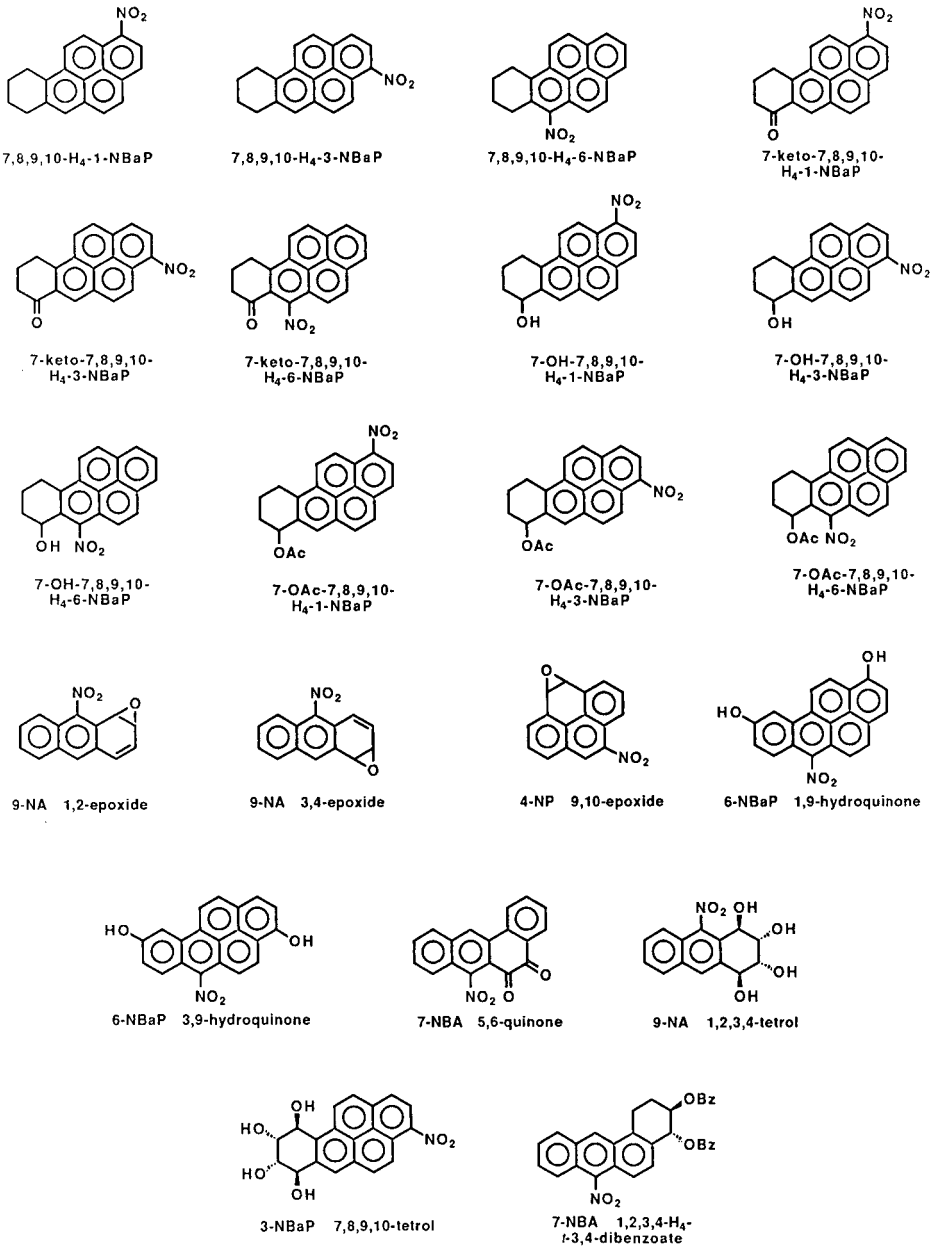

Fig. 2. Structures and abbreviations of 7-substituted nitro-7,8,9,10-tetrahydrobenzo[*a*]pyrene, nitro-PAH epoxides and other ring-oxidized derivatives.

were prepared by acetylation of the corresponding *cis*-dihydrodiols with acetic anhydride and pyridine[12]. 7-OAc-7,8,9,10-H_4-1-NBaP and 7-OAc-7,8,9,10-H_4-3-NBaP were prepared under similar conditions. 4-Hydroxy-9-nitroanthracene (4-OH-9-NA), 5-hydroxy-7-nitrobenz[*a*]anthracene (5-OH-7-NBA), 12-hydroxy-6-nitrochrysene(12-OH-6-NC), 5-hydroxy-3-nitrobenzo[*e*]pyrene (5-OH-3-NBeP), and 12-acetoxy-6-nitrochrysene (12-OAc-6-NC) were synthesized by acid-catalyzed dehydration of the corresponding *cis*-dihydrodiol precursors with *p*-toluenesulfonic acid in ben-zene[13]. All the *trans*-dihydrodiols, the remaining phenolic compounds and derivatives, epoxides, hydroquinones, and tetrahydrotetrols were obtained after metabolism of the corresponding parent nitro-PAHs by rat liver microsomes, as previously described[14–18]. The structures of the compounds synthesized were well characterized by spectral analysis of their UV absorption, mass, and high-resolution proton NMR data. The configuration and conformation of the dihydrodiol compounds and the orientation of the nitro substituents of each compound were also characterized by spectral analysis.

Chromatography

The HPLC system was composed of two Model 510 pumps, a Model 680 gradient controller, a U6K injector, a Model 440 absorbance detector set at 254 nm (all from Waters Assoc.), a Varian Associates (Walnut Creek, CA, U.S.A.) Model A-25 dual-pen strip-chart recorder, and optionally, a Hewlett-Packard (Palo Alto, CA, U.S.A.) Model 3390A reporting integrator. In addition, a Hewlett-Packard 1040A detection system with the data processing unit option was available to replace the Model 440 detector and the strip-chart recorder. The columns used were: Zorbax ODS (250 × 4.6 mm I.D.); Zorbax SIL (250 × 4.6 mm I.D.); Vydac 201TP54 ODS (250 × 4.6 mm I.D.); Deltabond C_8 (250 × 4.6 mm I.D.); Deltabond phenyl (250 × 4.6 mm I.D.); and μBondapak C_{18} (300 × 3.9 mm I.D.). All columns have a particle size of 5 μm except for the Waters μBondapak which has a 10-μm size. The flow-rate was set at 0.5 ml/min. All mobile phases were HPLC grade solvents and were premixed and degassed before use. Each injection was 20 μl or less in volume. The retention time was recorded by the 1040A detection system, and the ultra-violet absorption spectrum of the material in each chromatographic peak was measured, so that the identity of the chromatographic peak could be confirmed. After the retention time of each compound had been determined, a mixture of two or more compounds was chromatographed in order to confirm the relative elution order and reproducibility of retention times. To eliminate the possible UV photolytic decomposition of the compounds, a UV absorbing film was placed above the light diffusion panel.

RESULTS AND DISCUSSION

For studying the relationships of structure and retention order of the ring-oxidized derivatives of nitro-PAHs, a set of these compounds was prepared for HPLC analysis. For comparison, we have determined the retention times of these compounds by employing a Zorbax ODS column, a μBondapak C_{18} column, a Vydac ODS column, a normal-phase Zorbax SIL column, a Deltabond phenyl column, and a Deltabond C_8 column. The Zorbax ODS, the μBondapak C_{18}, and the Vydac ODS columns have a conventional bonding between the silicate hydroxy groups and the

substituents. However, the bonded phase of the Zorbax and μBondapak ODS columns is monomeric and the Vydac ODS is polymeric. The Deltabond reversed-phase phenyl and C_8 columns are packed with a uniform matrix of cross-linked polysiloxane functional groups. Thus, comparison of the separation efficiencies of the columns and the retention order of the compounds will promote an understanding of the mechanisms of interaction between the bonded phase and the solutes. Based on the types of functional groups, the ring-oxidized nitro-PAHs used in this study are divided into four groups. Their retention times on different HPLC columns are summarized in Tables I–IV. We have employed a number of different solvent systems and solvent flow-rates in order to obtain suitable retention times for each compound eluted from the different columns. The final conditions chosen are shown in Tables I–IV.

Separation of the ring-oxidized nitro-PAHs by reversed-phase and normal-phase HPLC

Under the chromatographic conditions used in this study, the monomeric Zorbax ODS column separates the nitro-PAH dihydrodiols and their ester derivatives well, with the retention times ranging from 6.0 to 19.7 min (Table I). As an illustration, the separation of a mixture of six nitro-PAH dihydrodiols and diacetates on a Zorbax ODS column is shown in Fig 3. The polymeric Vydac ODS column gave poor separation of the compounds shown in Table I and, with only one exception, gave retention times which were all within a range of 1.3 min (from 5.4 to 6.7 min). These results are in contrast to previous observations[19] that the Vydac ODS column resolves the monohydroxylated derivatives of benzo[*a*]pyrene, benz[*a*]anthracene and chrysene with a wider range of retention times than the monomeric Zorbax ODS column. Locke[20] suggested that the relative solubility of each PAH in the polar mobile phase was the basis of reversed-phase selectivity. Oxidation of nitro-PAHs to the ring-oxidized derivatives generates additional polar functional group(s), thus increasing the water solubility of the molecules, and affecting their partition coefficients between the stationary and the mobile phases. This may be the reason for the poor selectivity of the polymeric Vydac ODS column for ring-oxidized nitro-PAHs.

Neither the Deltabond phenyl column nor the Deltabond C_8 column separates these compounds well. All had retention times within 2.6 min (from 6.4 to 9.0 min). A similar lack of efficiency of these two columns was observed in the separation of other ring-oxidized nitro-PAHs (Tables II, III and IV). These columns are fully packed with a uniform matrix of cross-linked polysiloxane functional groups, which may well shield the remaining active sites in the silica support. Thus, our results suggest that interaction between the polar active sites of the silica support and the ring-oxidized nitro-PAH substrates is involved in the separation mechanism.

The phenolic nitro-PAHs and their derivatives are well separated by both the Zorbax and the Vydac ODS columns (Table II). The efficient separation by the Zorbax ODS column is illustrated in Fig 4. Although an acetoxy group is less polar than a hydroxy group, it can be eluted earlier than a hydroxylated nitro-PAH, if the former has a larger molecular size (*e.g.*, 3-OAc-6-NBaP and 11-OH-5,6-H_2-7-NBA). As expected, 7-NBA 4,5-quinone, which contains two keto functional groups, has a shorter retention time than the other compounds, which have only one hydroxyl or acetoxy group (Table II), The retention times of the compounds eluted from the μBondapak C_{18} column and the Zorbax SIL column were all close together.

To test the effect of a polar functional group in a nitro-PAH on the HPLC

TABLE I

HPLC RETENTION TIMES OF NITRO-POLYCYCLIC AROMATIC HYDROCARBON DIHYDRODIOLS AND THEIR DERIVATIVES ON DIFFERENT REVERSED- AND NORMAL-PHASE COLUMNS

The eluent for all reversed-phase HPLC analyses was methanol–water (95:5, v/v) at a flow-rate of 0.5 ml/min. The eluent for normal-phase HPLC was 30% of tetrahydrofuran in hexane at a flow-rate of 0.5 ml/min. ND = not determined. Due to apparent column inefficiency, the retention times of the compounds marked with a "–" were not determined.

	Retention time (min)					
	Zorbax ODS	*Vydac ODS*	*μBondapak ODS*	*Deltabond*		*Zorbax SIL*
				phenyl	C_8	
9-NA *t*-1,2-dihydrodiol	6.1	5.4	6.3	7.3	6.5	23.9
9-NA *t*-3,4-dihydrodiol	6.6	5.5	6.7	7.4	6.6	31.7
2-NA 5,6,7,8-H_4-7-keto-*t*-5,6-diol	6.0	5.4	6.3	7.2	6.4	12.7
6-NC *c*-11,12-dihydrodiol	6.8	5.7	7.0	7.5	6.7	25.0
7-NBA *c*-5,6-dihydrodiol	6.8	5.6	6.9	7.6	6.6	14.5
1-NBaP *t*-7,8-dihydrodiol	8.3	6.7	7.7	7.6	6.8	ND
1-NBaP 7,8,9,10-H_4-*t*-7,8-diol*	7.8	6.7	7.4	–	–	ND
1-NBaP *t*-9,10-dihydrodiol	6.3	5.4	6.5	–	–	ND
3-NBaP *t*-9,10-dihydrodiol	6.4	5.5	6.6	7.4	6.5	ND
1-NBeP *c*-4,5-dihydrodiol	6.8	5.7	7.1	7.6	6.6	12.8
3-NBeP *c*-4,5-dihydrodiol	7.1	5.8	7.3	7.7	6.7	16.5
6-NC *c*-11,12-diacetate	9.0	6.1	8.3	8.3	7.2	11.4
7-NBA *c*-5,6-diacetate	8.3	5.9	7.8	8.2	6.9	13.4
6-NBaP *c*-4,5-diacetate	9.7	6.7	8.8	8.7	7.3	14.3
1-NBaP 7,8,9,10-H_4-*t*-7,8-dibenzoate*	19.7	12.4	13.7	–	–	13.0
3-NBeP *c*-4,5-diacetate	9.2	6.5	8.3	–	–	15.6

* It has not been determined yet whether or not the nitro group is at the C_1 or the C_2 position.

retention time, a series of 7-substituted mononitrated 7,8,9,10-tetrahydrobenzo[*a*]-pyrene was used for HPLC analysis (Table III). The good separation of these compounds by a Vydac ODS column is shown in Fig. 5. The three mononitrated

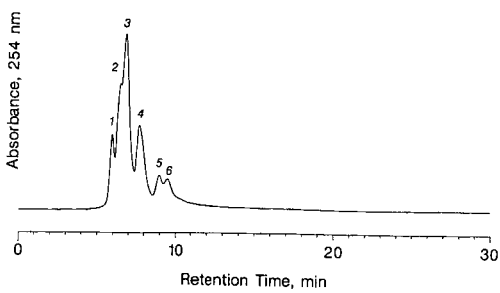

Fig. 3. Reversed-phase HPLC of some dihydrodiols and derivatives of nitro-polycyclic aromatic hydrocarbons on a Zorbax ODS column (250 × 4.6 mm I.D.), eluted with methanol–water (19:1, v/v) at a flow-rate of 0.5 ml/min. The compounds in the chromatographic peaks are: (1) 9-NA *t*-1,2-dihydrodiol; (2) 9-NA *t*-3,4-dihydrodiol; (3) 6-NC *c*-11,12-dihydrodiol; (4) 1- or 3-NBaP 7,8,9,10-H_4-*t*-7,8-diol, (5) 7-NBA *c*-5,6-diacetate; and (6) 6-NBaP *c*-4,5-diacetate.

TABLE II

HPLC RETENTION TIMES OF THE PHENOLIC AND ACETOXY DERIVATIVES OF NITRO-PO LYCYCLIC AROMATIC HYDROCARBONS ON DIFFERENT REVERSED- AND NORMAL-PHA SE COLUMNS

The eluent for all reversed-phase HPLC analyses was methanol–water (95:5, v/v) at a flow-rate of 0.5 ml/min. The eluent for normal-phase HPLC was 30% of tetrahydrofuran in hexane at a flow-rate of 0.5 ml/min. Due to apparent column inefficiency, the retention times of the compounds marked with a "–" were not determined. ND = not determined.

	Retention time (min)					
	Zorbax ODS	*Vydac ODS*	*μBondapak ODS*	*Deltabond*		*Zorbax SIL*
				phenyl	C_8	
4-OH-9-NA	7.8	5.9	7.5	–	6.9	ND
5-OH-7-NBA	8.4	6.1	7.7	–	–	14.2
11-OH-7-NBA	10.5	6.9	8.9	7.9	7.1	13.1
11-OH-5,6-H_2-7-NBA	7.8	5.9	7.6	7.9	6.8	13.5
12-OH-6-NC	11.3	7.4	9.2	7.8	7.2	ND
1-OH-6-NBaP	12.5	11.9	ND	–	–	ND
3-OH-6-NBaP	12.6	11.3	9.9	9.1	7.3	15.4
7-OH-6-NBaP	11.0	8.7	8.9	8.1	7.7	14.5
5-OH-3-NBeP	7.4	5.9	7.3	–	–	ND
11-OAc-7-NBA	11.1	7.2	9.2	8.3	7.5	12.5
12-OAc-6-NC	11.1	7.3	9.1	7.7	7.2	14.0
3-OAc-6-NBaP	13.5	9.8	10.2	8.6	7.7	13.9

H_4-BaPs (23, 24 and 25) have longer retention times than their 7-substituted derivatives. While the hydroxy-substituted derivatives (14, 15 and 16) and the acetoxy-substituted derivatives (18, 19 and 20) exhibit a poorer separation than the parent nitro-H_4-BaPs (23, 24 and 25), the keto derivatives (17, 21 and 22) are better separated than the parent compounds. Thus, these results exemplify that increasing the solubility in the polar mobile phase by introducing a functional group into a solute

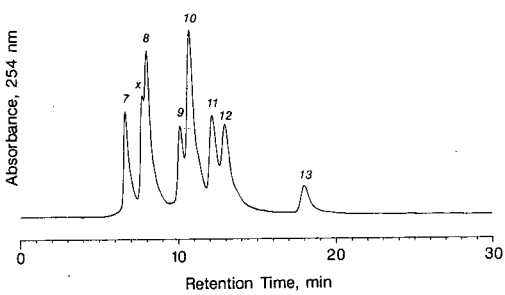

Fig. 4. Reversed-phase HPLC of some phenolic and acetoxy derivatives of nitro-polycyclic aromatic hydrocarbons on a DuPont Zorbax ODS column (250 × 4.6 mm I.D.), eluted with methanol–water (19:1, v/v) at a flow-rate of 0.5 ml/min. The compounds in the chromatographic peaks are: (7) 7-NBA 4,5-quinone; (8) 5-OH-7-NBA; (9) 11-OH-7-NBA; (10) 11-OAc-7-NBA; (11) 3-OH-6-NBaP; (12) 3-OAc-6-NBaP; and (13) 11-OH-5,6-H_2-7-NBA. The chromatographic peak marked with "X" contains an impurity.

TABLE III

HPLC RETENTION TIMES OF 1-, 3-, AND 6-NITRO-7,8,9,10-TETRAHYDROBENZO[*a*]PYRENE AND THEIR 7- AND 8-SUBSTITUTED DERIVATIVES ON DIFFERENT REVERSED- AND NORMAL-PHASE COLUMNS

The eluent for all reversed-phase HPLC analyses was methanol–water (95:5, v/v) at a flow-rate of 0.5 ml/min. The eluent for normal-phase HPLC was 30% of tetrahydrofuran in hexane at a flow-rate of 0.5 ml/min. Due to apparent column inefficiency, the retention times of the compounds marked with a "–" were not determined. ND = not determined.

	Retention time (min)					
	Zorbax ODS	*Vydac ODS*	*μBondapak ODS*	*Deltabond*		*Zorbax SIL*
				phenyl	C_8	
7,8,9,10-H_4-1-NBaP	47.3	25.1	ND	–	–	ND
7,8,9,10-H_4-3-NBaP	51.6	27.0	ND	–	–	ND
7,8,9,10-H_4-6-NBaP	20.5	22.7	ND	–	–	ND
7-Keto-7,8,9,10-H_4-1-NBaP	14.3	11.6	10.4	8.8	7.9	12.5
7-Keto-7,8,9,10-H_4-3-NBaP	14.1	13.4	10.7	9.0	8.0	12.1
7-Keto-7,8,9,10-H_4-6-NBaP	9.9	5.5	6.5	9.0	7.4	ND
7-OH-7,8,9,10-H_4-1-NBaP	10.5	8.1	8.9	8.0	7.2	23.4
7-OH-7,8,9,10-H_4-3-NBaP	10.3	7.8	8.9	8.0	7.2	20.6
7-OH-7,8,9,10-H_4-6-NBaP	10.0	7.2	8.6	8.1	7.2	12.2
7-OAc-7,8,9,10-H_4-1-NBaP	14.4	12.4	10.4	–	–	13.0
7-OAc-7,8,9,10-H_4-3-NBaP	16.4	10.7	11.3	–	–	12.2
7-OAc-7,8,9,10-H_4-6-NBaP	14.9	11.0	10.7	–	–	11.4
1-NBaP 7,8,9,10-H_4-*t*-7,8-dibenzoate	19.7	12.4	13.7	–	–	13.0
1-NBaP 7,8,9,10-H_4-*t*-7,8-diol	7.8	6.7	7.4	–	–	ND

does not always decrease the selectivity of the polymeric Vydac ODS column. HPLC analysis of additional nitro-PAHs with different types of substituents will be required to determine how substituents can affect the column selectivity.

The Zorbax ODS reversed-phase column gave a better separation of a number of

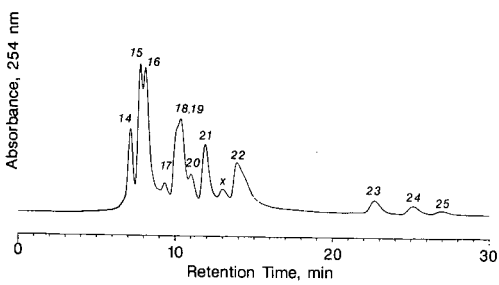

Fig. 5. Reversed-phase HPLC of 1-, 3, and 6-nitro-7,8,9,10-tetrahydrobenzo[*a*]pyrene and their 7- and 8-substituted derivatives on a Vydac ODS column (250 × 4.6 mm I.D.), eluted with methanol–water (19:1, v/v) at a flow-rate of 0.5 ml/min. The compounds in the chromatographic peaks are: (14) 7-OH-7,8,9,10-H_4-6-NBaP; (15) 7-OH-7,8,9,10-H_4-1-NBaP; (16) 7-OH-7,8,9,10-H_4-3-NBaP; (17) 7-keto-7,8,9,10-H_4-6-NBaP; (18) 7-OAc-7,8,9,10-H_4-6-NBaP; (19) 7-OAc-7,8,9,10-H_4-1-NBaP; (20) 7-OAc-7,8,9,10-H_4-3-NBaP; (21) 7-keto-7,8,9,10-1-NBaP; (22) 7-keto-7,8,9,10-H_4-3-NBaP; (23) 7,8,9,10-H_4-6-NBaP; (24) 7,8,9,10-H_4-1-NBaP; and (25) 7,8,9,10-H_4-3-NBaP. The chromatographic peak marked with "X" contains unidentified material.

TABLE IV

HPLC RETENTION TIMES OF RING-OXIDIZED NITRO-POLYCYCLIC AROMATIC HYDROCARBONS ON DIFFERENT REVERSED- AND NORMAL-PHASE COLUMNS

The eluent for all reversed-phase HPLC analyses was methanol–water (95:5, v/v) at a flow-rate of 0.5 ml/min. The eluent for normal-phase HPLC was 30% of tetrahydrofuran in hexane at a flow-rate of 0.5 ml/min. Due to apparent column inefficiency, the retention times of the compounds marked with a "—" were not determined. ND = not determined.

	Retention time (min)					
	Zorbax ODS	*Vydac ODS*	*μBondapak ODS*	*Deltabond*		*Zorbax SIL*
				phenyl	C_8	
9-NA 1,2-epoxide	7.7	5.5	6.7	7.9	—	12.2
9-NA 3,4-epoxide	7.7	5.9	7.4	7.9	7.0	13.6
4-NP 9,10-epoxide	7.1	6.1	7.1	7.7	6.7	14.0
6-NBaP 1,9-hydroquinone	7.9	6.7	7.8	—	—	ND
6-NBaP 3,9-hydroquinone	9.0	6.6	7.6	—	—	ND
9-NA 1,2,3,4-tetrol	5.7	5.3	6.1	7.1	6.4	ND
3-NBaP 7,8,9,10-tetrol	6.2	ND	6.5	—	—	ND
7-NBA 1,2,3,4-H_4-*t*-3,4-dibenzoate	21.1	12.2	13.8	—	—	14.0

ring-oxidized nitro-PAHs, as shown in Tables I–III. However, this column cannot separate 9-NA 1,2-epoxide from 9-NA 3,4-epoxide, by either isocratic or gradient elution. On the other hand, both the monomeric μBondapak C_{18} and the Vydac ODS column can effect this separation (Table IV). Although both Zorbax and μBondapak columns are packed with monomeric octadecyl-bonded phases on a silica gel support, the slight difference in support materials and/or phase preparation can result in different selectivity for polar functional groups[21,22]. Similar observations on the different selectivities for nitro-PAHs on monomeric ODS columns of different manufacturers have been reported elsewhere[23,24]. When chromatographed on the Zorbax SIL column with 30% of tetrahydrofuran in hexane, 9-NA 1,2-epoxide and 9-NA 3,4-epoxide were eluted at 12.2 and 13.6 min, respectively. We have previously found on many occasions that a mixture of two or more ring-oxidized PAHs inseparable by a reversed-phase HPLC column, can be well resolved in a normal-phase HPLC system[14,17,25,26]. Thus, the separation of many compounds, including PAHs, nitro-PAHs, and their ring-oxidized derivatives by HPLC will be facilitated by employing a combination of both reversed-phase and normal-phase HPLC systems.

Relationships between structures and HPLC retention times

(A) The polarity of the molecule is an important factor in determining the HPLC retention time. This can be well supported by the following observations.

(1) In the reversed-phase HPLC system, the general elution order of these compounds is: parent nitro-PAHs > tetrahydro-ketones = acetates > phenolic derivatives > epoxides > dihydrodiols > diol-ketones > tetrahydrotetrols. A specific example is the 9-nitroanthracene (9-NA) and its ring-oxidized derivatives, chromatographed on a Zorbax ODS analytical column:

9-NA tetrahydrotetrol < 9-NA *t*-1,2-dihydrodiol < 9-NA *t*-3,4-dihydrodiol <
(5.7 min) (6.1 min) (6.6 min)

9-NA 1,2-epoxide = 9-NA 3,4-epoxide < 4-OH-9-NA < 9-NA
(7.7 min) (7.7 min) (7.8 min) (8.8 min)

(2) Among the geometric isomers, *trans*-dihydrodiols with both hydroxyl groups in quasiaxial positions were eluted earlier than those with the hydroxyl groups in quasiequatorial positions. Examples include: 9-NA *t*-1,2-dihydrodiol < 9-NA *t*-3,4-dihydrodiol (as shown above) and 1-NBaP *t*-9,10-dihydrodiol < 1-NBaP *t*-7,8-dihydrodiol (see Table I).

(3) A compound having a nitro group perpendicular or nearly perpendicular to the aromatic ring was eluted earlier than the isomer(s) with the nitro group parallel or nearly parallel to the aromatic ring. For example, 7,8,9,10-H_4-6-NBaP and its derivatives were eluted earlier that their analogues having the nitro group at the C_1 and C_3 positions (see Table III).

(4) A phenolic compound having a hydroxyl group *peri* to the nitro substituent was eluted earlier than its isomers. For example, 7-OH-6-NBaP was eluted earlier than 1-OH-6-NBaP and 3-OH-6-NBaP.

(B) In general, retention times increase as the molecular size of the compound increases.

(C) For separation of ring-oxidized derivatives of nitro-PAHs by reversed-phase HPLC, the Zorbax ODS column gave the best resolution.

The results of this study provide increased understanding of the relationships between the structural features and the HPLC retention times of ring-oxidized derivatives of nitro-PAHs. The relation between HPLC retention times and structures of these has never before been studied. Since structural features have been found to be important factors in correlation with bacterial mutagenicity, DNA binding capability, and possibly the tumorigenicity of nitro-PAHs, our study may also facilitate our mechanistic study on the metabolic activation of nitro-PAHs.

REFERENCES

1 H. S. Rosenkranz and R. Mermelstein, *Mutat. Res.*, 114 (1983) 217.
2 C. M. White (Editor), *Nitrated Polycyclic Aromatic Hydrocarbons*, Hiedelberg, Huthig, 1985.
3 H. Tokiwa and Y. Ohnishi, *CRC Crit. Rev. Toxicol.*, 17 (1986) 23.
4 C. M. King, L J. Romano and D. Schuetzle (Editors), *Carcinogenic and Mutagenic Responses to Aromatic Amines and Nitroarenes*, Elsevier, Amsterdam, 1988.
5 P. P. Fu, M. W. Chou and F. A. Beland, in S. K. Yang and B. D. Silverman (Editors), *Polycyclic Aromatic Hydrocarbon Carcinogenesis: Structure-Activity Relationships*, Vol. II, CRC Press, Boca Raton, FL, 1988, pp. 37–65.
6 S. A. Wise, W. J. Bonnett, F. R. Guenther and W. E. May, *J Chromatogr. Sci.*, 19 (1981) 457.
7 M. A. Stadalius, H. S. Gold and L. R. Snyder, *J. Chromatogr.*, 296 (1984) 31.
8 M. W. Chou, R. H. Heflich, D. A. Casciano, D. W. Miller, J. P. Freeman, F. E. Evans and P. P. Fu, *J. Med. Chem.*, 27 (1984) 1156.
9 P. P. Fu, M. W. Chou, D. W. Miller, G. L. White, R. H. Heflich and F. A. Beland, *Mutat. Res.*, 143 (1985) 173.
10 Y. S. Wu, C. C. Lai, P. P. Fu and L. E. Unruh, *J. Chinese Chem. Soc.*, 35 (1988) 159.
11 K. El-Bayoumy and S. S. Hecht, *Cancer Res.*, 44 (1984) 3408.
12 P. P. Fu, C. C. Lai and S. K. Yang, *J. Org. Chem.*, 46 (1981) 220.

13 P. P. Fu, C. Cortez, K. B. Sukumaran and R. G. Harvey, *J. Org. Chem.*, 44 (1979) 4265.
14 P. P. Fu, M. W. Chou, S. K. Yang, F. A. Beland, F. F. Kadlubar, D. A. Casciano, R. H. Heflich and F. E. Evans, *Biochem. Biophys. Res. Commun.*, 105 (1982) 1037.
15 P. P. Fu and S. K. Yang, *Biochem. Biophys. Res. Commun.*, 115 (1983) 123.
16 P. P. Fu, L. S. Von Tungeln and M. W. Chou, *Carcinogenesis*, 6 (1985) 753.
17 P. P. Fu, R. H. Heflich, L. S. Von Tungeln, D. T. C. Yang, E. K. Fifer and F. A. Beland, *Carcinogenesis*, 7 (1986) 1819.
18 M. W. Chou, R. H. Heflich and P. P. Fu, *Carcinogenesis*, 7 (1986) 1837.
19 M. Mushtaq, Z. Bao and S. K. Yang, *J. Chromatogr.*, 385 (1987) 293.
20 D. C. Locke, *J. Chromatogr. Sci.*, 12 (1974) 433.
21 H. Colin and G. Guichion, *J. Chromatogr.*, 141 (1977) 289
22 L. R. Snyder and J. J. Kirkland, *Introduction to Modern Liquid Chromatography*, Wiley, New York, NY, 1979.
23 M. W. Chou, in W. M. Cooke and A. J. Dennis (Editors), *Ninth International Symposium on Polynuclear Aromatic Hydrocarbons*, Battelle Press, Columbus, OH, 1986, pp. 145–153.
24 M. W. Chou, *J. High Resolut. Chromatogr. Chromatogr. Commun.*, 8 (1985) 304.
25 M. W. Chou, D. W. Miller, J. P. Freeman and P. P. Fu, *Chem. Res. Toxicol.*, (1988) 115.
26 P. P. Fu, R. H. Heflich, L. S. Von Tungeln, H. Z. Miranda and F. E. Evans, *Carcinogenesis*, 9 (1988) 951.

Journal of Chromatography, 461 (1989) 327–336
Elsevier Science Publishers B.V., Amsterdam — Printed in The Netherlands

CHROMSYMP. 1435

SEPARATION OF AMINO- AND ACETYLAMINO-POLYCYCLIC AROMATIC HYDROCARBONS BY REVERSED- AND NORMAL-PHASE HIGH-PERFORMANCE LIQUID CHROMATOGRAPHY*

JENG-SHIOW LAI and SANDY S. HUNG
Institute of Applied Chemistry, Providence College, Taichung (Taiwan)
LEONARD E. UNRUH and HYEWOOK JUNG
National Center for Toxicological Research, Jefferson, AR 72079 (U.S.A.)
and
PETER P. FU*
Institute of Applied Chemistry, Providence College, Taichung (Taiwan) and National Center for Toxicological Research, Jefferson, AR 72079 (U.S.A.)

SUMMARY

In the field of chemical carcinogenesis, amino- and acetylamino-polycyclic aromatic hydrocarbons (PAHs) are among the most studied compounds. Many of these compounds have recently been detected in the environment. Presently, knowledge permitting predictions of the high-performance liquid chromatographic (HPLC) retention order of amino- and acetylamino-PAHs, particularly among their geometric isomers is lacking. In order to obtain a better understanding of the separation of these types of compounds, we have studied the separation of a series of structurally related amino- and acetylamino-PAHs derived from naphthalene, phenanthrene, anthracene, pyrene, benz[*a*]anthracene, benzo[*a*]pyrene, and benzo[*e*]pyrene by using reversed-phase and normal-phase HPLC columns of different types (monomeric, polymeric, and chiral stationary phase). The results indicate: (i) Pirkle-type chiral stationary phase columns and the Zorbax SIL column can efficiently separate both the amino-PAHs and acetylamino-PAHs; (ii) in general, there was no correlation between retention time and molecular size; (iii) when acetylamino-PAHs were separated on the monomeric Zorbax ODS column, the isomer with the acetylamino group located at the carbon position of higher electron density has a shorter retention time; and (iv) separation of the parent PAHs was better than that of the amino-PAHs and acetylamino-PAHs. Our results thus may provide useful information for the analysis of amino-PAHs, particularly for distinguishing the geometric isomers of environmental samples.

* The opinions or assertions contained herein are the private ones of the authors and are not to be construed as official or reflecting the views of the Food & Drug Administration.

0021-9673/89/$03.50

INTRODUCTION

Mechanistic studies of metabolic activation of aromatic amines and their amide derivatives is an important research area in chemical carcinogenesis[1,2]. Recent studies have indicated that large quantities of carcinogenic aromatic amines exist in the environment and in natural energy resources, *e.g.* coal distillates[3–8]. Consequently, it is important to detect and identify toxic aromatic amines in the environment. Amino-polycyclic aromatic hydrocarbons (amino-PAHs) constitute the major type of aromatic amines so far studied. There are many geometric isomers that are difficult to separate by conventional analytical methods, including high-performance liquid chromatography (HPLC). There are several reports describing the use of HPLC for the separation of aromatic amines in coal distillates[4–8]. However, the emphasis has been on the detection of these compounds in environmental samples. Little is known concerning the relationships between structural features, such as polarity and molecular size, and HPLC retention time[9–11]. It is known that when a compound is eluted from a HPLC column, polarity and molecular size of the molecule are important factors in determining the HPLC retention time. Polarity is largely related to the type, number, and location of the functional group(s) in the molecule. It has been reported that structural features of amino-PAHs can affect mutagenic and tumorigenic potencies as well as chemical properties of these compounds[12,13]. Consequently, a study of HPLC retention times of amino-PAHs on different types of HPLC columns will help in correlating their structures with mutagenicity–tumorigenicity. For this purpose, we have measured the HPLC retention time of some amino-PAHs and related acetylamino-PAHs on several different HPLC columns (reversed-phase and normal-phase; monomeric, polymeric, and chiral stationary phases).

EXPERIMENTAL

Materials

The structures and abbreviations of the amino-PAHs used in this study are shown in Fig. 1. The following amino-PAHs were purchased from Aldrich (Milwaukee, WI, U.S.A.): 1-A-N, 2-A-N, 1-A-A, 2-A-Ph, 3-A-Ph, 9-A-Ph, 6-A-Ch, 1-A-Py, 2-A-F, and 4-A-Bp. 4-, 6-, 11-, and 12-A-BaP were prepared as previously described[13]. 7-A-BA, 4-A-Py, 1- and 3-A-BeP, 1-, 3-, and 6-A-H_4-BaP, and 1- and 3-A-H_4-BeP were synthesized by reduction of the corresponding nitro-PAH precursors, either with hydrazine and palladium on charcoal in 95% ethanol, or with zinc powder in tetrahydrofuran, methanol, and ammonium chloride[14–17]. 1-, 3-, and 6-Nitro-7,8,9,10-tetrahydrobenzo[*a*]pyrenes and 1- and 3-nitro-9,10,11,12-tetrahydrobenzo[*e*]pyrenes, which were the precursors for preparing the corresponding amino-PAHs, were synthesized as previously described[17]. 6-A-H_2-BaP was synthesized by nitration of 4,5-dihydrobenzo[*a*]pyrene to yield the 6-nitro-4,5-dihydrobenz[*a*]pyrene, which was reduced with hydrazine and palladium on charcoal[15]. 3-A-Ch and 1-A-BaP were synthesized according to published procedures[15,18]. The acetylamino derivatives are similarily abbreviated by adding an additional "A" as a prefix to the abbreviation of the corresponding amino-PAH. For instance while 4-A-Bp designates 4-aminobiphenyl, 4-AA-Bp represents 4-acetylaminobiphenyl. The amido derivatives of the above described amino-PAHs were subsequently synthesized

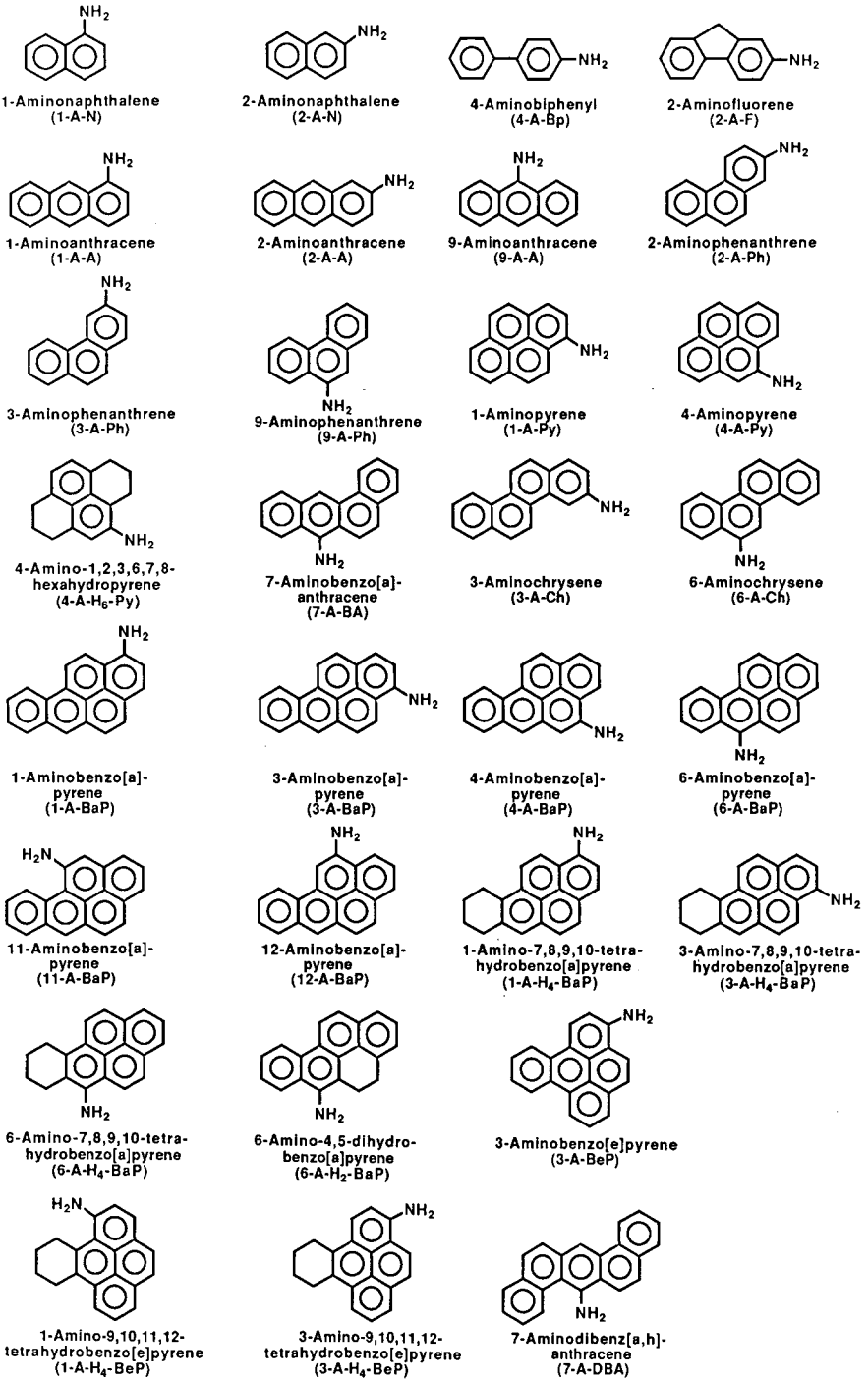

Fig. 1. The names, structure and abbreviations of the amino-PAHs used in this study.

by reacting the amino-PAHs with acetic anhydride and pyridine at ambient temperature for a period of 15 h (ref. 19). All the known, either purchased or synthesized, amino- and acetylamino-PAHs were characterized by comparison of their UV–VIS absorption and mass spectra with the published data. For the identification of the new compounds, high-resolution nuclear magnetic resonance spectral analysis was employed.

Chromatography

The HPLC system was composed of two Beckman/Altex (Fullerton, CA, U.S.A.) Model 100A pumps with prep heads, a Beckman/Altex Model 420 gradient controller, a Beckman/Altex Model 210 injector, a Waters Assoc. (Milford, MA, U.S.A.) Model 440 absorbance detector set at 254 nm, a Kipp & Zonen (Delft, the Netherlands) Model BD41 dual-pen strip-chart recorder, and, optionally, a Hewlett-Packard (Palo Alto, CA, U.S.A.) Model 3390A reporting integrator. A second HPLC system was composed of two Model 510 pump, a Model 680 gradient controller, a U6K injector, a Model 440 absorbance detector (all from Waters Assoc.) set at 254 nm, a Varian (Walnut Creek, CA, U.S.A.) Model A-25 dual-pen strip-chart recorder, and optionally, a Hewlett-Packard Model 3390A reporting integrator. In addition, a Hewlett-Packard 1040A detection system with the Data Processing Unit option was available to be used in place of the Waters Assoc. 440 detector and the appropriate strip-chart recorder. The following columns were used: Zorbax ODS (250 × 4.6 mm I.D.); Zorbax Sil (250 × 4.6 mm I.D.) (DuPont Medical Products, Wilmington, DE, U.S.A.); Vydac 201TP54 (250 × 4.6 mm I.D.) (the Separations Group, Hesperia, CA, U.S.A.); μBondapak Phenyl (250 × 4.6 mm I.D.) (Waters Assoc.); Deltabond C_8 (250 × 4.6 mm I.D.) (Keystone Scientific, State College, PA, U.S.A.) and a Pirkle-type chiral stationary-phase column (250 × 4.6 mm I.D.) (Regis, Morton Grove, IL, U.S.A.) packed with (*R*)-N-(3,5-dinitrobenzoyl)phenylglycine covalently bonded to spherical particles of 5-μm γ-aminopropylsilanized silica. To examine the separation efficiency, a semi-preparative Zorbax ODS column (250 × 21.2 mm I.D.) was employed. All the mobile phases, as described in the footnotes of Tables I and II, were premixed and degassed before use. For each injection 2 μl or less of the solution was used. To eliminate the possible UV photolytic decomposition of the compounds, a UV absorbing film was placed above the lightning diffusion panel.

RESULTS AND CONCLUSION

A set of structuraly related amino-PAHs and acetylamino-PAHs were prepared in order to study the relationships between structure and HPLC retention time. Compounds with slight differences in the structural geometry (*e.g.*, 7-aminobenz[*a*]anthracene *vs.* 6-aminochrysene), molecular size (*e.g.*, 6-aminochrysene *vs.* 6-aminobenzo[*a*]pyrene), and location of the amino/acetylamino functional group served as model compounds for studying the effect of molecular features on HPLC retention time. For comparison, we measured the retention times of these compounds on a monomeric Zorbax ODS column, a polymeric Vydac ODS column, a Deltabond revesed-phase C_8 column, a μBondapak phenyl column, a Zorbax SIL normal-phase column and a Pirkle-type chiral stationary-phase column. Both Zorbax ODS and Vydac ODS columns have a conventional bond between the silicate hydroxyl groups

and the alkyl substituents. Zorbax ODS is a monomeric column and the Vydac ODS is a polymeric column. The Deltabond reversed-phase C_8 column is packed with a uniform matrix of cross-linked polysiloxane functional groups. The findings are summarized below.

Separation of amino-PAHs by reversed-phase and normal-phase HPLC

In general, the Zorbax ODS column, the Zorbax SIL column, and the

TABLE I

HPLC RETENTION TIMES (IN MIN) OF AMINO-PAHs ELUTED FROM DIFFERENT COLUMNS

Compound	*Zorbax ODS**	*Vydac ODS***	*Vydac ODS****	*Zorbax SIL*§	*Deltabond C_8*§§	*Pirkle Ph-Gly*§§§	*Waters phenyl*†
1-A-N	6.5	1.8	2.6	9.7	8.4	4.9	3.2
2-A-N	7.4	1.9	2.7	16.6	8.4	8.0	3.2
4-A-Bp	7.7	2.0	2.8	8.5	8.6	13.1	3.7
2-A-F	9.0	2.1	3.1	9.1	8.8	9.2	3.6
1-A-A	6.2	1.8	2.9	15.6	8.0	8.5	3.2
2-A-A	8.4	2.3	3.4	7.5	8.0	13.6	3.4
9-A-A	6.0	1.7	2.6	19.6	8.0	3.2	2.8
2-A-Ph	8.0	2.4	3.4	9.6	8.4	14.0	3.3
3-A-Ph	8.8	3.6	5.6	9.2	8.4	13.8	3.4
9-A-Ph	7.6	1.9	2.9	14.6	8.6	4.6	3.5
7-A-BA	10.2	6.1	9.2	17.1	–	5.9	3.9
3-A-Ch	10.8	3.6	5.8	10.0	8.8	23.0	4.1
6-A-Ch	9.9	2.5	3.6	8.6	8.7	5.8	3.9
1-A-Py	3.8	8.6	8.0	8.6	8.0	11.4	3.7
4-A-Py	9.2	2.2	3.2	9.0	8.2	12.0	4.0
4-A-H_6-Py	14.3	2.7	3.8	5.7	–	5.5	3.9
1-A-BaP	5.84	1.7	2.6	9.0	–	7.6	3.4
3-A-BaP	5.7	1.7	2.5	15.5	–	8.7	3.4
4-A-BaP	5.8	1.7	2.6	8.9	8.0	9.2	3.4
6-A-BaP	14.2	4.7	7.0	7.8	8.4	41.0	3.8
11-A-BaP	6.2	1.8	2.8	9.6	8.0	9.1	3.4
12-A-BaP	5.6	1.7	2.6	9.1	8.0	9.8	3.4
1-A-H_4-BaP	6.0	1.8	2.6	7.1	10.8	6.3	5.2
3-A-H_4-BaP	5.9	1.7	2.5	9.1	8.0	9.7	3.3
6-A-H_4-BaP	19.1	5.4	8.0	5.8	10.8	20.0	4.2
6-A-H_2-BaP	19.4	4.8	2.7	11.4	–	6.1	3.8
3-A-BeP	5.96	1.9	2.9	9.5	9.6	16.1	3.4
1-A-H_4-BeP	6.1	1.8	2.6	9.6	8.0	10.0	3.1
3-A-H_4-BeP	5.92	1.7	2.5	7.0	10.0	9.5	3.2
7-A-DBA	31.0	3.2	6.6	6.9	–	5.9	–

* 250 × 4.6 mm I.D. column; methanol–water (90:10, v/v); 0.5 ml/min.

** 250 × 4.6 mm I.D. column; methanol–water (90:10, v/v); 1.5 ml/min.

*** 250 × 4.6 mm I.D. column; methanol–water (90:10, v/v); 1.0 ml/min.

§ 250 × 4.6 mm I.D. column; *n*-hexane containing 10% ethanol–acetonitrile (2:1, v/v); 1.0 ml/min.

§§ 250 × 4.6 mm I.D. column; methanol–water (90:10, v/v); 1.0 ml/min. Due to the apparent inefficient separation, the retention times of the compounds marked with "–" were not determined.

§§§ Pirkle-type covalent phenylglycine column (250 × 4.6 mm I.D.); *n*-hexane containing 10% ethanol–acetonitrile (2:1, v/v); 1.0 ml/min.

† 250 × 4.6 mm I.D. column; methanol–water (90:10, v/v); 1.0 ml/min.

Pirkle-type chiral stationary pase column can separate the amino-PAHs (see Table I), but not the Vydac ODS polymeric, the Deltabond column, or the μBondapak phenyl column. This contrasts with the previous report that the Vydac ODS column can separate PAHs and their methyl-substituted and hydroxylated derivatives more efficiently than the monomeric ODS column[20]. Nevertheless, the polymeric Vydac ODS column exhibits a better separation capability for some of the isomeric amino-PAH. For example, while the Zorbax ODS column shows poor separation of 3- and 6-aminochrysene, the Vydac column provides much better separation of these two isomers (Table I). On the other hand, as summarized in Scheme 1, the retention orders of amino-PAHs, separated on the polymeric Vydac ODS column and the monomeric Zorbax ODS column, are the same. These results suggest that the types of interaction of amino-PAHs with the monomeric ODS-bonded-phase adsorbent are similar to those with the polymeric ODS bonded phase adsorbent.

These compounds are not well separated either by the Deltabond C_8 column or by the μBondapak phenyl column (Table I), yielding a very narrow range of retention times of the tested compounds. Since all the active sites of the silica stationary phase in the Deltabond column have been completely shielded by te cross-linked polysiloxane functional groups, this suggests that the active polar sites are important in the separation of the amino-PAHs. The poor separation by the phenyl column indicates the π–π interactions between the bonded phase and amino-PAHs do not facilitate separation.

It is noteworthy to indicate that the separation of amino-PAH will be facilitated by employing a combination of both the reversed-phase and the normal-phase columns. For example, under the experimental conditions, 1- and 3-A-BaP cannot be separated by the Zorbax ODS column, but are well resolved by the Zorbax SIL normal-phase column (Table I and Fig. 2). Our previous reports have shown that on many occasions when a mixture of two or more PAHs, nitro-PAHs, and their ring-oxidized derivatives cannot be separated on a reversed-phase column, they can be nicely resolved on a normal-phase column[21–23].

Separation of the acetylamino-PAHs by reversed-phase and normal-phase HPLC

The results of the separation of acetylamino-PAHs by reversed- and normal-phase HPLC are shown in Table II. The Pirkle-type chiral stationary-phase column exhibits the best separation, and normal-phase HPLC shows a good separation. Like their amino-PAH analogues, these acetylamino-PAHs are not well separated on the Deltabond column. This further indicates that active sites in the silica matrix are involved in the separation mechanism.

Some amino-PAHs are unstable and may undergo air oxidation. Acetylation of an amino-PAH results in a more stable and less polar compound. Comparison of the separation of amino-PAHs and acetylamino-PAHs (Tables I and II) indicates that, in some cases, the acetylamino-PAH isomers are easier to separate than the corresponding amino-PAHs. A good example is the analysis of 3- and 6-A-Ch and 3- and 6-AA-Ch.

Separation of amino-PAHs and acetylamino-PAHs by the Pirkle-type chiral stationary phase column

The Pirkle-type chiral stationary phase column employed was packed with

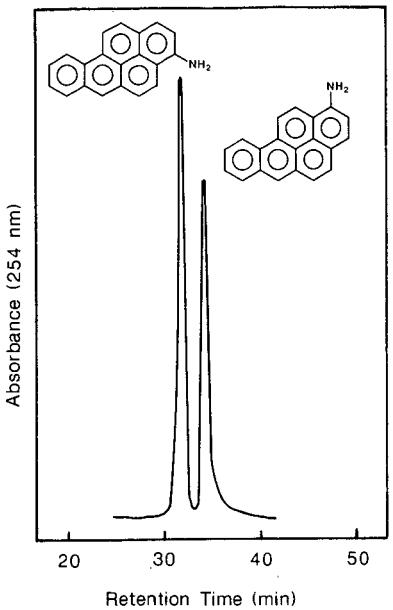

Fig. 2. Separation of 1- and 3-aminobenzo[*a*]pyrene by reversed-phase HPLC employing a semi-preparative Zorbax ODS column (250 × 21.2 mm I.D.).

optically active (R)-N-(3,5-dinitrobenzoyl)phenylglycine, covalently bonded to spherical particles of 5-μm γ-aminopropylsilanized silica. This column has been shown to resolve enantiomers of a large number of compounds, including the ring-oxidized derivatives of PAHs[24–26], and efficiently separates some nitro-PAHs[27,28]. A three-point interaction model was proposed by Pirkle and Finn[29] and others[25,27] for these separations. As shown in Tables I and II, the results indicate that the best separation of both amino-PAHs and acetylamino-PAHs are on the Pirkle-type column. In both cases, the compounds are separated over a wide range of retention times. There is no correlation between the retention time and molecular size of amino-PAH. However, a correlation exists for acetylamino-PAHs: an increased molecular size results in longer retention time. Based on the multiple-recognition-site mechanism, there are four different interaction sites: (i) π-bonding by the aromatic ring; (ii) hydrogen bonding by the amide hydrogen; (iii) hydrogen bonding by the amide carbonyl; and (iv) dipole formation by the amide linkage (Fig. 3A). We propose that there is an additional interaction that facilitates the separation: it is the hydrogen bonding between the nitro groups of the stationary phase and the amino and acetylamino groups of the substrate (Fig. 3B). Additionally, the electron-donating character of the amino and acetylamino groups makes the aromatic rings of the substrate more nucleophilic. This should enhance the π–π interaction of the aromatic ring with the stationary phase, which is electrophilic, due to the two electron-withdrawing nitro substituents. The existence of a correlation between the molecular size and retention time of the acetylamino-PAHs may suggest that acetylamino-PAHs can better fit into the interaction site than the amino-PAHs. Further studies are required for verification of this hypothesis.

TABLE II

HPLC RETENTION TIMES (IN MIN) OF ACETYLAMINO-PAHs ELUTED FROM DIFFERENT COLUMNS

Compound	*Zorbax ODS**	*Zorbax SIL***	*Vydac ODS****	*Deltabond* C_8§	*Pirkle Ph-Gly*§§
1-AA-N	10.4	22.6	4.2	8.4	14.5
2-AA-N	15.3	21.4	2.8	8.0	12.1
4-AA-Bp	4.3	22.1	2.6	–	10.9
2-AA-F	10.4	17.1	3.3	7.6	13.9
1-AA-A	8.8	26.5	3.0	8.0	20.5
2-AA-A	10.9	28.8	3.6	8.0	17.2
9-AA-A	8.5	34.2	2.8	8.0	20.8
2-AA-Ph	10.4	29.2	3.4	8.0	18.1
3-AA-Ph	10.5	27.5	3.2	8.4	14.4
9-AA-Ph	8.7	28.6	2.9	8.4	24.1
7-AA-BA	10.0	46.0	10.0	8.4	40.6
3-AA-Ch	15.6	38.0	6.3	8.8	24.5
6-AA-Ch	10.9	34.4	18.6	8.4	27.9
1-AA-Py	10.8	35.2	3.3	8.0	43.6
4-AA-Py	4.5	32.2	2.7	–	37.4
4-AA-H_6-Py	5.3	24.4	2.8	–	13.2
1-AA-BaP	6.1	41.4	5.4	–	64.8
3-AA-BaP	6.1	41.4	5.4	–	64.8
6-AA-BaP	4.8	52.4	3.3	–	65.7
11-AA-BaP	14.8	35.8	4.6	–	53.9
12-AA-BaP	12.8	36.2	4.5	–	54.2
1-AA-H_4-BaP	7.7	31.6	4.8	–	75.4
3-AA-H_4-BaP	7.7	31.6	4.8	–	75.4
6-AA-H_4-BaP	5.7	37.6	3.6	8.4	70.4
3-AA-H_4-BeP	5.5	24.7	3.2	–	

* 250 × 4.6 mm I.D. column; methanol–water (90:10, v/v); 1.0 ml/min.

** 250 × 4.6 mm I.D. column; *n*-hexane containing 20% tetrahydrofuran; 2.0 ml/min.

*** 250 × 4.6 mm I.D. column; methanol–water (90:10, v/v); 1.0 ml/min.

§ 250 × 4.6 mm I.D. column; methanol–water (90:10, v/v); 1.0 ml/min. Due to the apparent inefficient separation, the retention times of the compounds marked with "–" were not determined.

§§ Pirkle-type covalent phenylglycine column (250 × 4.6 mm I.D.); *n*-hexane containing 10% ethanol–acetonitrile (2:1, v/v); 2.0 ml/min.

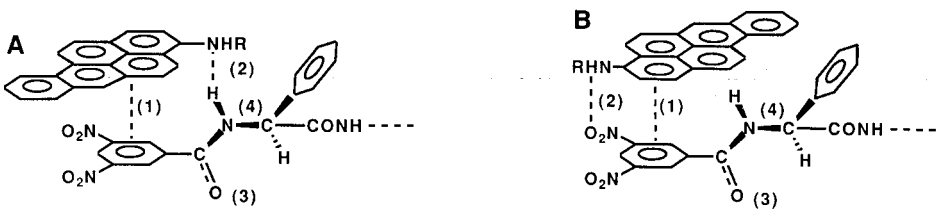

Fig. 3. Proposed three-point interaction model between Pirkle-type chiral stationary phase and the best orientations of 3-aminobenzo[*a*]pyrene (panel A and panel B) for maximum interaction. The number in parenthesis represents the type of interaction, as described in the text.

Relationships between structures and HPLC retention times

The following is a summary of our observations.

(1) For amino-PAHs, retention time in general does not correlate with molecular size (Tables I and II). However, in the case of acetylamino-PAHs, separation by the Pirkle-type chiral stationary-phase column and by normal-phase HPLC, the retention time does correlate with molecular size. Further study on larger series of amino-PAHs is required to determine the factor(s) which decide the retention order.

(2) The retention orders of the isomeric amino-PAHs and acetylamino-PAHs on different columns are summarized in Schemes 1 and 2. When acetylamino-PAHs were separated by the monomeric Zorbax ODS reversed-phase HPLC systems, an interesting phenomenon was observed, as shown in Scheme 2. The isomer having its acetylamino functional group located at the long axis of the aromatic moiety has the longest retention time, and the isomer having its acetylamino group at the shortest axis has the shortest retention time. For example, the retention order of the acetylaminoanthracene series is 2-AA-A > 1-AA-A > 9-AA-A. There exists a correlation in that the compound having its acetylamino group located at the carbon position with the highest electron density of the parent PAH has the sortest retention time. Similar results (with a few exceptions) were obtained with the polymeric Vydac ODS reversed-phase column (Scheme 2) and with the Pirkle-type chiral stationary-phase column. Similar results were also obtained when amino-PAHs were separated on a monomeric Zorbax ODS reversed-phase column.

(3) As shown in Tables I and II, there is no correlation between the retention of the parent PAHs and their amino or acetylamino derivatives. It shows that with an amino or acetylamino group, the resulting compounds are more difficult to separate on the monomeric Zorbax ODS column.

2-A-F > 4-A-Bp > 2-A-N > 1-A-N
2-A-A > 1-A-A > 9-A-A
3-A-Ph > 2-A-Ph > 9-A-Ph
3-A-Ch > 6-A-Ch
6-A-BaP > other A-BaP isomers
6-A-H_4-BaP > 1-A-H_4-BaP = 3-A-H_4-BaP

Scheme 1. HPLC retention times of the isomeric amino-PAHs, eluted from Zorbax ODS and Vydac ODS columns.

1. Eluted from the monomeric Zorbax ODS column
2-AA-N > 1-AA-N ⩾ 1-AA-Bp
2-AA-A > 1-AA-A > 9-AA-A
3-AA-Ph = 2-AA-Ph > 9-AA-Ph
3-AA-Ch > 6-AA-Ch
11-AA-BaP > 12-AA-BaP > 1-AA-BaP = 3-AA-BaP ⩾ 6-AA-BaP

2. Eluted with the polymeric Vydac ODS column
1-AA-N > 2-AA-N
2-AA-A > 1-AA-A > 9-AA-A
2-AA-Ph > 3-AA-Ph > 9-AA-Ph
6-AA-Ch > 3-AA-Ch
1-AA-BaP = 3-AA-BaP > 11-AA-BaP > 12-AA-BaP ⩾ 6-AA-BaP

Scheme 2. HPLC retention times of the isomeric acetylamino-PAHs.

REFERENCES

1 R. C. Garner, C. N. Martin and D. B. Clayson, in C. E. Searle (Editor), *Chemical Carcinogens*, ACS Monograph 182, American Chemical Society, Washington, DC, 2nd ed. 1984, pp. 175–276.
2 C. M. King, L. J. Romano and D. Schuetzle (Editors), *Carcinogenic and Mutagenic Responses to Aromatic Amines and Nitroarenes*, Elsevier, Amsterdam, 1988.
3 D. W. Later, T. G. Andros and M. L. Lee, *Anal. Chem.*, 55 (1983) 2126.
4 D. A. Haugen, M. J. Peak, K. M. Suhrbler and V. C. Stamoudis, *Anal. Chem.*, 54 (1982) 32.
5 L. J. Felic, R. E. Schirmer, D. L. Springer and C. V. Veverka, *J. Chromatogr.*, 354 (1986) 442.
6 V. Concialini, G. Chiavari and P. Vitali, *J. Chromatogr.*, 258 (1983) 244.
7 K. W. Sigvardson, J. M. Kennish and J. W. Birks, *Anal. Chem.*, 56 (1984) 1096.
8 W. L. Caudill, M. V. Novotný and R. M. Wightman, *J. Chromatogr.*, 261 (1983) 415.
9 S. A. Wise, W. J. Bonnett, F. R. Guenther and W. E. May, *J. Chromatogr. Sci.*, 19 (1981) 457.
10 L. R. Snyder and J. J. Kirkland, *Introduction to Modern Liquid Chromatography*, Wiley, NY, 1979.
11 H. Colin and G. Guiochon, *J. Chromatogr.*, 141 (1977) 289.
12 B. D. Silverman, in M. Cooke and A. J. Dennis (Editor), *Polynuclear Aromatic Hydrocarbons: Mechanisms, Methods and Metabolism*, Battelle Press, Columbus, OH, 1985, pp. 1213–1223.
13 P P. Fu, R. H. Heflich, D. A. Casciano, A. Y. Huang, W. M. Trie, F. F. Kadlubar and F. A. Beland, *Mutat. Res.*, 94 (1982) 13.
14 Y. S. Wu, Y. K. Wang, C. C. Lai, J. S. Lai, L. E. Unruh, F. E. Evans and P. P. Fu, in W. M. Cooke, D. Longfellow and W. May (Editors), *Eleventh International Symposium on Polynuclear Aromatic Hydrocarbons*, Washington, DC, in press.
15 L. F. Fieser and E. B. Hershberg, *J. Am. Chem. Soc.*, 61 (1939) 1565,
16 S. S. Hecht, E. El-Bayoumy, E. Tulley and E. J. LaVoie, *J. Med. Chem.*, 22 (1979) 981.
17 M. W. Chou, R. H. Heflich, D. A. Casciano, D. W. Miller, J. P. Freeman, F. E. Evans and P. P. Fu, *J. Med. Chem.*, 27 (1984) 1156.
18 W. E. Bachmann and C. H. Boatner, *J. Am. Chem. Soc.*, 58 (1936) 2097.
19 P. C. Howard, F. A. Beland and C. Cerniglia, *Carcinogenesis*, 4 (1983) 985.
20 M. Mushtaq, Z. Bao and S. K. Yang, *J. Chromatogr.*, 385 (1987) 293.
21 P. P. Fu, M. W. Chou, S. K. Yang, F. A. Beland, F. F. Kadlubar, D. A. Casciano, R. H. Heflich and F. E. Evans, *Biochem. Biophys. Res. Commun.*, 105 (1982) 1037.
22 P. P. Fu, R. H. Heflich, L. S. Von Tungeln, D. T. C. Yang, E. K. Fifer and F. A. Beland, *Carcinogenesis*, 7 (1986) 1819.
23 P. P. Fu, R. H. Heflich, L. S. Von Tungeln, H. Z. Miranda and F. E. Evans, *Carcinogenesis*, 9 (1988) 951.
24 S. K. Yang, H. B. Weems, M. Mushtaq and P. P. Fu, *J. Chromatogr.*, 316 (1984) 569.
25 S. K. Yang, M. Mushtaq and P. P. Fu, *J. Chromatogr.*, 371 (1986) 195.
26 H. B. Weems, M. Mushtaq, P. P. Fu and S. K. Yang, *J. Chromatogr.*, 371 (1986) 211.
27 M. W. Chou, in W. M. Cooke and A. J. Dennis (Editor), *Ninth International Symposium on Polynuclear Aromatic Hydrocarbons*, Battelle Press, Columbus, OH, 1986, p. 145–153.
28 M. W. Chou, *J. High Resolut. Chromatogr.*, 8 (1985) 304.
29 W. H. Pirkle and J. M. Finn, *J. Org. Chem.*, 46 (1981) 2935.

Journal of Chromatography, 461 (1989) 337–346
Elsevier Science Publishers B.V., Amsterdam — Printed in The Netherlands

CHROMSYMP. 1428

DETERMINATION OF PYRETHROID RESIDUES ON PADDY RICE BY REVERSED-PHASE HIGH-PERFORMANCE LIQUID CHROMATOGRAPHY

PAUL R. HADDAD*, JOHN G. BRAYAN, GERARD J. SHARP and SERGIO DILLI
Department of Analytical Chemistry, University of New South Wales, P.O. Box 1, Kensington, N.S.W. 2033 (Australia)
and
JAMES M. DESMARCHELIER
CSIRO Division of Entomology, P.O. Box 1700, Canberra, A.C.T. 2601 (Australia)

SUMMARY

Several synthetic pyrethroids and the synergist piperonyl butoxide have been determined as aged residues on paddy rice by reversed-phase high-performance liquid chromatography with detection at 225 nm. These compounds are commonly used as protectants for stored grains. Studies on the comparative rates of extraction of both the pesticides and interfering material from the grain were conducted with acetone, methanol, and hexane as extracting solvents. Acetone was the best of these solvents because it provided quantitative extraction of the pesticides over a 48-h period, and did not give high levels of ballast material. Pyrethroids present in the extract at levels in excess of 0.5 μg/ml could be determined by direct injection, but at lower concentrations, clean-up and preconcentration were required. Clean-up of acetone extracts was accomplished with either Florisil or alumina pre-columns, and up to a tenfold preconcentration was achieved by adsorption of the pesticide on a C_{18} pre-column, or by concentrating the extract through evaporation of the solvent. These approaches gave good recoveries and linear calibration plots. Detection limits were of the order of 0.05 μg/ml.

INTRODUCTION

Pyrethroid insecticides, such as bioresmethrin, phenothrin, fenvalerate, permethrin, and deltamethrin, together with the synergist piperonyl butoxide, are in current use as grain protectants. Since these pyrethroids are much more expensive than organophosphate pesticides, the levels at which they are applied are kept as low as possible. A commonly encountered situation is the application of a small amount of a pyrethroid in conjunction with a larger concentration of an organophosphate pesticide. This method is particularly suitable for the control of a specific pest that shows resistance to the organophosphate[1,2]. For example, 0.5–1 mg/kg of bioresmethrin can be applied to wheat with 10 mg/kg of fenitrothion, together with 5–10

0021-9673/89/$03.50

mg/kg of piperonyl butoxide, which acts a synergist increasing pesticide activity without having any insecticidal properties of its own.

It has been established[3–8] that polar solvents, such as methanol, are the most suitable for the extraction of aged residues of carbaryl and organophosphates from grain. Here, an aged residue refers to a pesticide that has been in contact with the grain for a substantial period of time. Little work has been performed on extraction of pyrethroids from grain, but it has been suggested that non-polar solvents may be useful for this purpose[4]. In this paper, studies are reported on the extraction of aged pyrethroid residues from grain with acetone, methanol, or hexane.

Reversed-phase high-performance liquid chromatography (HPLC) has been applied to the determination of piperonyl butoxide on a number of grains[9], and to the determination of pyrethroid residues on barley and wheat[10,11]. Fluorescence detection was used for piperonyl butoxide and UV absorption detection for the pyrethroids. A normal-phase HPLC method has also been reported for the determination of bioresmethrin on wheat[12]. In a previous communication[13], we have described the use of reversed-phase HPLC for the analysis of carbaryl and organoposphate pesticides, and in this paper we report a simple method for the analysis of pyrethroids and piperonyl butoxide on paddy rice for the purpose of monitoring rates of pesticide decay under controlled storage conditions. The concentrations of pesticide considered in this work are therefore those at which the efficacy of the pesticide is retained, and in all of the rice samples considered, the identities of the pesticides applied were known.

EXPERIMENTAL

Instrumentation

The liquid chromatograph consisted of Millipore Waters (Milford, MA, U.S.A.) Model 510 and 501 pumps, a Model 481 variable-wavelength detector, and Model 740 data module. The column was a Waters Novapak C_{18} stainless-steel column (150 × 3.9 mm I.D.), equipped with a Waters Guard Pak pre-column module. A Rheodyne (Cotati, CA, U.S.A.) 7000 six-port switching valve was used during the preconcentration step.

Reagents

Bioresmethrin, phenothrin, permethrin, deltamethrin, fenvalerate, and piperonyl butoxide standards were obtained from the Curator of Standards, Australian Government Analytical Laboratories (Melbourne, Australia). The solvents used were HPLC-grade methanol and acetonitrile and Nanograde hexane and acetone (Mallinkrodt, Oakleigh, Australia). Florisil Sep-Paks, obtained from Millipore, and basic alumina from Ajax (Sydney, Australia) were used for the clean-up of extracts.

The paddy rice, treated with phenothrin and permethrin, was obtained from a storage facility at Home Hill in Queensland, Australia. The rice was treated with pesticide as it was loaded into the silo on a conveyor belt, as is the normal practice in the industry. The pesticides were applied at a dosage rate of approximately 1 mg/kg, and the rice was stored for six months before extraction. The other pesticides used in this study were applied in the laboratory, *ca.* two months prior to analysis. In this case the pesticides were dissolved in 2 ml of acetone, and this was applied dropwise to 1 kg of rice in a large plastic bag. The application levels were 2 mg/kg for deltamethrin and 10 mg/kg for bioresmethrin, fenvalerate, and piperonyl butoxide.

Extraction

Extraction studies were performed by mixing 30 g of whole rice containing an aged pesticide with 50 ml of solvent in a stoppered conical flask and allowing the mixture to stand with occasional manual shaking. Each extraction was carried out in triplicate. For rice treated with permethrin, phenothrin, deltamethrin, and piperonyl butoxide, 1-ml aliquots of the extract were taken after 1, 4, 25, 48, and 72 h, whereas for the remaining pesticides, aliquots were taken after 48 and 72 h only. Comparative extraction studies were conducted on rice samples containing permethrin and phenothrin by either ginding the grain in a blender, followed by extraction with a solvent for 48 h, as described above, or by subjecting the whole grain to Soxhlet extraction for 8 h.

Sample clean-up

The following two clean-up methods were used.

(i) An aliquot (1 ml) of the extract was transferred to a small test tube and evaporated to near dryness, under a stream of nitrogen. The remaining few drops were shaken twice with 1 ml of hexane. With the aid of a syringe, the combined hexane phase was passed through a Florisil (Sep-Pak) cartridge, followed by 3 ml of acetone–hexane (15:85, v/v). Both eluates were collected and evaporated to dryness under a stream of nitrogen. Finally, the residue was dissolved in 1 ml of methanol for later analysis.

(ii) A small alumina column was made by plugging a Pasteur pipette with cotton and adding 0.5 g of basic alumina. Extract (1 ml) was then passed through the column, followed by 1 ml of pure acetone. The combined eluates were evaporated to 1 ml under a stream of nitrogen.

Analysis

Extracts containing pesticides at concentrations exceeding 0.5 μg/ml could be analysed by direct injection without clean-up. A suitable volume (10 μl) of extract was injected into the column and eluted with a mobile phase of 75% aq. acetonitrile at a flow-rate of 1 ml/min. For detection an absorption wavelength of 225 nm was used. Methanol and acetone extracts could be injected directly, but is was necessary to evaporate hexane extracts to dryness under a stream of nitrogen and to redissolve the residue in 1 ml of methanol prior to injection. The pesticides were identified in the chromatograms obtained by comparison of retention times with those of standards, and by confirmatory analysis using capillary gas chromatography with electron-capture or flame-ionization detection.

When the concentration of pesticide in the extract was less than 0.5 μg/ml, a sample preconcentration step was necessary. Two different preconcentration methods were used.

(i) Solid-phase extraction. This was process was accomplished with the aid of a six-port high-pressure switching valve, using the instrumental configuration shown in Fig. 1. The sample extract was first treated by the Florisil clean-up method described above, and 100 ml of the purified extract was injected into a C_{18} pre-column (Waters Guard Pak), using 40% aq. acetonitrile as the mobile phase. After 30 s, the mobile phase was changed to 75% aq. acetonitrile by rotating the switching valve, and the pyrethroid was passed into the analytical column. Both pumps were operated at a flow-rate of 1 ml/min.

(ii) Evaporation. Extract (10 ml) was evaporated to dryness in a rotary evaporator, and the residue was redissolved in 1–2 ml of acetone and purified by the alumina method described above.

RESULTS AND DISCUSSION

Extraction of aged residues

Three solvents, acetone, methanol, and hexane, were evaluated to determine which provided the most efficient extraction of the pesticides. The results for the extraction studies are shown in Table I, from which it can be seen that acetone and methanol generally extracted 10–15% more pyrethroid and about 50% more piperonyl butoxide than hexane. Grinding the grain or the use of Soxhlet extraction did not increase the levels of pesticide extracted. To investigate possible losses of pesticide from hexane extracts during the evaporation and redissolution steps necessary before injection, two equivalent series of pesticide standards were made up in methanol and hexane extracts of rice which had not been treated with a pesticide. The methanol extracts were injected directly onto the column, whilst the hexane extracts were evaporated to dryness and redissolved in methanol prior to injection. The results

TABLE I

EXTRACTION OF PESTICIDES FROM WHOLE GRAIN BY METHANOL, ACETONE AND HEXANE

Pesticide	*Approx. application rate (mg/kg)*	*Extraction time (h)*	*Amount extracted (mg/kg)*		
			Methanol	*Acetone*	*Hexane*
Permethrin	1	1	1.0	0.8	0.8
		4	1.1	1.0	0.8
		24	1.3	1.1	1.1
		48	1.3	1.1	1.2
		72	1.2	1.1	1.1
Phenothrin	1	1	0.7	0.7	0.5
		4	0.8	0.7	0.6
		24	1.0	1.0	0.9
		48	1.0	1.1	0.9
		72	1.1	1.1	0.9
Deltamethrin	2	1	2.0	1.8	1.3
		4	2.3	2.3	1.6
		24	2.3	2.3	2.2
		48	2.5	2.5	2.2
		72	2.5	2.5	2.2
Bioresmethrin	10	48	8.0	8.6	7.0
		72	8.2	8.5	6.7
Fenvalerate	10	48	7.8	9.0	7.3
		72	8.2	8.6	7.2
Piperonyl butoxide	10	1	5.8	4.8	3.8
		4	8.2	7.8	4.6
		24	11.2	10.6	5.9
		48	12.2	10.8	6.7
		72	11.5	10.7	7.2

TABLE II
RECOVERIES OBTAINED FOR THE FLORISIL AND ALUMINA CLEAN-UP PROCEDURES

Pesticide	*Concentration (μg/ml)*	*Recovery (%)*	
		Florisil clean-up	*Alumina clean-up*
Fenvalerate	1.0	96	100
Phenothrin	1.0	86	105
Bioresmethrin	1.0	84	100
Permethrin	1.0	88	105
Deltamethrin	1.0	83	100
Piperonyl butoxide	10.0	90	105

obtained by both methods were equivalent, indicating that no significant losses of pesticides from the hexane extracts had occurred.

Acetone was selected as the most suitable solvent for the extraction of pyrethroids from paddy rice, because the level of ballast material was much lower for this solvent than with methanol. The optimal extraction period was 48 h.

Sample clean-up

A Florisil clean-up procedure had been developed for the analysis of organophosphate pesticides in rice extracts[13] and was shown to give acceptable recoveries for typical organophosphates (*e.g.* 90 ± 7% for fenitrothion). This approach was found to be applicable to the pyrethroids, and Table II shows that recoveries in excess of 83% were obtained with this method. The optimal eluent was acetone–hexane (3:17), since this solvent eluted the pesticides but minimised the level of interfering material eluted from the Sep-Pak. Subsequent studies showed that much of the polar material extracted from rice by acetone, which ultimately interfered with the reversed-phase HPLC analysis of pesticides, could be removed by passing the extract through a column of basic alumina. Although this method was not always as effective as the Florisil clean-up, in many cases it was sufficient, and the alumina adsorbent showed no affinity for the pesticides, as indicated by the quantitative recoveries shown in Table II.

Analytical procedure

Calibration data and detection limits for the pyrethroids and piperonyl butoxide, injected at 225 nm without clean-up or preconcentration, are given in Table III. The detection limit was defined as the concentration of pesticide in a 10-μl injection which produced a signal-to-noise ratio of 3. Although the pesticides studied show stronger absorption at wavelengths below 225 nm, analysis at these wavelengths was impractical due to the presence of strongly absorbing contaminants. Under the chromatographic conditions described, all of the pyrethroids were eluted with retention times in the range 10–15 min, and piperonyl butoxide was eluted after about 5 min, as shown in Table IV. The *cis*- and *trans*-isomers of permethrin and phenothrin were separated. When the pesticide levels in the extract were greater than 0.5 μg/ml, analysis without clean-up was possible, but in some cases interference by extractives with piperonyl butoxide was observed. This could be prevented by changing the wavelength to 237 nm for the elution of piperonyl butoxide.

TABLE III

CALIBRATION DATA AND DETECTION LIMITS FOR DIRECT INJECTION OF PESTICIDES WITHOUT SAMPLE CLEAN-UP

Pesticide	*Working calibration range* (μg/ml)*	*Detection limit*	
		On rice (mg/kg)	*In extract (μg/kg)*
Fenvalerate	0.4–4	0.7	0.4
Phenothrin	1–4	1.0	0.6
Bioresmethrin	0.4–4	0.7	0.4
Permethrin	1–4	1.0	0.6
Deltamethrin	0.4–4	0.7	0.4
Piperonyl butoxide	4–40	1.7	1.0

* Correlation coefficients of 0.998 or higher were obtained for each of the stated ranges.

The pyrethroids are applied to grain at levels as low as 0.5 mg/kg, and the described extraction procedure would therefore produce concentrations of pesticide of *ca.* 0.3 μg/ml in the final extract. For this reason, preconcentration of the extract was necessary, and this was achieved by solid-phase extraction of the pesticides on a C_{18} pre-column. The sample extract containing pyrethroids was loaded onto a C_{18} pre-column conditioned with 40% aq. acetonitrile, and the bound pesticides were subsequently passed into the analytical column using 75% acetonitrile (Fig 1). The preconcentration procedure described under Experimental provided a ten-fold sample concentration factor. Table V shows calibration data for the preconcentration method with Florisil clean-up, and Fig. 2 compares the chromatograms obtained by direct injection and preconcentration of an extract which had been spiked with bioresmethrin, piperonyl butoxide, and the organophosphate fenitrothion. The extracts were subjected to Florisil clean-up prior to preconcentration in order to remove some of the extractives which accumulated on the pre-column. However, considerable amounts of early-eluted interfering material were still present (Fig. 2b), and this would limit adaptation of the preconcentration approach for on-line clean-up, unless further steps

TABLE IV

RETENTION TIMES OF PYRETHROIDS

Mobile phase, 75% aq. acetonitrile; flow-rate, 1 ml/min; Novapak C_{18} column.

Pesticide	*Retention time (min)*
Piperonyl butoxide	5.5
Deltamethrin	11.5
Bioresmethrin	11.5
Fenvalerate	12.2
trans-Permethrin	13.5
cis-Phenothrin	14.4
trans-Phenothrin	15.6
cis-Permethrin	16.2

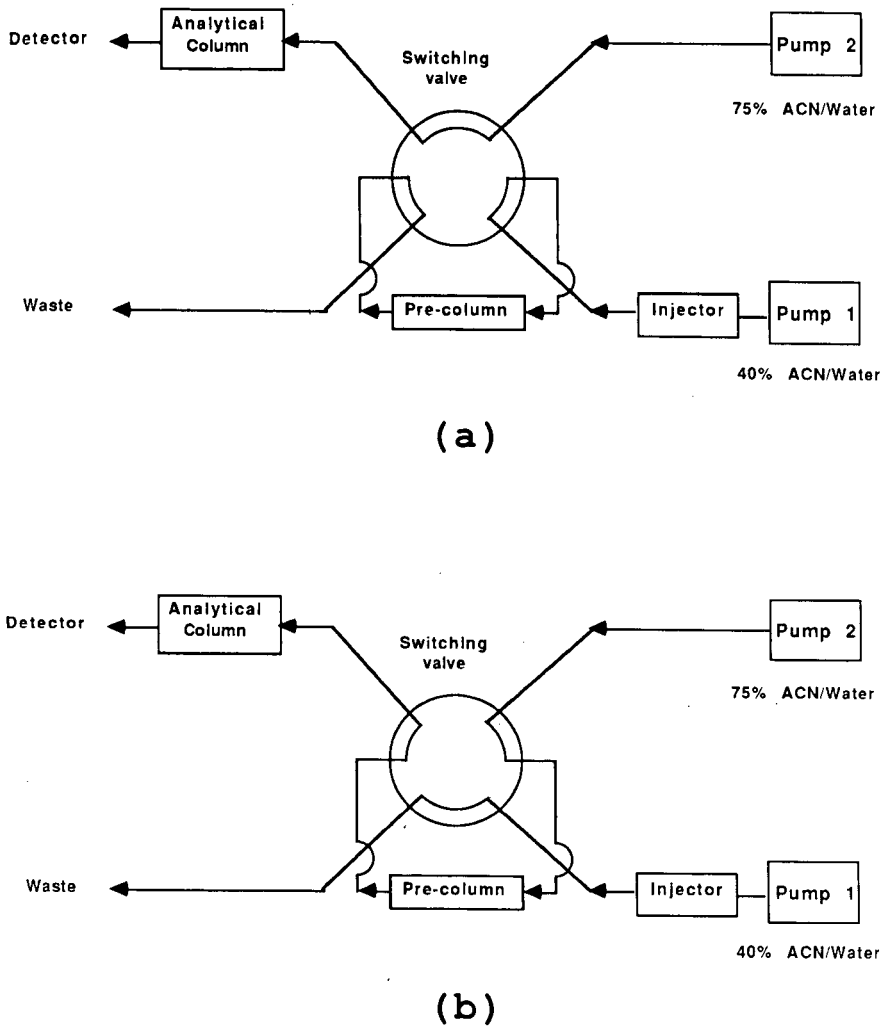

Fig 1. Schematic representation of the solid-phase preconcentration procedure, showing (a) loading of the sample and (b) transfer of the bound pesticide to the analytical column. ACN = acetonitrile.

were incorporated to clean the pre-column periodically. The chromatographic conditions employed in the preconcentration method were selected because they provided the best overall separation of all the pyrethroids and piperonyl butoxide. Further optimization of this approach could yield cleaner chromatograms for more limited mixtures.

One disadvantage of the above method was the requirement for an extra pump and switching valve, and changes in the tubing would be necessary if the HPLC was to be used for normal operation. Therefore, studies were undertaken in which the sample clean-up was combined with preconcentration by evaporation of the solvent. This was achieved by concentrating the sample from 10 ml to 1 ml in a rotary evaporator, and

TABLE V
CALIBRATION DATA AND DETECTION LIMITS FOR PESTICIDES AFTER CLEAN-UP AND PRECONCENTRATION

Preconcentration method	*Clean-up procedure*	*Pesticide*	*Working calibration range* (μg/ml)*	*Detection limit*	
				On rice (mg/kg)	*In extract (μg/ml)*
Solid-phase	Florisil	Fenvalerate	0.1–1	0.07	0.04
		Phenothrin	0.1–1	0.12	0.07
		Bioresmethrin	0.1–1	0.07	0.04
		Permethrin	0.1–1	0.07	0.04
		Deltamethrin	0.1–1	0.12	0.07
Evaporation	Alumina	Fenvalerate	0.06–0.6	0.07	0.04
		Phenothrin	0.1–0.6	0.17	0.1
		Permethrin	0.1–0.6	0.17	0.1
		Deltamethrin	0.06–0.6	0.07	0.04

* Correlation coefficients of 0.991 or higher were obtained for each of the stated ranges.

subsequent clean-up by the Florisil or alumina methods. The latter approach was preferred because of its simplicity. Calibration data and detection limits obtained by this method are listed in Table V. Piperonyl butoxide and bioresmethrin are not included, since early-eluted extractives made it difficult to quantitate the former pesticide, and the latter was volatilised to some extent during the evaporation step. Fig. 3 shows chromatograms obtained by injection of 2 μg/ml deltamethrin in an acetone extract of rice without preconcentration or clean-up (Fig. 3a), and an injection of 0.2 μg/ml deltamethrin after preconcentration and clean-up (Fig. 3b). These chromatograms show that quantitative preconcentration had been achieved, without undue interference by other extracted materials.

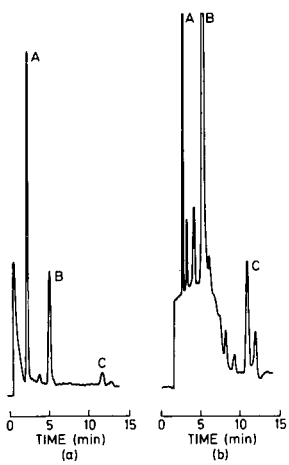

Fig. 2. Chromatograms of pyrethroids after Florisil clean-up, followed by (a) direct injection or (b) solid-phase preconcentration. Peaks: A = 5 μg/ml fenitrothion, B = 8 μg/ml piperonyl butoxide, C = 0.5 μg/ml bioresmethrin. Injection volumes: (a) 10 μl, (b) 100 μl; mobile phase, 75% aq. acetonitrile; flow-rate, 1.0 ml/min; detection, 225 nm.

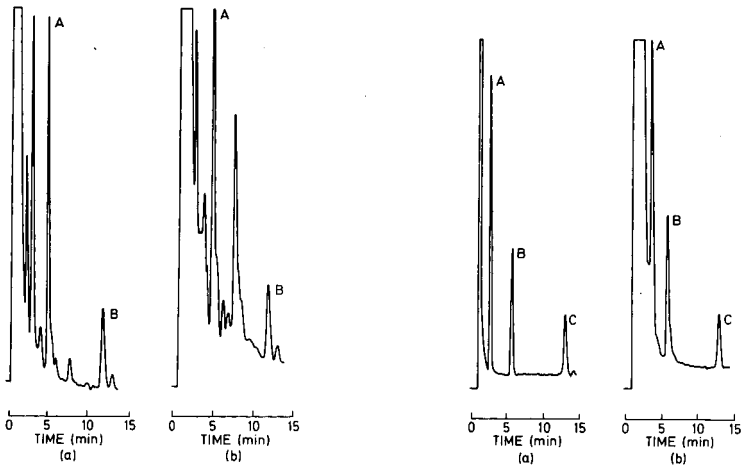

Fig. 3. Chromatograms of a spiked rice extract (a) without clean-up and (b) after preconcentration by solvent evaporation, followed by alumina clean-up. Sample: (a) 10 μl of extract, containing 20 μg/ml piperonyl butoxide (A) and 2 μg/ml deltamethrin (B): (b) 10 μl of extract, containing 2 μg/ml piperonyl butoxide (A) and 0.2 μg/ml deltamethrin (B), after evaporation, preconcentration, and alumina clean-up. Chromatographic conditions as for Fig. 2.

Fig. 4. Chromatograms of spiked rice extract (a) after and (b) before Florisil clean-up. Sample: 10 μl of extract, containing 5 μg/ml fenitrothion (A), 8 μg/ml piperonyl butoxide (B), and 2 μg/ml bioresmethrin (C). Chromatographic conditions as for Fig 2.

Both of the above preconcentration methods are limited to ten-fold preconcentration factors, because of the levels of interfering extractives present in acetone extracts, even after clean-up. In the evaporation method, a small peak appeared which was eluted close to the *trans*-permethrin and *trans*-phenothrin isomers, and in both methods a late-eluted, broad peak occasionally emerged and caused interference with subsequent analyses. This problem could be avoided by washing the column with 85% aq. acetonitrile for 5 min after every five or six injections. More extensive clean-up procedures would undoubtedly improve the detection limits and provide cleaner chromatograms, but the methods developed are adequate for grain screening purposes and have the advantage of being relatively rapid and straightforward.

Multiresidue analysis

As mentioned previously, pyrethroids are often applied to grain in conjunction with piperonyl butoxide and an organoposphate pesticide. Simultaneous analysis of these three types of compounds is possible, but clean-up is required for accurate quantitation. This is illustrated in Fig. 4, which shows the effect of Florisil clean-up on the determination of piperonyl butoxide, bioresmethrin and the organophosphate fenitrothion, in an acetone extract of rice. The relatively polar nature of the organophosphates enables them to be easily separated from the pyrethroids and piperonyl butoxide on a reversed-phase column. However, one organophosphate, pirimiphos methyl, was found to be inseparable from piperonyl butoxide under the chromatographic conditions used. The organophosphate pesticides and piperonyl butoxide are applied at levels that do not require preconcentration for their

determination. When concentration was necessary for pyrethroid analysis, it proved to be more reliable to analyse the extract for piperonyl butoxide and the organophosphate before the preconcentration step, because of the large number of early-eluted interfering materials present in the concentrated extracts (Figs. 2 and 3).

CONCLUSIONS

The method described is a simple technique for the analysis of organophosphates, piperonyl butoxide, and pyrethroids on paddy rice by reversed-phase HPLC. Altough this method lacks the sensitivity of gas chromatography with electron-capture detection, it permits the analysis of all pyrethroids, as well as piperonyl butoxide and organophosphate pesticides, in the concentration ranges likely to occur in stored grain.

ACKNOWLEDGEMENT

Financial assistance from the Australian Centre for International Agricultural Research (ACIAR) is gratefully acknowledged.

REFERENCES

1 J. M. Desmarchelier, *J. Stored Prod. Res.*, 13 (1977) 129.
2 M. Bengston, R. A. H. Davies, J. M. Desmarchelier, R. Hennig, W. Murray, B. W. Simpson, J. T. Snelson, R. Sticka and B. E. Wallbank, *Pestic. Sci.*, 14 (1983) 373.
3 J. M. Desmarchelier, M. Bengston, M. Connell, W. Minett, B. Moore, M. Phillps, J. Snelson, R. Sticka and K. Tucker, *Pestic. Sci.*, 8 (1977) 473.
4 J. M. Desmarchelier, *J. Pestic. Sci.*, 5 (1980) 521.
5 M. C. Bowman, M. Beroza and D. B. Leuck, *J. Agric. Food Chem.*, 16 (1968) 796.
6 P. A. Hargreaves and K. J. Melksham, *Pestic. Sci.*, 14 (1983) 347.
7 R. T. Krause, *J. Agric. Food Chem.*, 26 (1978) 1333.
8 R. T. Krause, *J. Assoc. Off. Anal. Chem.*, 63 (1980) 1114.
9 K. Isshiki, S. Tsumura and T. Watanabe, *Bull. Environ. Contam. Toxicol.*, 19 (1978) 518.
10 P. Bottomley and P. G. Baker, *Analyst (London)*, 109 (1984) 85.
11 R. M. Noble, D. J. Hamilton and W. J. Osborne, *Pestic. Sci.*, 13 1982) 246.
12 D. S. Gunew, in G. Zweig (Editor), *Analytical Methods for Pesticides and Plant Growth Regulators*, Vol. 10, Academic Press, New York, 1978, p. 19.
13 J. G. Brayan, P. R. Haddad, G. J. Sharp, S. Dilli and J. M. Desmarchelier, *J. Chromatogr.*, 447 (1988) 249.

Journal of Chromatography, 461 (1989) 347–352
Elsevier Science Publishers B.V., Amsterdam — Printed in The Netherlands

CHROMSYMP. 1489

HYDROCARBON GROUP TYPE ANALYSIS OF PETROLEUM PRODUCTS BY HIGH-PERFORMANCE LIQUID CHROMATOGRAPHY ON ORGANO-METALLIC DONOR/ACCEPTOR-BONDED SILICA

G. FÉLIX* and A. THIENPONT
Laboratoire de Chimie Organique et Organométallique (CNRS UA 35), Université de Bordeaux I, 351 Crs. de la Libération, F-33405 Talence (France)
and
M. EMMELIN and A. FAURE
Elf-France, C.R. Elf Solaize, BP 22, F-69360 Saint Symphorien d'Ozon (France)

SUMMARY

The preparation of a new organosilver bonded phase is described. The capacity ratios of 24 polynuclear aromatic hydrocarbons were determinated and showed a charge-transfer mechanism. The separation of olefins in several light petroleum products was resolved. The performance of the stationary phase in hydrocarbon group type analysis is discussed.

INTRODUCTION

The application of high-performance liquid chromatography (HPLC) to hydrocarbon group-type analysis (HGTA) of petroleum products was first reported in the 1970s, but only separations of light petroleum fractions were described. Accurate HGTA analyses are of vital importance for the refining industry. For instance, gasolines must meet severe specifications which are checked traditionally by normalized, although often inaccurate, tests (*e.g.*, FIA-ASTM D 1319)[1]. Several methods using high-performance liquid chromatography (HPLC) or supercritical fluid chromatography have been published[2–8] and some are currently under evaluation by the ASTM.

Recently, the preparation of new amino bonded phases has led to good separations of petroleum fractions, in particular heavier products[9,10]. Several papers have reported the use of column-switching HPLC using a silver column prepared by *in situ* flushing with aqueous silver nitrate. The column contained silica bonded with a strong cation-exchange phase [11–13]. The use of silver salts coated on silica gel for the separation of olefinic compounds[14] by charge-transfer chromatography is well known.

If we ligand a silver salt by an electron-acceptor molecule bonded on silica gel, it is possible to separate saturated compounds from aromatics (mono-, di-, poly-) with the acceptor molecules and to complex olefins strongly with the silver ions to

0021-9673/89/$03.50

achieve an HGTA analysis. We report here the sucessful synthesis and use of a new bonded acceptor stationary phase which ligands a silver salt for HGTA and was especially designed to show a high selectivity for petroleum fractions.

EXPERIMENTAL

Apparatus

HPLC was performed with a Knauer 64 pump equipped with a Iota differential refractometer (Jobin-Yvon). Packing of the HPLC column (150 × 4.6 mm I.D.) was achieved by the classical slurry packing technique. The bonded silica was suspended in carbon tetrachloride–methyl iodide (65:35) and the slurry was forced with acetone into the chromatographic column for 30 min under a pressure of 450 bar.

Materials

4-Aminophtalonitrile was obtained from Kodak and vinylacetic acid, dichloromethylsilane and silver tetrafluoroborate from Aldrich. The remaining chemicals and solvents were of analytical-reagent grade and were used as purchased.

The bonded stationary phase was formed on a matrix of LIChrosorb Si 60 gel of median particle size 5 μm having a reported surface area of approximately 480 m^2/g (Merck-Clevenot).

Preparation of phthalonitrile-bonded stationary phase. The new phase was synthesized according to the following scheme:

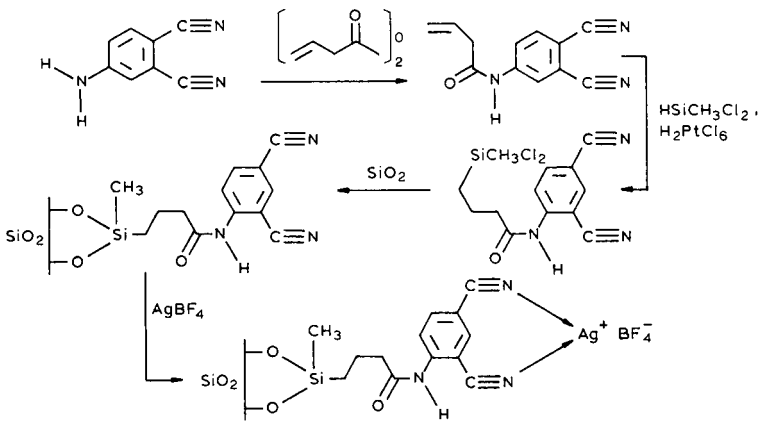

Vinylacetic anhydride. This compound was obtained according to the method of Kuhn and Low[15] by reaction of the acid with the acid chloride[16] in pyridine (yield, 72%; b.p., 115–120°C/70 mmHg).

N-(4-Phthalonitrile)vinylacetamide. To 1.1 g (0.0077 mole) of 4-aminophthalonitrile in 30 ml of glacial acetic acid were added 3 g (0.024 mole) of vinylacetic anhydride followed by two drops of concentrated sulphuric acid. The mixture was stirred at room temperature until the solution became homogeneous (about 30 min), then warmed at 40°C for 30 min. Boiling water (100 ml) was then added to yield overnight 1.1 g (70%) of a beige crystalline product (m.p., 174–176°C). NMR ([$^2H_6$]acetone):δ = 3.13 (2H, d, J = 7 Hz), 4.9–5.36 (2H, m), 5.63–6.33 (1H, m), 7.8

(2H, s + d), 8.14 (1H, d, J = 2 Hz), 9.16 (1H, s). IR (carbon tetrachloride):3300 and 3260 cm^{-1} (NH), 2220 cm^{-1} (CN), 1690 and 1680 cm^{-1} (CO).

N-(4-Phthalonitrile)-γ-dichloromethylsilylbutyramide. To 2.8 g (0.013 mole) of dichloromethylsilane (freshly distilled over magnesium powder) was added a crystal of H_2PtCl_4 followed by the dropwise addition of a solution of N-(4-phthalonitrile) vinylacetamide (2.3 g; 0.024 mole) in dry dichloromethane (80 ml). The mixture was stirred under relfux overnight and evaporated, yielding 4 g of a viscous, brown product. NMR (C^2HCl_3):δ = 0.1 (6H, S), 0.86–1.2 (2H, t, J = 7 Hz), 2.26–2.67 (2H, m), 2.9–3.33 (2H, t, J = 6 Hz), 7.7 (2H, s + d), 8.16 (1H, d, J = 2 Hz), 9.2 (1H, s).

Phthalonitrile-bonded stationary phase. To LiChrosorb Si 60 (5 g) in dry dichloromethane (20 ml) a solution of N-(4-phthalonitrile)-γ-chlorodimethylsilylbutyramide (4 g) in dry dichloromethane (50 ml) was added and the mixture was stirred under reflux for 12 h. After filtration, the product was washed twice with 100 ml of dichloromethane, 100 ml of tetrahydrofuran and 100 ml of hexane. The bonded silica was dried under vacuum at 80°C for 12 h.

Silver column. After packing, the column was washed with 30 ml of dichloromethane, 30 ml of hexane and 30 ml of toluene. The column was then flushed using the HPLC pump with a solution of silver tetrafluoroborate in toluene until the silver ions were detected in the eluate by reaction with hydrochloric acid. The column was backflushed with the silver solution until silver ions were detected. The operation was repeated five times. After equilibration with hexane, the column was ready for use.

RESULTS AND DISCUSSION

The calculation of surface coverage from carbon and nitrogen percentages gave a surface concentration[17] of α = 2.7 μmole/m^2.

Table I shows the elution of 24 polynuclear aromatic hydrocarbons (PAHs) with hexane as the mobile phase at a flow-rate of 1 ml/min. The retention times are in agreement with a charge-transfer retention mechanism, increasing with increasing

TABLE I

ELUTION OF AROMATIC HYDROCARBONS

Hydrocarbon	*Retention time (min)*	*Hydrocarbon*	*Retention time (min)*
Benzene	2.30	Pyrene	4.62
Indane	2.48	1,2,3,4-Tetrahydrotetracene	5.09
Indene	2.77	1,2-Benzanthracene	6.24
Biphenyl	2.80	Chrysene	6.62
Naphthalene	2.86	Benzo[*a*]pyrene	7.74
Acenaphthene	3.31	Benzo[*e*]pyrene	7.92
Acenaphthylene	3.53	7,12-Dimethylbenzanthracene	8.01
Fluorene	3.80	Perylene	9.45
1,2,3,6,7,8-Hexahydropyrene	4.05	Benzo[*g,h,i*]perylene	10.12
Anthracene	4.10	1,2,3,4-Dibenzoanthracene	11.47
Phenanthrene	4.17	1,2,5,6-Dibenzoanthracene	11.92
Fluoranthene	4.53	Coronene	12.48

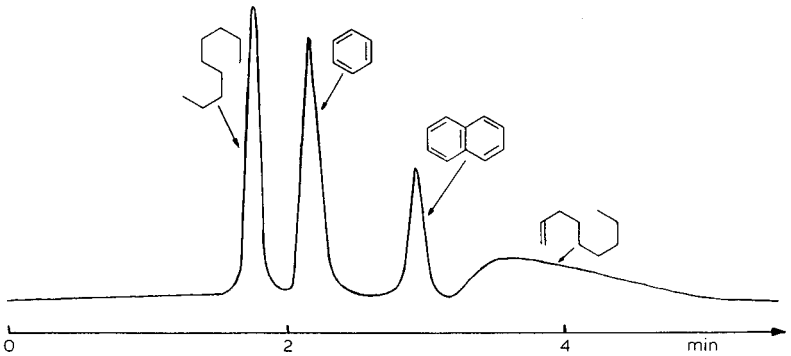

Fig. 1. Separation of test compounds. Mobile phase, hexane; flow-rate, 1 ml/min; detection, differential refractometer.

number of aromatic rings. It can be seen that naphthenic substitution (hexahydropyrene and tetrahydrotetracene) increases the retention owing to the effect of the benzylic groups as for the alkylated compounds (2, 6, 8, 19) compared with the corresponding non-alkylated compounds (1, 5, 15). Phthalonitrile can be classified as a weak acceptor like pentafluoro-bonded phases [18–21].

The column was first tested with a mixture of compounds containing nonane as the saturate, heptene as the olefin and benzene and naphthalene as the mono- and diaromatics. The separation (Fig. 1) shows that aromatics are normally retained, heptene is strongly retained and the peak is very broad.

No silver satls appeared to have contaminated the HPLC fractions. It is well known that nitrile groups are better ligands than water molecules so the nitrile ligand cannot be exchanged and shifted by water present in the mobile phase. The organometallic silver complex is very stable towards water even if the eluents are saturated with water, giving at the column a lifetime of several months.

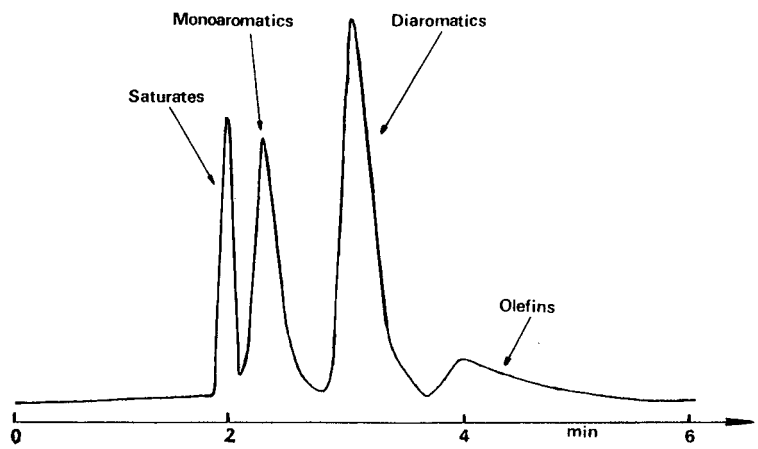

Fig. 2. Separation of a catalytic gasoline. Mobile phase, hexane; flow-rate, 1 ml/min; detection, differential refractometer.

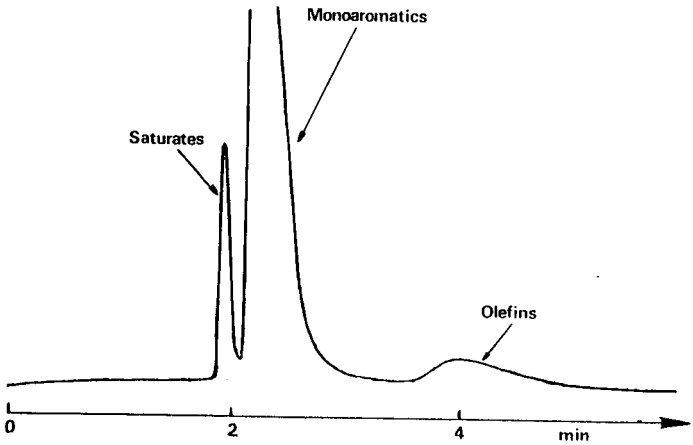

Fig. 3. Separation of a catalytic gas oil. Mobile phase, hexane; flow-rate, 1 ml/min; detection, differential refractometer.

However, this new phase was not compatible with several common HPLC solvents such as dichloromethane, which is a solvent of both silver complexes and silver salts. This incompatibility might be used for cleaning the column of accumulated polar compounds before flushing it with a new solution of silver tetrafluoroborate, thus increasing the lifetime of the column.

Figs. 2 and 3 show the separations obtained with two petroleum fractions (a catalytic gasoline and a catalytic gas oil). In addition to separating the different main hydrocarbon groups (saturates, aromatics, olefins), the aromatics are separated into mono- and diaromatics. With this bonded organometallic silver stationary phase, a complete HGTA analysis (saturates, olefins, mono- and diaromatics) can be achieved. This column can be used for the HPLC measurements of octane[22] and cetane indexes[23] in motor fuels. When the column is backflushed after the diaromat-

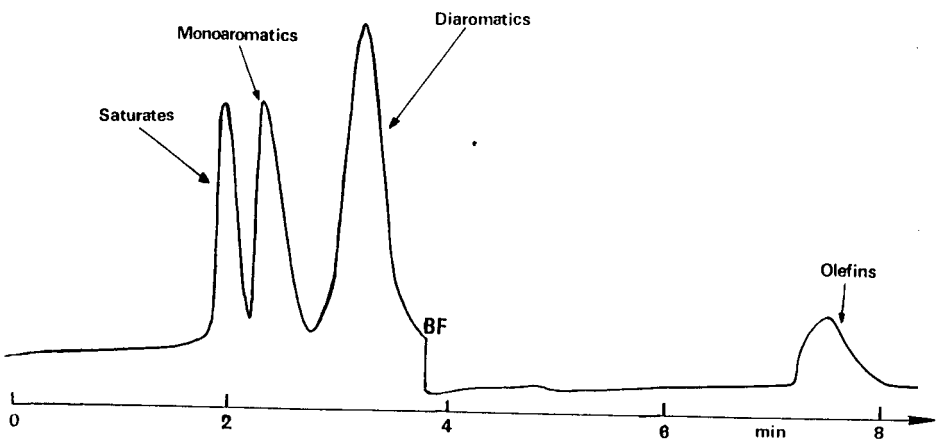

Fig. 4. Separation of a catalytic gas oil with backflushing. Mobile phase, hexane; flow-rate, 1 ml/min; detection, differential refractometer.

ics peak (Fig. 4), the olefins peak is sharper so the quantification is better. This technique cannot be used when the fuel samples contain PAHs with three or more rings because they coelute with the olefins.

This new organometallic silver bonded phase appears to be promising in its selectivity for the study of petroleum products, particularly light products such as gasoline and kerosene.

REFERENCES

1 *Annual Book of ASTM Standards, Part 23,* American Society for Testing and Materials, Philadelphia, PA, 1984.
2 K. Jinno, H. Nomura and Y. Hirata, *J. High Resolut. Chromatogr. Chromatogr. Commun.,* 3 (1980) 503.
3 S. Matsushita, Y. Tada and T. Ikushige, *J. Chromatogr.,* 208 (1981) 429.
4 T. V. Alfredson, *J. Chromatogr.,* 218 (1981) 715.
5 R. L. Miller, S. Ettre and N. G. Johansen, *J. Chromatogr.,* 259 (1983) 393.
6 J. M. Colin and G. Vion, *J. Chromatogr.,* 280 (1983) 152.
7 M. F. Rawdon, *Anal. Chem.,* 56 (1984) 715.
8 H. E. Schwartz and R. G. Brownlee, *J. Chromatogr.,* 353 (1986) 77.
9 G. Felix, E. Thoumazeau, J. M. Colin and G. Vion, *J. Liq. Chromatogr.,* 10 (1987) 2115.
10 M. Bouquet, J. M. Colin, J. P. Durand, R. Boulet and G. Félix, *J. Fuel Sci. Technol. Int.* submitted for publication.
11 P. C. Hayes, Jr. and S. D. Anderson, *Anal. Chem.,* 57 (1985) 2094.
12 P. C. Hayes, Jr. and S. D. Anderson, *Anal. Chem.,* 58 (1986) 2384.
13 P. C. Hayes, Jr. and S. D. Anderson, *J. Chromatogr.,* 387 (1987) 333.
14 O. K. Guha and J. Janák, *J. Chromatogr.,* 68 (1972) 325.
16 G. H. Jeffery and A. I. Vogel, *J. Chem. Soc.,* (1948) 661.
17 K. K. Unger, N. Becker and P. Roumeliotis, *J. Chromatogr.,* 125 (1976) 115.
18 G. Felix and C. Bertrand, *J. High Resolut. Chromatogr. Chromatogr. Commun.,* 8 (1985) 362.
19 G. Felix and C. Bertrand, *J. High Resolut. Chromatogr. Chromatogr. Commun.,* 10 (1987) 411.
20 G. Felix, A. Thienpont and C. Bertrand, *Chromatographia,* 23 (1987) 684.
21 G. Felix and C. Bertrand, *Analusis,* in press.
22 J. M. Colin, personal communication.
23 G. Felix, A. Lemorzellec, J. M. Colin and G. Vion, presented at *11th Symposium on Column Liquid Chromatography, Amsterdam,* 1987, paper MO-P-26.

Journal of Chromatography, 461 (1989) 353–359
Elsevier Science Publishers B.V., Amsterdam — Printed in The Netherlands

CHROMSYMP. 1460

PREPARATION, HIGH-PERFORMANCE LIQUID CHROMATOGRAPHIC SEPARATION AND CHARACTERIZATION OF HEXACARBOXYLIC PORPHYRINOGENS

FAMEI LI, C. K. LIM* and T. J. PETERS
Division of Clinical Cell Biology, MRC Clinical Research Centre, Watford Road, Harrow, Middlesex HA1 3UJ (U.K.)

SUMMARY

A simple method for the preparation and reversed-phase high-performance liquid chromatographic separation of hexacarboxylic porphyrinogen isomers is described. Uroporphyrin I or III was partially decarboxylated in 0.5 *M* hydrochloric acid at 150°C. Unreacted uroporphyrin and the hepta-, hexa- and pentacarboxylic porphyrins formed were esterified and then group-separated by thin-layer chromatography. After hydrolysis, the porphyrins were reduced to the corresponding porphyrinogens with 3% (w/w) sodium amalgam. The hexacarboxylic porphyrinogens were separated on an ODS-Hypersil column by elution with acetonitrile–methanol–1 *M* ammonium acetate, pH 5.16 (8:12:80, v/v/v) as mobile phase. Isomers were identified by high-performance liquid chromatography of the characteristic mixture of two pentacarboxylic porphyrins formed after partial decarboxylation of individual isomers. Except for the two type I isomers, resolution of the hexacarboxylic porphyrinogens was superior to that of the corresponding porphyrins.

INTRODUCTION

The enzymic decarboxylation of uroporphyrinogen I and III to coproporphyrinogen I and III, respectively, produces a mixture of hepta-, hexa- and pentacarboxylic porphyrinogen intermediates[1]. Among these, the hexacarboxylic porphyrinogen group is the most complex, consisting of two type I and six type III isomers (Fig. 1). The preparation, separation and characterization of these compounds are important for understanding the enzymic decarboxylation process and for the isolation of pure isomers for chemical and biochemical studies. We have reported the preparation, separation and characterization of protoporphyrinogen[2], copro- and uroporphyrinogens[3], pentacarboxylic porphyrinogens[4] and heptacarboxylic porphyrinogens[5]. This paper describes a simple method for the preparation and reversed-phase high-performance liquid chromatographic (HPLC) separation and characterization of the hexacarboxylic porphyrinogen isomers.

0021-9673/89/$03.50

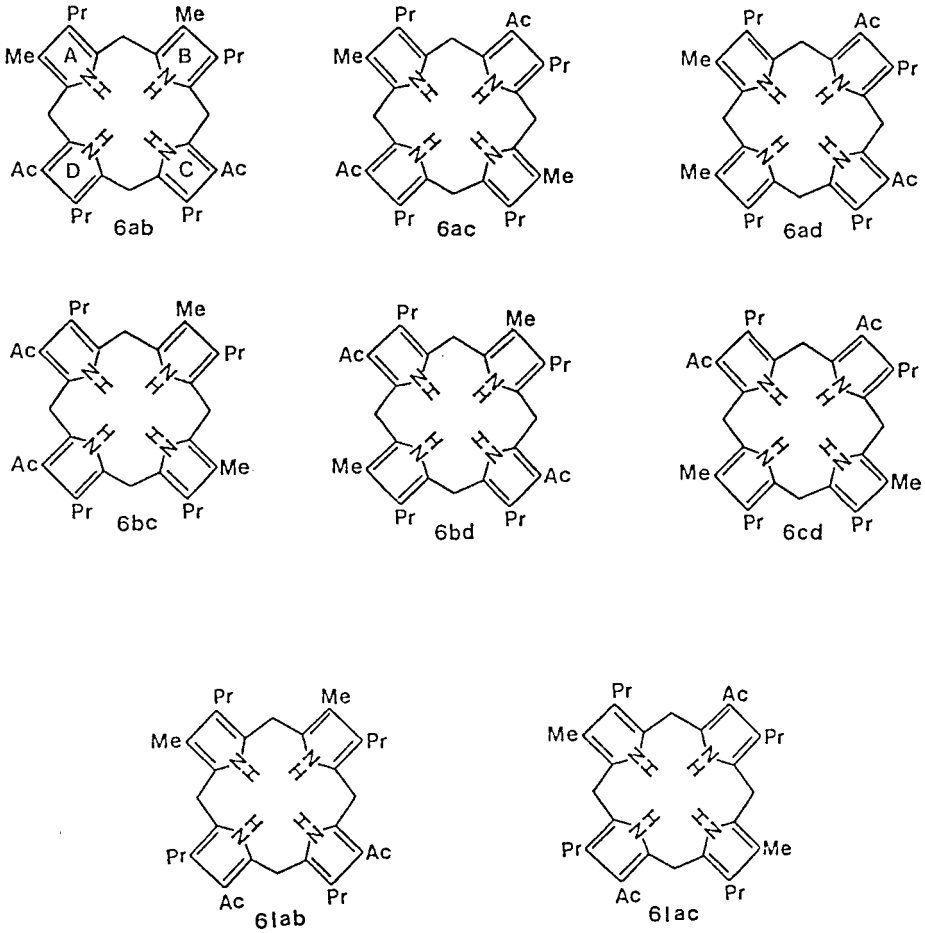

Fig. 1. Structures of hexacarboxylic porphyrinogen isomers. The letters a, b, c and d denote the positions of the methyl (Me) groups. Type I isomers are indicated with the letter I. Ac represents an acetic acid group and Pr a propionic acid group. Oxidation of the four methylene bridges to methine groups gives the corresponding porphyrins.

EXPERIMENTAL

Materials and reagents

Uroporphyrin I and III octamethyl esters were obtained from Sigma (Poole, U.K.) The esters were hydrolysed in 25% (w/v) hydrochloric acid for 96 h at room temperature in the dark.

Acetonitrile and methanol were of HPLC grade from Rathburn (Walkerburn, U.K.). Ammonium acetate, glacial acetic acid, carbon tetrachloride, chloroform, ethyl acetate and ethylenediaminetetraacetic acid (EDTA) were of AnalaR grade from BHD (Poole, U .K.).

Preparation of type I and type III hexacarboxylic porphyrinogen isomers

The method is based on that described for the preparation of penta- and heptacarboxylic porphyrinogens[4,5]. Uroporphyrin I or III was dissolved in 0.5 *M* hydrochloric acid in a Pyrex tube and heated at 150°C for 1 h in the dark. The solution was adjusted to pH 3.5 with aqueous ammonia after cooling and then extracted with ethyl acetate. The organic layer was evaporated to dryness and the residue was dissolved in 5 ml of methanol–concentrated sulphuric acid (19:1, v/v) and left to stand overnight in the dark. The resulting porphyrin methyl esters were extracted into chloroform and separated by preparative thin-layer chromatography (TLC), as previously described[5]. The band corresponding to hexacarboxylic porphyrin methyl esters, containing two type I or six type III isomers in almost equal proportions with a total yield of 30%, was collected. The reaction also produced about 25% hepta- and 20% pentacarboxylic porphyrin methyl esters. The esters were hydrolysed and extracted into ethyl acetate, as described above for uroporphyrins. Ethyl acetate was removed by evaporation and the residue was dissolved in 250 μl of 0.01 *M* potassium hydroxide solution. The solution was shaken vigorously with freshly prepared 3% (w/w) sodium amalgam until no fluorescence was detectable under a UV lamp. The prophyrinogen solution was transferred into a clean vial, flushed with nitrogen and kept on ice in the dark.

High-performance liquid chromatography

A Varian (Walnut Creek, CA, U.S.A.) Model 5000 liquid chromatograph was used. The separation was carried out on a 25 cm × 5 mm I.D. ODS-Hypersil (5 μm particle size) column (Shandon Southern, Runcorn, U.K.) with acetonitrile–methanol–1 *M* ammonium acetate, pH 5.16 (8:12:80, v/v/v), containing 0.27 m*M* EDTA, as eluent at a flow-rate of 1 ml/min. The mobile phase was thoroughly degassed with a stream of helium before use. The sample (20–100 μl, depending on concentrations) was injected via a Rheodyne 7125 injector (Cotati, CA, U.S.A.), fitted with a 100-μl loop. An LCA-15 electrochemical detector (EDT Research, London, U.K.) set at an operating potential of +0.70 V and a detector sensitivity of 30 nA was used for solute detection in analytical separation. The detector is of the wall-jet type, employing a glassy carbon working electrode and a silver–silver chloride reference electrode. For the small-scale preparative separation of isomers, a UV detector set at 240 nm was used. The purified porphyrinogens may be oxidized to the corresponding porphyrins simply by leaving the eluates on the bench for about 1 h under low-intensity white light.

Peak identification

Individual hexacarboxyl porphyrinogen isomers were isolated by small-scale preparative HPLC and oxidized to the corresponding porphyrins. Each porphyrin was partialy decarboxylated in 0.5 *M* hydrochloric acid at 150°C for 1 h. As each hexacarboxylic porphyrin gave a characteristic pair of pentacarboxylic porphyrin isomers on partial decarboxylation, analysis of these two isomers by the established HPLC system for pentacarboxylic porphyrin isomers[6] allows the positive identification of each hexacarboxylic porphyrinogen peaks. The pentacarboxylic porphyrins were separated on an ODS-Hypersil column with acetonitrile–1 *M* ammonium acetate, pH 5.16 (20:80, v/v) as mobile phase.

RESULTS AND DISCUSSION

Synthesis of hexacarboxylic porphyrinogens

The direct synthesis of porphyrinogens from pyrromethanes is impractical, because porphyrinogens are unstable to oxidation by air. The corresponding porphyrins were therefore prepared and then reduced to the porphyrinogens with sodium amalgam or sodium borohydride. The hexacarboxylic porphyrins have been synthesized by condensation of appropriate dipyrromethanes[1]. However, a mixture of isomeric hexacarboxylic porphyrins can also be easily and conveniently prepared by partial decarboxylation of uroporphyrin in 0.5 *M* hydrochloric acid at 150°C. As the reaction also produced penta- and heptacarboxylic porphyrins, preliminary group separation by TLC was performed[4,5] in order to simplify the subsequent HPLC purification. The isolated hexacarboxylic porphyrins were reduced to the porphyrinogens for HPLC separation. They were stable for at least 3 h when kept on ice in the dark.

High-performance liquid chromatography

The separation of a mixture containing two type I and six type III hexacarboxylic porphyrinogen isomers (see Fig. 1 for structures) is shown in Fig. 2. The ternary mobile phase acetonitrile–methanol–1 *M* ammonium acetate, pH 5.16 (8:12:80, v/v/v) was used, as it provided better resolution than binary systems with either acetonitrile or methanol as the organic modifier. The retention and resolution of the isomers were significantly influenced by the pH and the concentration of the ammonium acetate buffer used. Increasing the pH decreased the retention and consequently the resolution, the optimal pH being between 5.1 and 5.2. As with the separation of other porphyrinogens[2–5], a 1 *M* buffer solution was chosen for rapid separation without sacrificing resolution. Decreasing the buffer concentration increased the retention of all isomers without a significant improvement in resolution. Despite optimization of the mobile phase, only seven peaks were detected (Fig. 2), indicating that two of the isomers must have remained unresolved.

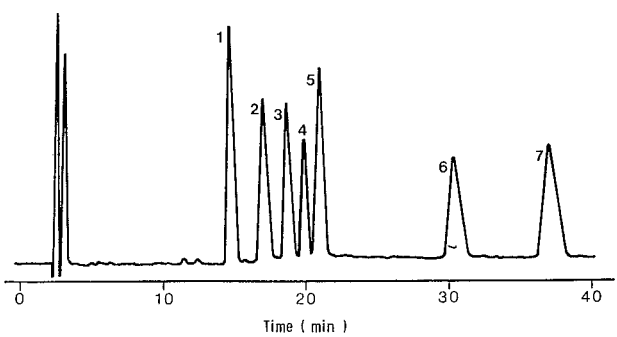

Fig. 2. HPLC separation of hexacarboxylic porphyrinogen isomers. The separation was carried out on a 25 cm × 5 mm I.D. ODS-Hypersil column with acetonitrile–methanol–1 *M* ammonium acetate, pH 5.16 (8:12:80, v/v/v) as mobile phase at a flow-rate of 1 ml/min; detection was amperometric at + 0.70 V. Peaks: 1 = isomer 6ab; 2 = isomer 6 cd; 3 = isomer 6bc; 4 = isomers 6Iab + 6Iac; 5 = isomer 6ac; 6 = isomer 6bd; 7 = isomer 6ad (see Fig. 1).

Peak identification

The two type I isomers (6Iab and 6Iac) were easily identified, as the corresponding porphyrins were available. The porphyrins have been prepared by partial decarboxylation of uroporphyrin I and then isolated by HPLC[6]. Sodium amalgam reduction followed by HPLC separation showed that 6ab and 6ac had identical retention times, corresponding to peak 4 in Fig. 2. These two isomers had therefore been eluted together under the HPLC conditions used. They were, however, completely separated from the six type III isomers.

For the identification of the type III isomers, a small-scale preparative HPLC isolation of isomers was performed. The purified isomers were oxidized to the corresponding porphyrins and then partially decarboxylated to pentacarboxylic porphyrins. As each type III hexacarboxylic porphyrin isomers can only give two type III pentacarboxylic porphyrins with fixed structures, analysis of these isomers allows the positive identification of individual hexacarboxylic porphyrins. The pentacarboxylic porphyrin pairs derived from each peak and the peak assignments are summarized in Table I. The elution order was 6ab, 6cd, 6bc, 6Iab + 6Iac, 6ac, 6bd and 6ad.

Comparison of the separation of hexacarboxylic porphyrins and porphyrinogens

Fig. 3 shows the separation of a standard mixture containing the eight hexacarboxylic porphyrin isomers using the reversed-phase system previously described[6]. Compared with the separation achieved in Fig. 2, it is obvious that the resolution of the porphyrinogens is superior to that of the porphyrins. The same trend has been observed for copro-[3], pentacarboxylic[4], and heptacarboxylic porphyrinogens[5]. In order to obtain pure isomers of the porphyrins, it is therefore necessary to reduce them to the porphyrinogens for purification. The purified porphyrinogens are then oxidized back to the porphyrins.

Reversed-phase chromatography of porphyrins has been shown to be dominated by hydrophobic interactions between the most hydrophobic side-chain substituents (methyl groups) and the hydrocarbonaceous stationary-phase surface[6]. In a

TABLE I

PENTACARBOXYLIC PORPHYRINS FORMED BY PARTIAL DECARBOXYLATION OF HEXACARBOXYLIC PORPHYRIN

The pentacarboxylic porphyrins were separated on an ODS-Hypersil column with acetonitrile in 1 *M* ammonium acetate, pH 5.16 (20:80, v/v) as mobile phase[6].

HPLC peak No. (Fig. 2)	*Pentacarboxylic porphyrins**	*Peak assignment**
1	5abc, 5abd	6ab
2	5acd, 5bcd	6cd
3	5abc, 5bcd	6bc
4	5I	6I
5	5abc, 5acd	6ac
6	5abd, 6bcd	6bd
7	5abd, 5acd	6ad

* The letters a, b, c and d denote the positions of methyl groups, *i.e.*, the position in which the acetic acid groups have been decarboxylated[1]. Type I isomers are indicated with the letter I.

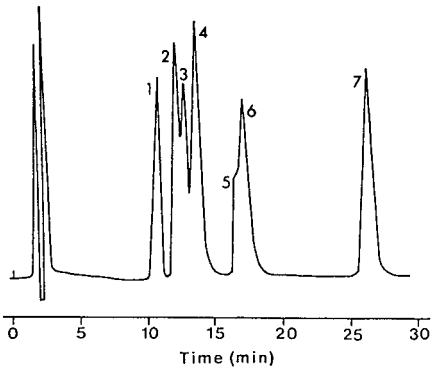

Fig. 3. HPLC separation of hexacarboxylic porphyrins. The separation was carried out on an ODS-Hypersil column with acetonitrile–1 *M* ammonium acetate, pH 5.16 (16:84, v/v) as eluent at a flow-rate of 1 ml/min; UV detection at 400 nm. Peaks: 1 = 6Iac; 2 = 6ac + 6bd; 3 = 6cd; 4 = 6Iab; 5 + 6 = 6ab + 6bc; 7 = 6ad (see Fig. 1).

hexacarboxylic porphyrin molecule there are two side-chain methyl substituents (see Fig. 1). The relative retention of the isomers is therefore governed by the distance between these two groups. The closer the methyl groups, the larger is the hydrophobic surface area available for interaction and the longer the compound is retained. The observed elution order of the hexacarboxylic porphyrin isomers (6Iac, 6ac + 6bd, 6cd, 6Iab, 6ab + 6bc and 6ad) is consistent with this hypothesis. However, the elution order of the hexacarboxylic porphyrinogen isomers deviated significantly from that predicted. This is probably due to the variable shielding of the methyl groups by the larger carboxylic acid groups in different isomers. Partial or complete shielding of one or both methyl groups will lead to a change in hydrophobicity and hence in elution order. Shielding of the methyl groups is possible in porphyrinogens because these molecules, with methylene instead of methine bridges, are flexible. The porphyrins are not affected by the shielding effect, because they are rigid molecules. Steric factors may have contributed to the improved resolution seen in the separation of porphyrinogens[3–5]. Separation of the two type I hexacarboxylic porphyrinogens, 6Iab and 6Iac, has not been achieved with the present system, although the corresponding porphyrins can be easily separated (Fig. 3, peaks 1 and 4). This is an exception to the general trend. A possible explanation is that one of the isomers adopted a conformation which resulted in an identical hydrophobicity to the other, resulting in an identical elution time.

CONCLUSIONS

Partial decarboxylation of uroporphyrin followed by reduction and HPLC separation of the hexacarboxylic porphyrinogens provided a simple and convenient route to the synthesis and isolation of pure hexacarboxylic porphyrin isomers. The porphyrinogens are easily converted to the porphyrins by oxidation. The resolution of the type III hexacarboxylic porphyrinogen isomers was superior to that of the corresponding porphyrins. The separation of the two type I isomers has not been achieved, although the corresponding porphyrins can be easily separated. The reten-

tion of the rigid hexacarboxylic porphyrins is dominated by hydrophobic interactions between the two side-chain methyl substituents and the hydrocarbonaceous stationary-phase surface. An additional important factor, partial or complete shielding of one or both of the methyl groups by the larger carboxy substituents, also affected the retention and resolution of the flexible hexacarboxylic porphyrinogen molecules.

REFERENCES

1 A. H. Jackson, H. A. Sancovich, A. M. Ferramola, N. Evans, D. E. Games, S. A. Matlin, G. H. Elder and S. G. Smith, *Philos. Trans. R. Soc. London, Ser. B,* 273 (1976) 191.
2 F. Li, C. K. Lim and T. J. Peters, *Biochem. J.,* 239 (1986) 481.
3 C. K. Lim, F. Li and T. J. Peters, *Biochem. J.,* 234 (1986) 629.
4 F. Li, C. K. Lim and T. J. Peters, *Biochem. J.,* 243 (1987) 621.
5 C. K. Lim, F. Li and T. J. Peters, *Biochem. J.,* 247 (1987) 229.
6 C. K. Lim, J. M. Rideout and D. J. Wright, *J. Chromatogr.,* 282 (1983) 629.

Journal of Chromatography, 461 (1989) 361–364
Elsevier Publishers B.V., Amsterdam — Printed in The Netherlands

CHROMSYMP. 1436

HIGH-PERFORMANCE LIQUID CHROMATOGRAPHY OF OXIDATION PRODUCTS OF 2,6-DIMETHYLPHENOL

H. LUETJE
BASF AG, Kunststofflaboratorium, 6700 Ludwigshafen/Rhein (F.R.G.)

SUMMARY

The oligomers of poly(2,6-dimethyl-1,4-phenylene oxide ($M < 1000$) have been separated by gradient elution. Poly(2,6-dimethyl-1,4-phenylene oxide) is prepared by oxidative coupling of 2,6-dimethylphenol. At low conversions the concentrations of the oligomers from $n = 2$ to $n = 10$ follow the normal distribution of Schulz and Flory. A linear extrapolation of these values ($n = 2$–10) yields a value for the monomer ($n = 1$), which amounts only to 1/20 of the experimental value. By a side reaction, 3,3′,5,5′-tetramethyl-4,4′-dipenoquinone (DPQ) is formed. From the chromatograms recorded simultaneously at different wavelengths, DPQ can be determined together with the oligomers during a single HPLC experiment. Experimental results confirming the principle of "equal reactivity" (Flory) for oligomers ($n < 10$) are presented.

INTRODUCTION

Polyphenylene ether (PPE) is a hard, tough material with exceptional properties[1]. Blends of PPE with high impact polystyrene are outstanding, combining excellent mechanical properties with good flame retardancy[2]. High-molecular-weight PPE is prepared by allowing 2,6-dimethylphenol (DMP) to react with oxygen in the presence of a catalyst (a cupric amine complex).

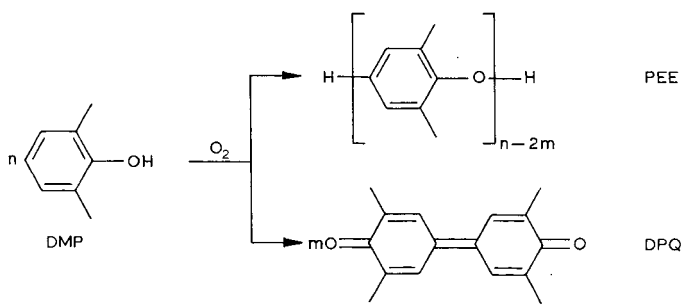

3,3′,5,5′-Tetramethyl-4,4′-diphenoquinone (DPQ)[3] is a by-product, which cannot be avoided. Hitherto the oligomeric reaction products have been investigated by gas chromatography as trimethylsilyl ethers[4] or by gel permeation chromatography

0021-9673/89/$03.50

(GPC)[5]. In this work a simple high-performance liquid chromatographic (HPLC) method is described, which allows a separation of the monomer and of the reaction products directly without any derivatization.

MATERIALS AND METHODS

Oxidation of 2,6-dimethylphenol

For the oxidative coupling of DMP the recipe reported by Brandt[1] was used. The reactor contained all of the monomer at the beginning of the oxidation (batch operation). The catalyst mixture, (a suspension of 0.36 g copper(I) bromide in 19.5 g dibutylamine and 13 g toluene), was added to a solution of 116 g 2,6-dimethylphenol in 374 g toluene. With vigorous agitation, air was passed into the solution at room temperature. (The use of air instead of pure oxygen reduced the reaction rate. Thus it was posible to withdraw samples having different degrees of conversion during a single experiment).

Analytical procedure

The oxidation reaction was stopped by adding a small sample of the reactor solution (2 ml) to an excess of methanol (10 ml) acidified with concentrated aqueous hydrochloric acid (0.5 ml). At low conversions, an homogenous mixture was obtained, which was washed with water after diluting it in choroform (20 ml). The chloroform solution was injected immediately into the chromatograph.

A HP 1090 liquid chromatograph (Hewlett-Packard, Analytical Division, Waldbronn, F.R.G.) equipped with an autosampler and diode-array detector HP 1040 was used. The eluents were delivered by two dual syringe metering pumps, operating at low pressure (around 3 bar).

Chromatographic conditions

Columns were from E. Merck (Darmstadt, F.R.G.) and were 250 mm × 4 mm. The stationary phase was LiChrosorb Si 60 (5 μm) (Merck) at an oven temperature of 40°C.

Gradient elution (0 to 95% B, 30 min) was used, with eluent A (73% dichloromethane + 27% cyclohexane), eluent B (99,2% dichoromethane + 0.8% tetrahydrofuran) and a flow-rate of 1 ml/min. The detection system was operated simultaneously at two wavelengths (277 and 420 nm). The data were evaluated by an analytical work station HP 79994 A (Hewlett-Packard).

RESULTS

Figs. 1 and 2 show chromatograms after 3 h of air oxidation. At 277 nm the monomer (DMP) peak appears after 5.8 min. Between 7 and 12 min, the oligomers $n=2$ to $n=10$ are separated. The polymer (PPE) appears after about 20 min (not shown). The by-product, diphenoquinone (DPQ) is eluted later (after 26 min). Optimum detection of DPQ is obtained at 420 nm. The oligomer distribution in Fig. 1 is close to equilibrium; the DMP content of the undiluted reactor sample shows little change (-5%) after standing overnight under nitrogen.

A single HPLC experiment is sufficient to determine the starting material, the oligomeric intermediates and the by-product.

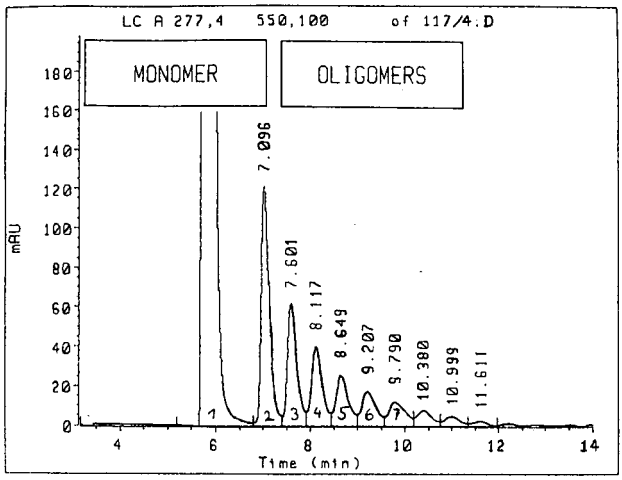

Fig. 1. HPLC separation of the reaction products after oxidation of dimethylphenol (DMP), detected at 277 nm.

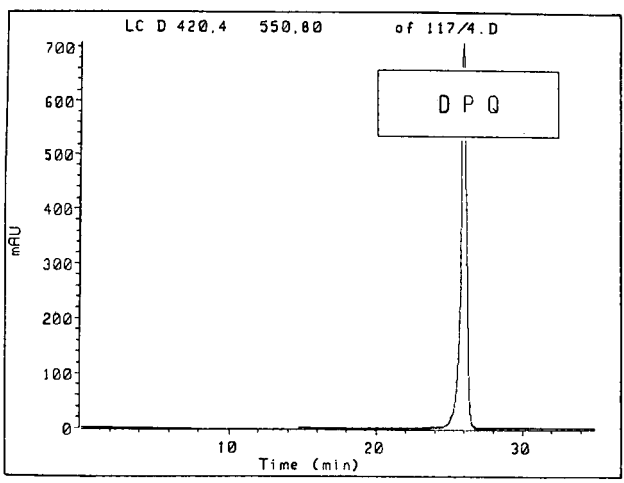

Fig. 2. HPLC separation of the reaction products after oxidation of dimethylphenol, detected at 420 nm; otherwise as in Fig. 1.

DISCUSSION

The oxidative coupling of DMP is reported to proceed in a manner analogous to a linear polycondensation[6]. Formally the coupling reaction can be treated as a polycondensation with elimination of hydrogen, the quinone ketal equilibration resulting in a redistribution reaction[4,7]. For a linear polycondensation a normal distribution of molecular weights as postulated by Schulz[8] and Flory[9] is expected.

For a normal distribution a linear plot of log (c_n/n) *vs.* n can be deduced (c_n = concentration by weight of the species with degree of polymerization (P)

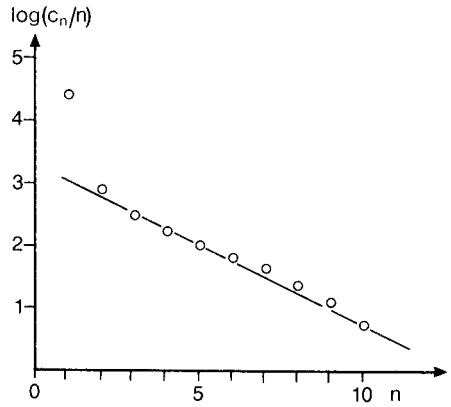

Fig. 3. Molar concentrations (c_n/n) of the oligomers (logarithmic plot). From the principle of equal reactivity, a linear plot is expected.

$= n$). c_n is proportional to a_n (a_n = HPLC peak area of the nth peak). When $\log(a_n/n)$ is plotted *vs.* n, the molar concentrations of the oligomers from $n = 2$ to $n = 10$ follow the normal distribution of Schulz and Flory. A linear extrapolation of these values yields a value for the monomer ($n = 1$) which amounts to only 1/20 of the experimental value (Fig. 3).

Flory[10] formulated a "principle of equal reactivity" for the functional groups of long chain molecules. Our chromatographic results confirm this principle for the oligomers in the range between $n = 2$ and $n = 10$. The reactivity is different for the first step in the oxidative coupling of DMP. Heitz[11] proposed a single electron process (SET)[12] in the growth reaction of PPE to explain the deviation of the concentration of DMP determined by his measurements (GPC)[5] at low conversion.

Apart from liquid chromatography, PPE oligomers have been investigated by gas chromatography after fractional distillation of derivatives[6] or by less specific methods such as thin-layer chromatography[13].

HPLC offers a rapid and specific method of separation for PPE oligomers. Equal reactivity is a fundamental principle of macromolecular chemistry. Its validity may be extended down to small molecules ($M > 200$) by our HPLC results.

REFERENCES

1 H. Brandt, in Houben, Weyl, *Methoden der Organischen Chemie, Makromolekulare Stoffe*, G. Thieme Verlag, Stuttgart, Vol. 2, 1987, p. 1380.
2 G. Brewer, *Modern Plastics Enzyclopedia*, McGraw-Hill, New York, 1988, p. 37.
3 C. G. Haynes, A. H. Turner and W. A. Waters, *J. Chem. Soc. (London)*, (1956) 2823.
4 D. M. White, *J. Org. Chem.*, 34 (1969) 297.
5 W. Koch, W. Risse and W. Heitz, *Makromol. Chem. Suppl.*, 12 (1985) 105.
6 G. F. Enders and G. F. Kwiateck, *J. Polym. Sci.*, 58 (1962) 593.
7 G. D. Cooper, *Ann. NY Acad. Sci.*, 159 (1969) 278.
8 G. V. Schulz, *Z. Phys. Chem.*, B 30 (1935) 379.
9 P. J. Flory, J. Am. Chem. Soc., 58 (1936) 1877.
10 P. J. Flory, *Chem. Rev.*, 39 (1946) 137.
11 W. Heitz, *Makromol. Chem. Makromol. Symp.*, 4 (1986) 35.
12 M. Chanon and M. L. Tobe, *Angew. Chem.*, 94 (1982) 27.
13 W. J. Mijs, H. van Dijk, W. G. B. Huysmans and J. G. Westra, *Tetrahedron*, 25 (1969) 4233.

Journal of Chromatography, 461 (1989) 365–375
Elsevier Science Publishers B.V., Amsterdam — Printed in The Netherlands

CHROMSYMP. 1508

CHROMATOGRAPHIC PROPERTIES OF A VINYL ALCOHOL COPOLYMER GEL COLUMN FOR THE ANALYSIS OF NON-IONIC SURFACTANTS

KOHJI NOGUCHI*, YUZO YANAGIHARA, MASAO KASAI and BUNJI KATAYAMA
Gel Separation Development Department, Asahi Chemical Industry Co., Ltd., 1-3-2, Yakoo Kawasaki-ku, Kawasaki-shi 210 (Japan)

SUMMARY

A high-performance size-exclusion chromatographic column packed with Asahipak GS-310 vinyl alcohol copolymer gel was investigated for its applicability to the analysis of non-ionic surfactants with mobile phases containing water and acetonitrile or other organic solvents in various ratios. The surfactant series consisted of $R(OCH_2CH_2)_nOH$, where R is an alkylaryl group and $n = 1$–100.

In the water-rich region, with acetonitrile concentrations of 0–30%, surfactants either were not eluted or their elution was extremely delayed, indicating a hydrophobic interaction between the gel and the alkylaryl group in the surfactant. In the acetonitrile-rich region, with acetonitrile concentrations of 60–100%, the surfactants were eluted relatively rapidly in order of decreasing molecular weight, without a fine separation between compounds with different n values. These results indicate that the organic solvent effectively inhibited the hydrophobic interaction and that size exclusion was the predominant separation mechanism. In the intermediate region, with 30–60% acetonitrile concentrations, the surfactants were eluted in the same order as for the acetonitrile-rich region, but less rapidly and with a fine separation between n values. The results indicate that the separation mechanism is mainly hydrophobic interaction between the alkylaryl groups and the gel, the hydrophobicity of the gel being too weak for effective interaction with the oxyethylene groups.

The results indicate that the Asahipak GS-310 hydrophilic polymer gel column can be effectively employed for the practical, efficient high-performance liquid chromatographic analysis of non-ionic surfactants.

INTRODUCTION

The Asahipak GS series consists of high-performance liquid chromatographic (HPLC) columns packed with vinyl alcohol copolymer gel, which were developed and are now widely utilized for aqueous size-exclusion chromatography (SEC). In a previous study[1], we found that two columns in the series, GS-310 and GS-510, could be characterized as "amphipathic SEC columns", capable of SEC of both pullulan with an aqueous mobile phase and polystyrene with chloroform as the mobile phase. Both columns were found to be characterized, in particular, by their stability and effective

0021-9673/89/$03.50

performance using mobile phases with a broad range of freely varied organic solvents and aqueous organic solvents of various concentration, because their gel volume is not significantly affected by changes in mobile-phase polarity. This characteristic led to the present investigation of the application of amphipathic Asahipak GS-310 to the analysis of non-ionic surfactants with mobile phases containing water and acetonitrile or other organic solvents in various ratios.

EXPERIMENTAL

Chromatography was performed with a Tri-Rotar HPLC apparatus (Jasco, Tokyo, Japan), equipped with a Shodex SE-51 refractometer (Showa Denko, Tokyo, Japan).

Asahipak GS-310 (500 mm × 7.6 mm I.D.) HPLC columns (Asahi Chemical Industries, Tokyo, Japan), packed with vinyl alcohol copolymer gel having a mean particle diameter of 9.0 μm and an exclusion limit of 40 000 Da, were employed.

Surfactants were obtained from Nippon Nyukazai (Tokyo, Japan), in the series described by the formula $R(OCH_2CH_2)_nOH$, where R = C_8H_{17}-*p*-C_6H_4– and C_9H_{19}-*p*-C_6H_4– and n = 1–100. Organic solvents were obtained from Wako (Osaka, Japan).

RESULTS AND DISCUSSION

The chromatographic behaviour of the non-ionic surfactants on isocratic elution with water–organic solvent mixtures using the vinyl alcohol copolymer gel column (GS-310) is shown in Fig. 1 in terms of the relationship between the retention volume of nonylphenoxyoligo(ethylene glycol)s and acetonitrile concentration in a water–acetonitrile mobile phase.

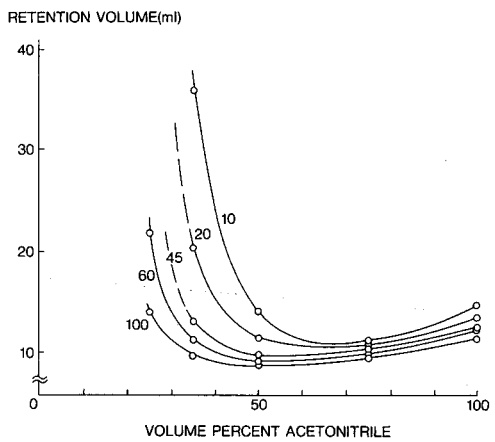

Fig. 1. Graphs illustrating plots of the retention volume (ml) against the composition of the acetonitrile–water mixture used as the eluent. The number on each curve indicates the number of EO units contained in the solute molecule. Column, Asahipak GS-310 (500 × 7.6 mm I.D.); temperature, 30°C; flow-rate, 1.0 ml/min; detection, 280 nm; samples, nonylphenoxy oligo(ethylene glycol)s.

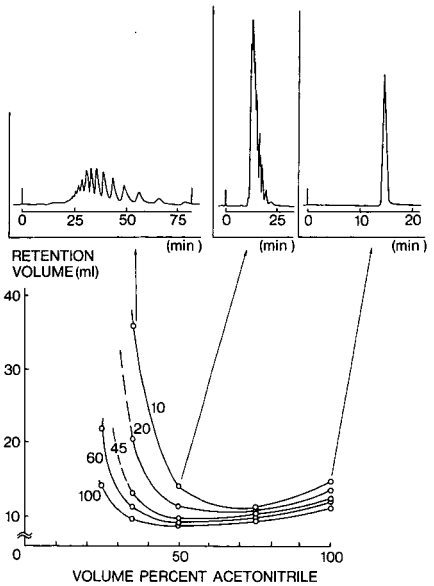

Fig. 2. Chromatograms of nonylphenoxy oligo(ethylene glycol)s with an average of 10 EO units at various acetonitrile concentrations, and graphs illustrating plots of the retention volume against the composition of the acetonitrile–water mixture used as the eluent. Column, Asahipak GS-310 (500 × 7.6 mm I.D.); temperature, 30°C; flow-rate, 1.0 ml/min; eluent, water–acetonitrile; detection, 280 nm.

The chromatograms in Fig. 2 are typical of those obtained for these surfactants on the GS-310 column. They were obtained with eluents containing acetonitrile at three concentrations for a homologous mixture containing an average of ten ethylene oxide (EO) units per solute molecule. These homologues were not eluted when the mobile phase was water alone or water containing up to 30% acetonitrile. In a series of analyses with successively higher acetonitrile concentrations, elution resulting in late, poorly defined peaks was first observed with about 30% acetonitrile, and further increases in the acetonitrile concentration resulted in increasingly rapid elution. It was also observed that, at a given acetonitrile concentration, smaller n values in C_9H_{19}-p-$C_6H_4(OCH_2CH_2)_n$–tended to result in longer elution times. Conversely, the acetonitrile concentration necessary to elute the non-ionic surfactant in a given time tended to increase with decreasing n.

In numerous similar analyses of these surfactants with n values ranging from 1 to 100, they were eluted in the intermediate region of about 30–60% acetonitrile with a fine separation between homologues with different n values. No reversal in the order of elution of these homologues occurred with changes in organic solvent concentration, in contrast to the results reported by Melander *et al.*[2] for similar analyses of phenyloligo(ethylene glycol)s on ODS columns.

It was therefore possible to analyse the non-ionic surfactants isocratically, despite the large variation in hydrophobicity known to occur with different n values. Under the given conditions that yielded this fine separation, moreover, the same homologue was eluted at the same elution volume, with excellent reproducibility, even when in different homologue mixtures, as shown in Fig. 3 and Table I.

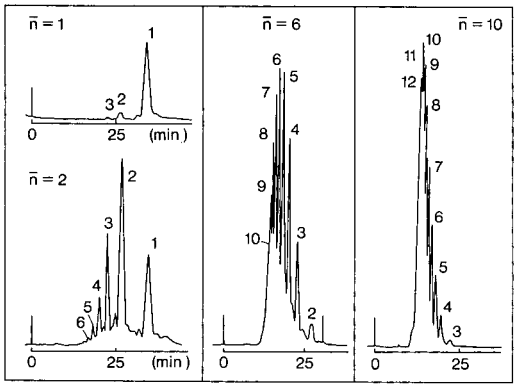

Fig. 3. Chromatograms for several nonylphenoxy oligo(ethylene glycol)s differing in the average number of EO units. Column, Asahipak GS-310 (500 × 7.6 mm I.D.); temperature, 30°C; flow-rate, 1.0 ml/min; eluent, water–acetonitrile (50:50); detection, 280 nm.

From these analyses, the number of theoretical plates (N) for these surfactants was determined to be about 5000–8000, with the value tending to increase with increasing k' value, as shown in Fig. 4. This indicates a capability for excellent separations of surfactants with small n values.

Fig. 5 shows the dependence of the logarithm of the retention factor for octylphenyloligo(ethylene glycol)s on the number of EO units with eluents of various acetonitrile concentrations. No inversion in the order of elution occurred with changes in the acetonitrile concentration, again in contrast to the behaviour of phenyloligo (ethylene glycol)s on ODS columns reported by Melander *et al.*[2].

As shown by the Van 't Hoff plots in Fig. 6, the retention factors decreased with increasing temperature for homologues with n values smaller than 10, as is usual in reversed-phase chromatography, but increased for those with larger n values. Although the elution order with respect to the n values in the homologous series is the reverse of that reported by Melander *et al.*[2] for phenyloligo(ethylene glycol)s on ODS columns, the tendency for the retention factors to decrease with increase in temperature for homologues with small n values and to increase for those with larger n values is similar.

TABLE I

REPRODUCIBILITY OF RETENTION VOLUMES

Average number of ethylene oxide units	*Retention volume (ml)*					
	*10**	*6**	*4**	*3**	*2**	*1**
2	–	16.91	20.14	22.76	27.01	35.10
6	13.99	16.96	20.09	22.70	27.01	–
10	14.15	16.91	19.99	22.70	–	–

* Number of ethylene oxide units in nonylphenoxyoligo(ethylene glycol)s.

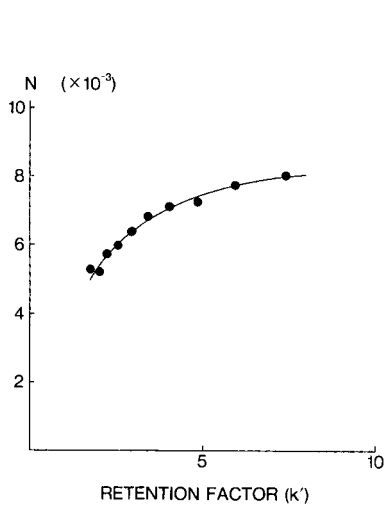

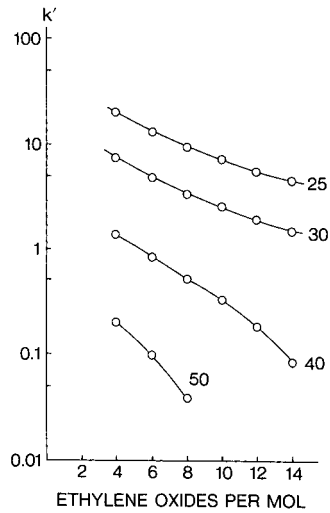

Fig. 4. Graph of the number of theoretical plates against retention factors (k'). Column, Asahipak GS-310 (500 × 7.6 mm I.D.); temperature, 30°C; flow-rate, 1.0 ml/min; eluent, water–acetonitrile (70:30); detection, 280 nm; sample, octylphenoxyoligo(ethylene glycol)s with an average of 10 EO units.

Fig. 5. Graphs of retention factors (k') on a logarithmic scale against number of EO units in octylphenoxy oligo(ethylene glycol)s with an average of 10 EO units. Column, Asahipak GS-310 (500 × 7.6 mm I.D.; temperature, 30°C; flow-rate, 1.0 ml/min; eluent, water–acetonitrile mixtures with the acetonitrile concentrations (%, v/v) indicated on the curves; detection, 280 nm.

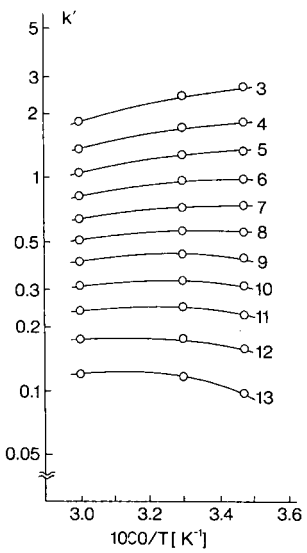

Fig. 6. Van 't Hoff plots of retention factors (k') for octylphenoxy oligo(ethylene glycol)s containing the number of EO units indicated on the curves. The retention data were measured with an Asahipak GS-310 column (500 × 7.6 mm I.D.) at an eluent flow-rate of 1.0 ml/min and with detection at 280 nm; eluent, water–acetonitrile (60:40).

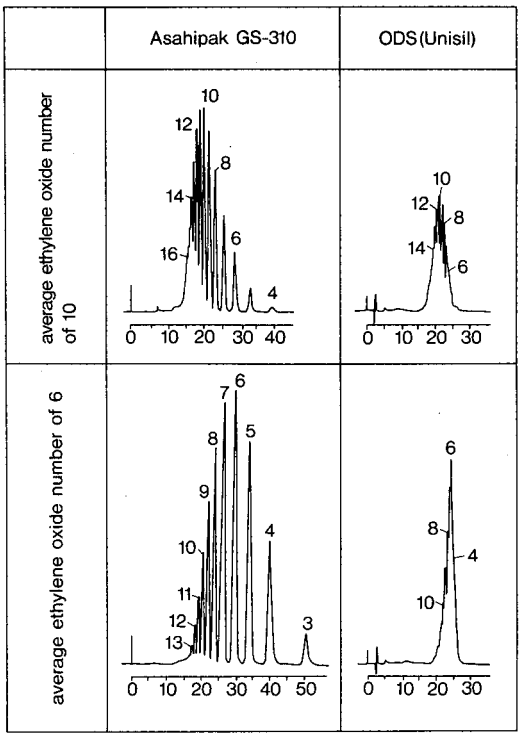

Fig. 7. Chromatograms of octylphenoxy oligo(ethylene glycol)s containing the number of EO units indicated on the peaks on an Asahipak GS-310 column (500 × 7.6 mm I.D.) at an eluent flow-rate of 1.0 ml/min and on a 5-μm Unisil Pack ODS column. Detection at 280 nm. Eluents: water–acetonitrile (60:40) on the Asahipak column and water–acetonitrile (45:55) on the ODS column. Temperature, 30°C.

For comparison, similar analyses were performed on a widely used ODS column. Fig. 7 shows typical examples of attempts to achieve a fine separation between homologous with different n values. The surfactants were eluted from the ODS column in order of decreasing n, as on Asahipak GS-310. However, the concentration of acetonitrile required to give similar retention factors was about 15–20% higher than on GS-310, indicating a higher hydrophobicity of the ODS column. The inferior separation between homologues with smaller n values on the ODS column corresponds to a far smaller difference between retention factors on the ODS column, especially for small n.

Elution mechanism

Three broad regions of non-ionic surfactant elution behaviour were observed, corresponding to different ranges of acetonitrile concentration: the water-rich region with acetonitrile concentrations of 0–30%, the intermediate region (30–60%) and the acetonitrile-rich region (60–100%).

In the water-rich region, elution of the non-ionic surfactants either did not occur or required very large eluent volumes, probably as a result of strong hydrophobic interactions between the alkylaryl groups in the surfactant and the gel skele-

ton. As an SEC column, on the other hand, GS-310 generally exhibits only weak hydrophobic interactions with poly(ethylene glycol)s and other hydrophilic solutes in water. It may therefore be expected to provide a means of effective removal of surfactants from protein–surfactant mixtures, with a capability for repeated use after washing with organic or aqueous–organic solvents to remove adsorbed surfactants.

In the acetonitrile-rich region, the non-ionic surfactants exhibited elution volumes of 9–14 ml, in order of decreasing molecular weight, with no fine separation between homologues with different n values. Plots of this relationship between molecular weight and elution volume are shown in Fig. 8, together with calibration graphs for standard polystyrenes in chloroform and for standard pullulans and poly(ethylene glycol)s in water. The plots for the non-ionic surfactants lie between the two calibration graphs; the K_d values, as calculated from the retention volume for each surfactant, ranged from 0.2 to 0.8. These results indicate that the organic solvent effectively inhibited hydrophobic interactions with the GS-310 gel, and that size exclusion was the predominant separation mechanism.

Essentially the same results, indicating a size-exclusion mechanism, were observed with methanol or n-propanol in place of acetonitrile. The organic solvent concentrations required for elution volumes similar to those obtained with acetonitrile were higher with methanol and lower with n-propanol, as shown in Fig. 9. The comparatively high efficiency of SEC with n-propanol indicates that organic solvents with longer alkyl groups inhibit more effectively the hydrophobic interactions between the nonylphenyl groups in the surfactant and the gel.

In the intermediate region, the surfactants were eluted in the same order as for the acetonitrile-rich region, but less rapidly and with a fine separation between n values. The K_d values for all of the homologues with smaller n values were greater than 1, as shown in Fig. 10, indicating that the separation mechanism is not predominantly one of size exclusion.

Fig. 11, obtained with three columns having different OH densities, shows that

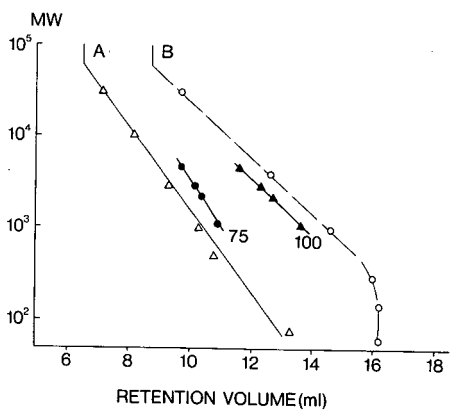

Fig. 8. Graphs of molecular weight on a logarithmic scale against retention volume. The number on each curve indicates the acetonitrile concentration in water–acetonitrile mixtures. Column, Asahipak GS-310 (500 × 7.6 mm I.D.); temperature, 30°C; flow-rate, 1.0 ml/min; detection at 280 nm; sample, nonylphenoxy oligo(ethylene glycol)s. (A) Calibration graph with standard polystyrene in chloroform; (B) calibration graph with standard poly(ethylene glycol)s in water.

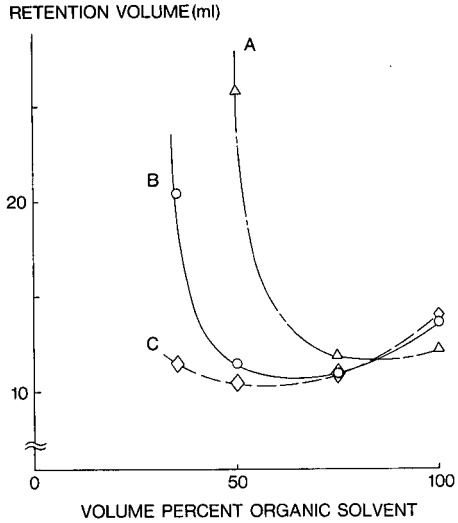

Fig. 9. Graphs of retention volume (ml) against composition of water–organic solvent mixtures used as eluent. Column, Asahipak GS-310 (500 × 7.6 mm I.D.); temperature, 30°C; flow-rate, 1.0 ml/min; detection at 280 nm; sample, nonylphenoxy oligo(ethylene glycol)s, average 20 EO units. Organic solvent: (A) methanol; (B) acetonitrile; (C) *n*-propanol.

the retention volume for surfactants with a given n value increases with decreasing OH density in the column gel. Hence with a gel of low OH density, as in GS-310, hydrophobic interactions predominate over hydrogen bonding.

Fig. 12 shows plots of retention volumes against n for GS-310 and ODS columns. With the ODS column, the slope is nearly constant throughout the investigated range of n values. With the GS-310 column, the slope increases rapidly with

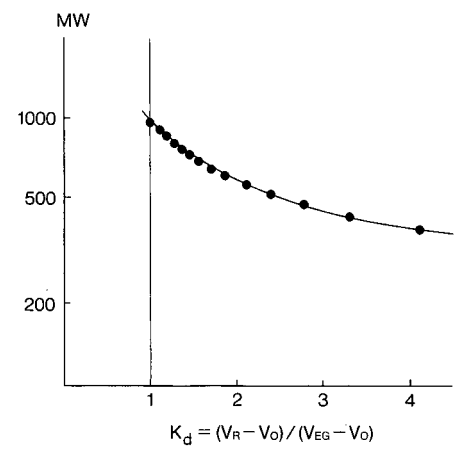

Fig. 10. Graphs of the molecular weight on a logarithmic scale against K_d value. Column, Asahipak GS-310 (500 × 7.6 mm I.D.); temperature, 30°C; flow-rate, 1.0 ml/min; detection at 280 nm; sample, octylphenoxy oligo(ethylene glycol)s, average 10 EO units; eluent, water–acetonitrile (60:40).

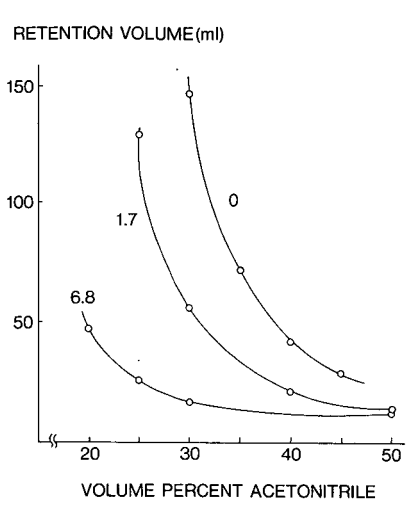

Fig. 11. Graphs of retention volume (ml) against composition of water–acetonitrile mixtures. The numbers on the curves indicate the density of OH groups in the gel (mequiv. per gram of dry resin). Columns, Asahipak GS-310 (500 × 7.6 mm I.D., OH group density 1.7), Asahipak GS-320 (500 × 7.6 mm I.D., OH group density 6.8) and a column packed with unhydrolysed gel (500 × 7.6 mm I.D., no OH groups); temperature, 30°C; flow-rate, 1.0 ml/min; detection at 280 nm; sample, octylphenoxy oligo(ethylene glycol)s, average 10 EO units.

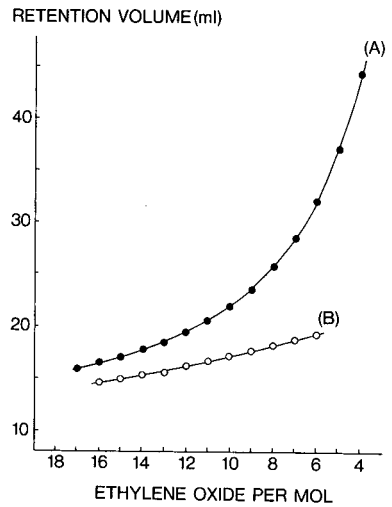

Fig. 12. Graphs of retention volume (ml) against the number of EO units in the solute molecule. The retention data were measured (A) on an Asahipak GS-310 column (500 × 7.6 mm I.D.) at a flow-rate of 1.0 ml/min and (B) on a 5-μm Unisil Pack ODS column (150 × 4.6 mm I.D.) at a flow-rate of 0.8 ml/min; detection 280 nm; temperature, 30°C; flow-rate, 1.0 ml/min; sample, octylphenoxy oligo(ethylene glycol)s; eluent, (A) water–acetonitrile (60:40) and (B) water–acetonitrile (45:55) solution.

diminishing n values, indicating a capability for far better separations of surfactants with small n values.

As shown in Fig. 13, poly(ethylene glycol)s were eluted by what is apparently a size exclusion mechanism from the GS-310 column, even with water alone as eluent, and hence they were also eluted in order of decreasing n with eluents containing organic solvents. For the ODS column, as shown here and also reported by Melander *et al.*[2], their elution occurs in order of increasing molecular weight. The reversal of the elution order between these two columns may be attributed to a difference in gel hydrophobicity. It appears that the strongly hydrophobic ODS, with C_{18} groups, effects a slower elution at higher moleculer weights because of its hydrophobic interaction with the dimethylene groups of the poly(ethylene glycol)s, whereas the lack of significant hydrophobic interactions between the weakly hydrophobic vinyl alcohol copolymer gel and the poly(ethylene glycol)s results in separation predominantly by size exclusion.

The difference between the capabilities of the two columns for fine separation of the non-ionic surfactants may also be explained on the basis of the reversed order of poly(ethylene glycol) elution, as related to the difference in hydrophobicities. It appears that significant hydrophobic interactions between the GS-310 gel and the surfactants involves only their alkylaryl groups, and that longer poly(ethylene glycol)

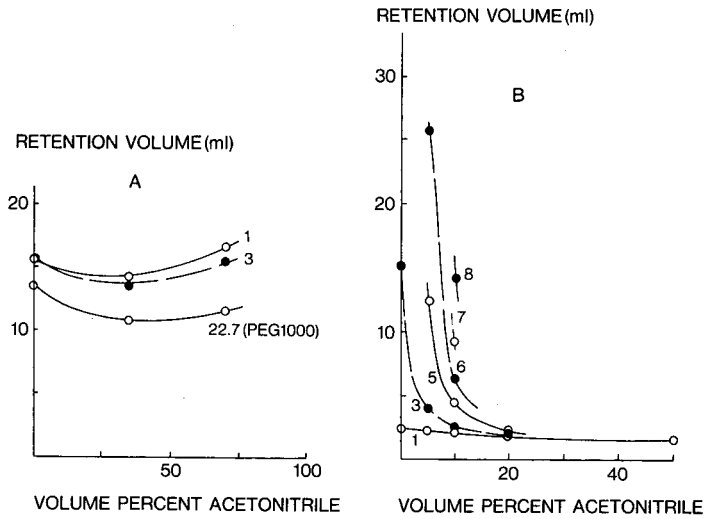

Fig. 13. Graphs of retention volume (ml) against composition of water–acetonitrile mixtures used as the eluent. The numbers on the curves indicate the number of EO units in the solute molecule. Columns (A) Asahipak GS-310 (500 × 7.6 mm I.D.) and (B) 5-μm Unisil Pack ODS (150 × 4.6 mm I.D.); sample, oligo(ethylene glycol)s; temperature, 30°C; flow-rate, (A) 1.0 ml/min and (B) 0.8 ml/min; detection, refractive index.

chains simply serve to interfere sterically with this interaction, these two effects in combination resulting in later elution of surfactants with smaller n values. On the other hand, the hydrophobic interaction between the ODS gel and the surfactants seems to involve both the alkylaryl and the poly(ethylene glycol) groups. Further, the interaction with the former groups is apparently stronger for the surfactants with smaller n values, whereas that with the latter groups appears stronger for those with larger n values. A cancelling effect therefore seems to occur, resulting particularly in a resolution between smaller n values that is poorer than that of the hydrophilic polymer gel column.

Any influence by micelle formation by the surfactants was considered to be negligible, as measurements were generally made with mobile phases having organic solvent concentrations known to prevent micelle formation, and also because essentially identical chromatograms were obtained at sample concentrations differing by as much as 10 000-fold.

CONCLUSION

The results of the analyses of alkylphenoxyoligo(ethylene glycol) non-ionic surfactants on GS-310 indicated that this column will be useful for various purposes, such as the selective removal of surfactants from protein–surfactant mixtures, the SEC of surfactants and the fine separation of surfactant series differing in the number of EO units. The surfactants were eluted in order of decreasing molecular weight, with no reversal in elution order for mobile phases with all water–organic solvent ratios.

Surfactants generally involve the presence of both a hydrophobic and a hydrophilic group in the same molecule. In the surfactants used in this study, these were alkylaryls and oligo(ethylene glycol)s, respectively. The ODS column apparently interacted hydrophobically with both of these groups, presumably more strongly with the former. It may further be assumed that the longer oligo(ethylene glycol) groups not only interacted hydrophobically with the ODS gel to effect a stronger retention, but also tended to interrupt sterically the interaction between the alkylaryl groups and the gel. Although the interactions appear to have a mutually cancelling effect, tending to impede fine separations, the stronger interaction between the ODS and the alkylaryl groups appears to predominate, thus determining the elution order.

GS-310, which is a hydrophilic polymer gel column with no C_{18} groups, apparently interacted hydrophobically only with the alkylaryl groups, at least at temperatures of 30°C and less, where longer oligo(ethylene glycol) chains simply tended to interrupt the interaction sterically. It may be presumed, furthermore, that this type of separation can be effected only on hydrophilic polymer gel columns which are amenable to various aqueous–organic solvent mobile phases and display weak hydrophobicity.

The results indicate that the GS-310 column can be effectively employed for practical, efficient HPLC analysis of various samples involving hydrophobic groups and hydrophilic groups in the same molecules, including surfactants.

REFERENCES

1 N. Hirata, M. Kasai, Y. Yanagihara and K. Noguchi, *J. Chromatogr.*, 396 (1987) 115–120.
2 W. R. Melander, A. Nahum and Cs. Horváth, *J. Chromatogr.*, 185 (1979) 129–152.

Journal of Chromatography, 461 (1989) 377–395
Elsevier Science Publishers B.V., Amsterdam — Printed in The Netherlands

CHROMSYMP. 1423

IMPROVED ENANTIOMERIC SEPARATION OF DIHYDRODIOLS OF POLYCYCLIC AROMATIC HYDROCARBONS ON CHIRAL STATIONARY PHASES BY DERIVATIZATION TO O-METHYL ETHERS

SHEN K. YANG*, MOHAMMAD MUSHTAQ, ZIPING BAO, HENRI B. WEEMS, MAGANG SHOU and XIANG-LIN LU

Department of Pharmacology, F. Edward Hébert School of Medicine, Uniformed Services University of the Health Sciences, Bethesda, MD 20814-4799 (U.S.A.)

SUMMARY

K-region *trans*-dihydrodiol derivatives of phenanthrene, 1-methylphenanthrene, 4,5-methylenephenanthrene, pyrene, 1-bromopyrene, chrysene, benzo[*c*]-phenanthrene, benz[*a*]anthracene, 1-, 4-, 6-, 7-, 11- and 12-methylbenz[*a*]anthracenes, 7,12-dimethylbenz[*a*]anthracene, 3-methylcholanthrene, and benzo[*a*]pyrene, and non-*K*-region *trans*-3,4-dihydrodiols of benz[*a*]anthracene, chrysene, and 7,12-dimethylbenz[*a*]anthracene are converted to O-methyl ethers. Enantiomers of these O-methyl ethers are generally more efficiently separated on Pirkle's chiral stationary phases than the enantiomers of underivatized dihydrodiols. O-Methyl ethers are substantially less polar than dihydrodiols, and O-methyl ethers are eluted with shorter retention times. Eluents of lower polarity can hence be used. This enhances chiral interactions between chiral stationary phase and solutes, allowing improved separation of enantiomers.

INTRODUCTION

Separation of dihydrodiol enantiomers of many polycyclic aromatic hydrocarbons (PAHs) has recently been studied by using columns packed with Pirkle's chiral stationary phases (CSP)[1–9]. Although enantiomers of many dihydrodiols are efficiently resolved, enantiomers of some dihydrodiols are either poorly resolved or not resolved at all. In order to explore means to improve enantiomeric resolution, unresolvable or poorly resolved dihydrodiols are derivatized to O-methyl ethers. Conversion to O-methyl ethers substantially reduces the polarity of dihydrodiols, hence an eluent with lower polarity can be used. The use of eluents with lower polarity helps to extend the useful lifetime of ionically bonded chiral stationary phase columns. The compounds studied are *K*-region *trans*-dihydrodiols of phenanthrene, 1-methylphenanthrene, 4,5-methylenephenanthrene, pyrene, 1-bromopyrene, chrysene, benzo-[*c*]phenanthrene, benz[*a*]anthracene, 1-, 4-, 6-, 7-, 11-, and 12-methylbenz[*a*]anthracenes, 7,12-dimethylbenz[*a*]anthracene, 3-methylcholanthrene, and benzo[*a*]pyrene, and non-*K*-region *trans*-3,4-dihydrodiols of benz[*a*]anthracene, chrysene, and 7,12-

0021-9673/89/$03.50

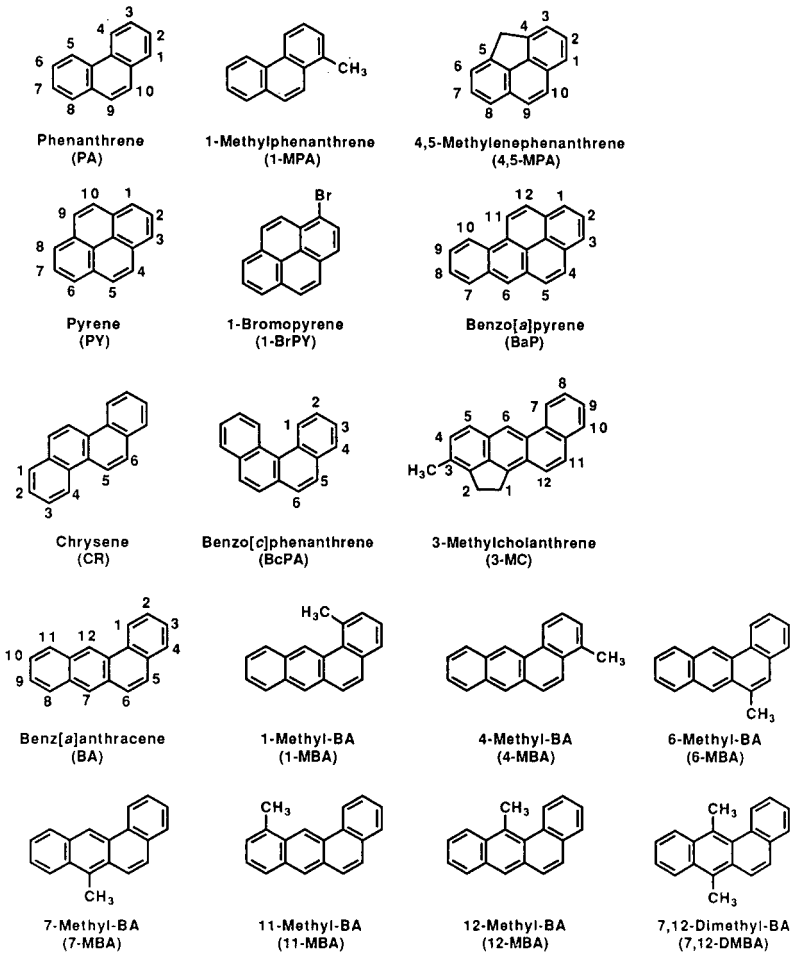

Fig. 1. Structures, numbering systems and abbreviations of PAHs described in this study.

dimethylbenz[*a*]anthracene. Structures, numbering systems, and abbreviations of parent PAHs included in this study are shown in Fig. 1. In the majority of cases, conversion of dihydrodiols to O-methyl ethers substantially improves enantiomeric separations.

EXPERIMENTAL

Chemicals

Epoxides and *trans*-dihydrodiols of PAHs were obtained either from the Chemical Repository of the National Cancer Institute or by incubation of the respective parent PAH with rat liver microsomes and an NADPH-regenerating system in the presence or in the absence of an epoxide hydrolase inhibitor[7,10,11].

High-performance liquid chromatography (HPLC)

HPLC was performed with a Waters Assoc. (Milford, MA, U.S.A.) liquid chromatograph, consisting of a Model 6000A solvent delivery system, a Model M45 solvent delivery system, a Model 660 solvent programmer, and a Model 440 absorbance detector (254 nm). Samples were injected via a Valco (Houston, TX, U.S.A.) Model N60 loop injector. Retention times and ratios of areas under the chromatographic peaks were recorded with a Hewlett-Packard (Palo Alto, CA, U.S.A.) Model 3390A integrator.

Normal-phase HPLC

O-Methyl ethers derived from *K*-region epoxides were separated on either a DuPont Golden Series SIL column (80 mm × 6.2 mm I.D.) or a DuPont Zorbax SIL column (250 mm × 6.2 mm I.D.). Eluents used for separation of isomeric O-methyl ethers are indicated in Table I.

TABLE I

NORMAL-PHASE HPLC SEPARATION OF ISOMERIC O-METHYL ETHERS OF DIHYDRODIOL DERIVATIVES OF SOME POLYCYCLIC AROMATIC HYDROCARBONS

*Dihydrodiol**	*Length of column (cm)***	*Eluent**** *(%)*	*Retention time (min) of O-methyl ether*§	
			Isomer 1	*Isomer 2*
PA 9,10-DHD§§	8	3.5% Eluent A	4.2 (9-O-methyl)	
1-MPA 9,10-DHD (AA)	8	1.8% Eluent A	7.2 (9-O-methyl)	9.4 (10-O-methyl)
4,5-MPA 9,10-DHD§§	25	5% Eluent A	14.1 (9-O-methyl)	
PY 4,5-DHD§§	8	3.5% Eluent A	5.2 (4-O-methyl)	
1-BrPY 4,5-DHD	25	2.5% Eluent A	14.8§§§	15.6§§§
1-BrPY 9,10-DHD (AA)	25	2.5% Eluent A	20.1§§§	22.6§§§
BaP 4,5-DHD	8	THF–MeOH–EtOAc–Hex (0.2:0.2:5:94.6)	17.1 (4-O-methyl)	18.0 (5-O-methyl)
CR 5,6-DHD (AA)	25†	EtOAc–Hex (7:13)	15.9 (6-O-methyl)	22.3 (5-O-methyl)
BcPA 5,6-DHD	8	0.5% Eluent A	9.8 (5-O-methyl)	10.8 (6-O-methyl)
3-MC 11,12-DHD (AA)	8	MeOH–THF–Hex (1.5:5:93.5)	6.5 (11-O-methyl)	7.3 (12-O-methyl)
BA 5,6-DHD	8	THF–MeOH–EtOAc–Hex (0.2:0.2:5:94.6)	13.3 (5-O-methyl)	14.0 (6-O-methyl)
1-MBA 5,6-DHD	25	EtOAc–EtOH–Hex (8:0.4:91.6)	20.4 (5-O-methyl)	21.5 (6-O-methyl)
4-MBA 5,6-DHD (AA)	8	2.5% Eluent A	7.1 (6-O-methyl)	8.6 (5-O-methyl)
6-MBA 5,6-DHD	8	0.5% Eluent A	7.0 (5-O-methyl)	9.4 (6-O-methyl)
7-MBA 5,6-DHD (AA)	8	2.5% Eluent A	7.2 (5-O-methyl)	8.9 (6-O-methyl)

(*Continued on p. 380*)

TABLE I (*continued*)

*Dihydrodiol**	*Length of column (cm)***	*Eluent**** *(%)*	*Retention time (min) of O-methyl ether*§*	
			Isomer 1	*Isomer 2*
11-MBA 5,6-DHD	25	1% Eluent A	22.0 (5-O-methyl)	22.6 (6-O-methyl)
12-MBA 5,6-DHD	25	EtOAc–MeOH–Hex (5:0.5:94.5)	19.8 (5-O-methyl)	20.3 (6-O-methyl)
7,12-DMBA 5,6-DHD (AA)	25	THF–Hex (1:4)	16.6 (5-O-methyl)	21.5 (6-O-methyl)
CR 3,4-DHD	8	3.6% Eluent A	9.0 (3-O-methyl)	10.7 (4-O-methyl)
BA 3,4-DHD	8	3.6% Eluent A	4.5 (3-O-methyl)	5.9 (4-O-methyl)
7,12-DMBA 3,4-DHD	8	3.6% Eluent A	4.4 (3-O-methyl)	5.8 (4-O-methyl)

* DHD = *trans*-dihydrodiol. Absolute configurations of resolved enantiomers are assigned as described in refs. 5, 7, 10 and 11. Dihydrodiols with hydroxyl groups preferentially in quasidiaxial conformation are indicated by AA in parenthesis.

** Unless otherwise stated, the column is indicated by its length and is either the DuPont Zorbax SIL column (250 × 6.2 mm I.D.) or DuPont Golden SIL column (80 × 6.2 mm I.D.).

*** The percentage of eluent A (ethanol–acetonitrile; 2:1, v/v) in hexane is indicated. The compositions of other elution solvents are as indicated. The flow-rate was 2 ml/min. Abbreviations for solvents are: THF = tetrahydrofuran; EtOAc = ethyl acetate; Hex = hexane, MeOH = methanol.

§ O-Methyl ethers are designed as isomers 1 and 2, according to their elution order on NP-HPLC. Normal-phase HPLC separations of O-methyl ethers, derived from *K*-region dihydrodiols of BaP[10], CR[5], BcPA[7], 3-MC[10], 12-MBA[11] and 7,12-DMBA[13], were partially described in earlier reports. The identity of each O-methyl ether is indicated in parenthesis. Bis-O-methyl ethers are eluted with much shorter retention times than O-methyl ethers.

§§ Due to symmetry, there is only one O-methyl ether.

§§§ The location of O-methyl group has not been established.

† A Resolvex SIL column (250 × 4.6 mm I.D.; Fisher Scientific) was used[5].

CSP HPLC

Enantiomeric separation of each dihydrodiol and O-methyl ether was tested by using a CSP column (250 mm × 4.6 mm I.D.; Regis, Morton Grove, IL, U.S.A.), packed with spherical particles of 5 μm diameter of γ-aminopropylsilanized silica to which either (*R*)-N-(3,5-dinitrobenzoyl)phenylglycine (*R*-DNBPG-I or *R*-DNBPG-C) or (*S*)-N-(3,5-dinitrobenzoyl)leucine (*S*-DNBL-I or *S*-DNBL-C) was bonded, either ionically (I) or covalently (C). The eluent was 0.1–10% (v/v) of eluent A (ethanol–acetonitrile; 2:1, v/v) in hexane at 2 ml/min.

Methoxylation of K-region epoxides

Racemic or enantiomeric epoxide was dissolved in methanol alone or in methanol, saturated with sodium methoxide and heated at 50°C for 1 h and then stored overnight at room temperature. The resulting two isomeric O-methyl ethers were separated by normal-phase HPLC. Enantiomers of each O-methyl ether were resolved by CSP-HPLC.

Methylation of trans-dihydrodiol

trans-Dihydrodiols were each methylated to a pair of isomeric O-methyl ethers by dissolving in sodium hydride-treated tetrahydrofuran (THF; 1 ml), methyl iodide (methyl iodide/O-methyl ether $\simeq$ 500, molar ratio), and a catalytic amount of sodium hydride, added at 0, 15, 30 and 45 min at room temperature in the dark. Fifteen minutes after the last addition of methyl iodide, the reaction was stopped by dropwise additions of methanol. The resulting isomeric O-methyl ethers were separated by normal-phase HPLC, as described above. Due to the use of excess amount of methyl iodide, a bis-O-methyl ether was formed in addition to O-methyl ethers. Relative amounts of O-methyl ethers and bis-O-methyl ether derived from each dihydrodiol varied greatly in repeated experiments under essentially the same experimental conditions.

Location of O-methyl group in O-methyl ethers

The location of O-methyl group in each O-methyl ether was established either by 500 MHz proton NMR spectroscopy[5,11] or by chemical methods[5,7,10,11] similarly as described in earlier reports.

Spectral analysis

All PAH derivatives in this study were analyzed by mass, UV–VIS, and circular dichroism (CD) spectral analyses. Mass spectral analysis was performed on a Finnigan Model 4000 gas chromatograph–mass spectrometer–data system (Finnigan MAT, San Jose, CA, U.S.A.) by electron impact with a solid probe at 70 eV and 250°C ionizer temperature. UV–VIS absorption spectra of samples in methanol were determined using a 1-cm path length quartz cuvette with a Varian Model Cary 118C spectrophotometer. CD spectra of samples in methanol in a quartz cell of 1-cm path length at room temperature were measured with a Jasco (Japan Scientific, Tokyo, Japan) Model 500A spectropolarimeter, equipped with a Model DP500 data processor.

RESULTS AND DISCUSSION

Normal-phase HPLC separation of O-methyl ethers

Due to symmetry, methoxylation of PA 9,10-epoxide, 4,5-MPA 9,10-epoxide, and PY 4,5-epoxide (or monomethylation of the corresponding dihydrodiol) each results in only one dihydrodiol O-methyl ether. Methoxylation of an epoxide (or monomethylation of a *trans*-dihydrodiol) of other PAHs each results in a pair of isomeric O-methyl ethers which can be separated by normal-phase HPLC (Table I). Structures, numbering systems, and abbreviations of dihydrodiols, O-methyl ethers, and bis-O-methyl ethers are shown in Figs. 2 and 3. Relative amounts of O-methyl ethers obtained by methoxylation of an epoxide and by methylation of a dihydrodiol are shown in Table II. Distribution of isomeric O-methyl ethers derived by methoxylation of an epoxide is reproducible. However, product ratios resulting from the reaction of methyl iodide and dihydrodiols are highly variable among repeated experiments.

K-region *trans*-dihydrodiols with hydroxyl groups preferentially in quasidiaxial conformation[12] are indicated by "AA" in Table I. The less strongly retained (hence, less polar) O-methyl ethers derived from quasidiaxial dihydrodiols (*e.g.*, 1-MPA

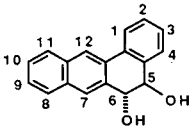

BA 5,6-DHD

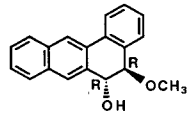

BA 5,6-DHD
5-O-methyl (#1)

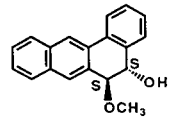

BA 5,6-DHD
6-O-methyl (#2)

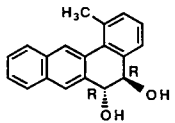

1-MBA 5,6-DHD

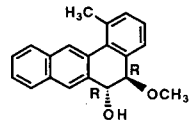

1-MBA 5,6-DHD
5-O-methyl (#1)

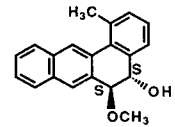

1-MBA 5,6-DHD
6-O-methyl (#2)

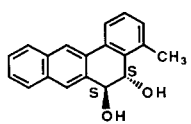

4-MBA 5,6-DHD

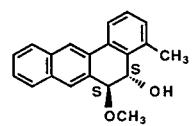

4-MBA 5,6-DHD
6-O-methyl (#1)

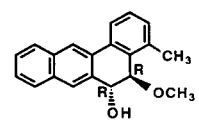

4-MBA 5,6-DHD
5-O-methyl (#2)

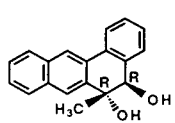

6-MBA 5,6-DHD

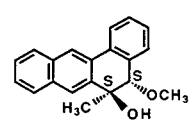

6-MBA 5,6-DHD
5-O-methyl (#1)

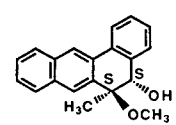

6-MBA 5,6-DHD
6-O-methyl (#2)

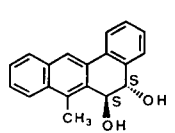

7-MBA 5,6-DHD

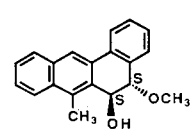

7-MBA 5,6-DHD
5-O-methyl (#1)

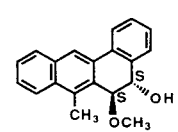

7-MBA 5,6-DHD
6-O-methyl (#2)

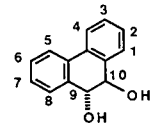

PA 9,10-DHD

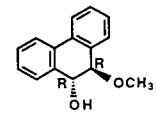

PA 9,10-DHD
9-O-methyl

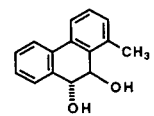

1-MPA 9,10-DHD

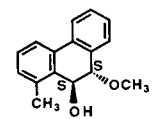

1-MPA 9,10-DHD
9-O-methyl (#1)

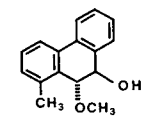

1-MPA 9,10-DHD
10-O-methyl (#2)

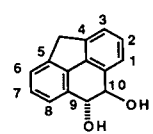

4,5-MPA 9,10-DHD

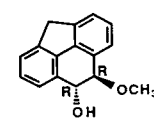

4,5-MPA 9,10-DHD
9-O-methyl

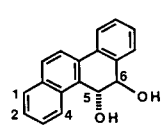

CR 5,6-DHD
(5S,6S on PG-C)

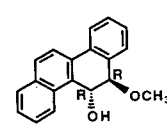

CR 5,6-DHD
6-O-methyl (#1)
(RV=0 on PG-C)

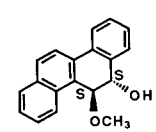

CR 5,6-DHD
5-O-methyl (#2)

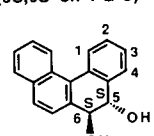

BcPA 5,6-DHD
(RV=0 on PG-C)

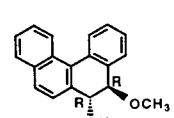

BcPA 5,6-DHD
5-O-methyl (#1)

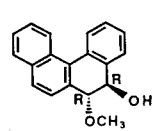

BcPA 5,6-DHD
6-O-methyl (#2)

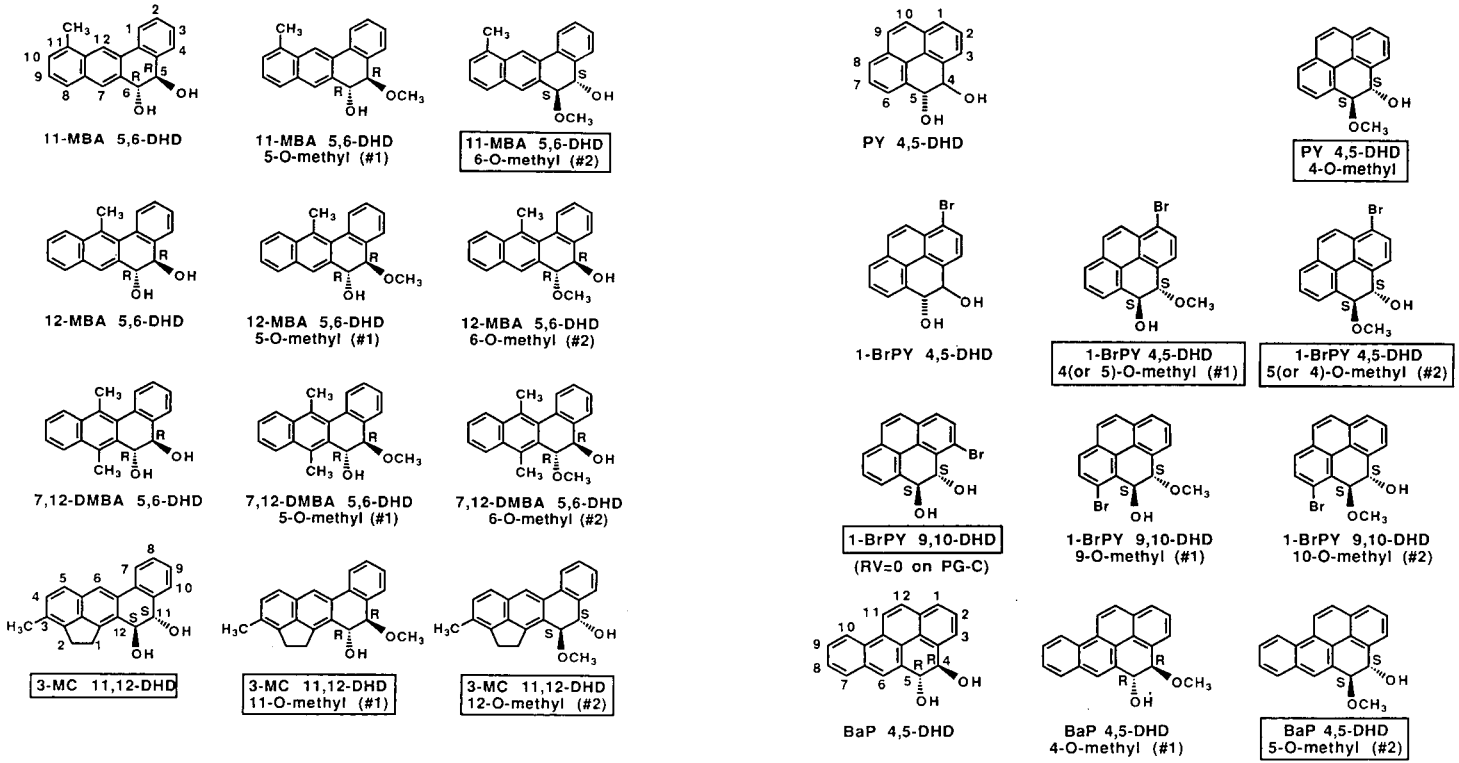

Fig. 2. Directions for reading this figure: (i) abbreviations of dihydrodiols (DHD) and O-methyl ethers are shown; (ii) two isomeric O-methyl ethers of each dihydrodiol are designated as 1 and 2 according to their elution order in normal-phase HPLC (Table I). Relative amounts of O-methyl ethers, obtained either by methoxylation of an epoxide or by methylation of a dihydrodiol, are indicated in Table II; (iii) absolute configurations of the more strongly retained enantiomers on the ionically bonded *R*-DNBPG column are shown; (iv) structures that do not have associated *R* and/or *S* designations indicate that enantiomers of dihydrodiol and/or O-methyl ether are not resolved by anyone of the four CSP columns used in this study; (v) enantiomeric separation on *R*-DNBPG-C, if different from that on *R*-DNBPG-I, is shown in parenthesis under the structure; (vi) a boxed-in name under the structure indicates that the same enantiomer is more strongly retained on *S*-DNBL-I and/or *S*-DNBL-C column; (vii) data on enantiomeric separations on four CSPs are shown in Table III.

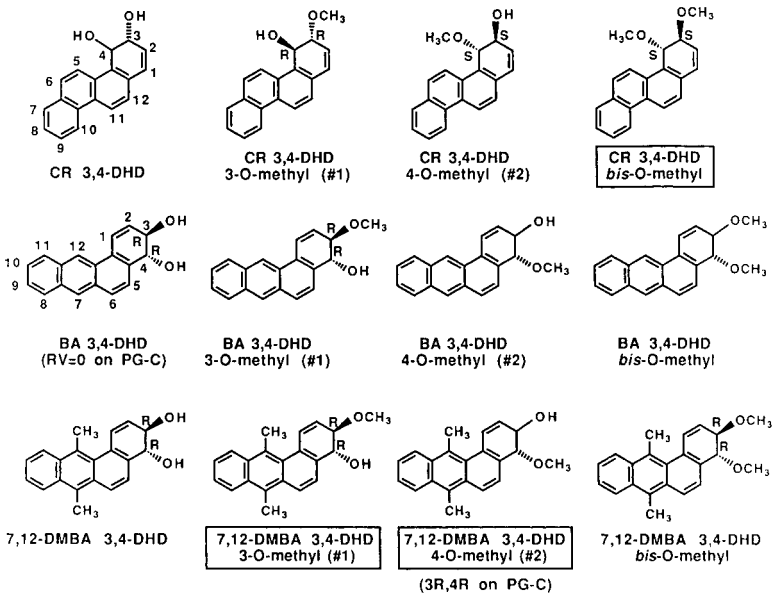

Fig. 3. Directions for reading this figure are similar to those described in the legend for Fig. 2.

9,10-DHD 9-O-methyl, CR 5,6-DHD 6-O-methyl, 4-MBA 5,6-DHD 6-O-methyl, 7-MBA 5,6-DHD 5-O-methyl, 7,12-DMBA 5,6-DHD 5-O-methyl, and 3-MC 11,12-DHD 11-O-methyl) all have their O-methyl groups located away from the sterically hindered region (Fig. 2a–d). Based on these observations, the less strongly retained O-methyl ether of 1-BrPY 9,10-DHD is tentatively assigned as the 9-O-methyl derivative (Fig. 2b). The less strongly retained O-methyl ethers derived from quasidiequatorial dihydrodiols with either a benz[*a*]anthracene or a benzo[*c*]phenanthrene nucleus all have their O-methyl groups at the C-5 position (Fig. 2a, c and d); the O-methyl group of BaP 4,5-DHD O-methyl No. 1 is similarly located at the C-4 position (Fig. 2b). However, structures of two isomeric O-methyl ethers derived from 1-BrPY 4,5-DHD cannot be established on the basis of the observation described above.

CSP HPLC resolution of enantiomers

Retention times, absolute configurations, and resolution values in the separation of enantiomeric dihydrodiols and O-methyl ethers, derived either by methoxylation of *K*-region epoxides or by methylation of *trans*-dihydrodiols by ionically and covalently bonded *R*-DNBPG and *S*-DNBL columns, are shown in Tables III and IV. Data on the enantiomeric resolutions of some *K*-region *trans*-dihydrodiols were partially reported earlier[1–10] and are included in Table III for comparison; new chromatographic data were obtained with different eluent compositions and/or CSP columns which were not previously reported. The major emphasis of the data in Tables III and IV is on the improvement of enantiomeric separation of O-methyl ethers as compared with that of dihydrodiols.

TABLE II

PERCENTAGES OF O-METHYL ETHERS DERIVED FROM METHOXYLATION OF EPOXIDES AND FROM METHYLATION OF DIHYDRODIOLS

*Epoxide or dihydrodiol**	*Methoxylation or methylation product***		
	Bis-O-methyl	*O-Methyl 1*	*O-Methyl 2*
1-MPA 9,10-epoxide	NF	36	64
1-MPA 9,10-DHD	ND	72	28
1-BrPY 4,5-epoxide	NF	51	49
1-BrPY 9,10-epoxide	NF	72	28
BaP 4,5-epoxide	NF	53	47
BaP 4,5-DHD	ND	52	48
	ND	66	34
CR 5,6-epoxide	NF	50	50
CR 5,6-DHD***	25	50	25
	50	44	6
BcPA 5,6-epoxide	NF	30	70
BcPA 5,6-DHD	ND	49	51
3MC 11,12-epoxide	NF	32	68
3MC 11,12-DHD	ND	87	13
	ND	83	17
BA 5,6-epoxide	NF	50	50
BA 5,6-DHD***	7	44	49
	18	40	42
1-MBA 5,6-epoxide	NF	58	42
1-MBA 5,6-DHD	ND	47	53
4-MBA 5,6-epoxide	NF	41	59
4-MBA 5,6-DHD	ND	82	18
6-MBA 5,6-epoxide	NF	85	15
7-MBA 5,6-epoxide	NF	42	58
11-MBA 5,6-epoxide	NF	48	52
11-MBA 5,6-DHD	ND	53	47
12-MBA 5,6-epoxide	NF	23	77
12-MBA 5,6-DHD***	ND	43	57
	29	55	16
7,12-DMBA 5,6-epoxide	NF	15	85
7,12-DMBA 5,6-DHD§	ND	80	20
CR 3,4-DHD	14	47	39
BA 3,4-DHD	10	26	64
7,12-DMBA 3,4-DHD	1	47	52

* Data on *K*-region derivatives of BaP[10], CR[5], BcPA[7], 3-MC[10], BA[11], 12-MBA[11] and 7,12-DMBA[13,17] are taken from earlier reports and are included for comparison.

** NF = not formed; ND = not detected in that particular experiment. Identities of O-methyl ethers are indicated in Table I.

*** Examples indicating that the relative amounts of O-methyl ethers by methylation of dihydrodiols varied substantially among repeated experiments.

§ Data from ref. 17.

TABLE III

CSP-HPLC RESOLUTION OF *K*-REGION *TRANS*-DIHYDRODIOLS AND THEIR MONOMETHYL ETHERS OF SOME POLYCYCLIC AROMATIC HYDROCARBONS

*Chemical**	*CSP***	*A (%)****	*Retention time (min)*§		*RV*§§
			Enantiomer 1	*Enantiomer 2*	
PA 9,10-DHD	*R*-DNBPG-I	2.5	37.5	37.5	0
	R-DNBPG-C	2.5	25.2	25.2	0
	S-DNBL-I	2.5	34.8	34.8	0
	S-DNBL-C	2.5	19.7	19.7	0
PA 9,10-DHD	*R*-DNBPG-I	0.5	25.6 (*S,S*)	26.1 (*R,R*)	0.3
9-O-methyl	*R*-DNBPG-C	0.5	30.5 (*S,S*)	30.9 (*R,R*)	0.2
	S-DNBL-I	0.5	20.7	20.7	0
	S-DNBL-C	0.5	17.7 (*R,R*)	18.1 (*S,S*)	0.3
1-MPA 9,10-DHD	*R*-DNBPG-I	5.0	34.9	34.9	0
	R-DNBPG-C	5.0	30.5	30.5	0
	S-DNBL-I	5.0	31.3	31.3	0
	S-DNBL-C	5.0	22.9	22.9	0
1-MPA 9,10-DHD	*R*-DNBPG-I	2.5	11.7 (*R,R*)	12.2 (*S,S*)	1.0
9-O-methyl (1)	*R*-DNBPG-C	2.5	12.0 (*R,R*)	12.7 (*S,S*)	1.2
	S-DNBL-I	2.5	9.9	9.9	0
	S-DNBL-C	2.5	8.6	8.6	0
1-MPA 9,10-DHD	*R*-DNBPG-I	2.5	15.8	15.8	0
10-O-methyl (2)	*R*-DNBPG-C	2.5	16.6	16.6	0
	S-DNBL-I	2.5	13.6	13.6	0
	S-DNBL-C	2.5	11.3	11.3	0
4,5-MPA 9,10-DHD	*R*-DNBPG-I	5.0	31.4	31.4	0
	R-DNBPG-C	5.0	20.9	20.9	0
	S-DNBL-I	5.0	24.7	24.7	0
	S-DNBL-C	5.0	15.0	15.0	0
4,5-MPA 9,10-DHD	*R*-DNBPG-I	1.0	23.2	23.2	0
9-O-methyl		0.5	66.6 (*S,S*)	69.7 (*R,R*)	1.0
	R-DNBPG-C	1.0	36.0 (*S,S*)	37.7 (*R,R*)	0.9
	S-DNBL-I	1.0	23.0	23.0	0
		0.5	37.2 (*R,R*)	38.0 (*S,S*)	0.4
	S-DNBL-C	1.0	32.7 (*R,R*)	35.3 (*S,S*)	1.5
CR 5,6-DHD	*R*-DNBPG-I	10	25.3	25.3	0
	R-DNBPG-C	10	20.2 (*R,R*)	20.8 (*S,S*)	0.7
	S-DNBL-I	10	24.1 (*R,R*)	25.1 (*S,S*)	1.1
	S-DNBL-C	10	14.2 (*R,R*)	14.6 (*S,S*)	0.5
CR 5,6-DHD	*R*-DNBPG-I	5	16.6 (*S,S*)	17.4 (*R,R*)	1.1
6-O-methyl (1)	*R*-DNBPG-C	5	15.2	15.2	0
	S-DNBL-I	5	10.0 (*R,R*)	10.3 (*S,S*)	0.6
	S-DNBL-C	5	9.0	9.0	0
CR 5,6-DHD	*R*-DNBPG-I	5	18.7 (*R,R*)	19.9 (*S,S*)	1.5
5-O-methyl (2)	*R*-DNBPG-C	5	17.1 (*R,R*)	18.6 (*S,S*)	1.9
	S-DNBL-I	5	11.7 (*R,R*)	12.2 (*S,S*)	0.9
	S-DNBL-C	5	10.8 (*R,R*)	10.9 (*S,S*)	0.1

TABLE III (*continued*)

*Chemical**	*CSP***	*A (%)****	*Retention time (min)*§		*RV*§§
			Enantiomer 1	*Enantiomer 2*	
BcPA 5,6-DHD	*R*-DNBPG-I	2.5	49.5 (*S,S*)	51.8 (*R,R*)	1.1
	R-DNBPG-C	2.5	30.3	30.3	0
	S-DNBL-I	2.5	38.8	38.8	0
	S-DNBL-C	2.5	22.6	22.6	0
BcPA 5,6-DHD 5-O-methyl (1)	*R*-DNBPG-I	0.5	27.8 (*S,S*)	31.3 (*R,R*)	2.5
	R-DNBPG-C	0.5	29.1 (*S,S*)	30.4 (*R,R*)	0.8
	S-DNBL-I	0.5	19.4 (*R,R*)	20.0 (*S,S*)	0.7
	S-DNBL-C	0.5	18.1 (*R,R*)	19.1 (*S,S*)	0.9
BcPA 5,6-DHD 6-O-methyl (2)	*R*-DNBPG-I	0.5	28.5 (*S,S*)	29.7 (*R,R*)	0.9
	R-DNBPG-C	0.5	28.8 (*S,S*)	29.0 (*R,R*)	0.2
	S-DNBL-I	0.5	21.7 (*R,R*)	22.7 (*S,S*)	0.8
	S-DNBL-C	0.5	21.1 (*R,R*)	21.8 (*S,S*)	0.5
PY 4,5-DHD	*R*-DNBPG-I	5.0	32.3	32.3	0
	R-DNBPG-C	5.0	20.3	20.3	0
	S-DNBL-I	5.0	22.3	22.3	0
	S-DNBL-C	5.0	17.2 (*R,R*)	18.0 (*S,S*)	0.6
		2.5	48.0 (*R,R*)	51.3 (*S,S*)	1.1
PY 4,5-DHD 4-O-methyl	*R*-DNBPG-I	2.0	21.7 (*R,R*)	22.4 (*S,S*)	0.7
	R-DNBPG-C	2.0	21.5 (*R,R*)	22.0 (*S,S*)	0.5
	S-DNBL-I	2.0	13.5	13.5	0
		1.0	25.7 (*R,R*)	26.3 (*S,S*)	0.4
	S-DNBL-C	2.0	12.7 (*R,R*)	13.2 (*S,S*)	0.6
		1.0	21.5 (*R,R*)	22.7 (*S,S*)	1.0
1-BrPY 4,5-DHD	*R*-DNBPG-I	5.0	16.0	16.0	0
		2.5	41.0	41.0	0
	R-DNBPG-C	5.0	15.7	15.7	0
	S-DNBL-I	5.0	23.0	23.0	0
	S-DNBL-C	2.5	34.0 (*R,R*)	35.2 (*S,S*)	0.6
1-BrPY 4,5-DHD 4 (or 5)-O-methyl (1)	*R*-DNBPG-I	2.5	14.1 (*R,R*)	14.6 (*S,S*)	0.6
	R-DNBPG-C	2.5	12.6 (*R,R*)	13.0 (*S,S*)	0.5
	S-DNBL-I	1.0	22.4	22.4	0
	S-DNBL-C	1.0	17.5 (*R,R*)	18.5 (*S,S*)	1.0
1-BrPY 4,5-DHD 5 (or 4)-O-methyl (2)	*R*-DNBPG-I	2.5	14.1 (*R,R*)	14.7 (*S,S*)	0.9
	R-DNBPG-C	2.5	12.9 (*R,R*)	13.4 (*S,S*)	0.6
	S-DNBL-I	1.0	23.2	23.2	0
	S-DNBL-C	1.0	17.3 (*R,R*)	18.0 (*S,S*)	0.7
1-BrPy 9,10-DHD	*R*-DNBPG-I	5.0	78.9(*R,R*)	80.1(*S,S*)	0.3
	R-DNBPG-C	2.5	31.9	31.9	0
	S-DNBL-I	5.0	54.2	54.2	0
	S-DNBL-C	5.0	40.9	40.9	0
		2.5	118.0(*R,R*)	124.0(*S,S*)	0.8
1-BrPY 9,10-DHD 9-O-methyl (1)	*R*-DNBPG-I	2.5	23.2(*R,R*)	26.0(*S,S*)	2.4
	R-DNBPG-C	2.5	18.6(*R,R*)	22.0(*S,S*)	3.0
	S-DNBL-I	1.0	35.5	35.5	0
	S-DNBL-C	1.0	28.3	28.3	0

(*continued on p. 388*)

TABLE III (*continued*)

*Chemical**	*CSP***	*A (%)****	*Retention time (min)*§		*RV*§§
			Enantiomer 1	*Enantiomer 2*	
1-BrPY 9,10-DHD	*R*-DNBPG-I	2.5	23.6(*R,R*)	24.3(*S,S*)	0.8
10-O-methyl (2)	*R*-DNBPG-C	2.5	22.8(*R,R*)	23.5(*S,S*)	0.6
	S-DNBL-I	1.0	46.1	46.1	0
	S-DNBL-C	1.0	36.3	36.3	0
BaP 4,5-DHD	*R*-DNBPG-I	10.0	24.4(*S,S*)	25.2(*R,R*)	0.8
	R-DNBPG-C	5.0	34.9(*S,S*)	35.3(*R,R*)	0.2
	S-DNBL-I	10.0	17.3(*R,R*)	17.6(*S,S*)	0.3
	S-DNBL-C	10.0	10.9(*R,R*)	11.1(*S,S*)	0.3
BaP 4,5-DHD	*R*-DNBPG-I	2.5	36.2(*S,S*)	38.6(*R,R*)	1.4
4-O-methyl (1)	*R*-DNBPG-C	2.5	36.0(*S,S*)	36.7(*R,R*)	0.3
	S-DNBL-I	5.0	10.5(*R,R*)	11.2(*S,S*)	1.1
	S-DNBL-C	5.0	9.6(*R,R*)	9.9(*S,S*)	0.4
BaP 4,5-DHD	*R*-DNBPG-I	5.0	19.0(*R,R*)	20.6(*S,S*)	2.0
5-O-methyl (2)	*R*-DNBPG-C	5.0	15.4(*R,R*)	17.4(*S,S*)	2.4
	S-DNBL-I	5.0	10.3(*R,R*)	10.5(*S,S*)	0.2
	S-DNBL-C	5.0	9.4(*R,R*)	9.5(*S,S*)	~0.1
BA 5,6-DHD	*R*-DNBPG-I	5.0	33.7	33.7	0.0
	R-DNBPG-C	5.0	18.8	18.8	0.0
	S-DNBL-I	5.0	24.0	24.0	0.0
	S-DNBL-C	5.0	14.2	14.2	0.0
BA 5,6-DHD	*R*-DNBPG-I	2.5	20.5(*S,S*)	22.6(*R,R*)	2.5
5-O-methyl (1)	*R*-DNBPG-C	2.5	17.6(*S,S*)	18.5(*R,R*)	1.2
	S-DNBL-I	2.5	12.4(*R,R*)	13.4(*S,S*)	1.8
	S-DNBL-C	2.5	10.7	10.7	0.0
		1.0	20.2(*R,R*)	21.5(*S,S*)	0.8
BA 5,6-DHD	*R*-DNBPG-I	2.5	18.4(*R,R*)	19.8(*S,S*)	1.7
6-O-methyl (2)	*R*-DNBPG-C	2.5	16.0(*R,R*)	17.8(*S,S*)	2.3
	S-DNBL-I	2.5	11.7(*R,R*)	12.2(*S,S*)	1.2
	S-DNBL-C	2.5	10.5	10.5	0.0
		1.0	19.4	19.4	0.0
1-MBA 5,6-DHD	*R*-DNBPG-I	5.0	23.0(*S,S*)	24.1(*R,R*)	1.1
	R-DNBPG-C	5.0	14.5	14.5	0
	S-DNBL-I	5.0	19.2(*R,R*)	19.6(*S,S*)	0.4
	S-DNBL-C	5.0	11.5	11.5	0
1-MBA 5,6-DHD	*R*-DNBPG-I	1.0	20.6(*S,S*)	24.3(*R,R*)	5.1
5-O-methyl (1)	*R*-DNBPG-C	1.0	17.6(*S,S*)	19.9(*R,R*)	3.1
	S-DNBL-I	1.0	13.1(*R,R*)	14.8(*S,S*)	3.2
	S-DNBL-C	1.0	9.4(*R,R*)	10.3(*S,S*)	1.8
1-MBA 5,6-DHD	*R*-DNBPG-I	2.5	10.6(*R,R*)	11.1(*S,S*)	0.9
6-O-methyl (2)	*R*-DNBPG-C	2.5	9.8(*R,R*)	10.5(*S,S*)	1.7
	S-DNBL-I	2.5	8.2(*R,R*)	8.6(*S,S*)	1.1
	S-DNBL-C	1.0	10.5(*R,R*)	11.0(*S,S*)	1.1
4-MBA 5,6-DHD	*R*-DNBPG-I	10.0	22.7(*R,R*)	23.4(*S,S*)	0.8
	R-DNBPG-C	10.0	20.8(*R,R*)	22.0(*S,S*)	1.2
	S-DNBL-I	10.0	18.4(*R,R*)	18.8(*S,S*)	~0.1
	S-DNBL-C	10.0	15.7(*R,R*)	16.2(*S,S*)	~0.1

TABLE III (*continued*)

*Chemical**	*CSP***	*A (%)****	*Retention time (min)*§		*RV*§§
			Enantiomer 1	*Enantiomer 2*	
4-MBA 5,6-DHD	*R*-DNBPG-I	2.5	20.7(*R*,*R*)	23.3(*S*,*S*)	2.7
6-O-methyl (1)	*R*-DNBPG-C	2.5	21.1(*R*,*R*)	25.1(*S*,*S*)	3.8
	S-DNBL-I	2.5	15.1(*R*,*R*)	15.4(*S*,*S*)	0.2
	S-DNBL-C	2.5	13.2(*R*,*R*)	14.2(*S*,*S*)	1.5
4-MBA 5,6-DHD	*R*-DNBPG-I	2.5	35.5(*S*,*S*)	36.3(*R*,*R*)	0.5
5-O-methyl (2)	*R*-DNBPG-C	2.5	35.6(*S*,*S*)	36.4(*R*,*R*)	0.5
	S-DNBL-I	2.5	21.2	21.2	0
	S-DNBL-C	2.5	20.4	20.4	0
6-MBA 5,6-DHD	*R*-DNBPG-I	5.0	16.8(*S*,*S*)	17.8(*R*,*R*)	1.3
	R-DNBPG-C	2.5	24.2(*S*,*S*)	25.4(*R*,*R*)	1.0
	S-DNBL-I	2.5	29.7	29.7	0
	S-DNBL-C	2.5	18.4(*S*,*S*)	19.0(*R*,*R*)	0.1
6-MBA 5,6-DHD	*R*-DNBPG-I	0.5	16.1(*R*,*R*)	16.4(*S*,*S*)	0.1
5-O-methyl (1)	*R*-DNBPG-C	0.5	17.7	17.7	0
	S-DNBL-I	0.5	11.9	11.9	0
	S-DNBL-C	0.5	10.6(*S*,*S*)	10.9(*R*,*R*)	0.1
		0.25	17.3(*S*,*S*)	18.0(*R*,*R*)	0.7
6-MBA 5,6-DHD	*R*-DNBPG-I	0.5	27.8(*R*,*R*)	29.6(*S*,*S*)	1.8
6-O-methyl (2)	*R*-DNBPG-C	0.5	23.6(*R*,*R*)	24.7(*S*,*S*)	1.0
	S-DNBL-I	0.5	20.4	20.4	0
	S-DNBL-C	0.5	15.4	15.4	0
7-MBA 5,6-DHD	*R*-DNBPG-I	10.0	30.9(*R*,*R*)	32.6(*S*,*S*)	1.1
	R-DNBPG-C	10.0	24.1(*R*,*R*)	30.0(*S*,*S*)	5.4
	S-DNBL-I	10.0	25.6(*R*,*R*)	27.2(*S*,*S*)	0.9
	S-DNBL-C	10.0	17.1(*R*,*R*)	17.5(*S*,*S*)	0.4
7-MBA 5,6-DHD	*R*-DNBPG-I	10.0	10.3(*R*,*R*)	11.3(*S*,*S*)	2.0
5-O-methyl (1)		5.0	20.5(*R*,*R*)	22.9(*S*,*S*)	3.2
	R-DNBPG-C	10.0	10.2(*R*,*R*)	11.8(*S*,*S*)	4.0
	S-DNBL-I	2.5	20.1	20.1	0
	S-DNBL-C	2.5	17.9(*R*,*R*)	18.2(*S*,*S*)	0.1
7-MBA 5,6-DHD	*R*-DNBPG-I	5.0	20.2(*R*,*R*)	23.6(*S*,*S*)	5.0
6-O-methyl (2)	*R*-DNBPG-C	5.0	20.0(*R*,*R*)	24.0(*S*,*S*)	5.7
	S-DNBL-I	5.0	12.4(*R*,*R*)	13.1(*S*,*S*)	1.1
		2.5	23.8(*R*,*R*)	25.3(*S*,*S*)	1.7
	S-DNBL-C	5.0	11.0(*R*,*R*)	11.7(*S*,*S*)	1.5
		2.5	18.2(*R*,*R*)	19.9(*S*,*S*)	2.1
11-MBA 5,6-DHD	*R*-DNBPG-I	6.0	25.0(*S*,*S*)	25.7(*R*,*R*)	0.6
	R-DNBPG-C	5.0	19.5	19.5	0
	S-DNBL-I	5.0	24.8(*R*,*R*)	25.5(*S*,*S*)	0.3
	S-DNBL-C	5.0	15.0(*R*,*R*)	15.0(*S*,*S*)	0.3
11-MBA 5,6-DHD	*R*-DNBPG-I	2.5	21.5(*S*,*S*)	24.2(*R*,*R*)	3.0
5-O-methyl (1)	*R*-DNBPG-C	2.5	19.4(*S*,*S*)	20.7(*R*,*R*)	1.7
	S-DNBL-I	2.5	12.2(*R*,*R*)	13.4(*S*,*S*)	1.7
	S-DNBL-C	2.5	12.1(*R*,*R*)	12.9(*S*,*S*)	1.5

(*continued on p. 390*)

TABLE III (*continued*)

*Chemical**	*CSP***	*A (%)****	*Retention time (min)*§		*RV*§§
			Enantiomer 1	*Enantiomer 2*	
11-MBA 5,6-DHD	*R*-DNBPG-I	2.5	17.5(*R*,*R*)	19.4(*S*,*S*)	2.6
6-O-methyl (2)	*R*-DNBPG-C	2.5	15.3(*R*,*R*)	17.5(*S*,*S*)	3.3
	S-DNBL-I	2.5	11.2(*R*,*R*)	11.5(*S*,*S*)	0.7
	S-DNBL-C	2.5	10.5(*R*,*R*)	11.1(*S*,*S*)	1.3
12-MBA 5,6-DHD	*R*-DNBPG-I	10.0	13.4(*S*,*S*)	14.5(*R*,*R*)	1.8
	R-DNBPG-C	5.0	18.3	18.3	0
	S-DNBL-I	10.0	11.4(*R*,*R*)	11.5(*S*,*S*)	<0.1
	S-DNBL-C	5.0	13.8	13.8	0
12-MBA 5,6-DHD	*R*-DNBPG-I	1.0	28.3(*S*,*S*)	32.5(*R*,*R*)	3.6
5-O-methyl (1)	*R*-DNBPG-C	1.0	23.7(*S*,*S*)	25.2(*R*,*R*)	1.1
	S-DNBL-I	1.0	16.2	16.2	0
		0.5	25.5(*R*,*R*)	27.4(*S*,*S*)	1.4
	S-DNBL-C	1.0	13.8	13.8	0
		0.5	31.8(*R*,*R*)	34.3(*S*,*S*)	1.1
12-MBA 5,6-DHD	*R*-DNBPG-I	1.0	23.0(*S*,*S*)	24.7(*R*,*R*)	1.5
6-O-methyl (2)	*R*-DNBPG-C	1.0	21.6	21.6	0
	S-DNBL-I	1.0	13.7(*R*,*R*)	15.3(*S*,*S*)	2.0
	S-DNBL-C	1.0	11.9(*R*,*R*)	12.9(*S*,*S*)	1.4
7,12-DMBA 5,6-DHD	*R*-DNBPG-I	10.0	21.8(*S*,*S*)	25.4(*R*,*R*)	2.6
	R-DNBPG-C	10.0	20.3(*R*,*R*)	20.8(*S*,*S*)	0.5
	S-DNBL-I	10.0	20.6(*R*,*R*)	28.6(*S*,*S*)	6.9
	S-DNBL-C	10.0	16.8(*R*,*R*)	18.9(*S*,*S*)	1.3
7,12-DMBA 5,6-DHD	*R*-DNBPG-I	2.5	35.5(*S*,*S*)	39.4(*R*,*R*)	2.8
5-O-methyl (1)	*R*-DNBPG-C	2.5	33.0(*R*,*R*)	37.7(*S*,*S*)	3.0
	S-DNBL-I	5.0	10.5(*R*,*R*)	11.5(*S*,*S*)	1.9
	S-DNBL-C	2.5	17.9(*S*,*S*)	18.4(*R*,*R*)	0.3
7,12-DMBA 5,6-DHD	*R*-DNBPG-I	5.0	16.7(*S*,*S*)	18.1(*R*,*R*)	2.3
6-O-methyl (2)	*R*-DNBPG-C	5.0	17.1(*R*,*R*)	18.5(*S*,*S*)	1.8
	S-DNBL-I	5.0	10.0(*R*,*R*)	14.9(*S*,*S*)	8.1
	S-DNBL-C	5.0	10.6(*R*,*R*)	13.0(*S*,*S*)	2.8
3-MC 11,12-DHD	*R*-DNBPG-I	10.0	20.4(*R*,*R*)	21.2(*S*,*S*)	0.8
	R-DNBPG-C	10.0	16.1(*R*,*R*)	17.8(*S*,*S*)	2.1
	S-DNBL-I	10.0	23.2(*R*,*R*)	24.5(*S*,*S*)	1.3
	S-DNBL-C	5.0	26.9	26.9	0.0
3-MC 11,12-DHD	*R*-DNBPG-I	5.0	32.8(*S*,*S*)	33.7(*R*,*R*)	0.6
11-O-methyl (1)		2.5	58.2(*S*,*S*)	63.6(*R*,*R*)	1.8
	R-DNBPG-C	5.0	27.6(*R*,*R*)	32.7(*S*,*S*)	3.4
	S-DNBL-I	5.0	15.2(*S*,*S*)	15.7(*R*,*R*)	0.5
	S-DNBL-C	5.0	11.1(*S*,*S*)	11.7(*R*,*R*)	1.0

TABLE III (*continued*)

*Chemical**	*CSP***	*A (%)****	*Retention time (min)*§		*RV*§§
			Enantiomer 1	*Enantiomer 2*	
3-MC 11,12-DHD	*R*-DNBPG-I	5.0	18.5(*R,R*)	22.4(*S,S*)	4.2
12-O-methyl (2)	*R*-DNBPG-C	5.0	17.7(*R,R*)	23.8(*S,S*)	6.1
	S-DNBL-I	5.0	9.9(*R,R*)	10.3(*S,S*)	1.0
	S-DNBL-C	5.0	11.5	11.5	0.0
		2.5	21.1	21.1	0.0

* O-Methyl ethers are designated as 1 and 2 according to their elution order on NP-HPLC. DHD = *trans*-dihydrodiol. Part of the data on CSP-HPLC resolutions of DHD enantiomers were reported earlier[1–10] and data shown in this table were updated from reanalysis.

** CSPs are defined in Materials and Methods.

*** Percentage of eluent A (ethanol–acetonitrile, 2:1, v/v) in hexane. The flow-rate was 2 ml/min, with a void volume of 2.4 ml.

§ See text for assignments of absolute configurations of resolved enantiomers. Enantiomers are designated as 1 and 2 according to their elution order on CSP-HPLC and have CD spectra that are mirror images of each other.

§§ RV = resolution value = $2(V_2 - V_1)/(W_2 + W_1)$, where V is retention volume and W is peak width at base.

TABLE IV

CSP-HPLC RESOLUTION OF SOME NON-*K*-REGION *TRANS*-DIHYDRODIOLS AND THEIR METHYL ETHERS OF CHRYSENE, BENZ[*a*]ANTHRACENE, AND 7,12-DIMETHYLBENZ[*a*]-ANTHRACENE

*Chemical**	*CSP***	*A (%)****	*Retention time* (min)§		*RV*§§
			Enantiomer 1	*Enantiomer 2*	
CR 3,4-DHD	*R*-DNBPG-I	10.0	38.1	38.1	0
	R-DNBPG-C	10.0	35.2	35.2	0
	S-DNBL-I	10.0	40.6(*R,R*)	42.0(*S,S*)	0.7
	S-DNBL-C	10.0	21.8	21.8	0
CR 3,4-DHD	*R*-DNBPG-I	5.0	26.4(*S,S*)	28.9(*R,R*)	1.9
3-O-methyl (1)	*R*-DNBPG-C	5.0	25.1(*S,S*)	26.1(*R,R*)	1.0
	S-DNBL-I	5.0	15.1(*R,R*)	15.9(*S,S*)	1.2
	S-DNBL-C	5.0	14.3	14.4	<0.1
		2.5	28.7(*R,R*)	30.1(*S,S*)	0.9
CR 3,4-DHD	*R*-DNBPG-I	5.0	29.7(*R,R*)	31.8(*S,S*)	2.2
4-O-methyl (2)	*R*-DNBPG-C	5.0	27.3(*R,R*)	29.6(*S,S*)	2.2
	S-DNBL-I	5.0	20.5	20.5	0
	S-DNBL-C	5.0	20.2	20.2	0
CR 3,4-DHD	*R*-DNBPG-I	1.25	11.0(*R,R*)	11.6(*S,S*)	1.1
bis-O-methyl	*R*-DNBPG-C	1.25	12.7(*R,R*)	13.3(*S,S*)	1.0
	S-DNBL-I	1.25	4.9	4.9	0
		0.5	10.0(*R,R*)	11.2(*S,S*)	1.6
	S-DNBL-C	1.25	6.0	6.0	0
		0.5	8.8(*R,R*)	9.1(*S,S*)	0.6

(*continued on p. 392*)

TABLE IV (*continued*)

*Chemical**	*CSP***	*A (%)****	*Retention time* (min)§		*RV*§§
			Enantiomer 1	*Enantiomer 2*	
BA 3,4-DHD	*R*-DNBPG-I	10.0	31.6(*S,S*)	32.1(*R,R*)	0.2
	R-DNBPG-C	10.0	19.6	19.6	0
	S-DNBL-I	10.0	20.6(*R,R*)	21.0(*S,S*)	0.2
	S-DNBL-C	10.0	14.0	14.0	0
BA 3,4-DHD 3-O-methyl (1)	*R*-DNBPG-I	2.5	28.1(*S,S*)	28.9(*R,R*)	1.0
	R-DNBPG-C	2.5	33.7(*S,S*)	34.6(*R,R*)	0.8
	S-DNBL-I	2.5	15.5	15.6	<0.1
	S-DNBL-C	1.0	28.5	28.5	0
BA 3,4-DHD 4-O-methyl (2)	*R*-DNBPG-I	2.5	35.7	35.7	0
	R-DNBPG-C	2.5	33.6	33.6	0
	S-DNBL-I	2.5	20.2	20.2	0
	S-DNBL-C	2.5	17.7	17.7	0
BA 3,4-DHD *bis*-O-methyl§§§	*R*-DNBPG-I	0.25	30.6	30.6	0
	R-DNBPG-C	0.25	36.1	36.1	0
	S-DNBL-I	0.25	13.9	13.9	0
		0.1	20.4	20.6	0.2
	S-DNBL-C	0.25	15.7	16.3	0.3
		0.1	21.8	22.8	0.8
7,12-DMBA 3,4-DHD	*R*-DNBPG-I	10.0	23.2(*S,S*)	24.5(*R,R*)	1.1
	R-DNBPG-C	10.0	16.5(*S,S*)	16.8(*R,R*)	0.1
	S-DNBL-I	10.0	24.9	24.9	0
	S-DNBL-C	10.0	15.6	15.6	0
7,12-DMBA 3,4-DHD 3-O-methyl (1)	*R*-DNBPG-I	2.5	25.9(*S,S*)	27.2(*R,R*)	1.4
	R-DNBPG-C	2.5	24.2(*S,S*)	25.5(*R,R*)	1.4
	S-DNBL-I	1.0	27.7(*S,S*)	28.8(*R,R*)	0.9
	S-DNBL-C	1.0	26.7(*S,S*)	27.4(*R,R*)	0.6
7,12-DMBA 3,4-DHD 4-O-methyl (2)	*R*-DNBPG-I	2.5	34.5	34.5	0
	R-DNBPG-C	2.5	33.8(*S,S*)	34.6(*R,R*)	0.5
	S-DNBL-I	2.5	18.8(*S,S*)	19.0(*R,R*)	~0.1
		1.0	46.2	46.2	0
	S-DNBL-C	2.5	17.7	17.7	0
7,12-DMBA 3,4-DHD *bis*-O-methyl	*R*-DNBPG-I	1.0	10.2(*S,S*)	10.6(*R,R*)	0.7
	R-DNBPG-C	1.0	9.8(*S,S*)	10.2(*R,R*)	0.9
	S-DNBL-I	0.1	14.6(*R,R*)	14.9(*S,S*)	<0.1
	S-DNBL-C	0.1	19.0(*R,R*)	19.8(*S,S*)	0.6

* Monomethyl ethers are designated as 1 and 2 according to their elution order on normal-phase HPLC.

** CSPs are defined in Materials and methods.

*** Percentage of eluent A (ethanol–acetonitrile, 2:1, v/v) in hexane. The flow-rate was 2 ml/min, with a void volume of 2.4 ml.

§ See text for the assignments of absolute configurations of resolved enantiomers. Enantiomers are designated as 1 and 2 according to their elution order on CSP-HPLC and have CD spectra that are mirror images of each other.

§§ RV = resolution value = $2(V_2 - V_1)/(W_2 + W_1)$, where V is retention volume and W is peak width at base.

§§§ Absolute configurations of resolved enantiomers were not established due to limited amounts of samples obtainable.

Enantiomers can be considered to have a baseline separation if the chromatographic peaks of separated enantiomers are both perfectly symmetrical and have a resolution value $\geqslant 1.0$. In practice, however, two compounds are said to show baseline separation when the resolution value is 1.5 or greater. Identities of resolved enantiomers were confirmed by UV–VIS absorption, CD, and mass spectral analyses[9–11,13–15].

Elution order of enantiomers

Enantiomers of 3-MC 11-O-methyl ether[10], 7,12-DMBA 5,6-DHD[2], 7,12-DMBA 5- and 6-O-methyl ethers have different elution orders on *R*-DNBPG-I and *R*-DNBPG-C. These observations are similar to the one reported earlier indicating that lacinilene C and lacinilene C methyl ether have reversed elution order of enantiomers on *R*-DNBPG-I[16]. Furthermore, enantiomers of 7,12-DMBA 5,6-DHD 5-O-methyl ether have different elution orders on ionically and covalently bonded *S*-DNBL columns; this is the only example so far indicating that elution orders of enantiomers are different on ionically and covalently bonded *S*-DNBL columns. The enantiomers of other compounds in Tables III and IV, if resolved on a particular CSP, were found to have the same elution order regardless whether the CSP was ionically or covalently bonded. The following compounds (their names are boxed-in in Figs. 2 and 3) have the same elution order of enantiomers on *R*-DNBPG and *S*-DNBL columns: PY 4,5-DHD 4-O-methyl, two isomeric 1-BrPY 4,5-DHD O-methyl ethers, 1-BrPY 9,10-DHD, CR 5,6-DHD, CR 5,6-DHD 5-O-methyl, 3-MC 11,12-DHD and both of its isomeric O-methyl ethers, BA 5,6-DHD 6-O-methyl, 1-MBA 5,6-DHD 6-O-methyl, 4-MBA 5,6-DHD and its 6-O-methyl ether, 6-MBA 5,6-DHD, 7-MBA 5,6-DHD and both of its isomeric O-methyl ethers, 3-MC 11,12-DHD and both of its isomeric O-methyl ethers, 7,12-DMBA 5,6-DHD and both of its isomeric O-methyl ethers, BaP 4,5-DHD 5-O-methyl, CR 3,4-DHD bis-O-methyl, and 7,12-DMBA 3- and 4-O-methyl ethers.

Resolution of enantiomers

Enantiomeric pairs of 4 dihydrodiols (PA 9,10-DHD, 1-MPA 9,10-DHD, 4,5-MPA 9,10-DHD, and BA 5,6-DHD) are not resolved on any of the four CSP columns (Table III). Except for the unresolvable enantiomeric pairs of 1-MPA 9,10-DHD 10-O-methyl (Table III) and BA 3,4-DHD 4-O-methyl (Table IV, the enantiomer pairs of other O-methyl derivatives are resolved on two or all four CSP columns with resolution values as high as 2.5 (Tables III and IV). The enantiomers of other dihydrodiol O-methyl ethers, are all more efficiently resolved on one or more CSP columns than those of underivatized dihydrodiols (Tables III and IV). By successively decreasing the percentage of eluent A in hexane, separations of enantiomeric pairs of some O-methyl ethers which are not resolved at higher eluent polarity become apparent. Examples of these are: 4,5-MPA 9,10-DHD 9-O-methyl, PY 4,5-DHD 4-O-methyl, 1-BrPY 9,10-DHD, 12-MBA 5,6-DHD 5-O-methyl, CR 3,4-DHD 3-O-methyl, and CR 3,4-DHD bis-O-methyl (Tables III and IV). Decrease in the polarity of the eluent apparently enhanced the chiral interactions between the CSP and solutes, permitting separation of enantiomers.

Elution order/absolute configuration relationship

There are no definitive rules that govern the elution order/absolute configuration of enantiomers. The following observations are summarized for those dihydrodiols and O-methyl ethers the enantiomers of which can be resolved:

(a) The *S,S*-enantiomers of dihydrodiols and O-methyl ethers of PY and 1-BrPY are more strongly retained by both ionically and covalently bonded *R*-DNBPG.

(b) Except that the *S,S*-enantiomers of quasidiaxial 1-BrPY 9,10-DHD, 4-MBA 5,6-DHD, 7-MBA 5,6-DHD, and 3-MC 11,12-DHD are more strongly retained by the *R*-DNBPG columns, the *R,R*-enantiomers of other dihydrodiols in Tables III and IV are more strongly retained. In contrast, the *R,R*-enantiomer of the quasidiaxial 7,12-DMBA 5,6-DHD is more strongly retained on *R*-DNBPG[2].

(c) There are no definitive rules on the elution order/absolute configuration relationship among the O-methyl ethers (isomer 1), which are less strongly retained in normal-phase HPLC on a silica (SIL) column.

(d) The *S,S*-enantiomers of most O-methyl ethers (isomers 2 in normal-phase HPLC) derived from *K*-region dihydrodiols are more strongly retained on *R*-DNBPG (Figs. 2 and 3, Tables III and IV). However, the *R,R*-enantiomers of O-methyl ethers 2, derived from BcPA 5,6-DHD, 4-MBA 5,6-DHD, 12-MBA 5,6-DHD, and 7,12-DMBA 5,6-DHD, are more strongly retained on *R*-DNBPG.

(e) Elution orders of enantiomers on *R*-DNBPG are not always reversed on *S*-DNBL. Those enantiomeric pairs that have the same elution order on *R*-DNBPG and *S*-DNBL are indicated with their names boxed-in in Figs. 2 and 3.

CONCLUSION

Derivatization of dihydrodiols of PAHs to O-methyl ethers generally improves enantiomeric separation on one or more kinds of Pirkle's CSPs. However, general rules are not apparent that can be used to predict the relationship between elution order and absolute configuration of resolved enantiomers. Nonetheless, the findings that dihydrodiol enantiomeric pairs can be separated either directly or following conversion to O-methyl ethers are very useful and have been applied with considerable success in the understanding of the detailed stereoselective pathways of metabolism of PAHs catalyzed by drug-metabolizing enzyme systems[1,5,7,8,11,12,18].

ACKNOWLEDGEMENT

This work was supported by Uniformed Services University of the Health Sciences Protocol RO7502 and U.S. Public Health Service grant CA29133. The opinions or assertions contained herein are the private ones of the authors and are not to be construed as official or reflecting the views of the Department of Defense or the Uniformed Services University of the Health Sciences.

REFERENCES

1 H. B. Weems and S. K. Yang, *Anal. Biochem.*, 125 (1982) 156.
2 S. K. Yang and H. B. Weems, *Anal. Chem.*, 56 (1984) 2658.
3 S. K. Yang, H. B. Weems, M. Mushtaq and P. P. Fu, *J. Chromatogr.*, 316 (1984) 569.
4 S. K. Yang, M. Mushtaq, H. B. Weems and P. P. Fu, *J. Liq. Chromatogr.*, 9 (1986) 473.

5 H. B. Weems, P. P. Fu and S. K. Yang, *Carcinogenesis*, 7 (1986) 1221.
6 S. K. Yang, M. Mushtaq and P. P. Fu, *J. Chromatogr.*, 371 (1986) 195.
7 S. K. Yang, M. Mushtaq and H. B. Weems, *Arch. Biochem. Biophys.*, 255 (1987) 48.
8 M. Shou and S. K. Yang, *Drug Metab. Disp.*, 16 (1988) 173.
9 H. B. Weems, M. Mushtaq, P. P. Fu and S. K. Yang, *J. Chromatogr.*, 371 (1986) 211.
10 H. B. Weems, M. Mushtaq and S. K. Yang, *Anal. Chem.*, 59 (1987) 2679.
11 S. K. Yang, M. Mushtaq, H. B. Weems, D. W. Miller and P. P. Fu, *Biochem. J.*, 245 (1987) 191.
12 P. P. Fu, F. E. Evans, D. W. Miller, M. W. Chou and S. K. Yang, *J. Chem. Res. Synop.*, (1983) 158.
13 M. Mushtaq, H. B. Weems and S. K. Yang, *Biochem. Biophys. Res. Commun.*, 125 (1984) 539.
14 S. K. Yang and P. P. Fu, *Chem.-Biol. Interac.*, 49 (1984) 71.
15 S. K. Yang and P. P. Fu, *Biochem. J.*, 223 (1984) 775.
16 R. D. Stipanovic, J. P. McCormick, E. O. Schlemper, B. C. Hamper, T. Shinmyozu and W. H. Pirkle, *J. Org. Chem.*, 51 (1986) 2500.
17 S. K. Balani, H. J. C. Yeh, D. E. Ryan, P. E. Thomas, W. Levin and D. M. Jerina, *Biochem. Biophys. Res. Commun.*, 130 (1985) 610.
18 S. K. Yang, *Biochem. Pharmacol.*, 37 (1988) 61.

Journal of Chromatography, 461 (1989) 397–405
Elsevier Science Publishers B.V., Amsterdam — Printed in The Netherlands

CHROMSYMP. 1432

GENERAL EVALUATION AND APPLICATION TO TRACE ANALYSIS OF A CHIRAL COLUMN FOR LIGAND-EXCHANGE CHROMATOGRAPHY

HIDEAKI KINIWA*, YUKA BABA, TOMOKO ISHIDA and HIROMASA KATOH
Mitsubishi Kasei Corporation, Research Centre, Yokohama, Kanagawa 227 (Japan)

SUMMARY

The direct optical resolution of more than twenty amino acids, including the separation of four isomers of *allo*-DL- and DL-isoleucine, can be achieved on a novel ligand-exchange column, MCI GEL CRS10W. The stationary phase, N,N-dioctyl-L-alanine-coated octadecylsilica, shows a stronger affinity for hydrophobic amino acids than for hydrophilic amino acids. General evaluation of the column clarified the effects of the column temperature and Cu^{II} concentration in the eluent on the chiral separation. The determination of trace enantiomers in some commercially available D- and L-amino acids was performed, revealing the presence of 0.03–0.5% of the trace enantiomer. The efficient resolution of strongly retained hydrophobic amino acids and hydroxycarboxylic acids was also achieved on a shortened column.

INTRODUCTION

The optical resolution of DL-amino acids by ligand-exchange chromatography has been intensively studied since the pioneering work of Davankov and co-workers in the late 1970s[1–5]. Following the modification of some of the initial ideas, several columns have become commercially available[6]. However, shortcomings of the commercially available ligand-exchange phases are that the number of amino acids separated on any given chiral column is limited and that the column temperature must be raised in order to increase the degree of resolution.

The column evaluated here, MCI GEL CRS10W, packed with N,N-dioctyl-L-alanine-coated octadecyl (ODS)-silica, demonstrated the efficient resolution of more than 20 amino acids on a single column at room temperature.

Considering reversed-phase packings coated with N-alkyl-L-amino acids, Davankov and Kurganov[5] first reported N-alkyl-L-hydroxyproline-coated ODS-silica as a novel stationary phase for ligand-exchange chromatography in 1980. Although the stationary phase demonstrated a very high selectivity for the optical resolution of various hydrophobic amino acids, the selectivity was not high for hydrophilic amino acids. This present paper describes a chiral stationary phase with a novel ligand that was developed to produce high selectivity for both hydrophilic and hydrophobic amino acids.

0021-9673/89/$03.50

EXPERIMENTAL

Reagents and reference materials

Amino acids and DL-mandelic acid were purchased from Sigma (St. Louis, MO, U.S.A.), DL-lactic acid from Kishida Kagaku (Osaka, Japan) and DL-leucic acid (DL-2-hydroxyisocaproic acid) from Tokyo Kasei (Tokyo, Japan). Copper(II) sulphate pentahydrate was purchased from Kishida Kagaku.

High-performance liquid chromatography

A Shimadzu (Kyoto, Japan) LC-6A system equipped with a Shimadzu SPD-6A UV spectrophotometric detector operating at 254 nm and a Waters Assoc. (Milford, MA, U.S.A.) column-temperature-controlling unit was used. The column, prepared by coating *ca.* 20 wt.-% of N,N-dioctyl-L-alanine on to ODS-silica, is commercially available as MCI GEL CRS10W (50 mm × 4.6 mm I.D.) from Mitsubishi Kasei (Tokyo, Japan). A column with a selectivity opposite to that of MCI GEL CRS10W, packed with N,N-dioctyl-D-alanine-coated ODS-silica, and a short column version (10 mm × 4.6 mm I.D.) of MCI GEL CRS10W were kindly supplied by Mitsubishi Kasei. The eluents evaluated included an aqueous solution of copper(II) sulphate

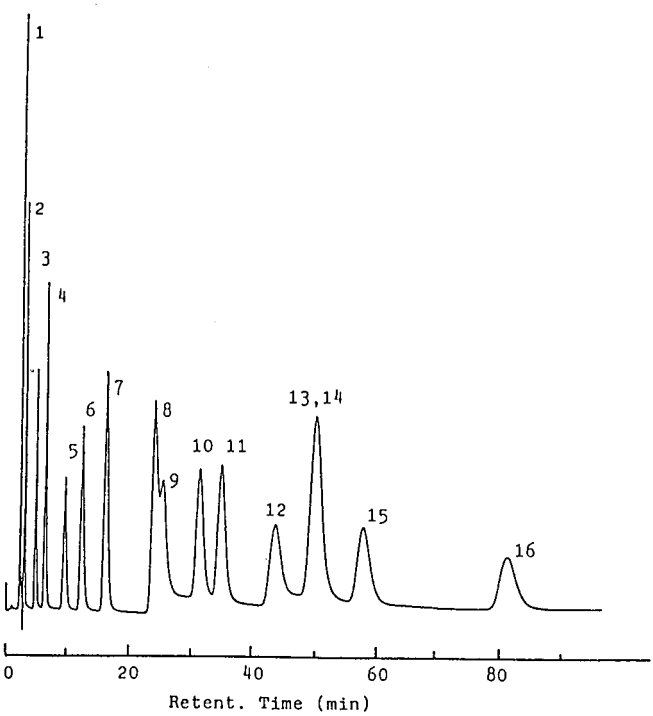

Fig. 1. Resolution of eight amino acid racemates. Column, MCI GEL CRS10W; eluent, 0.5 m*M* copper (II) sulphate solution; flow-rate, 1.0 ml/min; pressure, 110 kg/cm^2; column temperature, 32°C; UV detection, 254 nm. Peaks: 1 = D-Ala; 2 = L-Ala; 3 = D-Pro; 4 = D-Val; 5 = L-Pro; 6 = L-Val; 7 = D-Leu; 8 = D-Nle; 9 = D-Tyr; 10 = L-Leu; 11 = D-Eth; 12 = L-Tyr; 13 = L-Nle; 14 = D-Phe; 15 = L-Eth; 16 = L-Phe.

(between 0.1 and 2 m*M*) and a 2 m*M* solution of copper(II) sulphate in methanol–water (15:85, v/v). For trace analysis, a Shimadzu LC-5A system with a Shimadzu RF-530 fluorimetric detector was used.

RESULTS AND DISCUSSION

Resolution of amino acids

The MCI GEL CRS10W stationary phase is based on 3-μm ODS-silica of 100 Å mean pore diameter. It gave high separation factors, owing to a combination of ligand-exchange and hydrophobic interactions with N,N-dioctyl-L-alanine-coated ODS-silica. The column, although 50 mm long, gave sufficient retention and a high resolution even at ambient temperature (25–30°C). The durability of the column was also sufficient for practical use.

Fig. 1 shows the chiral separation of eight amino acids into their respective D- and L-enantiomers. The D-isomers were eluted ahead of the L-isomers in all instances, and hydrophilic amino acids were eluted ahead of hydrophobic amino acids. A remarkable baseline separation of four isomers of isoleucine was also achieved on this column, indicating that the amino acid contains 33% of *allo*-DL-isomers (Fig. 2).

The interaction between the amino acids to be resolved and the stationary phase can be understood in terms of a superposition of a complexing process and hydrophobic interaction. Hence the factors controlling retention and enantioselectivity, column temperature, Cu^{II} concentration in the eluent and the type of Cu^{II} salt, were varied and their effects were investigated.

Effect of column temperature

The column temperature was increased from 30 to 50°C at a constant eluent concentration [1 m*M* aqueous solution of copper(II) sulphate]. The chromatograms in Fig. 3 of a mixture of L-amino acids show a noticeable decrease in retention with increasing temperature. The separation factor also decreased with increasing temperature (Table I), suggesting that the temperature dependence of the complex stability must be greater for the later eluted isomer[1].

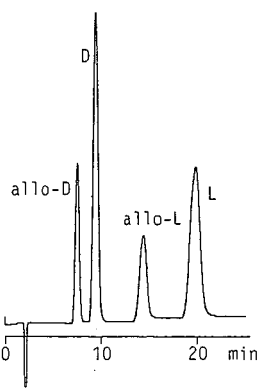

Fig. 2. Resolution of 20 μl of a 1 m*M* aqueous solution of DL-isoleucine. Conditions: eluent, 2 m*M* copper(II) sulphate solution; flow-rate, 1 ml/min; pressure, 100 kg/cm^2; temperature, 30°C; UV detection, 254 nm (0.04 a.u.f.s.).

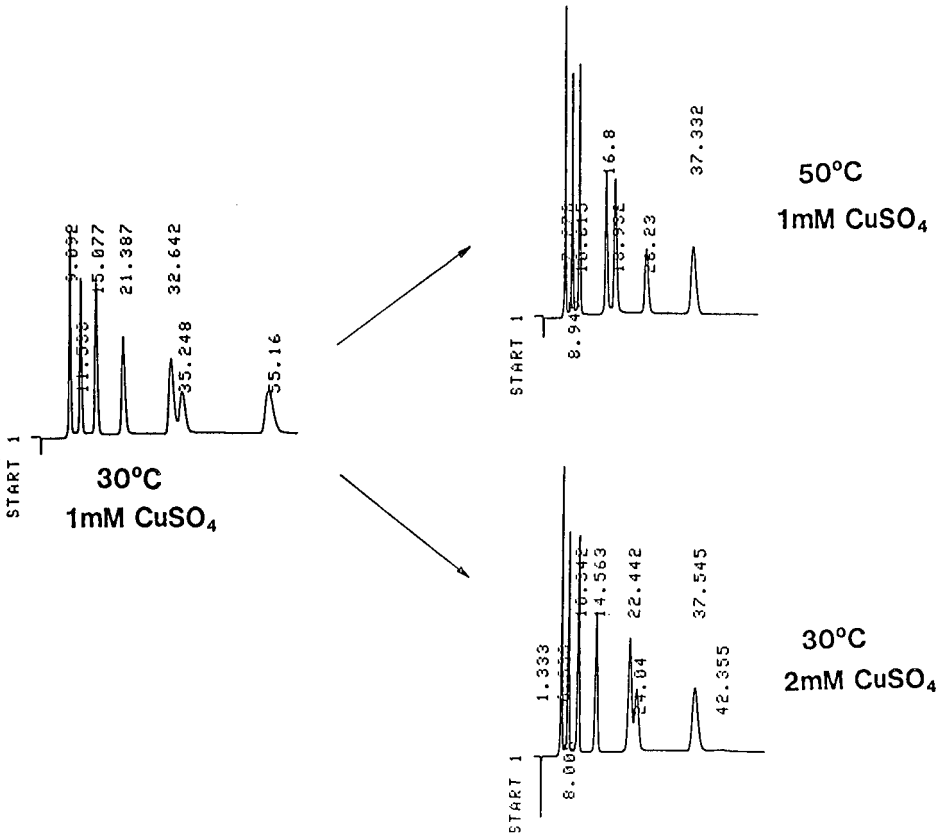

Fig. 3. Effect of temperature and copper(II) sulphate concentration on the resolution of an L-amino acid mixture. Order of elution: L-valine, L-norvaline, L-methionine, L-leucine, L-tyrosine, L-norleucine and L-phenylalanine.

Effect of Cu^{II} concentration and type of Cu^{II} salt

The copper(II) sulphate concentration in the eluent was increased from 1 to 2 m*M* at a constant temperature (30°C). It was observed that an increase in Cu^{II} con-

TABLE I

EFFECT OF TEMPERATURE AND COPPER(II) SULPHATE CONCENTRATION ON THE RESOLUTION OF DL-VALINE

Flow-rate, 1 ml/min; pressure, 110 kg/cm^2; detection, 254 nm.

$CuSO_4$ (mM)	*pH*	*Temperature (°C)*	k'_D	k'_L	α	R_s
1.0	5.30	30	7.32	14.93	2.04	5.01
1.0	5.30	50	6.05	11.68	1.93	4.26
2.0	5.15	30	5.04	10.30	2.04	4.59

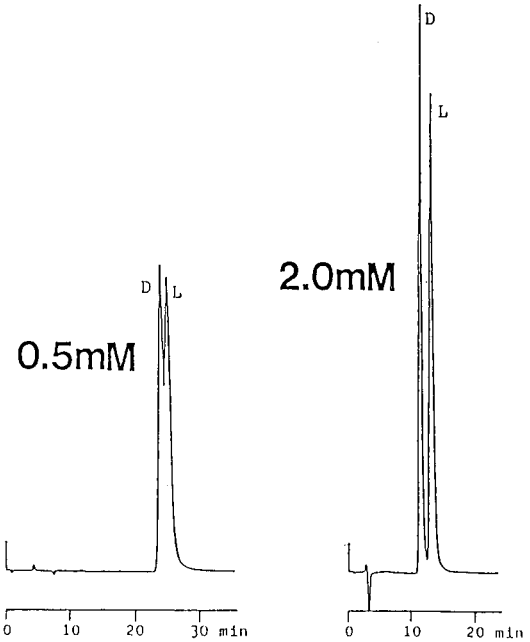

Fig. 4. Effect of copper(II) sulphate concentration in the eluent on the resolution of DL-aspartic acid (1 m*M* aqueous solution, 20 μl). Conditions: eluent, 0.5 m*M* (left) and 2 m*M* copper(II) sulphate solution (right); flow-rate, 1.0 ml/min; pressure, 110 kg/cm^2; temperature, 30°C; detection, 254 nm (0.16 a.u.f.s.).

centration decreases the retention time but has no effect on the resolution efficiency (Table I). The observed tendency can be explained by the fact that the lower the concentration of Cu^{II} in the eluent, the slower is the ligand exchange between the amino acid and the ligand on the stationary phase, which results in greater retention.

It is interesting to compare the changes in the pattern of the chromatograms in Fig. 3. It is clear that temperature affects the pattern of the chromatograms drastically, whereas the Cu^{II} concentration only affects the retention of the L-isomer. This tendency was also observed for D-isomers. Therefore, in order to weaken the interaction and consequently shorten the retention time, while maintaining the pattern of the chromatogram, an increase in the Cu^{II} concentration in the eluent seems favourable.

Subsequently, copper(II) sulphate was replaced with copper(II) acetate and the eluent concentration was altered. Comparison of the sulphate and acetate showed that the anions have no apparent effect on the enantioselectivity of the column, but in general copper(II) sulphate gave smaller retentions, probably owing to the lower ratio of copper(II) acetate [pH = 6.10 for 0.25 m*M* copper(II) acetate whereas pH = 5.50 for 0.25 m*M* copper(II) sulphate].

A striking effect of the copper(II) sulphate concentration on the resolution was observed for some acidic amino acids, especially DL-aspartic acid (Fig. 4). Copper(II) sulphate, rather than copper(II) acetate, and at a higher concentration gave a notably better resolution. Restriction of dissociation of the ω-carboxyl group of aspartic acid can be offered as an explanation.

TABLE II

OPTIMUM RESOLUTION CONDITIONS

Temperature, 32°C; detection, 254 nm.

Amino acid	$CuSO_4$ *(mM)*	*pH*	*Flow-rate (ml/min)*	*Retention time (min)*		k'_D	k'_L	α	R_s
				t_D	t_L				
Ornithine	0.1	5.60	0.2	6.00	6.83	1.15	1.45	1.26	–
Lysine	0.1	5.60	0.2	6.23	7.75	1.23	1.78	1.45	0.7
Alanine	0.1	5.60	0.5	8.22	10.99	6.34	8.81	1.39	1.4
Histidine	0.1	5.60	0.5	6.88	10.52	5.14	8.39	1.63	1.7
Serine	0.1	5.60	0.5	8.34	10.13	6.45	8.04	1.25	1.0
Threonine	0.1	5.60	0.5	9.04	11.34	7.07	9.13	1.29	1.3
Citrulline	0.5	5.35	0.5	6.42	10.40	4.73	8.29	1.75	2.3
Proline	1.0	5.25	1.0	3.72	7.31	5.64	12.04	2.13	4.5
Valine	1.0	5.25	1.0	4.66	8.92	7.32	14.93	2.04	5.0
Norvaline	1.0	5.25	1.0	5.85	11.51	9.45	19.55	2.07	4.7
Aspartic acid	2.0	5.15	0.5	11.52	13.22	5.20	6.11	1.18	0.9
Glutamic acid	2.0	5.15	1.0	10.76	16.22	18.21	27.96	1.54	2.3
Leucine	2.0	5.15	1.0	7.68	14.59	12.71	25.05	1.97	4.6
Tyrosine	2.0	5.15	1.0	12.42	22.45	21.18	39.09	1.85	5.3
Ethionine	2.0	5.15	1.0	15.84	26.37	27.29	46.09	1.69	5.0
Phenylalanine	2.0	5.15	1.0	20.75	37.79	36.05	66.48	1.84	6.3

Considering the effect of Cu^{II} concentration on retention and enantioselectivity, optimum resolution conditions for various racemic amino acids are summarized in Table II.

Effect of sample size on the number of theoretical plates

The maximum sample load capacity for a reasonable resolution was determined for L-methionine and L-alanine. The data in Fig. 5 indicate that, in order to attain a

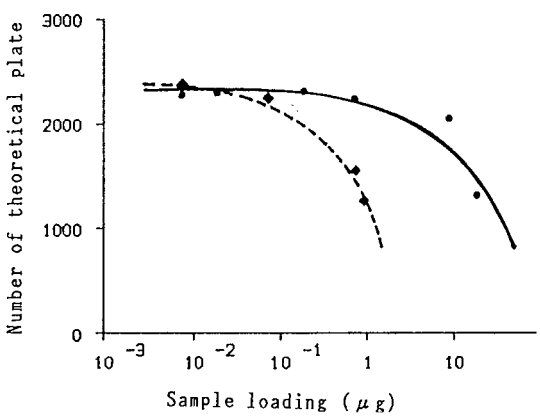

Fig. 5. Effect of sample load on the theoretical plate number for (◆) L-alanine and (●) L-methionine. Conditions for L-alanine: eluent, 0.1 m*M* copper(II) sulphate solution; flow-rate, 0.5 ml/min; pressure, 40 kg/cm^2; temperature, 30°C; detection, 254 nm. Conditions for L-methionine: eluent, 2 m*M* copper(II) sulphate solution; flow-rate, 1 ml/min; pressure, 97 kg/cm^2; temperature, 30°C; detection, 254 nm.

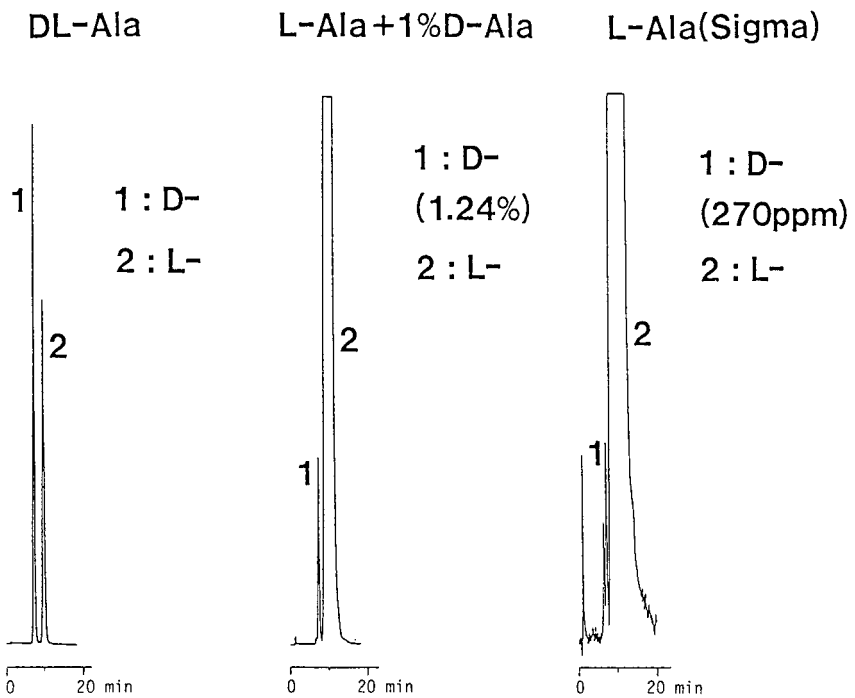

Fig. 6. Trace analysis of D-isomer content in L-alanine (100 ppm solution, 20 μl). Conditions: column, 50 mm × 4.6 mm I.D.; eluent, 0.1 m*M* copper(II) sulphate solution; flow-rate, 0.7 ml/min; temperature, ambient; fluorimetric detection (OPA post-column reaction method), exitation at 348 nm and emission at 450 nm, reaction temperature, 55°C.

theoretical plate number over 2000, 1 g of L-methionine and 0.1 g of L-alanine represent the maximum amount of sample.

After this investigation, the column was washed with distilled water. Subsequently, a decrease in the retention time for any given amino acid was observed. The retention was regained after passing 500 μl of 4% copper(II) acetate solution through the column. This indicates that Cu^{II} release from the Cu^{II}-complexed ligand on the stationary phase was the cause of the decrease in retention. It is not clear whether continuous overloading of the sample or the washing of the column causes the release of Cu^{II}. It should be noted that this was the only time that the column was washed with distilled water.

Effect of Cu^{II} salt in sample solutions

It was observed that sample solutions prepared with the eluent sometimes gave smaller peaks for the later eluted isomer, and not the expected 1:1 peak ratio for racemates. It was assumed that this phenomenon was due to the complex formation between the amino acids and Cu^{II} in the eluent solution and subsequent interaction with the stationary phase, causing elution of different ratios of Cu^{II}-complexed amino acids and non-complexed amino acids. This would create a difference in the mass of

the detectable Cu^{II}–amino acid complex. This assumption was verified by the 1:1 ratio of the peak areas of the resolved isomers when distilled water was used to dissolve the sample.

Resolution of hydroxycarboxylic acids

In addition to amino acids, organic acids that form complexes with Cu^{II} were also separated. A baseline separation of DL-lactic acid was achieved on this column by using 1 m*M* copper(II) sulphate solution as the eluent. In general, the elution of hydroxycarboxylic acids required a higher concentration of copper(II) sulphate in the eluent than did amino acids with similar side-chains. In most instances, faster elution was achieved by the addition of a small amount of methanol to the eluent. However, hydroxycarboxylic acids such as DL-leucic acid and DL-mandelic acid required more than 50 min for elution, even after addition of 15% (v/v) of methanol.

Table III summarizes the results for the resolution of some of the above-mentioned "long-retained" enantiomers on a short column (10 mm × 4.6 mm I.D.). Baseline separation of DL-leucic acid and DL-mandelic acid in less than 10 min was achieved on this column. The resolution of strongly retained hydrophobic amino acids, DL-phenylalanine and DL-tryptophane, was also possible.

Evaluation of the column durability

As the stationary phase is prepared by coating a hydrophobic ligand on to a reversed-phase packing, the stability of the immobilized ligand was of critical concern. The stability of the stationary phase was therefore evaluated. The changes in the capacity factors and separation coefficients after continuous analysis of some amino acids are shown in Table IV. When an aqueous solution was used as the eluent, no change was observed even after passing 21 l of the eluent. During that period, 800 analyses of the same sample were carried out, and no significant change of the chromatogram was obtained. On the other hand, when methanol was added to the eluent (15%, v/v), the capacity factors gradually decreased on increasing the elution volume. However, as the extent of the decrease was relatively small even after passing 21 l of

TABLE III

RESOLUTION OF AMINO ACIDS AND HYDROXYCARBOXYLIC ACIDS ON A SHORT COLUMN (10 mm × 4.6 mm I.D.)

Substance	*Conditions**	*Retention time (min)*		α	R_s
		t_D	t_L		
Phenylalanine	I	4.52	7.85	1.76	1.55
Tryptophan	II	3.49	5.95	1.71	1.14
Mandelic acid	II	4.35	6.68	1.54	0.94
Leucic acid	II	6.02	8.45	1.41	0.92

* (I) Sample, 1 m*M* aqueous solution, 20 μl; eluent, 2 m*M* copper(II) sulphate solution (pH 5.15); flow-rate, 1 ml/min; pressure, 7 kg/cm^2; temperature, 30°C; detection, 254 nm; (II) sample, 1 m*M* aqueous solution, 40 μl; eluent, 2 m*M* copper(II) sulphate solution in methanol–water (15:85, v/v) (pH 5.10); flow-rate, 2 ml/min; pressure, 37 kg/cm^2; temperature, 30°C; detection, 254 nm.

TABLE IV

CHANGE IN CAPACITY FACTORS AND ENANTIOSELECTIVITY WITH ELUTION VOLUME

Amino acid	*Conditions**	*Elution volume*							
		1 l				*21 l*			
		k'_D	k'_L	α	R_s	k'_D	k'_L	α	R_s
Proline	I	9.37	19.10	2.03	3.87	9.24	18.89	2.04	3.75
Valine	I	12.29	24.27	1.97	4.73	12.22	24.09	1.97	4.61
Phenylalanine	II	13.58	21.58	1.59	1.74	13.18	20.14	1.53	1.61

* (I) Sample, 0.5 m*M* aqueous solution, 20 μl; eluent, 0.5 m*M* copper(II) sulphate solution (pH 5.35); flow-rate, 1 ml/min; pressure, 110 kg/cm^2; temperature, 25°C; detection, 254 nm; (II) sample, 1.5 m*M* aqueous solution, 25 μl; eluent, 2 m*M* copper(II) sulphate solution in methanol–water (15:85, v/v) (pH 5.15); flow-rate, 1 ml/min; pressure, 126 kg/cm^2; temperature, 25°C; detection, 254 nm.

the eluent, and the separation coefficient remained almost constant, the decrease in the capacity factors would be a negligible problem in practical use.

Trace analysis

Sub-nanomole sensitivity is achieved by post-column derivatization with *o*-phthalaldehyde and subsequent fluorimetric detection[7], as shown in Fig. 6. For the trace analysis of L-isomers in D-amino acids, a column with opposite selectivity was used to enhance the detectability[8]. A straight line was obtained when the concentration of eluted L-isomer was plotted against incremental 100 ppm additions of L-isomer. The trace amount of initial L-isomer present in the corresponding D-isomer was determined by reading off the abscissa. The contents of L-isomers in D-aspartic acid and D-phenylalanine were 5000 and 800 ppm, respectively.

REFERENCES

1 V. A. Davankov, S. V. Rogozhin, A. V. Semechkin, V. A. Baranov and G. S. Sannikova, *J. Chromatogr.*, 93 (1974) 363.
2 V. A. Davankov and Yu. A. Zolotarev, *J. Chromatogr.*, 155 (1978) 285, 295, 303.
3 B. Lefebre, R. Audebert and C. Quivoron, *J. Liq. Chromatogr.*, 1 (1978) 761.
4 G. Gübitz, W. Jellenz, G. Lofler and W. Santi, *J. High Resolut. Chromatogr. Chromatogr. Commun.*, 2 (1979) 145.
5 V. A. Davankov and A. A. Kurganov, *Chromatographia*, 13 (1980) 339 and 677.
6 R. Däppen, H. Arm and V. R. Meyer, *J. Chromatogr.*, 373 (1986) 1.
7 J. A. Perry, J. D. Rateike and T. J. Szczerba, *J. Chromatogr.*, 389 (1987) 57.
8 Y. Ishida, T. Fujita and K. Asai, *J. Chromatogr.*, 204 (1981) 143.

Journal of Chromatography, 461 (1988) 407–418
Elsevier Science Publishers B.V., Amsterdam — Printed in The Netherlands

CHROMSYMP. 1433

MOBILE PHASE OPTIMIZATION OF A UREA-LINKED CHIRAL STATIONARY PHASE FOR THE HIGH-PERFORMANCE LIQUID CHROMATOGRAPHIC SEPARATION OF OPTICAL ISOMERS

SUBHASH C. DHANESAR* and DARYL J. GISCH*
Supelco, Inc., Supelco Park, Bellefonte, PA 16823-0048 (U.S.A.)

SUMMARY

A silica-based urea-linked chiral stationary phase, (*R*)-N-(1-naphthylethyl-N′-propylsilyl urea), was studied with binary, ternary, and single-component mobile phases, to determine the factors which most affect retention and selectivity. Binary mobile phases were prepared with hexane as the non-selective solvent, and 2-propanol, dichloromethane, or chloroform as the selective solvent. (±)-1-Phenylethyl-3,5-dinitrobenzamide was used as the enantiomer test mixture. Increasing the mobile phase strength reduced the retention of test solutes, while selectivity remained largely unchanged. Also, modifiers improved resolution and did not affect selectivity. Single-component mobile phases reduced the retention in the order of increasing solvent strength, selectivity being solvent-dependent.

INTRODUCTION

The resolution of optical isomers by high-performance liquid chromatography (HPLC) has become a much utilized technique. The importance of this technique is reflected in the fact that about 40% of all drugs used in therapy are chiral, and that their enantiomers differ to various degrees in that their pharmacological actions, as well as in their side-effects[1].

In a chiral solute mixture, the two enantiomers have identical internal energy before injection into the column and after elution from the column. The enantiomers can be separated if the chiral stationary phase (CSP) is able to produce a difference in internal energy between them. If there is chiral recognition between the solute molecules and the CSP, transient diastereomeric complexes of differing stability are formed. These transient complexes can be separated by chromatography.

Dalgliesh[2] was first to develop a mechanistic model for chiral recognition in a chromatographic system. The model postulates a three-point interaction between the CSP and the solute. Such interactions may consist of a combination of hydrogen bonding, dipole–dipole, π–π, and steric interactions, depending upon the system. Much understanding concerning the mechanism and the rationale for designing new CSPs has evolved from the work of Pirkle and co-workers[3,4], utilizing the three-point

* Present address: Barre-National, Inc., Baltimore, MD 21207 (U.S.A.)

0021-9673/89/$03.50

interaction model. A two-point interaction model was proposed by Lochmüller and Ryall[5], and by Dobashi and Hara[6], while a single-point mechanism was proposed by Lochmüller *et al.*[7], and by Wainer *et al.*[8]. Lochmüller and Souter[9] further proposed an environmental chirality with no specific points of interaction, for certain systems. Such studies have greatly expanded the range of enantiomers that have been separated on a wide variety of CSPs and have paved the way for the development of newer and more useful CSPs.

In this paper, we discuss how mobile phase variations affect retention and selectivity for chiral resolution upon a commercial naphthyl urea-linked π-donor brush-type CSP. Studies were conducted with binary and ternary mobile phases, the latter prepared by adding the modifiers methanol and acetonitrile to the binary phases. In the binary mobile phases, hexane and heptane were used as non-selective solvents, while alcohols, chloroform, and dichloromethane were used as selective solvents. 1,2-Dichloroethane, acetonitrile and methyl *tert.*-butyl ether were used as single-component mobile phases.

EXPERIMENTAL

Materials

A Supelcosil™ LC-(*R*)-Naphthyl Urea, 250 × 4.6 mm I.D. column (NU column) was used for the chiral separations (Supelco, Bellefonte, PA, U.S.A.). The chiral solute test mixture (±)-1-phenylethyl-3,5-dinitrobenzamide (PEDNBA) was obtained from Supelco, all other reagents, standards and mobile phase solvents were obtained from Anachemia (Champlain, NY, U.S.A.). All solvents were of HPLC grade.

Mobile phase mixtures

All binary and ternary mobile phases were hand-mixed. All mobile phase changes were made by equilibrating the column with a minimum of 150 ml of mobile phase. Chromatography was carried out at ambient temperatures. Mobile phases used for these studies are listed in Table I.

TABLE I

MOBILE PHASE MIXTURES

Mobile phase components	*Composition (v/v)*	*Polarity, P*
Binary mobile phases[10]		
Hexane–2-propanol	90:10	0.48
	80:20	0.86
	75:25	1.05
	70:30	1.24
	50:50	2.00
Heptane–2-propanol	134:12	0.50
	100:25	0.94
	75:21	1.01
	75:25	1.13
	75:35	1.38
	52:48	1.98

TABLE I (*continued*)

Mobile phase components	*Composition (v/v)*	*Polarity, P*
Hexane–dichloromethane	50:50	1.60
	45:55	1.75
	40:60	1.90
	35:65	2.05
	33:67	2.11
	30:70	2.20
	25:75	2.44
Hexane–chloroform	200:300	2.50
	200:325	2.58
	150:300	2.77
	100:300	3.10
	50:300	3.53
	20:300	3.85
Ternary mobile phases		
Hexane–2-propanol–acetonitrile	225:75:0	1.05
	225:75:0.4	1.06
	225:75:1.0	1.07
	225:75:2.0	1.08
	225:75:3.0	1.10
	225:75:4.0	1.11
	225:75:6.0	1.14
Hexane–2-propanol–methanol	75:25:0	1.05
	75:25:0.2	1.06
	75:25:0.5	1.07
	75:25:0.7	1.08
	75:25:1.0	1.09
	75:25:2.0	1.13
Hexane–chloroform–methanol	360:640:0	2.55
	360:640:0.025	2.56
	360:640:0.06	2.57
	360:640:0.12	2.58
	360:640:0.2	2.61
	360:640:0.5	2.67
Hexane–chloroform–acetonitrile	360:640:0	255
	360:640:0.03	2.56
	360:640:0.06	2.57
	360:640:0.12	2.61
	360:640:0.25	2.63
	360:640:0.5	2.71
	360:640:0.9	2.85
Alcohols containing mobile phases		
Hexane-ethanol	80:20	0.94
Hexane–*n*-propanol	80:20	0.88
Hexane–*n*-butanol	80:20	0.86
Hexane–*n*-octanol	80:20	0.93
Hexane–isobutanol	80:20	0.90
Hexane–2-propanol	80:20	0.86

Apparatus

Chromatography was performed with a Waters (Waters Assoc., Milford, MA, U.S.A.) 590 pump, a WISP 710B injector with a Waters 720 system controller, a Kratos (Ramsey, NY, U.S.A.) Spectroflow 757 variable-wavelength detector set at 254 nm, and a SP™-4270 recorder/integrator from Spectra-Physics (San Jose, CA, U.S.A.).

RESULTS AND DISCUSSION

The chiral phase is a π-donor brush-type stationary phase. The chiral bonded phase (Fig. 1A) interacts with solute molecules through a number of different interactions, depending on the functionality of the solute and solvent molecules. When PEDNBA (Fig. 1B) is used as the solute mixture, the CSP–solute interactions consist of a combination of a π–π interaction between the π-accepting 3,5-dinitrobenzoyl group of the solute and the electron-rich naphthyl group of the CSP, a dipole interaction between the carbonyl group of the solute and the amido group of the CSP, and a dipole interaction between the phenyl group of the solute and the carbonyl group of the CSP. The strength of these interactions determines the degree of chiral recognition, as seen by the order of elution of the enantiomers and the difference in their retention. These reflect the differences in strength of the transient diastereomeric complexes formed between the CSP and the solute enantiomers.

Furthermore, the solvent–CSP interactions depend on the chemical properties of the solvent used. Hexane or heptane are non-polar, non-selective solvents, serving only to adjust the strength of the mobile phase. In the binary mobile phases, 2-propanol interacts with the CSP through reciprocal hydrogen bonding at the amide group. Dichloromethane is a dipolar molecule, and interacts with the carbonyl group through a dipole–dipole interaction. Chloroform is a hydrogen donor that interacts with the amide group through non-reciprocal hydrogen bonding at the carbonyl oxygen. Each of these interactions is capable of reducing the strength of the solute–CSP interaction.

This model only reflects the solvation interaction of the polar solvent, with the functional groups of the bonded stationary phase (Fig. 1A) or the chiral solute (Fig. 1B). Such interactions may alter chiral recognition by the disruption of chemical interactions and/or by solvation of the phase or solute to a degree that steric bulk prevents interaction. This model does not address solute and solvent interactions with

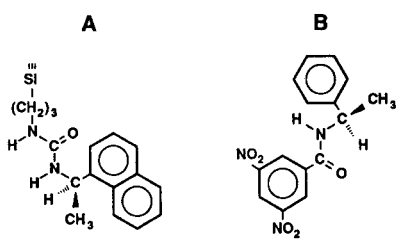

Fig. 1. Structures of the Supelcosil LC-(*R*)-naphthyl urea bonded-phase surface (A) and the PEDNBA test solute (B).

residual surface silanols upon the bonded phase support, as such interactions affect retention of each enantiomer equally and play no role in chiral recognition.

In this study, the effects of different binary and ternary mobile phases on retention and selectivity are examined. Retention of the enantiomers is reported as k'_{av}, the average capacity value for the enantiomers:

$$k'_{av} = \frac{k'_1 + k'_2}{2} \tag{1}$$

where k'_1 and k'_2 are the capacity factors of enantiomers 1 and 2, respectively. The difference in retention of the test solutes due to the binary and ternary mobile phases, dk', is reported as:

$$dk' = k'_{BMP} - k'_{TMP} \tag{2}$$

where k'_{BMP} and k'_{TMP} refer to the average capacity factors, k'_{av}, for the enantiomer pair in the binary and ternary mobile phases, respectively. Selectivity, α, is reported as:

$$\alpha = k'_2/k'_1 \tag{3}$$

For a further, in-depth discussion of general mobile phase optimization the work of Snyder *et al.*[11] is recommended. An in-depth discussion of the influence of mobile phase on k'_{av}, dk', and α for the NU column follows.

Binary mobile phases

Hexane–2-propanol and heptane–2-propanol. The non-polar solvents hexane and heptane by themselves play no active role in determining the strength of the solute–CSP interaction. Replacing hexane with heptane (Fig. 2A and B) produces no apparent difference in solute–CSP interaction, since, in each case, an increase in the 2-propanol concentration (increase in the mobile phase strength) produces a similar change in retention [k'_{av}]. Also, the selectivity (α) is similar with both mobile phases

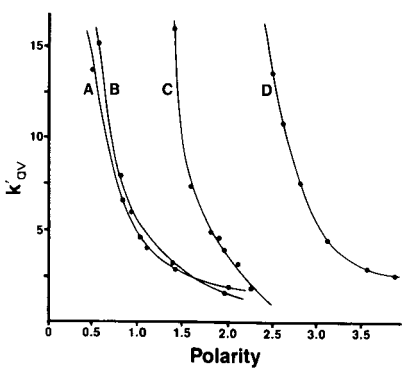

Fig. 2. Effect of mobile phase composition on retention of PEDNBA, showing k'_{av} *vs.* polarity for four binary mobile phases: hexane–2-propanol (A), heptane–2-propanol (B), hexane–chloroform (C), and hexane–dichloromethane (D). See Experimental for mobile phase compositions.

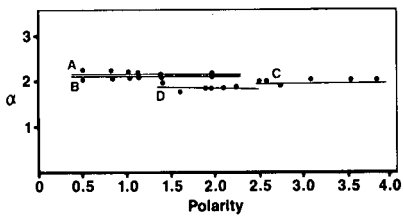

Fig. 3. Effect of mobile phase polarity on selectivity, showing α *vs.* polarity for four binary mobile phases: heptane–2-propanol (A), hexane–2-propanol (B), hexane–dichloromethane (C), and hexane–chloroform (D). See Experimental for mobile phase compositions.

(Fig. 3). This indicates that the stronger solvent, 2-propanol, competes more effectively at higher concentrations than the test solute for the polar sites on the CSP, thus causing a more rapid displacement of the latter. However, the difference in strength of the transient complexes remains equal, resulting in a constant α. Such effects are greatest for lower concentrations of 2-propanol (less than 0.5%), and fall off at higher concentrations. This could be due to nearly 1:1 interaction between 2-propanol and the CSP, indicating that solvation of the solute is not a major contributor to the reduction of k' with increasing 2-propanol concentration.

Hexane–dichloromethane. A trend similar to that discussed above is seen for hexane–dichloromethane mobile phases. In this case, a mobile phase polarity range of 1.6–2.4 gave k'_{av} reductions similar to those described before (Fig. 2C). This indicates that dichloromethane in a binary mobile phase produces a weaker mobile phase than 2-propanol. A higher mobile-phase strength is needed to elute the solute enantiomers. It is evident that, in competing with the solute–CSP interactions, the single dipole–dipole interaction produced by dichloromethane is not as effective as the reciprocal hydrogen bonding of 2-propanol.

Furthermore, when this mobile phase is used ($\alpha = 1.8$), the selectivity of the CSP is lower than with 2-propanol ($\alpha = 2.2$), but, as with hexane–2-propanol, α is independent of mobile phase strength. Selectivity is thus dependent on solvent type and not on mobile phase strength.

Hexane–chloroform. With chloroform in the mobile phase and polarity (P) ranging from 2.5 to 3.8, a higher mobile phase strength is required to produce a reduction in retention equivalent to that produced by the other binary mobile phases. This indicates that the proton-donating ability of chloroform is not as effective in reducing the overall solute–CSP interaction as the dipolar interaction of dichloromethane. The latter, in turn, is weaker than the reciprocal hydrogen bonding interaction of 2-propanol. In this case, also, the selectivity of the CSP remains constant ($\alpha = 2.0$) with increasing mobile phase strength, and is intermediate between that for 2-propanol and dichloromethane mobile phases.

From these observations, the active mobile phase components can be placed in the order 2-propanol > dichloromethane > chloroform for increasing solvent strength, and in the order 2-propanol > chloroform > dichloromethane for their ability to enhance the selectivity of the CSP. The minor variations in α, as observed in Fig. 3, also support the earlier statement that residuals play no significant role in chiral recognition influenced by polar mobile phase additives.

Ternary mobile phases

Hexane–2-propanol–methanol. Addition of methanol to hexane–2-propanol causes an initial increase in solute retention, k'_{av}, as seen in Fig. 4. In this figure k'_{av} and dk' are plotted against the change in polarity (ΔP) of the binary phase, caused by adding the modifier. As the methanol concentration increases from 0 to 2% (P increases from 0.01 to 0.05), dk' shows a negative deflection. The change in k'_{av} follows a similar but opposite trend, decreasing rapidly from 5.4 to 3.1. This implies that the change in k'_{av} is due entirely to the modifier. Addition of more than 2% methanol caused little additional change in retention.

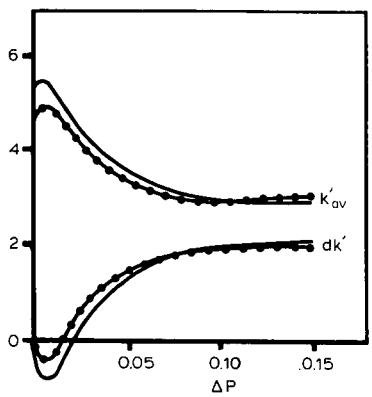

Fig. 4. Effect of mobile phase modifier concentration on PEDNBA retention, showing k'_{av} *vs.* ΔP and dk' *vs.* ΔP when hexane–2-propanol is modified with methanol (———) or acetonitrile (●—●). See Experimental for mobile phase compositions.

In Fig. 4, the increase in k'_{av} for $\Delta P < 0.02$ may be due to an initial interaction between 2-propanol and methanol, presumably weakening the solvent–CSP interaction and causing a stronger solute–CSP interaction. At higher concentrations, methanol displaces 2-propanol from the active sites on the CSP. When an equilibrium is established between methanol and the CSP, the methanol–solute competition lessens, and retention of the solute is no longer appreciably reduced by further addition of methanol.

Hexane–2-propanol–acetonitrile. When acetonitrile is added to a hexane–2-propanol mobile phase, in the same proportions as methanol, a similar trend is observed (Fig. 4): dk' initially decreases, then increases rapidly. A decrease in k'_{av} mirrors the increase in dk'. The initial interaction between acetonitrile and 2-propanol is somewhat smaller than that between methanol and 2-propanol, and the solvent–CSP interaction is larger, resulting in a reduction in the k'_{av} observed for acetonitrile. As for methanol, the fact that an increase in dk' corresponds to the decrease in k'_{av} shows that the decrease in k'_{av} is due solely to the increase in acetonitrile concentration.

It is interesting that the curves for methanol and acetonitrile in Fig. 4 flatten at approximately the same ΔP value (0.07). This could be related to the solvation strength of the solute–CSP interaction in the hexane–2-propanol binary phase.

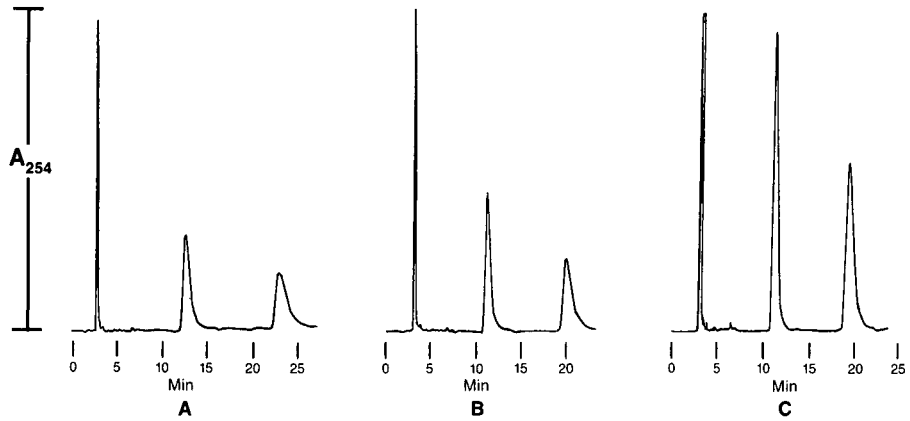

Fig. 5. Chromatograms showing the effects on retention and peak-shape, produced by adding 0.6% methanol (B) or acetonitrile (C) to hexane–2-propanol (75:25, v/v) (A).

Comparing the solvation interactions of methanol and acetonitrile, the effects caused by methanol are only minimally greater than with acetonitrile. The separation shown in Fig. 5A was obtained with hexane–2-propanol (75:25) as the mobile phase, while those in Fig. 5B and C were obtained by adding 0.6% methanol or acetonitrile, respectively. Both modifiers caused a reduction in k' and reduced peak tailing. Peak shape is most improved by using methanol, due to its stronger solvation effects.

Hexane–chloroform–methanol. When methanol is added to a hexane–chloroform mobile phase, k'_{av} decreases rapidly (Fig. 6) from 10.1 to 2.0 with a change in mobile-phase polarity of less than 0.02. As discussed previously, this decrease in k'_{av} is reflected in a corresponding increase in dk', indicating that the decrease in retention is due primarily to methanol in the mobile phase. Note that there is no initial methanol–chloroform interaction, as was seen with 2-propanol. Methanol competes directly with the solute for active sites on the CSP. Here, the drop in retention is more

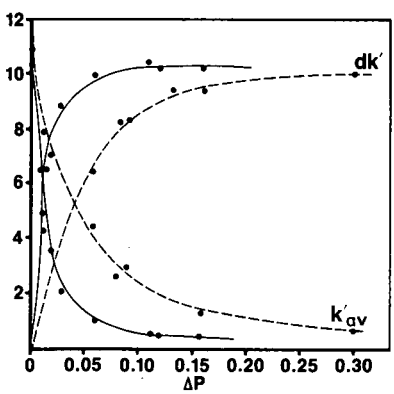

Fig. 6. Effect of mobile phase modifier concentration on PEDNBA retention, showing dk' *vs.* ΔP and k'_{av} *vs.* ΔP when hexane–chloroform is modified with methanol (———) or acetonitrile (– – –). See Experimental for mobile phase compositions.

rapid because methanol is a more interactive modifier in chloroform than in 2-propanol, and competes very strongly with the solute for active sites on the CSP.

Hexane–chloroform–acetonitrile. When acetonitrile is added to a hexane–chloroform mobile phase, k'_{av} drops less sharply than with methanol (Fig. 6), indicating that in this mobile phase, acetonitrile, although a polar modifier, is less interactive than methanol. Again, the corresponding rise in dk' indicates that the change in k'_{av} is due primarily to acetonitrile.

The difference in strength between methanol and acetonitrile is also seen in the polarity change required to cause k'_{av} to remain constant (flattened curve). For a similar decrease in retention, $\Delta P = 0.05$ and 0.17 for methanol and acetonitrile, respectively. Obviously, methanol is the stronger modifier.

The difference in the effects of the modifiers is seen in Fig. 7, in which the mobile phase is hexane–chloroform (38:62), and the modifier is 0.6% methanol or acetonitrile. Methanol has a much greater influence on retention and peak shape.

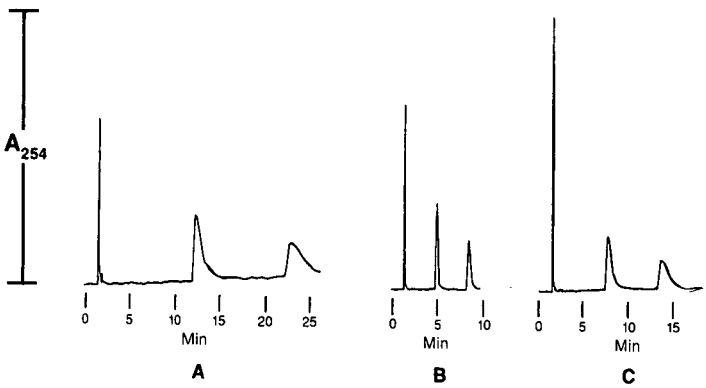

Fig. 7. Chromatograms showing the effects on retention and peak shape, produced by adding the methanol (B) or acetonitrile (C) to hexane–chloroform (A).

Hexane–dichloromethane–methanol. A ternary mobile phase, prepared by adding methanol to hexane–dichloromethane, shows a trend similar to that of the hexane–chloroform–methanol mobile phase (Fig. 8). This indicates that methanol is equally effective as a modifier in both binary mixtures, because it adjusts both to similar strengths. Retention becomes constant at $\Delta P = 0.05$.

Hexane–alcohol (80:20, v/v) binary phases

The effect of the steric bulk of mobile phase components on retention of the test solutes was investigated in mobile phases containing 20% (v/v) alcohol. Molarity differences for the various alcohols were not taken into account as the alcoholic portion of the varied mobile phases were in considerable molar excess when compared to the bonded stationary phase and chiral test solute in the chromatographic system. Fig. 9 shows that retention of the enantiomers increases, in a linear fashion, with the number of carbon atoms (steric bulk) of the alcohol in the mobile phase. Apparently, as steric interactions increase, the strength of the solute–CSP interactions decreases.

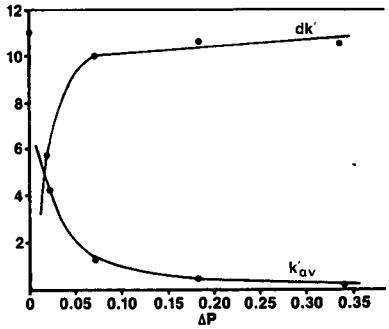

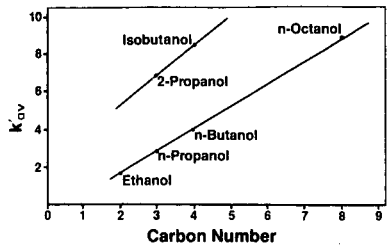

Fig. 8. Effect of modifier (methanol) concentration on PEDNBA retention, when added to a hexane–dichloromethane mobile phase. See Experimental for mobile phase compositions.

Fig. 9. Steric effect of alcohol modifiers on retention, showing k'_{av} *vs.* carbon number. Mobile phase, hexane–alcohol (80:20, v/v).

The two branched (hence more sterically hindered) alcohols produce greater retention of the test solute than their linear counterparts. In fact, 2-propanol and *n*-hexanol provide similar retention, and isobutanol provides retention similar to that from *n*-octanol. In other words, the branched alcohols provide retention similar to that of straight-chain alcohols having twice the carbon number. Compared to the linear alcohols, the steric bulk of the branched alcohols appears to reduce their ability to compete effectively with the solute for active sites on the CSP.

However, the branched alcohols impart greater selectivity to the CSP than their linear analogues. This is due to the fact that the branched alcohols allow the CSP to interact more strongly with the enantiomer that has the appropriate orientation, than with the less favorably oriented enantiomer. Chromatographically, the smaller alcohols allow better mass transfer than the larger alcohols (Fig. 10). Peak shapes in particular, are best with ethanol (Fig. 10A) or *n*-propanol (Fig. 10B).

Single-component mobile phases

Enantiomer separations obtained by using acetonitrile, 1,2-dichloroethane, and methyl *tert.*-butyl ether, as single-component mobile phases, are shown in Fig. 11. As expected, these solvents reduced retention of the test solutes in the order of increasing polarity: acetonitrile ($P = 5.87$) > 1,2-dichloroethane ($P = 3.5$) > methyl *tert.*-butyl ether ($P = 2.1$). The peak shape was best with acetonitrile and worst with methyl *tert.*-butyl ether. The strength of these solvents can be appropriately adjusted with weaker solvents, such as hexane.

General guidelines for method development

Although specific studies in this investigation were limited to one stationary phase and one test solute, these studies can serve as guidelines for developing methods, based on using the NU column or other π-donor, brush-type chiral stationary phases. The following summary of mobile phase trends, for PEDNBA, should apply generally for other chromatographic separations.

In the binary mobile phases, retention decreased when selective solvents were

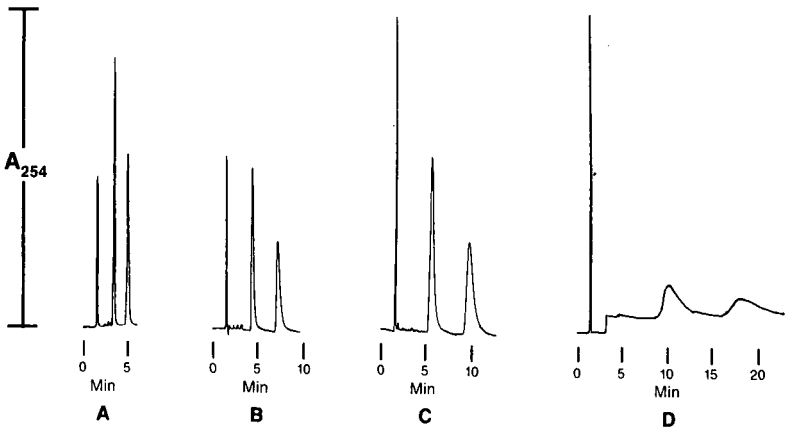

Fig. 10. Chromatograms showing the resolution of PEDNBA in hexane–ethanol (A), hexane–*n*-propanol (B), hexane–*n*-butanol (C), and hexane–*n*-octanol (D) (all 80:20, v/v).

added in the order 2-propanol > dichloromethane > chloroform (that is, proton acceptor > dipolar > proton donor). Also, k' increased with increasing chain length of *n*-alcohols when these were added (at the same concentration) to hexane. Branched alcohols caused longer retention than their linear analogues.

Addition of modifiers to the binary mobile phases caused a reduction in k' that corresponded with increasing modifier concentration. The largest decrease was seen with hexane–dichloromethane, and hexane–chloroform mobile phases to which methanol was added. In hexane–2-propanol, methanol and acetonitrile caused similar, but smaller, decreases in retention.

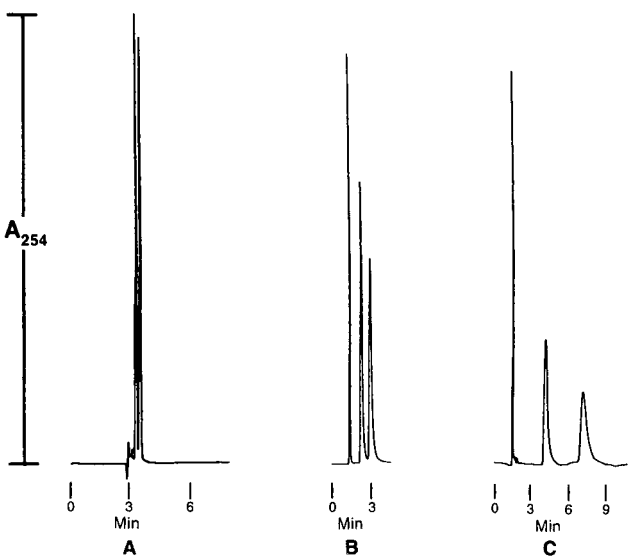

Fig. 11. Chromatograms showing the resolution of PEDNBA in the acetonitrile (A), 1,2-dichloroethane (B) and methyl *tert.*-butyl ether (C).

The separation factor for the isomers was largely independent of the composition of the mobile phase. Selectivity varied from 1.9 to 2.2 for 1,2-dichloroethane, acetonitrile, and methyl *tert.*-butyl ether single-component mobile phases, respectively. It was independent of component concentrations in all binary mobile phases and, in these cases, varied from 1.8 to 2.2. Selectivity was also unaffected by addition of small amounts of methanol or acetonitrile to a binary mobile phase. In all cases, sterically hindered (branched) alcohols gave higher α values than *n*-alcohols of the same carbon number.

Resolution of the isomers was greater in hexane–2-propanol than in any other binary mobile phase. Addition of modifiers increased resolution, methanol giving the largest increase, particularly in hexane–dichloromethane and hexane–chloroform.

CONCLUSIONS

The NU column shows good flexibility in use with numerous single-component, binary, and ternary mobile phases. Retention can be varied by changing mobile phase strength and composition. Selectivity was demonstrated to be mostly unaffected by changes in mobile phase strength, but was significantly influenced by mobile phase composition.

Organic modifiers, added to binary mobile phases at concentrations of less than 2%, influence both peak shape and retention. Methanol is a stronger mobile phase modifier than acetonitrile and exhibits a greater influence in a weak hexane–chloroform mobile phase than in hexane–2-propanol, suggesting that hydrogen bonding is the strongest modifier effect. At concentrations above 2.5%, such modifiers are only minimally effective at further reducing k'. Thus, a small quantity of a polar modifier can be used to modify a mobile phase to optimize a chiral separation.

REFERENCES

1 A. J. Roth and A. Kleeman, *Arzneistoffsynthese*, Thieme, Stuttgart/New York, 1982, p. XVII.
2 C. E. Dalgliesh, *J. Chem. Soc.*, 137 (1952) 3940.
3 W. H. Pirkle, M. H. Hyun and B. Bank, *J. Chromatogr.*, 316 (1984) 585.
4 W. H. Pirkle and T. C. Pochapsky, *Advan. Chromatogr.*, 27 (1987) 73.
5 C. H. Lochmüller and R. R. Ryall, *J. Chromatogr.*, 150 (1978) 511.
6 A. Dobashi and S. Hara, *J. Chromatogr.*, 267 (1983) 11.
7 C. H. Lochmüller, J. M. Harris and R. W. Souter, *J. Chromatogr.*, 71 (1972) 405.
8 I. W. Wainer, T. D. Doyle, F. S. Fry, Jr. and Z. Hamidzadeh, *J. Chromatogr.*, 355 (1986) 149.
9 C. H. Lochmüller and R. W. Souter, *J. Chromatogr.*, 113 (1975) 283.
10 M. Zief, L. J. Crane and J. Horvath, *J. Liq. Chromatogr.*, 7 (1984) 709.
11 L. R. Snyder, J. L. Glajch and J. J. Kirkland, *Practical HPLC Method Development*, Wiley-Interscience, New York, NY, 1988.

Journal of Chromatography, 461 (1989) 419–428
Elsevier Science Publishers B.V., Amsterdam — Printed in The Netherlands

CHROMSYMP. 1437

DETERMINATION OF THE ENANTIOMERS OF α-AMINO ACIDS AND α-AMINO ACID AMIDES BY HIGH-PERFORMANCE LIQUID CHROMATOGRAPHY WITH A CHIRAL MOBILE PHASE

A. DUCHATEAU*, M. CROMBACH, M. AUSSEMS and J. BONGERS
DSM Research, P.O. Box 18, 6160 MD Geleen (The Netherlands)

SUMMARY

A high-performance liquid chromatographic method for the enantiomeric analysis of a mixture of an α-amino acid and the corresponding acid amide is described. Reversed-phase chromatography with copper(II) acetate and N,N-di-*n*-propyl-L-alanine in the mobile phase are used for the separation. For Val and Val-NH_2, several parameters affecting retention and enantioselectivity were investigated. The results indicate that by manipulation of pH, ionic strength, temperature, concentration of Cu^{II}, N,N-di-*n*-propyl-L-alanine and ion-pairing reagent, good control of enantiomeric separation can be achieved. For α-amino acid amides a mechanism is proposed which may account for the retention and enantioselectivity. Examples of enantiomeric analysis of mixtures of α-amino acids and α-amino acid amides with aliphatic, aromatic and polar side-chains are given. The method can be used for the control of the enantiomeric purity of α-amino acids and the corresponding acid amides obtained by enantioselective synthesis.

INTRODUCTION

One of the routes to optically pure α-amino acids (α-AA) is through organic synthesis of racemic α-amino acid amides (α-AA-NH_2), followed by the use of a broad-specificity peptidase to achieve resolution on a large scale. In conjunction with this synthesis, analytical methods are required for the control of the enantiomeric purity of both α-AA and α-AA-NH_2. High-performance liquid chromatographic (HPLC) methods for the enantiomeric resolution of α-AA using a chiral copper complex as an additive to the mobile phase have been known for several years. Lindner and Hirschböck[1] recently summarized enantioselective HPLC systems generated by the mobile-phase additive mode. Copper complexes of N,N-di-*n*-propyl-L-alanine (L-DPA) were introduced by Weinstein *et al.*[2] and appeared to resolve the common protein amino acids. Davankov *et al.*[3] reported the resolution of valinamide into its enantiomers by ligand-exchange chromatography.

The aim of this work was to develop an HPLC method for the enantiomeric resolution of an α-AA together with the corresponding α-AA-NH_2. For this, we made use of copper complexes of L-DPA. We studied the influence of several mobile phase

0021-9673/89/$03.50

parameters in order to optimize the enantiomeric separation of the α-AA and the corresponding α-AA-NH_2. A model is proposed for the enantiomeric resolution of α-AA-NH_2 by the use of copper complexes of L-DPA.

EXPERIMENTAL

Materials

α-AA and α-AA-NH_2 were obtained from Sigma (St. Louis, MO, U.S.A.) or synthesized in our laboratory[4]. For each compound, both the racemic form and at least one optically pure enantiomer were available. L-DPA was prepared according to the method of Bowman and Stroud[5]. The pairing ion laurylsulphonate and *o*-phthalaldehyde (OPA) were obtained from Merck (Darmstadt, F.R.G.). 2-Mercaptoethanol (MCE) was supplied by Fluka (Buchs, Switzerland). Water was purified with a Milli-Q system. HPLC-grade acetonitrile and ethanol were obtained from Merck and used as supplied. All other chemicals were of analytical-reagent grade.

Instrumentation

The chromatographic system consisted of a Hewlett-Packard (Palo Alto, CA, U.S.A.) Model 1081B liquid chromatograph, a Rheodyne (Cotati, CA, U.S.A.) 7010 injection valve for manual injection or a Micromeritics (Norcross, GA, U.S.A.) Model 725 autosampler for automated injection. The injection loop had a 20-μl capacity. The columns used were Nucleosil 120-C_{18} (250 × 4.0 mm I.D., 5 μm, and 125 × 4.0 mm I.D., 3 μm) and Polygosil 60-C_{18} (125 × 4.0 mm I.D., 5 μm) from Macherey, Nagel & Co. (Düren, F.R.G.) and Hypersil-ODS (200 × 4.6 mm I.D., 5 μm) from Hewlett-Packard. The flow-rate was 1 ml/min and the column temperature was kept at 40°C.

For reaction detection with OPA–MCE, the reagent was added to the column effluent by a mixing T. Post-column addition of reagent was effected with a Gilson (Villiers-le-Bel, France) Model 302 pump at a flow-rate of 1 ml/min. The OPA–MCE reaction was carried out in a coiled capillary stainless-steel tube (12 m × 0.35 mm I.D., coil diameter 12 mm) at 40°C. The fluorophores were monitored with a Waters Assoc. (Milford, MA, U.S.A.) Model 420 fluorescence detector. For excitation a 338-nm band-pass filter and for emission a 415-nm long-pass filter were used. Quantitation was performed with a Hewlett-Packard 3350 Laboratory Automation System.

Eluent, reagent and sample preparation

The mobile phase consisted of copper(II) acetate, L-DPA and triethylamine (TEA), titrated to the required pH with acetic acid. The concentration of the mobile phase components and the eluent pH varied, depending on the experiment, and are indicated in the figures. The OPA–MCE reagent was a mixture of potassium borate buffer (0.4 *M*, pH 10.0), OPA (6 m*M*), MCE (0.1%), ethanol (1.0%) and EDTA (30 m*M*). The chelating agent, EDTA, was added to the reagent in order to avoid precipitation of copper(II) hydroxide in the reaction coil under the alkaline conditions applied. The Cu(L-DPA)$_2$ solution consisted of copper(II) acetate and L-DPA in a concentration ratio of 1:2. Standards and samples were dissolved in the eluent.

RESULTS AND DISCUSSION

Effects controlling retention and enantioselectivity

With Val–Val-NH_2 and α-Ph-Gly–α-Ph-Gly-NH_2 as model compounds, we initially used the chromatographic conditions described by Weinstein *et al.*[2] to obtain enantiomeric resolution. Under these conditions, the α-AA-NH_2 showed tailing peaks and the enantiomers were only partially resolved. For the α-AA, good enantioselectivity was obtained ($\alpha > 2$). However, with Val–Val-NH_2, the L-Val-NH_2 peak overlapped with the D-Val peak.

In order to optimize the enantiomeric separation of a mixture of an α-AA and the corresponding α-AA-NH_2, we studied the influence of the following factors on the chromatographic behaviour of Val and Val-NH_2 enantiomers: TEA concentration, pH of the eluent, concentrations of Cu^{II}, L-DPA and Cu(L-DPA)$_2$, column temperature, ionic strength and concentration of laurylsulphonate in the eluent.

Effect of triethylamine

The peak tailing that we observed for α-AA-NH_2 may result from interactions of the polar amide function with free silanol sites on the reversed-phase column. A well known technique to suppress this tailing phenomenon is the addition of a competitive amine (*e.g.*, TEA) to the mobile phase. Fig. 1A shows the asymmetry factor (A_s) and resolution (R_s) of the enantiomers of Val-NH_2 as a function of TEA concentration from 0 to 5 m*M*. As shown by A_s, the peak symmetry of the enantiomers is improved by the addition of TEA to the eluent, and consequently the enantiomeric resolution increases. With respect to the capacity factors (k') and separation factors (α) of the enantiomers of Val and Val-NH_2, a decrease in these parameters can be seen when TEA is used in the concentration range 0.5–5 m*M* (Fig. 1B). Because TEA forms complexes with Cu^{II}, the TEA molecules will compete as ligands with the Val and Val-NH_2 enantiomers for the formation of the mixed-ligand complex, thus lowering k' with increasing TEA concentration. Use of a 5 m*M* concentration of TEA resulted in increased background noise and an unstable baseline. In subsequent experiments, we therefore used the minimum TEA concentration (0.5–1.0 m*M*) at which baseline resolution for the enantiomers of Val-NH_2 is obtained.

Effect of pH

For the enantiomeric separation of amino acids, Weinstein[6] suggested that ligand exchange may take place between the binary Cu(L-DPA)$_2$ complex and the enantiomers of the amino acids. In order to be coordinated as a bidentate ligand to Cu^{II}, the amino acid must possess an unprotonated amine group and an acid function in the anionic form[7–9]. With an α-AA-NH_2, coordination may take place via interactions of Cu^{II} with the unprotonated α-amino group and nitrogen of the acid amide group.

As a result, the formation of copper amino acid (amide) complexes will be strongly pH dependent. The influence of the eluent pH on the k' and α values of the enantiomers of Val and Val-NH_2 was studied over the pH range 3.5–5.5 (Fig. 1C). In order to avoid precipitation of copper(II) hydroxide, pH values above 5.5 were not studied.

The k' values of the Val enantiomers increase as the eluent pH rises. A similar

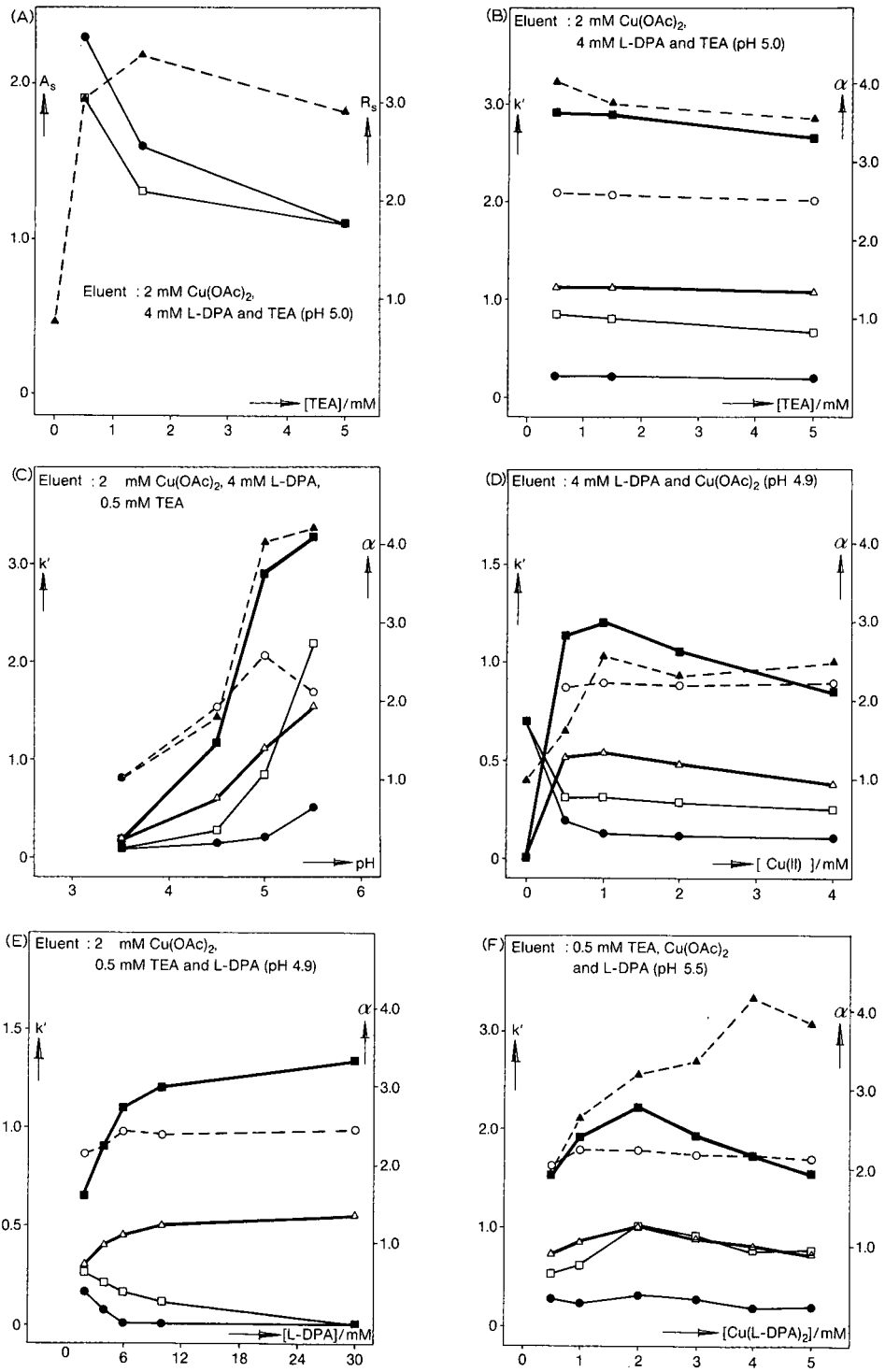
(A)
A_s
R_s
Eluent : 2 mM $Cu(OAc)_2$,
4 mM L-DPA and TEA (pH 5.0)
[TEA]/mM
(B)
Eluent : 2 mM $Cu(OAc)_2$,
4 mM L-DPA and TEA (pH 5.0)
k'
α
[TEA]/mM
(C)
Eluent : 2 mM $Cu(OAc)_2$, 4 mM L-DPA,
0.5 mM TEA
k'
α
pH
(D)
Eluent : 4 mM L-DPA and $Cu(OAc)_2$ (pH 4.9)
k'
α
[Cu(II)]/mM
(E)
Eluent : 2 mM $Cu(OAc)_2$,
0.5 mM TEA and L-DPA (pH 4.9)
k'
α
[L-DPA]/mM
(F)
Eluent : 0.5 mM TEA, $Cu(OAc)_2$
and L-DPA (pH 5.5)
k'
α
$[Cu(L\text{-}DPA)_2]$/mM

Fig. 1.

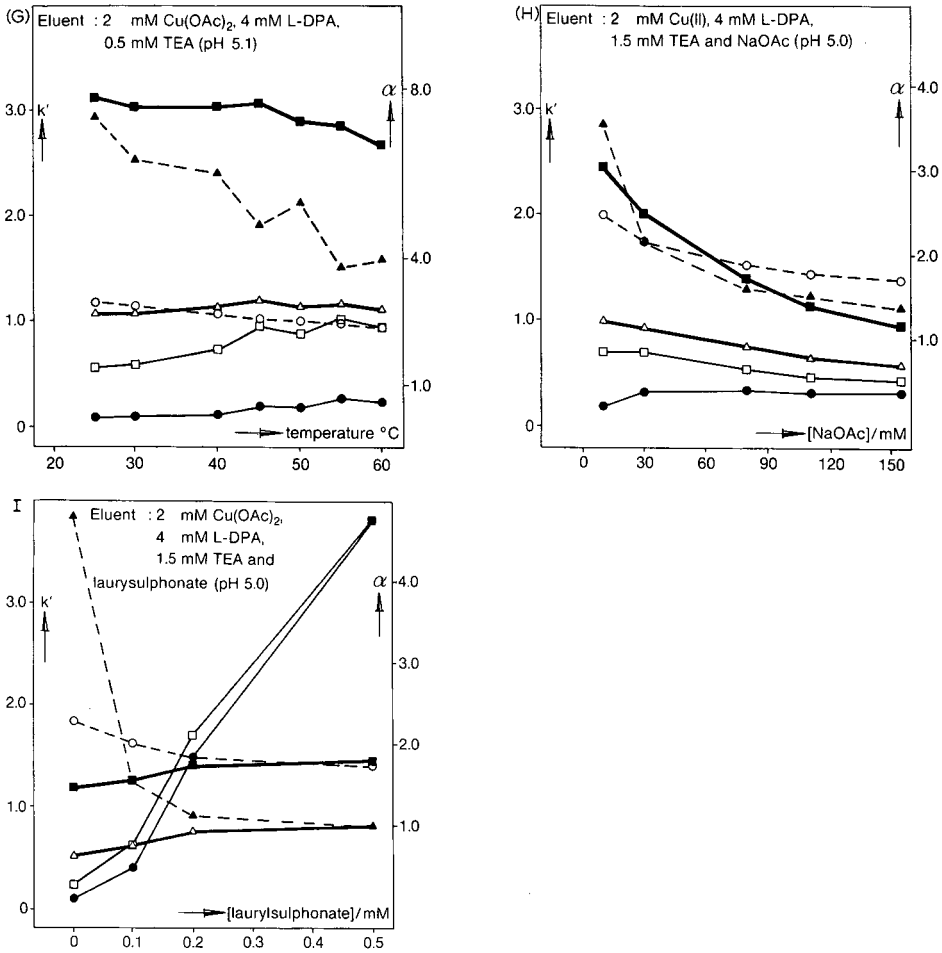

Fig. 1. Effect of (A, B) triethylamine concentration, (C) eluent pH, concentrations of (D) Cu^{II}, (E) L-DPA and (F) Cu(L-DPA)$_2$, (G) column temperature, (H) ionic strength and (I) laurylsulphonate concentration on the retention and selectivity of Val and Val-NH_2 enantiomers. Columns: (A, B, C, G, H) Hypersil ODS and (D, E, F, I) Polygosil 60-C_{18}. For other conditions, see Experimental. k': △, D-Val; ■, L-Val; ●, D-Val-NH_2; □, L-Val-NH_2. α: ○, D,L-Val; ▲, D,L-Val-NH_2.

effect is observed for the α-value. For the Val-NH_2 enantiomers, the retention and selectivity also increase with increasing pH. However, the increase is much steeper than with Val. Above pH 5, the elution order of L-Val-NH_2 and D-Val is reversed. The increase in k' and α of the compounds studied can be explained as follows: decreasing the acidity of the eluent favours deprotonation of the ammonium group of Val and Val-NH_2 and thus enhances the formation of mixed-ligand copper complexes, which are assumed to be primarily responsible for both the retention and enantioselectivity. The marked increase in the k' value of Val-NH_2 compared with Val can be explained in terms of the basicity of these compounds. The α-NH_2-function of Val-NH_2 is less basic than that of Val (Δ p$K_a \approx 2$).

Starting from the ammonium form of Val and Val-NH_2 at pH 3.5, an increase in the eluent pH will first generate the unprotonated α-NH_2 of Val-NH_2 and only after a further increase in the pH will the α-NH_2 function of Val be deprotonated and thus be able to form mixed-ligand copper complexes. From this study, it is clear that the eluent pH is a powerful device for tailoring the resolution of the enantiomers of an α-AA and the corresponding α-AA-NH_2.

Effect of Cu^{II}

At a constant concentration of L-DPA, the influence of the Cu^{II} concentration in the eluent on the k' and α values of the enantiomers of Val and Val-NH_2 was studied (Fig. 1D). In the absence of Cu^{II}, no retention was obtained for Val. On addition of 0.5 m*M* Cu^{II}, retention occurred for the Val enantiomers. At Cu^{II} concentrations above 1 m*M*, a slight decrease in k' for both Val enantiomers was seen. However, the enantioselectivity remained constant at Cu^{II} concentrations above 1 m*M*.

The effect of the Cu^{II} concentration on the retention and enantioselectivity of Val-NH_2 is remarkable. In the absence of Cu^{II}, a higher k' for the enantiomers is obtained than in the presence of Cu^{II}. An increase in the Cu^{II} concentration results in a further decrease in the retention of the Val-NH_2 enantiomers. The increase in k' and α of the Val enantiomers in the Cu^{II} concentration range 0–1 m*M* is caused by the formation of Cu^{II}–L-DPA complexes, which will act as exchange sites for the enantiomers for the formation of mixed-ligand complexes.

An explanation for the decrease of the k' values of the Val-NH_2 enantiomers in the Cu^{II} concentration range 0–1 m*M* may be as follows: in the absence of Cu^{II}, the interaction of the hydrophobic part of the Val-NH_2 molecules with the reversed-phase matrix will produce retention. However, the tailing peak of Val-NH_2, in the absence of a competitive base, points to another interaction with the stationary phase, namely the interaction of the polar acid amide groups with the free silanol sites in the matrix. This interaction will give an additional increase in retention. In the presence of Cu^{II}, mixed-ligand complexes of Val-NH_2 with Cu^{II}–L-DPA will be formed. In the resulting complex the polar acid amide group will be coordinated with Cu^{II} and thus be unavailable to undergo interaction with the free silanol sites in the matrix. The absence of the latter interaction may explain the observed decrease in retention when the Cu^{II}–L-DPA system is used.

The addition of copper(II) acetate to the mobile phase will cause an increase in ionic strength, which may explain the slight decrease in the retention of both Val and Val-NH_2 enantiomers at Cu^{II} concentrations above 1 m*M*.

Effect of L-DPA

The influence of the L-DPA concentration in the eluent at a constant Cu^{II} concentration on the k' and α values of the enantiomers of Val and Val-NH_2 was studied (Fig. 1E). An increase in the L-DPA concentration results in an increase in the α and k' values of the Val enantiomers.

For the acid amide enantiomers, an opposite effect can be seen. Increasing the L-DPA concentration leads to a decrease in the k' values of the Val-NH_2 enantiomers and a diminution of enantioselectivity. The equilibrium reactions for the formation of the binary Cu (L-DPA)$_2$ complex can be written as

$$Cu^{2+} + \text{L-DPA}^- \rightleftharpoons [Cu(\text{L-DPA})]^+ \quad (1)$$

$$[Cu(\text{L-DPA})]^+ + \text{L-DPA}^- \rightleftharpoons [Cu(\text{L-DPA})_2] \quad (2)$$

These equilibria will be influenced by the pH of the eluent, which will determine the ionization state of the L-DPA (anion, zwitterion or cation) and by the Cu^{II}:L-DPA concentration ratio. Considering the starting conditions in Fig. 1E (2 m*M* Cu^{II}, 2 m*M* L-DPA, pH 4.9), both $[Cu(\text{L-DPA})]^+$ and $[Cu(\text{L-DPA})_2]$ will be present in the eluent. On introduction of the α-AA and α-AA-NH_2 enantiomers into the eluent, two reactions can lead to mixed-ligand complex formation. For example, for the L-form of the α-AA these reactions can be written as

$$[Cu(\text{L-DPA})_2] + \text{L-AA}^- \rightleftharpoons [(\text{L-AA})Cu\ (\text{L-DPA})] + \text{L-DPA}^- \quad (3)$$

$$[Cu(\text{L-DPA})]^+ + \text{L-AA}^- \rightleftharpoons [(\text{L-AA})Cu\ (\text{L-DPA})] \quad (4)$$

Only in reaction 3 does ligand exchange take place. In reaction 4 mixed-ligand complexes are formed without exchange. Increasing the L-DPA concentration in the eluent at a constant Cu^{II} concentration will shift the equilibria of reactions 1 and 2 to the right, resulting in a higher concentration of $Cu(\text{L-DPA})_2$ complexes. This implies that more interaction sites become available for the enantiomers to form mixed-ligand complexes.

The increase in the *k'* values for the Val enantiomers can therefore be explained in terms of an increase in mixed (L-Val)Cu(L-DPA) and (D-Val)Cu(L-DPA) complexes formed by ligand exchange. For the Val-NH_2 enantiomers it is unlikely that the formation of mixed-ligand complexes will proceed via ligand exchange. This can be seen by comparing tabulated equilibrium constants[10] for the reaction

$$Cu^{II} + L \rightleftharpoons Cu^{II}L \quad (5)$$

With Gly–Gly-NH_2 the highest equilibrium constant is found for the α-AA. This indicates that the coordination of an α-AA to Cu^{II} is much stronger than that of an α-AA-NH_2. Therefore, it is very doubtful that an α-AA-NH_2 (*e.g.*, Val-NH_2) will displace an α-AA (*e.g.*, L-DPA) from Cu^{II}. The data we found for the Val-NH_2 enantiomers (Fig. 1E) can be explained on the basis of reaction 4. Increasing the L-DPA concentration in the eluent will lead to an increase in $Cu(\text{L-DPA})_2$ complexes and a decrease in $[Cu(\text{L-DPA})]^+$. This decrease means that the equilibrium of reaction 4 is shifted to the left, resulting in fewer $[(\text{L-Val-NH}_2)Cu(\text{L-DPA})]^+$ and $[(\text{D-Val-NH}_2)Cu(\text{L-DPA})]^+$ complexes. This in turn results in a decrease in the *k'* values of the Val-NH_2 enantiomers (Fig. 1E). The formation of mixed-ligand complexes involving α-Val-NH_2 may therefore proceed preferentially under the conditions where the L-DPA:Cu^{II} concentration ratio is 1 rather than at higher ratios. For α-hydroxy acids it has also been suggested that a 1:1 ratio of Cu^{II} and L-Pro (as chiral selector) is important for the formation of mixed-ligand complexes[7].

Effect of Cu(L-DPA)$_2$ concentration

The influence of the $Cu(\text{L-DPA})_2$ concentration in the eluent on the *k'* and α values of Val and Val-NH_2 enantiomers is presented in Fig. 1F. From 0.5 to 2 m*M*

Cu(L-DPA)$_2$, the k' values for both Val and Val-NH$_2$ enantiomers increase, whereas above 2 m*M* Cu(L-DPA)$_2$ a decrease in the k' values of all enantiomers can be seen. The α value for the Val enantiomers slowly decreases, whereas for the Val-NH$_2$ enantiomers the increase in α continues at Cu(L-DPA)$_2$ concentrations above 2 m*M*. If the Cu(L-DPA)$_2$ concentration in the eluent is lower than the concentration at which the stationary phase is saturated, retention and selectivity will be determined by the amount of [Cu(L-DPA)$_2$] and [Cu(L-DPA)]$^+$ adsorbed on the stationary phase. The behaviour of k' and α in the range 0.5–2 m*M* Cu(L-DPA)$_2$ therefore seems to originate from the loading of the stationary phase with the chiral complexes. Once the stationary phase is saturated with [Cu(L-DPA)$_2$] and [Cu(L-DPA)]$^+$, further addition of Cu(L-DPA)$_2$ will increase its concentration in the mobile phase. The enhancement of the electrolyte concentration probably accounts for the decrease in retention observed at Cu(L-DPA)$_2$ concentrations above 2 m*M*.

The two *n*-propyl chains of L-DPA may play an important role in the observed behaviour of the enantiomers studied, as a similar mechanism for the retention and enantioselectivity has been proposed for other chiral ligands with long alkyl side-chains[8,11–13].

Effect of column temperature

As the equilibria in the present system should be temperature-dependent, the effect of column temperature was studied. In Fig. 1G, the influence of temperature on the k' and α values of Val and Val-NH$_2$ enantiomers is given. For L-Val a decrease in k' can be seen, whereas the k' of D-Val remains nearly constant on raising the column temperature. The enantioselectivity for Val decreases. For the Val-NH$_2$ enantiomers the k' values increase on increasing the temperature. The latter effect could be explained by a shift of equilibrium 4 towards the mixed-ligand complex. However, in this instance one would expect an increase in the enantioselectivity of Val-NH$_2$; however, this is not observed (Fig. 1G). The explanation of the increase in the k' values of Val-NH$_2$ enantiomers, together with the decrease in enantioselectivity, is therefore not clear to us.

Effect of ionic strength

To investigate the importance of electrostatic effects, the influence of ionic strength on the k' and α values of Val and Val-NH$_2$ enantiomers was studied (Fig. 1H). The ionic strength of the eluent was regulated by means of sodium acetate. Over the concentration range studied the k' and α values of Val and Val-NH$_2$ enantiomers decreased. The decrease was most noticeable at low concentrations of acetate, where the drop in k' and α is fairly rapid. At higher concentrations the change in k' and α is much more moderate.

Effect of alkylsulphonate

Aliphatic α-AA and α-AA-NH$_2$ with small hydrophobic side-chains (*e.g.*, Ala–Ala-NH$_2$) had low k' values in the chromatographic system employed. In order to increase the retention of these compounds, the influence of an ion-pairing reagent in the eluent on the k' and α values of the enantiomers of Val and Val-NH$_2$ was studied (Fig. 1I). Laurylsulphonate was chosen for ion-pair formation.

For the Val enantiomers, a moderate increase in the k' values was obtained over

the range 0–0.5 m*M*. The enantioselectivity decreased over this range. The Val-NH_2 enantiomers showed a steep increase in k' at increasing sulphonate concentration, while a rapid drop in enantioselectivity occurred, resulting in a loss of selectivity at a concentration of 0.5 m*M*. The increase in retention and the decrease in enantioselectivity can be explained by assuming a competition between mixed-ligand formation and ion-pair formation. Because the coordination of an α-AA-NH_2 to Cu^{II} is much weaker than that of an α-AA[10], the effect of the ion-pairing reagent is greatest on Val-NH_2 (Fig. 1I). This study indicates that the use of an ion-pairing reagent may be a device for enhancing the retention of enantiomers with low k' values; however, its use is limited to some extent as the enantioselectivity decreases. Another important aspect of the use of an ion-pairing reagent is the fact that it is a powerful device for discriminating between an α-AA and α-AA-NH_2. If enantiomeric reolution of an α-AA is vitiated by overlap with the corresponding α-AA-NH_2, the use of an ion-pairing reagent may be useful in eliminating the interference effect.

Chromatography

The feasibility of the separation system was tested for DL-β-methyl-Ala, DL-Met, DL-α-phenyl-Gly, DL-Phe, DL-β-benzyl-Ala and their corresponding amides. For all compounds tested a separation of the amino acid and the amide enantiomers could be achieved. The α-AA-NH_2 enantiomers were eluted before the α-AA enantiomers and in all instances the D-enantiomer was eluted before the L-enantiomer. With the hydrophobic β-benzyl-Ala and β-benzyl-Ala-NH_2, acetonitrile was added to the mobile phase to shorten the retention times. A representative chromatogram of a sample from a process stream is given in Fig. 2.

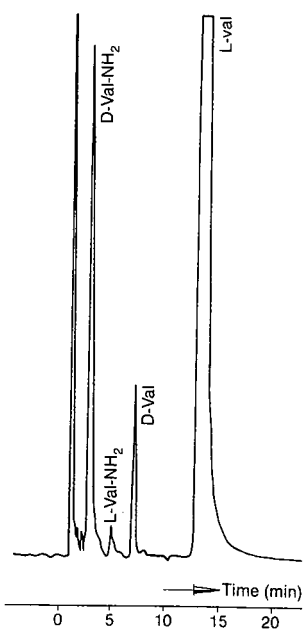

Fig. 2. Chromatogram of a sample from L-Val synthesis. Column: Nucleosil 120-5C_{18}. Mobile phase: 2 m*M* copper(II) acetate–4 m*M* L-DPA–1 m*M* TEA (pH 5.1). For other conditions, see Experimental.

Quantitative determinations were carried out by comparing the peak areas of samples with those of standard solutions, employing the external standard method. As an example of the linearity, precision and detection limit of the method, these data are given for Val and Val-NH_2. The linearity of the amount *versus* response relationship was established over the ranges 3–40 nmol (DL-Val) and 10–75 nmol (DL-Val-NH_2). Linear regression analysis from calibration graphs indicated that the correlation coefficients for the enantiomers were 0.9997 (Val) and 0.9998 (Val-NH_2). The within-run precision of the assay gave a coefficient of variation of $\leqslant 2\%$ for both Val and Val-NH_2. The detection limits, calculated as two times the noise ratio, and expressed in terms of picomoles of the compounds injected, were 20 and 400 for Val and Val-NH_2, respectively.

REFERENCES

1 W. F. Lindner and I. Hirschböck, *J. Liq. Chromatogr.*, 9 (1986) 551.
2 S. Weinstein, M. H. Engel and P. E. Hare, *Anal. Biochem.*, 121 (1982) 370.
3 V. A. Davankov, S. V. Rogoshin, I. I. Peslyakas, A. V. Semichkin and T. P. Sachkova, *Dokl. Akad. Nauk SSR*, 201 (1971) 854.
4 E. M. Meijer, W. H. J. Boesten, H. E. Schoemaker and J. A. M. van Balken, in J. Tramper, H. C. van der Plas and P. Linko (Editors), *Biocatalysis in Organic Synthesis*, Elsevier, Amsterdam, 1985, p. 135.
5 R. E. Bowman and H. H. Stroud, *J. Chem. Soc.*, (1950) 1342.
6 S. Weinstein, *Angew. Chem., Int. Ed. Engl.*, 21 (1982) 218.
7 R. Horikawa, H. Sakamoto and T. Tanimura, *J. Liq. Chromatogr.*, 9 (1986) 537.
8 V. A. Davankov, A. S. Bochkov, A. A. Kurganov, P. Roumeliotis and K. K. Unger, *Chromatographia*, 13 (1980) 677.
9 P. E. Hare and E. Gil-Av, *Science (Washington, D.C.)*, 204 (1979) 1226.
10 A. E. Martell (Editor), *Stability Constants, Supplement No. 1*, Special Publication No. 25, Chemical Society, London, 1971.
11 J. N. LePage, W. Lindner, G. Davies, D. E. Seitz and B. L. Karger, *Anal. Chem.*, 51 (1979) 433.
12 W. Lindner, J. N. LePage, G. Davies, D. E. Seitz and B. L. Karger, *J. Chromatogr.*, 185 (1979) 323.
13 Y. Tapuhi, N. Miller and B. L. Karger, *J. Chromatogr.*, 205 (1981) 325.

Journal of Chromatography, 461 (1989) 429–441
Elsevier Science Publishers B.V., Amsterdam — Printed in The Netherlands

CHROMSYMP. 1507

INDIRECT DETECTION IN REVERSED-PHASE LIQUID CHROMATOGRAPHY

RESPONSE DEVIATIONS IN ION-PAIRING SYSTEMS

E. ARVIDSSON

Department of Analytical Pharmaceutical Chemistry, Uppsala University Biomedical Center, P.O. Box 574, S-751 23 Uppsala (Sweden)

J. CROMMEN

Department of Analytical Chemistry, Institute of Pharmacy, University of Liège, rue Fusch 5, B-4000 Liège (Belgium)

G. SCHILL and D. WESTERLUND*

Department of Analytical Pharmaceutical Chemistry, Uppsala University Biomedical Center, P.O. Box 574, S-751 23 Uppsala (Sweden)

SUMMARY

Deviation effects in indirect detection have been studied in ion-pairing systems with several retained components in the eluent. The response extinction or reversal that appears in certain retention ranges have been given a theoretical explanation. Other response disturbances and peak deformations have been explained as due to pH instability and/or protolysis of the detectable eluent component (the probe) in the migrating compound zones. Principles are given for the design of indirect detection systems to optimize the sensitivity and avoid detection disturbances.

INTRODUCTION

Indirect detection is a technique applied in chromatography to visualize compounds with low or no inherent detectable (UV, fluorescence, electrochemical) properties[1–3]. It is technically based on the use of a mobile phase containing a component with a detector response. The detectable component (the probe) can be charged, and it is then distributed to the solid phase as an ion pair(s) and its retention can then easily be regulated by the nature and the concentration of the counter ion(s). Uncharged compounds can also be used as probes[4], but the regulation of the retention must then be made by other means.

The indirect detection effects are due to disturbances of established equilibria that occur in the injection zone on application of a sample. These disturbances will affect all components in the system that are coupled by a common interaction, which in reversed-phase chromatography normally is the competition for the limited binding capacity of the adsorbent. The equilibrium displacements will affect the concen-

0021-9673/89/$03.50

trations of all retained mobile phase components, and all affected compounds will migrate as separate zones through the column. The migrating zones of the solutes injected as well as of the eluent components will contain a mobile phase with a composition different from the normal one and will appear as peaks in the chromatogram, even though only one mobile phase component, the probe, gives detectable response. The peaks representing the analytes (solute peaks) and the mobile phase components (system peaks) can be positive or negative depending on the charge and the retention of the compound relative to that of the probe.

The theoretical background for the indirect detection technique has been presented in recent publications[5–7]. Quantitative expressions for the response in reversed-phase ion-pairing systems have been developed. They are valid for systems where one ion pair of the probe is the dominating competitor for the solute, as demonstrated by the existence of only one system peak with significant retention. Such conditions can occur when the remaining components in the mobile phase are hydrophilic buffering agents and the adsorbent is alkyl- or aryl-bonded silica. The simple relationship between the response and the retention of the solute relative to the probe is not valid when several retained system peaks appear in the chromatogram. This indicates that several ion pairs in the mobile phase compete for the adsorbent, and it can occur, *e.g.*, when the solid phase is highly hydrophobic. A theoretical approach to the response in such systems is presented in this paper.

The indirect detection is due to changes in the baseline absorbance that often are smaller than $\pm$ 1%. Solute and system peaks show good symmetry and have about the same width as in direct detection. However, extra peaks and peak deformation are sometimes observed in ion-pairing systems. The deviations can be combined with changes in retention that depend on the amount of sample, which indicates that the systems are unstable. The background to the disturbances is discussed in this paper and recommendations for the construction of ion-pairing indirect detection systems are given.

EXPERIMENTAL

Butylamine hydrochloride and 1-methylpyridinium hydrogensulphate (MP) were obtained from Eastman-Kodak (Rochester, NY, U.S.A.). Sodium 6-hydroxy-naphthalene-2-sulphonate (60HNS) and 3-hydroxybenzoic acid (30HBA) were obtained from E. Merck (Darmstadt, F.R.G.). They were recrystallized from water before use. All other chemicals were of analytical grade and were used without further purification.

The detector used was a LDC Spectromonitor III. The pump was an Altex 100 A, and the injector a Rheodyne 7125 with a loop volume of 25 μl.

μBondapak Phenyl (10 μm) (Waters Assoc., Milford, MA, U.SA.) and PRP-1 (10 μm) (Hamilton, Bonaduz, Switzerland) were used as the solid phases. They were packed by the slurry technique in columns of sizes 100 mm $\times$ 4.6 mm I.D. or 100 mm $\times$ 3.2 mm I.D. Part of the studies was performed with a PLRP-S (5 μm) prepacked column, 150 mm $\times$ 4.6 mm I.D., from Polymer Laboratories (Amherst, MA, U.S.A.).

The mobile phases were aqueous solutions, containing a detectable ion, NP, 60HNS or 30HBA, buffering agents and in some cases an organic solvent in low concentrations. The mobile phase flow-rate was 0.50 ml/min.

The eluent reservoir, injector column and connecting tubes were thermostatted at 25.0°C in a water-bath in order to eliminate the disturbances of temperature fluctuations.

The samples were injected, dissolved in the mobile phase. The capacity factors were calculated from $k' = (V_R - V_m)/V_m$, where V_m, the volume of mobile phase in the column, was obtained from the front peak of the chromatogram.

The detection wavelength was 254 nm when using 60HNS or 30HBA as the probe, 272 nm when using MP and 270 nm when 40HBA was the detectable component.

RESULTS AND DISCUSSION

Theoretical background for indirect detection in ion-pairing systems

Reversed-phase ion-pair chromatography gives many possibilities for adjusting the retention of the ionic compounds in the system. Ionic analytes and mobile phase components compete for the limited binding capacity of the adsorbent. The injection of a solute gives rise to a change in the distribution at the injection zone of the adsorbed compounds. In analytical applications the disturbances are so small that the distribution behaviour of the different compounds can be described by linear expressions, such as

$$\Delta C_{i,s} = C_{i,s} - C^{\circ}_{i,s} = \sum_{j=1}^{n} a_{i,j} \cdot \Delta C_{j,m} \quad (1)$$

where $C_{j,m}$ is the concentration of j in the mobile phase, $C_{i,s}$ is the quotient of the amount of i in the stationary phase to the volume of mobile phase in the column, $\Delta C_{i,s}$ is the change in the concentration of any compound i in the stationary phase, $C^{\circ}_{i,s}$ is the initial concentration and

$$a_{i,j} = \partial C_{i,s}/\partial C_{j,m} \quad (2)$$

for each compound (solute or mobile phase additive) is evaluated for the starting concentration in the mobile phase reservoir, *i.e.*, zero for a solute and differing from zero for a mobile phase component. When n compounds are involved in the same interaction, n^2 $a_{i,j}$ terms are obtained, representing the elements of a quadratic matrix. The diagonal elements in this matrix, *i.e.* $a_{i,i}$, which correspond to the capacity factors of i, are the eigenvalues of the matrix. The relative changes of compounds i and j in a peak are given by the corresponding eigenvectors and can be used to express the relative response[5,6], as discussed below. The background to the interaction in these multicomponent systems has been extensively discussed by Helfferich and Klein[8] and by Riedo and Kováts[9].

In a previous paper[6], response models were developed for a system containing a hydrophobic adsorbent in an aqueous mobile phase with three components: *e.g.*, a cationic probe, Q^+, an anion, X^-, and a further cationic component, B^+, which is so hydrophilic that its distribution to the adsorbent is negligible. A solute injection will give rise to changes in the distribution of Q^+ and X^- at the injection zone, and the resulting chromatogram will show one solute peak and one retained system peak.

The discussion below deals with chromatographic systems in which mobile phase components are distributed to the adsorbent as two different ion pairs, resulting in chromatograms with two retained system peaks. The mobile phase is assumed to contain a buffering agent in excess. A theoretical expression for the response can be developed according to the same principles as previously published[6], if the concentration of one of the buffering components can be considered to be constant.

Constant $[H^+]$ in the mobile phase

The mobile phase contains a cationic probe, Q^+, and a buffering agent, HX. The solute, HA^+, has the same charge as the probe. The buffering anion, X^-, participates in the distribution of Q^+, HA^+ and H^+, and it is likely that $[X^-]$ in the migrating zones deviates from its normal value in the eluent. The most hydrophilic cation is H^+, and it is distributed only as an ion pair with X^-. The assumption of constant $[H^+]$ in the mobile phase is therefore a reasonable approximation.

Electroneutrality conditions give:

$$[X^-] = [HA^+] + [Q^+] + [H^+] \tag{3}$$

Ion pairs of HA^+, Q^+ and H^+ compete for the binding capacity of the adsorbent. If they compete according to a Langmuir model, and the surface is homogeneous, the concentrations of Q^+ and HA^+ on the solid phase can be expressed by

$$C_{Q,s} = \frac{A \cdot K_{QX}[Q^+]\,([H^+] + [Q^+] + [HA^+])}{N_1} \tag{4}$$

$$C_{HA,s} = \frac{A \cdot K_{HAX}[HA^+]\,([H^+] + [Q^+] + [HA^+])}{N_1} \tag{5}$$

where

$$N_1 = 1 + (K_{HAX}[HA^+] + K_{QX}[Q^+] + K_{HX}[H^+])\,([HA^+] + [Q^+] + [H^+]) \tag{6}$$

and A is the product of the binding capacity of the solid phase and the phase volume ratio in the column; K_{QX}, K_{HX} and K_{HAX} are the equilibrium constants for the distribution of Q^+, H^+ and HA^+ to the solid phase as ion pairs with X^-. The partial derivatives for the probe, Q^+, and the solute, HA^+ (*cf.*, eqn. 2), then are:

$$a_{HA,HA} = \frac{\partial C_{HA,s}}{\partial C_{HA,m}} = A \cdot K_{HAX}([H^+] + [Q^+])\,(1 - \theta_{Q,H}) = k'_{HA} \tag{7}$$

$$a_{Q,Q} = \frac{\partial C_{Q,s}}{\partial C_{Q,m}} = (A \cdot K_{QX}[H^+] + 2A \cdot K_{QX}[Q^+])\,(1 + K_{HX}[H^+]^2) + A \cdot K_{QX}[Q^+]^2 K_{HX}[H^+](1 - \theta_{Q,H})^2 = k'_Q \tag{8}$$

The fraction of the solid phase that is not covered by Q^+ or H^+ is represented by:

$$(1 - \theta_{Q,H}) = \frac{1}{\{1 + (K_{QX}[Q^+] + K_{HX}[H^+])\,[X^-]\}} \tag{9}$$

Eqns. 7 and 8 represent the eigenvalues of the matrix and correspond to the capacity factors of HA^+ and Q^+, *i.e.*, the k' values of the solute peak and the most retained system peak, respectively.

The interaction term, $a_{Q,HA}$, can be given the form:

$$a_{Q,HA} = -k'_{HA}\theta_Q\left(1 - \frac{1}{K_{HAX}([H^+] + [Q^+])^2}\right) \tag{10}$$

An expression for k'_{HA} is given by eqn. 7. θ_Q, the fractional coverage of the solid phase by Q^+, is defined by:

$$\theta_Q = \frac{C_{Q,s}}{A} = \frac{K_{QX}[Q^+][X^-]}{1 + (K_{QX}[Q^+] + K_{HX}[H^+])[X^-]} \tag{11}$$

The relative changes of the concentrations of HA^+ and Q^+ in the eluted solute peak are given by the corresponding eigenvector, derived from the matrix. The relative response can be expressed as (*cf.*, ref. 6)

$$\frac{\Delta C_Q}{\Delta C_{HA}} = \frac{\varepsilon^*_{HA}}{\varepsilon_Q} = \theta_Q\left(1 - \frac{1}{K_{HAX}([H^+] + [Q^+])^2}\right) \cdot \frac{\alpha_s}{1 - \alpha_s} \tag{12}$$

where ε^*_{HA} isthe apparent molar absorptivity of the slute HA^+, ε_Q is the molar absorptivity of the mobile phase component Q^+ and $\alpha_s = k'_{HA}/k'_Q$. When $[H^+] \gg [Q^+]$, eqn. 12 gives:

$$\frac{\varepsilon^*_{HA}}{\varepsilon_Q} = \theta_Q\left(1 - \frac{1}{K_{HAX}[H^+]^2}\right) \cdot \frac{\alpha_s}{1 - \alpha_s} \tag{13}$$

Eqn. 13 shows that the relative response increases with increased load, *i.e.*, an higher concentration of Q^+ in the mobile phase leads to a larger distribution of Q^+ to the solid phase and a higher response. The response has a maximum when α_s is close to unity, as shown earlier[6].

It should be emphasized that eqn. 13 is an approximation, since changes of $[H^+]$ in the solute zone have not been taken into consideration due to mathematical restrictions.

K_{HAX} increases with increasing hydrophobicity of the solute, HA^+. This has a large influence on the relative response, particularly when k'_{HA} is smaller than k'_Q, as summarized in Table I.

When HA^+ is hydrophilic with a low retention, $K_{HAX}[H^+]^2$ is small, and the expression $\{1 - (1/K_{HAX}[H^+]^2)\}$ will then be negative and the relative response will assume a negative value. With increasing K_{HAX}, the quotient, $1/(K_{HAX}[H^+]^2)$ will

TABLE I
DIRECTION OF SOLUTE PEAK WITH INCREASING HYDROPHOBICITY OF HA^+

α_s	$\frac{1}{K_{HAX}[H^+]^2}$	$\frac{\varepsilon^*_{HA}}{\varepsilon_Q}$
<1	>1	Negative
<1	1	0
<1	<1	Positive
>1	<1	Negative

decrease and, when its value is equal to 1, the relative response will be equal to zero. With further increase of K_{HAX} and k'_{HA} the relative response will reach an increasingly positive value until α_s is higher than 1 when the response changes to negative in the same way as in a system with a single system peak.

The concentration $[H^+]$ mainly influences the response for solutes with own K_{HAX}; $\varepsilon^*_{HA}/\varepsilon_Q$ of such solutes increases with increasing $[H^+]$.

The expressions for the capacity factors and the relative response for an uncharged solute, S, derived according to the same general principles are very simple and equal to those obtained in systems with a single system peak:

$$k'_s = a_{S,S} = A \cdot K_S(1 - \theta_{Q,H}) \tag{14}$$

and

$$\frac{\Delta C_Q}{\Delta C_S} = \frac{\varepsilon^*_S}{\varepsilon_Q} = \theta_Q \cdot \frac{\alpha_s}{1 - \alpha_s} \tag{15}$$

Reversal of the response direction between two system peaks

A study of the response in a reversed-phase chromatographic system with two system peaks was made with methylpyridinium ion as the detectable component and cyclamic acid as the buffering agent, using a polystyrene copolymer as the solid phase. The chromatographic system is denoted as No. 1 in Table II.

The response pattern for solutes in a system with one retained system peak has been presented in several previous papers. When the solute is uncharged or has the

TABLE II
CHROMATOGRAPHIC SYSTEMS
HCy = Cyclamic acid; HP = phosphoric acid; Phenyl = μBondapak Phenyl.

System No.	*Detectable component*	*Counter/buffer ions*	*Organic solvent*	*Solid phase*
1	10^{-4} *M* MP	0.01 *M* HCy	4% Methanol	PLRP-S
2	$(0.26–15) \cdot 10^{-5}$ *M* 60HNS	0.01 *M* HP	4% Methanol	PRP-1
3	10^{-3} *M* 30HBA	$3.7 \cdot 10^{-4}$ *M* TPrA Sodium hydroxide to pH 6		Phenyl

same charge as the probe, the solute peak is positive before the system peak and negative after; when the solute and probe have opposite charges, the response pattern is reversed. However, in the present system, cationic solutes, i.e., solutes with the same charge as the probe, show a deviating response pattern.

The peaks originating from the mobile phase components (system peaks) were identified by comparison of the chromatograms obtained for a series of solutes with different hydrophobicities. The k' values are given in Table III. The third system peak was the largest and was found to originate from the probe, methylpyridinium ion. The origin of the remaining three system peaks has not been elucidated.

The response pattern of alkylamines with k' values between k'_{SP2} and k'_{SP3} are demonstrated in Fig. 1A–C. Methylamine and ethylamine, which appear rather close to SP2, give negative peaks, whereas propylamine, which comes just before SP3, gives a positive peak. It should furthermore be noted that, on injection of the same amounts of methylamine and ethylamine, methylamine gave a much larger peak. This is a deviation from the normal response behaviour. Ethylamine is more strongly retained and is eluted closer to SP3 (the system peak of the probe) than methylamine. In a system with one retained system peak this should give an higher response.

Capacity factors and peak directions for these amines as well as for some cations and uncharged solutes are summarized in Table III. The results are in agreement with the theoretical predictions above based on eqns. 13 and 15.

Peak deformation

The ideal chromatographic system, designed for indirect detection, shows a stable baseline as well as symmetrical solute and system peaks with the same peak width as those obtained in direct detection. However, peak deformation and extra peaks can appear under certain chromatographic conditions. Some examples of deviations and possible explanations are given below. The discussion will deal only with deformations such as wave-shaped peaks and extra peaks that are specific for the

TABLE III
RETENTION AND PEAK DIRECTION
System 1 (see Table II).

Compound	*k'*	*Peak direction*
Mobile phase components	0.48 1.07 4.9* 5.6	
Methylamine	1.30	Neg.
Ethylamine	1.80	Neg. (small)
Propylamine	4.10	Pos.
Butylamine	13.4	Neg.
Triethylamine	13.3	Neg.
Ethyltrimethylammonium ion	3.7	Pos.
Triethylmethylammonium ion	12.9	Neg.
Diaminobutane	7.5	Neg.
1,5-Pentanediol	3.0	Pos.
1,3-Cyclohexanediol	2.9	Pos.
Acetonitrile	2.5	Pos.

* System peak originating from methylpyridinium ion.

indirect detection systems. Peak asymmetry and related effects that are due to overloading of the solid phase will not be treated.

The indirect detection systems that show deformation of solute or system peaks all have a low buffer capacity and/or a low fractional loading of the probe on the adsorbent. The specific deformations mentioned above, are as a rule, seen only in systems containing an ion-pairing probe, and it is probable that they are due to changes in the ionic composition in the zone of the migrating compound.

Peak deformations have been observed on highly hydrophobic adsorbents such as PRP-1 as well as on alkyl- or aryl-bonded silica. The background to the disturbances may, to some extent, change with the hydrophobicity of the adsorbent and, therefore, examples of both kinds of solid phases are presented.

PRP-1 as adsorbent with low loading of probe. The use of a probe with high molar absorptivity is one important way to achieve high detection sensitivity. However, such a probe can be used only in low concentration in order to avoid a very high baseline absorbance that might give rise to errors due to excessive noise and a non-linear response of the detector. The problems that can occur in such a system are illustrated by the results obtained with 60HNS ($\varepsilon \approx 5400$) as the detectable mobile phase component. It was added as the sodium salt to the mobile phase, which also contained a constant concentration of phosphoric acid and 4% of methanol. The probe concentration varied between $2.6 \cdot 10^{-6}$ and $1.5 \cdot 10^{-4}$ *M*. The chromatographic system is denoted as No. 2 in Table II.

When water or an excess of the probe was injected, the main system peak had good symmetry and its capacity factor was stable, with a relative standard deviation of 1.0–2.4% on repeated injections of the same solution. However, for injected solutes, the retention showed large variations on repeated applications of the same sample solution. The chromatograms of ionic solutes showed deviations from the normal pattern. Injection of butanesulphonate gave a solute peak without disturbing

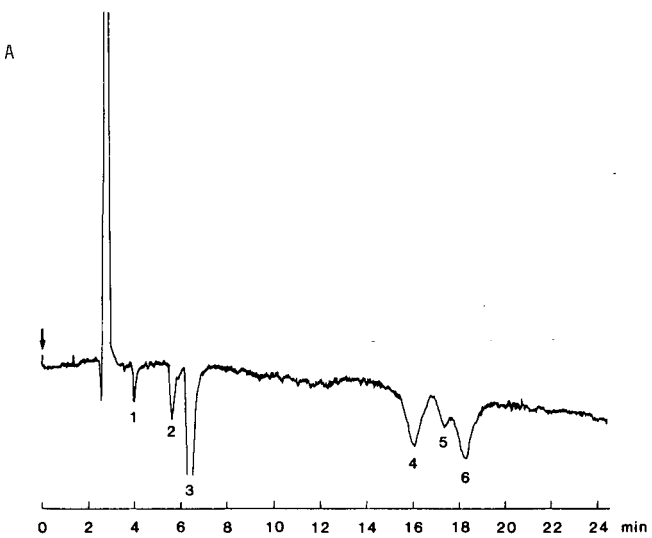

Fig. 1.

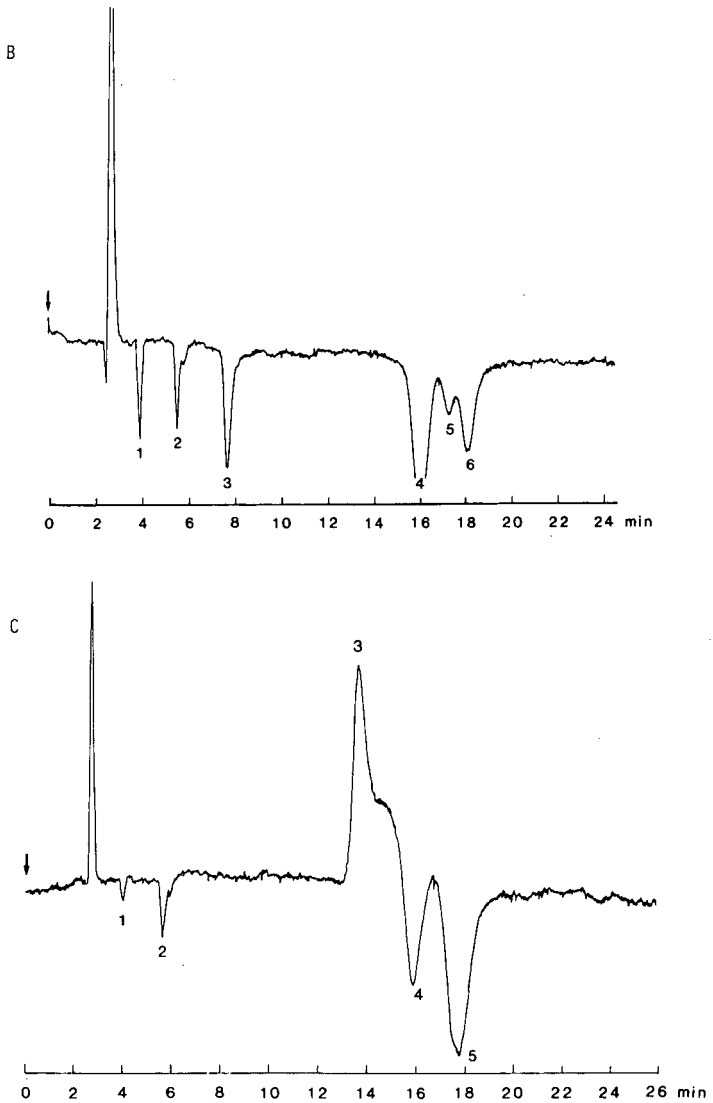

Fig. 1. (A) Reversed response of solute. Solid phase: PLRP-S 5 μm. Mobile phase: 10^{-4} M methylpyridinium–10^{-2} M cyclamic acid–4% methanol. Solute: methylamine. Peaks: 1, 2, 4 and 6 = system peaks; 3 = methylamine; 5 = unidentified impurity. (B) Solute: ethylamine (peak 3); other peaks as in (A). (C) Normal response of solute. Solute: propylamine. Peaks: 1, 2, 4 and 5 are system peaks; 3 = propylamine.

asymmetry but a wave-shaped system peak at a probe concentration of $5 \cdot 10^{-6}$ M (Fig. 2A). At a probe concentration of $1.5 \cdot 10^{-4}$ M there is also a tendency for the solute peak to assume a wave shape (Fig. 2B). Peak deformation was also observed on injection of butylamine. On the other hand, acetonitrile as a solute gave a normal chromatogram.

A low fractional coverage, θ_Q, of the probe on the adsorbent is a possible cause of the peak deformation. Low-fractional-coverage systems are known to be less stable[2],

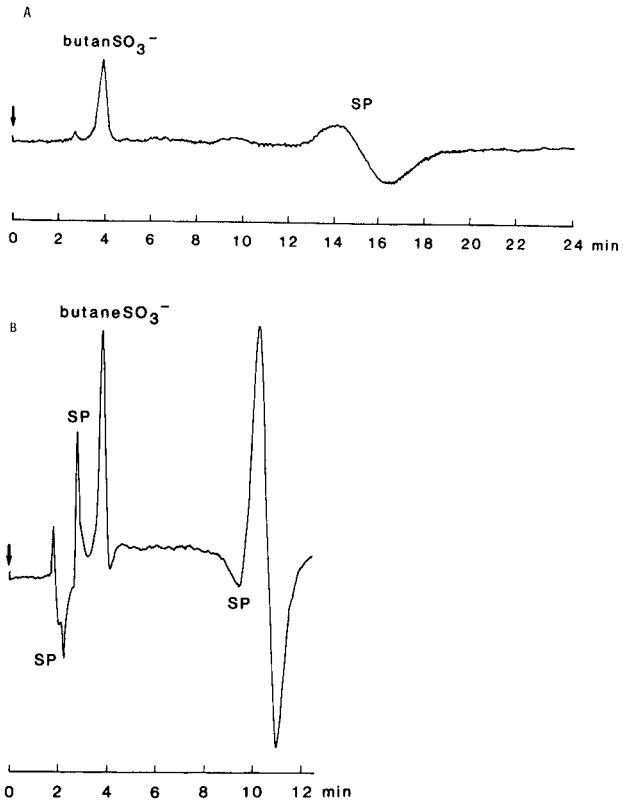

Fig 2. Wave-shaped system peaks. Solid phase: PRP-1. Solute: butanesulphonate. Mobile phases: (A) $5 \cdot 10^{-6}$ *M* 60HNS–0.01 *M* phosphoric acid–4% methanol; (B) $1.5 \cdot 10^{-4}$ *M* 60HNS–0.01 *M* phosphoric acid–4% methanol. SP = system peaks.

and this may result in multipeak chromatograms. However, a low θ_Q does not seem to be the main reason for the disturbances in this particular example. Wave-shaped system peaks appear at probe concentrations of $5 \cdot 10^{-6}$ as well as at $15 \cdot 10^{-4}$ *M* and there is no indication of less deformation of system peaks at probe concentrations as high as 30 times the lower probe concentration.

A low buffer capacity, β, of the chromatographic system can also be the reason for deformation of the peaks. The total concentration of phosphoric acid is 0.01 *M*, and the resulting pH is close to the first pK_a value of phosphoric acid, which gives $\beta = 0.006$. However, this low buffer capacity is not sufficient to prevent a pH change within the system peak zone if the retention of the probe is high and the aprotic anion of 60HNS is bound as ion pair with H^+ or exchanged for $H_2PO_4^-$ in the stationary phase. For example, when the concentration of the probe, 60HNS, is $1.5 \cdot 10^{-4}$ *M*, the system peak has $k' = 3.8$. Approximate calculations based on $\Delta C_{H_2PO_4}/\Delta pH = \beta = 0.006$ give $\Delta pH = 0.002$, which will affect the distribution of 60HNS.

Previous studies[10,11] have shown that the solid phase, PRP-1, is highly hydrophobic and can bind hydrophilic buffer components. Fig. 2A and B show that at least two system peaks appear in the chromatograms. This indicated that the buffer

components, H^+, and dihydrogenphosphate, p^-, are bound. If the peak distortion is due to a pH change, the disturbances should be different, depending on the nature of the buffer components. The disturbances would also increase with decreasing concentration of the buffer and increasing binding of the buffer to the adsorbent.

Experiment at a concentration of 60HNS of $5 \cdot 10^{-5}$ *M* showed that the systems became more unstable when the concentration of phosphoric acid decreased from 10^{-2} to 10^{-3} *M*. Increasing the pH from 2.3 to 6.9 at a constant analytical concentration of phosphoric acid also resulted in a less stable system.

Phenyl-bonded silica as adsorbent with a protolytic probe. Unstable systems giving wave-shaped system and solute peaks as well as extra peaks were also observed when alkyl- or aryl-bonded silica were used as the adsorbents. Examples of such chromatograms are seen in Figs. 3 and 4. The chromatographic system is denoted as No. 3 in Table II. It has a low buffer capacity, and the fractional coverage of the probe is probably fairly low. The probe is protolytic, and the system contains no further buffering agent.

The mobile phase contains three ions, Na^+, 30HBA and tetrapropylammonium, TPrA, and gives two retained system peaks, SP2 originating from 30HBA and SP3 from TPrA. The two chromatograms show distortions but to different extents. The sample peaks are asymmetric but the hexanoic acid peak (Fig. 4) is less distorted than the hexylamine peak in Fig. 3, which ends in an extra peak just before SP3. SP2 is more wave-shaped in Fig. 3. The peak distortion is due to the fact that the probe has a buffering function in the system, and a change in probe concentration can change the pH of the mobile phase significantly, since the buffer capacity is very low. The large distortion on injection of hexylamine could be due to the fact that 30HBA acts as a counter ion in the distribution of the cationic sample.

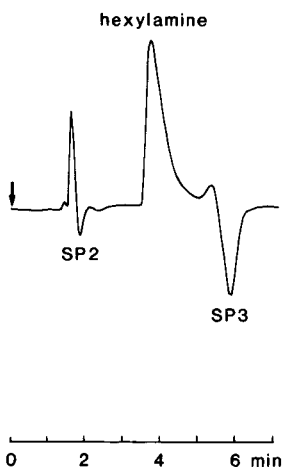

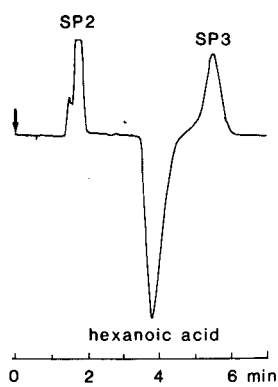

Fig. 3. Unstable chromatographic system. Solid phase: μBondapak Phenyl. Mobile phase: 10^{-3} *M* 30HBA–$3.7 \cdot 10^{-4}$ *M* TPrA–sodium hydroxide to pH 6. Solute: hexylamine. From ref. 2. Reprinted with permission.

Fig. 4. Unstable chromatographic system as in Fig. 3 but solute was hexanoic acid. From ref. 2. Reprinted with permission.

The peak distortions due to low system stability, *e.g.*, low buffer capacity, could be initiated at the injection zone, but it seems likely that they are amplified and, in fact, mainly created during the migration of the compound zone in the column.

Direction of extra peaks

The extra peaks appearing close to the main peaks in insufficiently buffered solutions can have the same or the opposite direction as the main peak (*cf.*, Fig. 2B). A discussion may be based on the basic expression for the indirect response, given below. It is valid for a solute HA^+ in a chromatographic system containing two components, the probe, Q^+, and the counter ion, X^-, that can be distributed to the adsorbent. The third component, B^+, is so hydrophilic that its distribution is negligible (*cf.*, ref. 6)

$$\frac{\varepsilon^*_{HA}}{\varepsilon_Q} = L - M \tag{16}$$

where

$$L = \frac{\alpha_s}{1 - \alpha_s} \cdot \theta_Q \tag{17}$$

and

$$M = \frac{1}{1 - \alpha_s} \cdot \frac{C_Q}{2C_Q + C_B} \tag{18}$$

The M term is usually negliglible when C_B is much larger than C_Q. If this is not the case and C_B changes within the solute zone, due to, *e.g.*, protolysis, it can have a significant effect on the response. An increase in C_B will increase the absolute value of the response, and a shoulder or second maximum may appear in the peak. A decrease in C_B has the opposite effect, and if L and M are of similar magnitude, it can even change the direction of the response, which may result in a wave-shaped peak.

Design of ion-pairing systems for indirect detection

From the basic expression for indirect detection in ion-pairing systems (eqn. 16) it follows that optimum sensitivity is obtained when the retention of the solute is close to that of the probe (α_s close to 1) and when the detector response of the probe, *e.g.*, the molar absorptivity is high. For solutes that are uncharged or have the same charge as that of the probe, the sensitivity increases with the fractional loading of the probe on the adsorbent, θ_Q.

To avoid disturbances in sensitivity and peak shape, it is important to use mobile phases which contain only a few components: if possible only the probe and hydrophilic buffer. More than one hydrophobic component in the mobile phase may result in several retained system peaks and decrease the detection sensitivity for the components that are eluted between them.

The probe should be aprotic to avoid detection disturbances due to protolysis.

The buffer should have a capacity and concentration such that changes in the distribution of the probe are avoided.

REFERENCES

1 L. Hackzell, M. Denkert, G. Schill and E. Sjögren, *J. Chromatogr.*, 218 (1982) 31.
2 L. Hackzell and G. Schill, *Chromatographia.*, 15 (1982) 437.
3 L. Hackzell, T. Rydberg and G. Schill, *J. Chromatogr.*, 282 (1983) 197.
4 P. Herné, M. Renson and J. Crommen, *Chromatographia.*, 19 (1984) 274.
5 G. Schill and J. Crommen, *Trends Anal. Chem.*, 6 (1987) 111.
6 J. Crommen, G. Schill, D. Westerlund and L. Hackzell, *Chromatographia.*, 24 (1987) 252.
7 J. Crommen, G. Schill and P. Herné, *Chromatographia.*, 25 (1988) 397.
8 F. Helfferich and G. Klein, *Multicomponent Chromatography*, Marcel Dekker, New York, 1970.
9 F. Riedo and E. sz. Kováts, *J. Chromatogr.*, 239 (1982) 1.
10 E. Arvidsson, J. Crommen, G. Schill and D. Westerlund, *J. Chromatographia*, 24 (1987) 460.
11 E. Arvidsson, J. Crommen, G. Schill and D. Westerlund, *J. Chromatographia*, in press.

Author Index

Vol. 461

journal of
chromatography news section

SHORT CONFERENCE REPORT

HPLC '88, 12th INTERNATIONAL SYMPOSIUM ON COLUMN LIQUID CHROMATOGRAPHY, WASHINGTON, DC, U.S.A., JUNE 19–24, 1988

HPLC '88 was held at the Sheraton Washington Hotel which although somewhat eccentric was readily accessible from the centre of Washington by Metro. Attendance was high at some 1200 souls, and there was a well-visited and extensive exhibit featuring instruments and publishers.

It was quite generally opined that the level of the papers was excellent, and the kind reader will be able to form his own opinion on this after perusing these three volumes of the Proceedings.

The Sheraton Washington fortunately is notable for the efficiency of its air conditioning system. This effectively kept the participants prisoner in the scientific sessions as the temperatures outside were record highs for this week in June. The humidity was also often in the region of 100%.

Fig. 1. The Chairman of the symposium Georges Guiochon, starting things off in the Sheraton Washington Hotel.

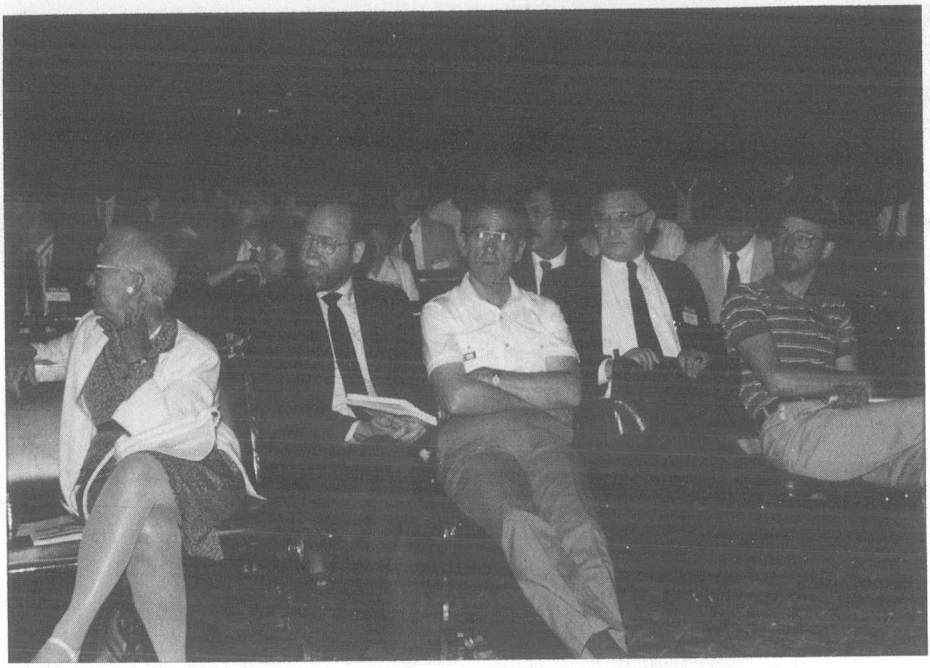

Fig. 2. Part of the audience at the opening session whilst clearly something of interest was happening off left. We see Phyllis Brown, Wayne Melander, Lloyd Snyder, Csaba Horváth and John Dolan.

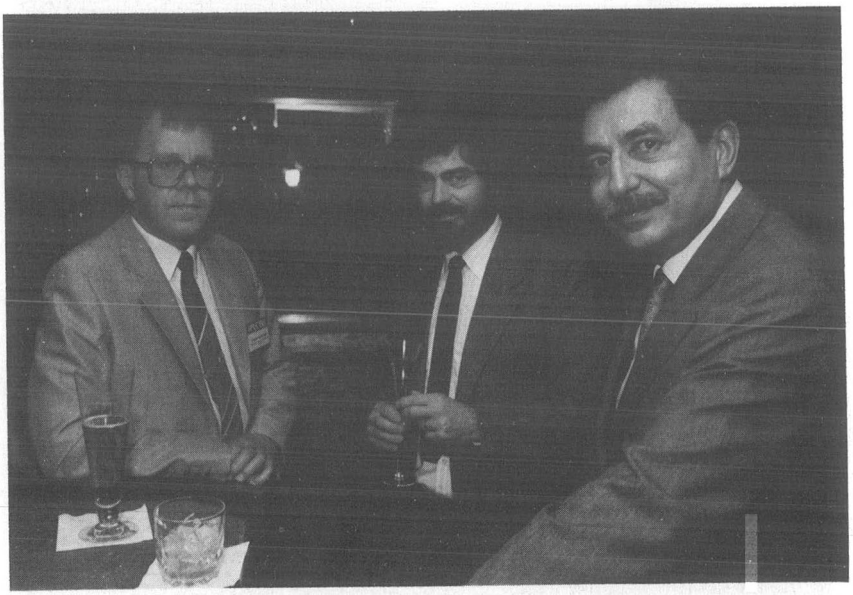

Fig. 3. Douglas Westerlund looks worried in the company of Michel Martin and Claude Guillemin. He is perhaps reflecting on the cares of organising CLC'89 (the next in the series, with an alternative abbreviation) in Stockholm. It is the thirteenth.

Fig. 4. A panoramic view of the opening session chaired by Josef Huber. The attentive reader will be able to locate a great many prominent chromatographers in the audience.

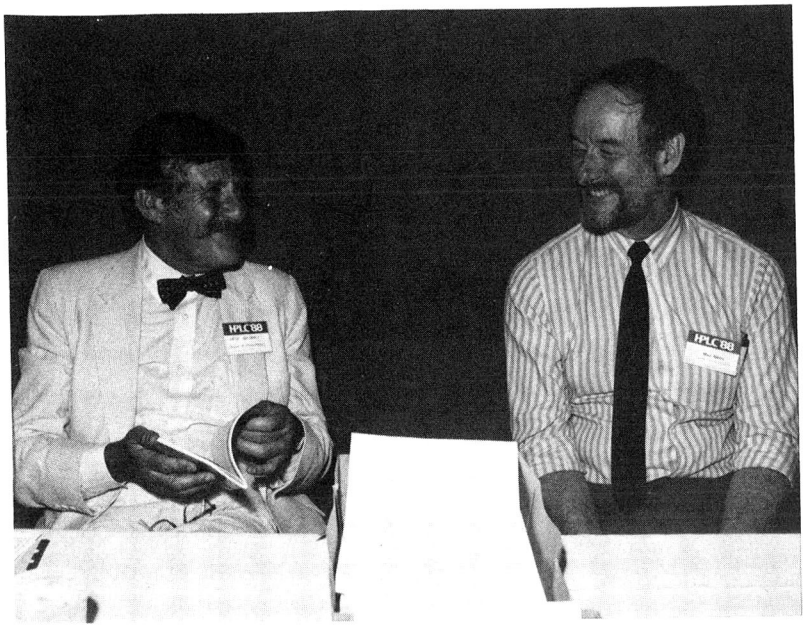

Fig. 7. Erich Heftmann, editor of the Proceedings, is clearly delighted with the way the manuscripts are coming in. There are none actually to be seen, having been stored carefully in large cardbord boxes off right.

Fig.8. Arriving at one of the functions we see the Chairman accompanying his beautiful wife Lois and two other attractive participants.

(All photos courtesy of Panoramic Visions, Reston, VA 22091, U.S.A.)

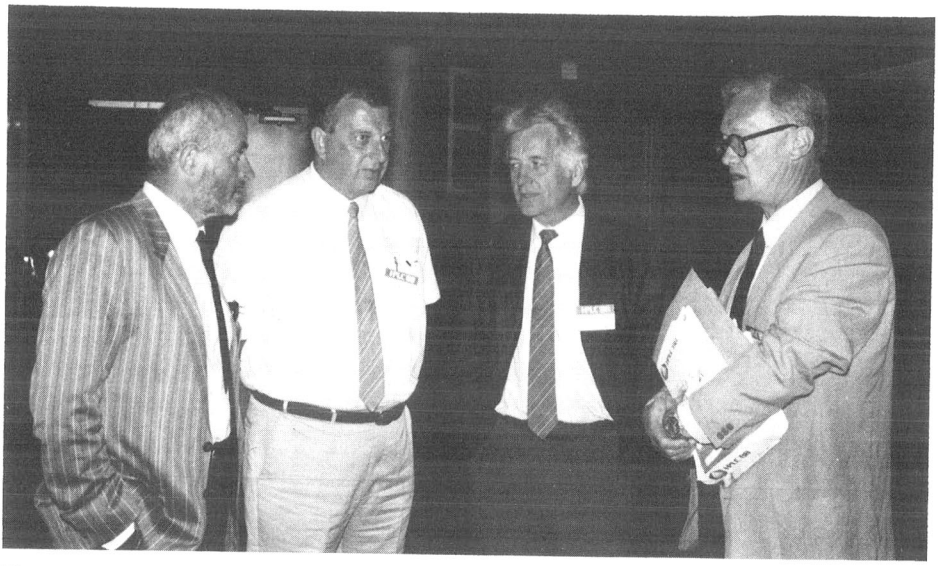

Fig. 5. A very serious discussion underway amongst a national group during a coffee break. It is not difficult to guess which language was being spoken. From left to right Klaus Unger, Heinz Engelhardt, Peter Hupe and Gerhard Schomburg. The last appears not yet to have handed his manuscript to Erich Heftmann.

Fig. 6. There were several delightful receptions during the symposium. Here we see a coolly-clad but apparently surprised John Knox in the company of Shmuel Shaltiel and Barry Karger, Chairman of HPLC '90 (back to the original abbreviation) in Boston.

Analytical Artifacts

GC, MS, HPLC, TLC and PC

by **B.S. MIDDLEDITCH**, *Dept. of Biochemical and Biophysical Sciences, University of Houston, Houston, TX, USA*

(Journal of Chromatography Library, 44)

This encyclopaedic catalogue of the pitfalls and problems that all analysts encounter in their work is destined to spend more time on the analyst's workbench than on a library shelf. The author has dedicated the book to "the innumerable scientists who made mistakes, used impure chemicals and solvents, suffered the consequences of unanticipated side-reactions, and were otherwise exposed to mayhem yet were too embarrassed to publish their findings".

Traditionally, the mass spectroscopist or gas chromatographer learnt his trade by participating in a 4-6 year apprenticeship as graduate student and post-doctoral researcher. Generally, no formal training was provided on the things that go wrong, but this information was accumulated by sharing in the experiences of colleagues. Nowadays, many novice scientists simply purchase a computerized instrument, plug it in, and use it. Much time can be wasted in studying and resolving problems due to artifacts and there is also a strong possibility that artifacts will not be recognized as such. For example, most analysts realize that they should use glass rather than plastic containers; but few of them would anticipate the possibility of plasticizer residues on glassware washed using detergent from a plastic bottle.

This book is an easy-to-use compendium of problems encountered when using various commonly used analytical techniques. Emphasis is on impurities, by-products, contaminants and other artifacts. A separate entry is provided for each artifact. For specific chemicals, this entry provides the common name, mass spectrum, gas chromatographic data, CAS name and registry number, synonyms and a narrative discussion. More than 1100 entries are included. Mass spectral data are indexed in a 6-peak index (molecular ion, base peak, second peak, third peak) and there are also formula, author and subject indexes. An extensive bibliography contains complete literature citations.

The book is designed to be *used*. It will not only allow experienced analysts to profit from the mistakes of others, but it will also be invaluable to other scientists who use analytical instruments in their work.

1989 xxiv + 1028 pages
US$ 241.50 / Dfl. 495.00
ISBN 0-444-87158-6

ELSEVIER SCIENCE PUBLISHERS

P.O. Box 211, 1000 AE Amsterdam, The Netherlands
P.O. Box 882, Madison Square Station, New York, NY 10159, USA

Quantitative Gas Chromatography for Laboratory Analyses and On-line Process Control

by G. GUIOCHON and C.L. GUILLEMIN

(Journal of Chromatography Library, 42)

This is a book which no chemical analyst should be without!

It explains how quantitative gas chromatography can - or should - be used for accurate and precise analysis. All the problems involved in the achievement of quantitative analysis by GC are covered, whether in the research lab, the routine analysis lab or in process control.

The discussion of the theoretical background is restricted to essentials. It is presented in a way that is simple enough to be understood by all analytical chemists, while being complete and up-to-date.

Extensive and detailed descriptions are given of the various steps involved in the derivation of precise and accurate data. This starts with the selection of the instrumentation and column, continues with the choice of optimum experimental conditions, then calibration and ends with the use of correct procedures for data acquisition and calculations.

Finally, there is almost always a way to reduce errors and an entire chapter deals with this single issue. Numerous examples are provided.

A lexicon explaining the most important chromatographic terms and a detailed index complete the book.

This is a book which should be on the library shelf of all universities, instrument companies and any laboratory and plant where gas chromatography is used.

1988 780 pages
US$ 165.75 / Dfl. 315.00
ISBN 0-444-42857-7

A brochure describing the contents of this book in detail is available on request from the publisher

Elsevier Science Publishers

P.O. Box 211, 1000 AE Amsterdam, The Netherlands
P.O. Box 1663, Grand Central Station, New York, NY 10163, USA

PUBLICATION SCHEDULE FOR 1989

Journal of Chromatography and Journal of Chromatography, Biomedical Applications

MONTH	J	F	M	
Journal of Chromatography	461 462 463/1	463/2 464/1	The publication schedule for further issues will be published later	
Bibliography Section		486/1		
Biomedical Applications	487/1	487/2	488/1 488/2	

INFORMATION FOR AUTHORS

(Detailed *Instructions to Authors* were published in Vol. 445, pp. 453–456. A free reprint can be obtained by application to the publisher, Elsevier Science Publishers B.V., P.O. Box 330, 1000 AH Amsterdam, The Netherlands.)

Types of Contributions. The following types of papers are published in the *Journal of Chromatography* and the section on *Biomedical Applications:* Regular research papers (Full-length papers), Notes, Review articles and Letters to the Editor. Notes are usually descriptions of short investigations and reflect the same quality of research as Full-length papers, but should preferably not exceed six printed pages. Letters to the Editor can comment on (parts of) previously published articles, or they can report minor technical improvements of previously published procedures; they should preferably not exceed two printed pages. For review articles, see inside front cover under Submission of Papers.

Submission. Every paper must be accompanied by a letter from the senior author, stating that he is submitting the paper for publication in the *Journal of Chromatography*. Please do not send a letter signed by the director of the institute or the professor unless he is one of the authors.

Manuscripts. Manuscripts should be typed in double spacing on consecutively numbered pages of uniform size. The manuscript should be preceded by a sheet of manuscript paper carrying the title of the paper and the name and full postal address of the person to whom the proofs are to be sent. Authors of papers in French or German are requested to supply an English translation of the title of the paper. As a rule, papers should be divided into sections, headed by a caption (*e.g.*, Summary, Introduction, Experimental, Results, Discussion, etc.). All illustrations, photographs, tables, etc., should be on separate sheets.

Introduction. Every paper must have a concise introduction mentioning what has been done before on the topic described, and stating clearly what is new in the paper now submitted.

Summary. Full-length papers and Review articles should have a summary of 50–100 words which clearly and briefly indicates what is new, different and significant. In the case of French or German articles an additional summary in English, headed by an English translation of the title, should also be provided. (Notes and Letters to the Editor are published without a summary.)

Illustrations. The figures should be submitted in a form suitable for reproduction, drawn in Indian ink on drawing or tracing paper. Each illustration should have a legend, all the *legends* being typed (with double spacing) together on a *separate sheet*. If structures are given in the text, the original drawings should be supplied. Coloured illustrations are reproduced at the author's expense, the cost being determined by the number of pages and by the number of colours needed. The written permission of the author and publisher must be obtained for the use of any figure already published. Its source must be indicated in the legend.

References. References should be numbered in the order in which they are cited in the text, and listed in numerical sequence on a separate sheet at the end of the article. Please check a recent issue for the layout of the reference list. Abbreviations for the titles of journals should follow the system used by *Chemical Abstracts*. Articles not yet published should be given as "in press" (journal should be specified), "submitted for publication" (journal should be specified), "in preparation" or "personal communication".

Dispatch. Before sending the manuscript to the Editor please check that the envelope contains three copies of the paper complete with references, legends and figures. One of the sets of figures must be the originals suitable for direct reproduction. Please also ensure that permission to publish has been obtained from your institute.

Proofs. One set of proofs will be sent to the author to be carefully checked for printer's errors. Corrections must be restricted to instances in which the proof is at variance with the manuscript. "Extra corrections" will be inserted at the author's expense.

Reprints. Fifty reprints of Full-length papers, Notes and Letters to the Editor will be supplied free of charge. Additional reprints can be ordered by the authors. An order form containing price quotations will be sent to the authors together with the proofs of their article.

Advertisements. Advertisement rates are available from the publisher on request. The Editors of the journal accept no responsibility for the contents of the advertisements.

For Superior Chiral Separation

CHIRALCEL, CHIRALPAK and CROWNPAK are now available from DAICEL and include 15types of HPLC columns which provide superior resolution of racemic compounds.

Drugs directly resolved on our DAICEL columns are given as follows;

SUBSTANCE	α	column
Alprenolol	3.87	OD
Amphetamine	1.2	CR
Atenoloi	1.58	OD
Atropine	1.62	OD
Baclofen	1.39	CR
Carbinoxamine	1.39	OD
Carteolol	1.86	OD
Chlophedianol	2.82	OJ
Chlormezanone	1.47	OJ
Cyclopentolate	2.47	OJ
Diltiazem	1.46	OD
	2.36	OF
	1.75	OG
Disopyramide	2.46	OF
Ethiazide	1.54	OF
Ethotoin	1.40	OJ
Fenoprofen	1.35	OJ
Glutethimide	2.48	OJ

SUBSTANCE	α	column
Gauifenesin	2.40	OD
Hexobarbital	1.7	CA-1
Homatropine	3.13	OD
Hydroxyzine	1.17	OD
Indapamide	1.58	OJ
Ketamine	complete resolution	CA-1
Ketoprofen	1.46	OJ
Mephobarbital	5.9	OJ
	2.3	CA-1
Methaqualone	2.8	CA-1
	7.3	OJ
Methsuximide	2.68	OJ
Metoprolol	complete resolution	OD
Mianserin	1.75	OJ
Nilvadipine	complete resolution	OT

SUBSTANCE	α	column
Oxapadol	complete resolution	CA-1
Oxazepan	4.36	OC
Oxazolam	1.67	OF
Oxprenolol	6.03	OD
Perisoxal	1.33	OF
	1.27	OD
Pindolol	5.07	OD
Piprozolin	1.7	CA-1
Praziquantal	complete resolution	CA-1
Propranolol	2.29	OD
Rolipram	complete resolution	CA-1
Sulconazole	1.68	OJ
Suprofen	1.6	OJ
Trimebutine	1.81	OJ
Warfarin	1.96	OC

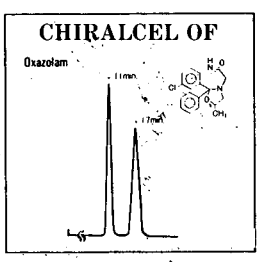

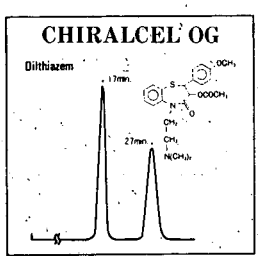

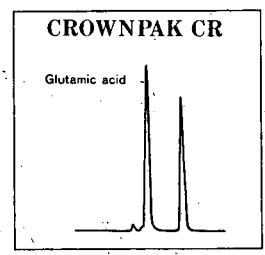

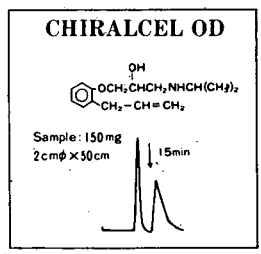

In addition to the drugs listed above, our chiral columns permit resolution also of the following: FMOC amino acids and Carboxylic acids, and Pesticides, for example Isofenfos, EPN and Acephate, and Synthetic intermediate 4-hydroxy cyclophentenone etc, Many other compounds besides these can be readily resolved.

▷ *Separation Service*

- A pure enantiomer separation in the amount of 100g~10kg is now available.
- Please contact us for additional information regarding the manner of use and application of our chiral columns and how to procure our separation service.

For more information about our Chiral Separation Service and Columns, please contact us!

DAICEL CHEMICAL INDUSTRIES, LTD.

Tokyo
8-1, Kasumigaseki 3-chome,
Chiyoda-ku, Tokyo 100, Japan
Phone: 03(507)3151, 3189
Telex: 222-4632 DAICEL J
FAX: 03(507)3193

New York
Pan-Am Bldg. 200 Park Avenue,
New York, N.Y. 10166-0130, U.S.A.
Phone: (212)878-6765, 6766
Telex: (23)236154 DCC UR
FAX: (212)983-8190

DAICEL (U.S.A.) INC.
611 west 6th Street, Room 2152
Los Angeles California 90017, U.S.A.
Phone: (213)629-3656
Telex: 215515 DCIL UR
FAX: (213)629-2109

DAICEL (EUROPA) GmbH
Königsallee 92a
4000 Düsseldorf 1, F.R. Germany
Phone: (0211)134158
Telex: (41)8588042 DCEL D
FAX: (0211)879-8329